Illustrations

to

Phase Equilibrium Studies of Some Basalt-like Compositions in the System $CaO-MgO-Al_2O_3-SiO_2-Na_2O-Fe-O_2$

by

David John Humphries, B.A.

Thesis presented for the Degree of Doctor of Philosophy of the University of Edinburgh in the Faculty of Science

1975

EDINBURGEN. EX BIBL. UNIV.

CONTENTS

Volume 2 - Illustrations

CHAPTER 2 EXPERIMENTAL TECHNIQUE

Figures 2.1-2.8

CHAPTER 3 METHOD OF PRESENTATION OF RESULTS

Figures 3.1-3.6

CHAPTER 4 THE SYSTEM $CaO-MgO-Al_2O_3-SiO_2$

Figures 4.1-4.13

CHAPTER 5 THE SYSTEM $CaO-MgO-Al_2O_3-SiO_2-Na_2O$

Figures 5.1-5.20

CHAPTER 6 THE SYSTEM $CaO-MgO-Al_2O_3-SiO_2-Fe-O_2$

Figures 6.1-6.102

CHAPTER 7 THE SYSTEM $CaO-MgO-Al_2O_3-SiO_2-Na_2O-Fe-O_2$

Figures 7.1-7.4

CHAPTER 8 MELTING STUDIES ON NATURAL ROCKS

Figures 8.1-8.36

Abbreviations are given in Appendix A (Volume 1). The shorthand notation for the equilibria is explained in section 3.3

CHAPTER 2

EXPERIMENTAL TECHNIQUE

Figures 2.1 - 2.8

Figure 2.1

The thermal profile for the temperature range 1000-1400°C, of Furnace 6 used in this study, typical of each furnace used. The depth indicated is the depth of the tip of the axial thermocouple from a fixed reference point on the furnace shell. Note the development of the temperature maximum (dashed line) as the nominal temperature increases. The position chosen for the running depth (262 mm) allows for the minimum of temperature differences for slight errors in running depth, and for no overshoot of temperature when the probe is lowered into the furnace, assuming runs are to be made in the temperature range 1000-1400°C.

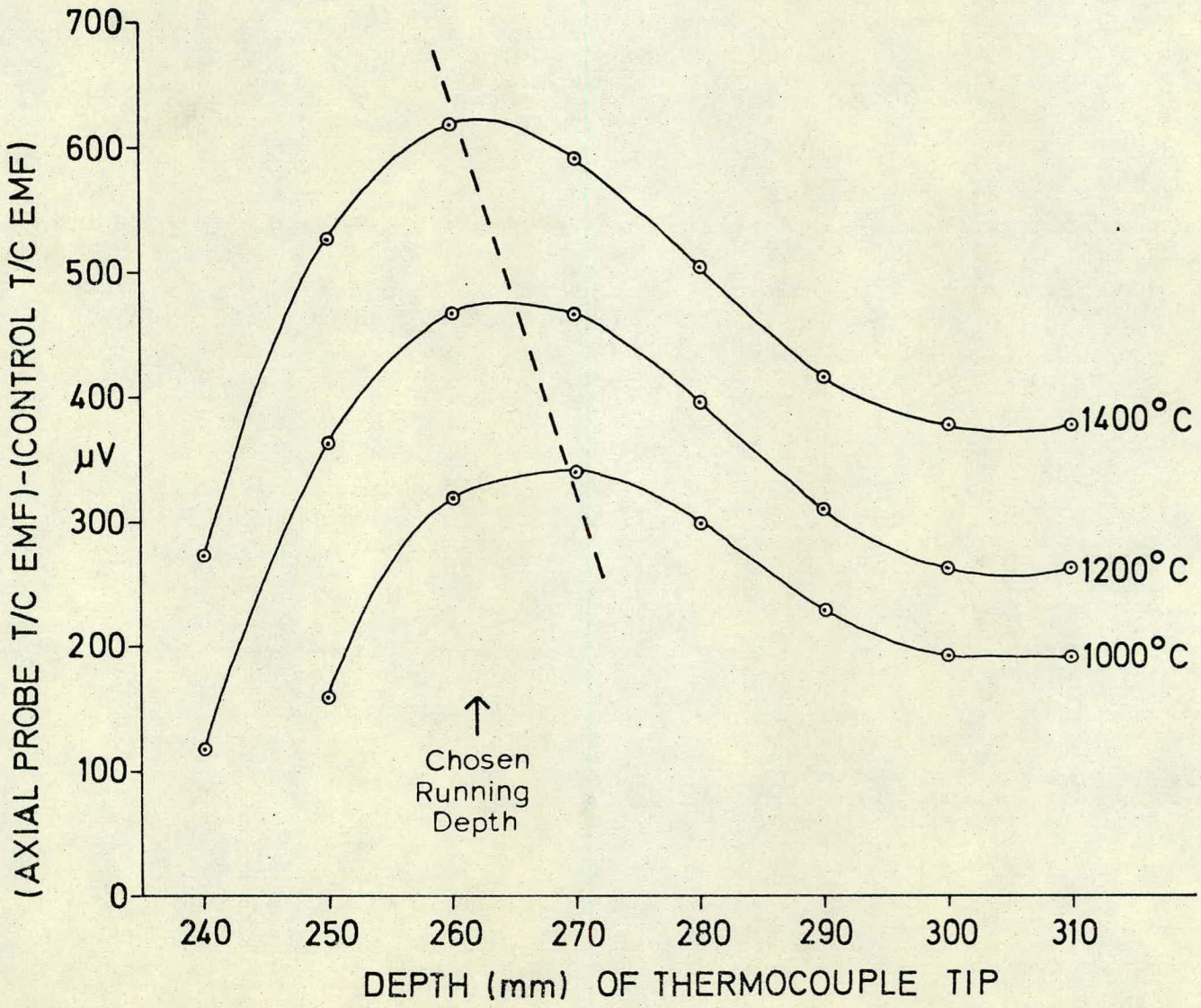
700
600
500
400
μV
300
200
100
0
(AXIAL PROBE T/C EMF)-(CONTROL T/C EMF)
1400°C
1200°C
1000°C
Chosen
Running
Depth
240
250
260
270
280
290
300
310
DEPTH (mm) OF THERMOCOUPLE TIP

Fig 2.1

Figure 2.2

A trace of the emf recorded on the axial thermocouple from the moment the probe reaches its final running depth, until the emf has stabilised at the run emf value. Note that no overshoot occurs with this steady lowering technique.

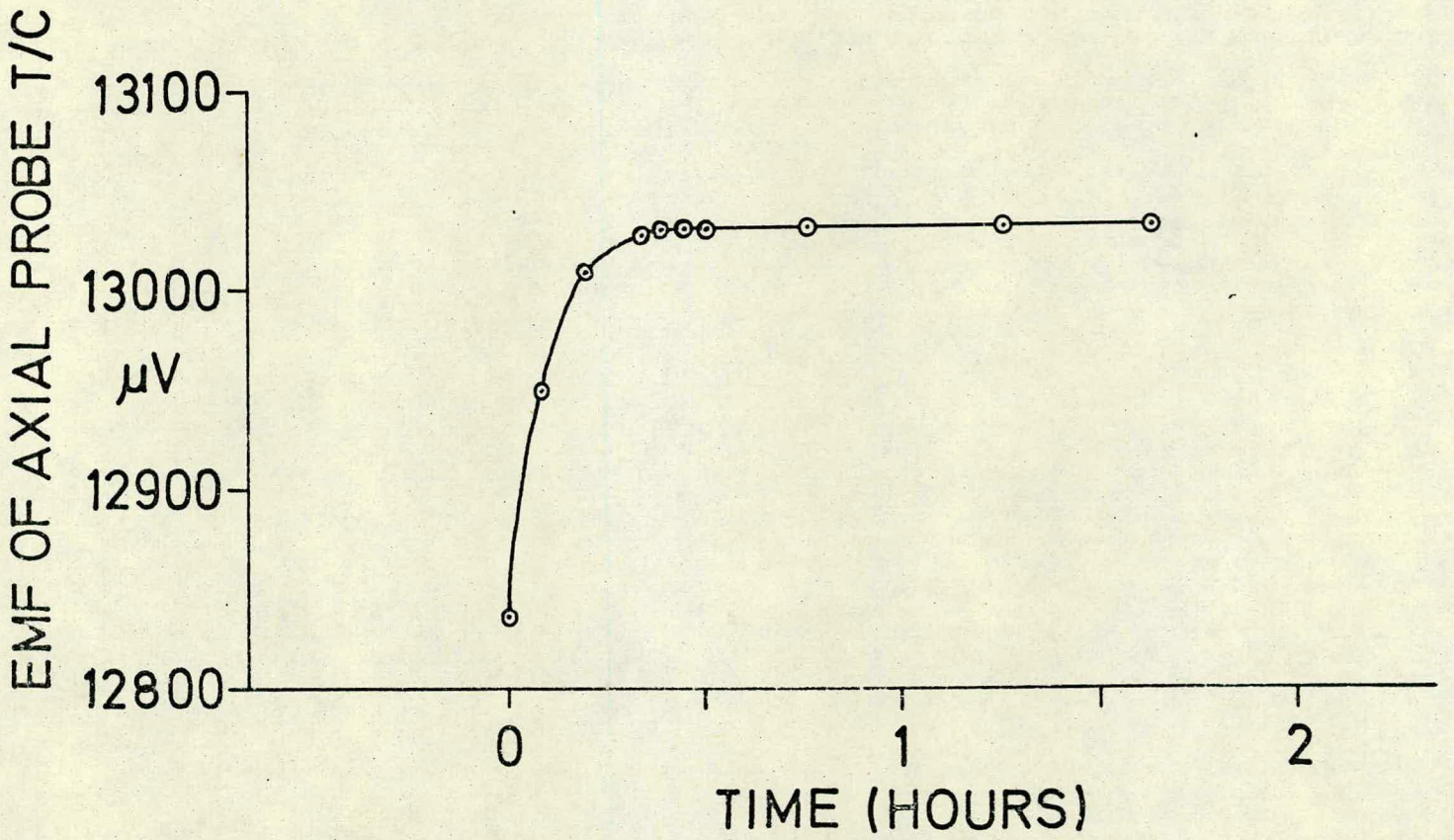
EMF OF AXIAL PROBE T/C
13100
13000
μV
12900
12800
0
1
2
TIME (HOURS)

Fig 2.2

Figure 2.3

Diagram showing the pO_2-temperature relationship measured in a cooling magma lake (dashed line through circles, from Sato and Wright, 1966), and inferred from a study of opaque minerals in trachybasalt lavas (dashed lines through crosses, from Anderson, 1968), and the pO_2 of the reference equilibria at which the controlled atmosphere experiments were conducted.

Also shown are the capsule materials which can be used at particular temperature-pO_2 conditions. The curve labelled Ag-Pd marks the upper temperature and lower pO_2 limits of the optimum silver-palladium alloy compositions for use as containers for iron-bearing charges, from Muan (1963).

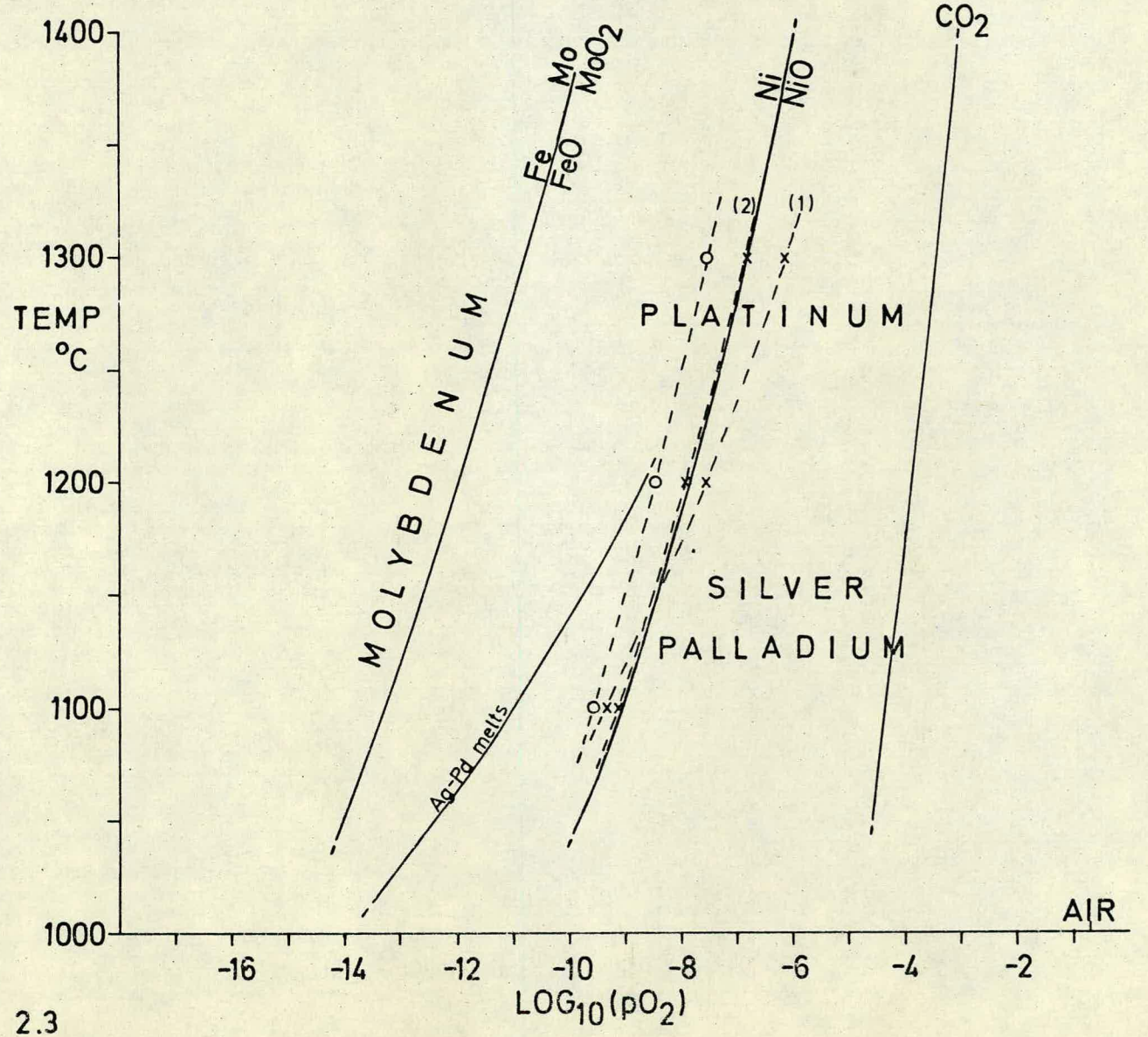
1400
1300
1200
1100
1000
TEMP
°C
Mo
MoO2
Fe
FeO
Ni
NiO
CO2
(2)
(1)
MOLYBDENUM
PLATINUM
SILVER
PALLADIUM
Ag-Pd melts
AIR
-16
-14
-12
-10
-8
-6
-4
-2
LOG10(pO2)

Fig 2.3

Figures 2.4 to 2.7

Temperature-pO_2 plots of the calibration data for each of the atmospheric controlled furnaces used. On each diagram is shown the reference curve (solid line) - for the Ni/NiO equilibrium from Eugster and Wones (1962) equation; for the Fe/FeO equilibrium from the data of Darken and Gurry (1945) - and the actual calibration curve (dashed line) determined for each furnace. The appropriate value to correct the experimental value to the "true" value of the reference curve was calculated based on these figures.

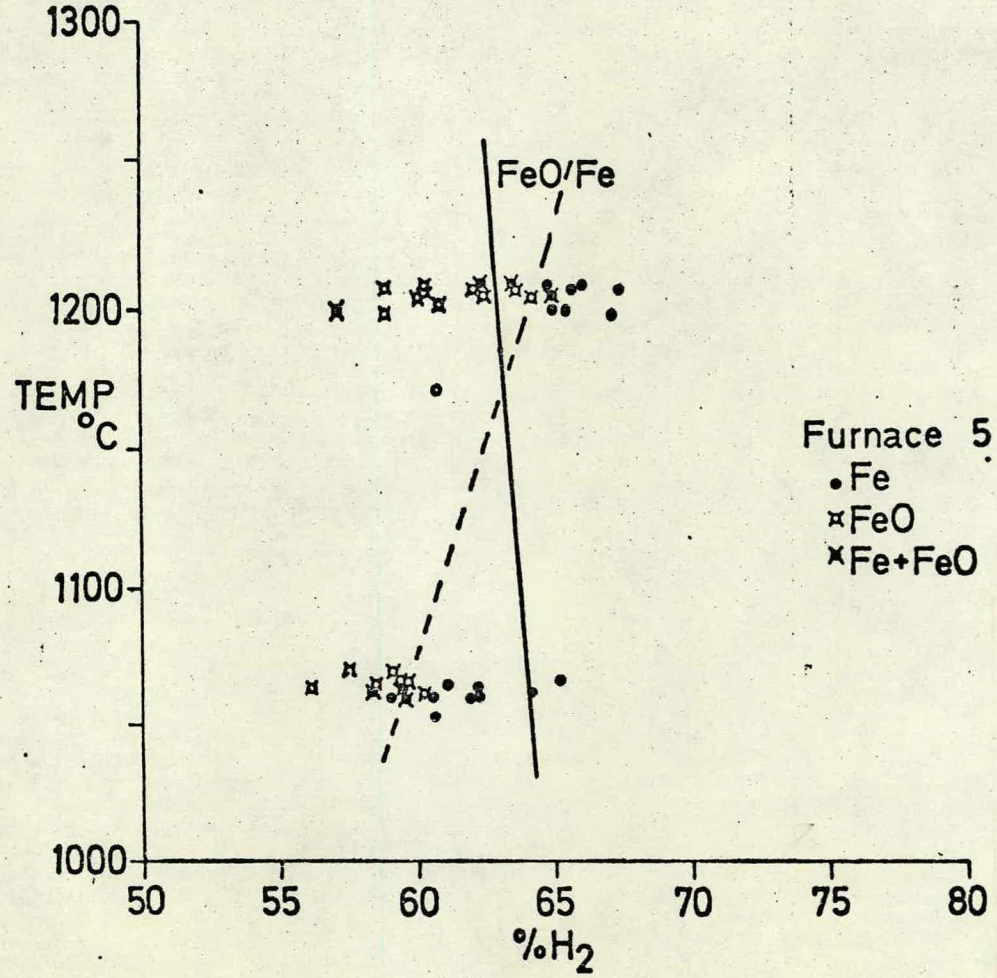
1300
1200
1100
1000
TEMP °C
FeO/Fe
Furnace 5
• Fe
¤ FeO
✕ Fe+FeO
50
55
60
65
70
75
80
%H2

Fig 2.4

Figure 2.5

See figure 2.4

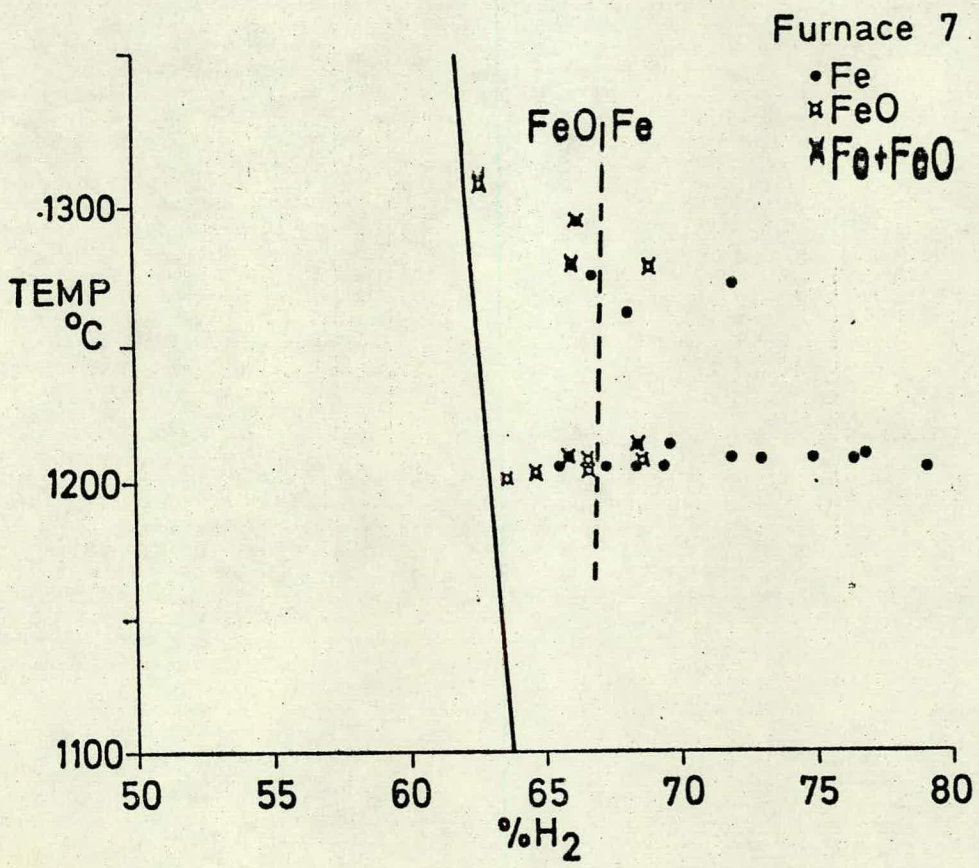
Furnace 7
• Fe
¤ FeO
✱ Fe+FeO
FeO | Fe
1300
TEMP °C
1200
1100
50
55
60
65
70
75
80
%H2

Fig 2.5

Figure 2.6

See figure 2.4

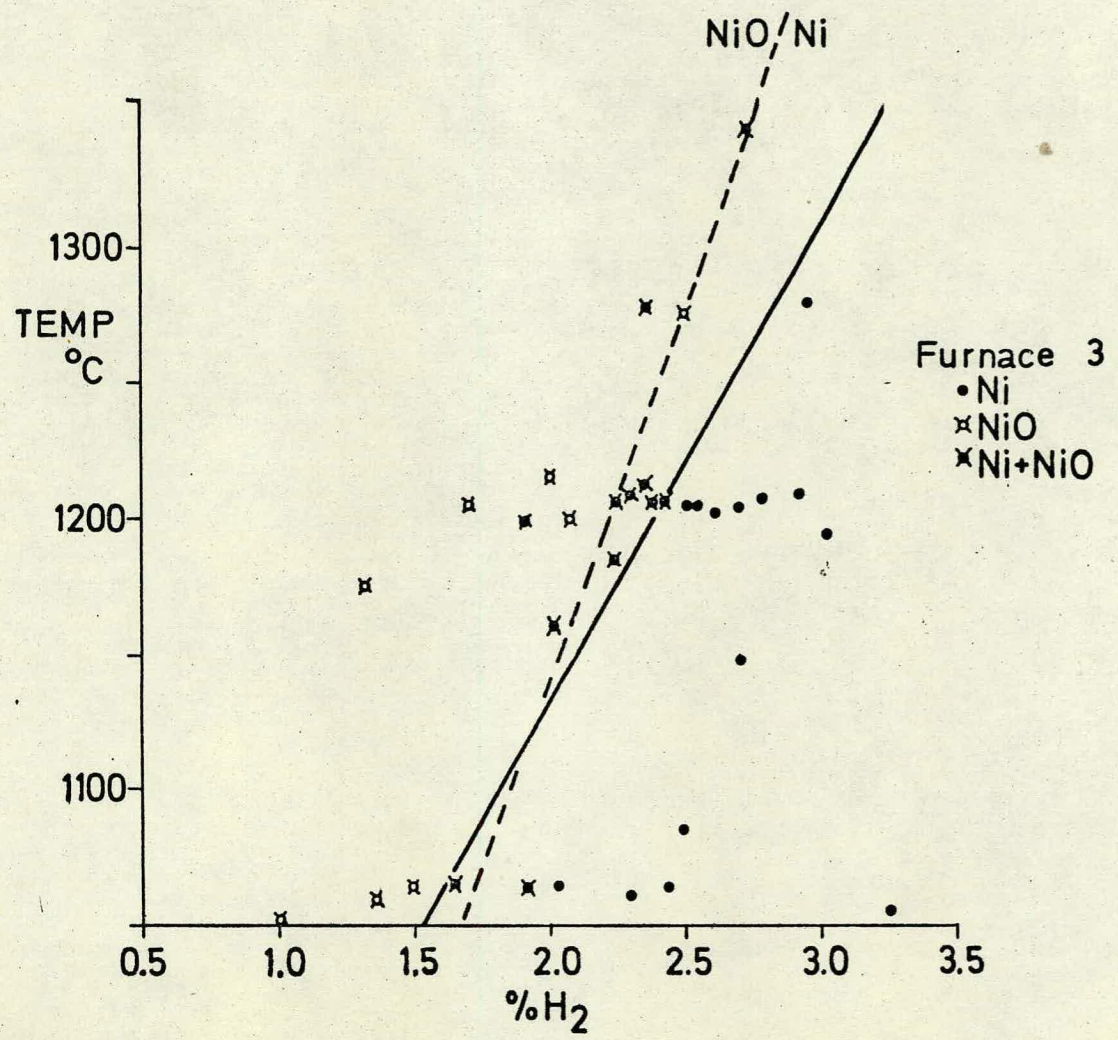
NiO/Ni
1300
TEMP
°C
1200
1100
0.5
1.0
1.5
2.0
2.5
3.0
3.5
%H2
Furnace 3
•Ni
¤NiO
✱Ni+NiO

Fig 2.6

Figure 2.7

See figure 2.4

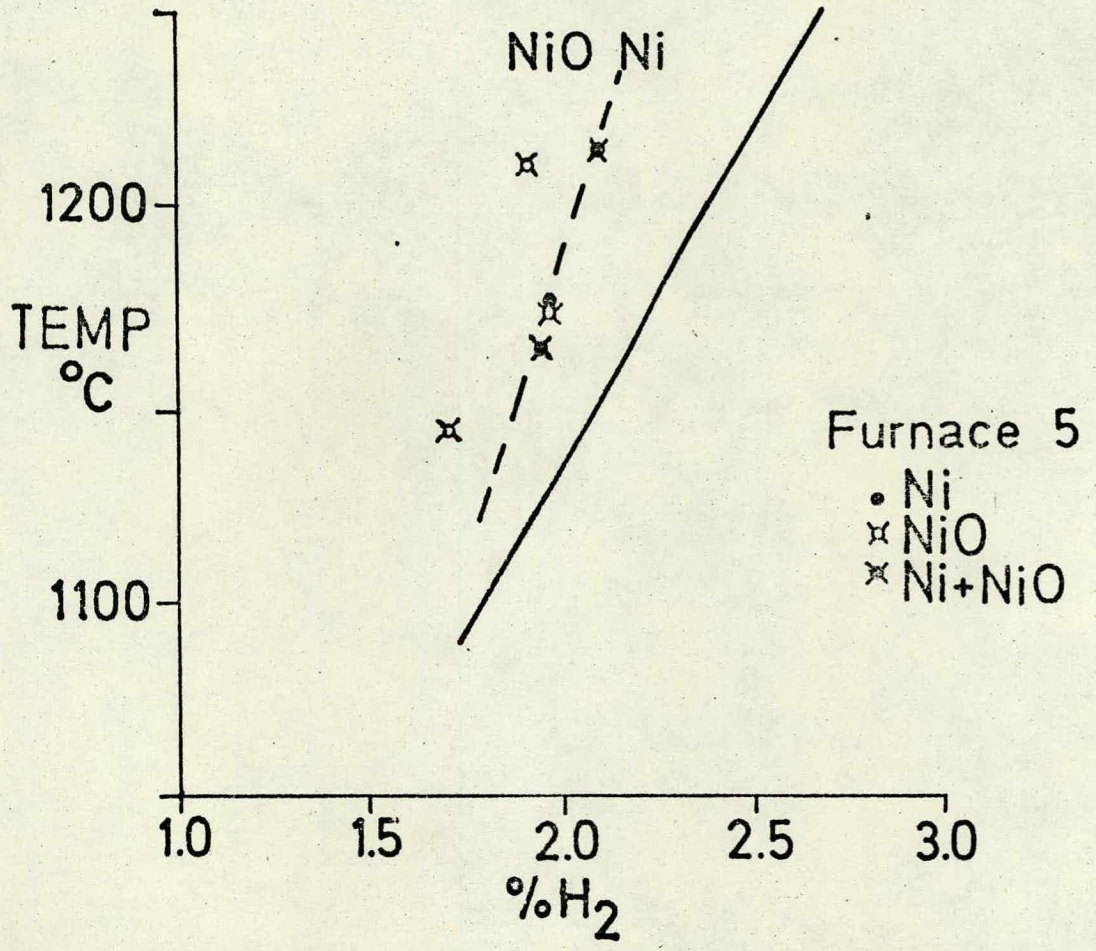

Fig 2.7

Figure 2.8

Diagrammatic layout of the gas supply system to each of the atmospheric controlled furnaces. The values a and b are used to calculate the CO_2 and H_2 ccs in the gas stream to the furnace.

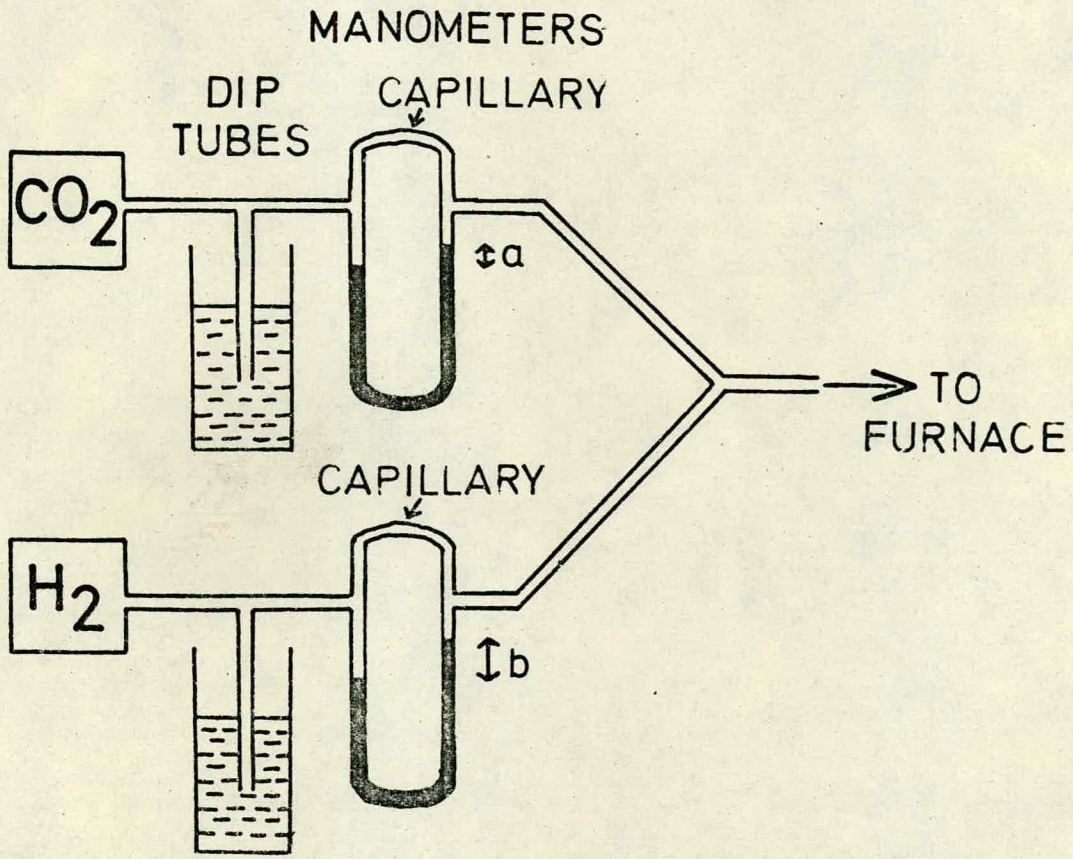
MANOMETERS
DIP TUBES
CAPILLARY
CO_2
a
TO FURNACE
CAPILLARY
H_2
b

Fig 2.8

CHAPTER 3

METHOD OF PRESENTATION OF RESULTS

Figures 3.1 - 3.6

Figure 3.1

The tetrahedron XO-YO-R_2O_3-ZO_2 showing the location of the phases encountered in this study and the names of their CMAS counterparts. The two planes $XO.ZO_2$-$YO.ZO_2$-R_2O_3 (CS-MS-A) and $3XO.R_2O_3$-YO-ZO_2 (C_3A-M-S) are also shown.

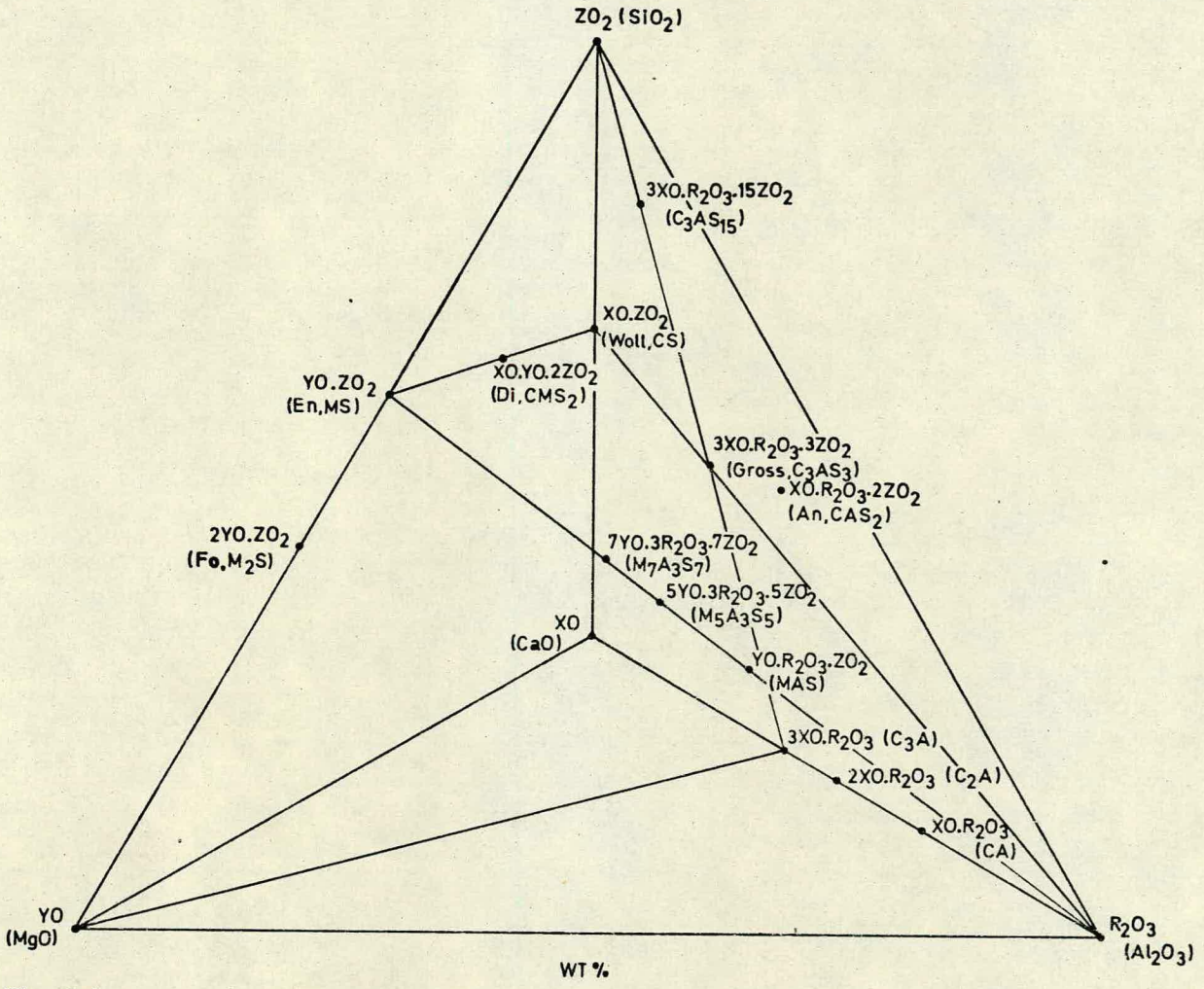
ZO_2 (SiO_2)
$3XO.R_2O_3.15ZO_2$
(C_3AS_{15})
$XO.ZO_2$
(Woll,CS)
$XO.YO.2ZO_2$
(Di,CMS_2)
$YO.ZO_2$
(En,MS)
$3XO.R_2O_3.3ZO_2$
(Gross,C_3AS_3)
$XO.R_2O_3.2ZO_2$
(An,CAS_2)
$2YO.ZO_2$
(Fo,M_2S)
$7YO.3R_2O_3.7ZO_2$
($M_7A_3S_7$)
$5YO.3R_2O_3.5ZO_2$
($M_5A_3S_5$)
XO
(CaO)
$YO.R_2O_3.ZO_2$
(MAS)
$3XO.R_2O_3$ (C_3A)
$2XO.R_2O_3$ (C_2A)
$XO.R_2O_3$
(CA)
YO
(MgO)
R_2O_3
(Al_2O_3)
WT %

Fig 3.1

Figure 3.2

The plane $XO.ZO_2$-$YO.ZO_2$-R_2O_3 (CS-MS-A) showing the locations of the joins studied and relevant piercing points.

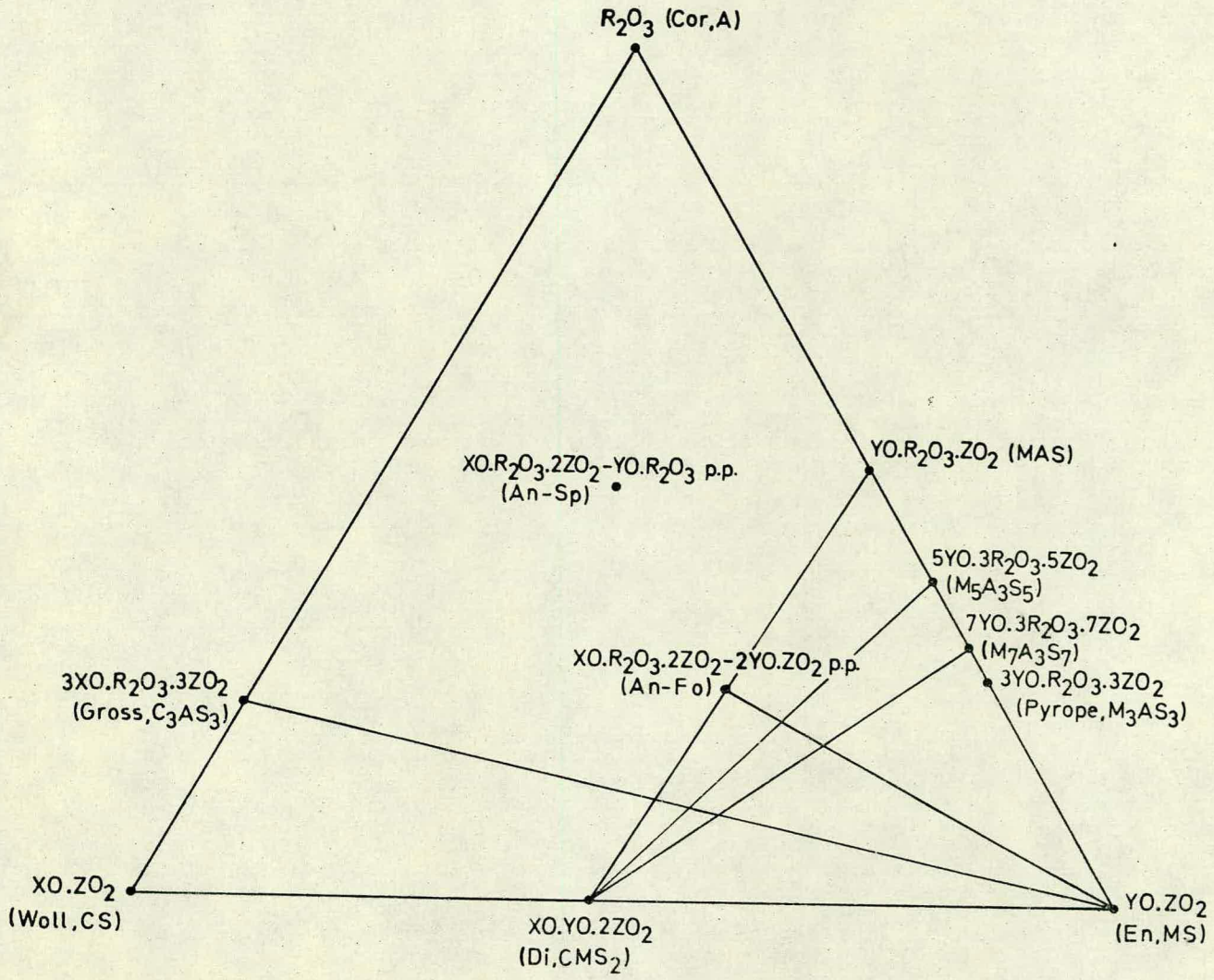
R_2O_3 (Cor,A)
$XO.R_2O_3.2ZO_2$-$YO.R_2O_3$ p.p.
(An-Sp)
$YO.R_2O_3.ZO_2$ (MAS)
$5YO.3R_2O_3.5ZO_2$
($M_5A_3S_5$)
$7YO.3R_2O_3.7ZO_2$
($M_7A_3S_7$)
$XO.R_2O_3.2ZO_2$-$2YO.ZO_2$ p.p.
(An-Fo)
$3YO.R_2O_3.3ZO_2$
(Pyrope, M_3AS_3)
$3XO.R_2O_3.3ZO_2$
(Gross, C_3AS_3)
$XO.ZO_2$
(Woll, CS)
$XO.YO.2ZO_2$
(Di, CMS_2)
$YO.ZO_2$
(En, MS)
WT%

Fig 3.2

Figure 3.3

The plane $3XO.R_2O_3$-YO-ZO_2 (C_3A-M-S) showing the locations of the joins studied and relevant piercing points.

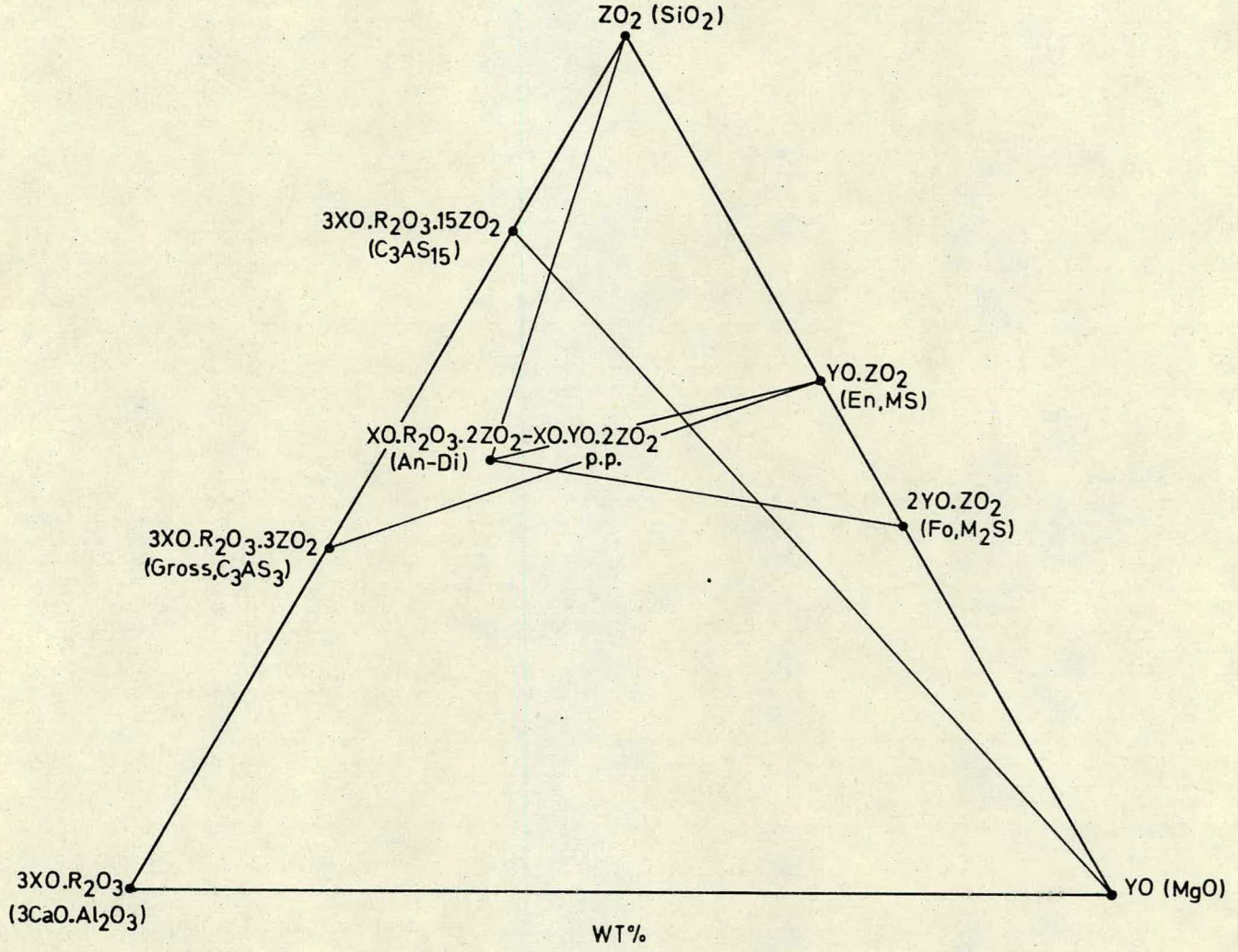
ZO_2 (SiO_2)
$3XO.R_2O_3.15ZO_2$
(C_3AS_{15})
$YO.ZO_2$
(En, MS)
$XO.R_2O_3.2ZO_2$-$XO.YO.2ZO_2$
(An-Di)
p.p.
$2YO.ZO_2$
(Fo, M_2S)
$3XO.R_2O_3.3ZO_2$
(Gross, C_3AS_3)
$3XO.R_2O_3$
($3CaO.Al_2O_3$)
YO (MgO)
WT%

Fig 3.3

Figure 3.4

Part of the plane CS-MS-A showing the variation in CIPW normative constituents. The forsterite contents in the assemblage An-Di-Fo-En are not shown, but can be obtained by difference.

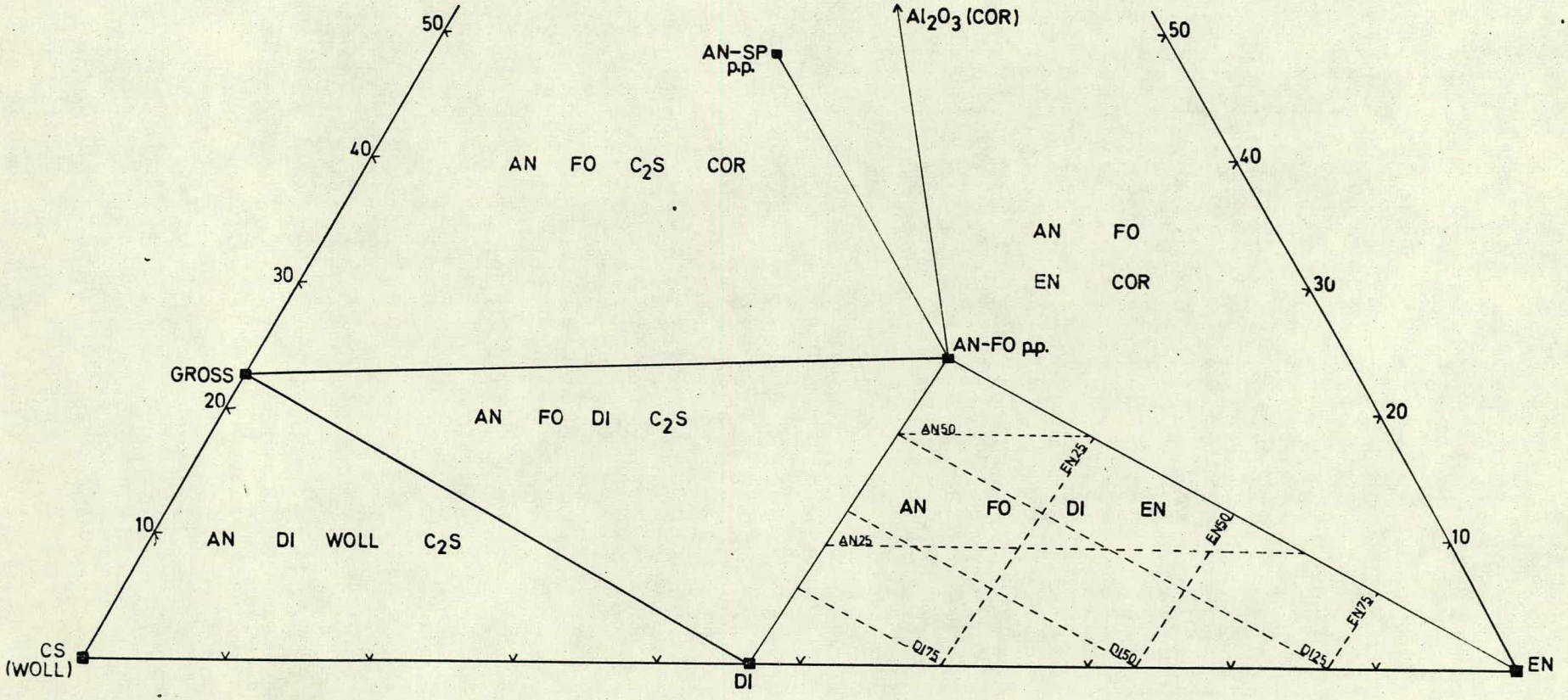
Al_2O_3 (COR)
AN-SP p.p.
AN-FO p.p.
GROSS
CS (WOLL)
DI
EN
AN FO C_2S COR
AN FO DI C_2S
AN DI WOLL C_2S
AN FO EN COR
AN FO DI EN
AN50
AN25
EN25
EN50
EN75
DI75
DI50
DI25
50
40
30
20
10
WT%

Fig 3.4

Figure 3.5

Part of the plane $XO.ZO_2$-$YO.ZO_2$-R_2O_3 (CS-MS-A) showing the variation in CIPW normative constituents when the bulk normative plagioclase is albite. The $2YO.ZO_2$ (forsterite) contents in the assemblage $XO.R_2O_3.2ZO_2$-$XO.YO.2ZO_2$-$2YO.ZO_2$-$YO.ZO_2$ (Ab-Di-Fo-En) are not shown, but can be obtained by difference.

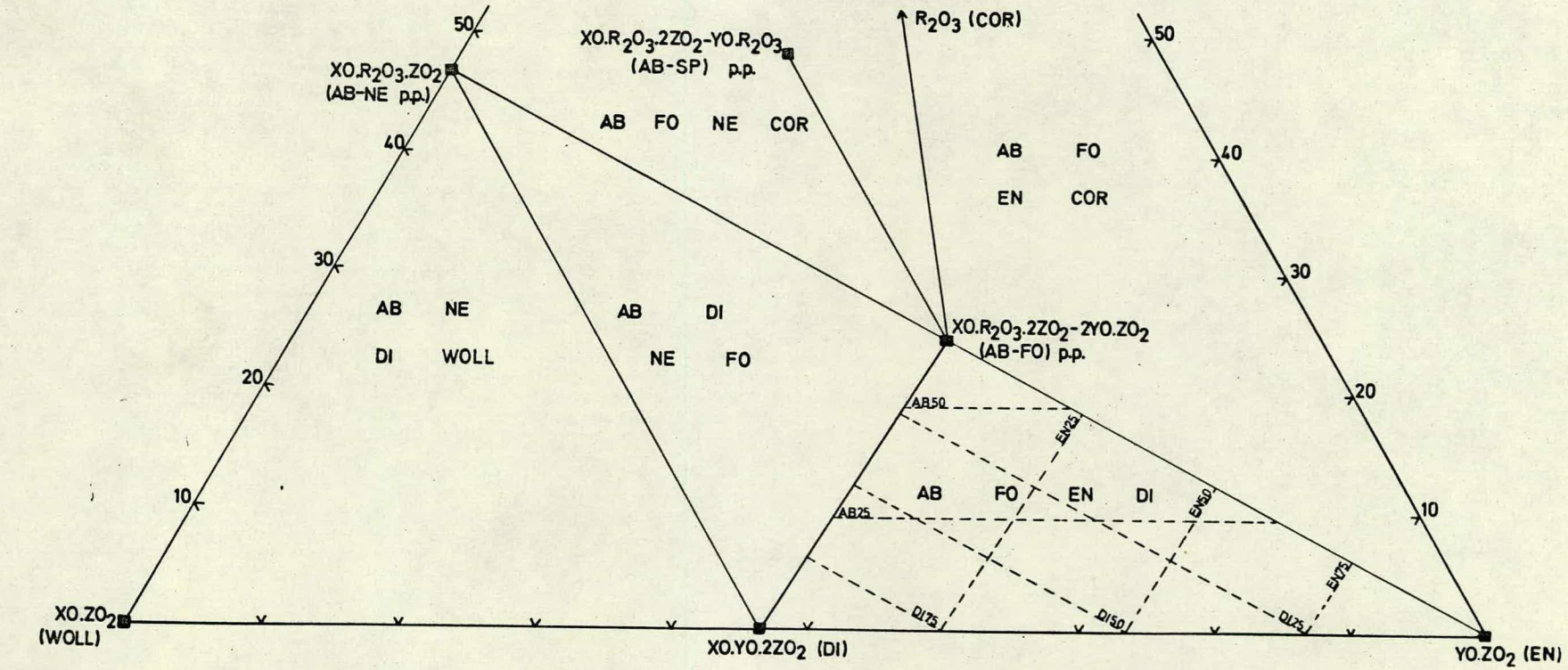
XO.R2O3.ZO2
(AB-NE p.p.)
XO.R2O3.2ZO2-YO.R2O3
(AB-SP) p.p.
R2O3 (COR)
XO.R2O3.2ZO2-2YO.ZO2
(AB-FO) p.p.
AB FO NE COR
AB NE
DI WOLL
AB DI
NE FO
AB FO
EN COR
AB FO EN DI
AB50
AB25
EN25
EN50
EN75
DI75
DI50
DI25
50
40
30
20
10
XO.ZO2
(WOLL)
XO.YO.2ZO2 (DI)
YO.ZO2 (EN)
WT %

Fig 3.5

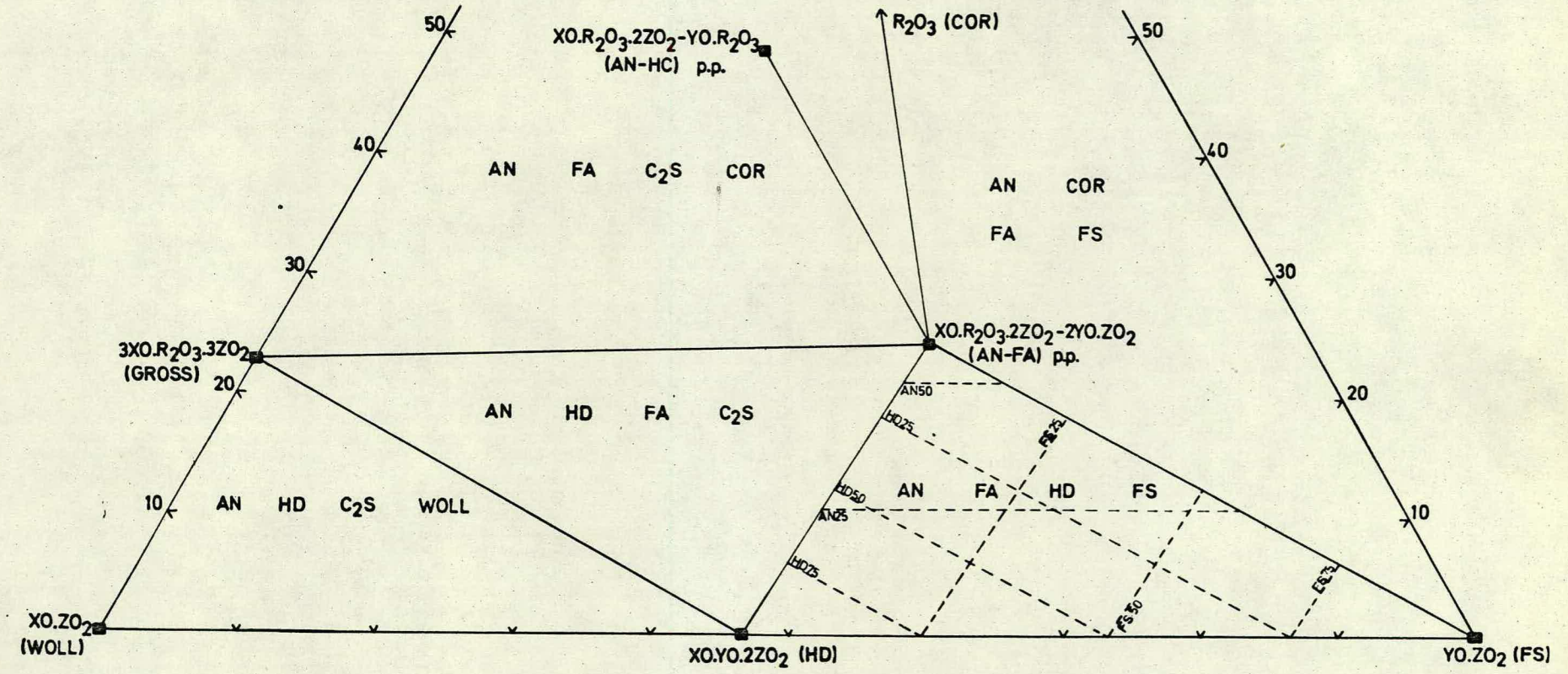
50
40
30
20
10
XO.R2O3.2ZO2-YO.R2O3
(AN-HC) p.p.
R2O3 (COR)
AN FA C2S COR
AN COR
FA FS
3XO.R2O3.3ZO2
(GROSS)
XO.R2O3.2ZO2-2YO.ZO2
(AN-FA) p.p.
AN HD FA C2S
AN50
HD25
FA25
AN HD C2S WOLL
HD50
AN25
AN FA HD FS
HD75
FS50
FS75
XO.ZO2
(WOLL)
XO.YO.2ZO2 (HD)
YO.ZO2 (FS)
WT %

Fig 3.6

CHAPTER 4

THE SYSTEM $CaO-MgO-Al_2O_3-SiO_2$

Figures 4.1 - 4.13

Figure 4.1

Liquidus diagram for the plane Anorthite-Diopside-Forsterite, redrawn slightly modified from Osborn and Tait (1952). The compositions studied are shown by circles, the composition names can be found by referring to figure 5.10. The light dashed lines are the temperature contours, the solid lines the phase equilibrium boundaries. The trace of the join Diopside-MAS is also shown, its intersection with the join Anorthite-Forsterite being the An-Fo piercing point in the plane CS-MS-A. The dotted line is the trace of L. 4 E 2 sp,fo,an,liq for compositions in this plane having a spinel liquidus.

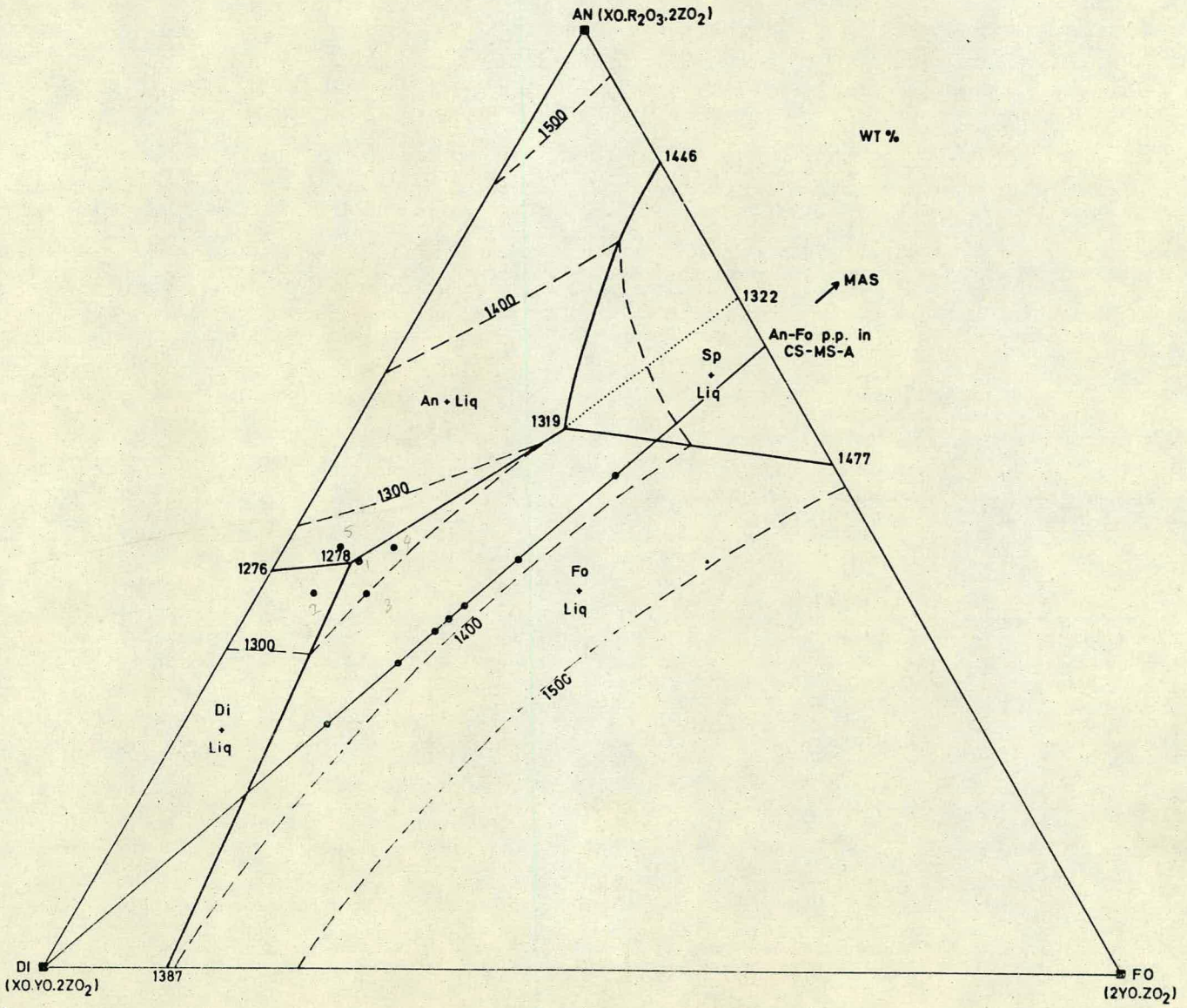
AN ($XO.R_2O_3.2ZO_2$)
WT %
1500
1446
1400
1322
MAS
An-Fo p.p. in CS-MS-A
Sp + Liq
An + Liq
1319
1477
1300
1276
1278
Fo + Liq
1300
1400
1500
Di + Liq
DI ($XO.YO.2ZO_2$)
1387
FO ($2YO.ZO_2$)

Fig 4.1

Figure 4.2

Liquidus diagram for part of the plane CS-MS-A, constructed entirely from previously published data. The phase boundaries are indicated by thick solid lines, the joins studied by thin solid lines, and the dashed lines are temperature contours where known.

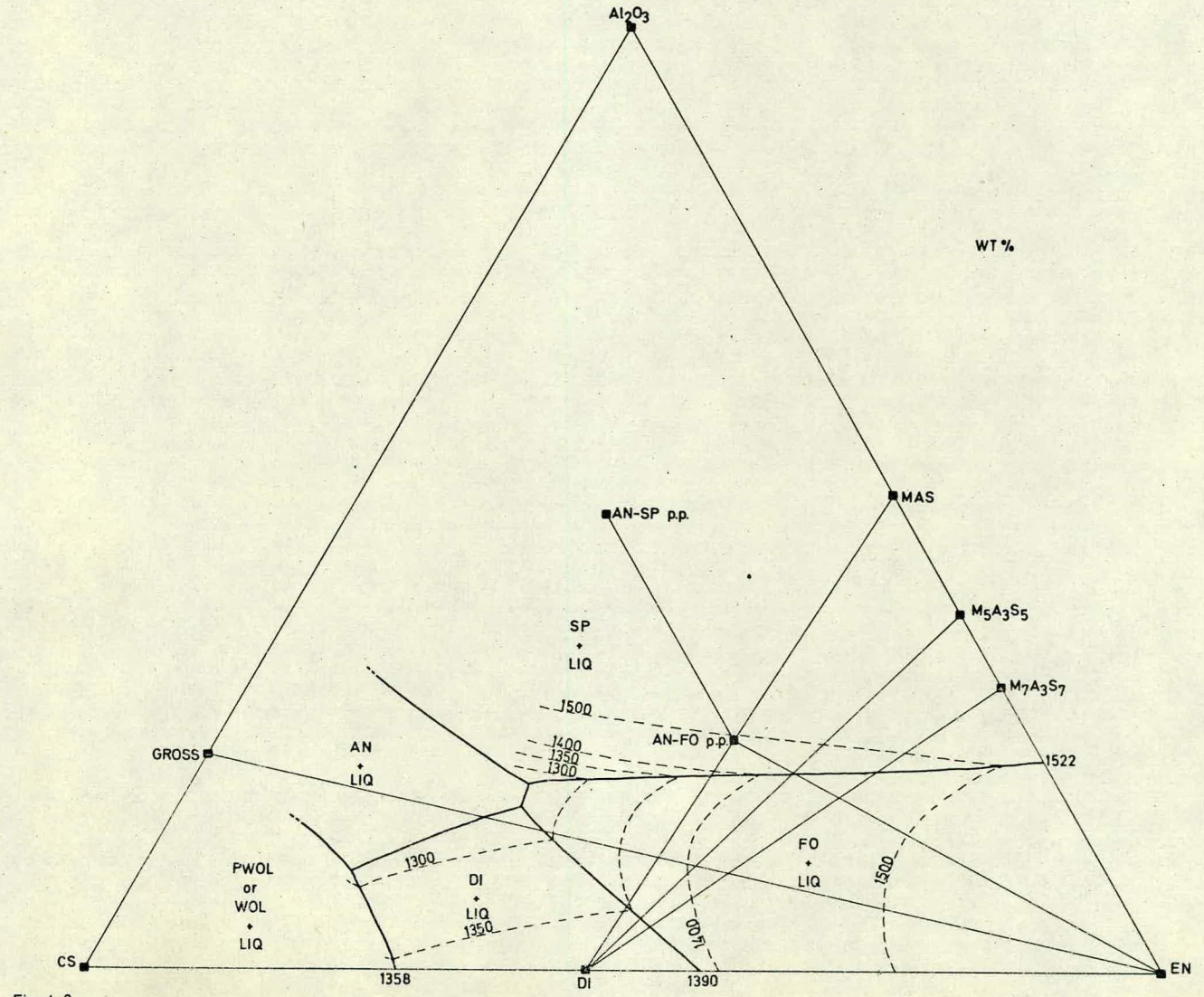
Al2O3
WT %
MAS
AN-SP p.p.
M5A3S5
M7A3S7
SP
+
LIQ
1500
AN-FO p.p.
1400
1350
1300
1522
GROSS
AN
+
LIQ
1300
PWOL
or
WOL
+
LIQ
DI
+
LIQ
1350
FO
+
LIQ
1500
1400
CS
1358
DI
1390
EN

Fig 4.2

Figure 4.3

Part of the forsterite projection into the plane CS-MS-A, drawn on the basis of results presented, and previously published data.

The filled circles (labelled 3-6) are the projected positions of the compositions studied by Yang (1973), and the areas labelled pig and pen are the projected positions of those phases analysed in experiments on those compositions. The projected position of L.4E1 fo, di, pig, pen, liq was determined using the quenching data of Yang (1973), on these compositions.

The solid lines are the projection phase boundaries, the dashed lines are the temperature contours where known, for the appearnace of the second phase indicated. The dotted line enclosed those liquids on the surface of the olivine phase volume which are silica saturated in the CIPW norm.

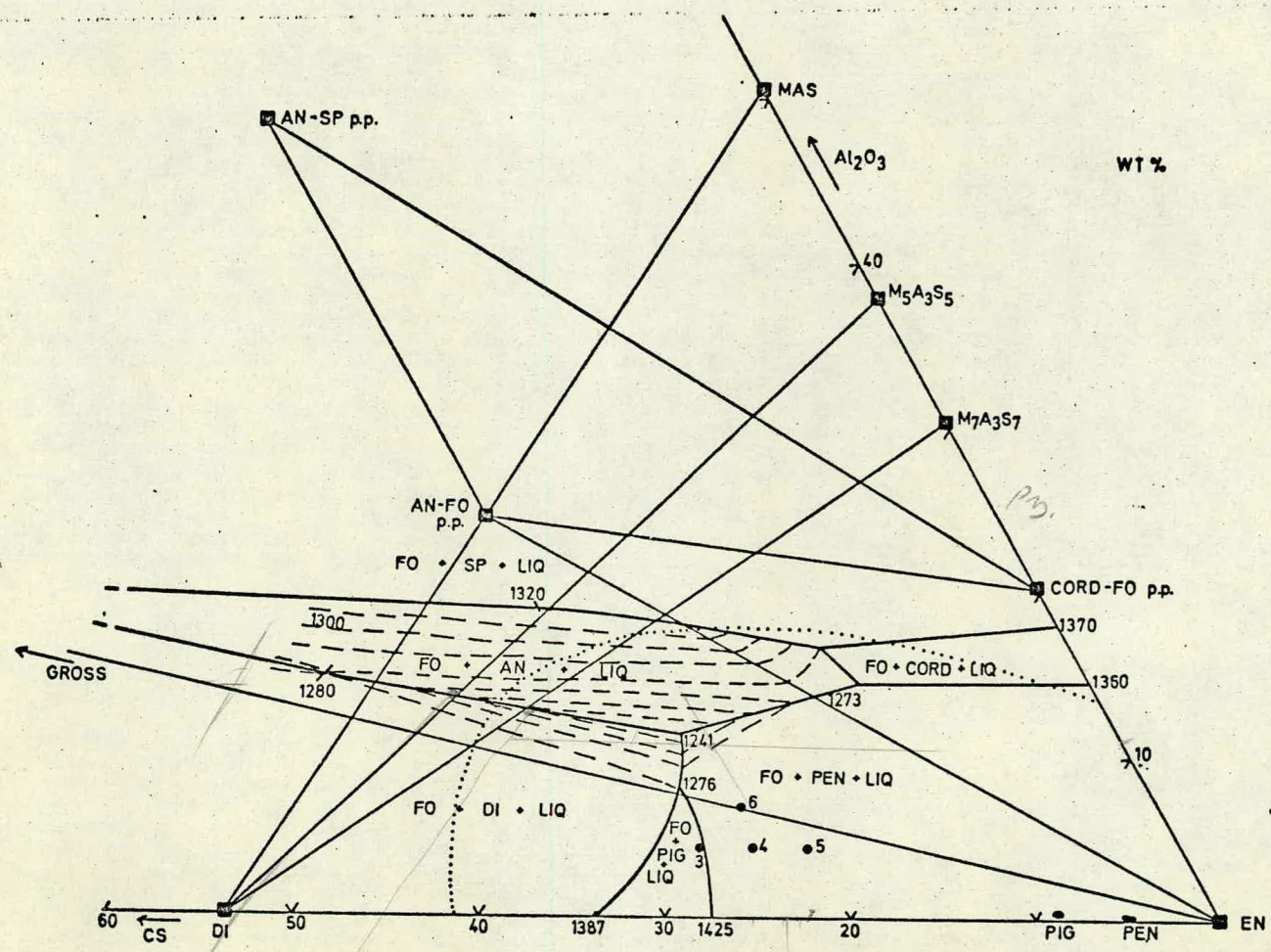
MAS
AN-SP p.p.
Al_2O_3
WT %
40
$M_5A_3S_5$
$M_7A_3S_7$
AN-FO p.p.
FO + SP + LIQ
1320
1300
CORD-FO p.p.
1370
GROSS
FO + AN + LIQ
1280
FO + CORD + LIQ
1360
273
1241
10
1276
FO + PEN + LIQ
6
FO + DI + LIQ
FO + PIG + LIQ
3
4
5
60
CS
DI
50
40
1387
30
1425
20
PIG
PEN
EN

Fig 4.3

Figure 4.4

T - X section for the join Enstatite-Grossular, redrawn after Ford and O'Hara (1972), to include the pigeonite stability fields. The extent of pigeonite occurrence with forsterite was obtained from the forsterite projection (figure 4.3).

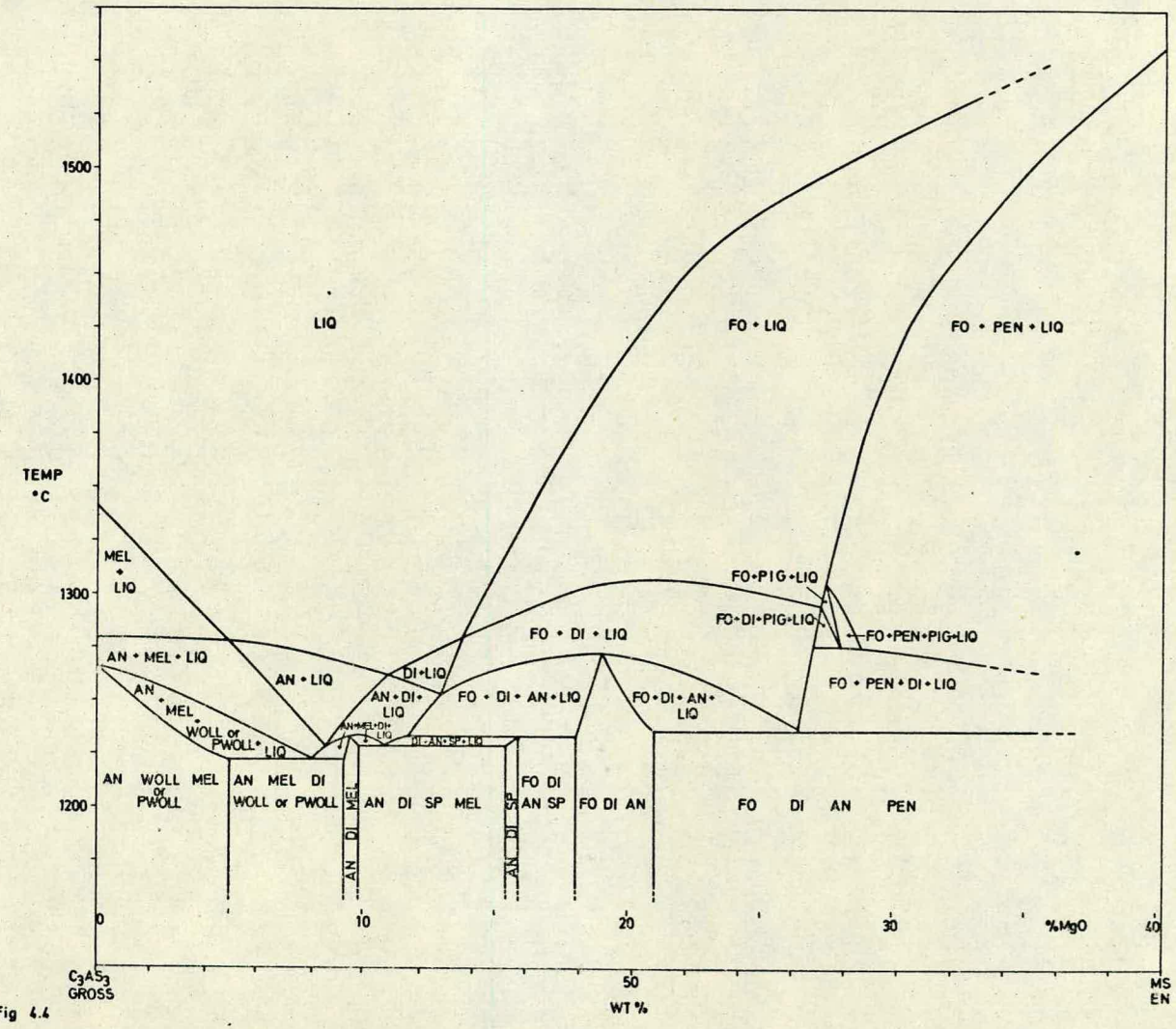
LIQ
FO + LIQ
FO + PEN + LIQ
MEL + LIQ
FO+PIG+LIQ
FO+DI+PIG+LIQ
FO+PEN+PIG+LIQ
FO + DI + LIQ
AN + MEL + LIQ
AN + LIQ
DI+LIQ
AN+DI+ LIQ
FO + DI + AN + LIQ
FO+DI+AN+ LIQ
FO + PEN + DI + LIQ
AN + MEL + WOLL or PWOLL + LIQ
AN+MEL+DI+LIQ
DI+AN+SP+LIQ
AN WOLL MEL or PWOLL
AN MEL DI WOLL or PWOLL
AN DI MEL
AN DI SP MEL
AN DI SP
FO DI AN SP
FO DI AN
FO DI AN PEN
TEMP °C
1500
1400
1300
1200
0
10
20
30
%MgO
40
C3AS3 GROSS
50
WT %
MS EN

Fig 4.4

Figure 4.5

T - X section for part of the join $C_3^*AS_{15}$-M, redrawn after O'Hara and Biggar (1969), to include the pigeonite stability fields. The extent of pigeonite occurrence with forsterite was obtained from the forsterite projection (figure 4.3), its occurrence with silica, however, is unknown, but is assumed to be similar.

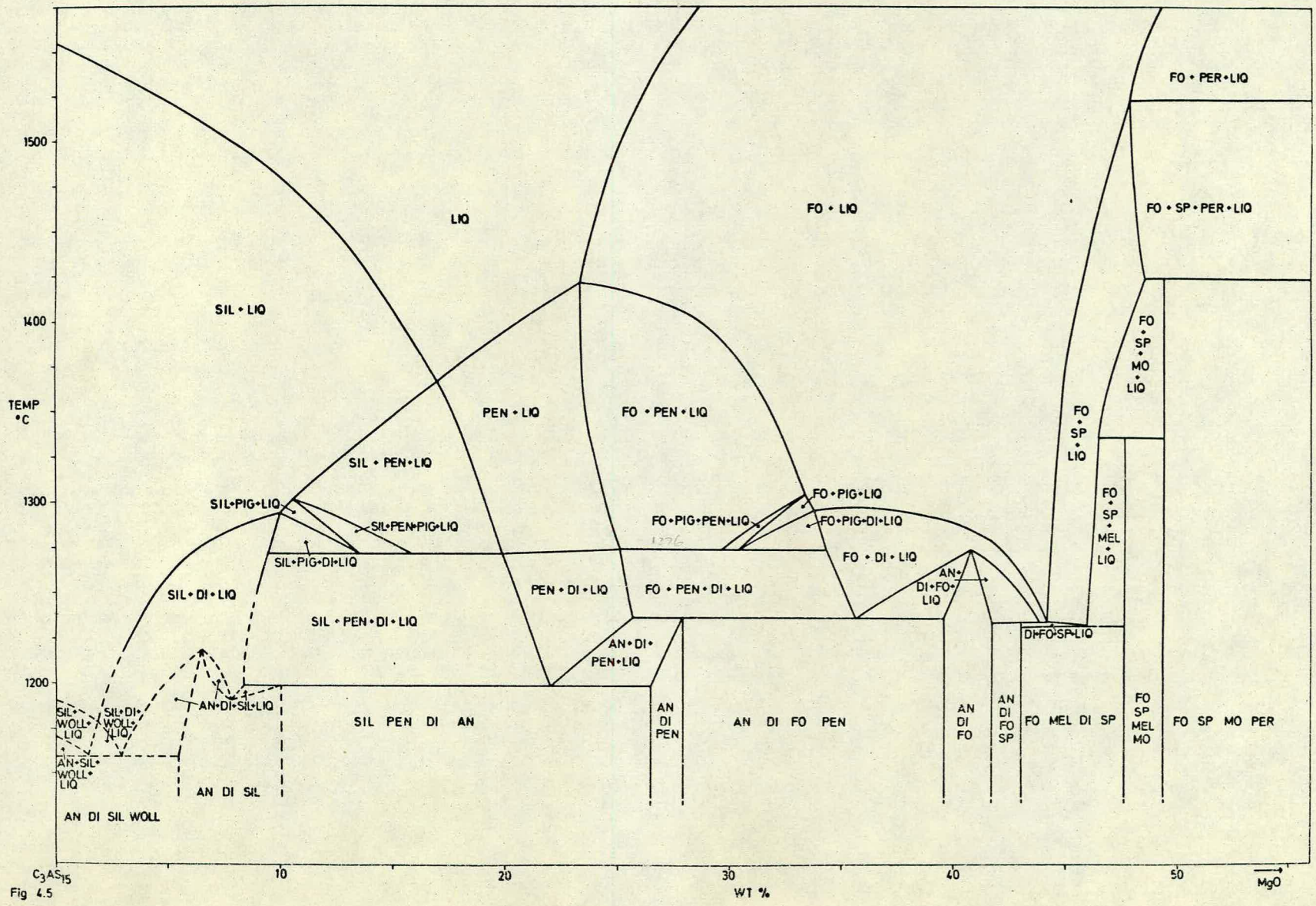
LIQ
FO + LIQ
FO + PER + LIQ
FO + SP + PER + LIQ
SIL + LIQ
PEN + LIQ
FO + PEN + LIQ
FO + SP + MO + LIQ
FO + SP + LIQ
SIL + PEN + LIQ
SIL + PIG + LIQ
FO + PIG + LIQ
FO + PIG + PEN + LIQ
FO + PIG + DI + LIQ
SIL + PEN + PIG + LIQ
SIL + PIG + DI + LIQ
FO + SP + MEL + LIQ
FO + DI + LIQ
AN + DI + FO + LIQ
SIL + DI + LIQ
PEN + DI + LIQ
FO + PEN + DI + LIQ
SIL + PEN + DI + LIQ
DI + FO + SP + LIQ
AN + DI + PEN + LIQ
SIL + WOLL + LIQ
SIL + DI + WOLL + LIQ
AN + DI + SIL + LIQ
SIL PEN DI AN
AN DI PEN
AN DI FO PEN
AN DI FO
AN DI FO SP
FO MEL DI SP
FO SP MEL MO
FO SP MO PER
AN + SIL + WOLL + LIQ
AN DI SIL
AN DI SIL WOLL
1500
1400
1300
1200
TEMP °C
10
20
30
40
50
C3AS15
MgO
WT %

Fig 4.5

Figure 4.6

Liquidus diagram for part of the plane C_3A-M-S constructed on the basis of previously published data. The phase boundaries are indicated by thick solid lines, the joins of interest by thin solid lines, the dashed lines are temperature contours where known. The small field of pigeonite is known to occur on this plane from the forsterite projection diagram (figure 4.3), though its extent against the silica volume is unknown.

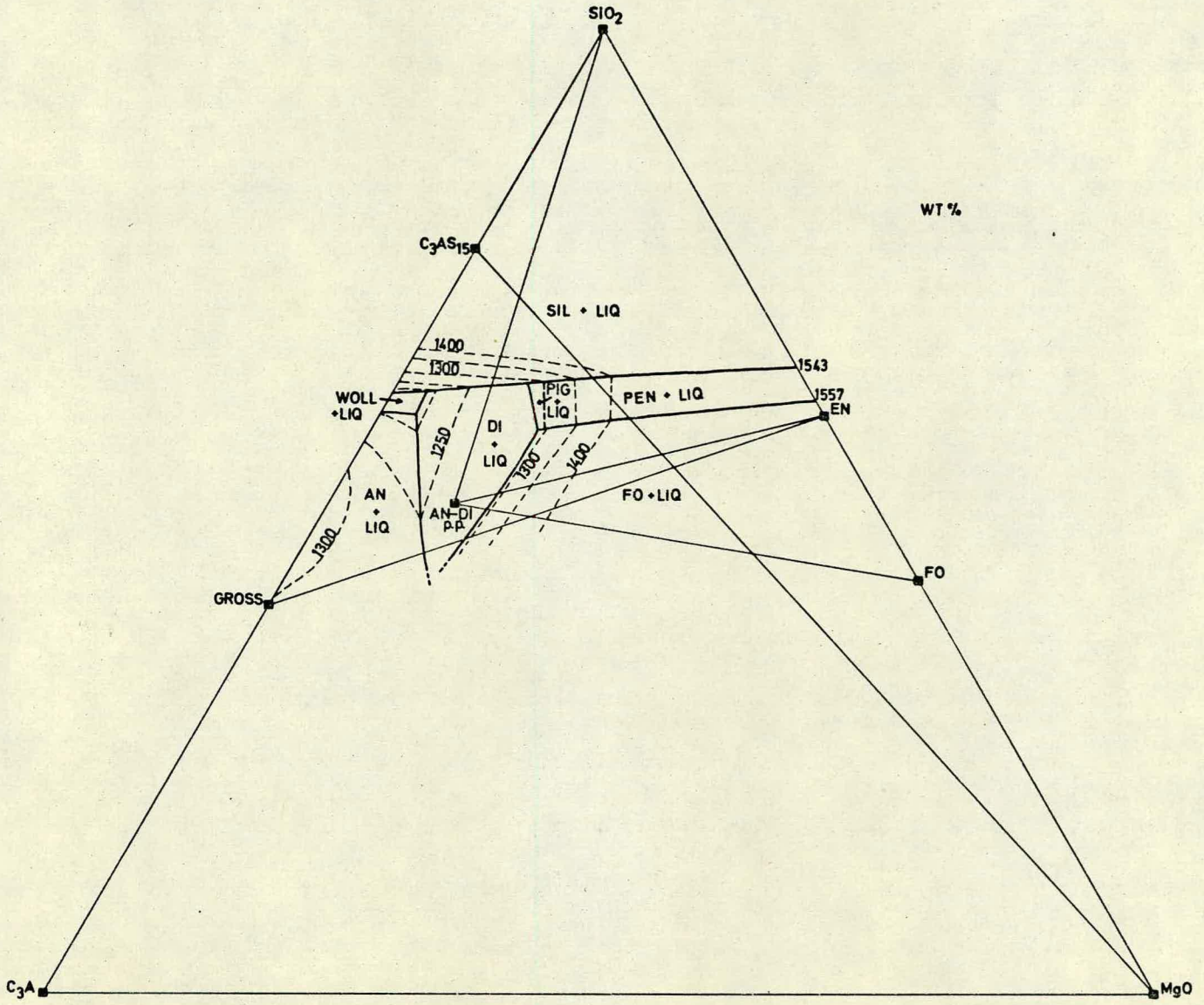
SiO2
WT %
C3AS15
SIL + LIQ
1400
1300
1543
WOLL
+LIQ
PIG
+
LIQ
PEN + LIQ
1557
EN
DI
+
LIQ
1250
1300
1400
AN
+
LIQ
AN-DI
P.P.
FO + LIQ
1300
GROSS
FO
C3A
MgO

Fig 4.6

Figure 4.7

Diopside projection into part of the plane CA-M-S on the basis of previously published data, showing the relationship between olivine-bearing equilibria and silica-bearing equilibria. The field of protoenstatite+diopside+liquid has been assumed to extend to the silica phase volume, as in the previous diagrams. The solid lines are the projection phase boundaries, the dashed lines are temperature contours where known. The piercing points in this plane of the joins studied are also indicated.

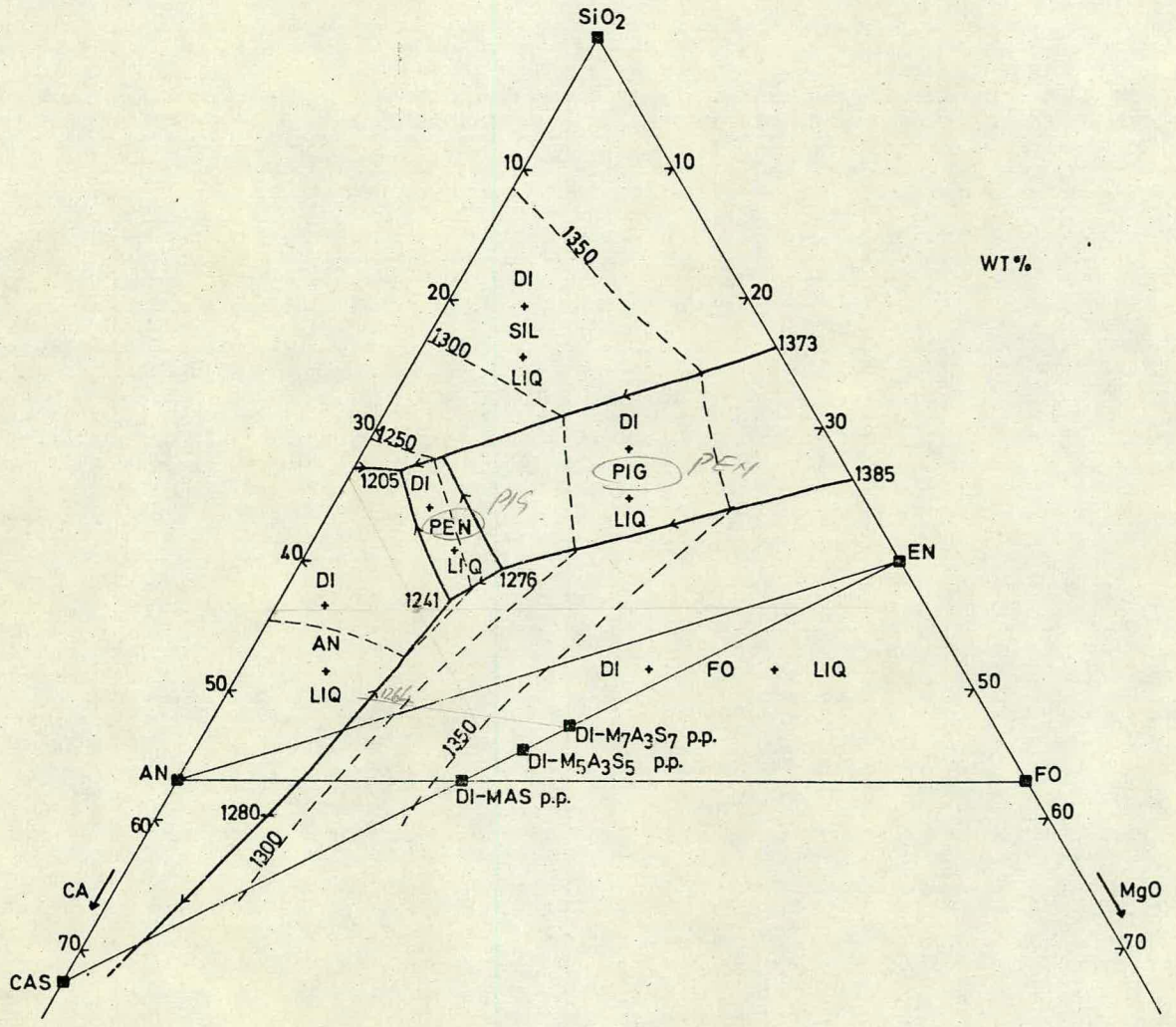
SiO2
WT%
10
20
30
40
50
60
70
1350
1300
1250
1205
1373
1385
1276
1241
1280
DI
+
SIL
LIQ
PIG
PEN
AN
FO
EN
CAS
CA
MgO
DI-M7A3S7 p.p.
DI-M5A3S5 p.p.
DI-MAS p.p.

Fig 4.7

Figure 4.8

Anorthite projection into part of the plane CM-A-S, drawn on the basis of previously published data. The solid lines are the projected phase boundaries, the phase fields being indicated.

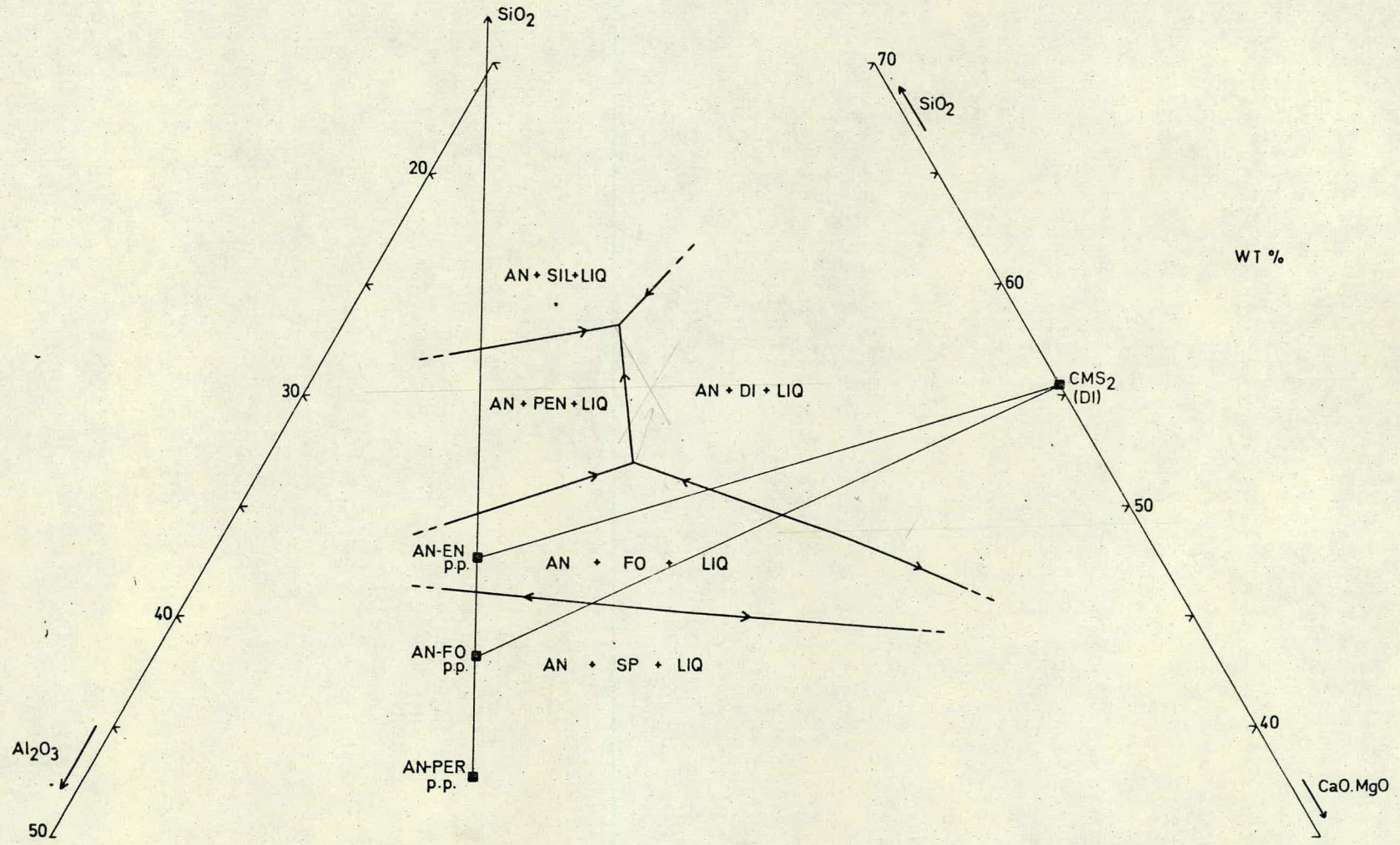
SiO2
70
SiO2
20
AN + SIL + LIQ
WT %
60
30
AN + PEN + LIQ
AN + DI + LIQ
CMS2
(DI)
AN-EN
p.p.
AN + FO + LIQ
50
40
AN-FO
p.p.
AN + SP + LIQ
Al2O3
40
AN-PER
p.p.
50
CaO.MgO

Fig 4.8

Figure 4.9

Flow sheet for the geological part of the system $CaO-MgO-Al_2O_3-SiO_2$.

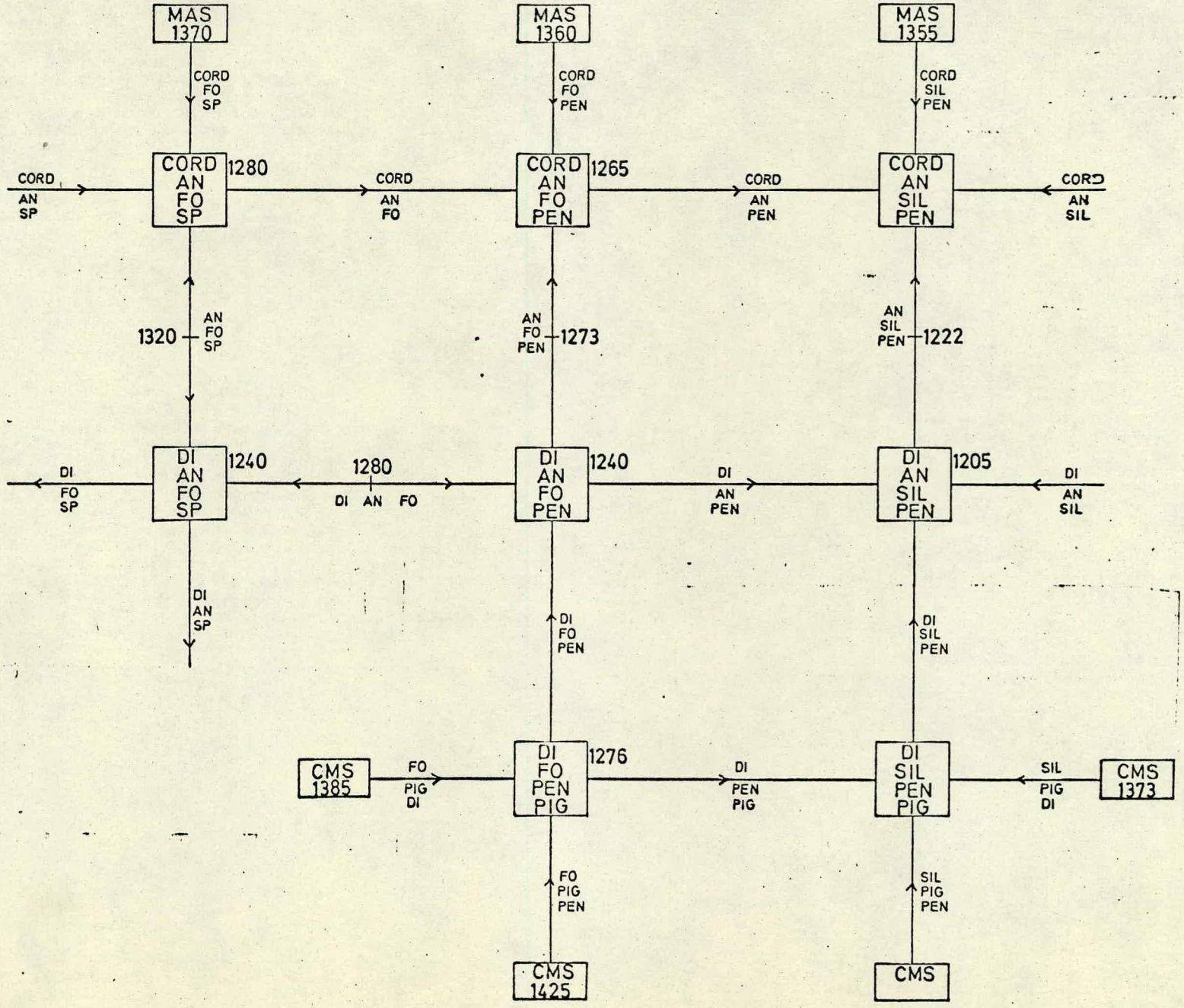
MAS 1370
MAS 1360
MAS 1355
CORD FO SP
CORD FO PEN
CORD SIL PEN
CORD AN SP
CORD AN FO SP
1280
CORD AN FO
CORD AN FO PEN
1265
CORD AN PEN
CORD AN SIL PEN
CORD AN SIL
1320
AN FO SP
AN FO PEN
1273
AN SIL PEN
1222
DI AN FO SP
1240
1280
DI AN FO
DI AN FO PEN
1240
DI AN PEN
DI AN SIL PEN
1205
DI FO SP
DI AN SIL
DI AN SP
DI FO PEN
DI SIL PEN
CMS 1385
FO PIG DI
DI FO PEN PIG
1276
DI PEN PIG
DI SIL PEN PIG
SIL PIG DI
CMS 1373
FO PIG PEN
SIL PIG PEN
CMS 1425
CMS

Fig 4.9

Figure 4.10

A forsterite projection into part of the plane CS-MS-A from figure 4.3, outlining the areas of like crystallisation histories under perfect equilibrium crystallisation conditions for forsterite saturated compositions. Each area is numbered to correspond with the numbering given in table 4.1, in which the crystallisation histories for compositions projecting in each area are given. The letter associated with each area indicates the change in CIPW normative character of the residual liquids produced from compositions projecting in that area. (A more detailed discussion of the crystallisation of such compositions is given by O'Hara (1969)). The letters have the following meanings

a residual liquids always undersaturated* in the CIPW norm

b residual liquids begin undersaturated, become saturated,* then return to being undersaturated again

c residual liquids always saturated in the norm

d residual liquids begin undersaturated, but become saturated

---

* The term undersaturated represents the presence of corundum or larnite in the CIPW norm; saturated represents the absence of such minerals in the norm.

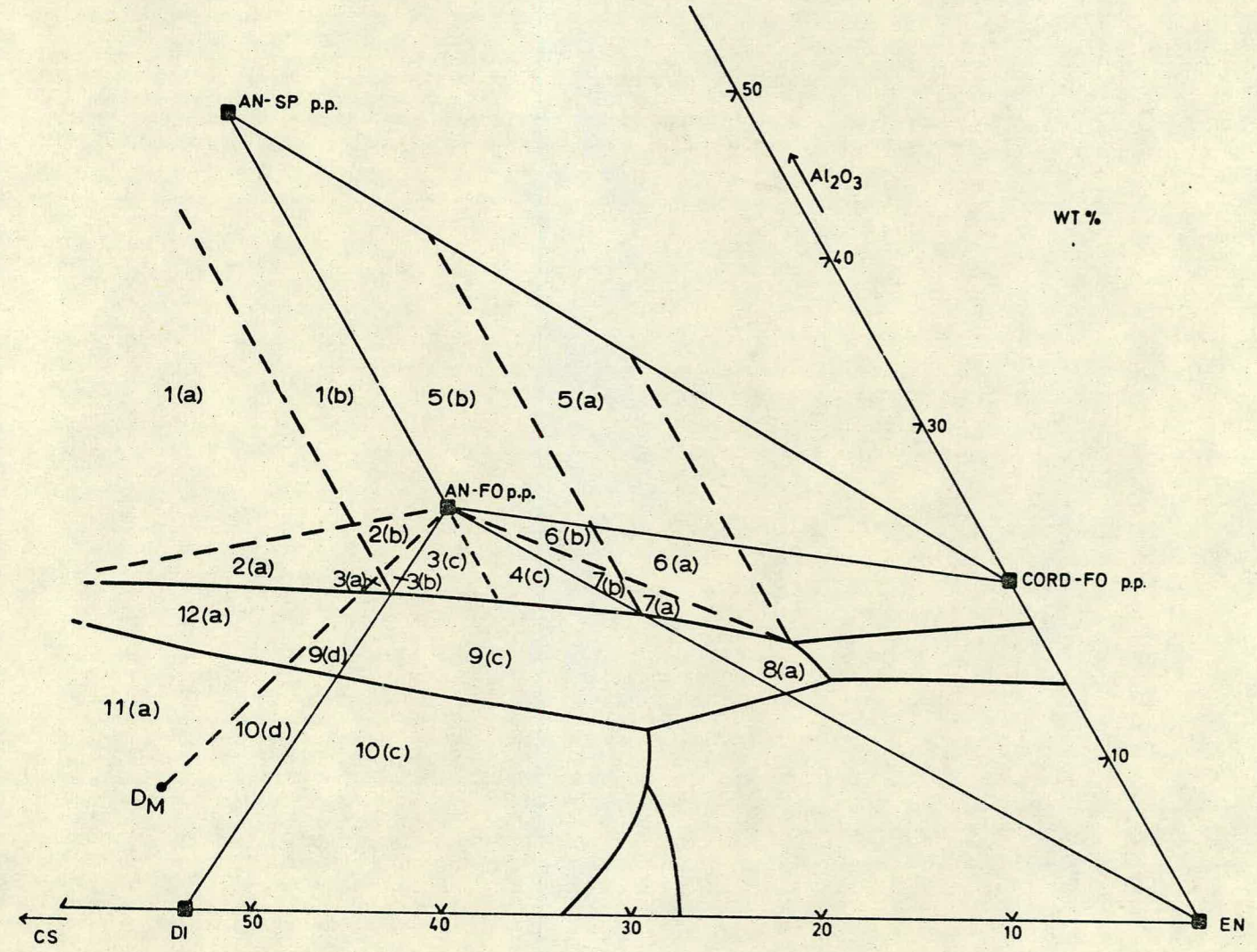
AN-SP p.p.
50
Al_2O_3
WT %
40
30
1(a)
1(b)
5(b)
5(a)
AN-FO p.p.
2(b)
6(b)
3(c)
2(a)
3(a)
3(b)
4(c)
7(b)
6(a)
CORD-FO p.p.
7(a)
12(a)
9(d)
9(c)
8(a)
11(a)
10(d)
10(c)
10
D_M
CS
DI
50
40
30
20
10
EN

Fig 4.10

Figure 4.11

A forsterite projection into part of the plane CS-MS-A from figure 4.3, outlining the areas of like crystallisation histories under perfect fractional crystallisation conditions for forsterite saturated compositions. Each area is numbered to correspond with the numbering given in table 4.2, in which the crystallisation histories for compositions projecting in each area are given. The letter associated with each area indicates the change in CIPW normative character of the residual liquids produced from compositions projecting in that area. (A more detailed discussion of the crystallisation of such compositions is given by O'Hara (1969)). The letters have the following meanings

a residual liquids begin undersaturated, later become saturated in the CIPW norm

b residual liquids always saturated in the norm

c residual liquids always undersaturated in the norm

The area enclosed by the hatched lines includes those projected compositions which can produce undersaturated residual liquids during equilibrium crystallisation (figure 4.10), and saturated residual liquids under perfect fractional crystallisation (this figure).

The terms undersaturated and saturated are explained in figure 4.10.

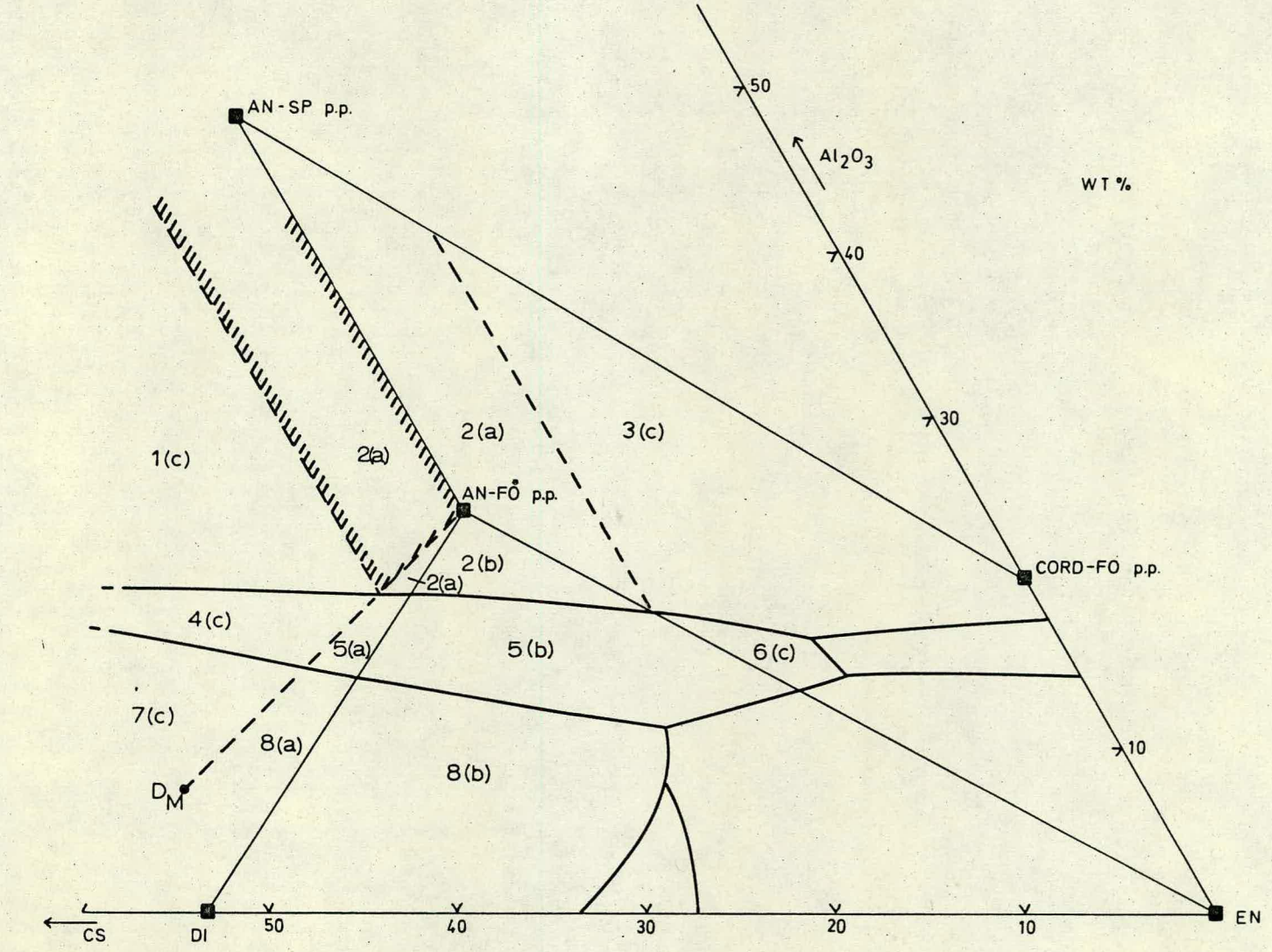
AN-SP p.p.
50
Al_2O_3
WT %
40
30
2(a)
3(c)
1(c)
2(a)
AN-FO p.p.
2(b)
2(a)
CORD-FO p.p.
4(c)
5(a)
5(b)
6(c)
7(c)
8(a)
10
8(b)
D_M
CS
DI
50
40
30
20
10
EN

Fig 4.11

Figure 4.12

A diopside projection into part of the plane CA-M-S from figure 4.7, outlining the areas of like crystallisation histories under perfect equilibrium crystallisation conditions for diopside saturated compositions. Each area is numbered to correspond with the numbering given in table 4.3, in which the crystallisation histories for compositions projecting in each area are given.

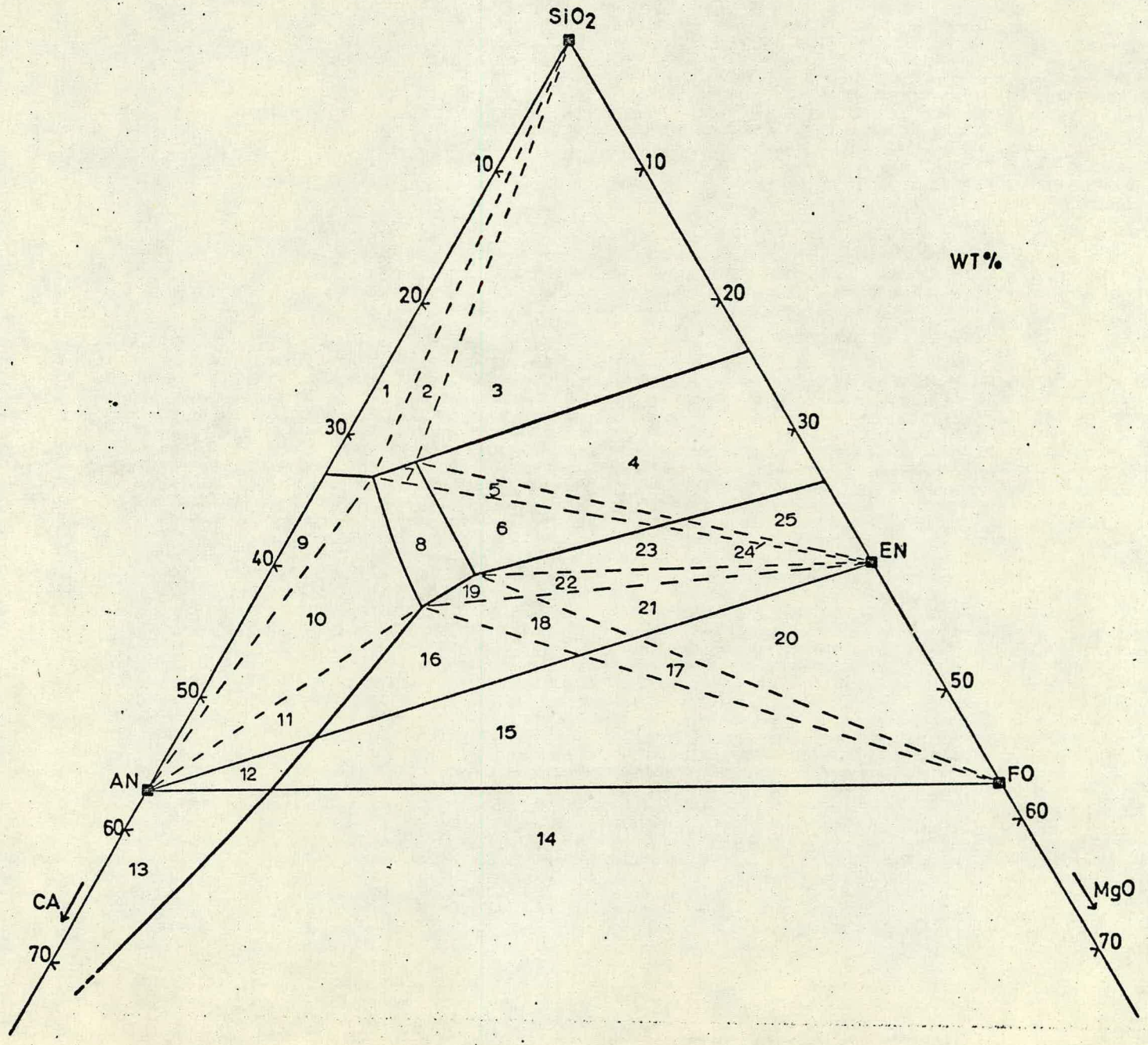
SiO2
WT%
10
10
20
20
30
30
40
50
50
60
60
70
70
1
2
3
4
5
6
7
8
9
10
11
12
13
14
15
16
17
18
19
20
21
22
23
24
25
EN
AN
FO
CA
MgO

Fig 4.12

Figure 4.13

A diopside projection into part of the plane CA-M-S from figure 4.7, outlining the areas of like crystallisation histories under perfect fractional crystallisation conditions for diopside saturated compositions. Each area is numbered to correspond with the numbering given in table 4.4, in which the crystallisation histories for compositions projecting in each area are given.

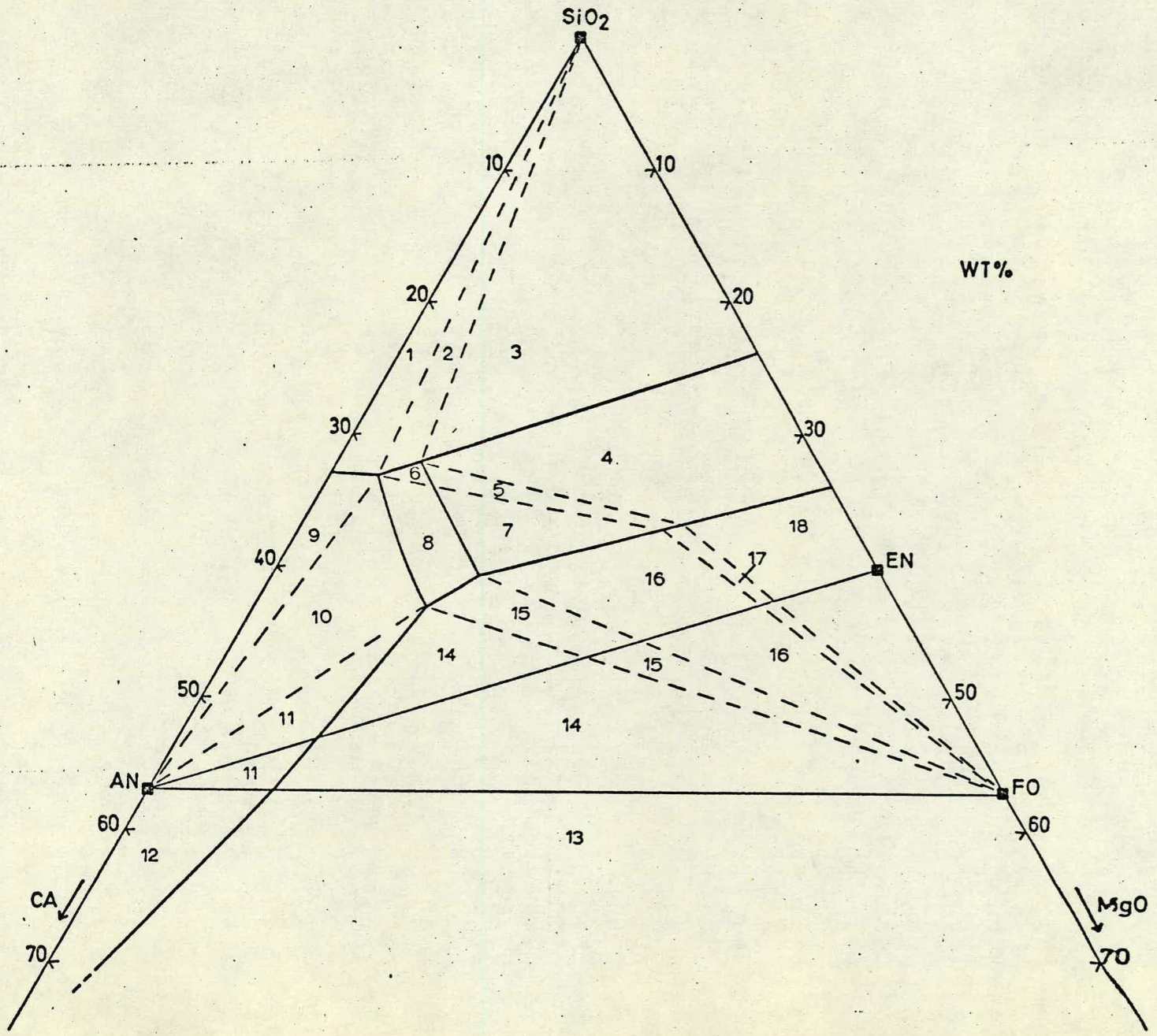
SiO2
10
10
20
20
30
30
40
50
50
60
60
70
70
WT%
1
2
3
4
5
6
7
8
9
10
11
12
13
14
15
16
17
18
EN
AN
FO
CA
MgO

Fig. 4.12

CHAPTER 5

THE SYSTEM $CaO-MgO-Al_2O_3-SiO_2-Na_2O$

Figures 5.1 - 5.20

Figure 5.1

Liquidus diagram for the plane $XO.ZO_2$-$YO.ZO_2$-R_2O_3 ($NA_{-1}S_4$-MS-A) in the system NMAS, that is, no CaO present, drawn on the basis of previously published data. The thick solid lines indicate the liquidus phase boundaries.

Within the olivine phase volume, the projection phase boundaries are shown by thick dashed lines, the second phase to crystallise for each area being indicated. The thin dashed lines are temperature contours where known. The area enclosed by the dotted line shows the projected position of liquids which are silica saturated in the CIPW norm.

The lower area $XO.ZO_2$-$YO.ZO_2$-$2XO.R_2O_3.2ZO_2$ ($NA_{-1}S_4$-MS-NS_4) is not utilised, as discussed in the text.

EDINBURGEN. EX BIBL. UNIV.

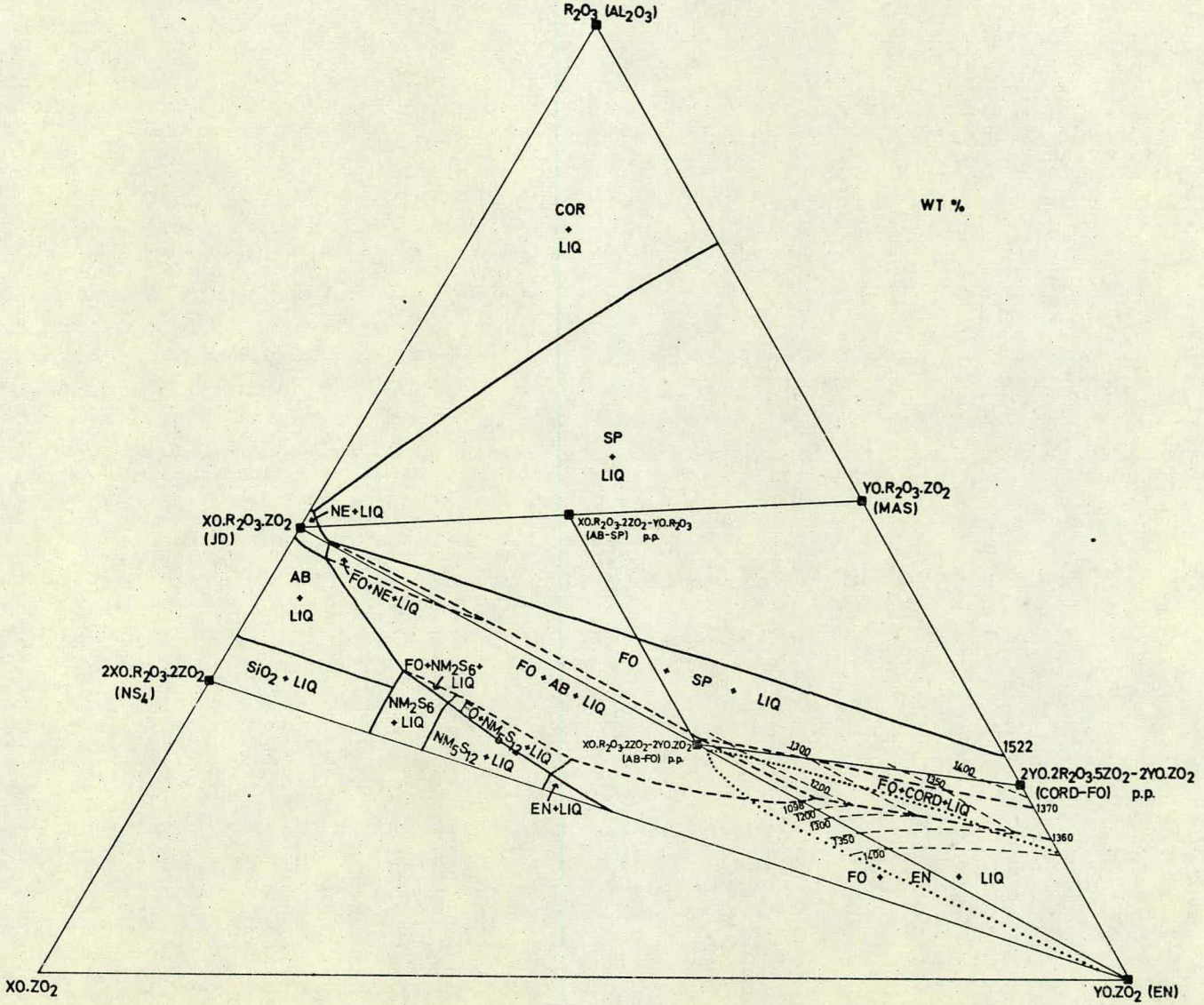
R_2O_3 (AL_2O_3)
COR
+
LIQ
WT %
SP
+
LIQ
$YO.R_2O_3.ZO_2$
(MAS)
$XO.R_2O_3.ZO_2$
(JD)
NE+LIQ
$XO.R_2O_3.2ZO_2$-$YO.R_2O_3$
(AB-SP) p.p.
AB
+
LIQ
FO+NE+LIQ
FO
+
SP
+
LIQ
$2XO.R_2O_3.2ZO_2$
(NS_4)
SiO_2 + LIQ
FO+NM_2S_6+
LIQ
FO+AB+LIQ
NM_2S_6
+LIQ
FO+NM_5S_{12}+LIQ
NM_5S_{12}+LIQ
$XO.R_2O_3.2ZO_2$-2YO.ZO_2
(AB-FO) p.p.
1300
1400
1522
$2YO.2R_2O_3.5ZO_2$-2YO.ZO_2
(CORD-FO) p.p.
1350
1200
FO+CORD+LIQ
1370
1360
1300
1350
1400
FO
+
EN
+
LIQ
EN+LIQ
$XO.ZO_2$
$YO.ZO_2$ (EN)

Fig 5.1

Figure 5.2

A $2YO.ZO_2$ (forsterite) projection into part of the plane $XO.ZO_2$-$YO.ZO_2$-R_2O_3 (CS-MS-A) of some of the forsterite-bearing equilibria at the bulk normative plagioclase ratio of An_0Ab_{100}, based on previously published data. The thick solid lines are the projection boundaries, the phase fields being indicated. The continuation of L. 5 E 3 fo,pig,pen, liq into the diagram is unknown. The dashed lines are the temperature contours of the appearance of the second phase where known, and the dotted line encloses those liquids on the surface of the olivine phase volume which are silica saturated.

The piercing point labelled AOpp. is the piercing point of the join $XO.R_2O_3.2ZO_2$-$2YO.ZO_2$ (Albite-Forsterite) in this plane.

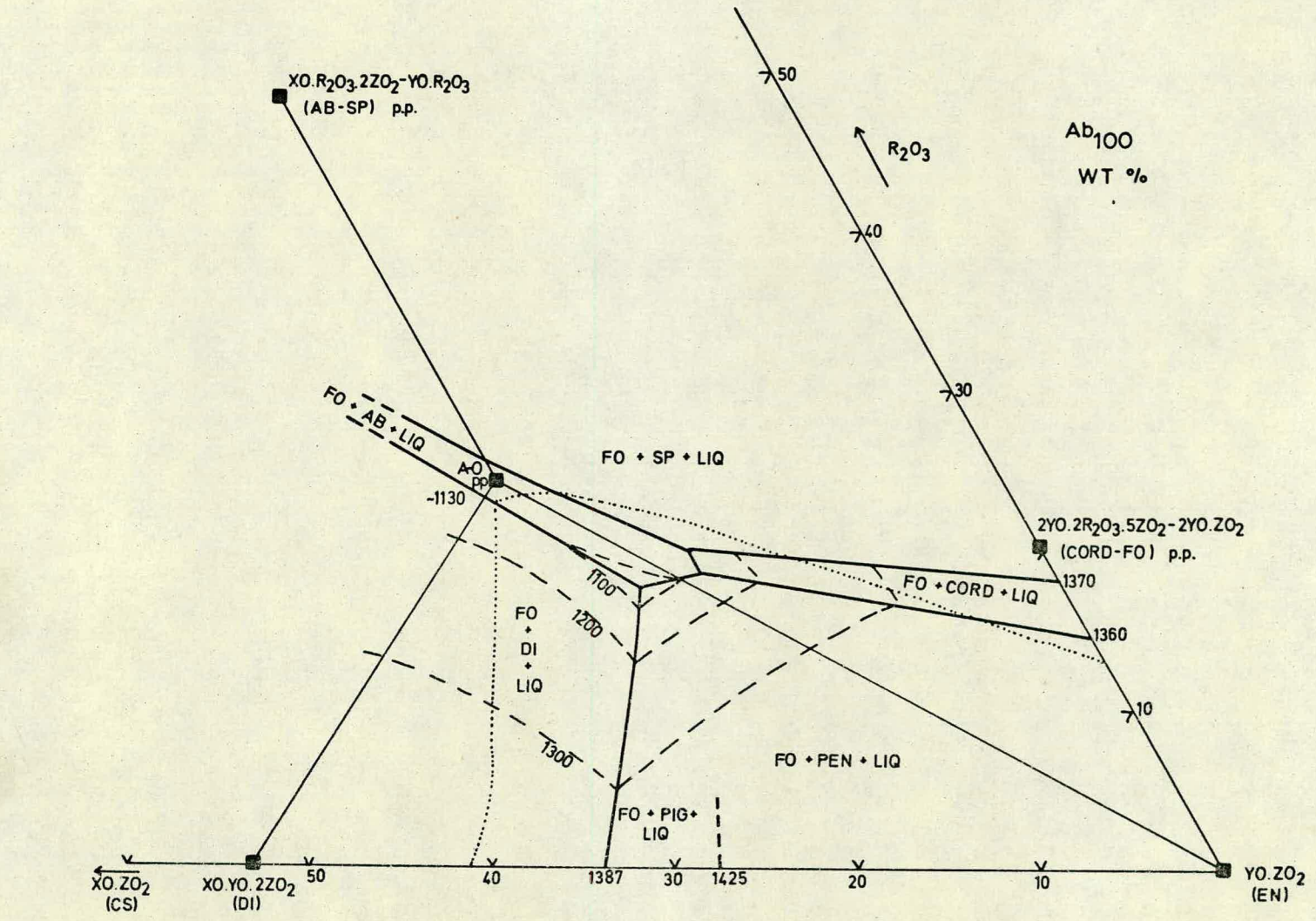
XO.R2O3.2ZO2-YO.R2O3
(AB-SP) p.p.
50
40
30
10
R2O3
Ab100
WT %
FO + AB + LIQ
A-O
pp
~1130
FO + SP + LIQ
2YO.2R2O3.5ZO2-2YO.ZO2
(CORD-FO) p.p.
1370
FO + CORD + LIQ
1360
1100
1200
FO
+
DI
+
LIQ
1300
FO + PEN + LIQ
FO + PIG +
LIQ
XO.ZO2
(CS)
XO.YO.2ZO2
(DI)
50
40
1387
30
1425
20
10
YO.ZO2
(EN)

Fig 5.2

Figures 5.3 to 5.6

Liquidus diagrams for the plane $XO.R_2O_3.2ZO_2$-$XO.YO.2ZO_2$-$2YO.ZO_2$ (An-Di-Fo) for compositions having bulk normative plagioclase contents of $An_{67.97}Ab_{32.03}$, $An_{51.48}Ab_{48.52}$, $An_{34.66}Ab_{65.34}$, and An_0Ab_{100} (wt%). The compositions studied are shown by circles and lie on the trace of the join $XO.YO.2ZO_2$-$YO.R_2O_3.ZO_2$ (Diopside-MAS) in this plane. The composition names can be found by referring to figure 5.10. The light dashed lines are temperature contours, the solid lines are the phase equilibrium boundaries. Data from the joins Diopside-Albite-Anorthite (Bowen (1915)) and Forsterite-Albite-Anorthite (Schairer and Yoder (1967)) were also used to construct the diagram.

The dotted line on figure 5.3 is the trace of L. 5 E 3 sp,fo,plag,liq for compositions in this plane having a spinel liquidus.

Figure 5.6 (An_0Ab_{100}) is redrawn after Schairer and Morimoto (1958).

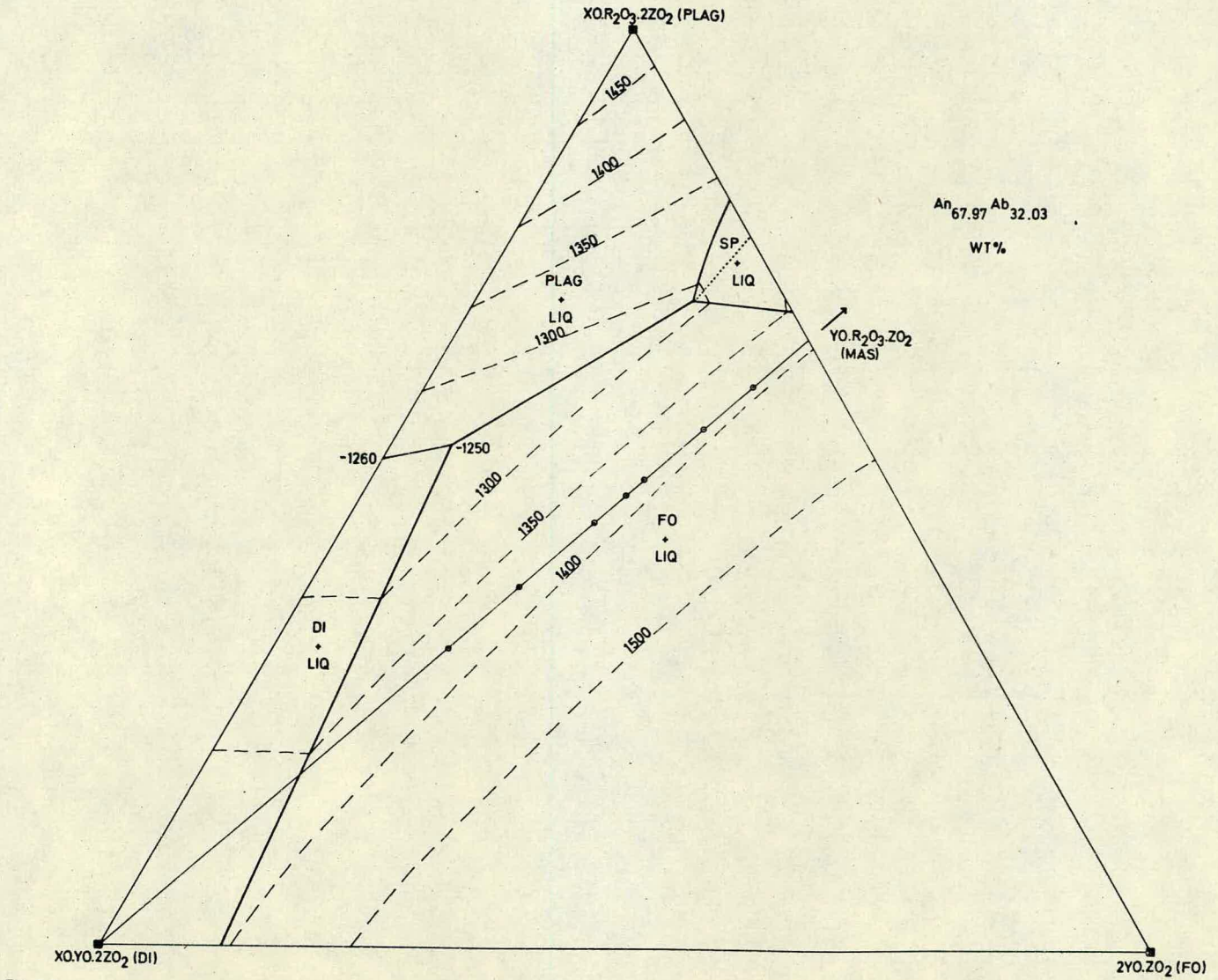
XO.R2O3.2ZO2 (PLAG)
1450
1400
1350
1300
PLAG
+
LIQ
SP
+
LIQ
An67.97 Ab32.03
WT%
YO.R2O3.ZO2
(MAS)
~1260
~1250
1300
1350
1400
1500
FO
+
LIQ
DI
+
LIQ
XO.YO.2ZO2 (DI)
2YO.ZO2 (FO)

Fig 5.3

Figure 5.4

See figure 5.3

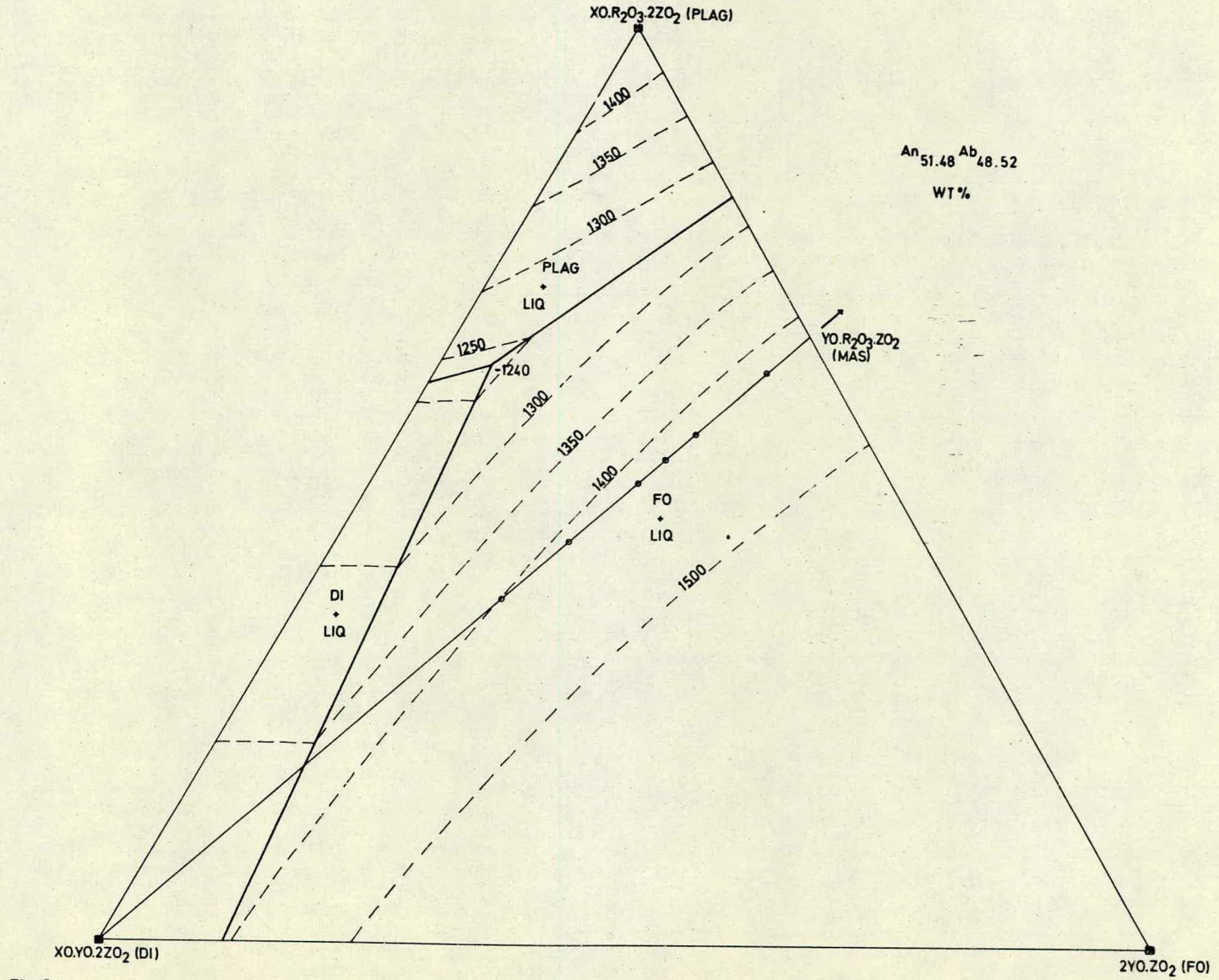
XO.R2O3.2ZO2 (PLAG)
An51.48 Ab48.52
WT%
1400
1350
1300
PLAG
+
LIQ
1250
1240
YO.R2O3.ZO2
(MAS)
1300
1350
1400
FO
+
LIQ
1500
DI
+
LIQ
XO.YO.2ZO2 (DI)
2YO.ZO2 (FO)

Fig 5 4

Figure 5.5

See figure 5.3

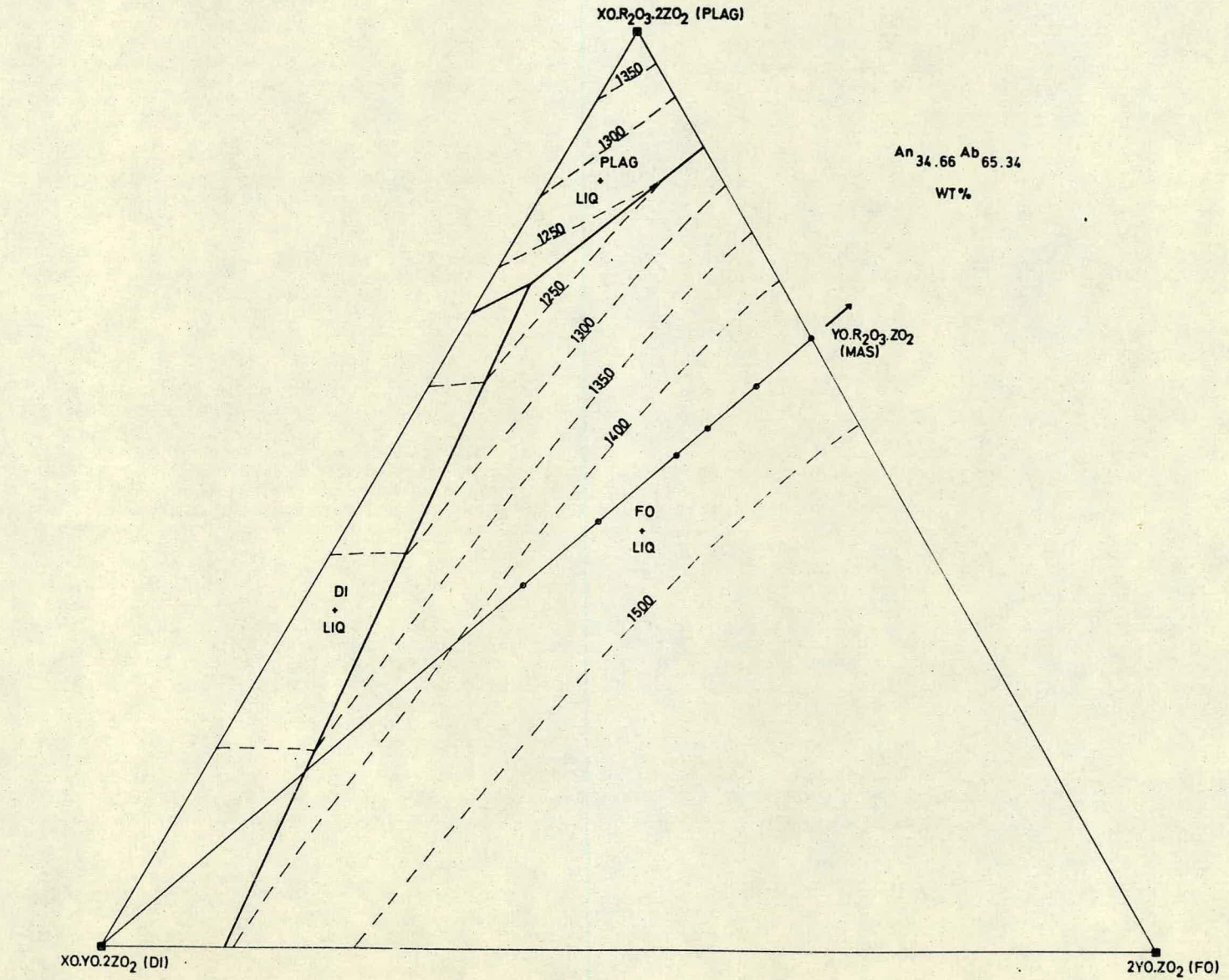
XO.R2O3.2ZO2 (PLAG)
1350
1300
PLAG
+
LIQ
1250
An34.66 Ab65.34
WT%
1250
1300
1350
1400
YO.R2O3.ZO2
(MAS)
FO
+
LIQ
DI
+
LIQ
1500
XO.YO.2ZO2 (DI)
2YO.ZO2 (FO)

Fig 5.5

Figure 5.6

See figure 5.3

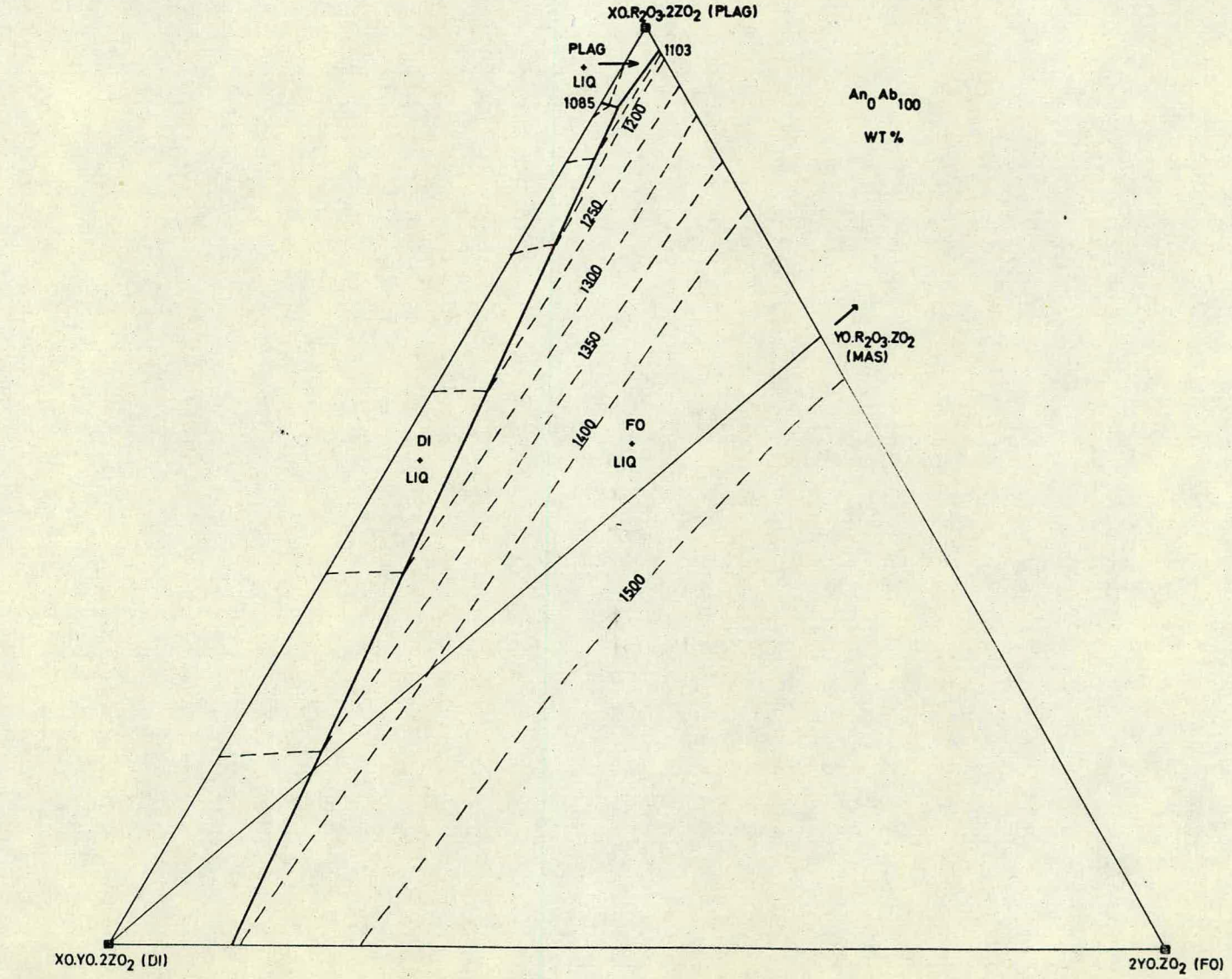
XO.R2O3.2ZO2 (PLAG)
PLAG
+
LIQ
1085
1103
1200
1250
1300
1350
1400
1500
An0 Ab100
WT %
YO.R2O3.ZO2
(MAS)
DI
+
LIQ
FO
+
LIQ
XO.YO.2ZO2 (DI)
2YO.ZO2 (FO)

Fig 5.6

Figures 5.7 to 5.9

$2YO.ZO_2$ (forsterite) projection diagrams into part of the plane $XO.ZO_2$-$YO.ZO_2$-R_2O_3 (CS-MS-A) for compositions having bulk normative plagioclase contents of $An_{67.97}Ab_{32.03}$, $An_{51.48}Ab_{48.52}$, and $An_{34.66}Ab_{65.34}$ (wt%). The compositions studied are indicated by filled circles, the composition names can be found by referring to figures 5.10 to 5.12 as necessary. The light dashed lines are temperature contours where known, the thick lines the projected phase equilibrium boundaries.

Also shown on figure 5.8 (⊗) is the projected position of L. 5 E 3 fo,plag,pyx,liq in the join Fe-O_2-MgO-SiO_2-$Anorthite_{50}Albite_{50}$ from Eggler (1974).

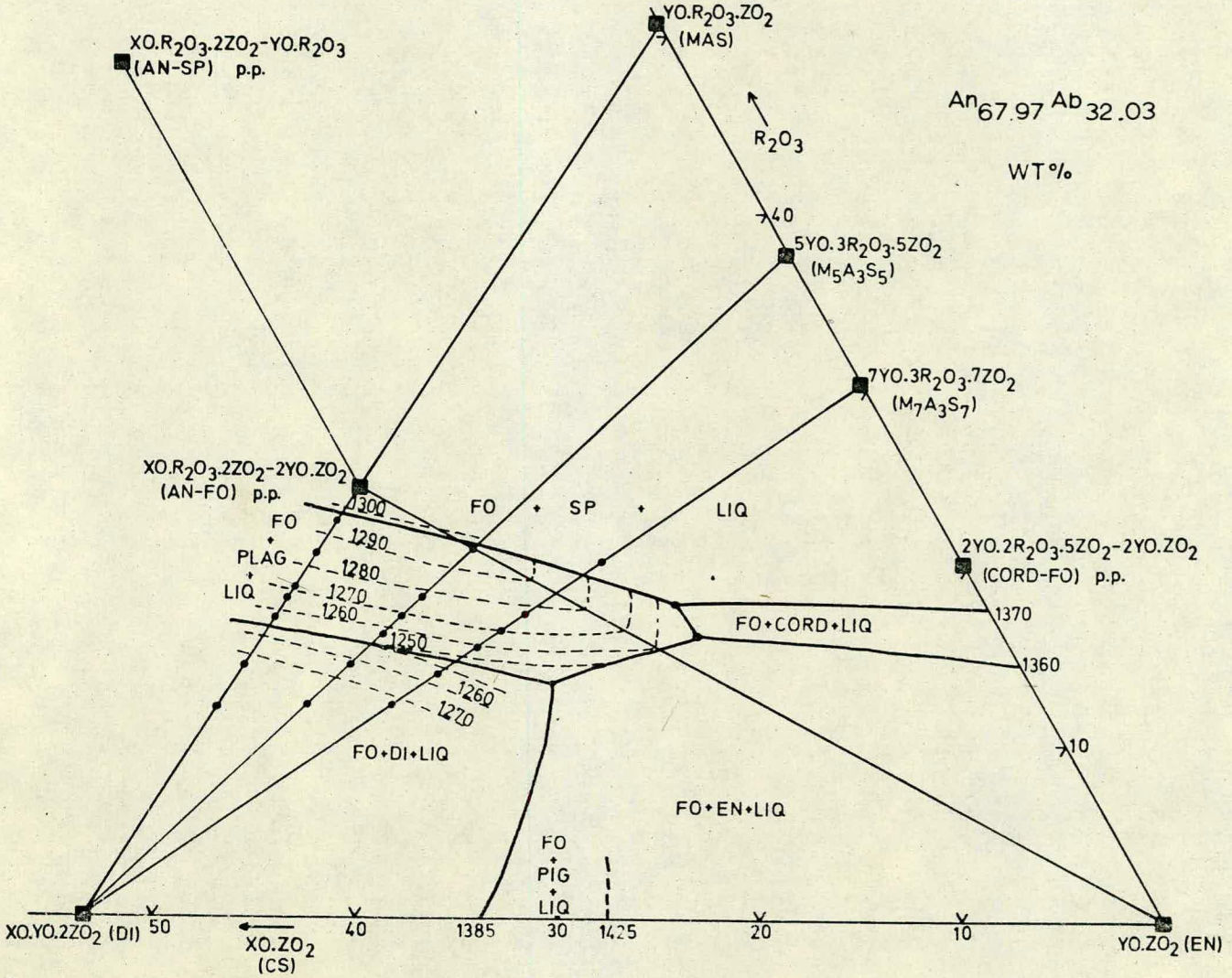
XO.R2O3.2ZO2-YO.R2O3
(AN-SP) p.p.
YO.R2O3.ZO2
(MAS)
An67.97 Ab32.03
WT%
R2O3
40
5YO.3R2O3.5ZO2
(M5A3S5)
7YO.3R2O3.7ZO2
(M7A3S7)
XO.R2O3.2ZO2-2YO.ZO2
(AN-FO) p.p.
1300
FO + SP + LIQ
FO
+
PLAG
+
LIQ
1290
1280
1270
1260
1250
1260
1270
2YO.2R2O3.5ZO2-2YO.ZO2
(CORD-FO) p.p.
1370
FO+CORD+LIQ
1360
10
FO+DI+LIQ
FO+EN+LIQ
FO
+
PIG
+
LIQ
XO.YO.2ZO2 (DI)
50
XO.ZO2
(CS)
40
1385
30
1425
20
10
YO.ZO2 (EN)

Fig 5.7

Figure 5.8

See figure 5.7

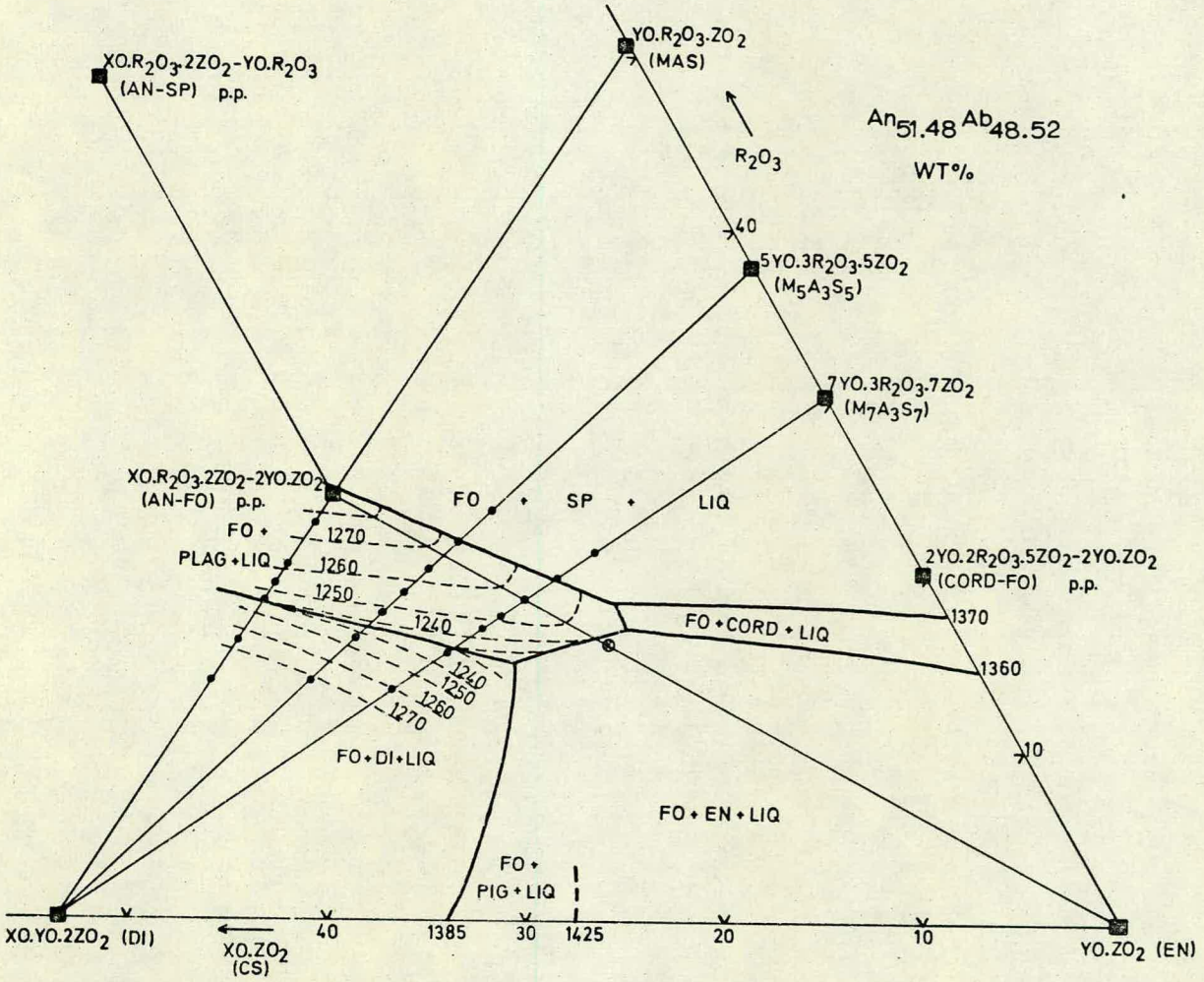
XO.R2O3.2ZO2-YO.R2O3
(AN-SP) p.p.
YO.R2O3.ZO2
(MAS)
An51.48 Ab48.52
WT%
R2O3
40
5YO.3R2O3.5ZO2
(M5A3S5)
7YO.3R2O3.7ZO2
(M7A3S7)
XO.R2O3.2ZO2-2YO.ZO2
(AN-FO) p.p.
FO + SP + LIQ
FO +
PLAG+LIQ
1270
1260
1250
1240
2YO.2R2O3.5ZO2-2YO.ZO2
(CORD-FO) p.p.
1370
FO+CORD + LIQ
1360
1240
1250
1260
1270
10
FO+DI+LIQ
FO + EN + LIQ
FO +
PIG + LIQ
XO.YO.2ZO2 (DI)
XO.ZO2
(CS)
40
1385
30
1425
20
10
YO.ZO2 (EN)

Fig 5.8

Figure 5.9

See figure 5.7

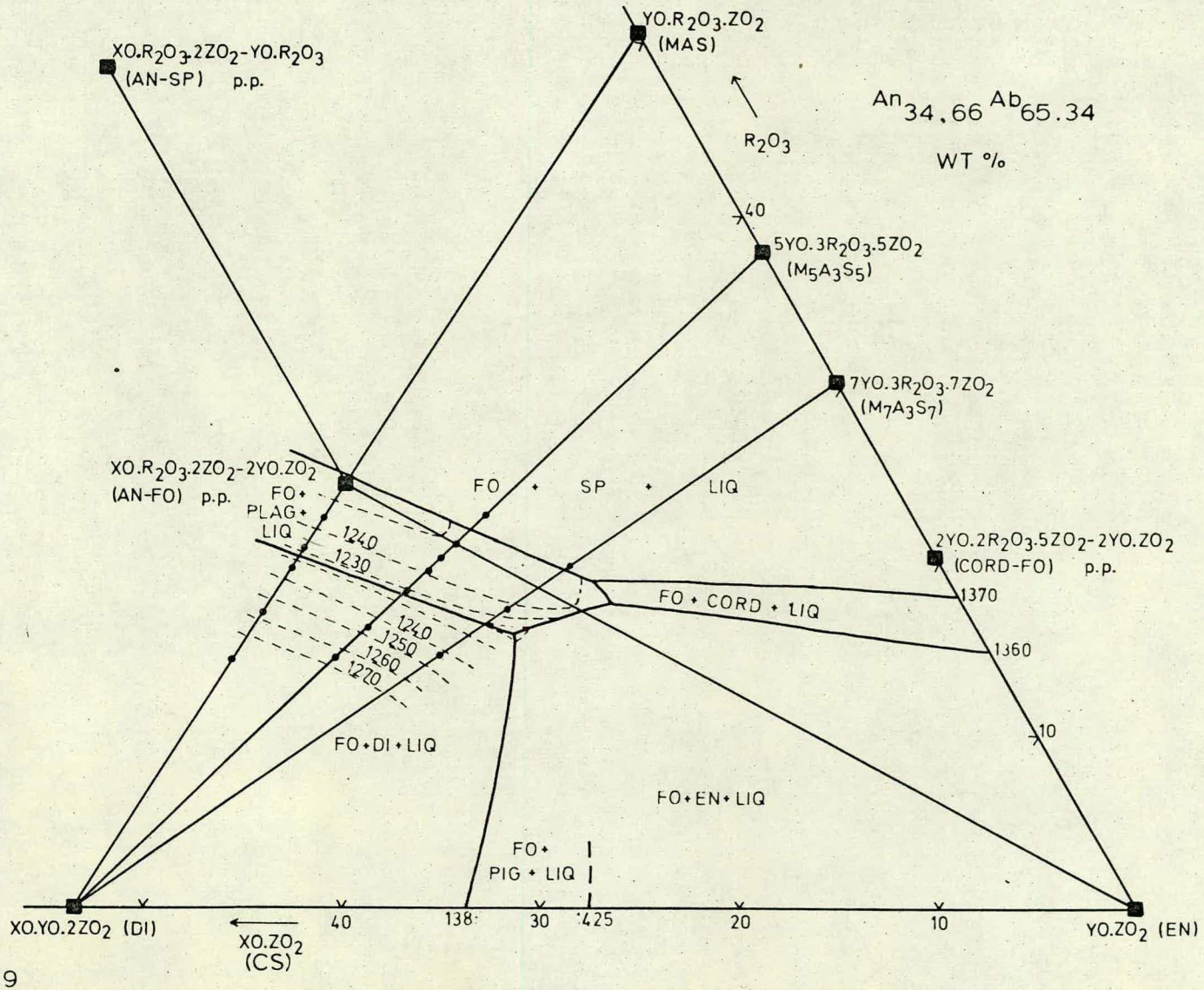
XO.R2O3.2ZO2-YO.R2O3
(AN-SP) p.p.
YO.R2O3.ZO2
(MAS)
R2O3
An34.66 Ab65.34
WT %
40
5YO.3R2O3.5ZO2
(M5A3S5)
7YO.3R2O3.7ZO2
(M7A3S7)
XO.R2O3.2ZO2-2YO.ZO2
(AN-FO) p.p.
FO + SP + LIQ
FO + PLAG + LIQ
1240
1230
2YO.2R2O3.5ZO2-2YO.ZO2
(CORD-FO) p.p.
FO + CORD + LIQ
1370
1360
1240
1250
1260
1270
10
FO+DI+LIQ
FO+EN+LIQ
FO + PIG + LIQ
XO.YO.2ZO2 (DI)
XO.ZO2
(CS)
40
138
30
425
20
10
YO.ZO2 (EN)

Fig 5.9

Figure 5.10

Diagram showing the effect of replacing anorthite by albite in the equilibrium L. 5 E 3 fo,plag,di,liq, plotted in the join $XO.YO.2ZO_2$-$YO.R_2O_3.ZO_2$ (Diopside-MAS) of the $2YO.ZO_2$ (forsterite) projection into the plane $XO.ZO_2$-$YO.ZO_2$-R_2O_3 (CS-MS-A). The compositions studied are shown by circles at the bulk normative plagioclase ratios studied; the composition names are also indicated. The light dashed lines are the temperature contours where known, the thick solid lines the phase equilibrium projection boundaries.

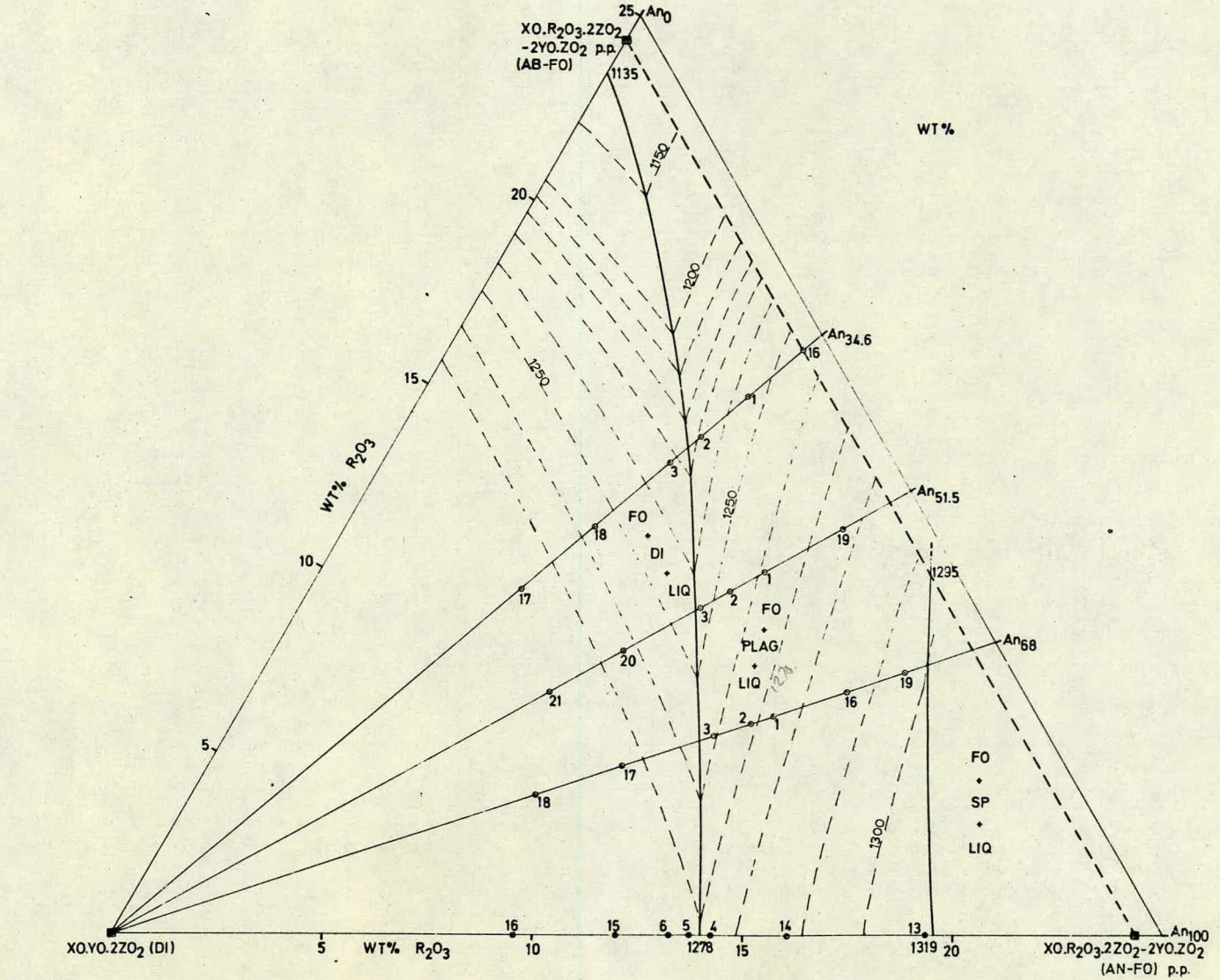
XO.R2O3.2ZO2
-2YO.ZO2 p.p.
(AB-FO)
An0
1135
1150
1200
1250
WT%
An34.6
An51.5
An68
An100
1235
1278
1300
1319
FO
DI
LIQ
PLAG
SP
WT% R2O3
XO.YO.2ZO2 (DI)
XO.R2O3.2ZO2-2YO.ZO2
(AN-FO) p.p.

Fig 5.10

Figure 5.11

Diagram showing the effect of replacing anorthite by albite in the equilibrium L. 5 E 3 fo,plag,di,liq, plotted in the join $XO.YO.2ZO_2$-$5YO.3R_2O_3.5ZO_2$ (Diopside-$M_5A_3S_5$) of the $2YO.ZO_2$ (forsterite) projection into the plane $XO.ZO_2$-$YO.ZO_2$-R_2O_3 (CS-MS-A). The compositions studied are shown by circles at the bulk normative plagioclase ratios studied; the composition names are also indicated. The light dashed lines are the temperature contours where known, the thick solid lines the phase equilibrium projection boundaries.

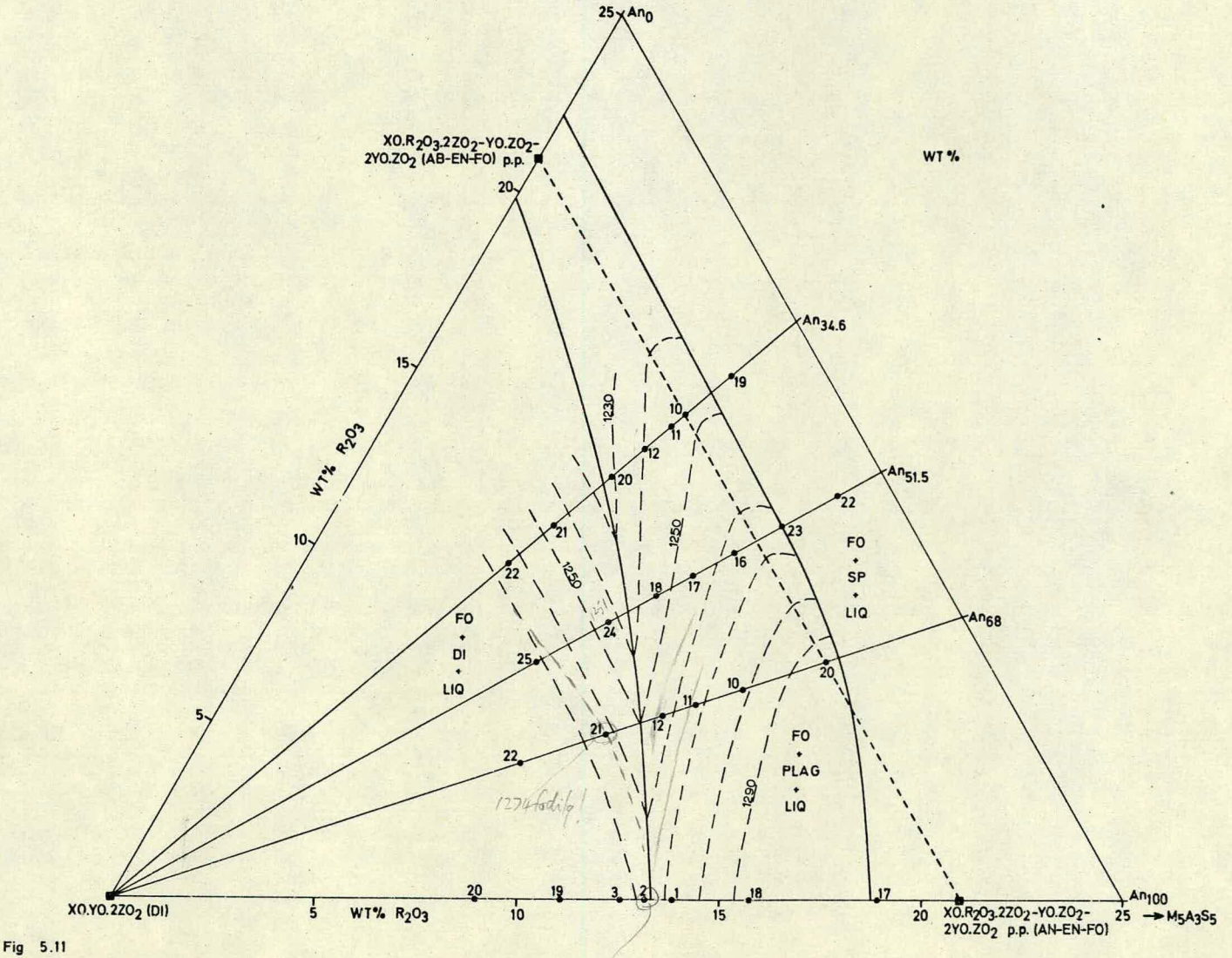
25 An0
X0.R2O3.2ZO2-YO.ZO2-
2YO.ZO2 (AB-EN-FO) p.p.
WT %
20
An34.6
15
WT% R2O3
19
10
11
12
1230
20
An51.5
22
10
21
23
1250
22
16
FO
+
SP
+
LIQ
18
17
1250
An68
24
FO
+
DI
+
LIQ
25
10
20
11
12
21
FO
+
PLAG
+
LIQ
22
1290
5
20
19
3
2
1
18
17
An100
X0.YO.2ZO2 (DI)
5
WT% R2O3
10
15
20
X0.R2O3.2ZO2-YO.ZO2-
2YO.ZO2 p.p. (AN-EN-FO)
25 → M5A3S5

Fig 5.11

Figure 5.12

Diagram showing the effect of replacing anorthite by albite in the equilibrium L. 5 E 3 fo,plag,di,liq, plotted in the join $XO.YO.2ZO_2$-$7YO.3R_2O_3.7ZO_2$ (Diopside-$M_7A_3S_7$) of the $2YO.ZO_2$ (forsterite) projection into the plane $XO.ZO_2$-$YO.ZO_2$-R_2O_3 (CS-MS-A). The compositions studied are shown by circles at the bulk normative plagioclase ratios studied; the composition names are also indicated. The light dashed lines are the temperature contours where known, the thick solid lines the phase equilibrium projection boundaries.

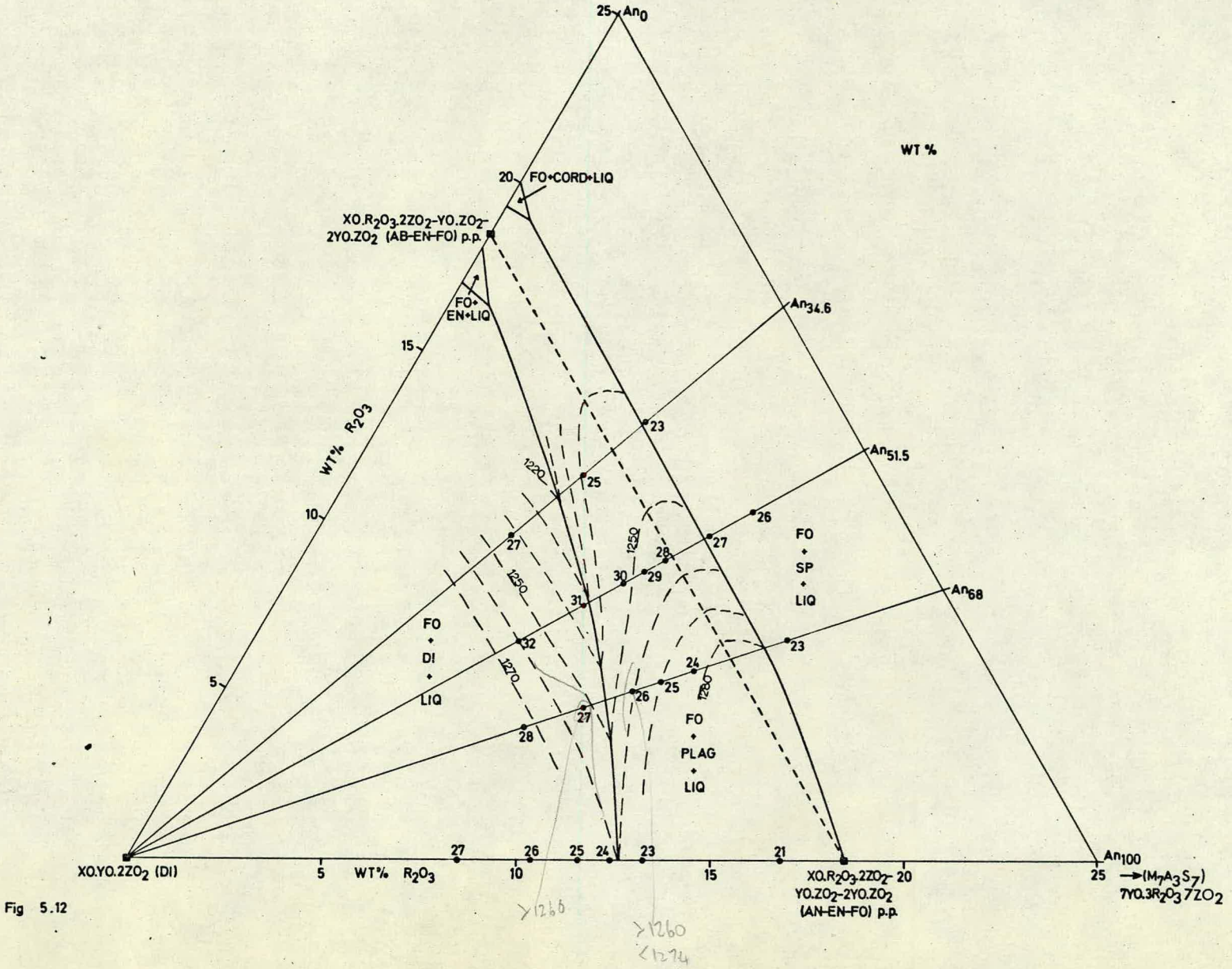
WT %
25 An0
20
FO+CORD+LIQ
XO.R2O3.2ZO2-YO.ZO2-
2YO.ZO2 (AB-EN-FO) p.p.
FO+
EN+LIQ
15
WT% R2O3
10
5
An34.6
An51.5
An68
An100
1220
1250
1270
1280
FO
+
DI
+
LIQ
FO
+
SP
+
LIQ
FO
+
PLAG
+
LIQ
XO.YO.2ZO2 (DI)
WT% R2O3
XO.R2O3.2ZO2-
YO.ZO2-2YO.ZO2
(AN-EN-FO) p.p.
(M7A3S7)
7YO.3R2O3.7ZO2
>1260
>1260
<1274

Fig 5.12

Figure 5.13

Summary diagram of the change in liquidus phase volumes in the plane $XO.R_2O_3.2ZO_2$-$XO.YO.2ZO_2$-$2YO.ZO_2$ (Anorthite-Diopside-Forsterite) with changing anorthite/albite content of the bulk normative plagioclase. The solid lines are the phase boundaries at $An_{100}Ab_0$ and An_0Ab_{100} ratios; intermediate positions are shown —·—·— (—∘—∘—on the L. 5 E 4 plag,sp,liq (AML) surface to avoid confusion). The thick solid lines labelled ADOL, AMOL show the change in position of the piercing points of L. 5 E 3 plag,di,fo,liq (ADOL) and L. 5 E 3 plag,fo,sp,liq (AOML) in this plane, as the anorthite/albite ratio changes. Temperature contours on the changing surfaces are shown by light dashed lines (dotted lines on L. 5 E 4 plag,sp,liq (AML) surface to avoid confusion).

Abbreviations used for the equilibria are

ADL = L. 5 E 4 plag,di,liq

AML = L. 5 E 4 plag,sp,liq

AOL = L. 5 E 4 plag,fo,liq

ODL = L. 5 E 4 fo,di,liq

OML = L. 5 E 4 fo,sp,liq

ADOL = L. 5 E 3 plag,di,fo,liq

AOML = L.5 E 3 plag,fo,sp,liq

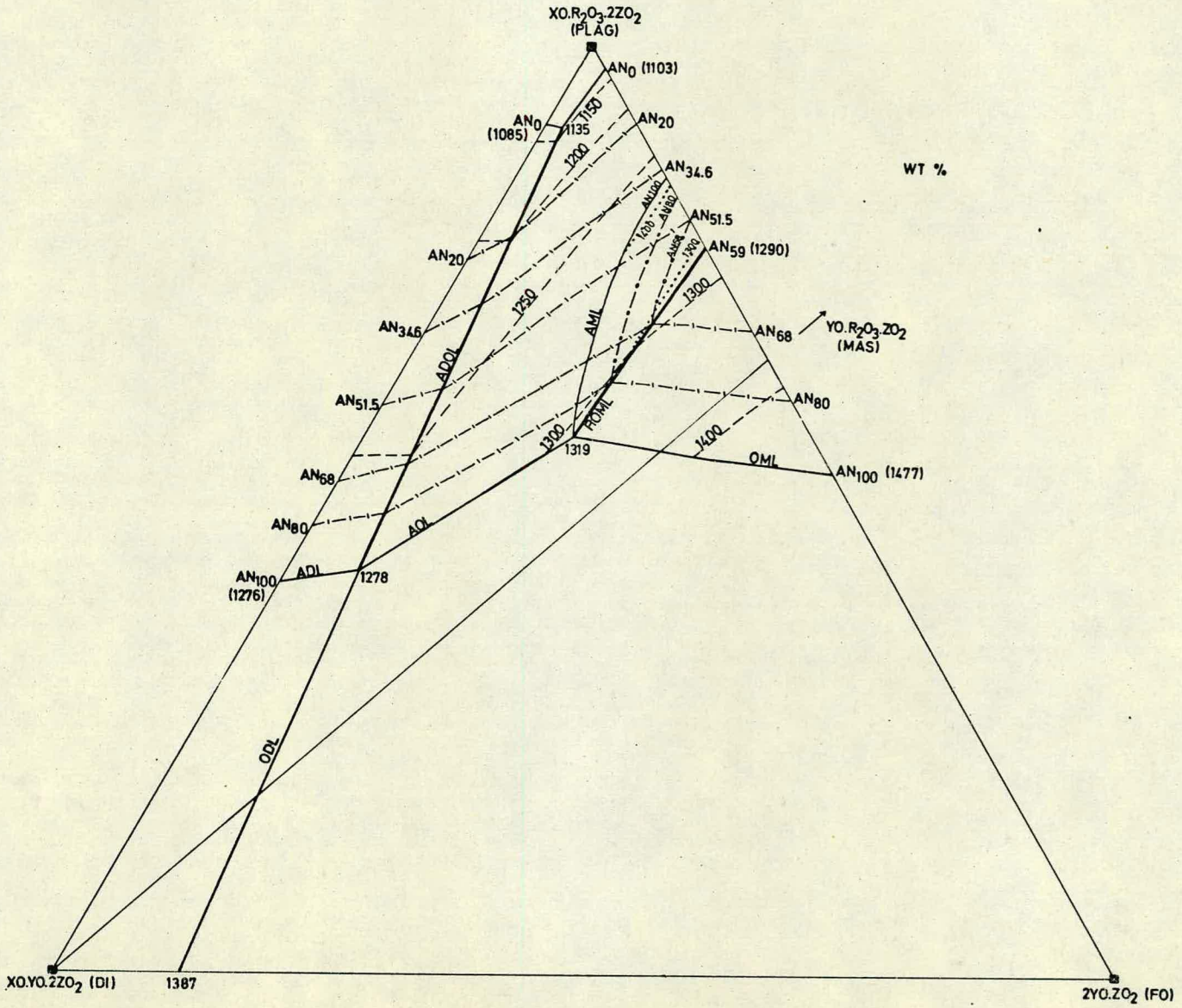
XO.R2O3.2ZO2
(PLAG)
AN0 (1103)
AN0
(1085)
1150
1135
AN20
1200
AN34.6
WT %
AN51.5
AN59 (1290)
AN20
1250
AN34.6
AML
1300
AN68
YO.R2O3.ZO2
(MAS)
AN51.5
ADOL
AN80
PDML
1300
1319
1400
OML
AN68
AN100 (1477)
AN80
ADL
AN100
(1276)
ADL
1278
ODL
XO.YO.2ZO2 (DI)
1387
2YO.ZO2 (FO)

Fig 5.13

Figure 5.14

A summary diagram of the $2YO.ZO_2$ (forsterite) projection diagrams into the plane $XO.ZO_2$-$YO.ZO_2$-R_2O_3 (CS-MS-A) presented as figures 5.7 - 5.9, to show the change in position in projection of some of the forsterite-bearing equilibria, with changing bulk normative plagioclase ratio. The thin solid lines are the projection boundaries for the bulk normative plagioclase ratios of $An_{100}Ab_0$ (labelled 0) from figure 4.3, and An_0Ab_{100} (labelled 100) from figure 5.2; intermediate positions are shown —+— —+— —+— and the appropriate plagioclase ratio indicated. The thick solid lines are the change in projection position of L. 5 E 2 from plagioclase ratio $An_{100}Ab_0$ to An_0Ab_{100}. The extension of L. 5 E 2 fo,pig,pen,di,liq from $An_{100}Ab_0$ ratio is unknown. The projected position of the $Diopside_{ss}$ composition in the equilibrium L. 5 E 3 fo,di,an,liq and the thermal divide Anorthite-$Diopside_{ss}$-Forsterite is shown for reference (D_M —•—).

The point (⊗) is the piercing point of L. 5 E 3 fo,di,plag,liq in the plane Diopside-Enstatite-$Albite_{38.6}$-$Anorthite_{61.4}$ from Emslie (1971).

The dotted lines show the extent of liquids on the surface of the forsterite volume which are silica saturated at $An_{100}Ab_0$ (labelled 0) and An_0Ab_{100} (labelled 100), to show the gradual expansion of the area of silica saturated olivine-bearing liquids.

The piercing point labelled AOpp is the piercing point of the join $XO.R_2O_3.2ZO_2$-$2YO.ZO_2$ (Anorthite-Forsterite) in this plane.

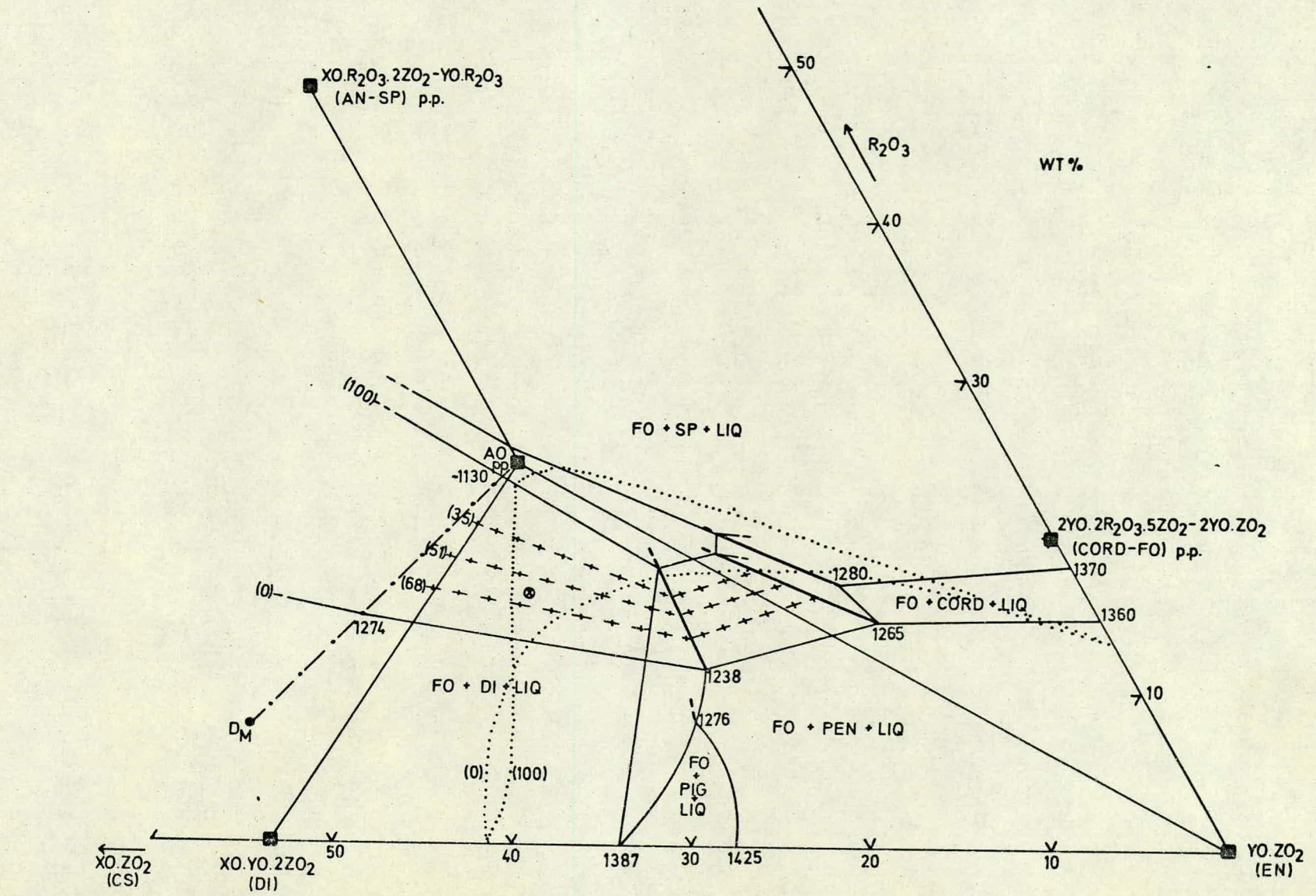
XO.R2O3.2ZO2-YO.R2O3
(AN-SP) p.p.
50
R2O3
WT %
40
30
(100)
FO + SP + LIQ
AO
pp
1130
(35)
(51)
(68)
(0)
1274
1280
2YO.2R2O3.5ZO2-2YO.ZO2
(CORD-FO) p.p.
1370
FO + CORD + LIQ
1360
1265
1238
FO + DI + LIQ
10
1276
FO + PEN + LIQ
DM
(0)
(100)
FO
+
PIG
+
LIQ
XO.ZO2
(CS)
XO.YO.2ZO2
(DI)
50
40
1387
30
1425
20
10
YO.ZO2
(EN)

Fig 5.14

Figure 5.15

Summary diagram of part of the $XO.YO.2ZO_2$ (diopside) projection into the plane $XO.R_2O_3$-YO-ZO_2 (CA-M-S) showing the relationship between the forsterite+diopside+liquid equilibria and the silica+diposide+liquid equilibria as the anorthite/albite content of the bulk normative plagioclase changes. The projection phase boundaries at An_0Ab_{100} and $An_{100}Ab_0$ are shown as solid lines, the change in projection of AODPL (L. 5 E 2 plag,fo,di,pyx,liq) and ASDPL (L. 5 E 2 plag,sil,di,pyx,liq) being indicated. The thick dashed line is an estimate of the change in projection of the diopside+protoenstatite+pigeonite+liquid surface. The thin dashed lines are temperature contours where known for the diopside projection surface for the ratio $An_{100}Ab_0$ (figure 4.7); the figures in parenthesis after the equilibria abbreviations are the albite contents of the bulk normative plagioclase.

Abbreviations used for the equilibria are

ADPL = L. 5 E 3 plag,di,pyx,liq

AODL = L. 5 E 3 plag,fo,di,liq

ASDL = L. 5 E 3 plag,sil,di,liq

ODPL = L. 5 E 3 fo,di,pyx,liq

SDPL = L. 5 E 3 sil,di,pyx,liq

AODPL = L. 5 E 2 plag,fo,di,pyx,liq

ASDPL = L. 5 E 2 plag,sil,di,pyx,liq

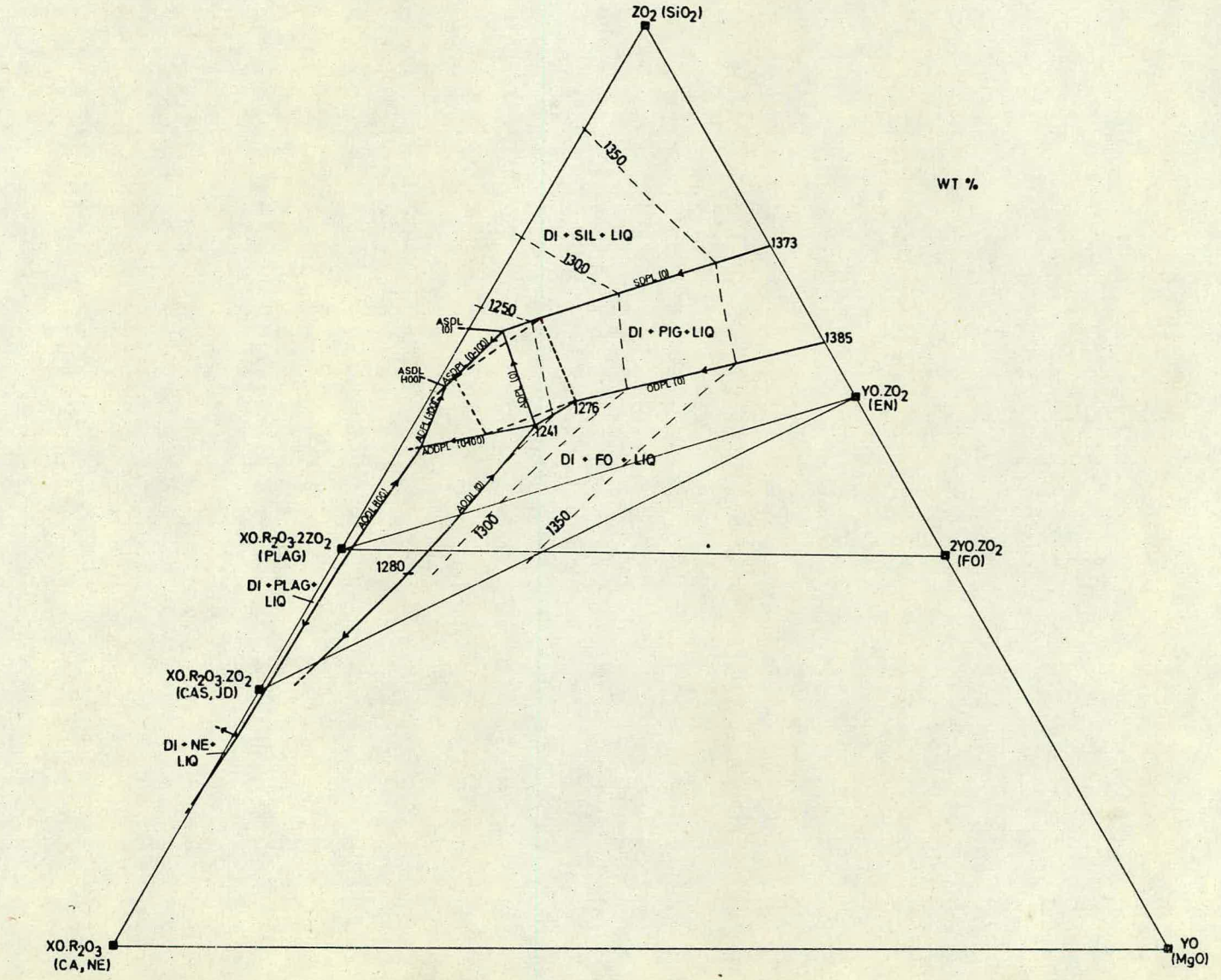
ZO2 (SiO2)
WT %
1350
DI + SIL + LIQ
1373
1300
SDPL (O)
1250
ASDL (O)
DI + PIG + LIQ
1385
ASDL (HOO)
ODPL (O)
YO.ZO2 (EN)
1276
1241
ADDPL (O+OO)
DI + FO + LIQ
ADDL (OO)
ADDL (O)
1300
1350
XO.R2O3.2ZO2 (PLAG)
1280
2YO.ZO2 (FO)
DI + PLAG + LIQ
XO.R2O3.ZO2 (CAS, JD)
DI + NE + LIQ
XO.R2O3 (CA, NE)
YO (MgO)

Fig 5.15

Figure 5.16

A $2YO.ZO_2$ (forsterite) projection into the join $YO.R_2O_3$-$XO.R_2O_3.2ZO_2$ (spinel-plagioclase) extended versus anorthite/albite ratio to show the change in forsterite projection boundaries and the change in nature of L. 5 E 3 fo,plag,sp,liq from one of spinel reaction to one of coprecipitation. This join is represented in the plane $XO.ZO_2$-$YO.ZO_2$-R_2O_3 (CS-MS-A) as the line from $XO.R_2O_3.2ZO_2$-$YO.R_2O_3$ (AnSp) to $XO.R_2O_3.2ZO_2$-$2YO.ZO_2$ (AnFo) piercing points extended.

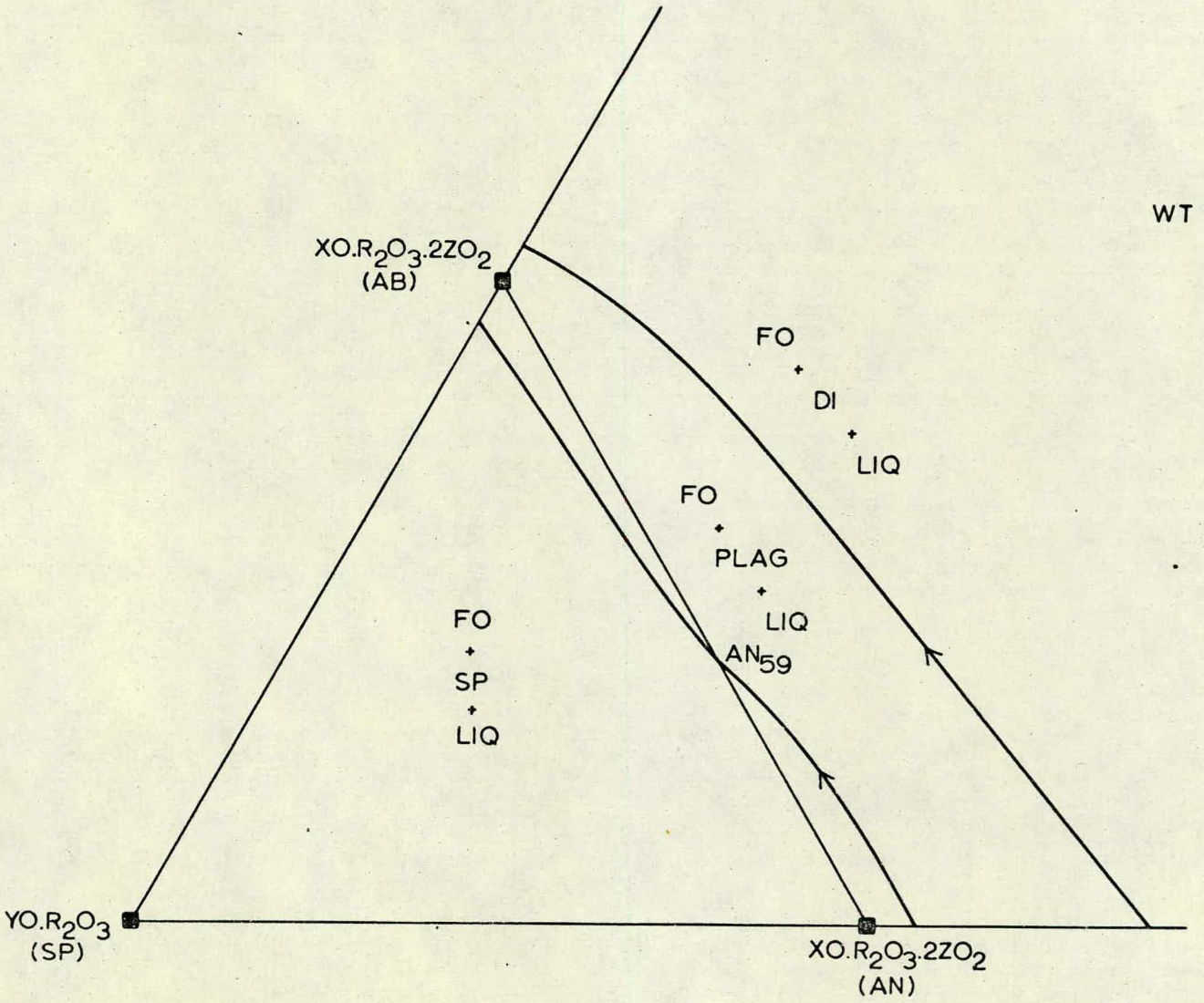
WT %
XO.R2O3.2ZO2
(AB)
FO
DI
LIQ
FO
PLAG
LIQ
AN59
FO
SP
LIQ
YO.R2O3
(SP)
XO.R2O3.2ZO2
(AN)

Fig 5.16

Figure 5.17

The areas of like crystallisation histories under perfect equilibrium crystallisation conditions for forsterite saturated compositions projecting in the join $YO.R_2O_3$-$XO.R_2O_3.2ZO_2$ (spinel-plagioclase), presented as figure 5.16. Each area is numbered to correspond with the numbering given in table 5.1, in which the crystallisation histories for compositions projecting in each area are given. Further discussion is given in the text.

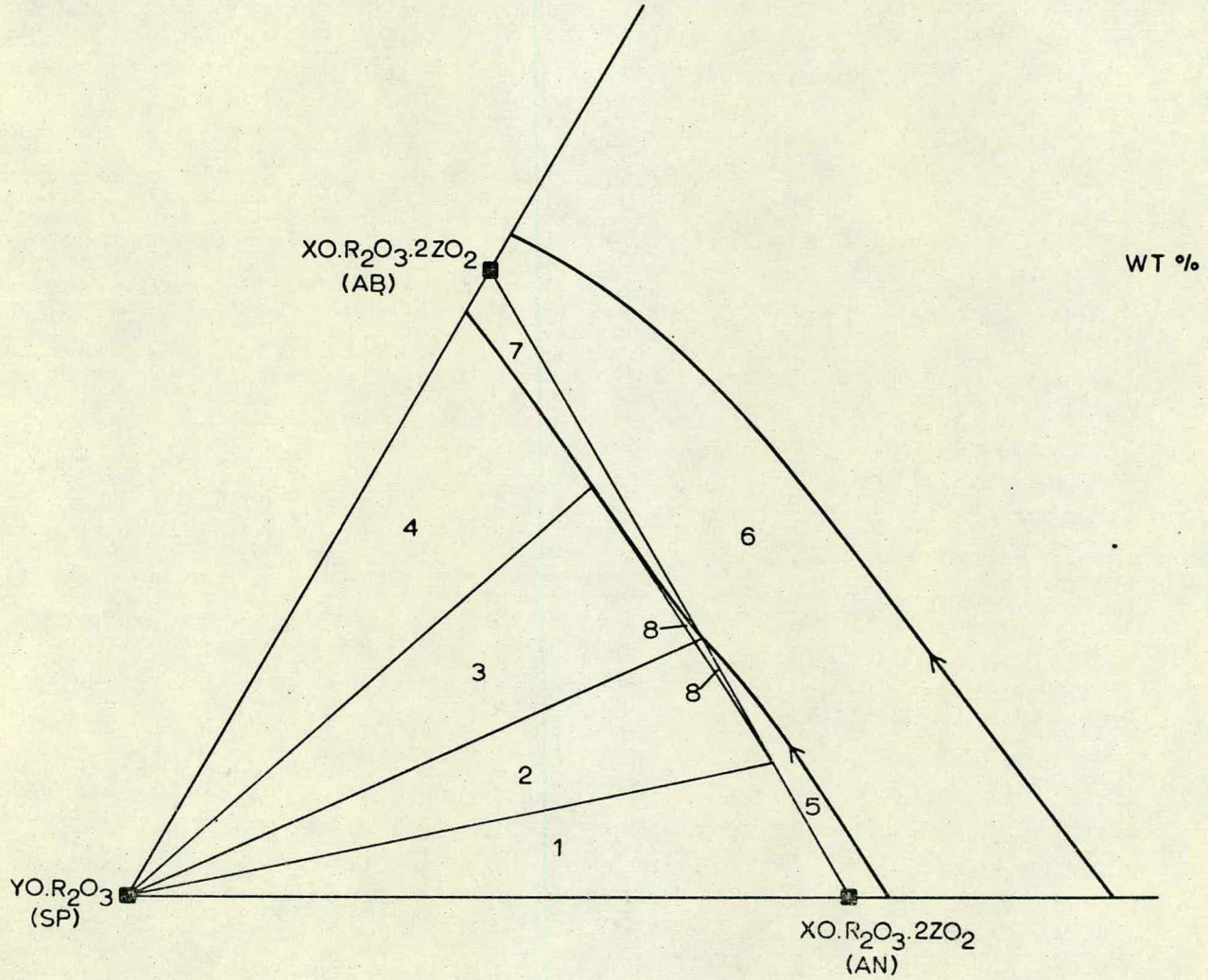

Fig 5.17

Figure 5.18

The areas of like crystallisation histories under perfect fractional crystallisation conditions for forsterite saturated compositions projecting in the join $YO.R_2O_3$-$XO.R_2O_3.2ZO_2$ (spinel-plagioclase), presented as figure 5.16. Each area is numbered to correspond with the numbering given in table 5.2, in which the crystallisation histories for compositions projecting in each area are given. Further discussion is given in the text.

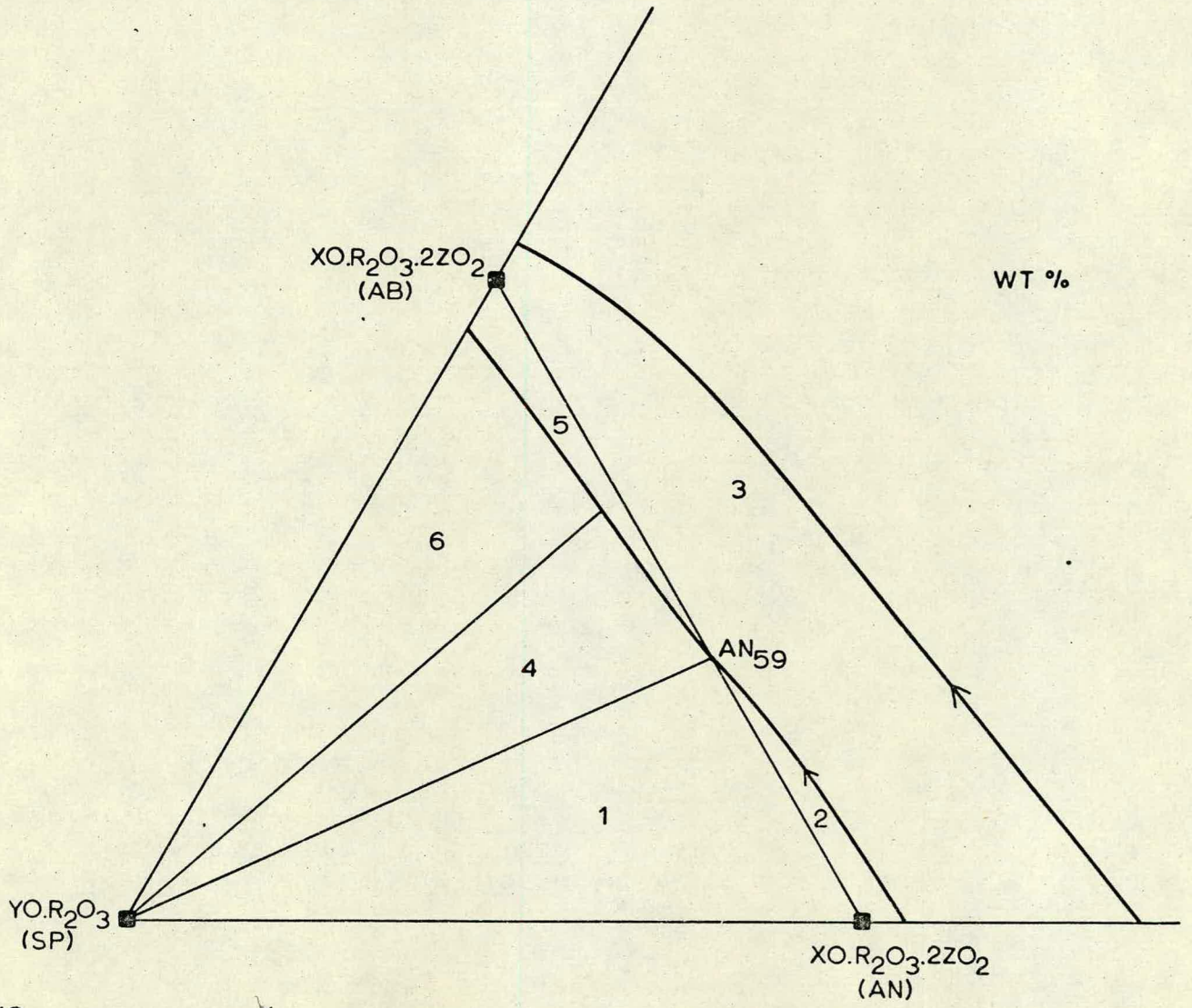

Fig 5.18

Figure 5.19

A $2YO.ZO_2$ (forsterite) projection into part of the plane $XO.ZO_2$-$YO.ZO_2$-R_2O_3 (CS-MS-A) for compositions having a bulk normative plagioclase ratio of $An_{34.6}Ab_{65.4}$ (from figure 5.9), outlining areas of like crystallisation histories under perfect equilibrium crystallisation conditions for forsterite saturated compositions. Each area is numbered to correspond with the numbering given in table 5.3, in which the crystallisation histories for compositions projecting in each area are given. The letter associated with each area indicates the change in CIPW normative character of the residual liquids produced from compositions projecting in that area. The letters have the following meanings.

a residual liquids always undersaturated* in the CIPW norm

c residual liquids always saturated* in the norm

d residual liquids begin undersaturated, but become saturated.

The extent of the undersaturated parts of areas 9 and 10 are only approximate and will depend upon the diopside solid solution composition at the maximum on 5 E 3 fo,plag,di,liq.

A similar diagram can be drawn for each plagioclase ratio from $An_{59}Ab_{41}$ to An_0Ab_{100}. Further discussion is given in the text.

---

* The term undersaturated represents the presence of corundum or nepheline or larnite in the CIPW norm; saturated represents the absence of such minerals in the norm.

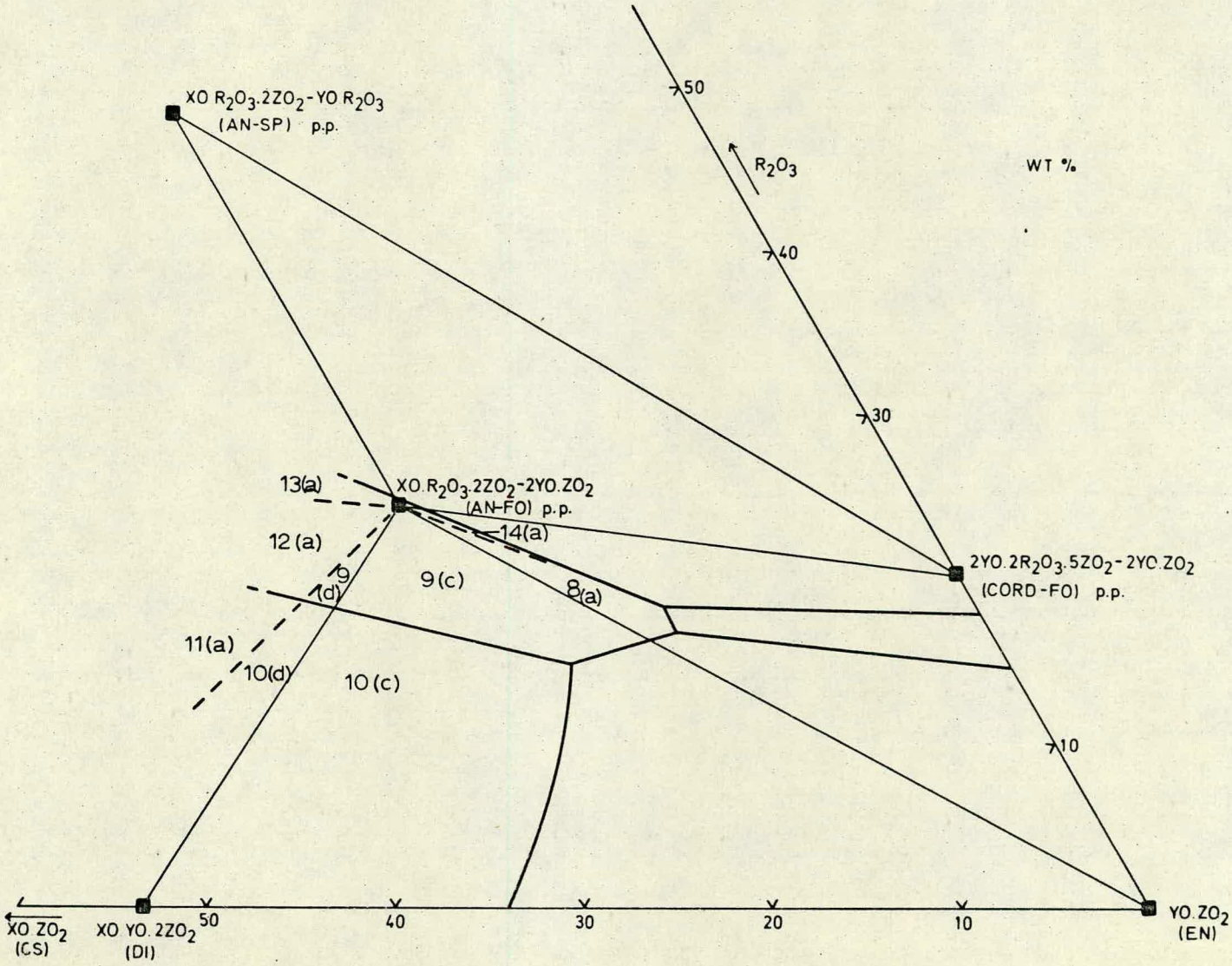
XO R_2O_3.2ZO_2-YO R_2O_3
(AN-SP) p.p.
50
R_2O_3
WT %
40
30
13(a)
XO.R_2O_3.2ZO_2-2YO.ZO_2
(AN-FO) p.p.
14(a)
12 (a)
9
9(d)
9 (c)
8(a)
2YO.2R_2O_3.5ZO_2-2YO.ZO_2
(CORD-FO) p.p.
11(a)
10(d)
10 (c)
10
XO ZO_2
(CS)
XO YO.2ZO_2
(DI)
50
40
30
20
10
YO.ZO_2
(EN)

Fig 5.19

Figure 5.20

A $2YO.ZO_2$ (forsterite) projection into part of the plane $XO.ZO_2$-$YO.ZO_2$-R_2O_3 (CS-MS-A) for compositions having a bulk normative plagioclase ratio of $An_{34.6}Ab_{65.4}$ (from figure 5.9), outlining areas of like crystallisation histories under perfect fractional crystallisation conditions for forsterite saturated compositions. Each area is numbered to correspond with the numbering given in table 5.4, in which the crystallisation histories for compositions projecting in each area are given. The letter associated with each area indicates the change in CIPW normative character of the residual liquids produced from compositions projecting in that area. The letters have the following meanings

a residual liquids begin undersaturated, later become saturated in the CIPW norm

b residual liquids always saturated in the norm

c residual liquids always undersaturated in the norm

The terms undersaturated and saturated are explained in figure 5.19.

The extent of the undersaturated parts of areas 5 and 8 are only approximate and will depend upon the diopside solid solution composition at the maximum on 5 E 3 fo,plag,di,liq.

The area of compositions producing saturated and undersaturated residual liquids (see figure 4.10) has now vanished.

A similar diagram can be drawn for each plagioclase ratio from $An_{59}Ab_{41}$ to An_0Ab_{100}. Further discussion is given in the text.

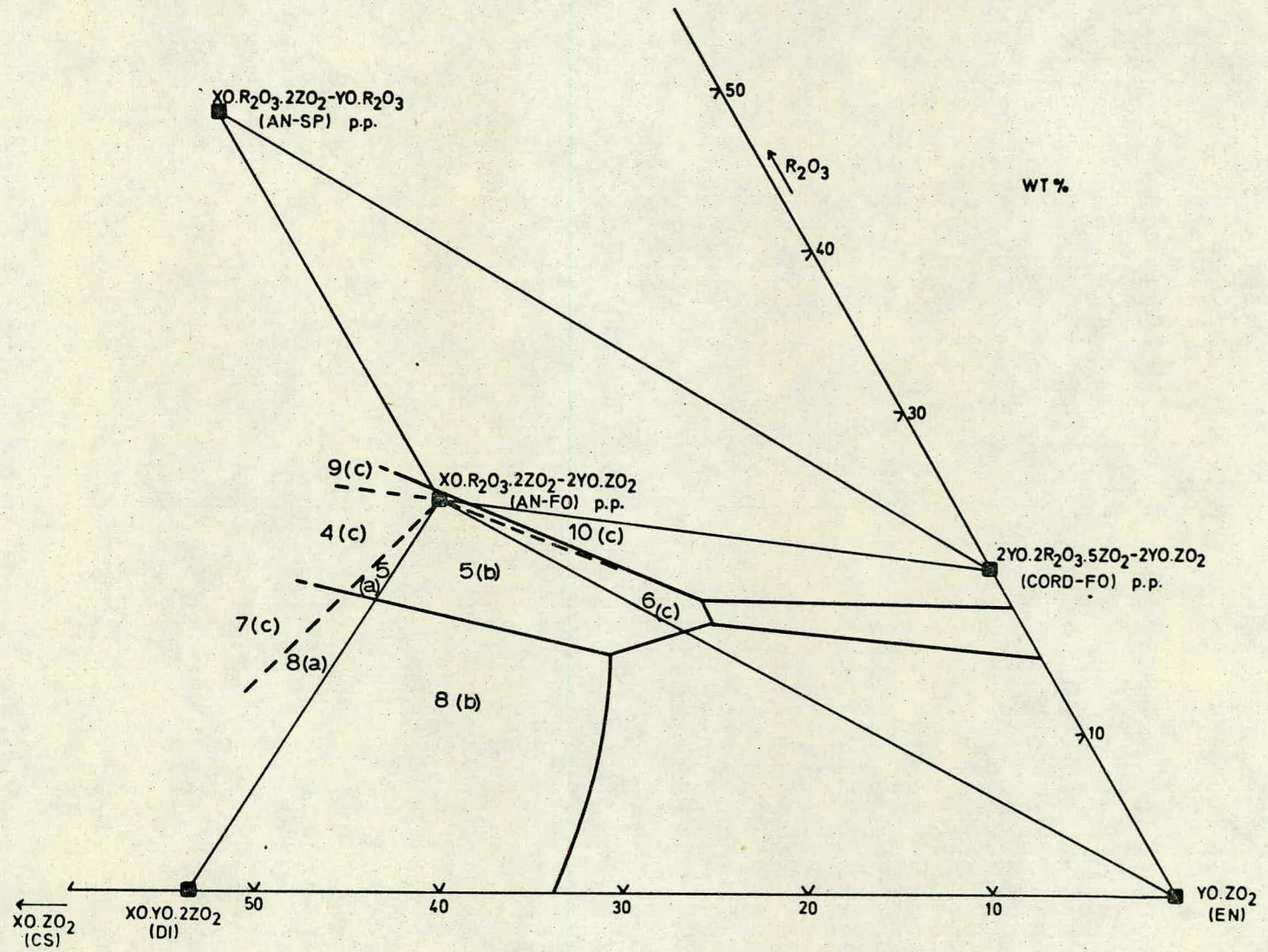
XO.R2O3.2ZO2-YO.R2O3
(AN-SP) p.p.
50
R2O3
WT %
40
30
9(c)
XO.R2O3.2ZO2-2YO.ZO2
(AN-FO) p.p.
4(c)
10 (c)
2YO.2R2O3.5ZO2-2YO.ZO2
(CORD-FO) p.p.
5
(a)
5(b)
6(c)
7(c)
8(a)
8 (b)
10
XO.ZO2
(CS)
XO.YO.2ZO2
(DI)
50
40
30
20
10
YO.ZO2
(EN)

Fig 5.20

CHAPTER 6

THE SYSTEM $CaO-MgO-Al_2O_3-SiO_2-Fe-O_2$

Figures 6.1 - 6.102

Figure 6.1

Temperature versus pO_2 plot of some of the equilibria within the system $MgO-SiO_2-Fe-O_2$ (thick solid lines), redrawn after Speidel and Nafziger (1968). The light lines are equilibria within the bounding system SiO_2-Fe-O_2 shown for reference. Also shown, as dashed lines, are the reference curves of the Ni/NiO, Fe/FeO and CO_2 equilibria used in this study, and the curve for the CO_2/H_2 constant mixing ratio of 50 mentioned in the text.

Abbreviations used for the equilibria are

OIWL = L. 6 E 4 ol,Fe,wu,liq

OMWL = L. 6 E 4 ol,sp,wu,liq

OPIL = L. 6 E 4 ol,pyx,Fe,liq

OPML = L. 6 E 4 ol,pyx,sp,liq

OSIL = L. 6 E 4 ol,sil,Fe,liq

OSML = L. 6 E 4 ol,sil,sp,liq

OSPL = L. 6 E 4 ol,sil,pyx,liq

SPIL = L. 6 E 4 sil,pyx,Fe,liq

SPML = L. 6 E 4 sil,pyx,sp,liq

OSPIL = L. 6 E 3 ol,sil,pyx,Fe,liq

OSPML = L. 6 E 3 ol,sil,pyx,sp,liq

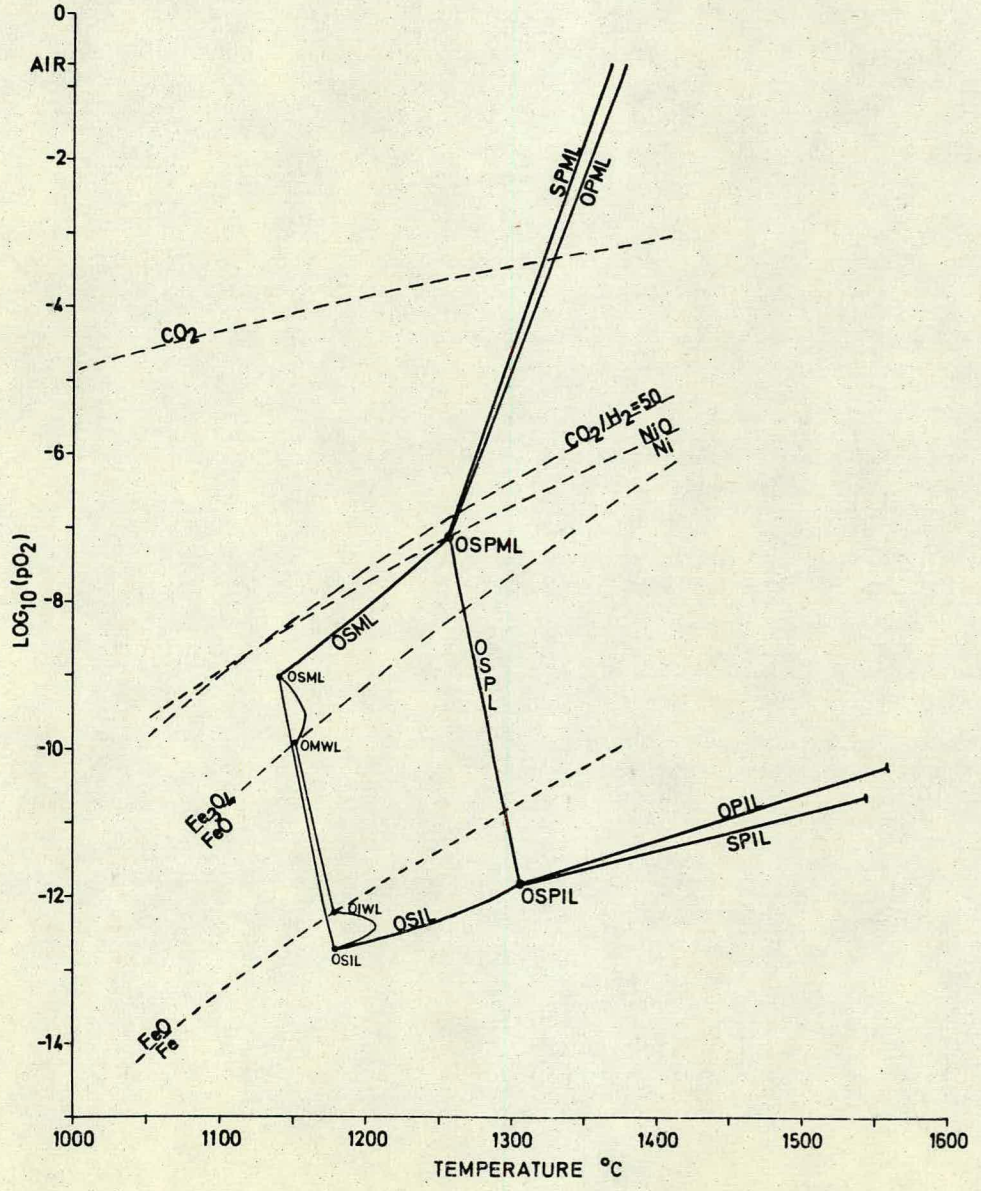
0
AIR
-2
-4
-6
-8
-10
-12
-14
$LOG_{10}(pO_2)$
1000
1100
1200
1300
1400
1500
1600
TEMPERATURE °C
SPML
OPML
CO_2
$CO_2/H_2=50$
NiO
Ni
OSPML
OSML
OSPL
OSML
OMWL
Fe_3O_4
FeO
OPIL
SPIL
OSPIL
OIWL
OSIL
OSIL
FeO
Fe

Fig 6.1

Figure 6.2

Multi-pO_2 plot of the system $MgO-SiO_2-Fe-O_2$, drawn as an oxygen projection into the plane $MgO-SiO_2-FeO$. The thick solid lines are the L. 6 E 4 which intersect this plane, the pO_2 and temperature of some of the liquids being indicated. The names of the equilibria are shown in the inset to the right.

Also shown are the liquidus phase boundaries at the pO_2=Fe metal just present (thin solid lines), and at the pO_2=air (thin dashed lines), to show how the phase diagram at any pO_2 can be drawn.

The data of Muan and Osborn (1956), Bowen and Schairer (1935), Muan (1955) and Presnall (1966) were used to construct this diagram.

Abbreviations used for the equilibria are

IOSL = L. 6 E 4 Fe,ol,sil,liq

IPOL = L. 6 E 4 Fe,pyx,ol,liq

IPSL = L. 6 E 4 Fe,pyx,sil,liq

OMWL = L. 6 E 4 ol,sp,wu,liq

OPML = L. 6 E 4 ol,pyx,sp,liq

OPSL = L. 6 E 4 ol,pyx,sil,liq

OSML = L. 6 E 4 ol,sil,sp,liq

SPML = L. 6 E 4 sil,pyx,sp,liq

IPOSL = L. 6 E 3 Fe,pyx,ol,sil,liq

OPSML = L. 6 E 3 ol,pyx,sil,sp,liq

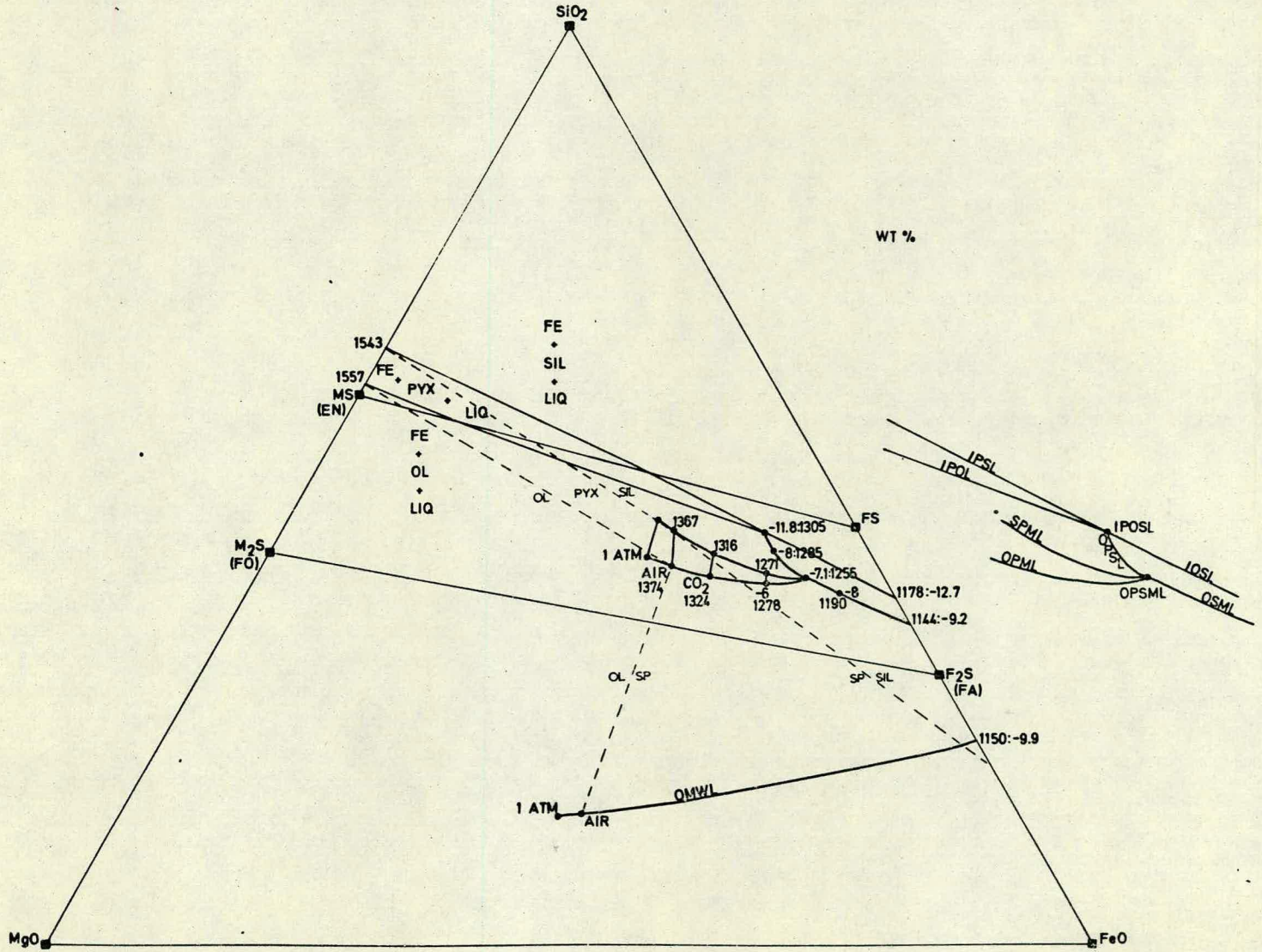
SiO2
WT %
1543
1557
MS
(EN)
FE
PYX
LIQ
FE
SIL
LIQ
FE
OL
LIQ
OL
PYX
SIL
1367
1316
1271
1374
1324
1278
1190
1 ATM
AIR
CO2
-11.8:1305
-8:1285
-7.1:1255
-6
-8
1178:-12.7
1144:-9.2
FS
M2S
(FO)
F2S
(FA)
OL
SP
SP
SIL
1150:-9.9
1 ATM
AIR
QMWL
IPSL
IPOL
SPML
OPSL
IPOSL
IQSL
OPML
OPSML
QSML
MgO
FeO

Fig 6.2

Figures 6.3 to 6.4

The liquidus phase diagrams for compositions in the join $MgO-SiO_2-FeO$ at the pO_2 of the Ni/NiO and Fe/FeO equilibria, drawn from the multi-pO_2 plot presented as figure 6.2. Each diagram is in effect an oxygen projection since at both these pO_2 conditions some Fe_2O_3 will be present in the compositions.

The Ni/NiO diagram intersects L. 6 E 3 ol,pyx,sil, sp,liq (OPSML).

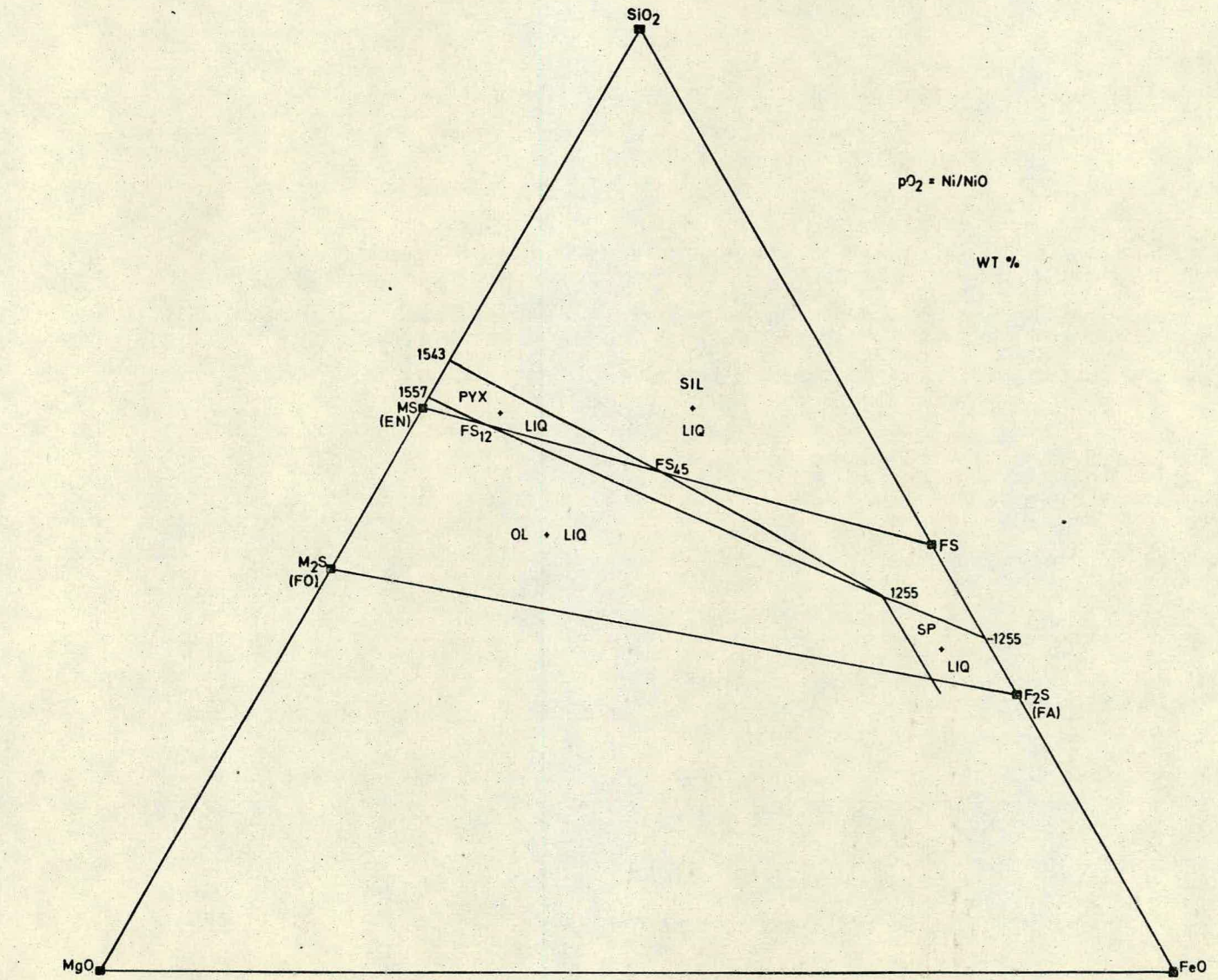
SiO2
pO2 = Ni/NiO
WT %
1543
1557
MS
(EN)
PYX
LIQ
FS12
SIL
LIQ
FS45
OL + LIQ
FS
M2S
(FO)
1255
SP
LIQ
1255
F2S
(FA)
MgO
FeO

Fig 6.3

Figure 6.4

See figure 6.3

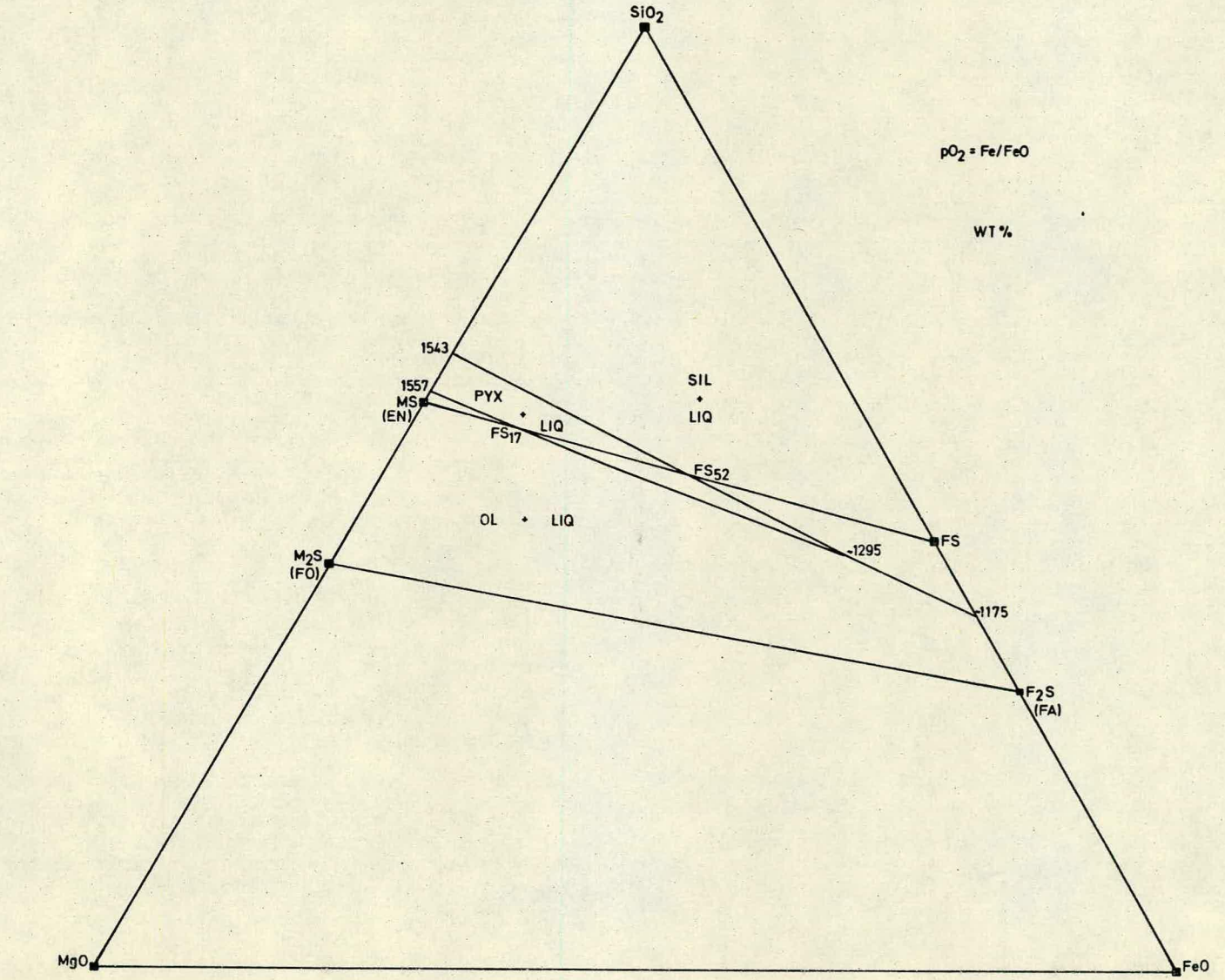
SiO2
pO2 = Fe/FeO
WT %
1543
1557
MS
(EN)
PYX
LIQ
FS17
SIL
LIQ
FS52
OL
LIQ
FS
1295
1175
M2S
(FO)
F2S
(FA)
MgO
FeO

Fig 6.4

Figure 6.5

Composition versus pO_2 plot for the join En-FS, to show the change in liquidus phase with changing pO_2, drawn from figure 6.2. The reference curves for the pO_2 of the Ni/NiO and Fe/FeO equilibria are also shown. The thin dashed lines are the liquidus temperature contours, the thick solid lines the phase equilibrium boundaries.

Abbreviations used for the equilibria are

OIL = L. 6 E 5 ol,Fe,liq

OPL = L. 6 E 5 ol,pyx,liq

PIL = L. 6 E 5 pyx,Fe,liq

PSL = L. 6 E 5 pyx,sil,liq

SIL = L. 6 E 5 sil,Fe,liq

OPIL = L. 6 E 4 ol,pyx,Fe,liq

SPIL = L. 6 E 4 sil,pyx,Fe,liq

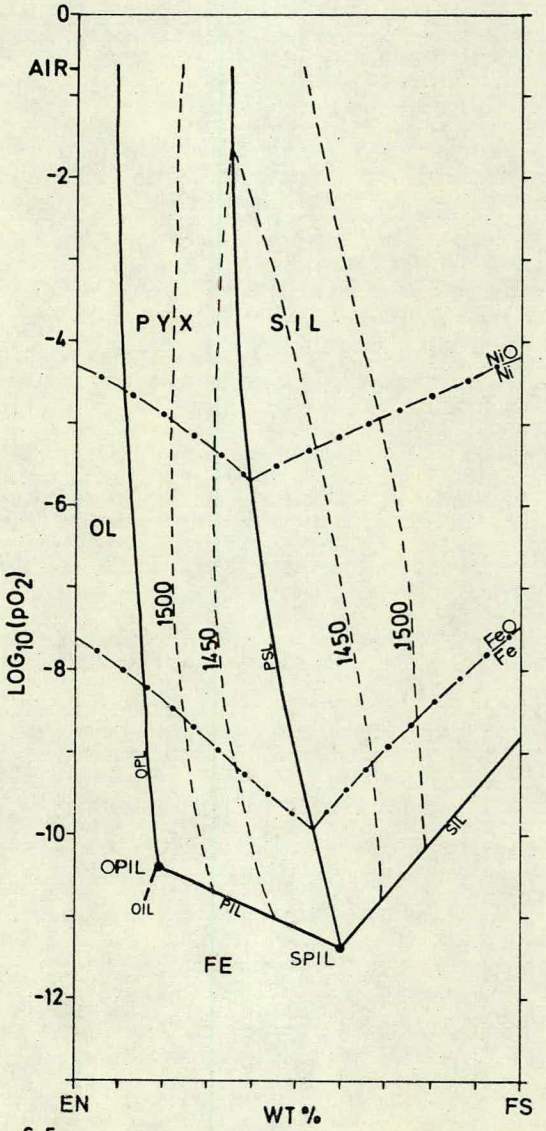
0
AIR
-2
-4
-6
-8
-10
-12
PYX
SIL
OL
1500
1450
PSL
1450
1500
Ni/NiO
Fe3O4/Fe
OPL
OPIL
OIL
PIL
FE
SPIL
SIL
LOG10(pO2)
EN
WT %
FS

Fig 6.5

Figure 6.6

The join CMS_2-M_2S-S-Fe_3O_4 at the CO_2/H_2 mixing ratio = 50, reinterpreted from Nafziger (1970). The phase equilibrium boundaries are shown as light lines on the faces of the tetrahedron, the front face shown to the left of the diagram. Within the volume, the phase boundaries are shown by thick dashed lines, the dotted lines represent some of these equilibria outside the volume shown, but within the larger C-M-S-Fe_3O_4 volume. A detailed explanation of the figure is given in the text. All equilibria have liquid present (L).

Abbreviations used are

O = Ol; D = cpx; M = sp; P = pyx; S = sil;
W = Wustite.

ODM = L. 6 E 4 ol,cpx,sp,liq
ODP = L. 6 E 4 ol,cpx,pyx,liq
OMW = L. 6 E 4 ol,sp,wu,liq
OPM = L. 6 E 4 ol,pyx,sp,liq
OPS = L. 6 E 4 ol,pyx,sil,liq
OSD = L. 6 E 4 ol,sil,cpx,liq
OSM = L. 6 E 4 ol,sil,sp,liq
SDM = L. 6 E 4 sil,cpx,sp,liq
SDP = L. 6 E 4 sil,cpx,pyx,liq
SPM = L. 6 E 4 sil,pyx,sp,liq
OSDM = L. 6 E 3 ol,sil,cpx,sp,liq
SOPD = L. 6 E 3 sil,ol,pyx,cpx,liq
SOPM = L. 6 E 3 sil,ol,pyx,sp,liq

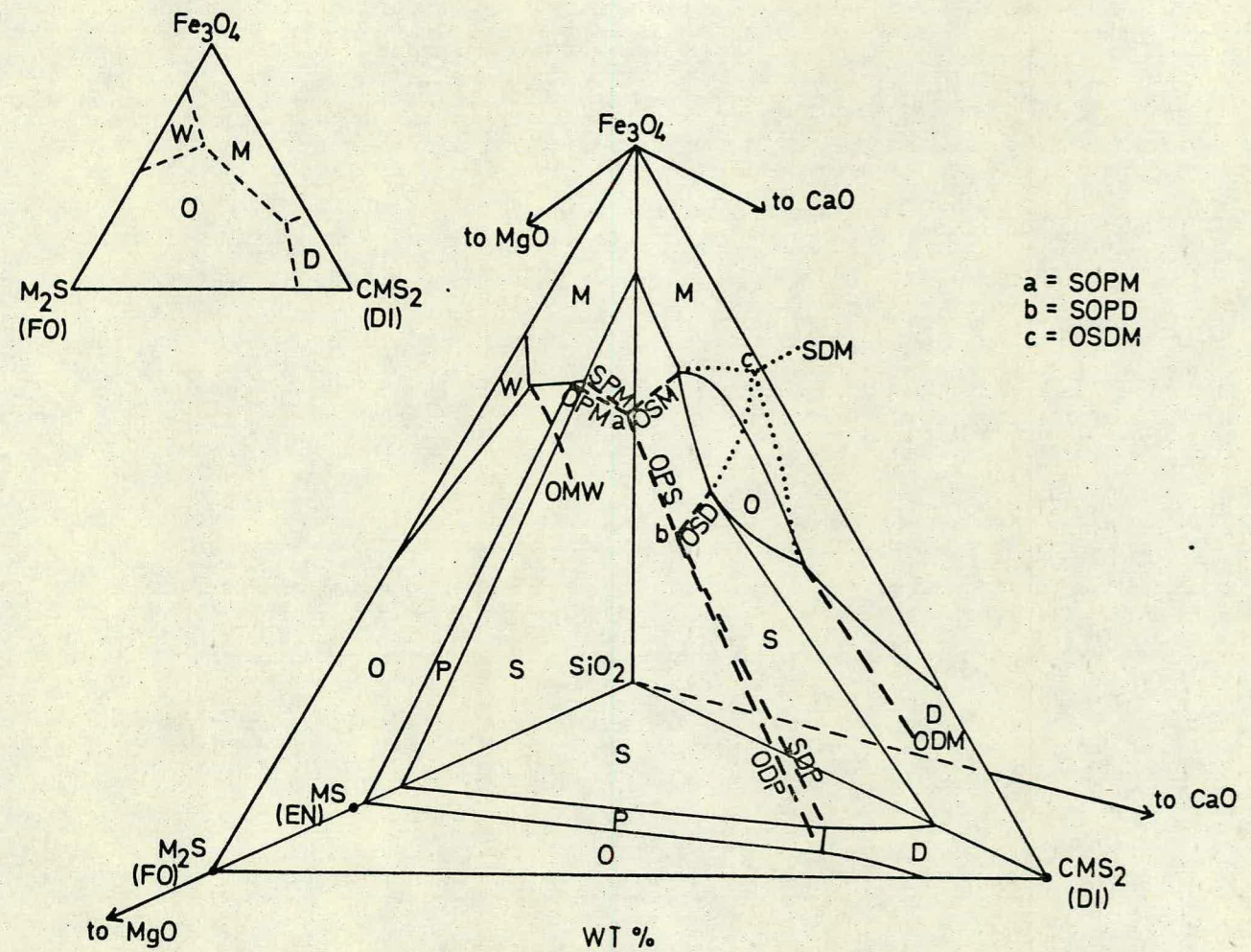
Fe3O4
W
M
O
D
M2S
(FO)
CMS2
(DI)
Fe3O4
to MgO
to CaO
a = SOPM
b = SOPD
c = OSDM
M
M
SDM
C
W
SPM
OPM
OSM
OMW
OPS
b
OSD
O
S
O
P
S
SiO2
D
ODM
S
SPP
OPP
to CaO
MS
(EN)
P
M2S
(FO)
O
D
CMS2
(DI)
to MgO
WT %

Fig 6.6

Figure 6.7

PO_2 versus temperature plot of some of the equilibria in the join $XO.YO.2ZO_2$-YO-ZO_2 (Diopside-M-S), reinterpreted from the data of Presnall (1966) and Nafziger (1970), showing SOPDML (L. 6 E 2 sil,ol,pyx,cpx,sp,liq) to occur at a more oxidising pO_2 than that of the Ni/NiO equilibria and the CO_2/H_2 constant mixing ratio of 50. The actual pO_2:temperature locations of the equilibria are unknown, except for part of OPSML (L. 6 E 3 ol,pyx,sil,sp,liq) and SODML (L. 6 E 3 sil,ol,cpx,sp,liq).

Abbreviations used for the equilibria are

OPDML = L. 6 E 3 ol,pyx,cpx,sp,liq

OPSML = L. 6 E 3 ol,pyx,sil,sp,liq

SODML = L. 6 E 3 sil,ol,cpx,sp,liq

SODPL = L. 6 E 3 sil,ol,cpx,pyx,liq

SPDML = L. 6 E 3 sil,pyx,cpx,sp,liq

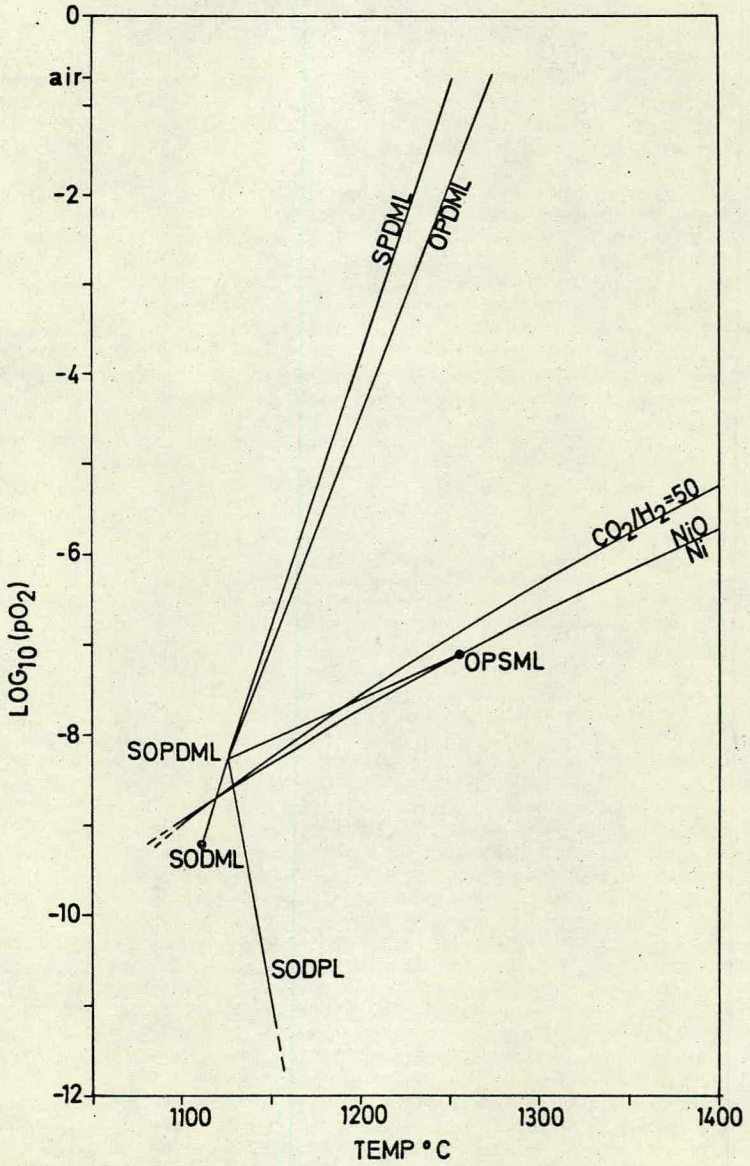
0
air
-2
-4
-6
-8
-10
-12
LOG10 (pO2)
SPDML
OPDML
CO2/H2=50
NiO
Ni
OPSML
SOPDML
SODML
SODPL
1100
1200
1300
1400
TEMP °C

Fig 6.7

Figure 6.8

Multi-Fe/Mg ratio plot of the join XO-YO-ZO_2 (C-M-S) at the pO_2 at which Fe metal is just present. Data from Muan and Osborn (1965), Ricker (reported in Muan and Osborn (1965)) and from figure 6.2, were used to construct this figure. The intersection of L. 6 E 3 sil,cpx,woll,Fe,liq (SDWIL) with the pyroxene quadrilateral at these pO_2 is shown to be most unlikely, and contradicts that estimated by Yoder, Tilley and Schairer (1963) at these pO_2. Values in parentheses are 100 x FeO/(FeO+MgO) (wt%), and the arrows indicate the direction of increasing Fe/Mg content in L. 6 E 3. The locations of the L. 6 E 2 are all tentative, except for SDWOIL (L. 6 E 2 sil,cpx,woll,ol,Fe,liq) from Ricker.

Abbreviations used for the equilibria are

DWOIL = L. 6 E 3 cpx,woll,ol,Fe,liq

OPDIL = L. 6 E 3 ol,pyx,cpx,Fe,liq

OSPIL = L. 6 E 3 ol,sil,pyx,Fe,liq

SDOIL = L. 6 E 3 sil,cpx,ol,Fe,liq

SDPIL = L. 6 E 3 sil,cpx,pyx,Fe,liq

SDWIL = L. 6 E 3 sil,cpx,woll,Fe,liq

SOWIL = L. 6 E 3 sil,ol,woll,Fe,liq

SDWOIL = L. 6 E 2 sil,cpx,woll,ol,Fe,liq

SOPDIL = L. 6 E 2 sil,ol,pyx,cpx,Fe,liq

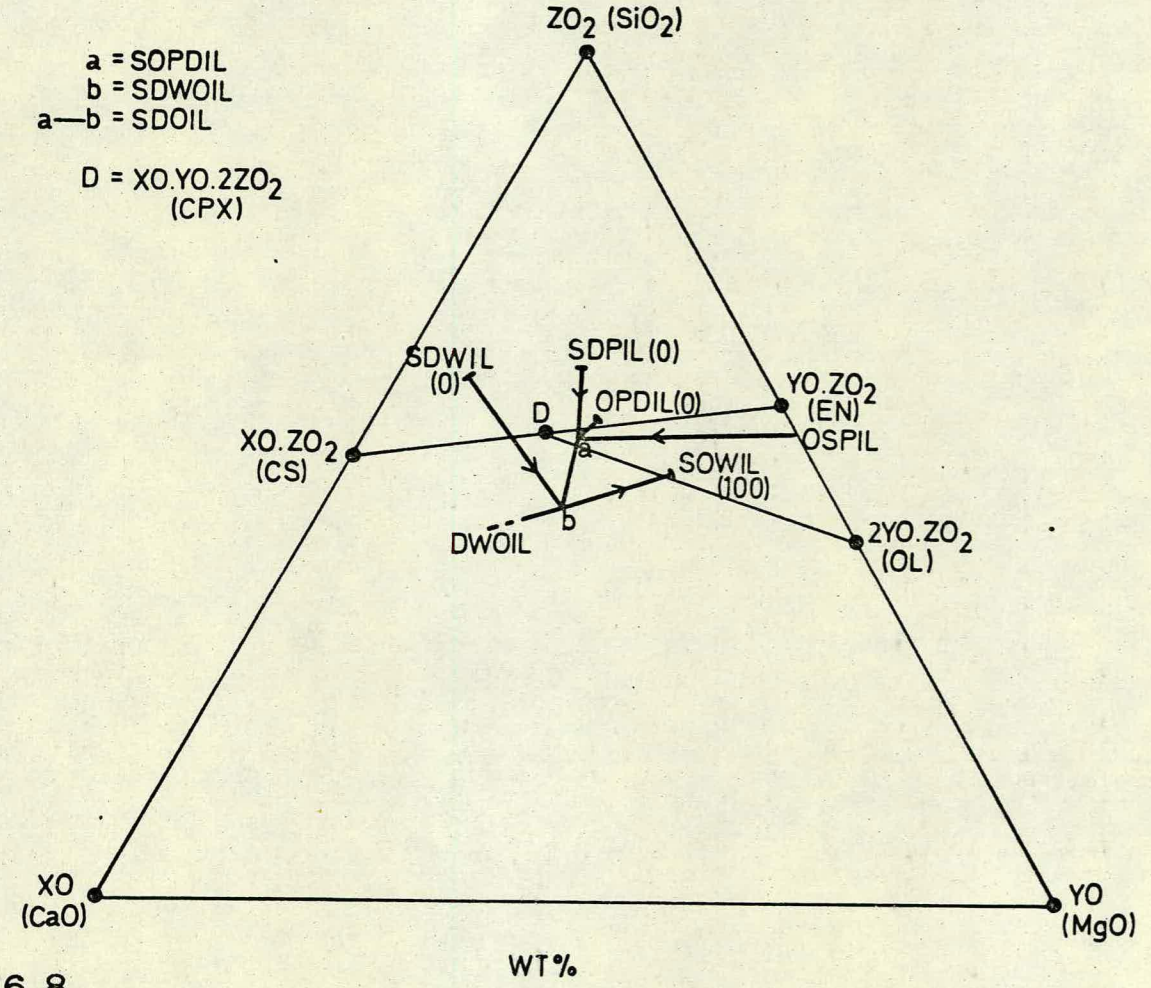
a = SOPDIL
b = SDWOIL
a—b = SDOIL
D = XO.YO.2ZO2
(CPX)
ZO2 (SiO2)
SDWIL
(0)
SDPIL (0)
OPDIL(0)
YO.ZO2
(EN)
D
XO.ZO2
(CS)
a
OSPIL
SOWIL
(100)
b
DWOIL
2YO.ZO2
(OL)
XO
(CaO)
YO
(MgO)
WT%

Fig 6.8

Figure 6.9

Multi-pO_2 plot of the anorthite saturation (projection) diagrams into part of the plane MgO-SiO_2-FeO from Roeder and Osborn (1966), all iron recalculated as FeO. The resulting diagram shows the change in projected position of some of the L. 6 E 3 which pierce this join, and the inferred projected position of L. 6 E 2 an,pyx,ol,sil,sp,liq (APOSML). The temperature and pO_2 of some of the liquids is indicated where known, from the data of Roeder and Osborn (1966).

Abbreviations used for the equilibria are

AOPSL = L. 6 E 3 an,ol,pyx,sil,liq

AOSML = L. 6 E 3 an,ol,sil,sp,liq

APOML = L. 6 E 3 an,pyx,ol,sp,liq

APSML = L. 6 E 3 an,pyx,sil,sp,liq

APOSML = L. 6 E 2 an,pyx,ol,sil,sp,liq

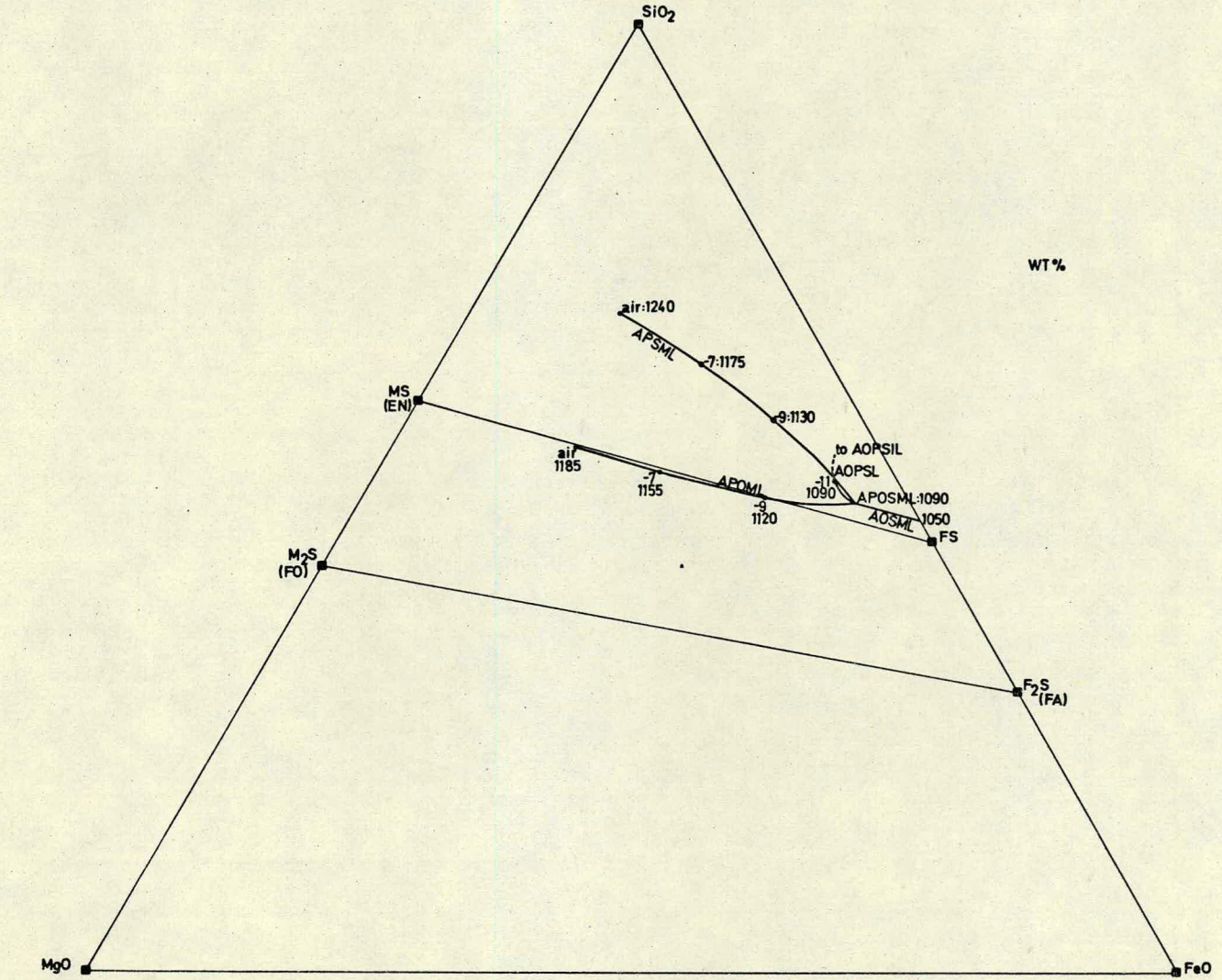
SiO2
WT%
air:1240
APSML
-7:1175
MS
(EN)
-9:1130
to AOPSIL
AOPSL
air
1185
-7
1155
APOML
-11
1090
APOSML:1090
-9
1120
AOSML
1050
FS
M2S
(FO)
F2S
(FA)
MgO
FeO

Fig 6.9

Figure 6.10

Multi-pO_2 and multi-Fe/Mg ratio plot of the join $XO.R_2O_3.2ZO_2$-YO-ZO_2 (Anorthite-M-S), showing the change in anorthite content of some of the L. 6 E 3 which pierce this join. The pO_2 and temperature of some of these liquids is indicated where known. Values for 100 x FeO/(FeO+MgO) (wt%) are indicated in parentheses taken from the multi-pO_2 plot of the anorthite saturation surface in this join (figure 6.9). The arrows on the locus of liquids of the equilibria indicate the direction of increasing FeO/FeO+MgO content.

The piercing point labelled AO p.p. is the piercing point of the join $XO.R_2O_3.2ZO_2$-$2YO.ZO_2$ (Anorthite-Olivine) in this plane.

Abbreviations used for the equilibria are

AOPML = L. 6 E 3 an,ol,pyx,sp,liq

AOPSL = L. 6 E 3 an,ol,pyx,sil,liq

AOSML = L. 6 E 3 an,ol,sil,sp,liq

APSML = L. 6 E 3 an,pyx,sil,sp,liq

APOSML = L. 6 E 2 an,pyx,ol,sil,sp,liq

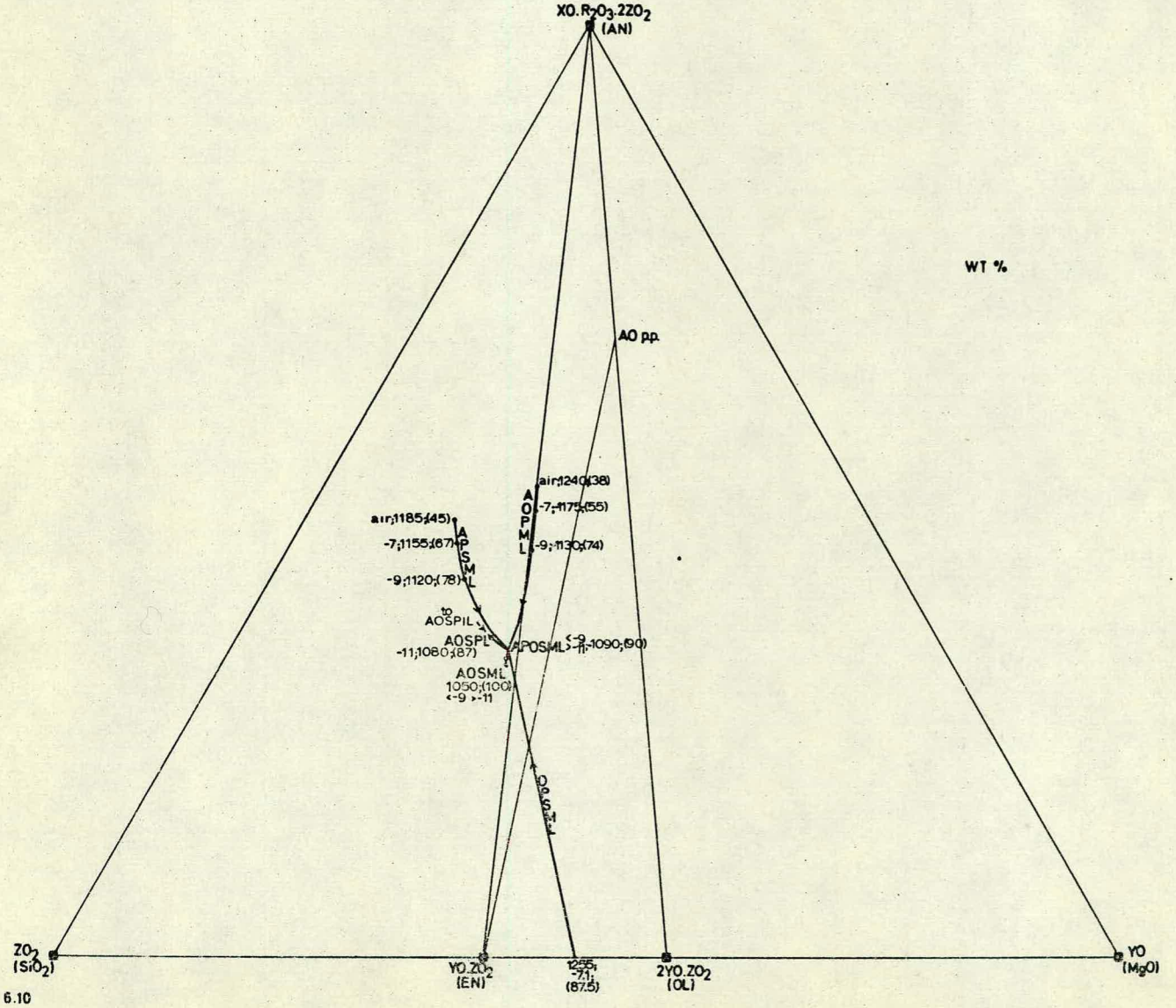
XO.R2O3.2ZO2
(AN)
WT %
AO pp.
air;1240;(38)
-7;1175;(55)
-9;1130;(74)
AOPML
air;1185;(45)
-7;1155;(67)
-9;1120;(78)
AOSPIL
to
AOSPL
-11;1080;(87)
AOSPML
-9;1090;(90)
AOSML
1050;(100)
<-9 >-11
AOSML
ZO2
(SiO2)
YO.ZO2
(EN)
1255
-7.1
(87.5)
2YO.ZO2
(OL)
YO
(MgO)

Fig 6.10

Figure 6.11

Temperature versus pO_2 plot of some of the L. 6 E 3 which pierce the join Anorthite-MgO-SiO_2-Fe-O_2, from the data of Roeder and Osborn (1966). The same equilibria are shown on figures 6.9, 6.10. The reference curves for the pO_2 of the Ni/NiO and Fe/FeO equilibria are also shown .

Abbreviations used for the equilibria are

AOSML = L. 6 E 3 an,ol,sil,sp,liq

APOML = L. 6 E 3 an,pyx,ol,sp,liq

APSML = L. 6 E 3 an,pyx,sil,sp,liq

OSPAL = L. 6 E 3 ol,sil,pyx,an,liq

OSPML = L. 6 E 3 ol,sil,pyx,sp,liq

AOSPIL = L. 6 E 2 an,ol,sil,pyx,Fe,liq

APOSML = L. 6 E 2 an,pyx,ol,sil,sp,liq

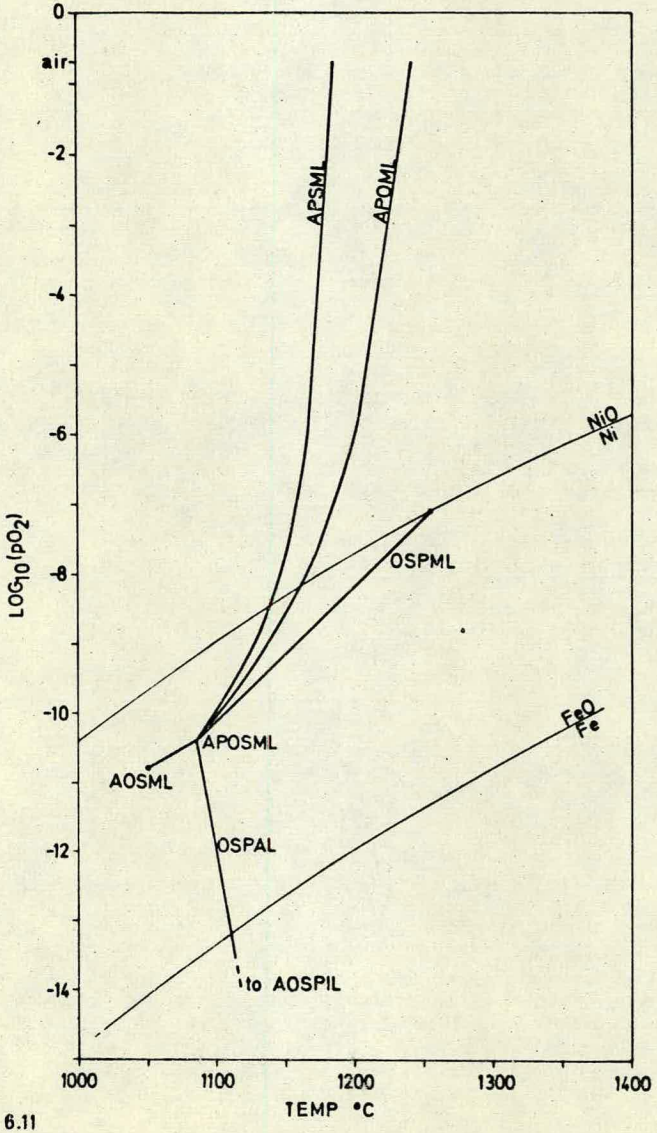
0
air
-2
-4
-6
-8
-10
-12
-14
$LOG_{10}(pO_2)$
APSML
APOML
NiO
Ni
OSPML
APOSML
AOSML
OSPAL
to AOSPIL
FeO
Fe
1000
1100
1200
1300
1400
TEMP °C

Fig 6.11

Figures 6.12 to 6.13

Anorthite saturation (projection) diagrams into part of the plane $MgO-SiO_2-FeO$, at the pO_2 of the Ni/NiO and Fe/FeO equilibria, drawn from the multi-pO_2 plot presented as figure 6.9. The phase boundaries are shown by thick solid lines.

Abbreviations used for the equilibria are

APOML = L. 6 E 3 an,pyx,ol,sp,liq

APOSL = L. 6 E 3 an,pyx,ol,sil,liq

APSML = L. 6 E 3 an,pyx,sil,sp,liq

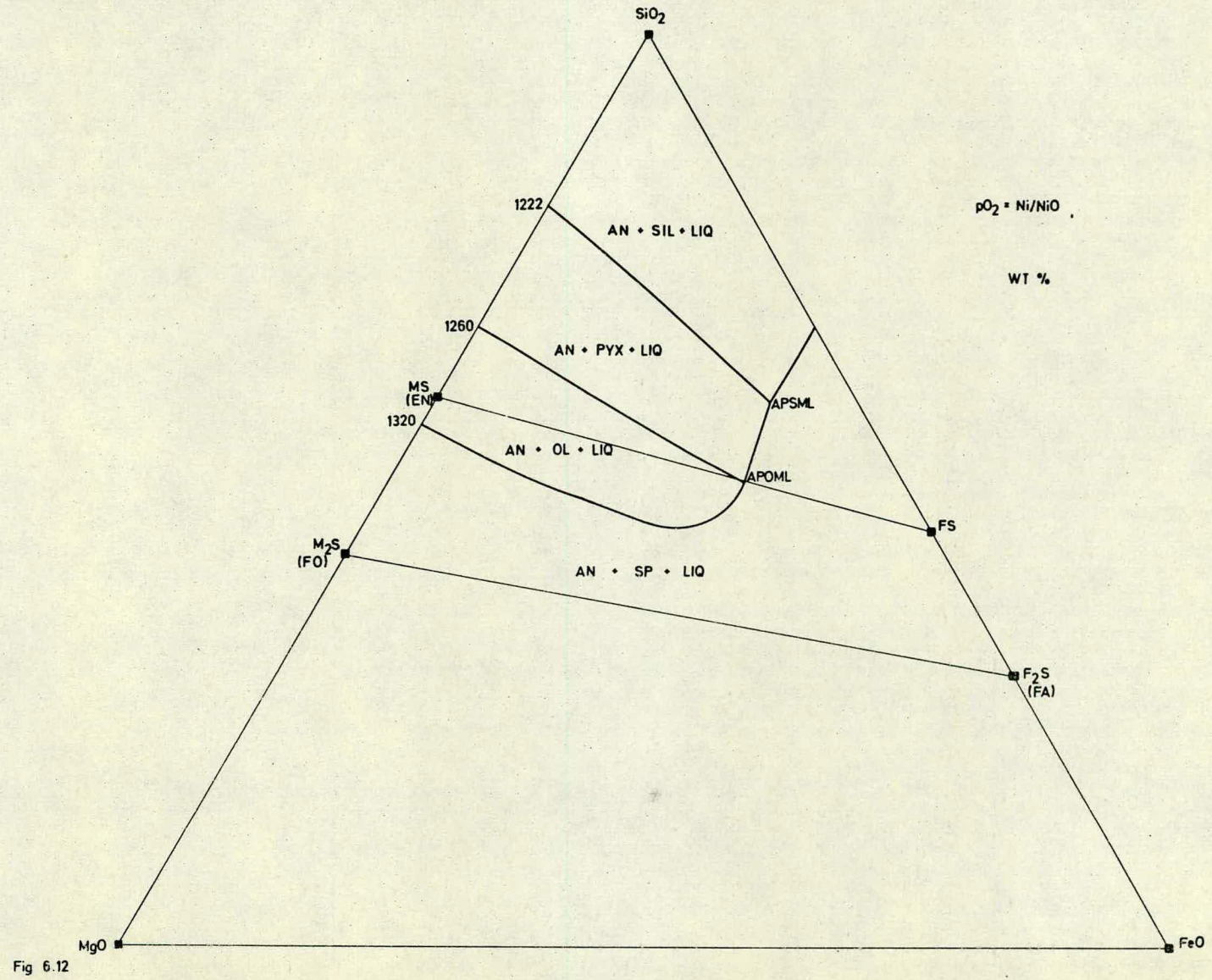
SiO2
1222
AN + SIL + LIQ
pO2 = Ni/NiO
WT %
1260
AN + PYX + LIQ
MS
(EN)
APSML
1320
AN + OL + LIQ
APOML
FS
M2S
(FO)
AN + SP + LIQ
F2S
(FA)
MgO
FeO

Fig 6.12

Figure 6.13

See figure 6.12

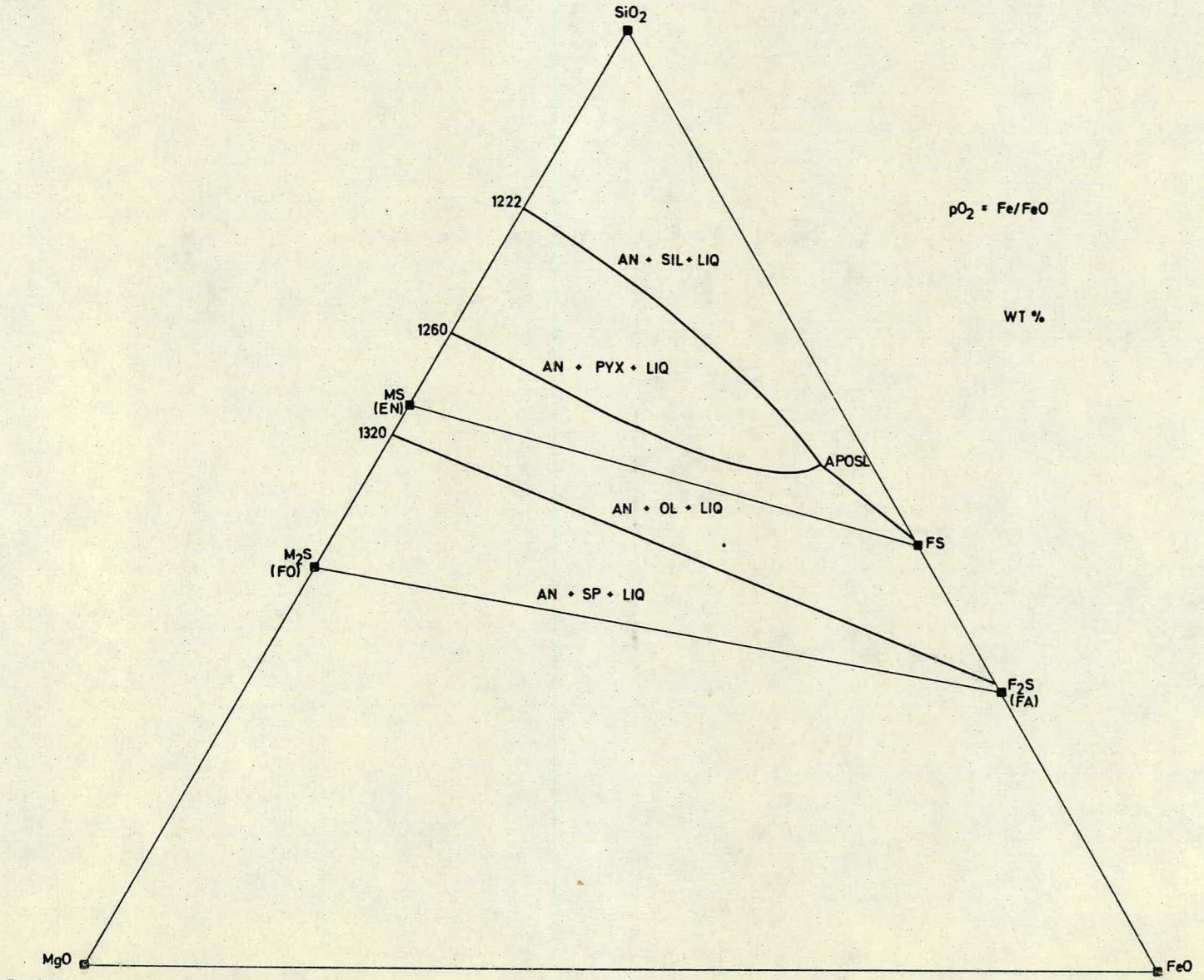
SiO2
1222
AN + SIL + LIQ
pO2 = Fe/FeO
WT %
1260
AN + PYX + LIQ
MS
(EN)
1320
APOSL
AN + OL + LIQ
FS
M2S
(FO)
AN + SP + LIQ
F2S
(FA)
MgO
FeO

Fig 6.13

Figures 6.14 to 6.15

Multi-Fe/Mg ratio plot of the join $XO.R_2O_3.2ZO_2$-YO-ZO_2 (Anorthite-M-S) at the pO_2 of the Ni/NiO and Fe/FeO equilibria, drawn using the multi-pO_2 plot for this join (figure 6.10), and the anorthite saturation diagrams at these pO_2 (figures 6.12, 6.13). The thin solid lines are the phase boundaries in the iron-free system (labelled 0), and the MgO-free system (labelled 100), the latter being only approximate locations. The intermediate phase boundaries are indicated and labelled with the value 100 x FeO/(FeO+MgO) (wt%) for which they represent. The thick solid lines are the L. 6 E 4 which pierce this join at these pO_2 and have a variable FeO/MgO ratio. The arrows indicate the direction of increasing FeO/FeO+MgO content where known.

The piercing point labelled AO p.p. is the piercing point of the join $XO.R_2O_3.2ZO_2$-$2YO.ZO_2$ (Anorthite-olivine) in this plane.

Abbreviations used for the equilibria are

AOL = L. 6 E 5 an,ol,liq
AML = L. 6 E 5 an,sp,liq
APL = L. 6 E 5 an,pyx,liq
ASL = L. 6 E 5 an,sil,liq
OML = L. 6 E 5 ol,sp,liq
OPL = L. 6 E 5 ol,pyx,liq
OSL = L. 6 E 5 ol,sil,liq
SPL = L.6 E 5 sil,pyx,liq
AOML = L. 6 E 4 an,ol,sp,liq
AOPL = L. 6 E 4 an,ol,pyx,liq
AOSL = L. 6 E 4 an,ol,sil,liq
APML = L. 6 E 4 an,pyx,sp,liq
ASML = L. 6 E 4 an,sil,sp,liq
ASPL = L. 6 E 4 an,sil,pyx,liq
OPML = L. 6 E 4 ol,pyx,sp,liq
SOPL = L. 6 E 4 sil,ol,pyx,liq
SPML = L. 6 E 4 sil,pyx,sp,liq
AOMPL = L. 6 E 3 an,ol,sp,pyx,liq
AOPSL = L. 6 E 3 an,ol,pyx,sil,liq
ASPML = L. 6 E 3 an,sil,pyx,sp,liq
OSPML = L. 6 E 3 ol,sil,pyx,sp,liq

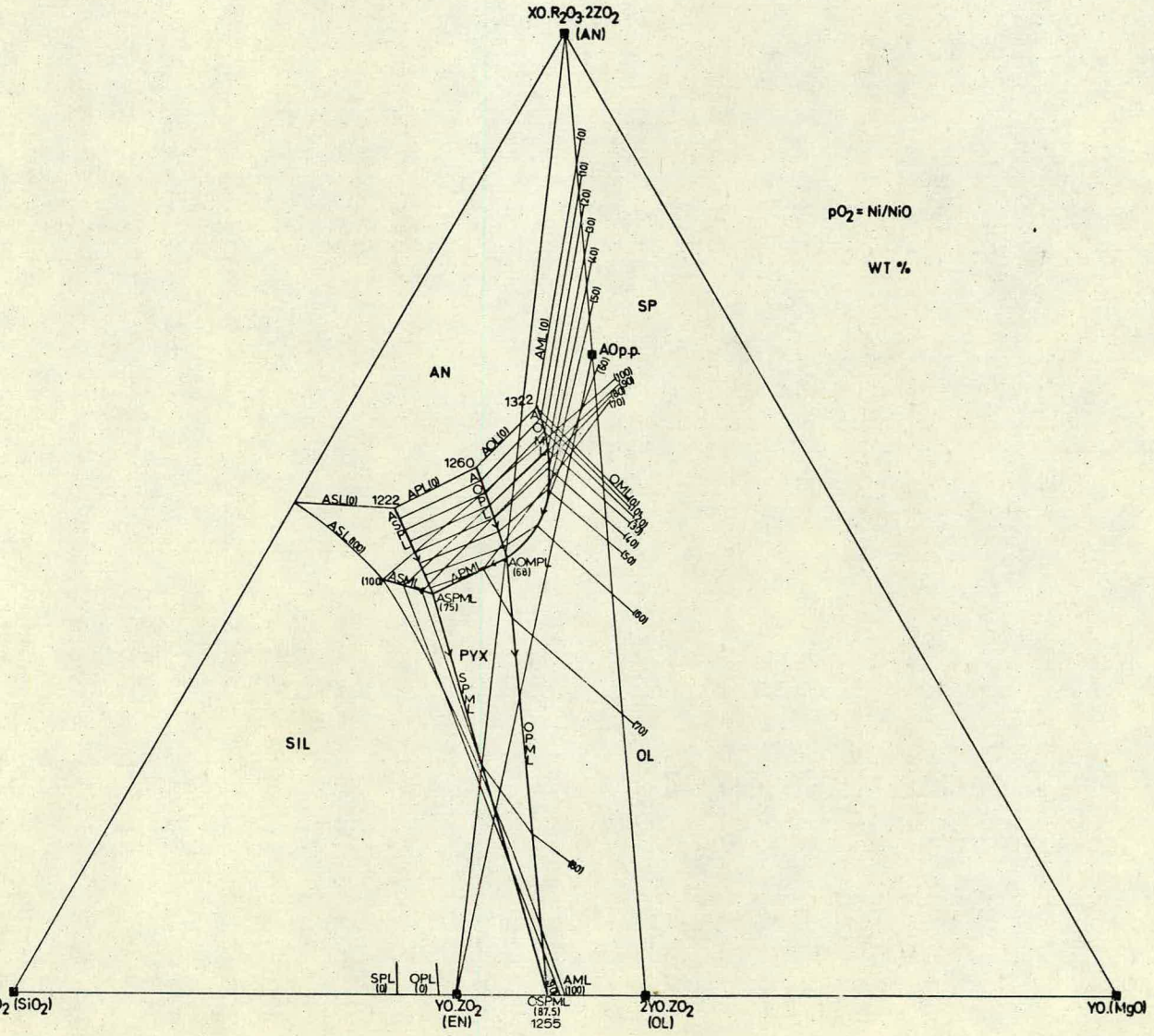
XO.R2O3.2ZO2
(AN)
pO2 = Ni/NiO
WT %
SP
AN
AOp.p.
(70)
1322
1260
1222
ASL(0)
ASL(100)
(100)
AOPL
AOML
APL(0)
AOL(0)
AML(0)
QML(0)
(10)
(20)
(30)
(40)
(50)
(60)
(70)
ASL
APL
AOML
AOPL
AOMPL
(68)
ASPML
(75)
PYX
SPML
OPL
SIL
OL
(80)
(90)
SPL
(0)
OPL
(0)
AML
(100)
CSPML
(87.5)
1255
ZO2 (SiO2)
YO.ZO2
(EN)
2YO.ZO2
(OL)
YO.(MgO)

Fig 6.14

Figure 6.15

See figure 6.14

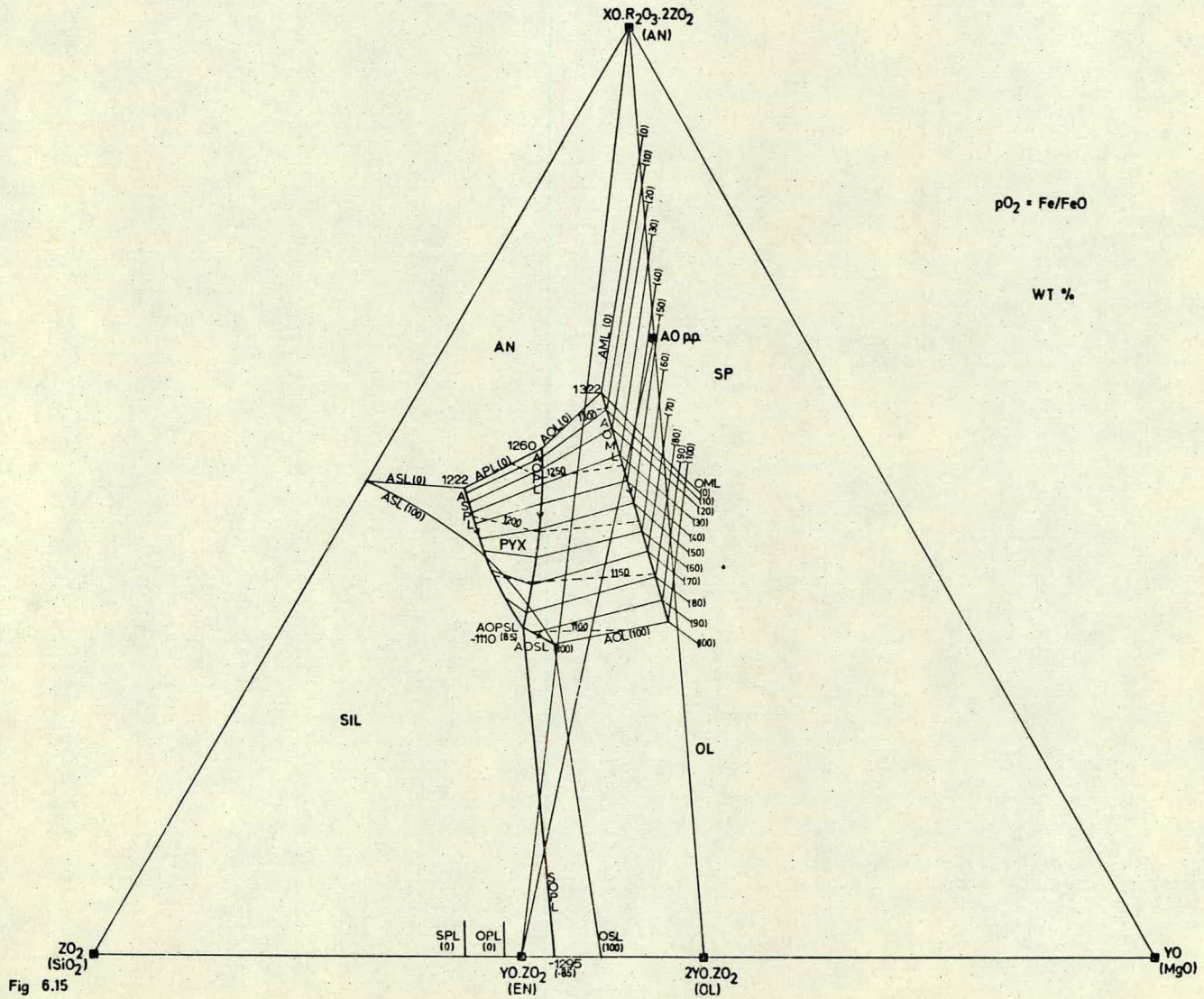
XO.R2O3.2ZO2
(AN)
pO2 = Fe/FeO
WT %
AN
AO pp
SP
PYX
SIL
OL
ASL(0)
ASL(100)
APL(0)
AOL(0)
AOL(100)
AML(0)
OML
AOPSL
-1110 (85)
ADSL
1322
1260
1222
1250
1200
1150
1100
SPL
(0)
OPL
(0)
OSL
(100)
-1295
(85)
ZO2
(SiO2)
YO.ZO2
(EN)
2YO.ZO2
(OL)
YO
(MgO)

Fig 6.15

Figures 6.16 to 6.17

Liquidus diagrams for the join $YO.ZO_2$-$XO.R_2O_3$. $2ZO_2$:$2YO.ZO_2$ (Enstatite-AnorthiteForsterite) piercing point in the plane $XO.ZO_2$-$YO.ZO_2$-R_2O_3 (CS-MS-A) versus FeO/MgO ratio, at the pO_2 of the Ni/NiO and Fe/FeO equilibria. The diagrams are constructed from the multi-Fe/Mg ratio plots of the join $XO.R_2O_3.2ZO_2$-YO-ZO_2 (Anorthite-M-S) presented as figures 6.14, 6.15, and are used in the construction of the liquidus diagrams for the plane $XO.ZO_2$-$YO.ZO_2$-R_2O_3 (CS-MS-A) (figures 6.44-6.48 and 6.86-6.90). The thin dashed lines are the temperature contours where known.

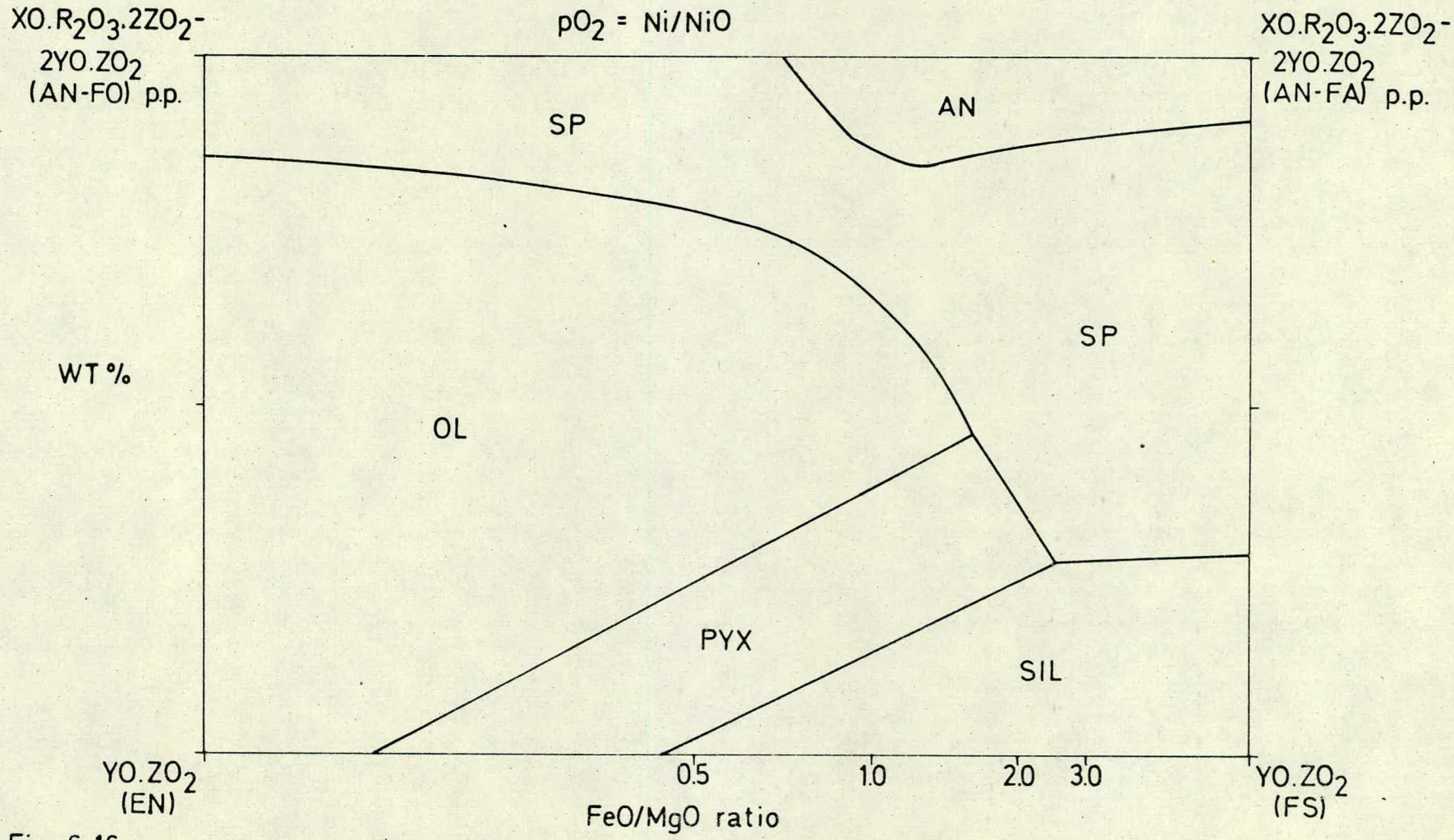
XO.R2O3.2ZO2-
2YO.ZO2
(AN-FO) p.p.
pO2 = Ni/NiO
XO.R2O3.2ZO2-
2YO.ZO2
(AN-FA) p.p.
SP
AN
SP
WT %
OL
PYX
SIL
YO.ZO2
(EN)
0.5
1.0
2.0
3.0
YO.ZO2
(FS)
FeO/MgO ratio

Fig 6.16

Figure 6.17

See figure 6.16

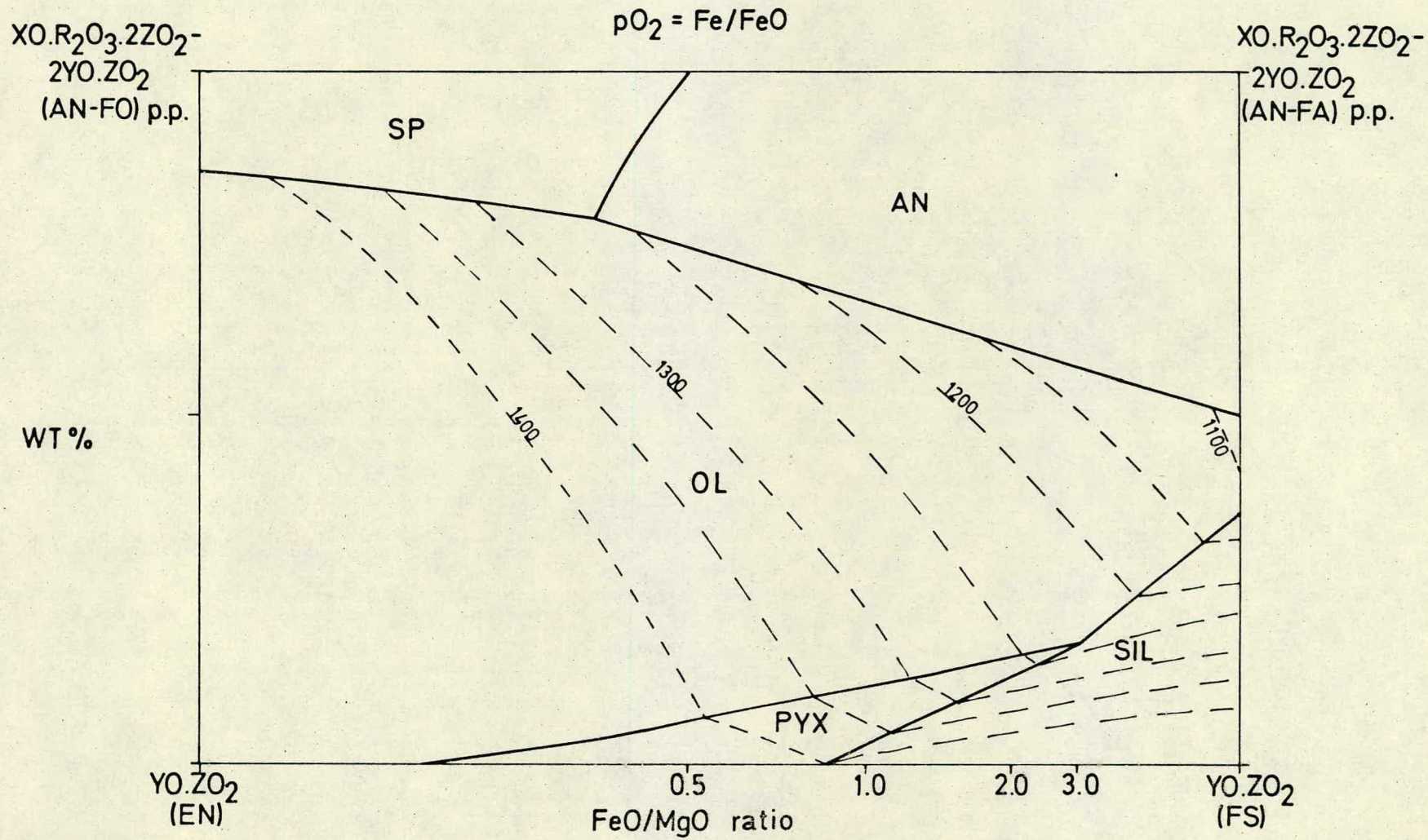
pO_2 = Fe/FeO
$XO.R_2O_3.2ZO_2$-
$2YO.ZO_2$
(AN-FO) p.p.
$XO.R_2O_3.2ZO_2$-
$2YO.ZO_2$
(AN-FA) p.p.
SP
AN
1300
1200
1400
1100
OL
SIL
PYX
WT %
$YO.ZO_2$
(EN)
0.5
1.0
2.0
3.0
$YO.ZO_2$
(FS)
FeO/MgO ratio

Fig 6.17

Figures 6.18 to 6.19

$2YO.ZO_2$ (olivine) projection diagrams into the join $YO.ZO_2$-$XO.R_2O_3.2ZO_2$:$2YO.ZO_2$ (Enstatite-AnorthiteForsterite) piercing point in the plane $XO.ZO_2$-$YO.ZO_2$-R_2O_3 (CS-MS-A) versus FeO/MgO ratio, at the pO_2 of the Ni/NiO and Fe/FeO equilibria. The projection boundaries are shown by solid lines for compositions lying in this join having an olivine liquidus. The boundaries are extended beyond the olivine liquidus boundaries in this join, to show the bounding surface of the olivine volume over a wider area, the bounding surface there being more olivine-rich than the compositions in this plane.

The dashed lines (figure 6.19) are the olivine projection boundaries assuming no olivine crystallisation, and occur at higher FeO/MgO ratios. The dotted line on figure 6.19 encloses the area of liquids containing olivine which are silica saturated.

Abbreviations used for the equilibria are

OAML = L. 6 E 4 ol,an,sp,liq

OAPL = L. 6 E 4 ol,an,pyx,liq

OASL = L. 6 E 4 ol,an,sil,liq

OPML = L. 6 E 4 ol,pyx,sp,liq

OPSL = L. 6 E 4 ol,pyx,sil,liq

OAPML = L. 6 E 3 ol,an,pyx,sp,liq

OAPSL = L. 6 E 3 ol,an,pyx,sil,liq

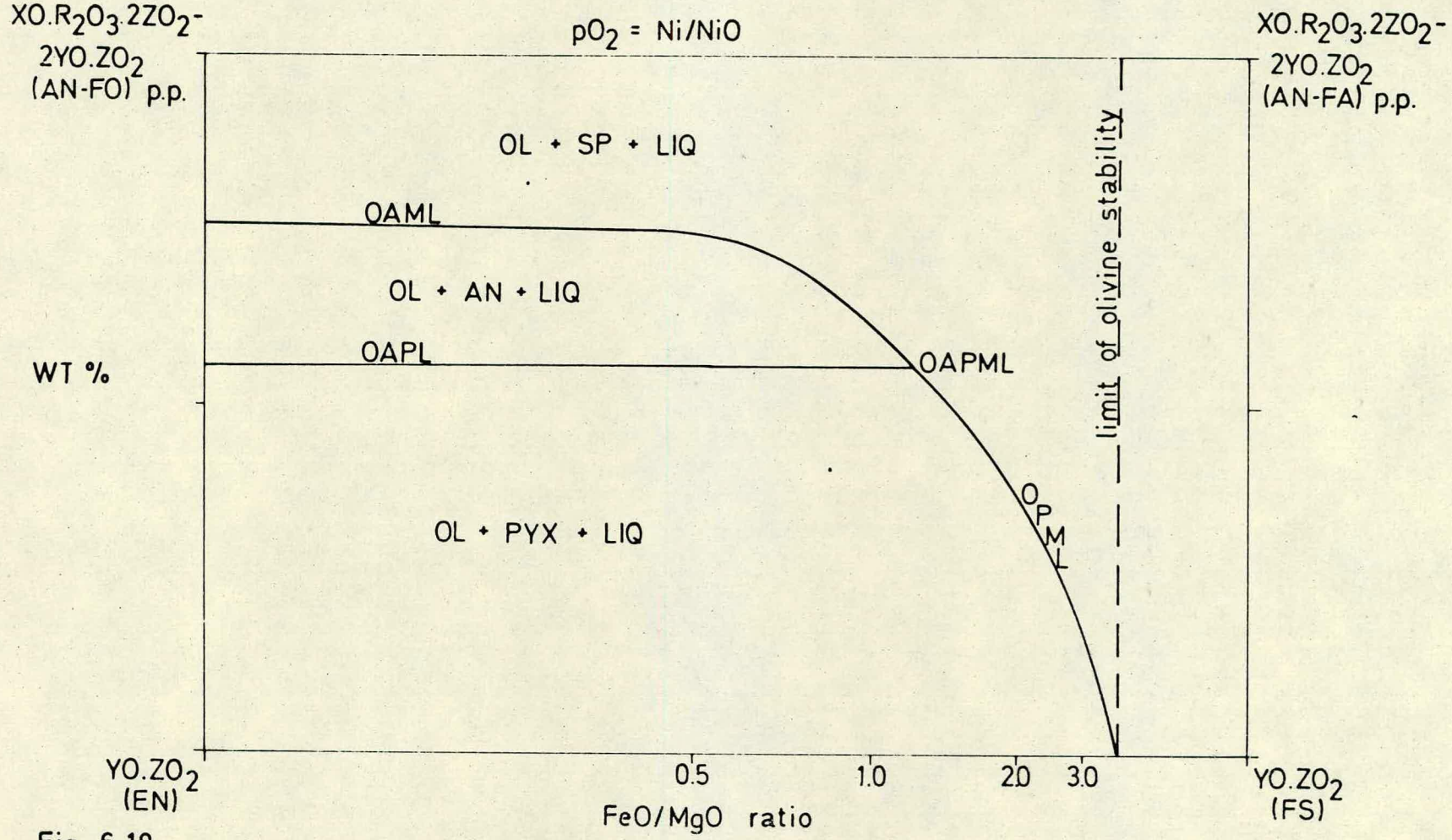
XO.R2O3.2ZO2-
2YO.ZO2
(AN-FO) p.p.
pO2 = Ni/NiO
XO.R2O3.2ZO2-
2YO.ZO2
(AN-FA) p.p.
OL + SP + LIQ
OAML
OL + AN + LIQ
OAPL
OAPML
OPML
limit of olivine stability
WT %
OL + PYX + LIQ
YO.ZO2
(EN)
0.5
1.0
2.0
3.0
FeO/MgO ratio
YO.ZO2
(FS)

Fig 6.18

Figure 6.19

See figure 6.18

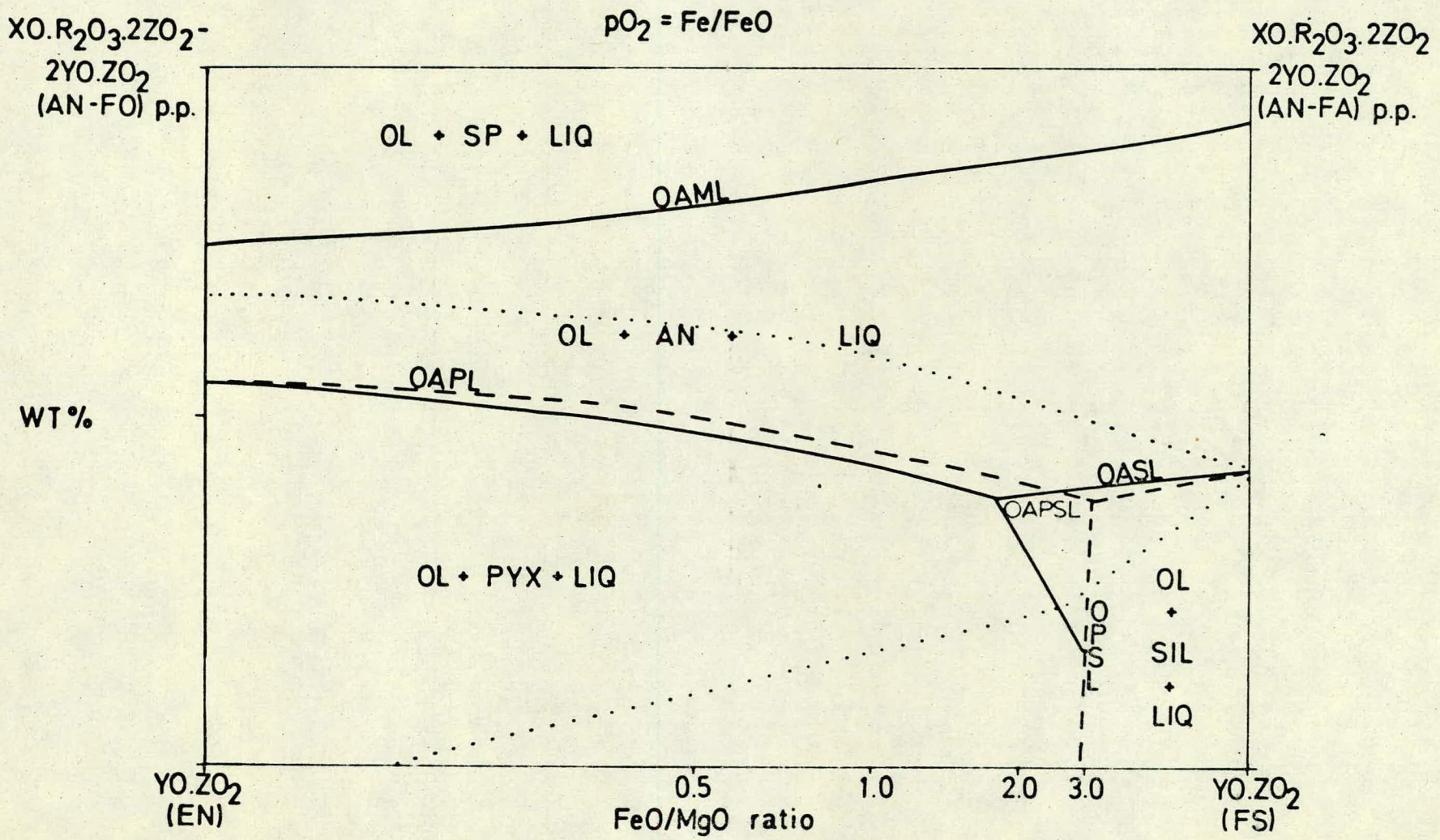
XO.R2O3.2ZO2-
2YO.ZO2
(AN-FO) p.p.
pO2 = Fe/FeO
XO.R2O3.2ZO2
2YO.ZO2
(AN-FA) p.p.
OL + SP + LIQ
OAML
OL + AN + LIQ
OAPL
WT%
OASL
OAPSL
OL + PYX + LIQ
OL
+
SIL
+
LIQ
OPSL
YO.ZO2
(EN)
0.5
1.0
2.0
3.0
YO.ZO2
(FS)
FeO/MgO ratio

Fig 6.19

Figures 6.20 to 6.22

T - X sections for part of the join $XO.YO.2ZO_2$-$YO.R_2O_3.ZO_2$ (Diopside-MAS) at FeO/MgO mole ratios of 0.18, 0.5, and 1.0, and the pO_2 of the Fe/FeO equilibrium. The experiments on each composition are shown at the appropriate temperatures by filled circles, the composition names are indicated beneath each composition studied. The phase boundaries are drawn using the combined data plots presented in figures 6.23, 6.24.

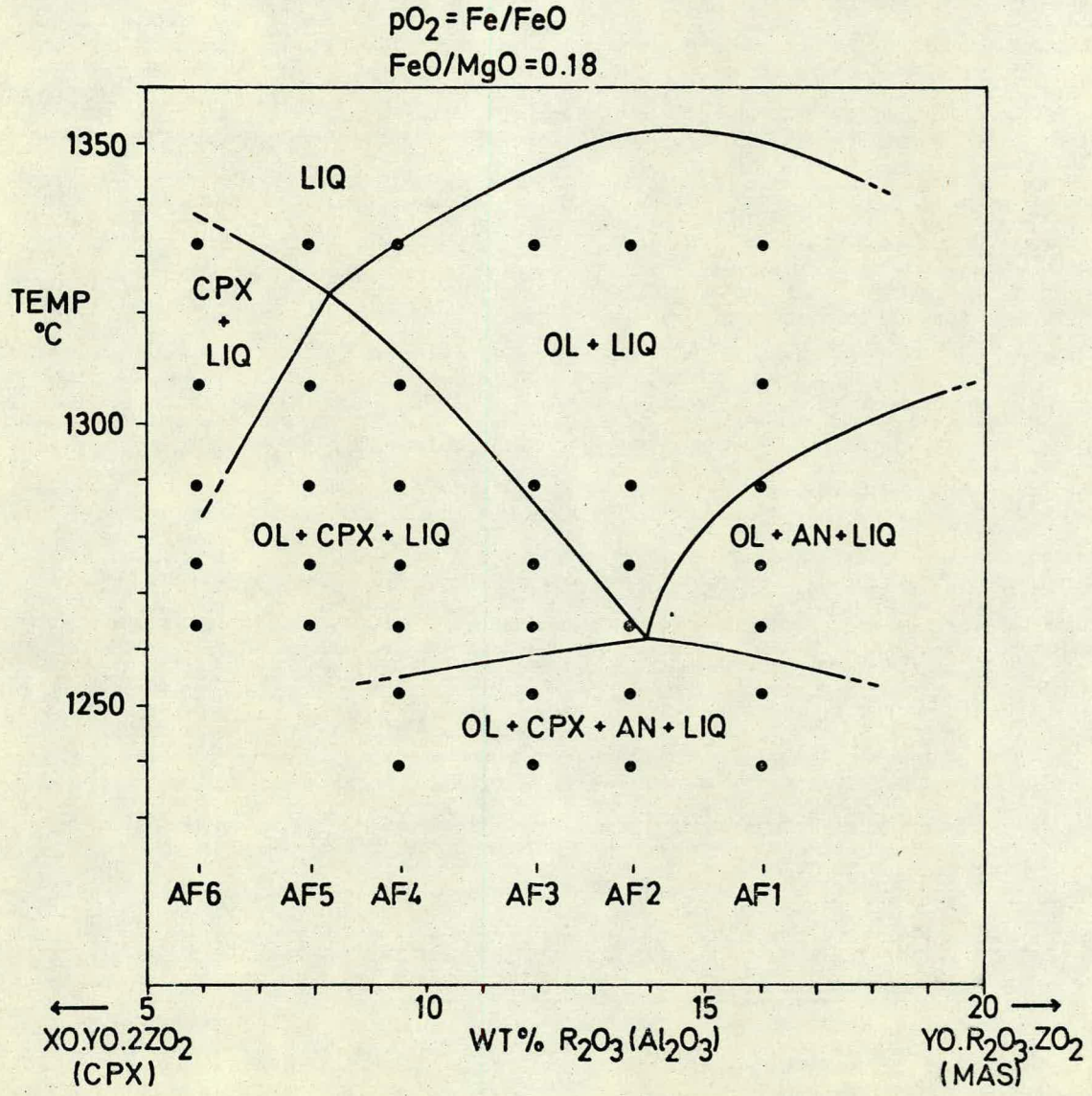
pO_2 = Fe/FeO
FeO/MgO = 0.18
1350
1300
1250
TEMP °C
LIQ
CPX + LIQ
OL + LIQ
OL + CPX + LIQ
OL + AN + LIQ
OL + CPX + AN + LIQ
AF6
AF5
AF4
AF3
AF2
AF1
5
10
15
20
XO.YO.2ZO2 (CPX)
WT% R2O3 (Al2O3)
YO.R2O3.ZO2 (MAS)

Fig 6.20

Figure 6.21

See figure 6.20

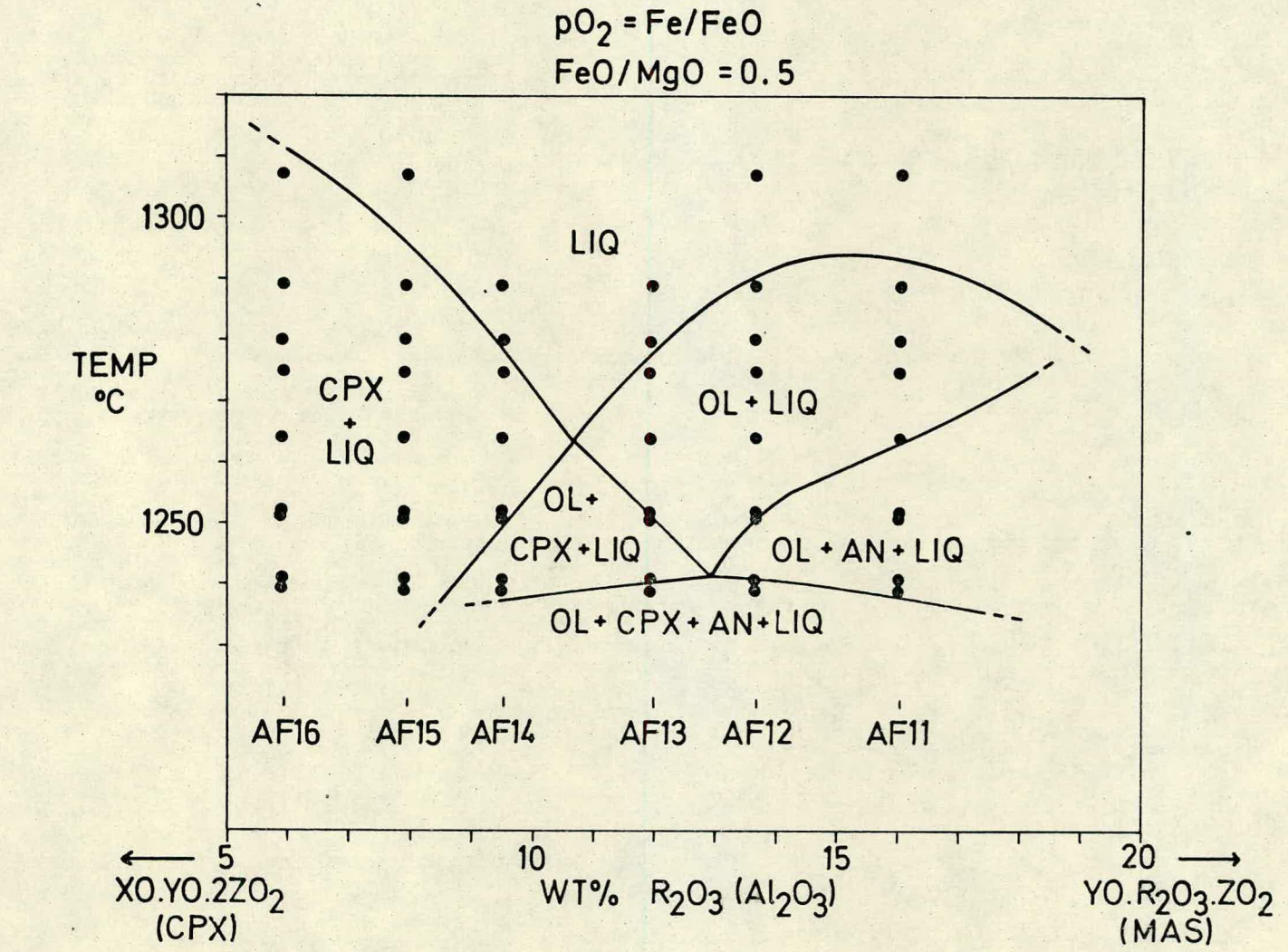
pO_2 = Fe/FeO
FeO/MgO = 0.5
1300
1250
TEMP
°C
LIQ
CPX
+
LIQ
OL + LIQ
OL +
CPX + LIQ
OL + AN + LIQ
OL + CPX + AN + LIQ
AF16
AF15
AF14
AF13
AF12
AF11
5
10
15
20
XO.YO.2ZO2
(CPX)
WT% R2O3 (Al2O3)
YO.R2O3.ZO2
(MAS)

Fig 6.21

Figure 6.22

See figure 6.20

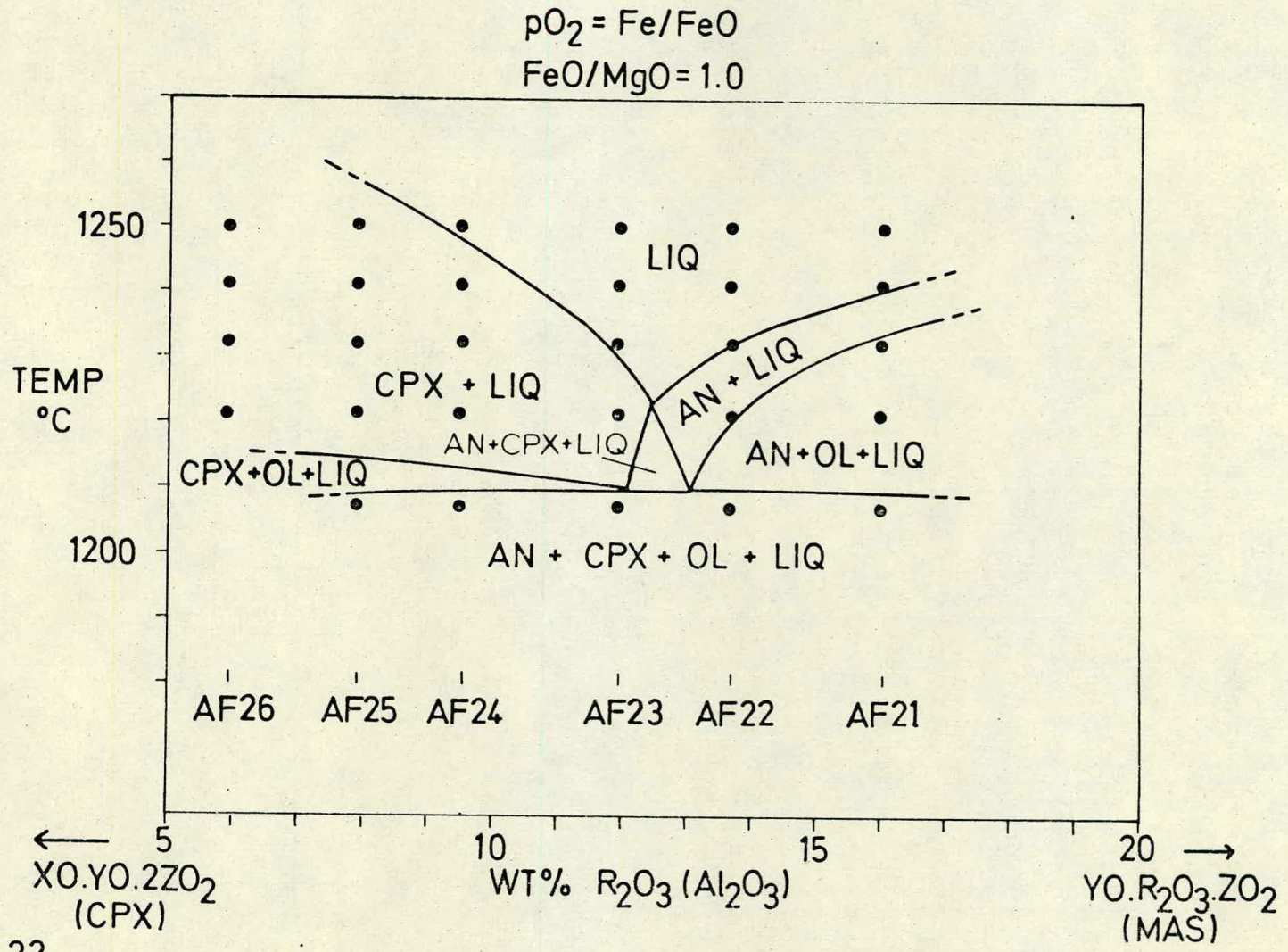
pO_2 = Fe/FeO
FeO/MgO = 1.0
1250
1200
TEMP
°C
LIQ
CPX + LIQ
AN + LIQ
AN+CPX+LIQ
CPX+OL+LIQ
AN+OL+LIQ
AN + CPX + OL + LIQ
AF26
AF25
AF24
AF23
AF22
AF21
5
10
15
20
XO.YO.2ZO2
(CPX)
WT% R2O3 (Al2O3)
YO.R2O3.ZO2
(MAS)

Fig 6.22

Figure 6.23

Liquidus diagram for part of the join $XO.YO.2ZO_2$-$YO.R_2O_3.ZO_2$ (Diopside-MAS), to show the change in liquidus phase for molecularly equivalent compositions with changing FeO/MgO ratio, at the pO_2 of the Fe/FeO equilibrium. The compositions studied are shown by filled circles, the composition name can be found by referring to the individual T - X sections for this join (figures 6.20-6.22). Compositions at other FeO/MgO ratios lie in the join Enstatite-Grossular, their names can be found by referring to the T - X sections for that join (figures 6.30-6.36). The phase boundaries are indicated by thick solid lines, the dashed lines are the temperature contours where known.

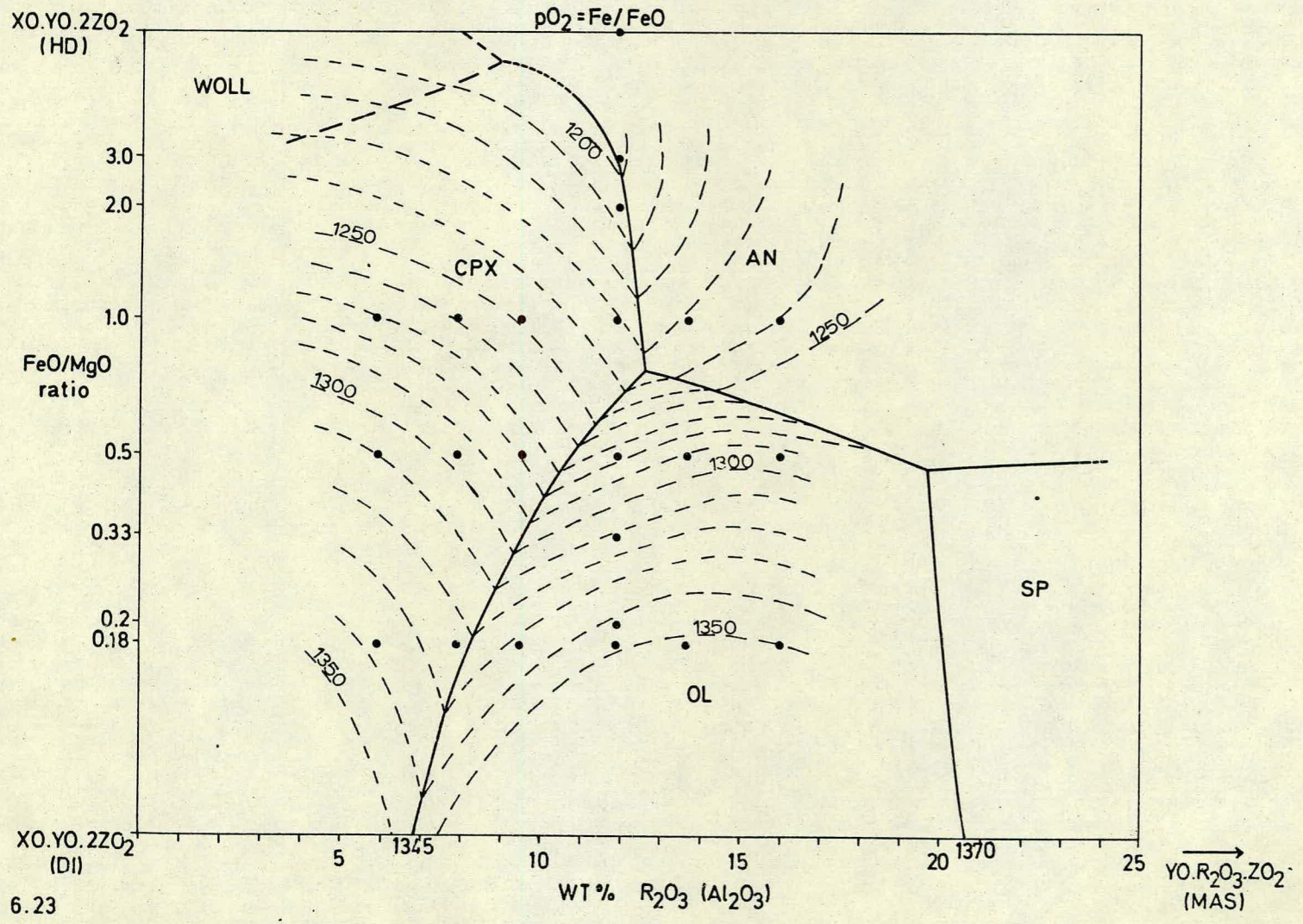
XO.YO.2ZO2
(HD)
pO2 = Fe/FeO
WOLL
1200
3.0
2.0
1250
CPX
AN
1250
1.0
FeO/MgO
ratio
1300
0.5
1300
0.33
SP
0.2
0.18
1350
1350
OL
XO.YO.2ZO2
(DI)
5
1345
10
15
20
1370
25
YO.R2O3.ZO2
(MAS)
WT % R2O3 (Al2O3)

Fig 6.23

Figure 6.24

Diagram to show the change in second phase to crystallise for molecularly equivalent compositions in part of the join $XO.YO.2ZO_2$-$YO.R_2O_3.ZO_2$ (Diopside-MAS) with changing FeO/MgO ratio, at the pO_2 of the Fe/FeO equilibrium. The compositions studied are shown by filled circles, the composition name can be found by referring to the individual T - X sections for this join (figures 6.20-6.22). Compositions at other FeO/MgO ratios lie in the join Enstatite-Grossular, their names can be found by referring to the T - X sections for that join (figures 6.30-6.36). The liquidus phase boundaries are indicated by thick solid lines, the projected phase boundaries within each phase volume are indicated where known by thin solid lines. The phase assemblage for each area is also indicated. The dashed lines are the temperature contours for the appearance of the second phase in each composition in the join where known.

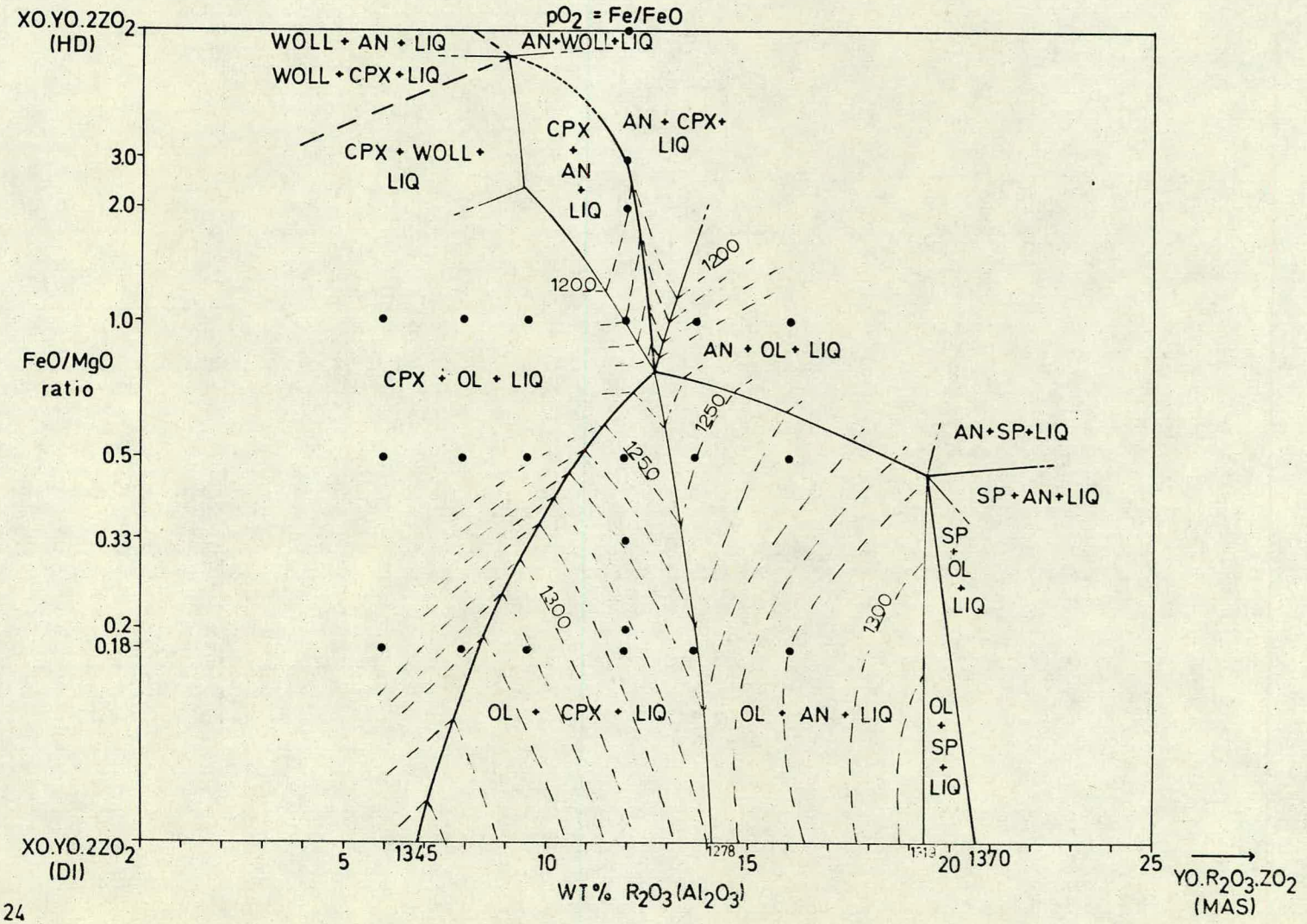
XO.YO.2ZO2
(HD)
pO2 = Fe/FeO
WOLL + AN + LIQ
AN+WOLL+LIQ
WOLL + CPX + LIQ
CPX + WOLL + LIQ
CPX + AN + LIQ
AN + CPX + LIQ
3.0
2.0
1.0
FeO/MgO ratio
0.5
0.33
0.2
0.18
1200
1200
1250
1250
1300
1300
AN + OL + LIQ
CPX + OL + LIQ
AN+SP+LIQ
SP + AN + LIQ
SP + OL + LIQ
OL + CPX + LIQ
OL + AN + LIQ
OL + SP + LIQ
XO.YO.2ZO2
(DI)
5
1345
10
1278
15
1313
20
1370
25
WT% R2O3 (Al2O3)
YO.R2O3.ZO2
(MAS)

Fig 6.24

Figures 6.25 to 6.27

T - X sections for part of the join $XO.YO.2ZO_2$-$5YO.3R_2O_3.5ZO_2$ (Diopside-$M_5A_3S_5$) at FeO/MgO mole ratios of 0.18, 0.5, and 1.0, and the pO_2 of the Fe/FeO equilibrium. The experiments on each composition are shown at the appropriate temperatures by filled circles, the composition names are indicated beneath each composition studied. The phase boundaries are drawn using the combined data plots presented in figures 6.28, 6.29.

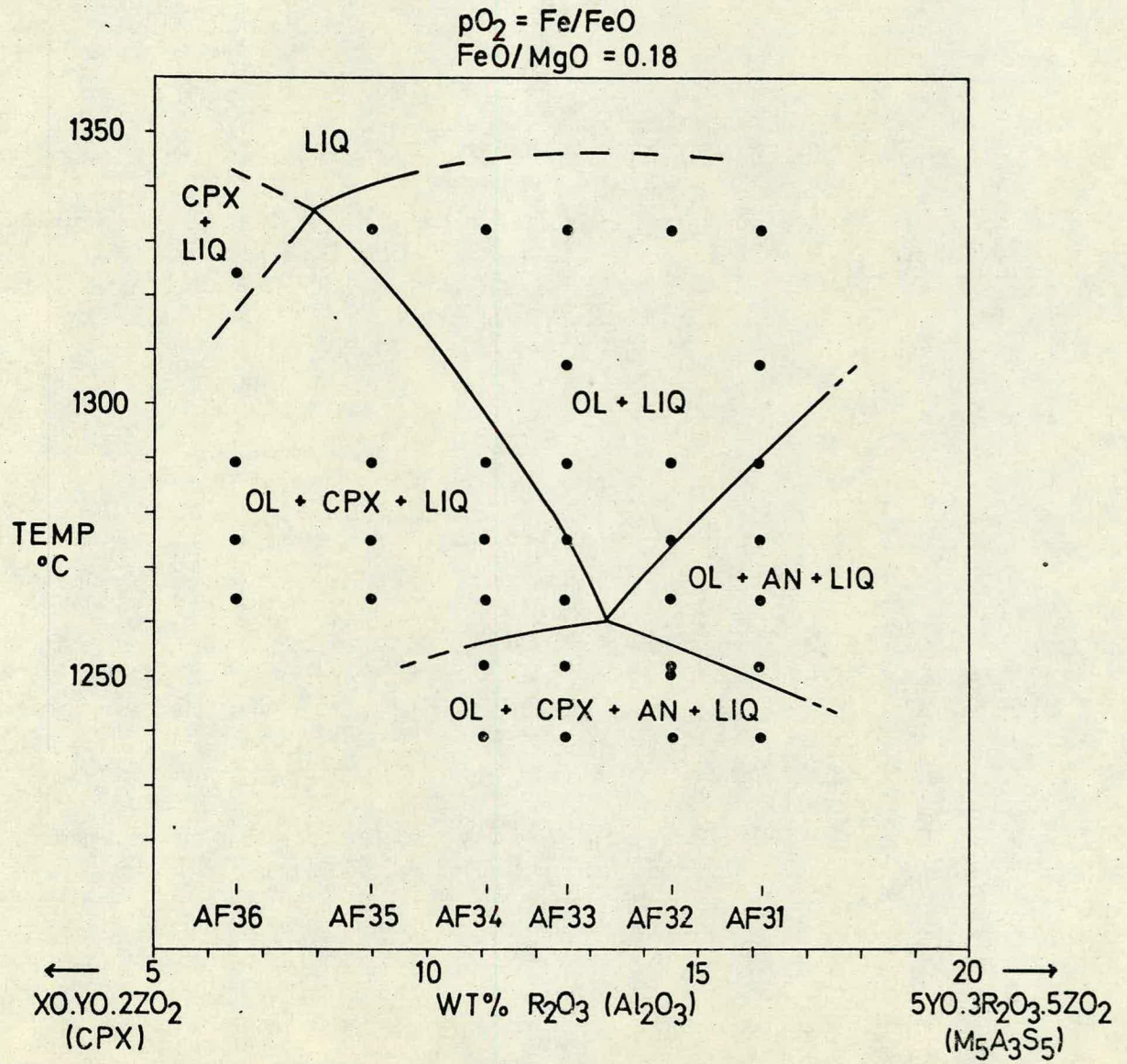
pO_2 = Fe/FeO
FeO/MgO = 0.18
1350
1300
1250
TEMP °C
LIQ
CPX + LIQ
OL + LIQ
OL + CPX + LIQ
OL + AN + LIQ
OL + CPX + AN + LIQ
AF36
AF35
AF34
AF33
AF32
AF31
5
10
15
20
XO.YO.2ZO2 (CPX)
WT% R2O3 (Al2O3)
5YO.3R2O3.5ZO2 (M5A3S5)

Fig 6.25

Figure 6.26

See figure 6.25

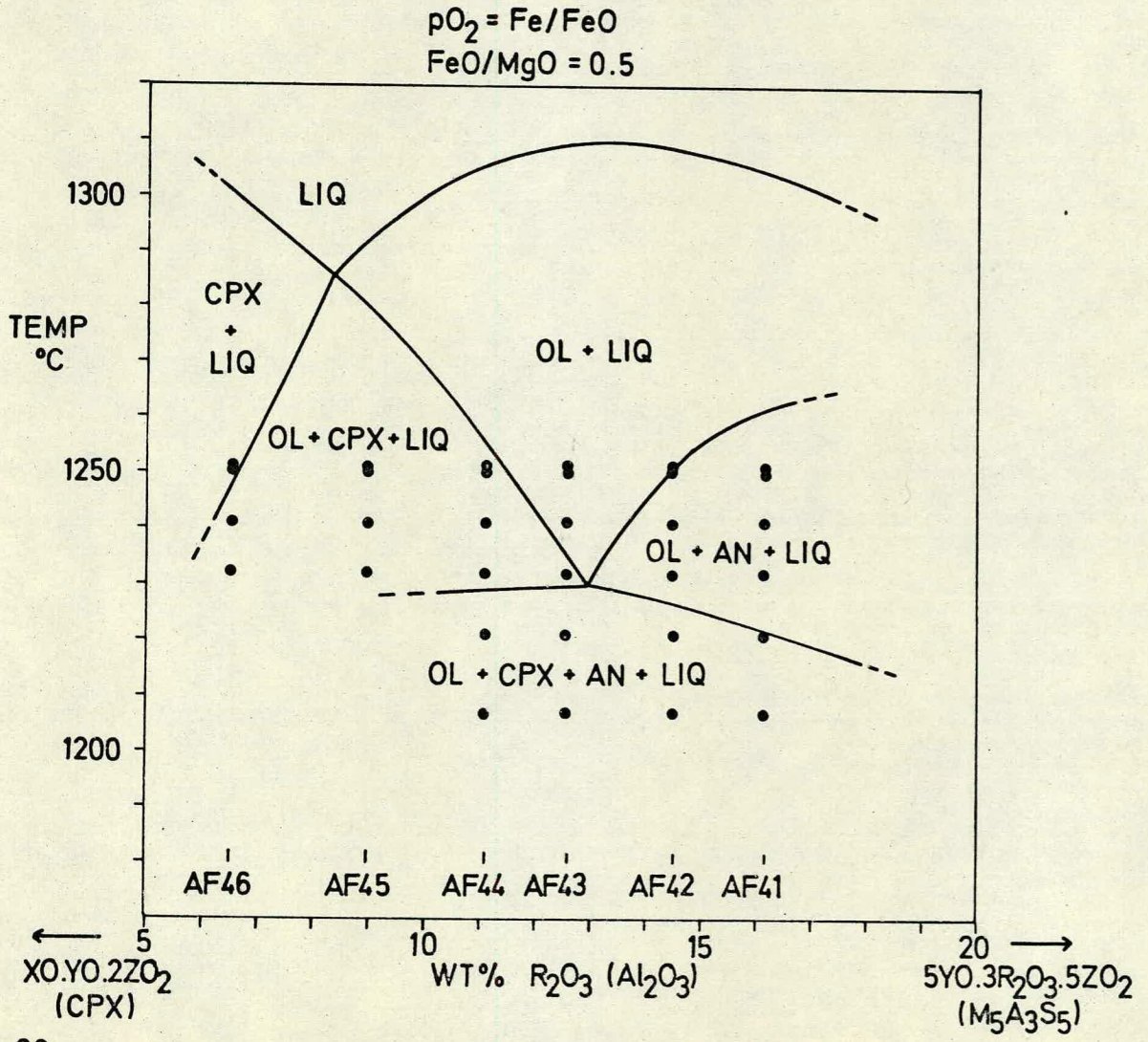
pO_2 = Fe/FeO
FeO/MgO = 0.5
1300
1250
1200
TEMP °C
LIQ
CPX + LIQ
OL + LIQ
OL + CPX + LIQ
OL + AN + LIQ
OL + CPX + AN + LIQ
AF46
AF45
AF44
AF43
AF42
AF41
5
10
15
20
XO.YO.2ZO2 (CPX)
WT% R_2O_3 (Al_2O_3)
5YO.3R_2O_3.5ZO2 ($M_5A_3S_5$)

Fig 6.26

Figure 6.27

See figure 6.25

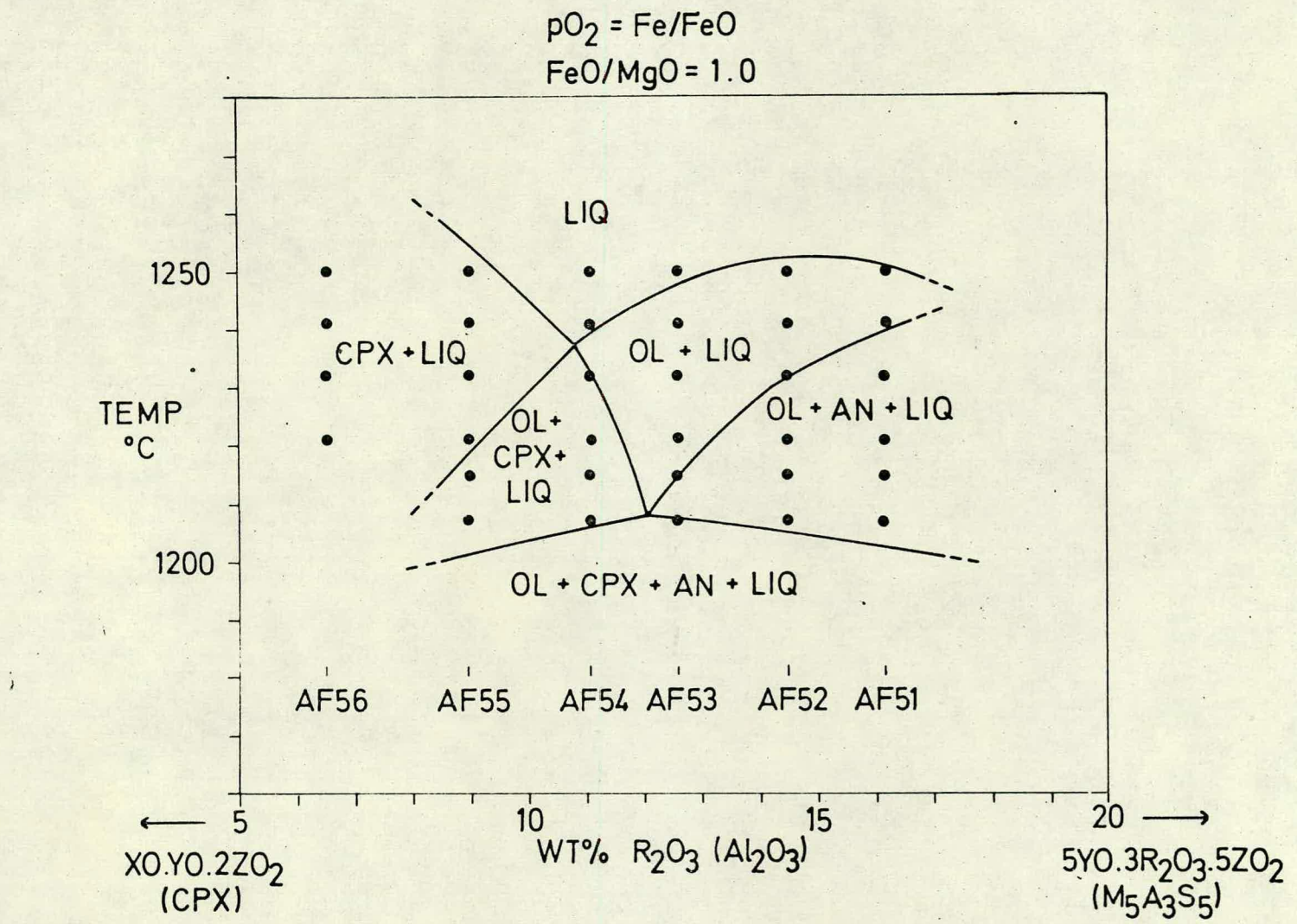
pO2 = Fe/FeO
FeO/MgO = 1.0
LIQ
1250
CPX + LIQ
OL + LIQ
TEMP
°C
OL + AN + LIQ
OL+
CPX+
LIQ
1200
OL + CPX + AN + LIQ
AF56
AF55
AF54
AF53
AF52
AF51
5
10
15
20
XO.YO.2ZO2
(CPX)
WT% R2O3 (Al2O3)
5YO.3R2O3.5ZO2
(M5A3S5)

Fig 6.27

Figure 6.28

Liquidus diagram for part of the join $XO.YO.2ZO_2$-$5YO.3R_2O_3.5ZO_2$ (Diopside-$M_5A_3S_5$), to show the change in liquidus phase for molecularly equivalent compositions with changing FeO/MgO ratio, at the pO_2 of the Fe/FeO equilibrium. The compositions studied are shown by filled circles, the composition name can be found by referring to the individual T - X sections for this join (figures 6.25-6.27). The phase boundaries are indicated by thick solid lines, the dashed lines are the temperature contours where known.

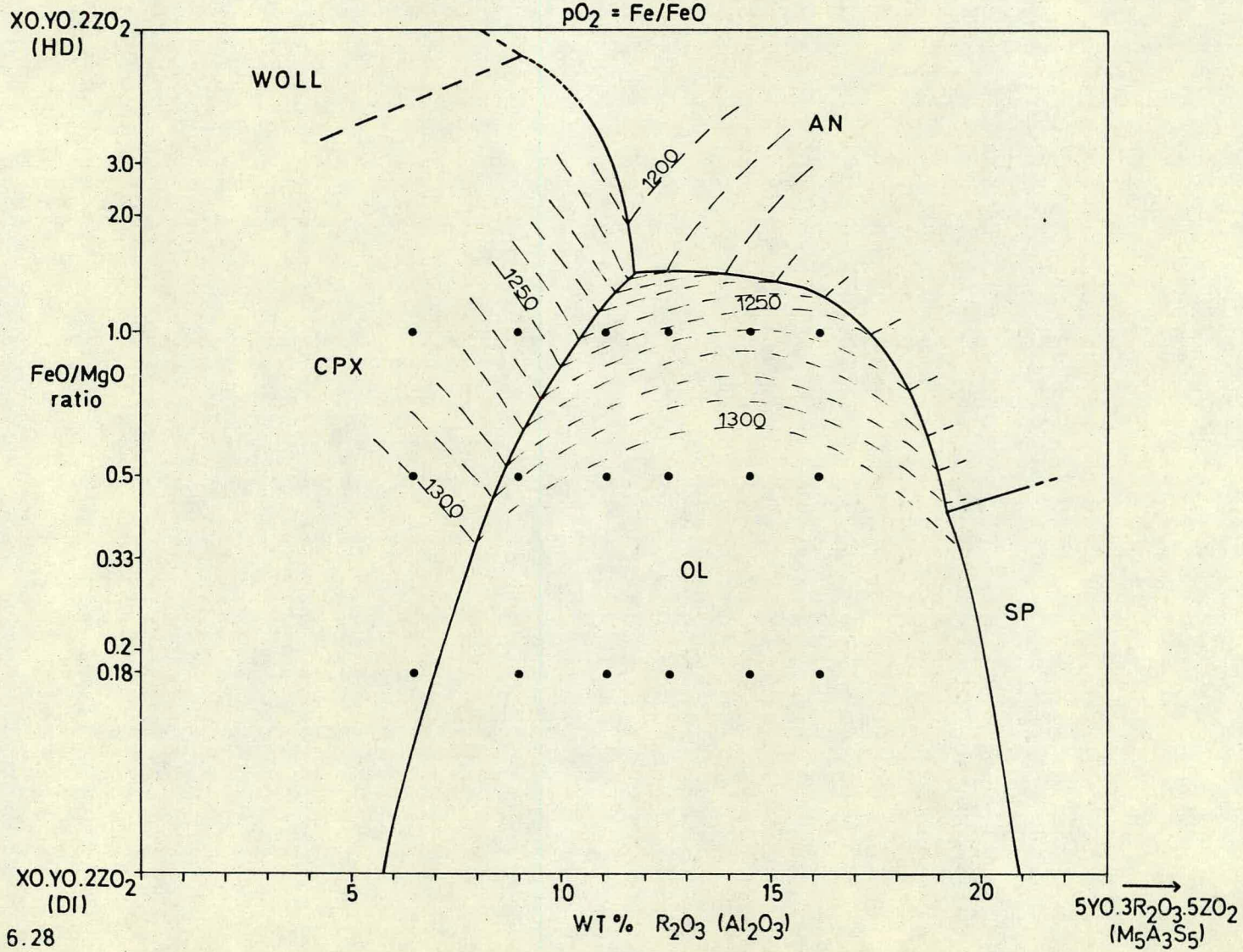
pO_2 = Fe/FeO
XO.YO.2ZO$_2$
(HD)
WOLL
AN
1200
1250
1250
1300
1300
CPX
OL
SP
3.0
2.0
1.0
0.5
0.33
0.2
0.18
FeO/MgO
ratio
XO.YO.2ZO$_2$
(DI)
5
10
15
20
WT % R_2O_3 (Al_2O_3)
5YO.3R_2O_3.5ZO_2
($M_5A_3S_5$)

Fig 6.28

Figure 6.29

Diagram to show the change in second phase to crystallise for molecularly equivalent compositions in part of the join $XO.YO.2ZO_2$-$5YO.3R_2O_3.5ZO_2$ (Diopside-$M_5A_3S_5$) with changing FeO/MgO ratio, at the pO_2 of the Fe/FeO equilibrium. The compositions studied are shown by filled circles, the composition names can be found by referring to the individual T - X sections for this join (figures 6.25-6.27). The liquidus phase boundaries are indicated by thick solid lines, the projected phase boundaries within each phase volume are indicated by thin solid lines. The phase assemblage for each area is indicated where known. The dashed lines are the temperature contours for the appearance of the second phase in each composition in the join where known.

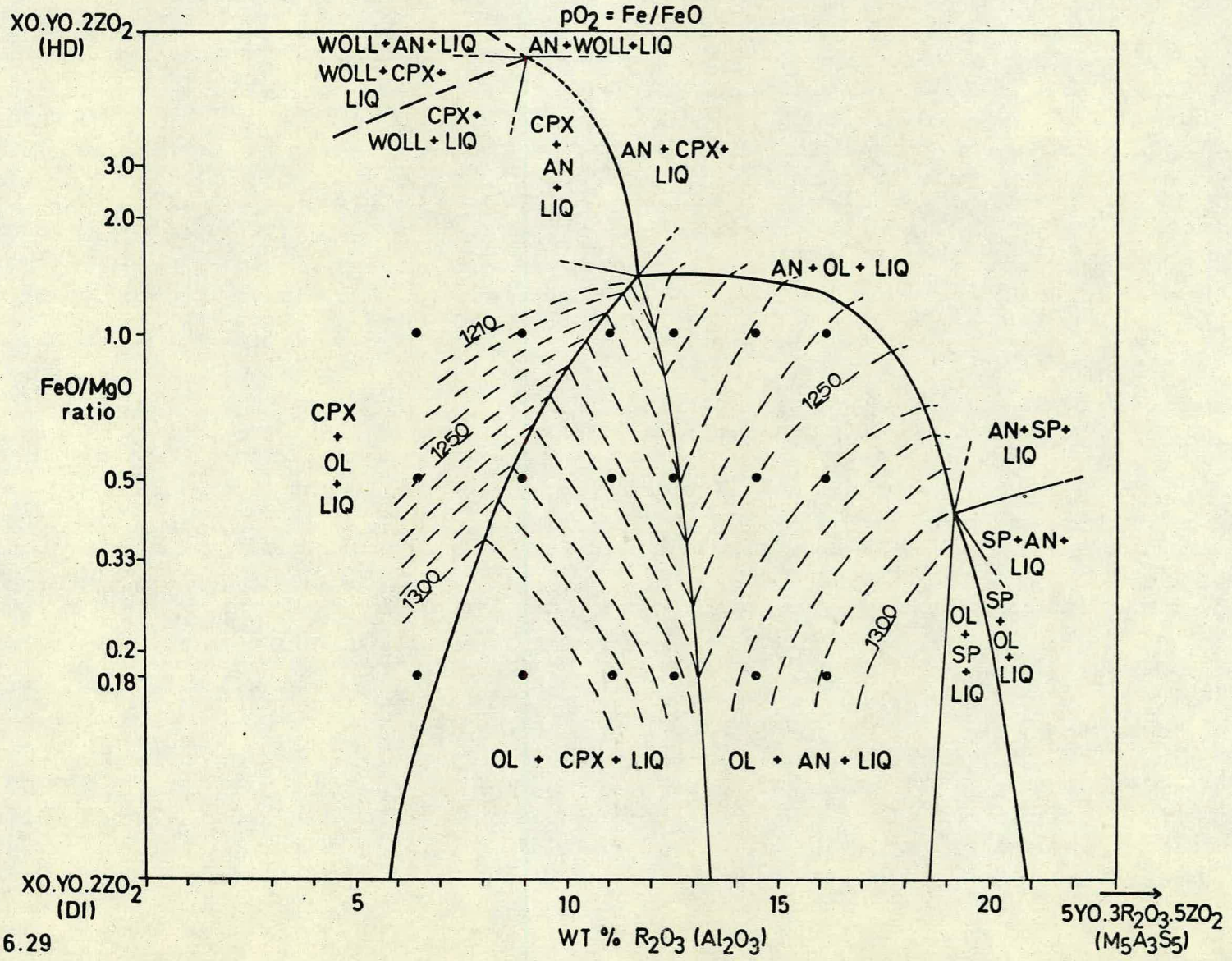
pO2 = Fe/FeO
XO.YO.2ZO2 (HD)
WOLL + AN + LIQ
AN + WOLL + LIQ
WOLL + CPX + LIQ
CPX + WOLL + LIQ
CPX + AN + LIQ
AN + CPX + LIQ
AN + OL + LIQ
AN + SP + LIQ
SP + AN + LIQ
SP + OL + LIQ
OL + SP + LIQ
CPX + OL + LIQ
OL + CPX + LIQ
OL + AN + LIQ
1210
1250
1250
1300
1300
3.0
2.0
1.0
0.5
0.33
0.2
0.18
FeO/MgO ratio
XO.YO.2ZO2 (DI)
5
10
15
20
WT % R2O3 (Al2O3)
5YO.3R2O3.5ZO2 (M5A3S5)

Fig 6.29

Figures 6.30 to 6.36

T - X sections for part of the join $YO.ZO_2$-$3XO.R_2O_3.3ZO_2$ (Enstatite-Grossular) at FeO/MgO mole ratios of 0.2, 0.33, 0.5, 1.0, 2.0, 3.0, and X (MgO-free) and the pO_2 of the Fe/FeO equilibrium. The experiments on each composition are shown at the appropriate temperatures by filled circles. The composition names are generated from the information beneath each composition studied, using the format

FeO/MgO mole ratio - moles MgO - 3 - 1 - moles SiO_2.

The phase boundaries are drawn using the combined data plots presented in figures 6.37, 6.38. Some data points are inconsistent with these phase boundaries, but generally only by a small temperature error.

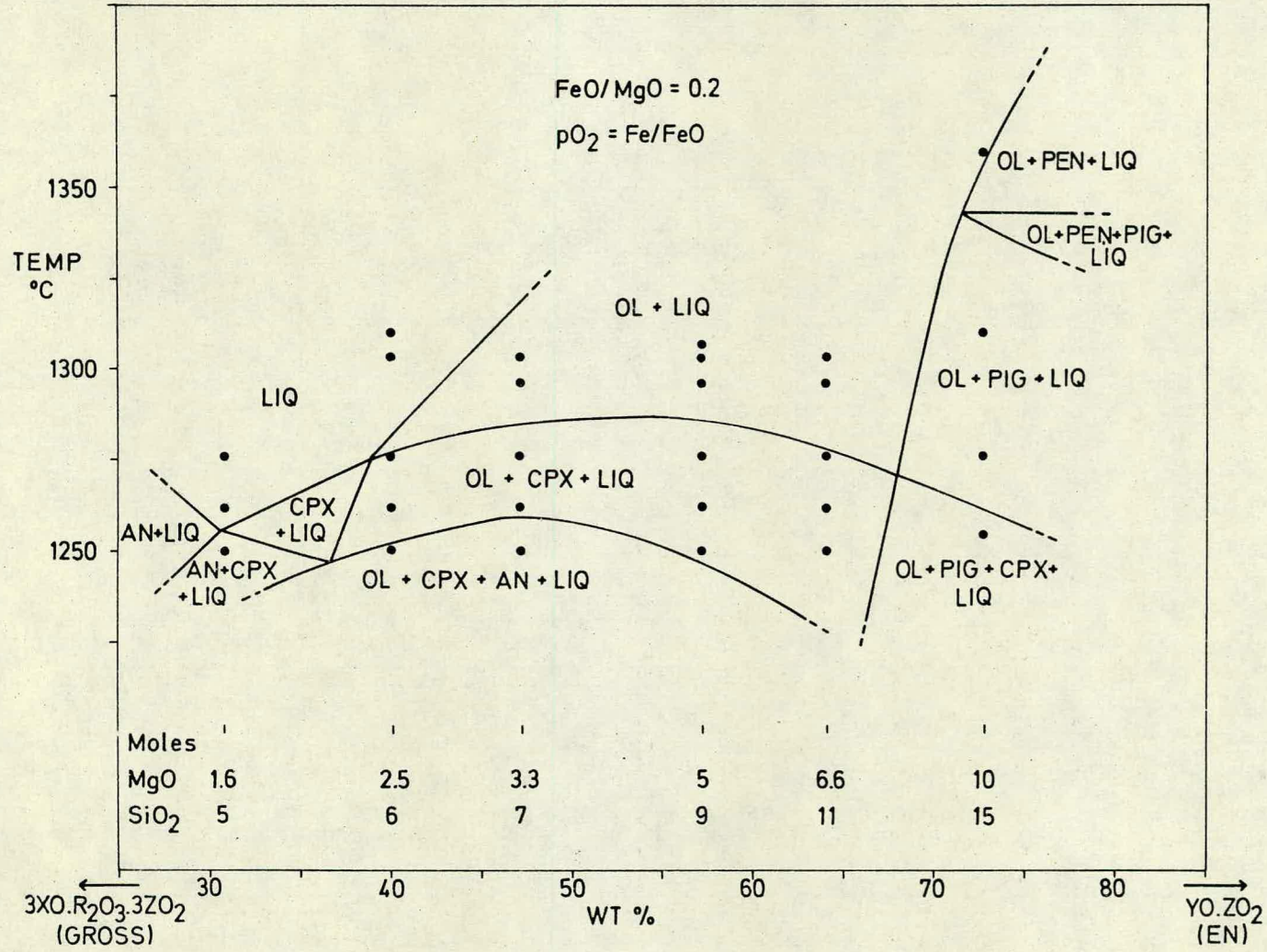
FeO/MgO = 0.2
pO_2 = Fe/FeO
1350
TEMP °C
1300
1250
LIQ
OL + LIQ
OL + PEN + LIQ
OL + PEN + PIG + LIQ
OL + PIG + LIQ
OL + CPX + LIQ
CPX + LIQ
AN + LIQ
AN + CPX + LIQ
OL + CPX + AN + LIQ
OL + PIG + CPX + LIQ
Moles
MgO 1.6 2.5 3.3 5 6.6 10
SiO_2 5 6 7 9 11 15
30
40
50
60
70
80
WT %
$3XO.R_2O_3.3ZO_2$ (GROSS)
$YO.ZO_2$ (EN)

Fig 6.30

Figure 6.31

See figure 6.30

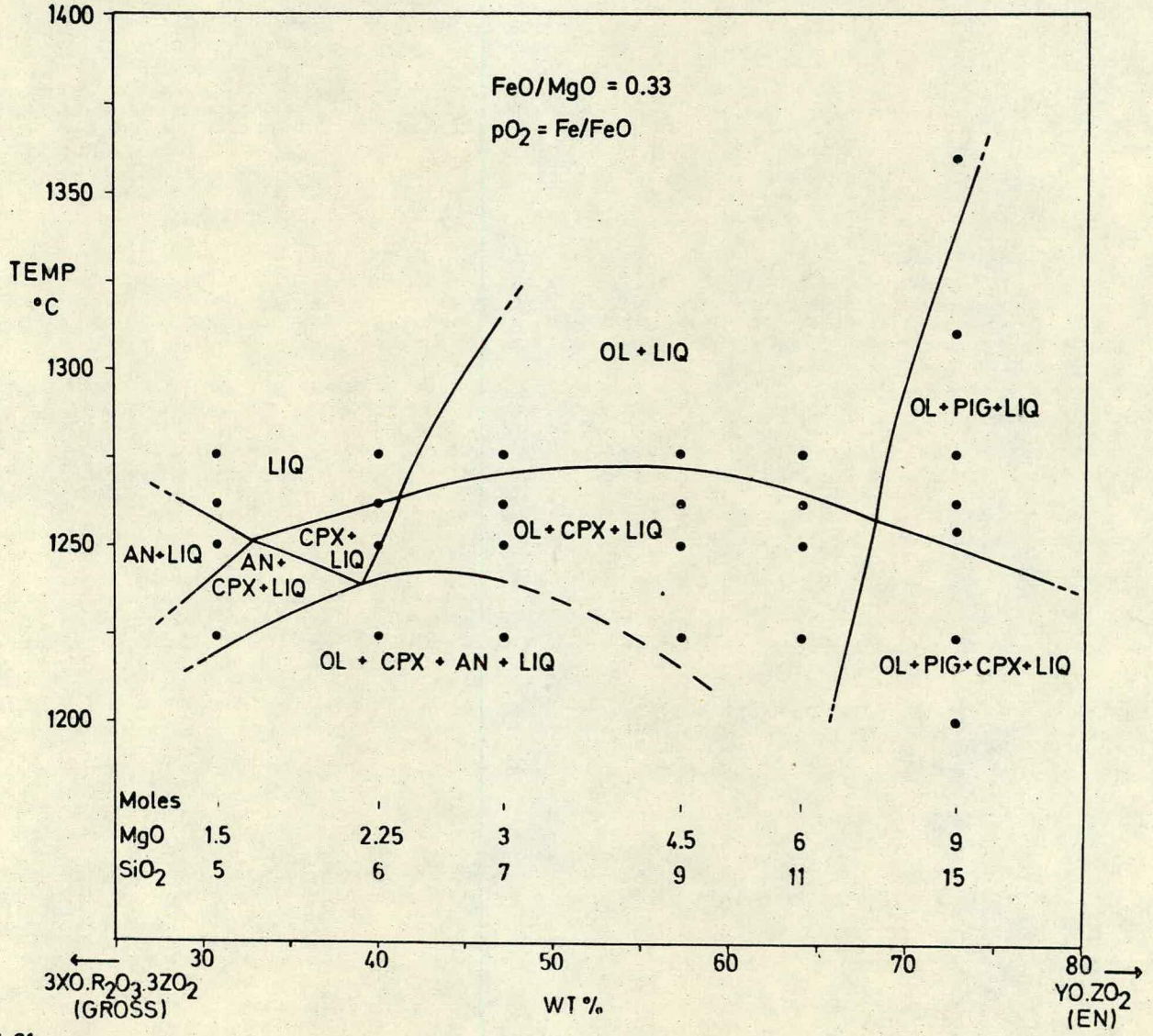
1400
1350
TEMP
°C
1300
1250
1200
FeO/MgO = 0.33
pO2 = Fe/FeO
OL + LIQ
OL+PIG+LIQ
LIQ
AN+LIQ
CPX+
LIQ
AN+
CPX+LIQ
OL+CPX+LIQ
OL + CPX + AN + LIQ
OL+PIG+CPX+LIQ
Moles
MgO 1.5 2.25 3 4.5 6 9
SiO2 5 6 7 9 11 15
30
40
50
60
70
80
3XO.R2O3.3ZO2
(GROSS)
WT %
YO.ZO2
(EN)

Fig 6.31

Figure 6.32

See figure 6.30

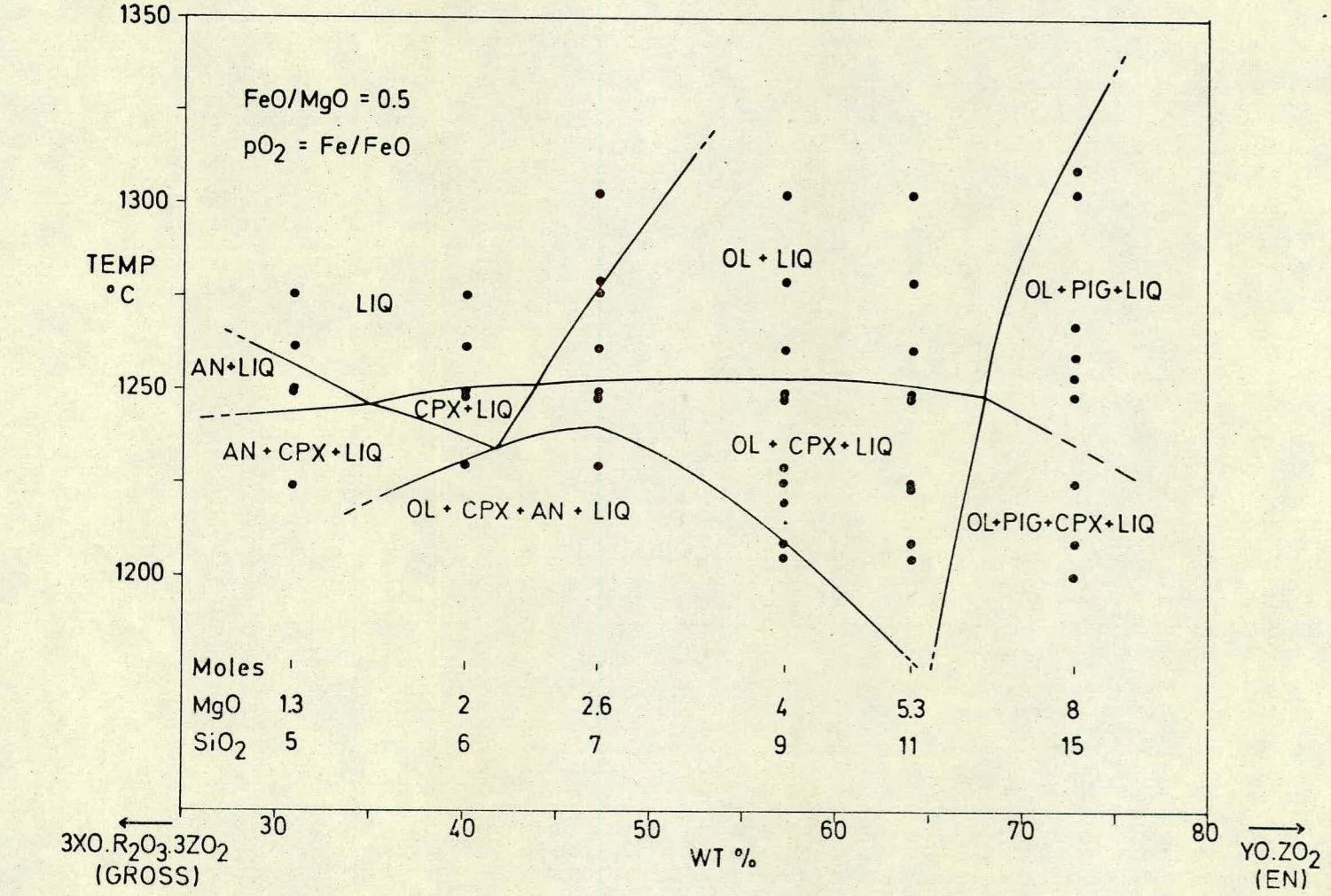
1350
1300
1250
1200
TEMP
°C
FeO/MgO = 0.5
pO2 = Fe/FeO
LIQ
OL + LIQ
OL + PIG + LIQ
AN+LIQ
CPX+LIQ
AN + CPX + LIQ
OL + CPX + LIQ
OL + CPX + AN + LIQ
OL+PIG+CPX+LIQ
Moles
MgO 1.3 2 2.6 4 5.3 8
SiO2 5 6 7 9 11 15
30
40
50
60
70
80
WT %
3XO.R2O3.3ZO2
(GROSS)
YO.ZO2
(EN)

Fig 6.32

Figure 6.33

See figure 6.30

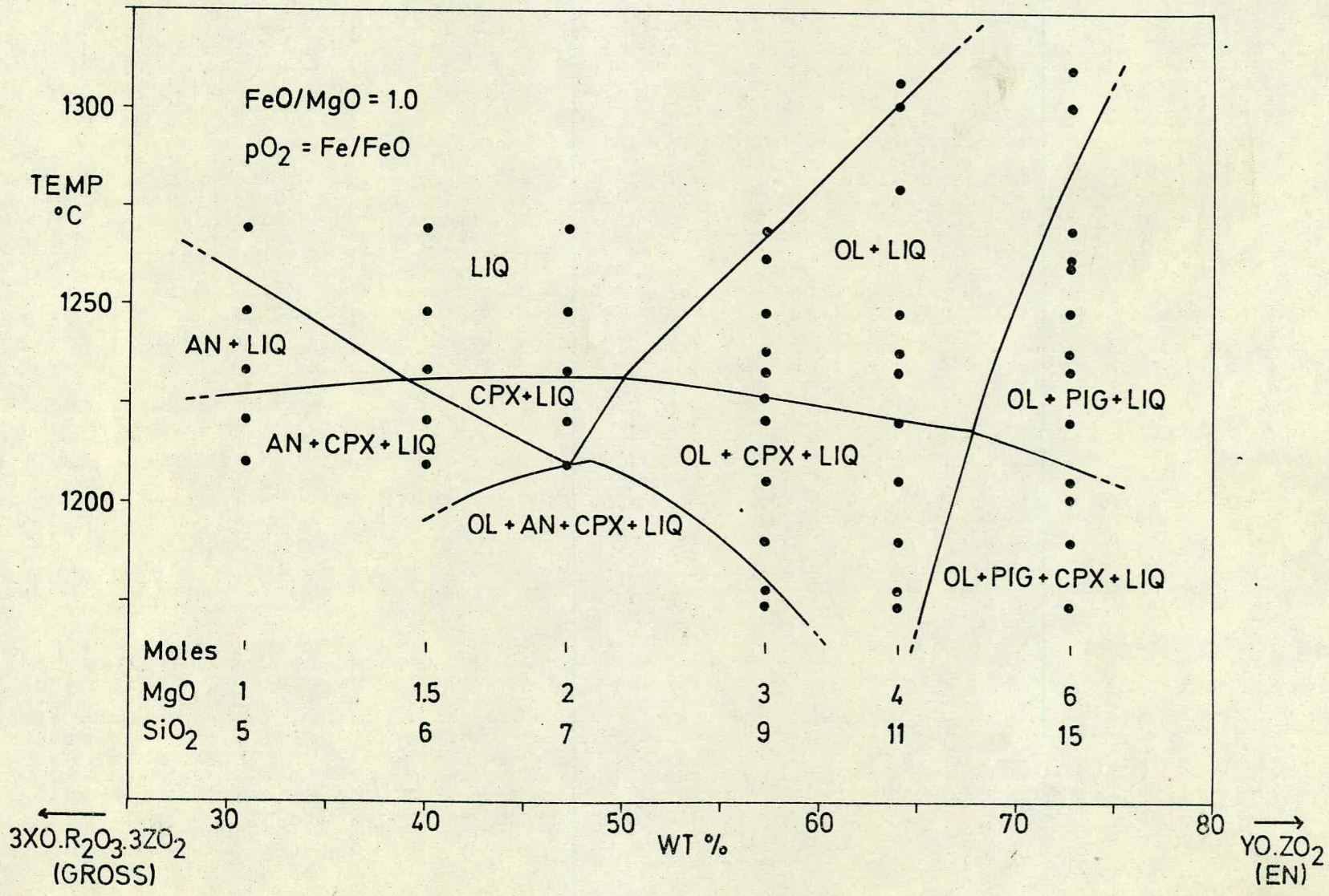
FeO/MgO = 1.0
pO2 = Fe/FeO
TEMP °C
1300
1250
1200
LIQ
OL + LIQ
AN + LIQ
CPX+LIQ
OL + PIG+LIQ
AN + CPX + LIQ
OL + CPX + LIQ
OL + AN + CPX + LIQ
OL+PIG + CPX + LIQ
Moles
MgO 1 1.5 2 3 4 6
SiO2 5 6 7 9 11 15
30 40 50 60 70 80
WT %
3XO.R2O3.3ZO2 (GROSS)
YO.ZO2 (EN)

Fig 6.33

Figure 6.34

See figure 6.30

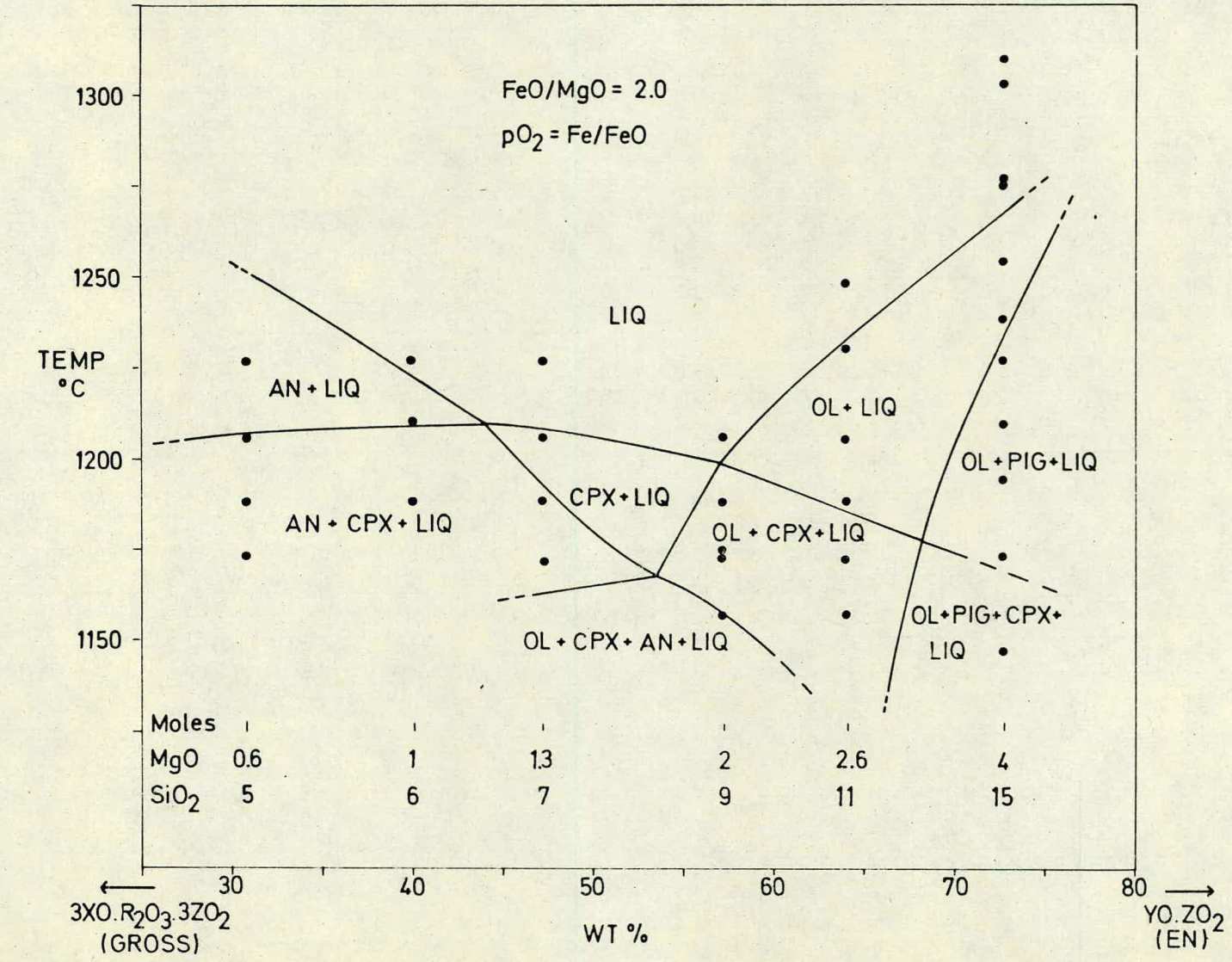
FeO/MgO = 2.0
pO_2 = Fe/FeO
1300
1250
1200
1150
TEMP °C
LIQ
AN + LIQ
OL + LIQ
OL + PIG + LIQ
CPX + LIQ
AN + CPX + LIQ
OL + CPX + LIQ
OL + PIG + CPX + LIQ
OL + CPX + AN + LIQ
Moles
MgO 0.6 1 1.3 2 2.6 4
SiO_2 5 6 7 9 11 15
30 40 50 60 70 80
← $3XO.R_2O_3.3ZO_2$ (GROSS)
WT %
$YO.ZO_2$ (EN) →

Fig 6.34

Figure 6.35

See figure 6.30

Found missing Jan 1980 GWB.

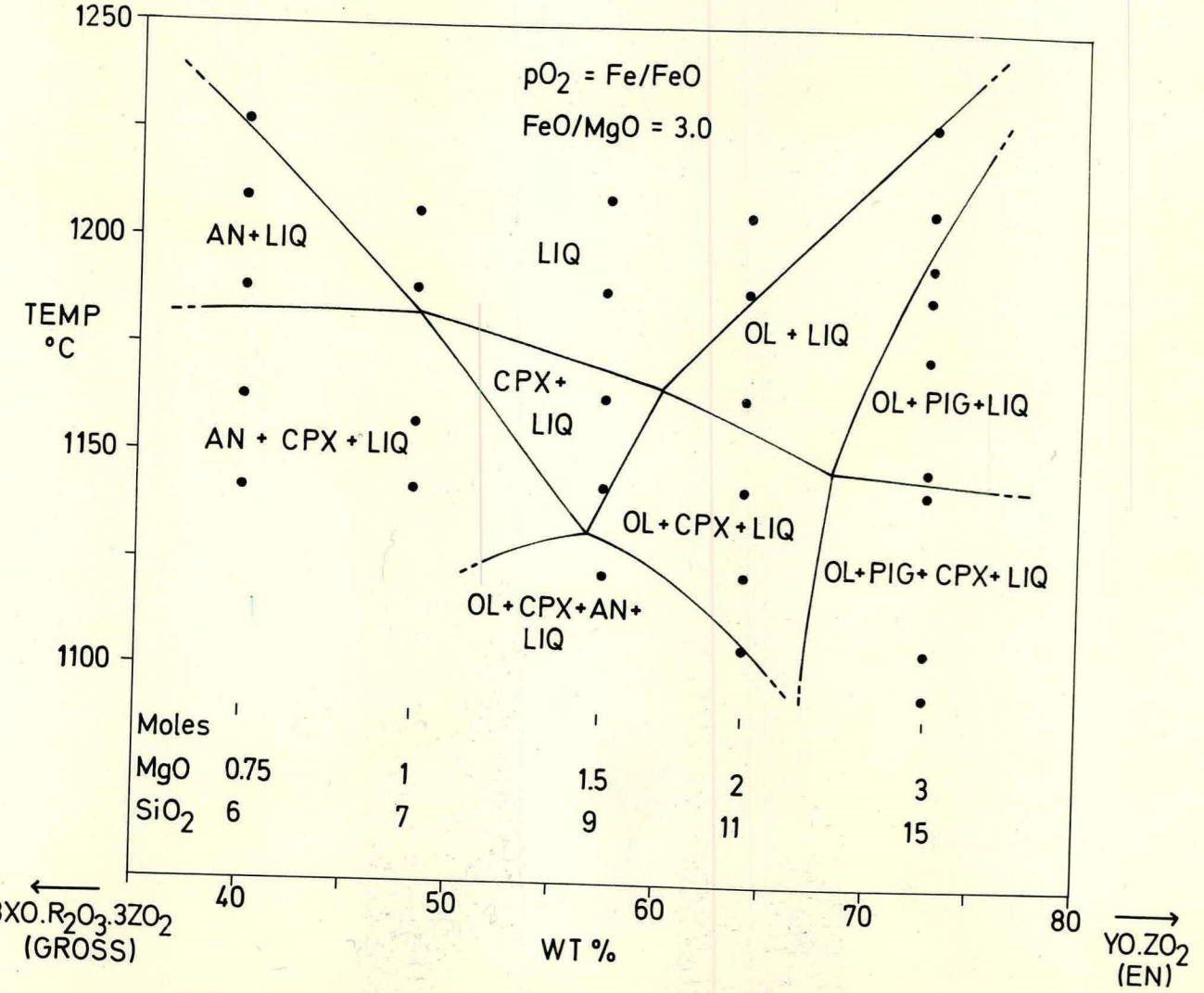
1250
1200
1150
1100
TEMP °C
pO_2 = Fe/FeO
FeO/MgO = 3.0
AN+LIQ
LIQ
OL + LIQ
CPX+ LIQ
OL+ PIG+LIQ
AN + CPX + LIQ
OL+CPX+LIQ
OL+PIG+ CPX+ LIQ
OL+CPX+AN+ LIQ
Moles
MgO 0.75 1 1.5 2 3
SiO_2 6 7 9 11 15
40
50
60
70
80
WT %
$3XO.R_2O_3.3ZO_2$ (GROSS)
$YO.ZO_2$ (EN)

Fig 6.35

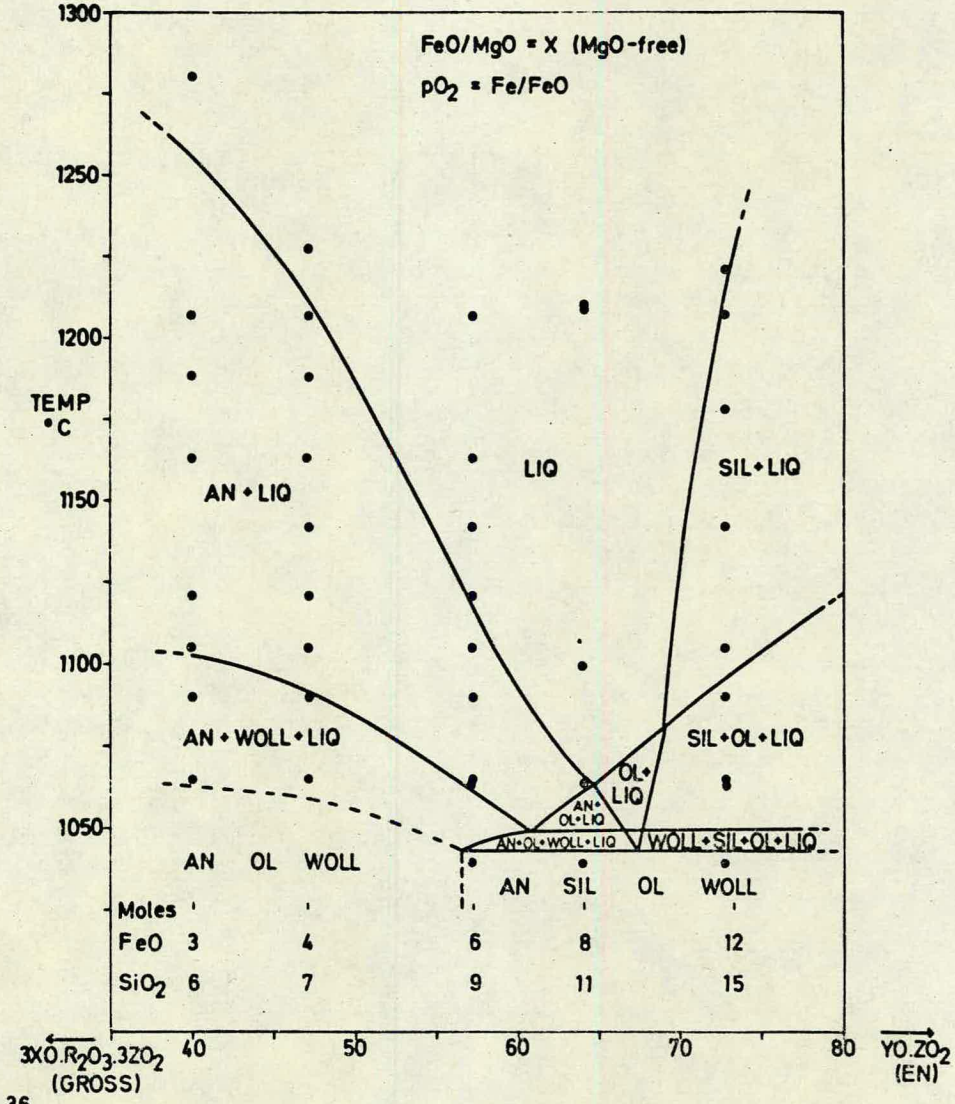
FeO/MgO = X (MgO-free)
pO_2 = Fe/FeO
TEMP °C
1300
1250
1200
1150
1100
1050
AN + LIQ
LIQ
SIL + LIQ
AN + WOLL + LIQ
SIL + OL + LIQ
OL + LIQ
AN + OL + LIQ
AN + OL + WOLL + LIQ
WOLL + SIL + OL + LIQ
AN OL WOLL
AN SIL OL WOLL
Moles
FeO 3 4 6 8 12
SiO_2 6 7 9 11 15
40 50 60 70 80
$3XO.R_2O_3.3ZO_2$ (GROSS)
$YO.ZO_2$ (EN)

Fig 6.36

Figure 6.37

Liquidus diagram for part of the join $YO.ZO_2$-$3XO.R_2O_3.3ZO_2$ (Enstatite-Grossular), to show the change in liquidus phase with changing FeO/MgO ratio for molecularly equivalent compositions, at the pO_2 of the Fe/FeO equilibrium. The compositions studied are shown by filled circles, the composition name can be found by referring to the individual T - X sections for this join (figures 6.30-6.36). The phase boundaries are indicated by thick solid lines, the dashed lines are the temperature contours, where known. Data from the join MgO-SiO_2-Fe-O_2 at these pO_2 (figure 6.5) was used along the join "MS"-"FS".

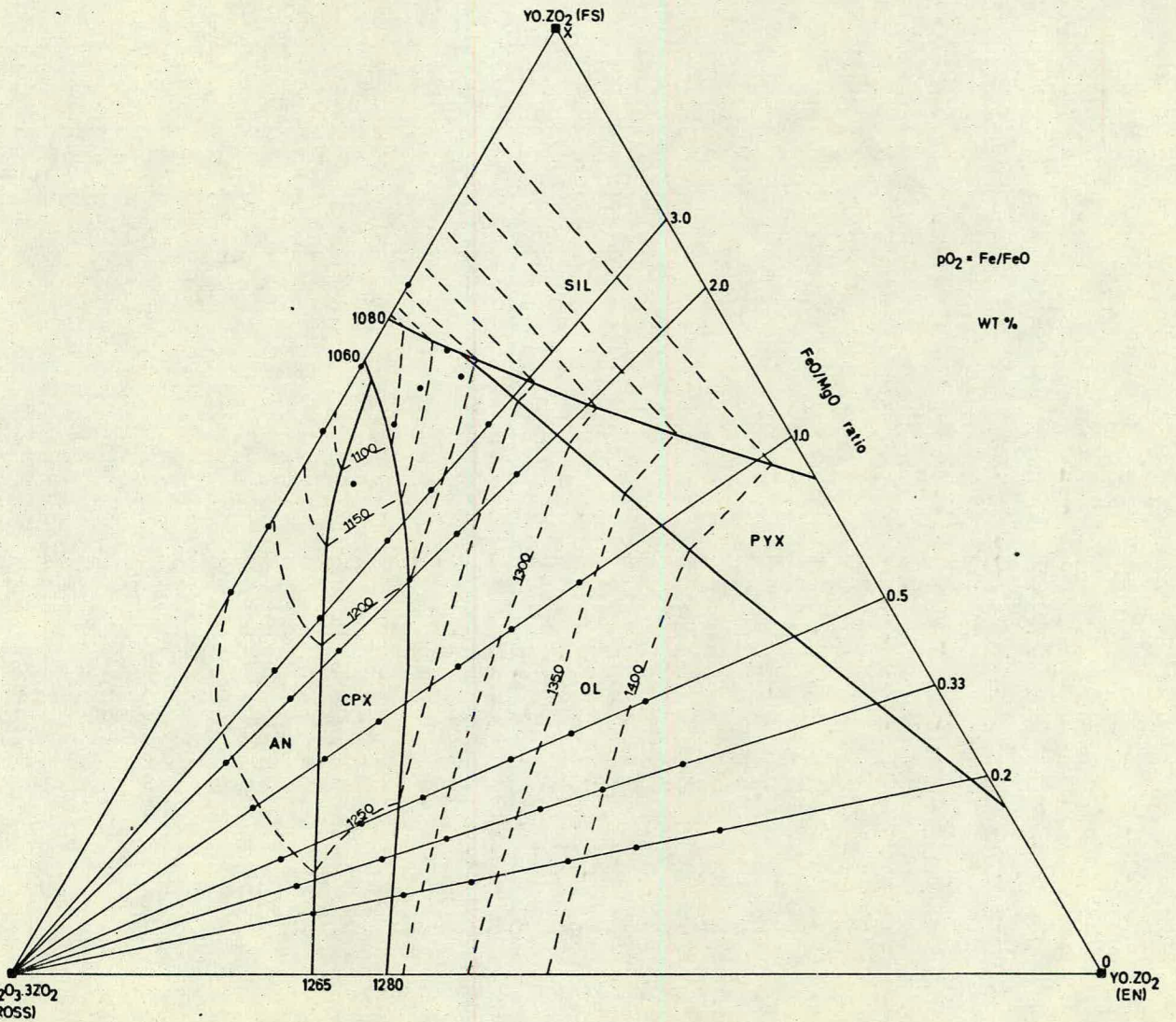
YO.ZO2 (FS)
X
3.0
2.0
1.0
0.5
0.33
0.2
0
pO2 = Fe/FeO
WT %
FeO/MgO ratio
SIL
PYX
CPX
AN
OL
1080
1060
1100
1150
1200
1300
1350
1400
1250
1265
1280
3XO.R2O3.3ZO2
(GROSS)
YO.ZO2
(EN)

Fig 6.37

Figure 6.38

Diagram to show the change in second phase to crystallise for molecularly equivalent compositions in part of the join $YO.ZO_2$-$3XO.R_2O_3.3ZO_2$ (Enstatite-Grossular), with changing FeO/MgO ratio, at the pO_2 of the Fe/FeO equilibrium. The compositions studied are shown by filled circles, the composition names can be found by referring to the individual T - X sections for this join (figures 6.30-6.36). The liquidus phase boundaries are indicated by thick solid lines, the projected phase boundaries within each phase volume by thin solid lines. The phase assemblage for each area is indicated. The dashed lines are the temperature contours for the appearance of the second phase in each composition in the join where known.

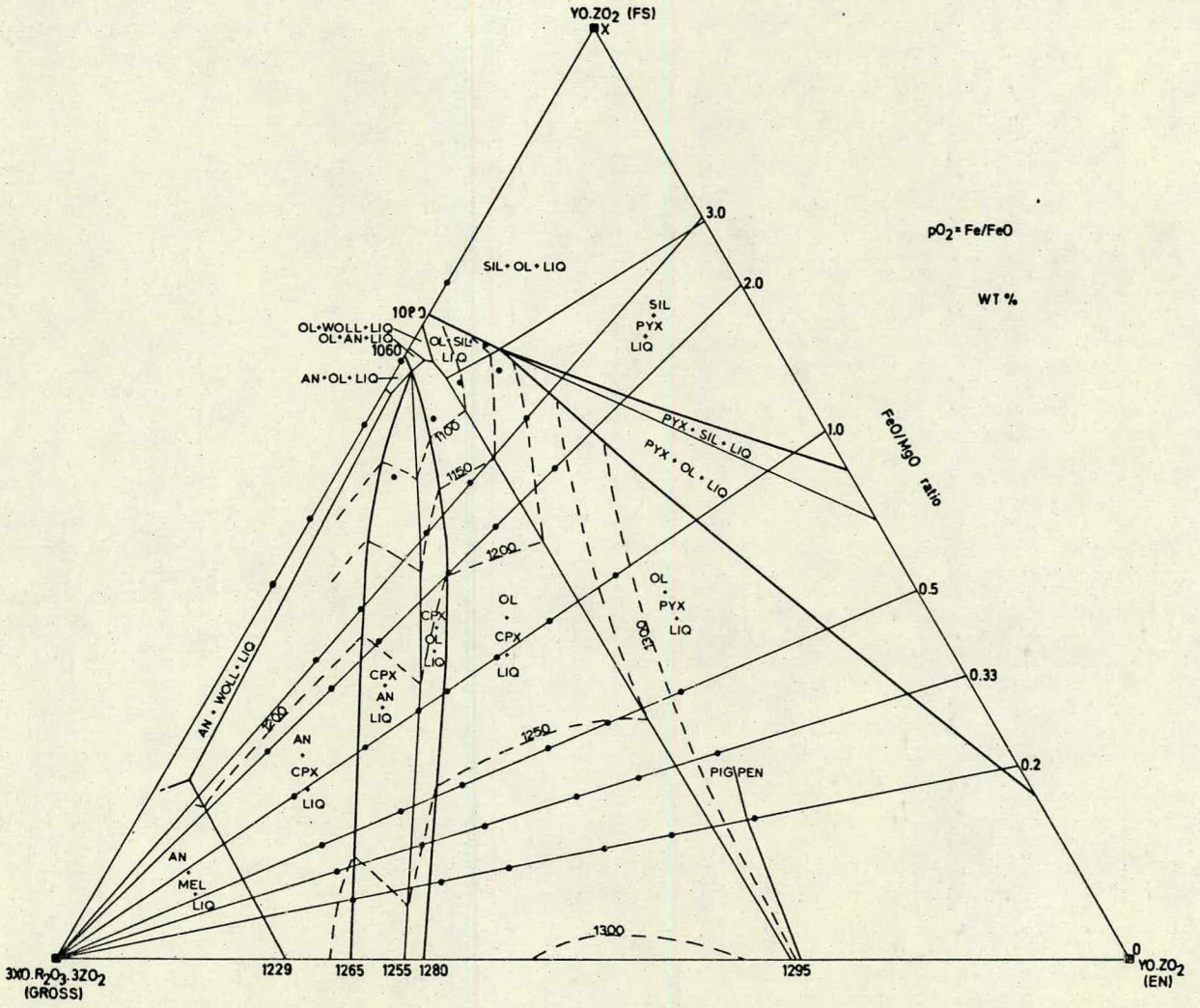
YO.ZO2 (FS)
X
3.0
2.0
1.0
0.5
0.33
0.2
0
pO2 = Fe/FeO
WT %
FeO/MgO ratio
SIL • OL • LIQ
SIL
PYX
LIQ
1060
OL • WOLL • LIQ
OL • AN • LIQ
AN • OL • LIQ
OL
SIL
LIQ
PYX • SIL • LIQ
PYX • OL • LIQ
1100
1150
1200
1250
1300
OL
PYX
LIQ
OL
CPX
LIQ
CPX
OL
LIQ
CPX
AN
LIQ
AN • WOLL • LIQ
AN
CPX
LIQ
AN
MEL
LIQ
OPX
PIG/PEN
3XO.R2O3.3ZO2
(GROSS)
1229
1265
1255
1280
1295
YO.ZO2
(EN)

Fig 6.38

Figures 6.39 to 6.41

T - X sections for part of the join $3XO.R_2O_3.15ZO_2$-YO (C_3AS_{15}-M) at FeO/MgO mole ratios of 0.5, 1.0, and 2.0, and the pO_2 of the Fe/FeO equilibrium. The experiments on each composition are shown at the appropriate temperatures by filled circles. The composition names are generated from the information beneath each composition studied, using the format

FeO/MgO mole ratio - moles MgO - 3 - 1 - moles SiO_2.

The phase boundaries are drawn using the combined data plots presented in figures 6.42, 6.43. Some data points are inconsistent with these phase boundaries, but generally only by a small temperature error.

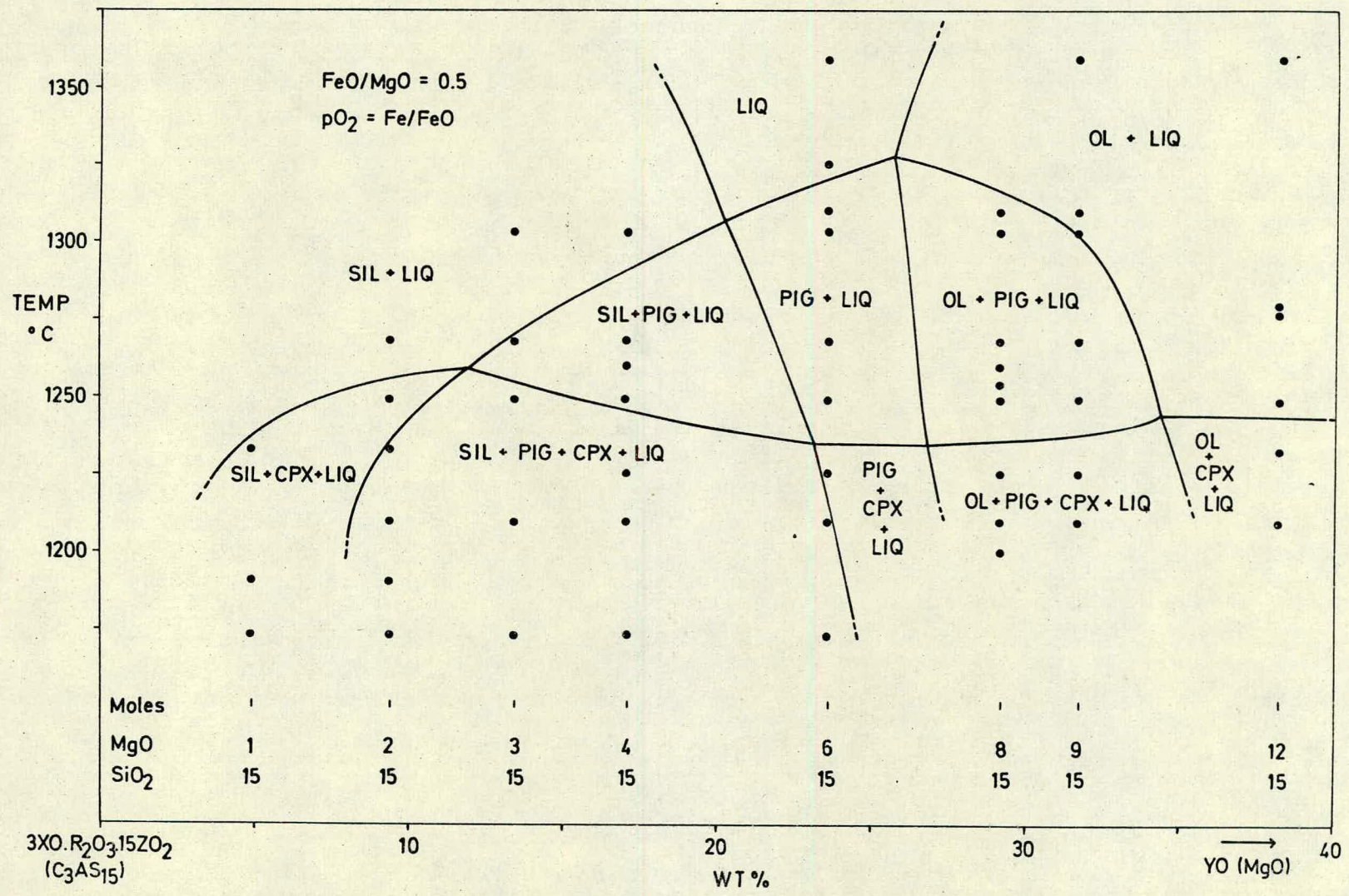
FeO/MgO = 0.5
pO_2 = Fe/FeO
LIQ
OL + LIQ
SIL + LIQ
SIL+PIG+LIQ
PIG + LIQ
OL + PIG + LIQ
SIL+CPX+LIQ
SIL + PIG + CPX + LIQ
PIG + CPX + LIQ
OL + PIG + CPX + LIQ
OL + CPX + LIQ
TEMP °C
1350
1300
1250
1200
Moles
MgO 1 2 3 4 6 8 9 12
SiO_2 15 15 15 15 15 15 15 15
$3XO.R_2O_3.15ZO_2$
(C_3AS_{15})
10
20
30
40
WT %
YO (MgO)

Fig 6.39

Figure 6.40

See figure 6.39

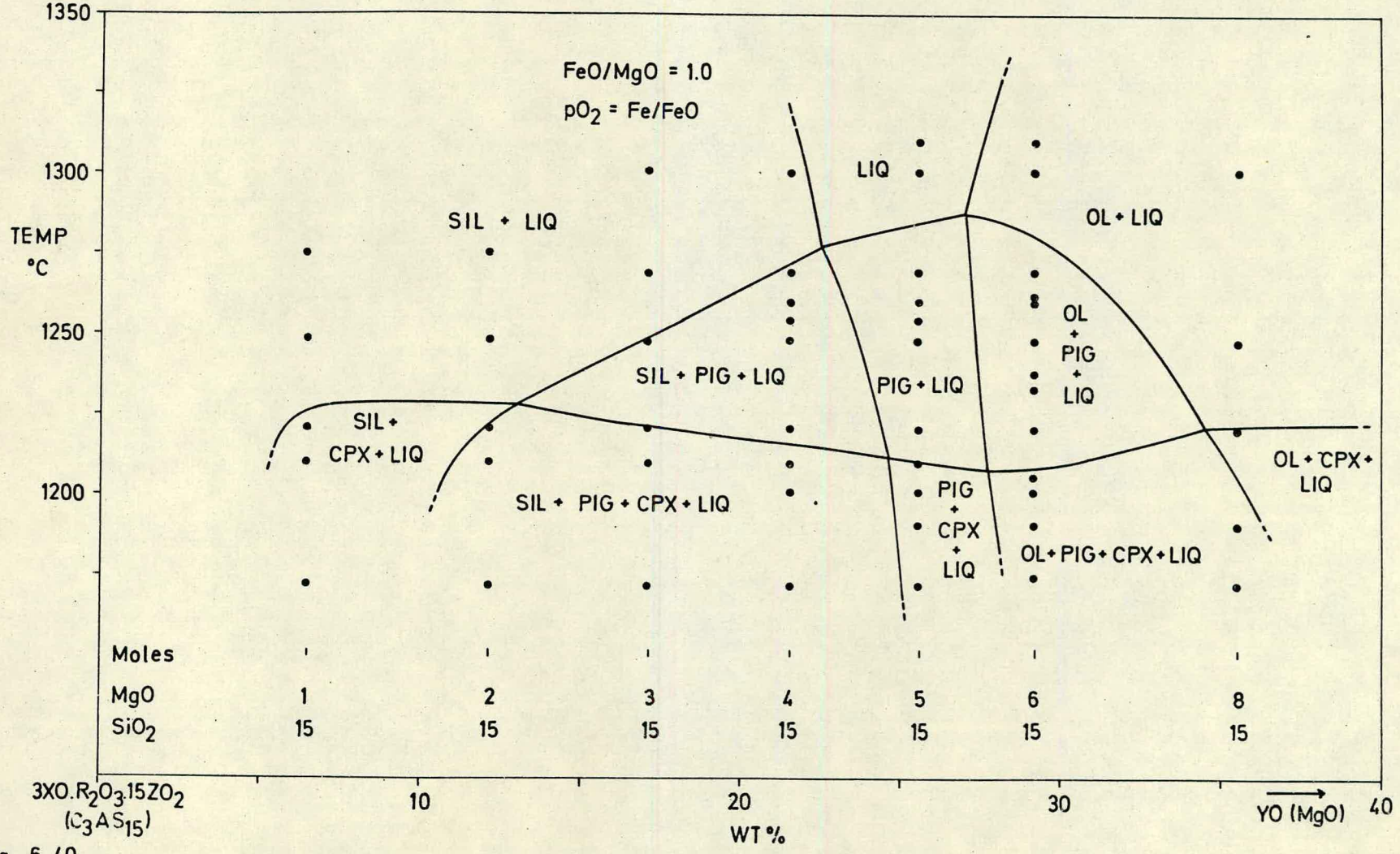
FeO/MgO = 1.0
pO_2 = Fe/FeO
LIQ
SIL + LIQ
OL + LIQ
SIL + PIG + LIQ
PIG + LIQ
OL + PIG + LIQ
SIL + CPX + LIQ
SIL + PIG + CPX + LIQ
PIG + CPX + LIQ
OL + CPX + LIQ
OL + PIG + CPX + LIQ
TEMP °C
1350
1300
1250
1200
Moles
MgO 1 2 3 4 5 6 8
SiO_2 15 15 15 15 15 15 15
$3XO.R_2O_3.15ZO_2$
(C_3AS_{15})
10
20
30
40
WT %
YO (MgO)

Fig 6.40

Figure 6.41

See figure 6.39

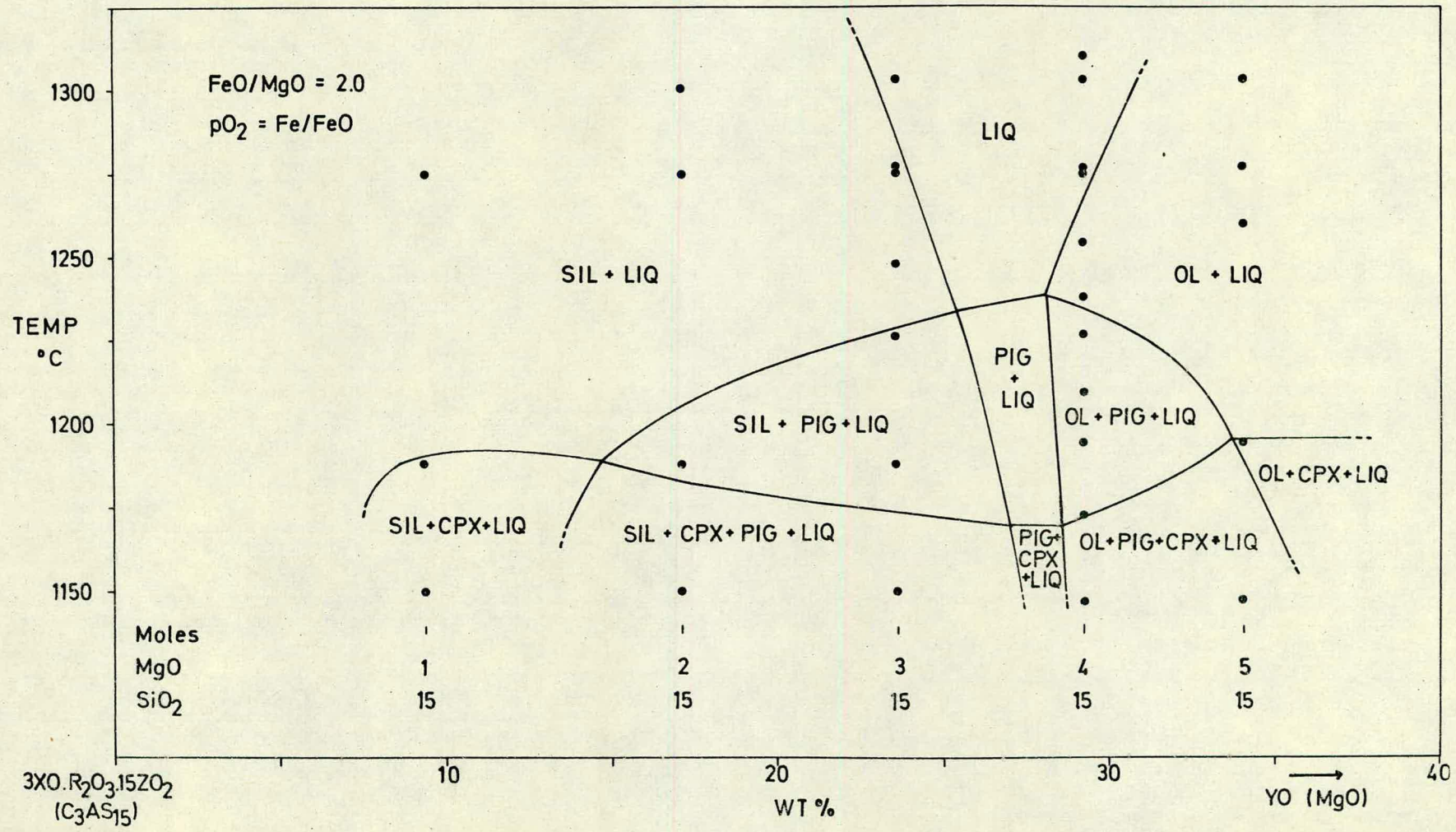
FeO/MgO = 2.0
pO_2 = Fe/FeO
LIQ
SIL + LIQ
OL + LIQ
PIG + LIQ
SIL + PIG + LIQ
OL + PIG + LIQ
OL+CPX+LIQ
SIL+CPX+LIQ
SIL + CPX + PIG + LIQ
PIG+ CPX +LIQ
OL+PIG+CPX+LIQ
TEMP °C
1300
1250
1200
1150
Moles MgO
Moles SiO_2
1
2
3
4
5
15
15
15
15
15
10
20
30
40
WT %
YO (MgO)
3XO.R_2O_3.15ZO_2
(C_3AS_{15})

Fig 6.41

Figure 6.42

Liquidus diagram for part of the join $3XO.R_2O_3.15ZO_2$-YO (C_3AS_{15}-M), to show the change in liquidus phase with changing FeO/MgO ratio for molecularly equivalent compositions, at the pO_2 of the Fe/FeO equilibrium. The compositions studied are shown by filled circles, the composition names can be found by referring to the individual T - X sections for this join (figures 6.39-6.41). The phase boundaries are indicated by thick solid lines, the dashed lines are the temperature contours, where known.

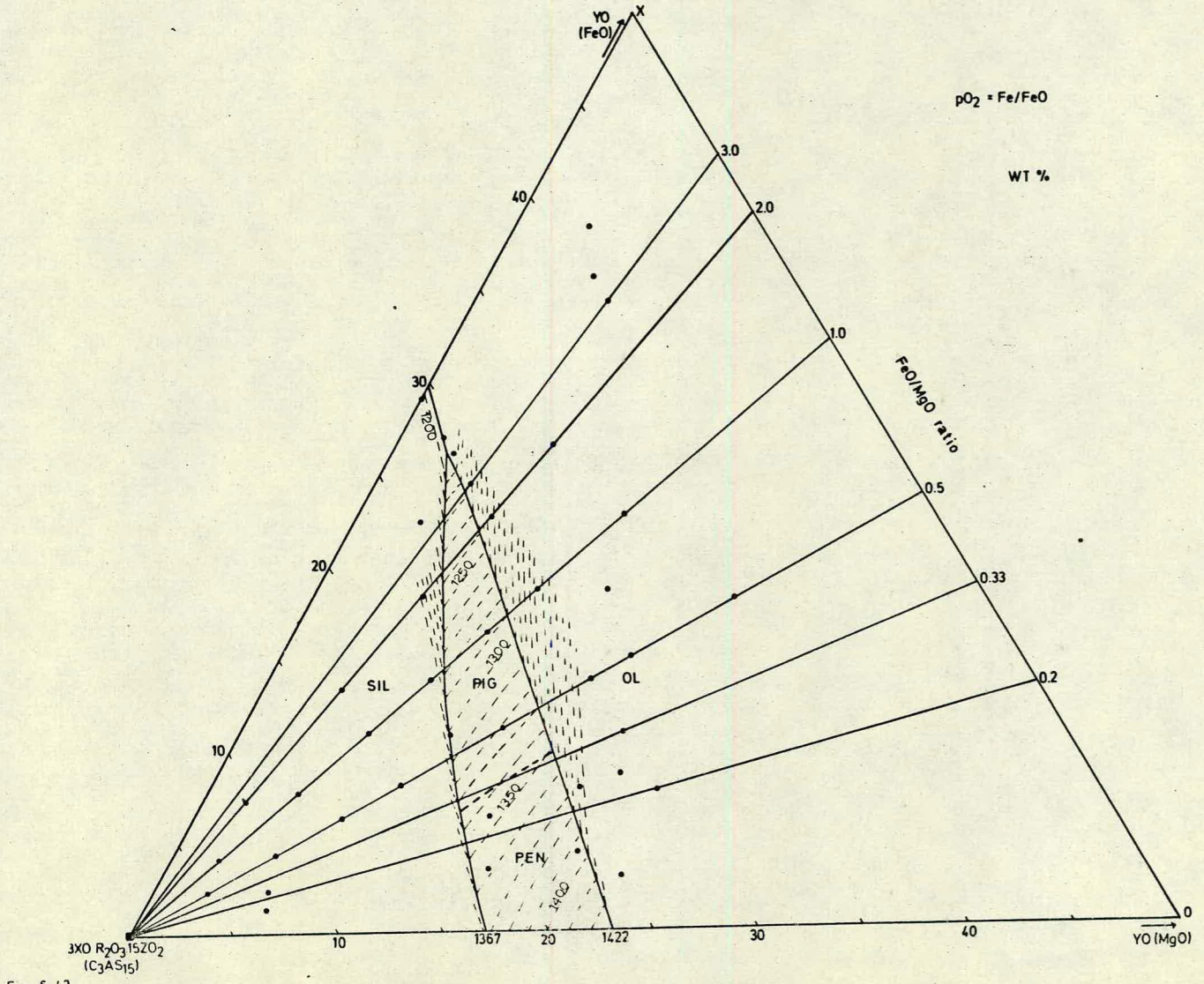
YO
(FeO)
X
pO_2 = Fe/FeO
WT %
3.0
2.0
1.0
0.5
0.33
0.2
0
FeO/MgO ratio
40
30
20
10
1200
1250
1300
1350
1400
SIL
PIG
OL
PEN
3XO R_2O_3 15ZO_2
(C_3AS_{15})
10
1367
20
1422
30
40
YO (MgO)

Fig 6.42

Figure 6.43

Diagram to show the change in second phase to crystallise for molecularly equivalent compositions in part of the join $3XO.R_2O_3.15ZO_2$-YO (C_3AS_{15}-M), with changing FeO/MgO ratio, at the pO_2 of the Fe/FeO equilibrium. The compositions studied are shown by filled circles, the composition names can be found by referring to the individual T - X sections for this join (figures 6.39-6.41). The liquidus phase boundaries are indicated by thick solid lines, the projected phase boundaries within each phase volume are indicated by thin solid lines. The phase assemblage for each area is indicated. The dashed lines are the temperature contours for the appearance of the second phase in each composition in this part of the join, where known.

The thick dashed line marks the approximate maximum extent of pen occurrence in this join. The dash-dot line marks the area in which pen does not react with the liquid, pig therefore not occurring.

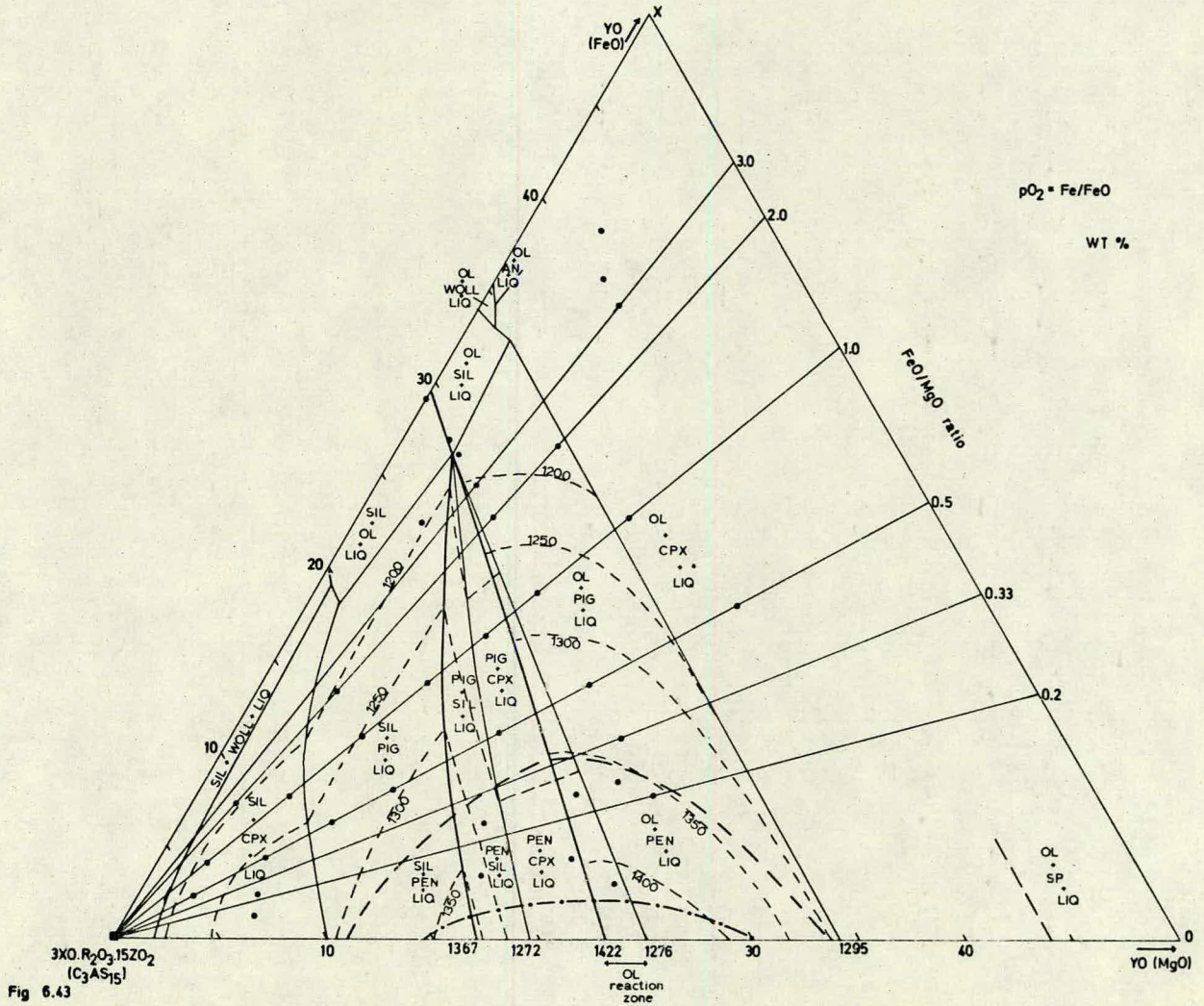
YO (FeO)
X
3.0
2.0
1.0
0.5
0.33
0.2
0
40
30
20
10
pO_2 = Fe/FeO
WT %
FeO/MgO ratio
OL + WOLL + LIQ
OL + AN + LIQ
OL + SIL + LIQ
SIL + OL + LIQ
OL + CPX + LIQ
OL + PIG + LIQ
PIG + CPX + LIQ
PIG + SIL + LIQ
SIL + PIG + LIQ
SIL + CPX + LIQ
OL + PEN + LIQ
PEN + CPX + LIQ
PEN + SIL + LIQ
SIL + PEN + LIQ
OL + SP + LIQ
1200
1250
1300
1350
1400
1450
1500
3XO.R_2O_3.15ZO_2
(C_3AS_{15})
10
1367
1272
1422
1276
30
1295
40
YO (MgO)
OL reaction zone

Fig 6.43

Figures 6.44 to 6.48

Liquidus diagrams for part of the plane $XO.ZO_2$-$YO.ZO_2$-R_2O_3 (CS-MS-A) at FeO/MgO mole ratios of 0.5, 1.0, 2.0, 3.0, and X (MgO-free), and the pO_2 of the Fe/FeO equilibrium. The diagrams show the relationship between the joins $XO.YO.2ZO_2$-$YO.R_2O_3.ZO_2$ (Diopside-MAS), $XO.YO.2ZO_2$-$5YO.3R_2O_3.5ZO_2$ (Diopside-$M_5A_3S_5$), and $YO.ZO_2$-$3XO.R_2O_3.3ZO_2$ (Enstatite-Grossular) studied here, and the join $YO.ZO_2$-$XO.R_2O_3.2ZO_2$:$2YO.ZO_2$ (Enstatite-Anorthite Forsterite piercing point) from Roeder and Osborn (1966), presented as figure 6.17 for these pO_2. The compositions studied are shown by filled circles, the composition name can be found by referring to the T - X sections for the join in question. The phase boundaries are indicated by thick solid lines, the dashed lines are the temperature contours where known.

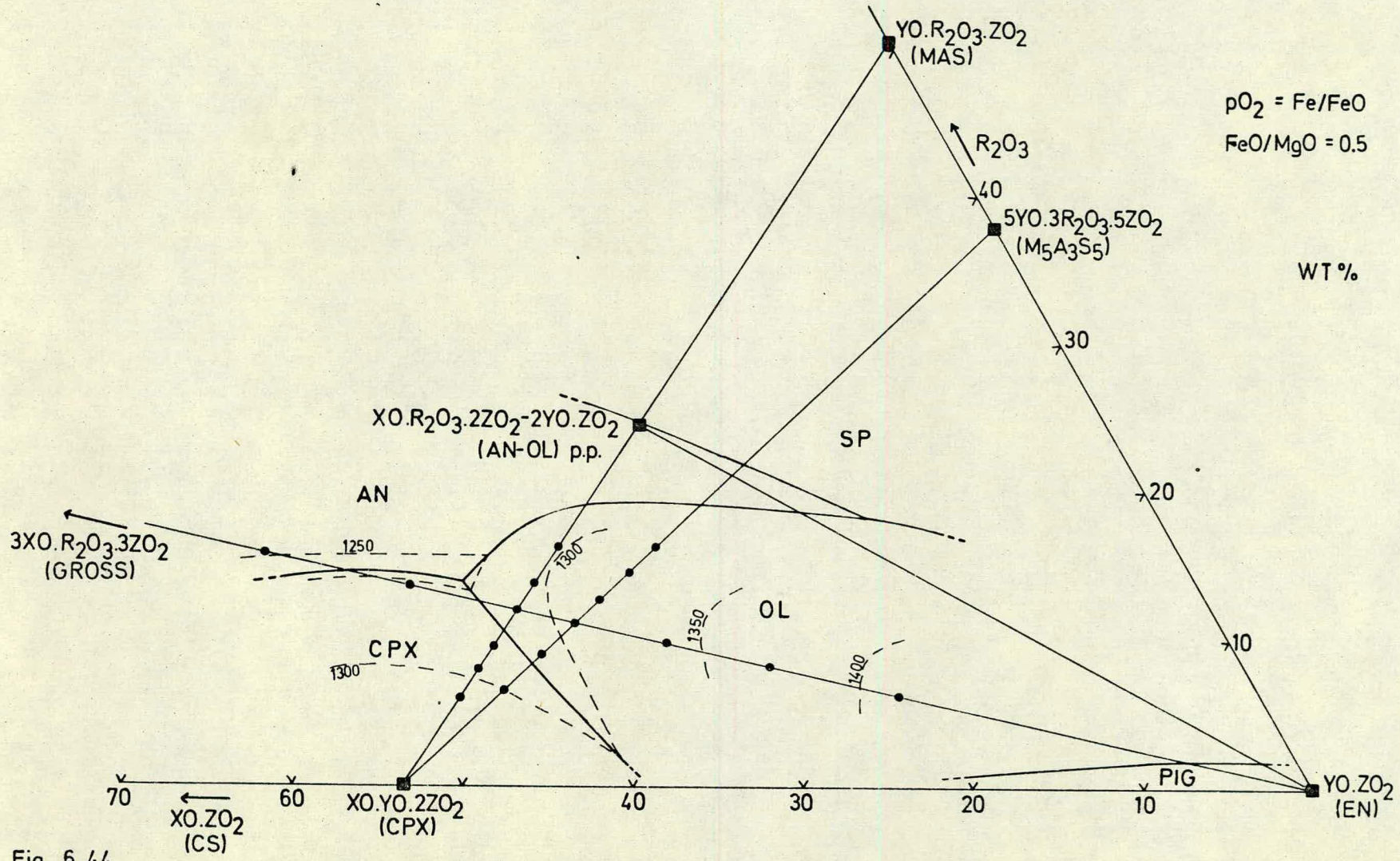
YO.R2O3.ZO2
(MAS)
pO2 = Fe/FeO
FeO/MgO = 0.5
R2O3
40
5YO.3R2O3.5ZO2
(M5A3S5)
WT %
30
XO.R2O3.2ZO2-2YO.ZO2
(AN-OL) p.p.
SP
20
AN
3XO.R2O3.3ZO2
(GROSS)
1250
1300
1350
OL
CPX
1300
1400
10
PIG
70
60
XO.ZO2
(CS)
XO.YO.2ZO2
(CPX)
40
30
20
10
YO.ZO2
(EN)

Fig 6.44

Figure 6.45

See figure 6.44

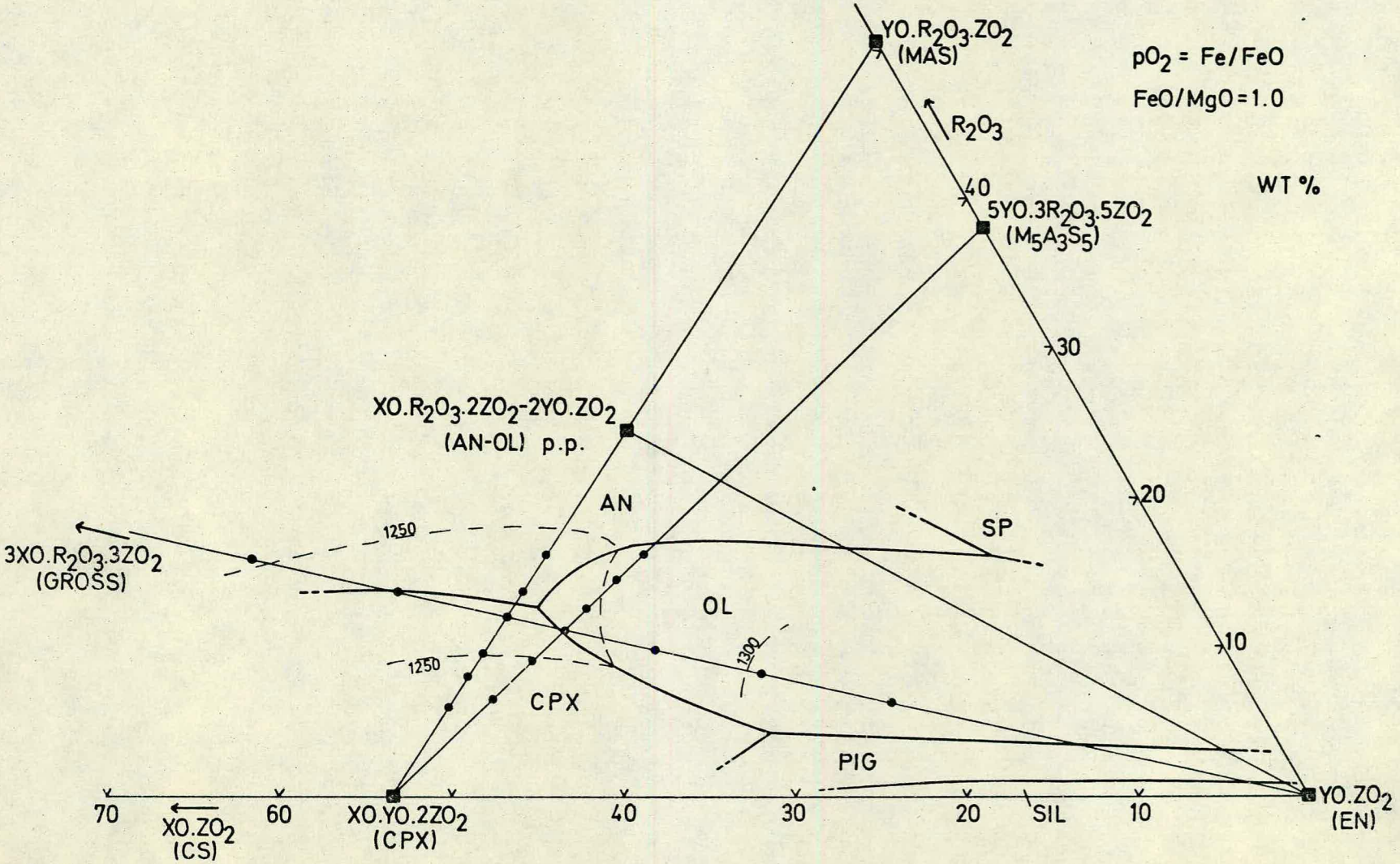
YO.R2O3.ZO2
(MAS)
pO2 = Fe/FeO
FeO/MgO=1.0
R2O3
WT %
40
5YO.3R2O3.5ZO2
(M5A3S5)
30
XO.R2O3.2ZO2-2YO.ZO2
(AN-OL) p.p.
AN
20
SP
1250
3XO.R2O3.3ZO2
(GROSS)
OL
10
1300
1250
CPX
PIG
70
60
XO.YO.2ZO2
(CPX)
40
30
20
SIL
10
YO.ZO2
(EN)
XO.ZO2
(CS)

Fig 6.45

Figure 6.46

See figure 6.44

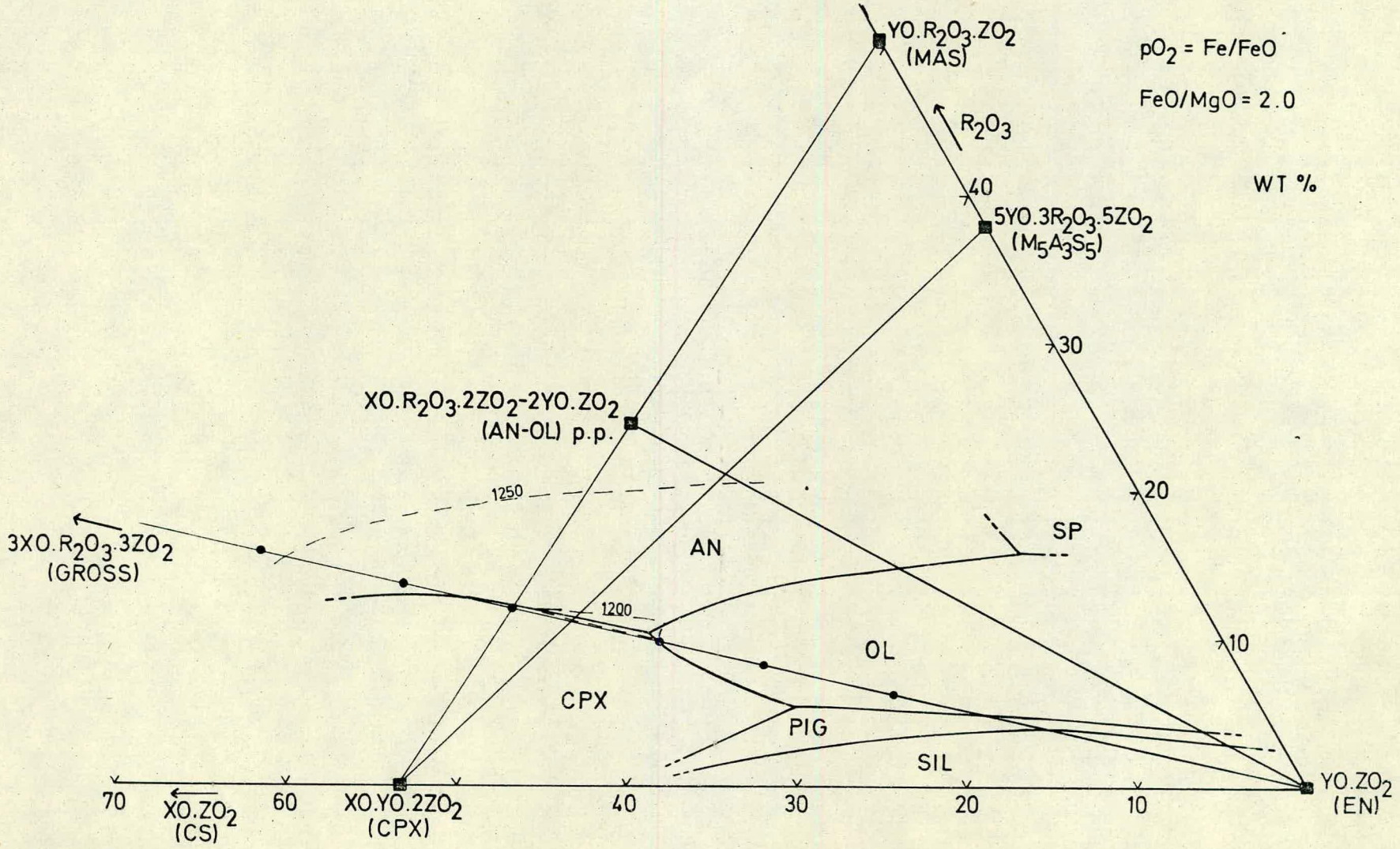
YO.R2O3.ZO2
(MAS)
pO2 = Fe/FeO
FeO/MgO = 2.0
R2O3
WT %
40
5YO.3R2O3.5ZO2
(M5A3S5)
30
XO.R2O3.2ZO2-2YO.ZO2
(AN-OL) p.p.
20
1250
SP
3XO.R2O3.3ZO2
(GROSS)
AN
1200
10
OL
CPX
PIG
SIL
70
XO.ZO2
(CS)
60
XO.YO.2ZO2
(CPX)
40
30
20
10
YO.ZO2
(EN)

Fig 6.46

Figure 6.47

See figure 6.44

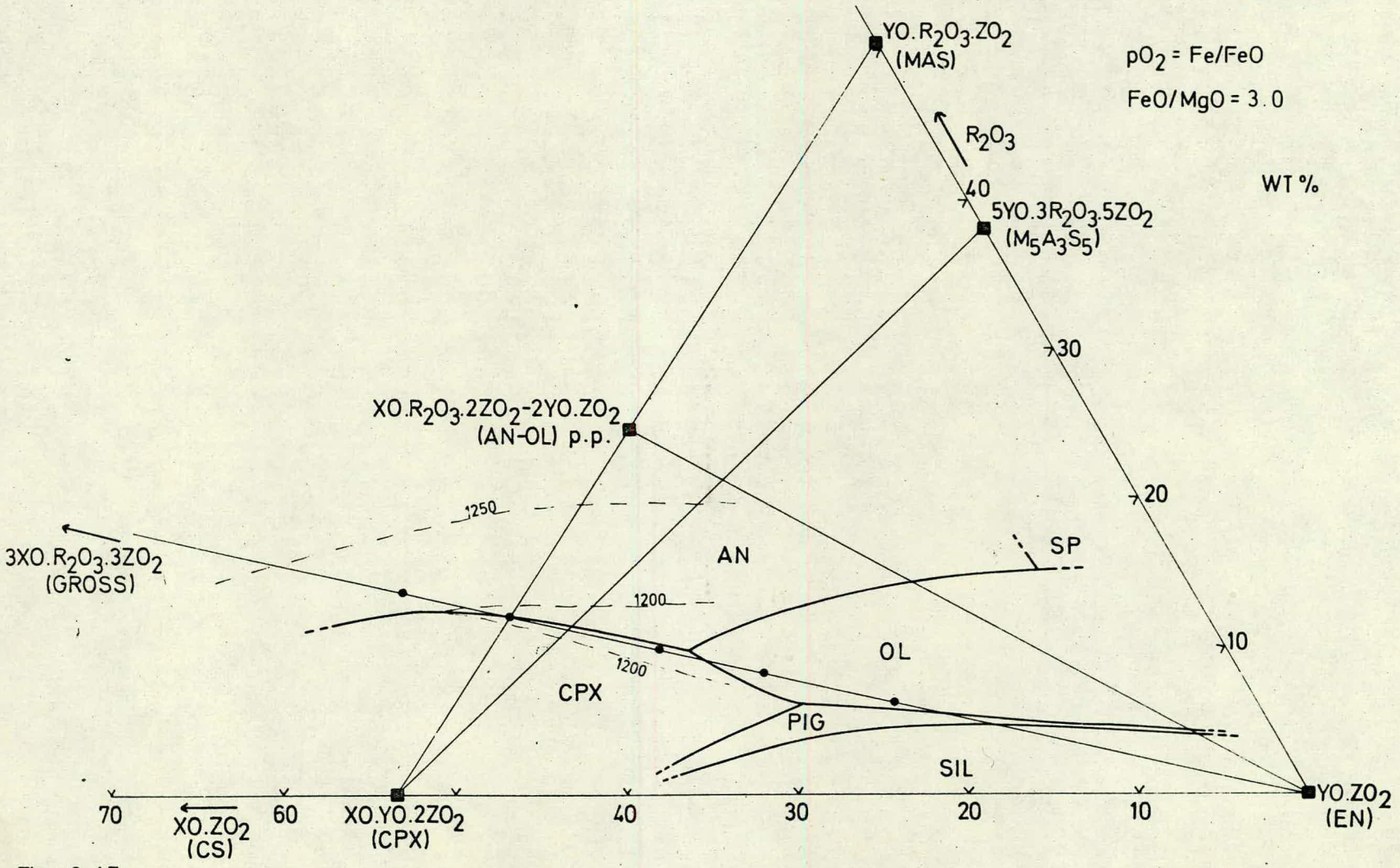
YO.R2O3.ZO2
(MAS)
pO2 = Fe/FeO
FeO/MgO = 3.0
R2O3
WT %
40
5YO.3R2O3.5ZO2
(M5A3S5)
30
XO.R2O3.2ZO2-2YO.ZO2
(AN-OL) p.p.
20
1250
3XO.R2O3.3ZO2
(GROSS)
AN
SP
1200
10
OL
1200
CPX
PIG
SIL
70
XO.ZO2
(CS)
60
XO.YO.2ZO2
(CPX)
40
30
20
10
YO.ZO2
(EN)

Fig 6.47

Figure 6.48

See figure 6.44

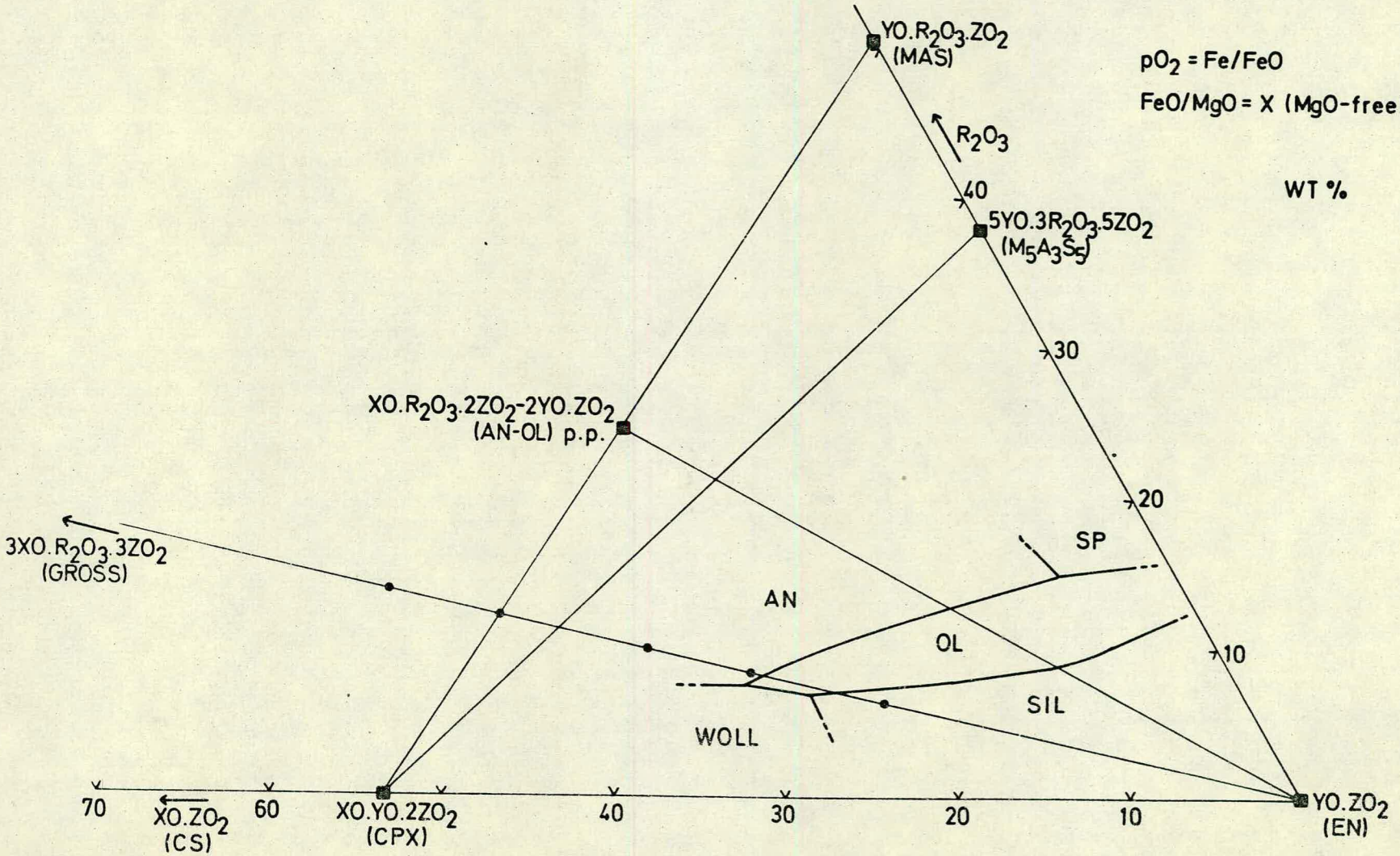
YO.R2O3.ZO2
(MAS)
pO2 = Fe/FeO
FeO/MgO = X (MgO-free)
R2O3
WT %
40
5YO.3R2O3.5ZO2
(M5A3S5)
30
XO.R2O3.2ZO2-2YO.ZO2
(AN-OL) p.p.
20
3XO.R2O3.3ZO2
(GROSS)
SP
AN
OL
10
SIL
WOLL
70
XO.ZO2
(CS)
60
XO.YO.2ZO2
(CPX)
40
30
20
10
YO.ZO2
(EN)

Fig 6.48

Figures 6.49 to 6.53

Liquidus diagrams for part of the plane $3XO.R_2O_3$-YO-ZO_2 (C_3A-M-S) at FeO/MgO mole ratios of 0.5, 1.0, 2.0, 3.0, and X (MgO-free), and the pO_2 of the Fe/FeO equilibrium. The diagrams show the relationship between the joins $YO.ZO_2$-$3XO.R_2O_3.3ZO_2$ (Enstatite-Grossular) and $3XO.R_2O_3.15ZO_2$-YO (C_3AS_{15}-M) studied here, and the join YO-ZO_2 (M-S) at these pO_2 (figure 6.4). The compositions studied are shown by filled circles, the composition name can be found by referring to the T - X sections for the join in question. The phase boundaries are indicated by thick solid lines, the dashed lines are the temperature contours where known.

The piercing point labelled AD p.p. is the piercing point of the join $XO.R_2O_3.2ZO_2$-$XO.YO.2ZO_2$ (Anorthite-Diopside) in this plane.

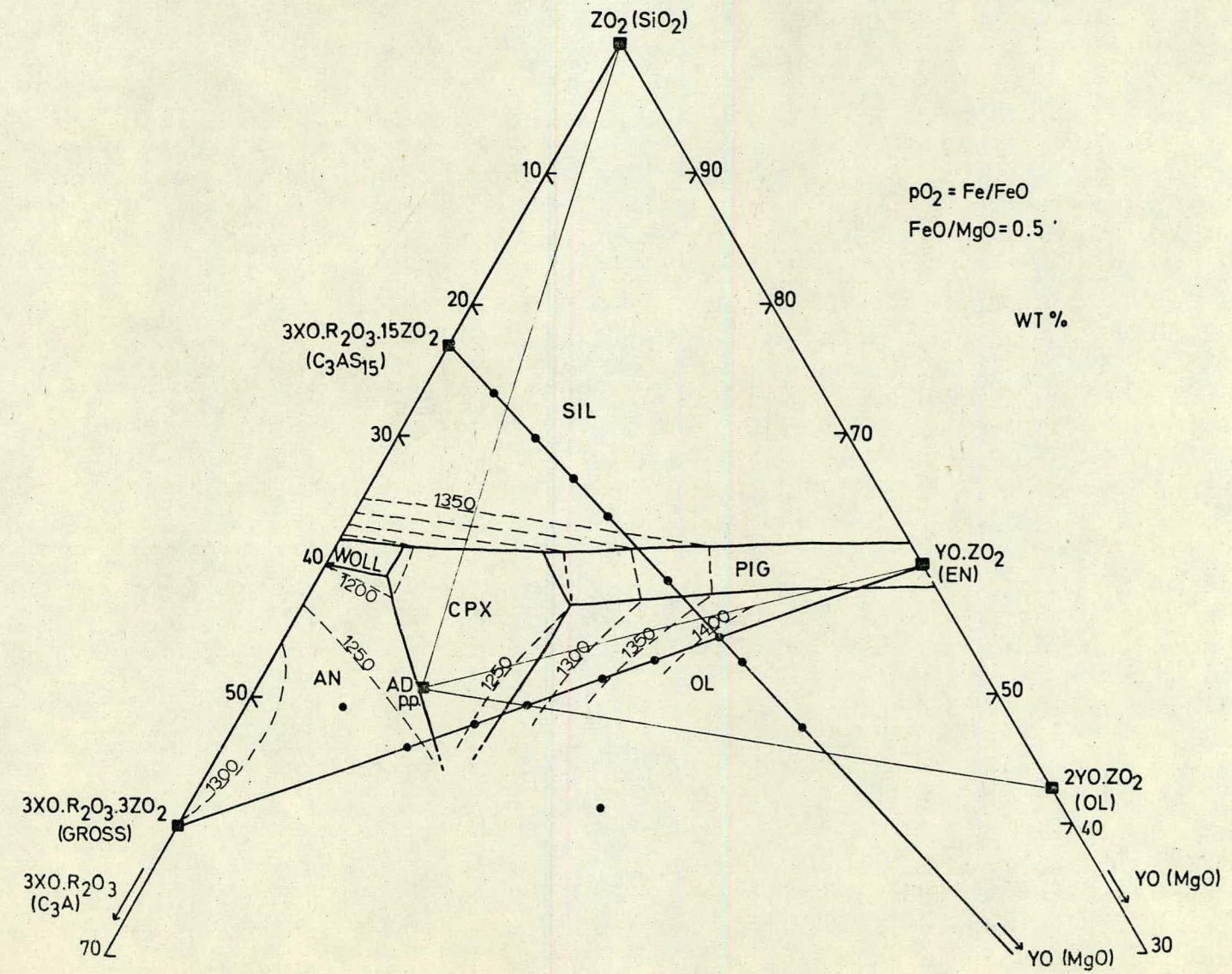
ZO_2 (SiO_2)
10
90
20
80
30
70
40
50
50
70
$3XO.R_2O_3.15ZO_2$
(C_3AS_{15})
$3XO.R_2O_3.3ZO_2$
(GROSS)
$3XO.R_2O_3$
(C_3A)
$YO.ZO_2$
(EN)
$2YO.ZO_2$
(OL)
40
30
YO (MgO)
YO (MgO)
WOLL
PIG
CPX
AN
AD
pp
OL
SIL
1350
1200
1250
1300
1250
1300
1350
1400
pO_2 = Fe/FeO
FeO/MgO = 0.5
WT %

Fig 6.49

Figure 6.50

See figure 6.49

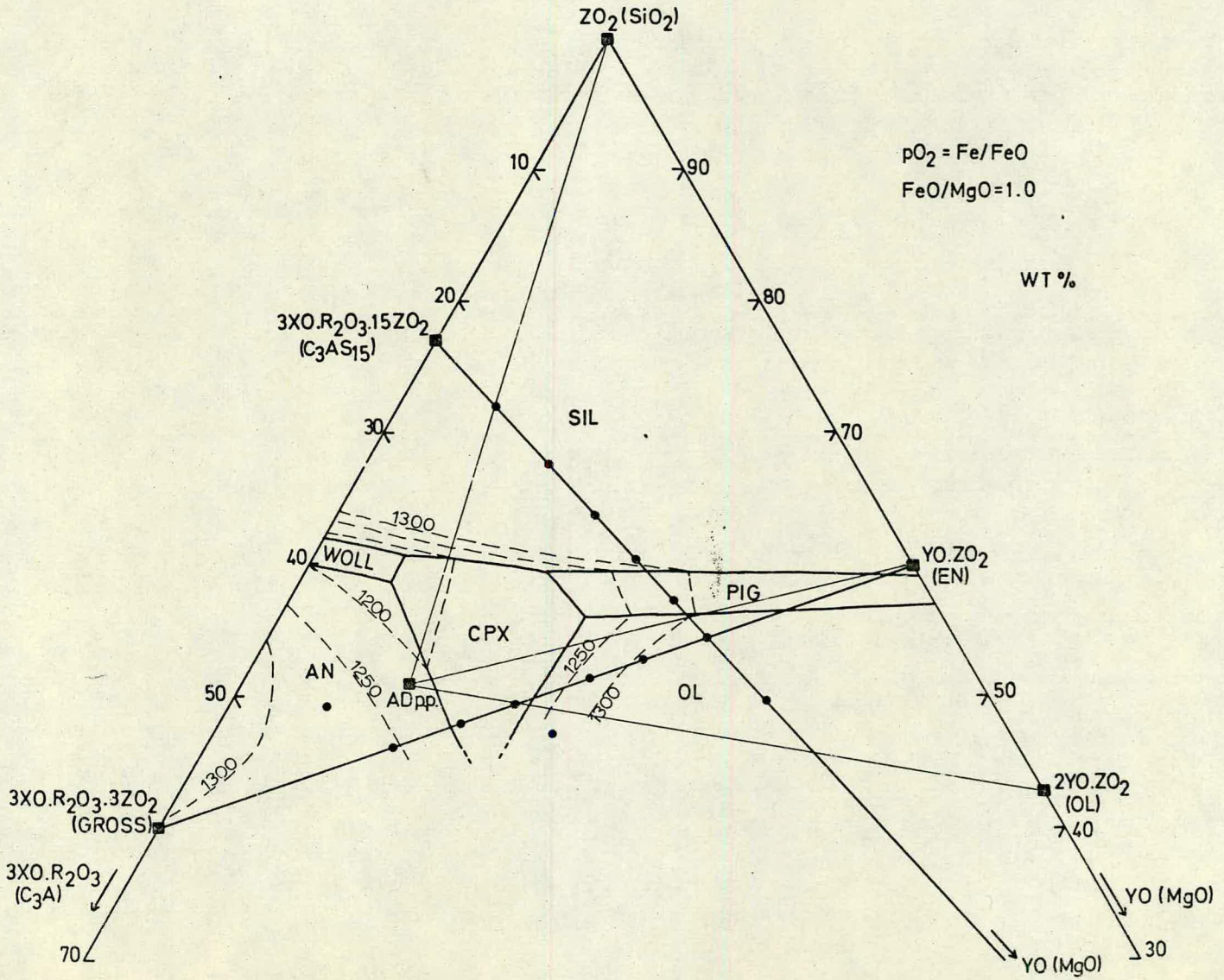
ZO_2 (SiO_2)
pO_2 = Fe/FeO
FeO/MgO=1.0
WT %
10
90
20
80
$3XO.R_2O_3.15ZO_2$
(C_3AS_{15})
30
SIL
70
1300
40
WOLL
$YO.ZO_2$
(EN)
1200
PIG
CPX
AN
1250
1250
50
ADpp.
OL
50
1300
1300
$3XO.R_2O_3.3ZO_2$
(GROSS)
$2YO.ZO_2$
(OL)
40
$3XO.R_2O_3$
(C_3A)
YO (MgO)
70
YO (MgO)
30

Fig 6.50

Figure 6.51

See figure 6.49

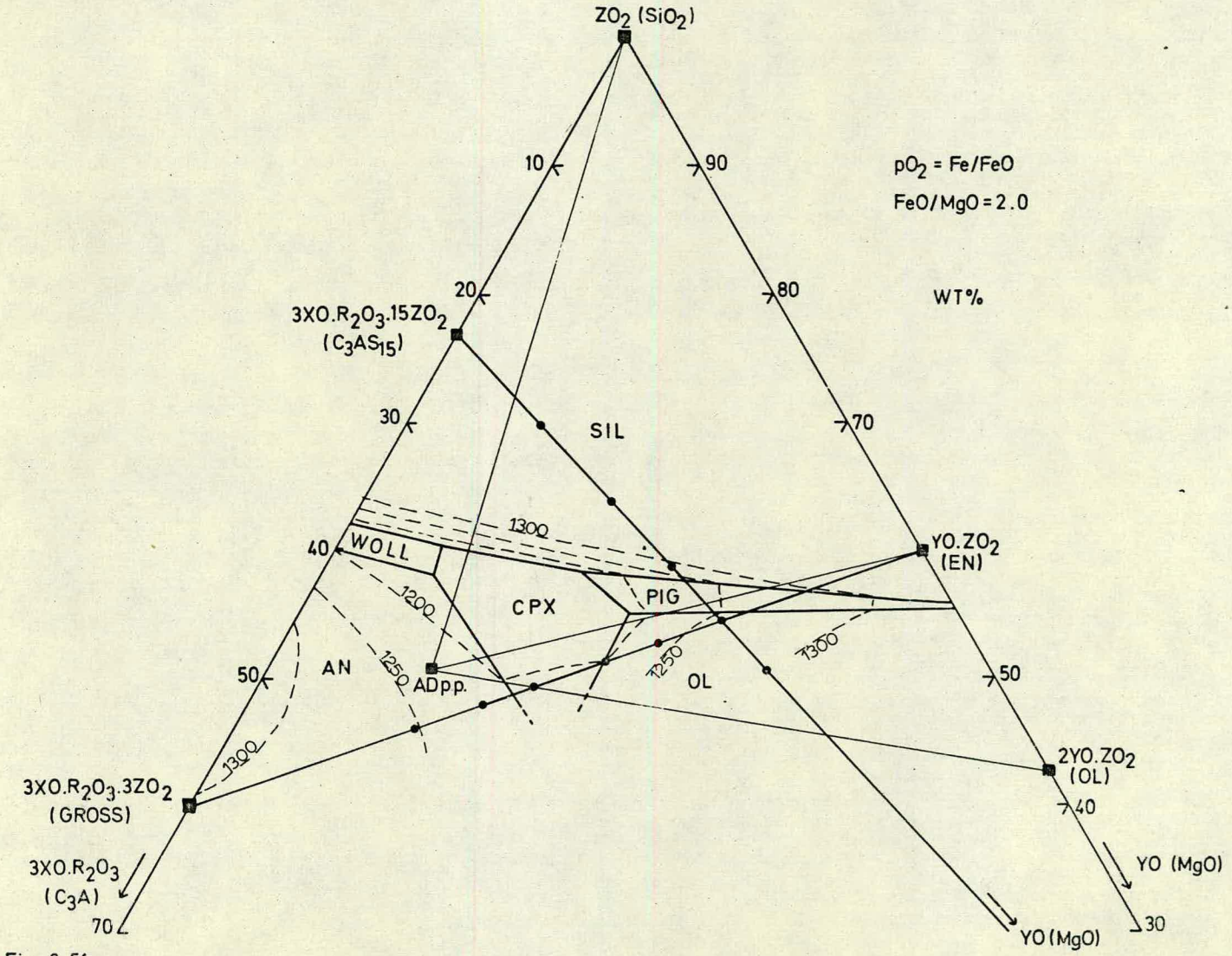
ZO2 (SiO2)
pO2 = Fe/FeO
FeO/MgO = 2.0
WT%
10
90
20
80
3XO.R2O3.15ZO2
(C3AS15)
30
70
SIL
1300
40
WOLL
YO.ZO2
(EN)
1200
CPX
PIG
1300
50
AN
1250
ADpp.
1250
OL
50
1300
2YO.ZO2
(OL)
40
3XO.R2O3.3ZO2
(GROSS)
3XO.R2O3
(C3A)
70
YO (MgO)
YO (MgO)
30

Fig 6.51

Figure 6.52

See figure 6.49

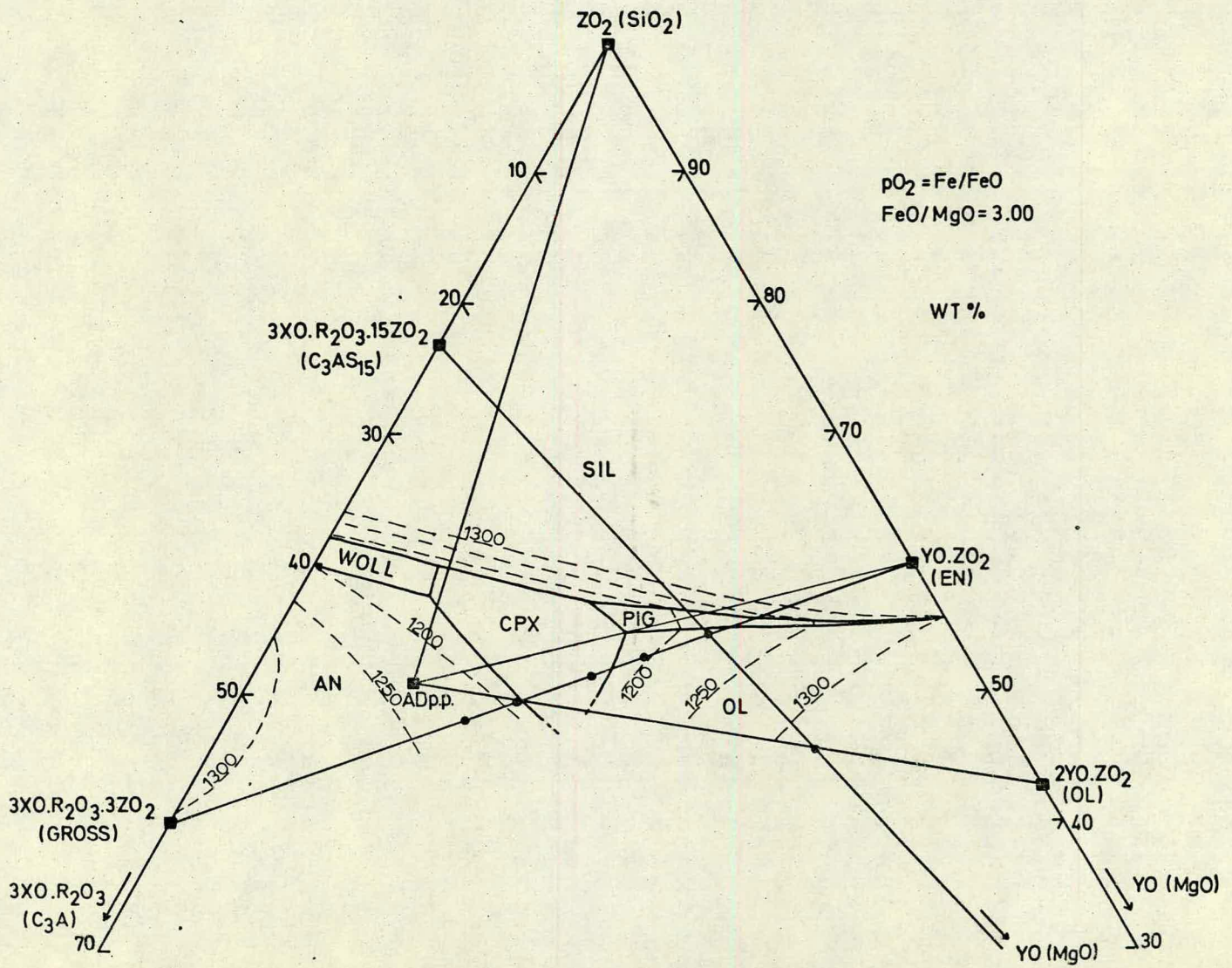
ZO2 (SiO2)
10
90
pO2 = Fe/FeO
FeO/MgO = 3.00
20
80
WT %
3XO.R2O3.15ZO2
(C3AS15)
30
70
SIL
1300
40
WOLL
YO.ZO2
(EN)
CPX
PIG
1200
50
AN
1250
ADpp.
1200
1250
OL
1300
50
1300
2YO.ZO2
(OL)
40
3XO.R2O3.3ZO2
(GROSS)
YO (MgO)
3XO.R2O3
(C3A)
70
YO (MgO)
30

Fig 6.52

Figure 6.53

See figure 6.49

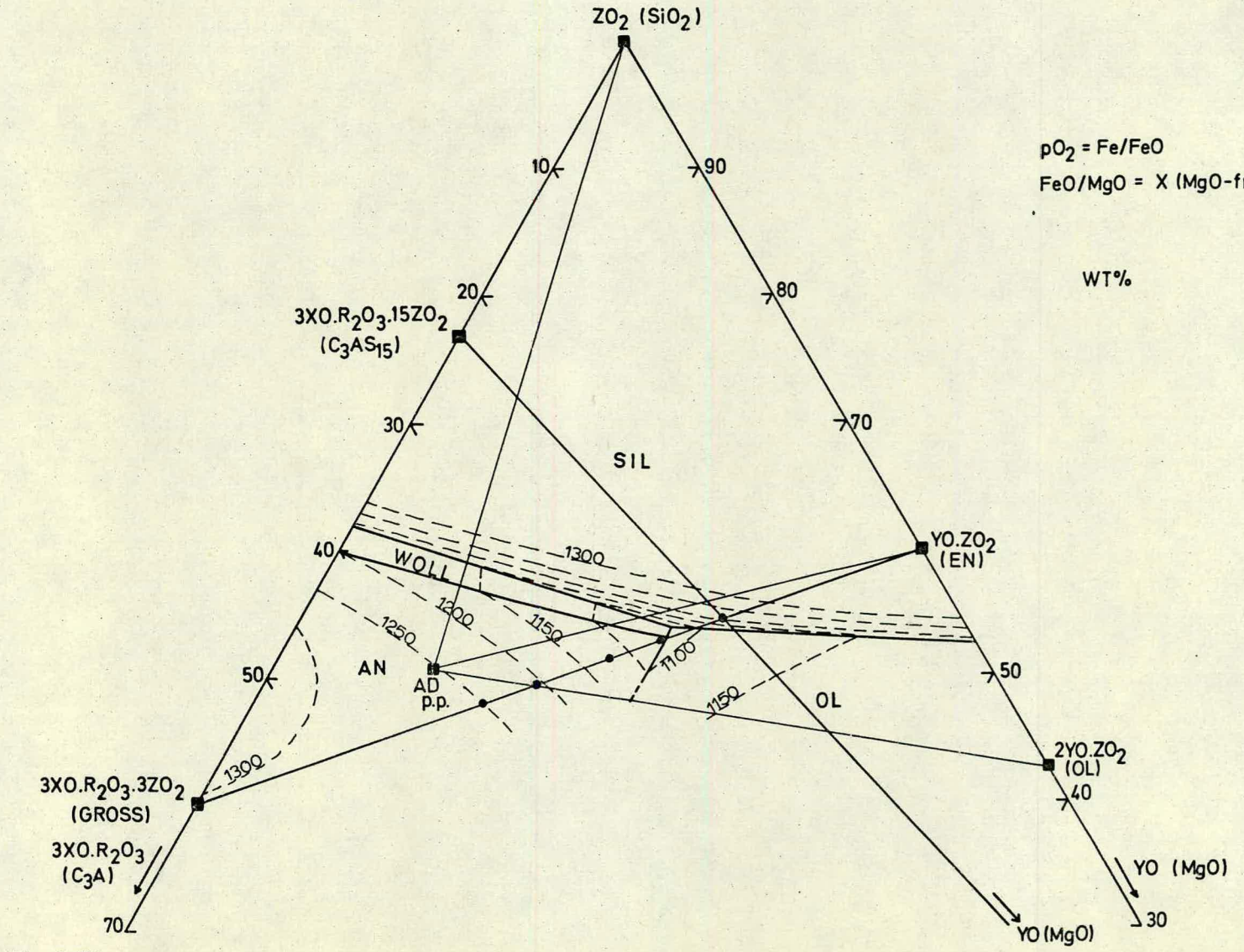
ZO_2 (SiO_2)
pO_2 = Fe/FeO
FeO/MgO = X (MgO-free)
WT%
10
90
20
80
$3XO.R_2O_3.15ZO_2$
(C_3AS_{15})
30
70
SIL
40
WOLL
1300
1200
1250
1150
1100
$YO.ZO_2$
(EN)
50
AN
AD
p.p.
OL
1150
50
1300
$2YO.ZO_2$
(OL)
40
$3XO.R_2O_3.3ZO_2$
(GROSS)
$3XO.R_2O_3$
(C_3A)
YO (MgO)
70
30
YO (MgO)

Fig 6.53

Figures 6.54 to 6.58

Projections from $2YO.ZO_2$ (olivine) into part of the plane $XO.ZO_2$-$YO.ZO_2$-R_2O_3 (CS-MS-A) of the bounding surface of the olivine volume at the FeO/MgO mole ratios 0.5, 1.0, 2.0, 3.0, and X (MgO-free) and the pO_2 of the Fe/FeO equilibrium, for those compositions lying in the plane $XO.ZO_2$-$YO.ZO_2$-R_2O_3 (CS-MS-A). Data from the joins $XO.YO.2ZO_2$-$YO.R_2O_3.ZO_2$ (Diopside-MAS), $XO.YO.2ZO_2$-$5YO.3R_2O_3.5ZO_2$ (Diopside-$M_5A_3S_5$) and $YO.ZO_2$-$3XO.R_2O_3.3ZO_2$ (Enstatite-Grossular) studied here were utilised, and from $YO.ZO_2$-$XO.R_2O_3.2ZO_2$: $2YO.ZO_2$ (Enstatite-AnorthiteForsterite piercing point) from Roeder and Osborn (1966), presented as figure 6.19 for these pO_2. The projection boundaries are shown by thick solid lines, the dashed lines are temperature contours, where known. The projection boundaries are continued outside the olivine phase volume in this plane, to obtain an impression of the projected positions of the equilibria.

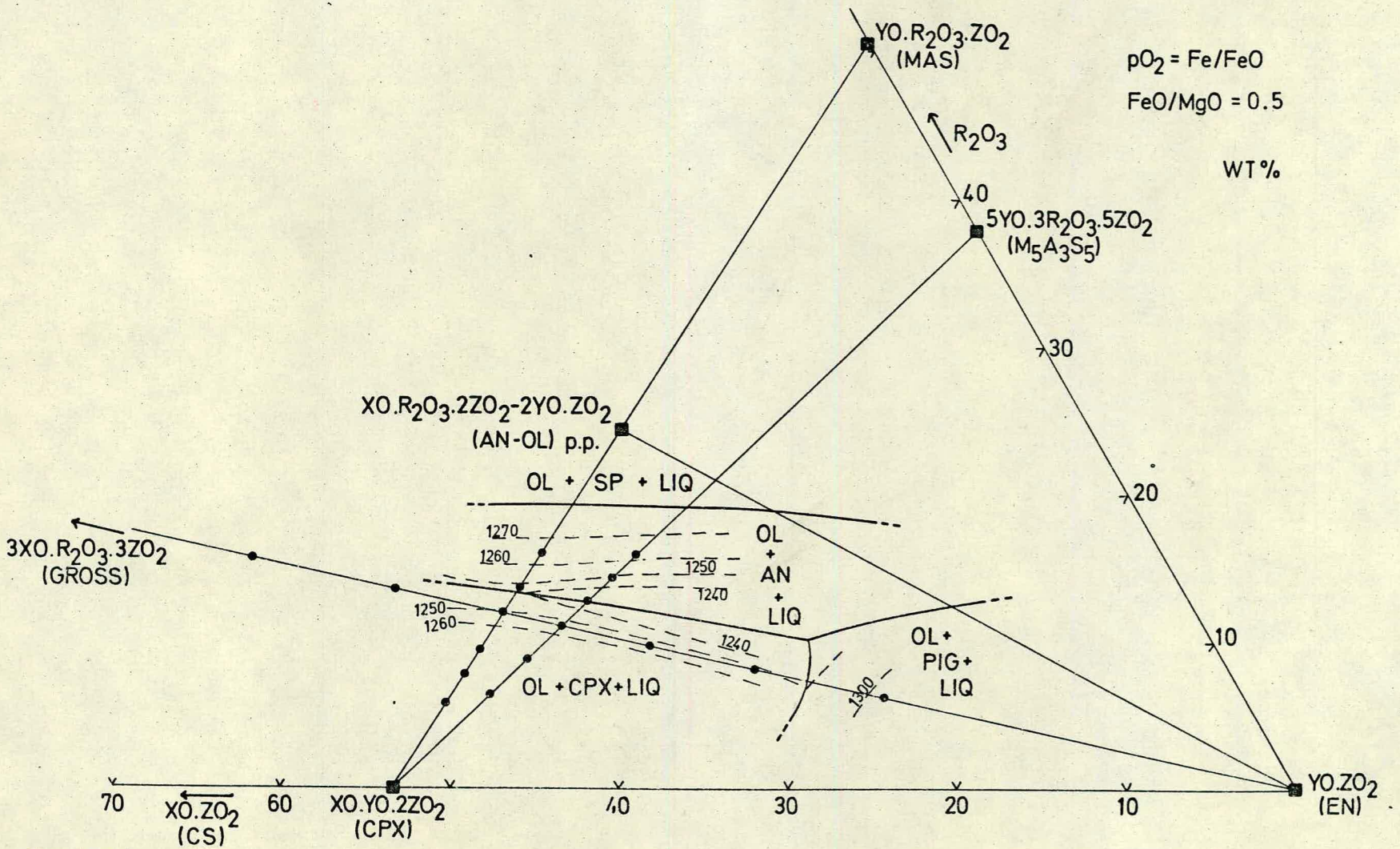
YO.R2O3.ZO2
(MAS)
pO2 = Fe/FeO
FeO/MgO = 0.5
WT%
R2O3
40
5YO.3R2O3.5ZO2
(M5A3S5)
30
XO.R2O3.2ZO2-2YO.ZO2
(AN-OL) p.p.
20
OL + SP + LIQ
3XO.R2O3.3ZO2
(GROSS)
1270
1260
OL
+
AN
+
LIQ
1250
1240
1250
1260
1240
10
OL +
PIG +
LIQ
OL + CPX + LIQ
1300
70
XO.ZO2
(CS)
60
XO.YO.2ZO2
(CPX)
40
30
20
10
YO.ZO2
(EN)

Fig 6.54

Figure 6.55

See figure 6.54

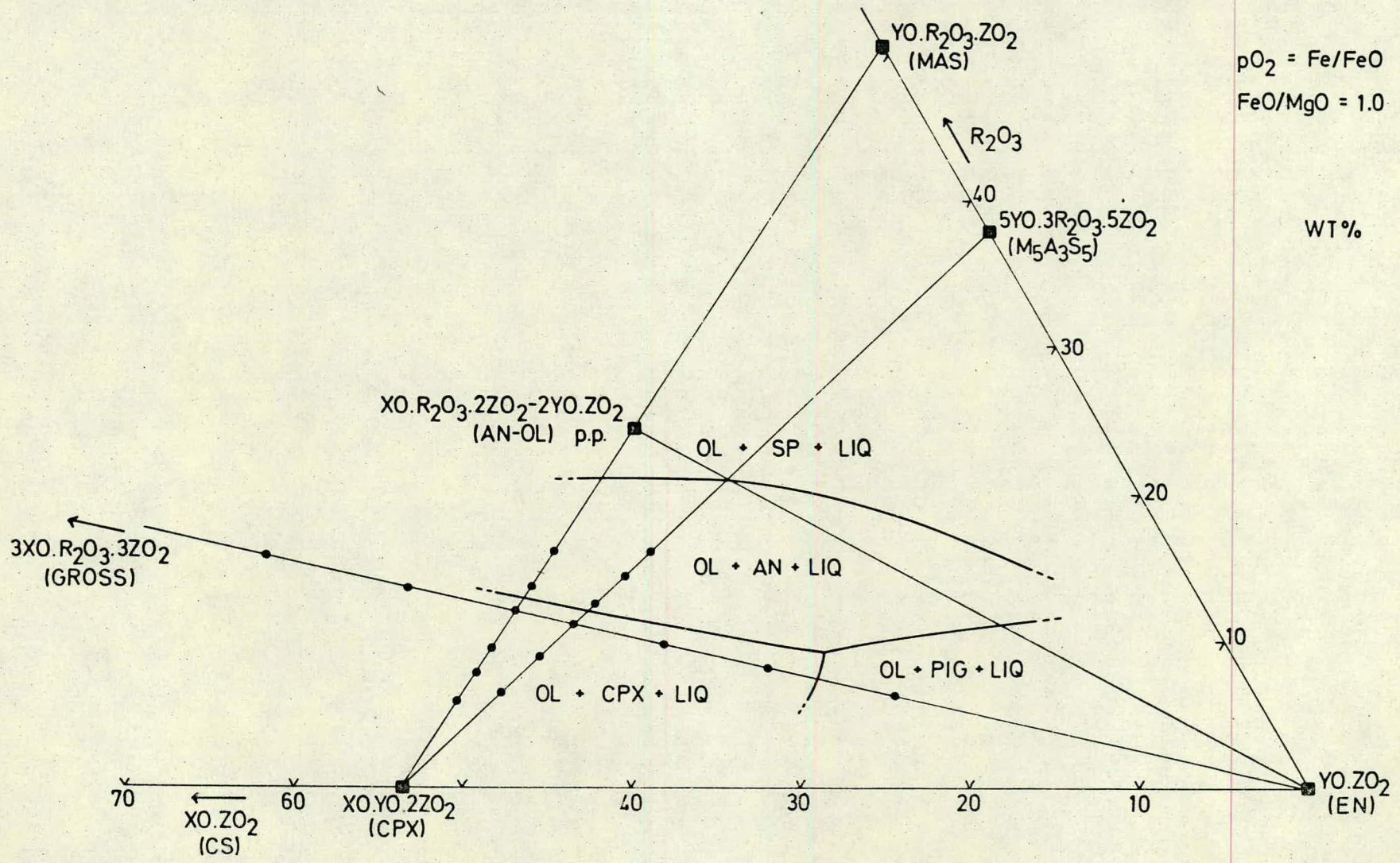
YO.R2O3.ZO2
(MAS)
pO2 = Fe/FeO
FeO/MgO = 1.0
R2O3
40
5YO.3R2O3.5ZO2
(M5A3S5)
WT%
30
XO.R2O3.2ZO2-2YO.ZO2
(AN-OL) p.p.
OL + SP + LIQ
20
3XO.R2O3.3ZO2
(GROSS)
OL + AN + LIQ
10
OL + PIG + LIQ
OL + CPX + LIQ
70
60
XO.YO.2ZO2
(CPX)
40
30
20
10
YO.ZO2
(EN)
XO.ZO2
(CS)

Fig 6.55

Figure 6.56

See figure 6.54

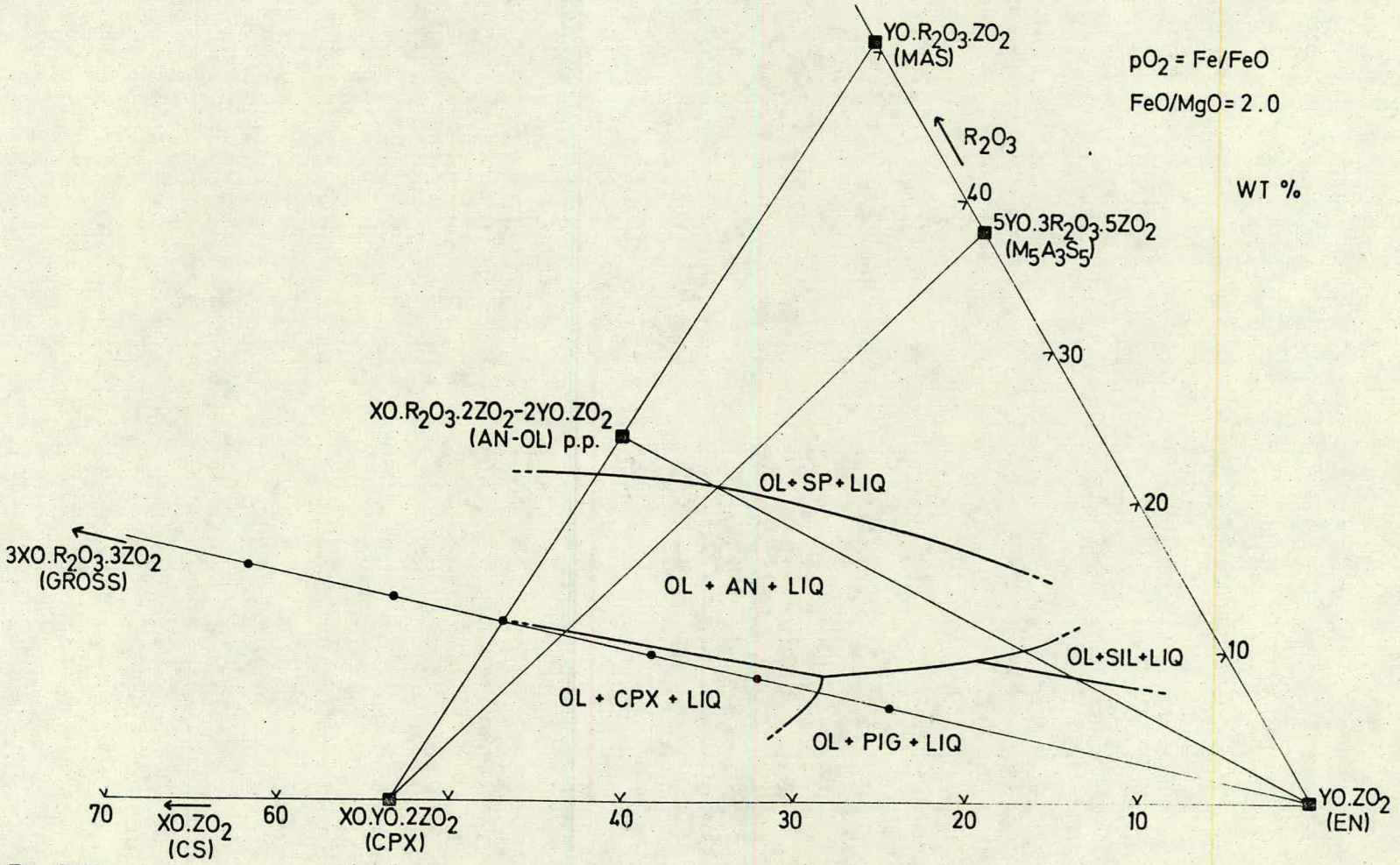
YO.R2O3.ZO2
(MAS)
pO2 = Fe/FeO
FeO/MgO= 2.0
R2O3
WT %
40
5YO.3R2O3.5ZO2
(M5A3S5)
30
XO.R2O3.2ZO2-2YO.ZO2
(AN-OL) p.p.
OL+SP+LIQ
20
3XO.R2O3.3ZO2
(GROSS)
OL + AN + LIQ
OL+SIL+LIQ
10
OL + CPX + LIQ
OL + PIG + LIQ
70
XO.ZO2
(CS)
60
XO.YO.2ZO2
(CPX)
40
30
20
10
YO.ZO2
(EN)

Fig 6.56

Figure 6.57

See figure 6.54

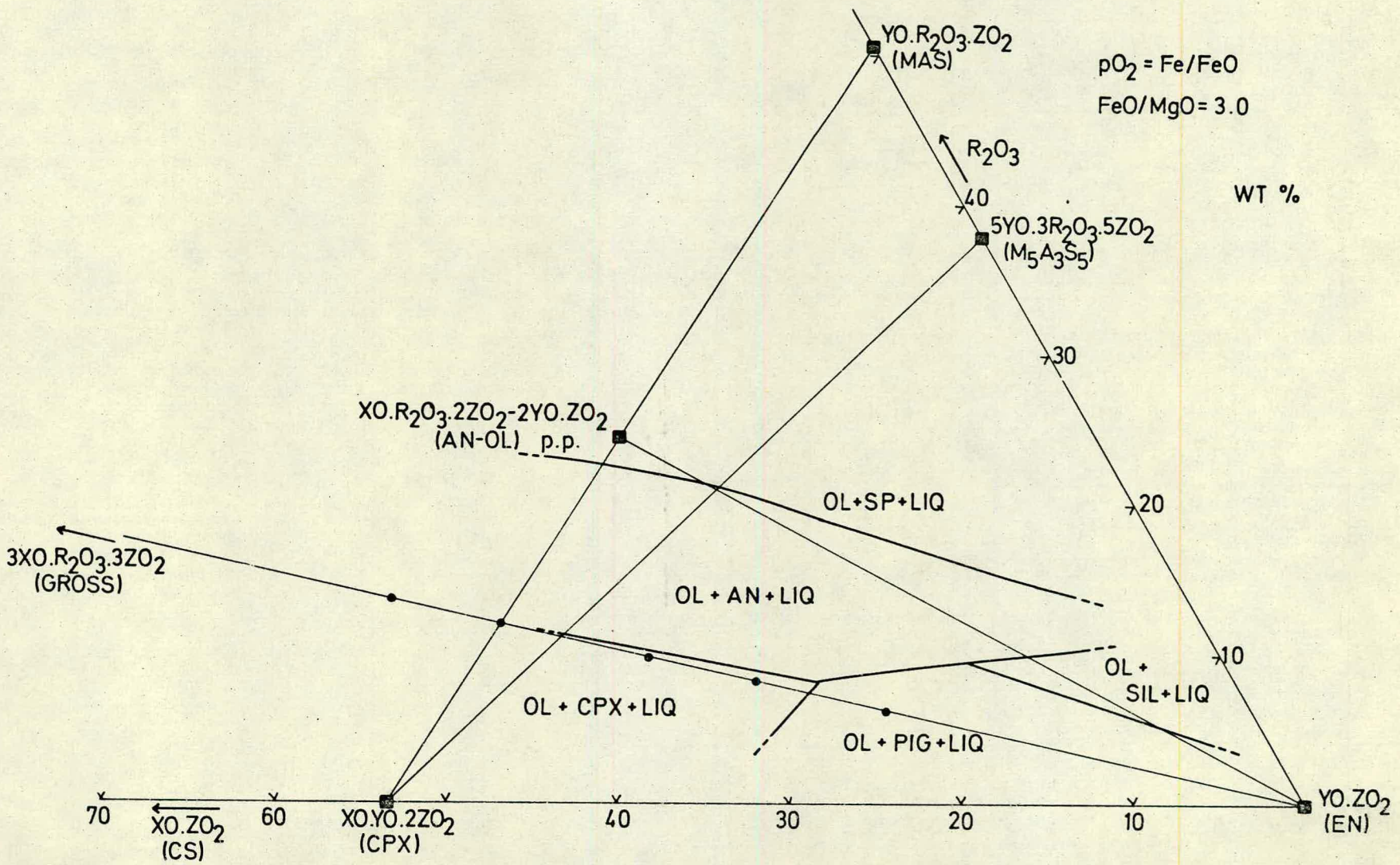
YO.R2O3.ZO2
(MAS)
pO2 = Fe/FeO
FeO/MgO = 3.0
R2O3
WT %
40
5YO.3R2O3.5ZO2
(M5A3S5)
30
XO.R2O3.2ZO2-2YO.ZO2
(AN-OL) p.p.
OL+SP+LIQ
20
3XO.R2O3.3ZO2
(GROSS)
OL + AN + LIQ
10
OL +
SIL+LIQ
OL + CPX + LIQ
OL + PIG+LIQ
70
XO.ZO2
(CS)
60
XO.YO.2ZO2
(CPX)
40
30
20
10
YO.ZO2
(EN)

Fig 6.57

Figure 6.58

See figure 6.54

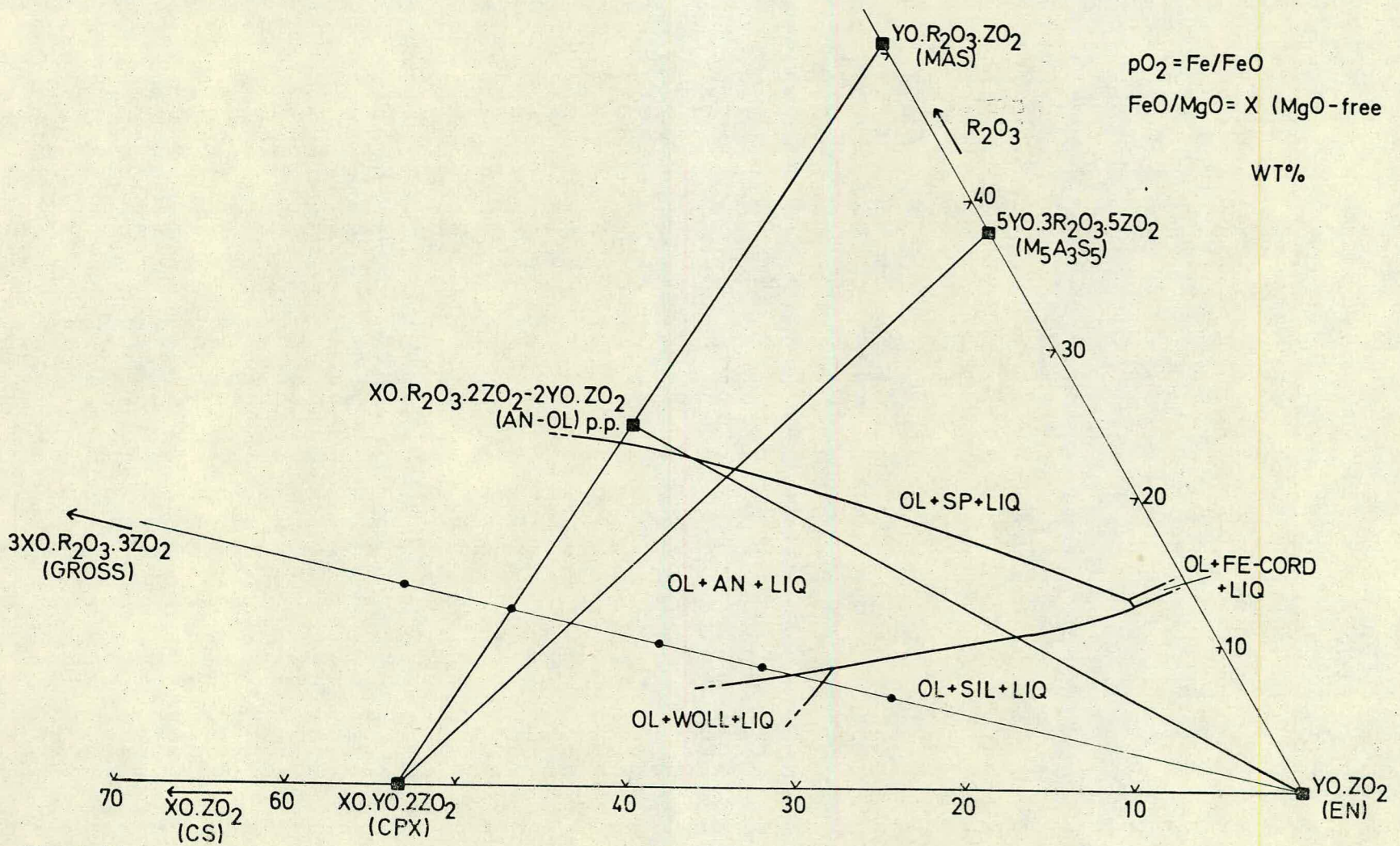
YO.R2O3.ZO2
(MAS)
pO2 = Fe/FeO
FeO/MgO = X (MgO-free
R2O3
WT%
40
5YO.3R2O3.5ZO2
(M5A3S5)
30
XO.R2O3.2ZO2-2YO.ZO2
(AN-OL) p.p.
OL+SP+LIQ
20
3XO.R2O3.3ZO2
(GROSS)
OL+FE-CORD
+LIQ
OL+AN+LIQ
10
OL+SIL+LIQ
OL+WOLL+LIQ
70
XO.ZO2
(CS)
60
XO.YO.2ZO2
(CPX)
40
30
20
10
YO.ZO2
(EN)

Fig 6.58

Figure 6.59

A summary figure of the liquidus data for the plane $XO.ZO_2$-$YO.ZO_2$-R_2O_3 (CS-MS-A), combining the L. 6 E 4 piercing points present at each FeO/MgO mole ratio studied (figures 6.44-6.48), to present a multi-Fe/Mg perspective of L. 6 E 3 piercing points which occur in this plane, at the pO_2 of the Fe/FeO equilibrium. The locations of L. 6 E 3 are tentative only. Values in parenthesis are 100 x FeO/(FeO+MgO) (wt%), and the arrows indicate the direction of increasing Fe/Mg ratio of the L. 6 E 4.

Abbreviations used for the equilibria are

AWDL = L. 6 E 4 an,woll,cpx,liq

DOPL = L. 6 E 4 cpx,ol,pyx,liq

DOSL = L. 6 E 4 cpx,ol,sil,liq

DOWL = L. 6 E 4 cpx,ol,woll,liq

OADL = L. 6 E 4 ol,an,cpx,liq

OAML = L. 6 E 4 ol,an,sp,liq

SOPL = L. 6 E 4 sil,ol,pyx,liq

SOWL = L. 6 E 4 sil,ol,woll,liq

SPDL = L. 6 E 4 sil,pyx,cpx,liq

SWDL = L. 6 E 4 sil,woll,cpx,liq

WOAL = L. 6 E 4 woll,ol,an,liq

DOPSL = L. 6 E 3 cpx,ol,pyx,sil,liq

DWOAL = L. 6 E 3 cpx,woll,ol,an,liq

SODWL = L. 6 E 3 sil,ol,cpx,woll,liq

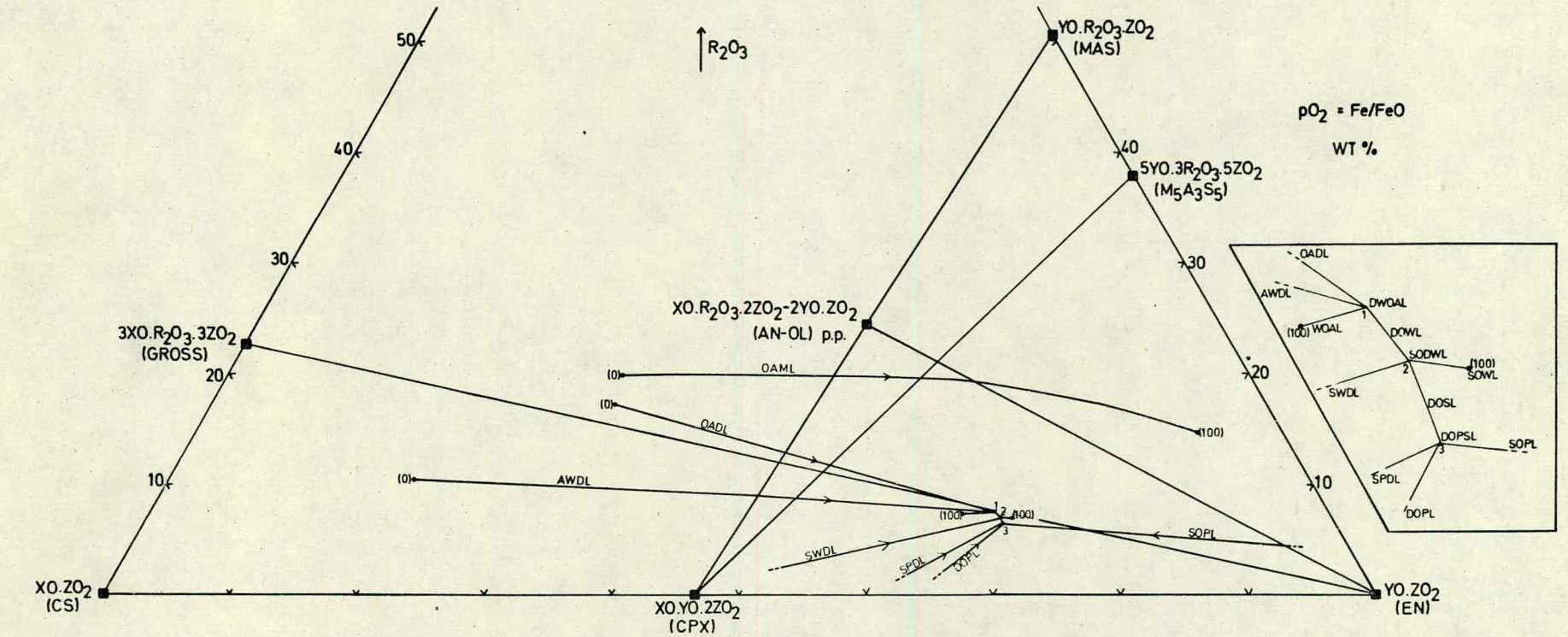
R_2O_3
pO_2 = Fe/FeO
WT %
$YO.R_2O_3.ZO_2$
(MAS)
$5YO.3R_2O_3.5ZO_2$
$(M_5A_3S_5)$
$3XO.R_2O_3.3ZO_2$
(GROSS)
$XO.R_2O_3.2ZO_2$-$2YO.ZO_2$
(AN-OL) p.p.
$XO.ZO_2$
(CS)
$XO.YO.2ZO_2$
(CPX)
$YO.ZO_2$
(EN)
50
40
30
20
10
OAML
OADL
AWDL
SWDL
SPDL
DOPL
SOPL
(0)
(100)
OADL
AWDL
DWOAL
WOAL
DOWL
SODWL
SOWL
SWDL
DOSL
DOPSL
SOPL
SPDL
DOPL

Fig 6.59

Figure 6.60

A summary figure of the liquidus data for the plane $3XO.R_2O_3$-YO-ZO_2 (C_3A-M-S) combining the L. 6 E 4 piercing points present at each FeO/MgO mole ratio studied (figures 6.49-6.53), to present a multi-Fe/Mg perspective of L. 6 E 3 piercing points which occur in this plane, at the pO_2 of the Fe/FeO equilibrium. The locations of L. 6 E 3 are tentative only. Values in parentheses are 100 x FeO/(FeO+MgO) (wt%), and the arrows indicate the direction of increasing Fe/Mg ratio of the L. 6 E 4.

The piercing point labelled AD p.p. is the piercing point of the join $XO.R_2O_3.2ZO_2$-XO.YO.$2ZO_2$ (Anorthite-Diopside) in this plane.

Abbreviations used for the equilibria are

ADOL = L. 6 E 4 an,cpx,ol,liq

AWDL = L. 6 E 4 an,woll,cpx,liq

AWOL = L. 6 E 4 an,woll,ol,liq

ODPL = L. 6 E 4 ol,cpx,pyx,liq

OWSL = L. 6 E 4 ol,woll,sil,liq

SDOL = L. 6 E 4 sil,cpx,ol,liq

SDPL = L. 6 E 4 sil,cpx,pyx,liq

SPOL = L. 6 E 4 sil,pyx,ol,liq

SWDL = L. 6 E 4 sil,woll,cpx,liq

WDOL = L. 6 E 4 woll,cpx,ol,liq

AWDOL = L. 6 E 3 an,woll,cpx,ol,liq

OWSDL = L. 6 E 3 ol,woll,sil,cpx,liq

SDPOL = L. 6 E 3 sil,cpx,pyx,ol,liq

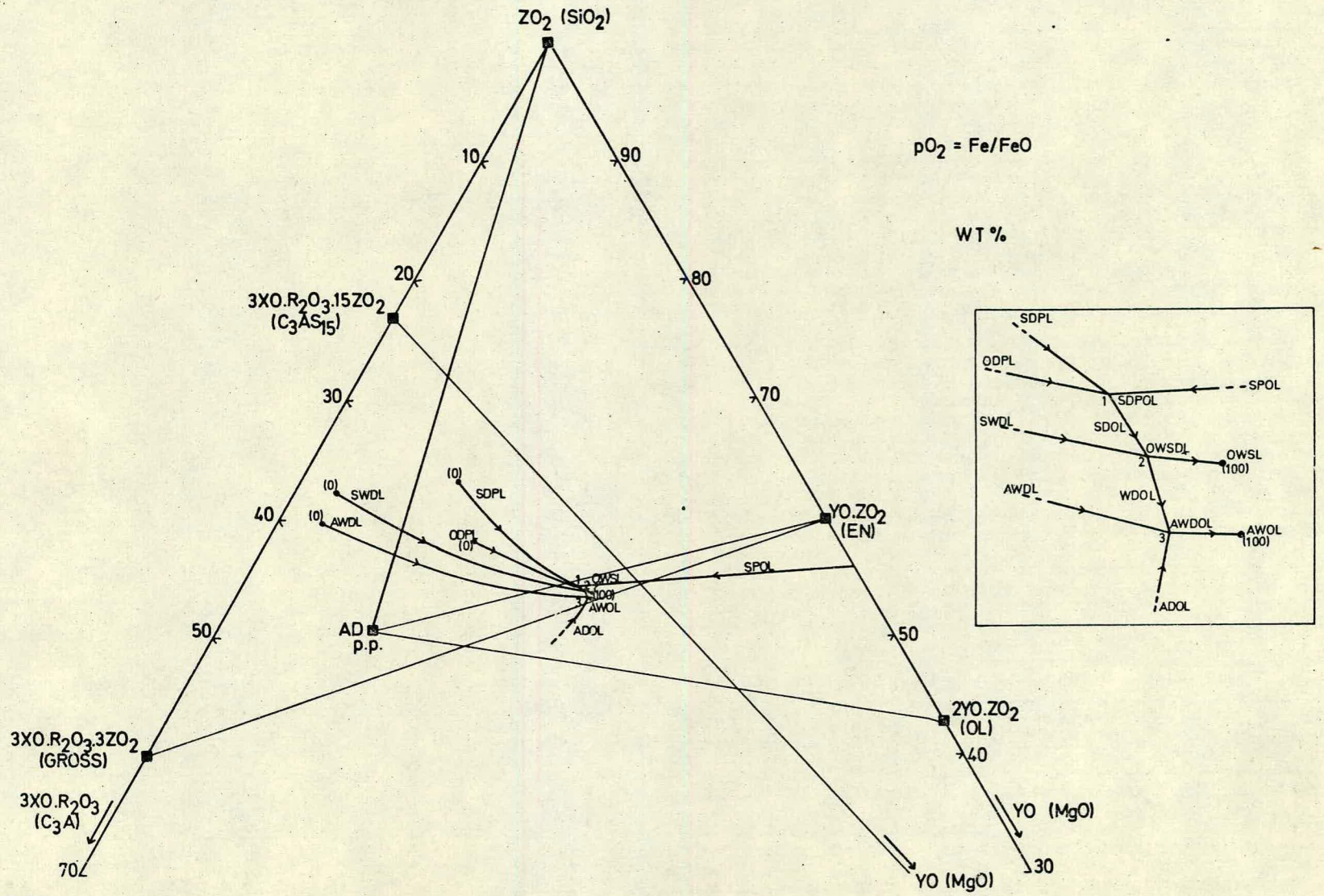
ZO2 (SiO2)
10
90
20
80
3XO.R2O3.1.5ZO2
(C3AS1.5)
30
70
40
YO.ZO2
(EN)
50
50
AD
p.p.
2YO.ZO2
(OL)
40
3XO.R2O3.3ZO2
(GROSS)
3XO.R2O3
(C3A)
70
YO (MgO)
30
YO (MgO)
pO2 = Fe/FeO
WT %
SDPL
ODPL
SPOL
1 SDPOL
SWDL
SDOL
OWSDL
OWSL
(100)
2
AWDL
WDOL
AWDOL
AWOL
(100)
3
ADOL
(0) SWDL
(0) AWDL
(0) SDPL
ODPL
(0)
SPOL
OWSL
(100)
AWOL
ADOL

Fig 6.60

Figure 6.61

A summary figure of the 2YO.ZO (olivine) projection into the plane $XO.ZO_2$-$YO.ZO_2$-R_2O_3 (CS-MS-A), combining the L. 6 E 3 data from figures 6.54 - 6.60, to give an impression of the L. 6 E 2 occurring at the pO_2 of the Fe/FeO equilibrium. The locations of L. 6 E 2 are tentative only. Values in parentheses are 100 x FeO/(FeO+MgO) (wt%), and the arrows indicate the direction of increasing Fe/Mg ratio of the L. 6 E 3.

Abbreviations used for the equilibria are

ADOSL = L. 6 E 3 an,cpx,ol,sil,liq

AWDOL = L. 6 E 3 an,woll,cpx,ol,liq

OAMCL = L. 6 E 3 ol,an,sp,cord,liq

OAPCL = L. 6 E 3 ol,an,pyx,cord,liq

OAPDL = L. 6 E 3 ol,an,pyx,cpx,liq

OAWSL = L. 6 E 3 ol,an,woll,sil,liq

OSPAL = L. 6 E 3 ol,sil,pyx,an,liq

OSPDL = L. 6 E 3 ol,sil,pyx,cpx,liq

SWDOL = L. 6 E 3 sil,woll,cpx,ol,liq

AWDOSL = L. 6 E 2 an,woll,cpx,ol,sil,liq

OSPADL = L. 6 E 2 ol,sil,pyx,an,cpx,liq

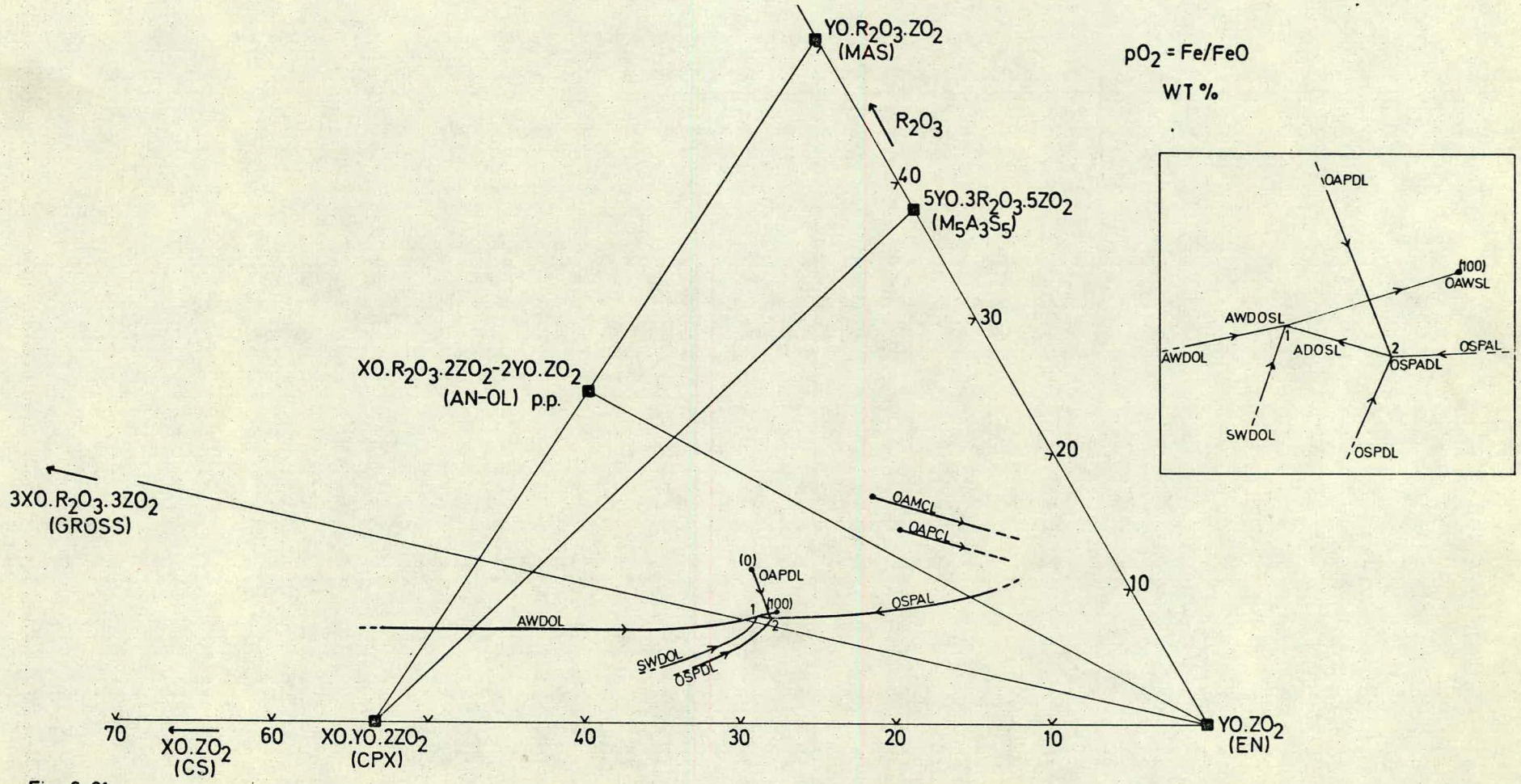
YO.R2O3.ZO2
(MAS)
pO2 = Fe/FeO
WT %
R2O3
40
5YO.3R2O3.5ZO2
(M5A3S5)
30
XO.R2O3.2ZO2-2YO.ZO2
(AN-OL) p.p.
20
3XO.R2O3.3ZO2
(GROSS)
OAMCL
OAPCL
(0)
OAPDL
1
(100)
2
OSPAL
AWDOL
SWDOL
OSPDL
10
70
XO.ZO2
(CS)
60
XO.YO.2ZO2
(CPX)
40
30
20
10
YO.ZO2
(EN)
OAPDL
(100)
OAWSL
AWDOSL
1
ADOSL
2
OSPAL
AWDOL
OSPADL
SWDOL
OSPDL

Fig 6.61

Figures 6.62 to 6.64

T - X sections for part of the join $XO.YO.2ZO_2$-$YO.R_2O_3.ZO_2$ (Diopside-MAS) at FeO/MgO mole ratios of 0.18, 0.5, and 1.0, and the pO_2 of the Ni/NiO equilibrium. The experiments on each composition are shown at the appropriate temperatures by filled circles, the composition names are indicated beneath each composition studied. The phase boundaries are drawn using the combined data plots presented in figures 6.65, 6.66.

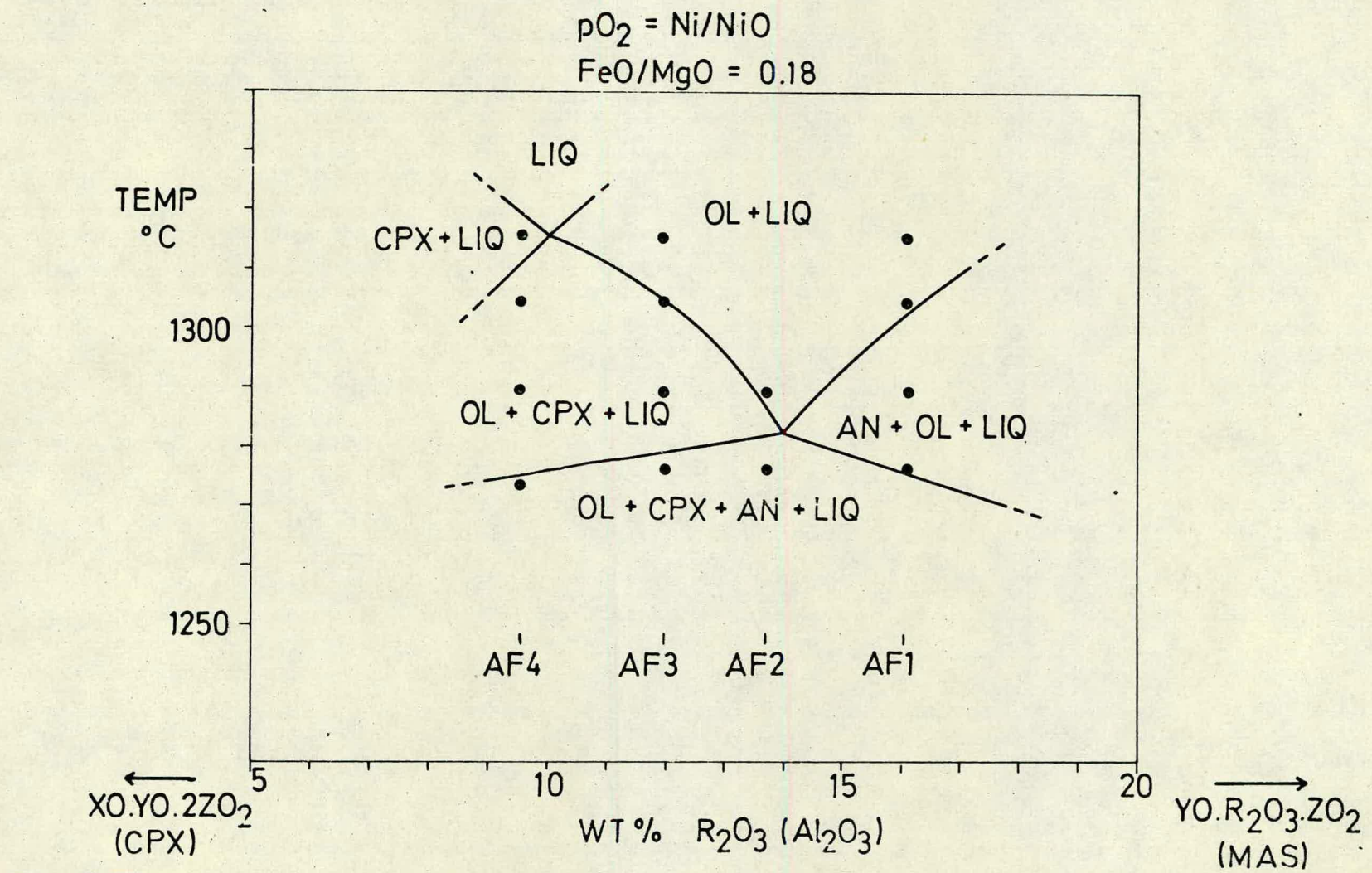
pO_2 = Ni/NiO
FeO/MgO = 0.18
LIQ
TEMP °C
CPX + LIQ
OL + LIQ
1300
OL + CPX + LIQ
AN + OL + LIQ
OL + CPX + AN + LIQ
1250
AF4
AF3
AF2
AF1
5
10
15
20
XO.YO.2ZO2 (CPX)
WT % R2O3 (Al2O3)
YO.R2O3.ZO2 (MAS)

Fig 6.62

Figure 6.63

See figure 6.62

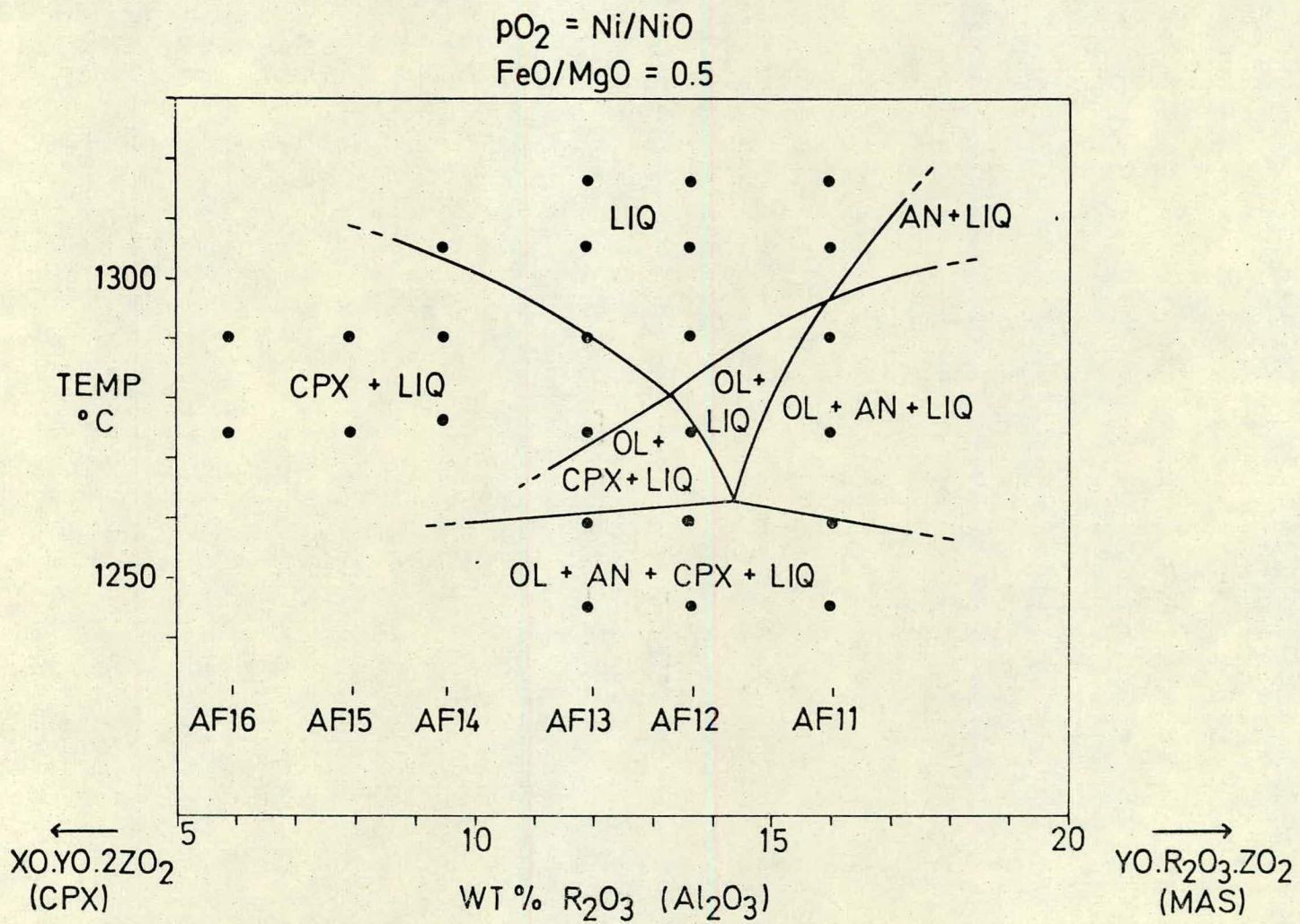
pO2 = Ni/NiO
FeO/MgO = 0.5
LIQ
AN+LIQ
1300
TEMP
°C
CPX + LIQ
OL+
LIQ
OL + AN + LIQ
OL+
CPX+LIQ
1250
OL + AN + CPX + LIQ
AF16
AF15
AF14
AF13
AF12
AF11
5
10
15
20
XO.YO.2ZO2
(CPX)
WT % R2O3 (Al2O3)
YO.R2O3.ZO2
(MAS)

Fig 6.63

Figure 6.64

See figure 6.62

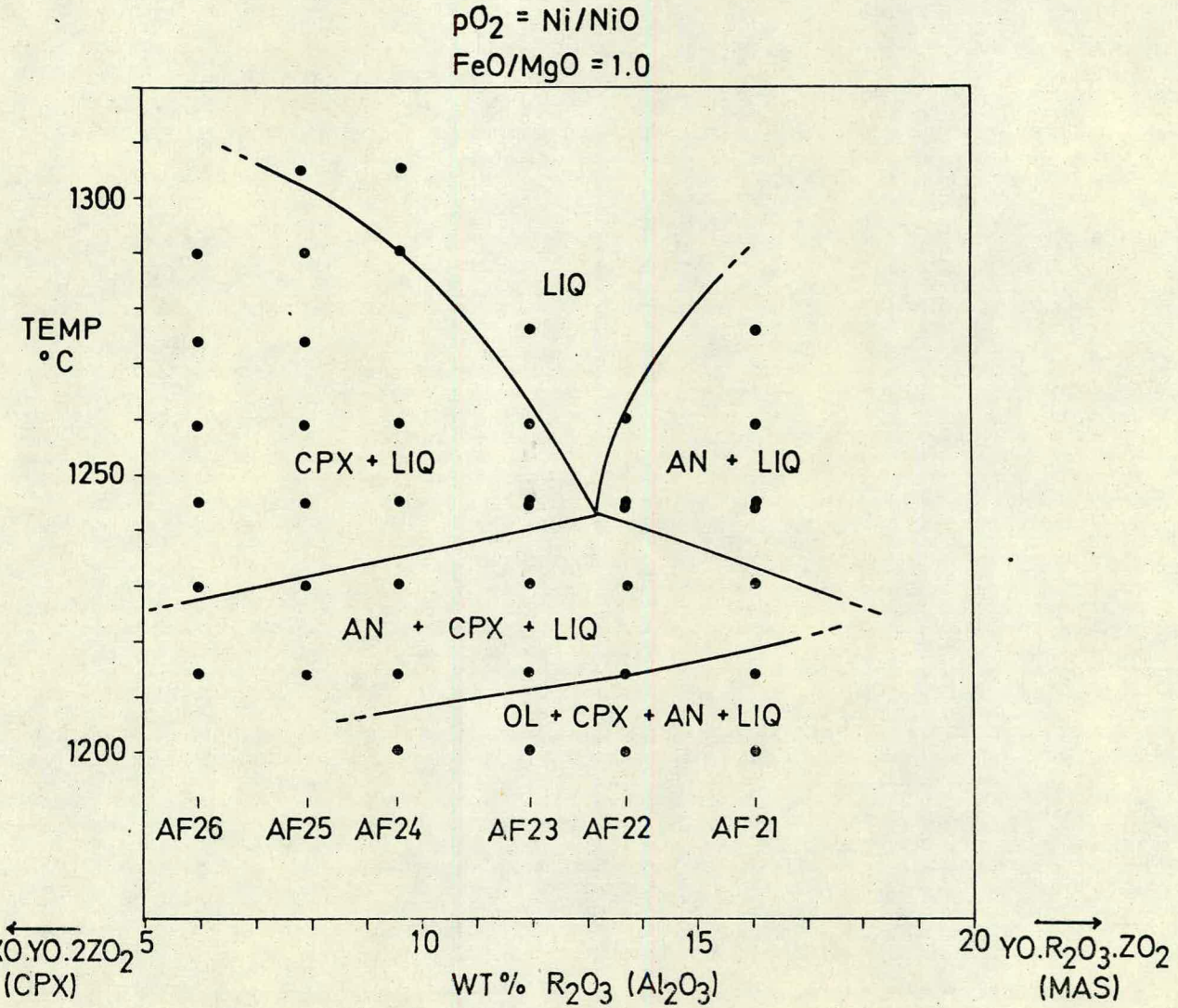
pO_2 = Ni/NiO
FeO/MgO = 1.0
TEMP °C
1300
1250
1200
LIQ
CPX + LIQ
AN + LIQ
AN + CPX + LIQ
OL + CPX + AN + LIQ
AF26
AF25
AF24
AF23
AF22
AF21
5
10
15
20
WT% R_2O_3 (Al_2O_3)
$XO.YO.2ZO_2$ (CPX)
$YO.R_2O_3.ZO_2$ (MAS)

Fig 6.64

Figure 6.65

Liquidus diagram for part of the join $XO.YO.2ZO_2$-$YO.R_2O_3.ZO_2$ (Diopside-MAS), to show the change in liquidus phase for molecularly equivalent compositions with changing FeO/MgO ratio, at the pO_2 of the Ni/NiO equilibrium. The compositions studied are shown by filled circles, the composition names can be found by referring to the individual T - X sections for this join (figures 6.62-6.64). Compositions at other FeO/MgO ratios lie in the join Enstatite-Grossular, their names can be found by referring to the T - X sections for that join (figures 6.72-6.78). The phase boundaries are indicated by thick solid lines, the dashed lines are the temperature contours where known.

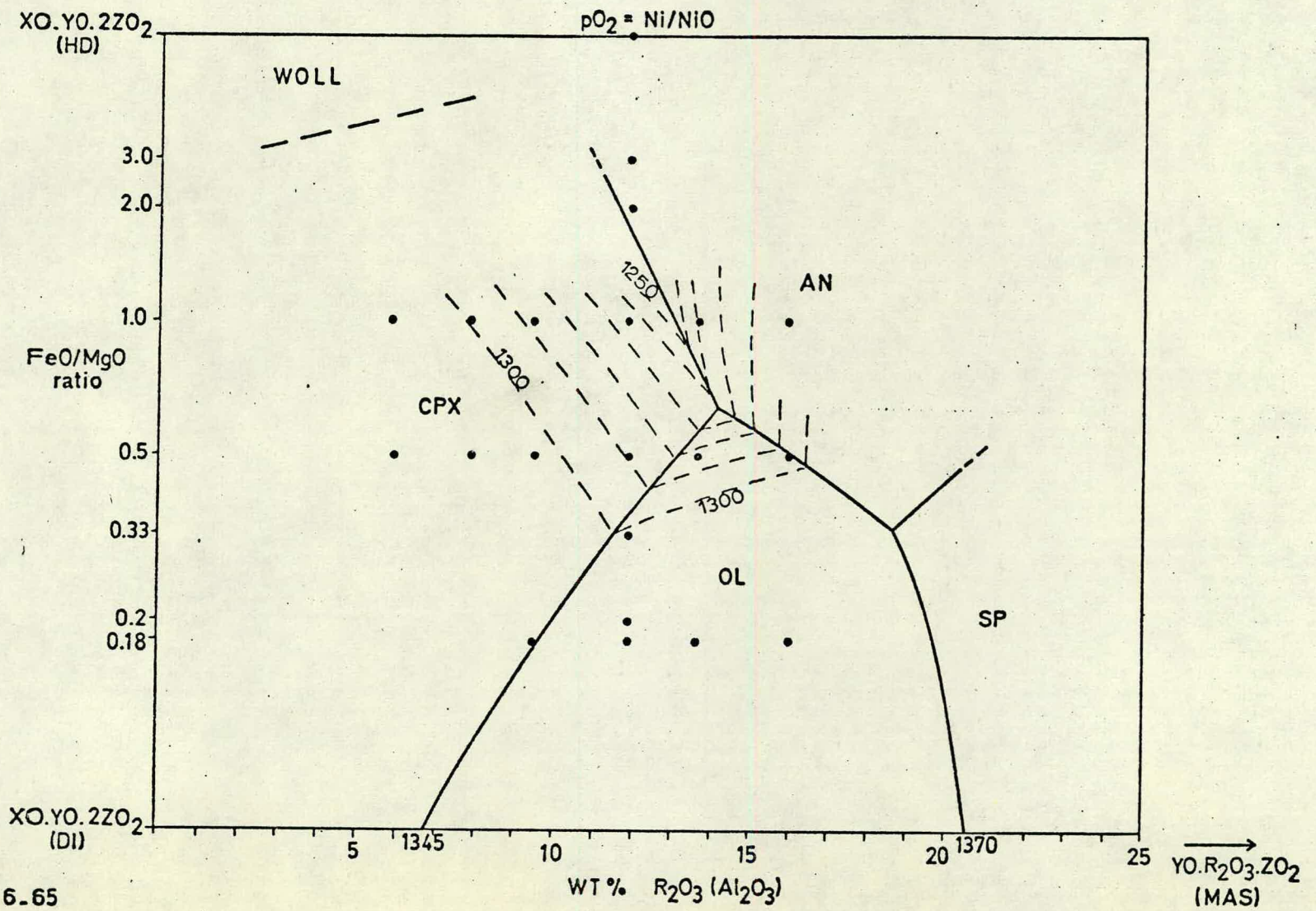
XO.YO.2ZO2
(HD)
pO2 = Ni/NiO
WOLL
3.0
2.0
1.0
Fe0/Mg0
ratio
0.5
0.33
0.2
0.18
XO.YO.2ZO2
(DI)
1250
1300
1300
AN
CPX
OL
SP
5
1345
10
15
20
1370
25
WT % R2O3 (Al2O3)
YO.R2O3.ZO2
(MAS)

Fig 6-65

Figure 6.66

Diagram to show the change in the second phase to crystallise for molecularly equivalent compositions in part of the join $XO.YO.2ZO_2$-$YO.R_2O_3.ZO_2$ (Diopside-MAS) with changing FeO/MgO ratio, at the pO_2 of the Ni/NiO equilibrium. The compositions studied are shown by filled circles, the composition names can be found by referring to the individual T - X sections for this join (figures 6.62-6.64). Compositions at other FeO/MgO ratios lie in the join Enstatite-Grossular, their names can be found by referring to the T - X sections for that join (figures 6.72-6.78). The liquidus phase boundaries are indicated by thick solid lines, the projected phase boundaries within each phase volume are indicated where known by thin solid lines. The phase assemblage for each area is also indicated. The dashed lines are the temperature contours for the appearance of the second phase in each composition in the join where known.

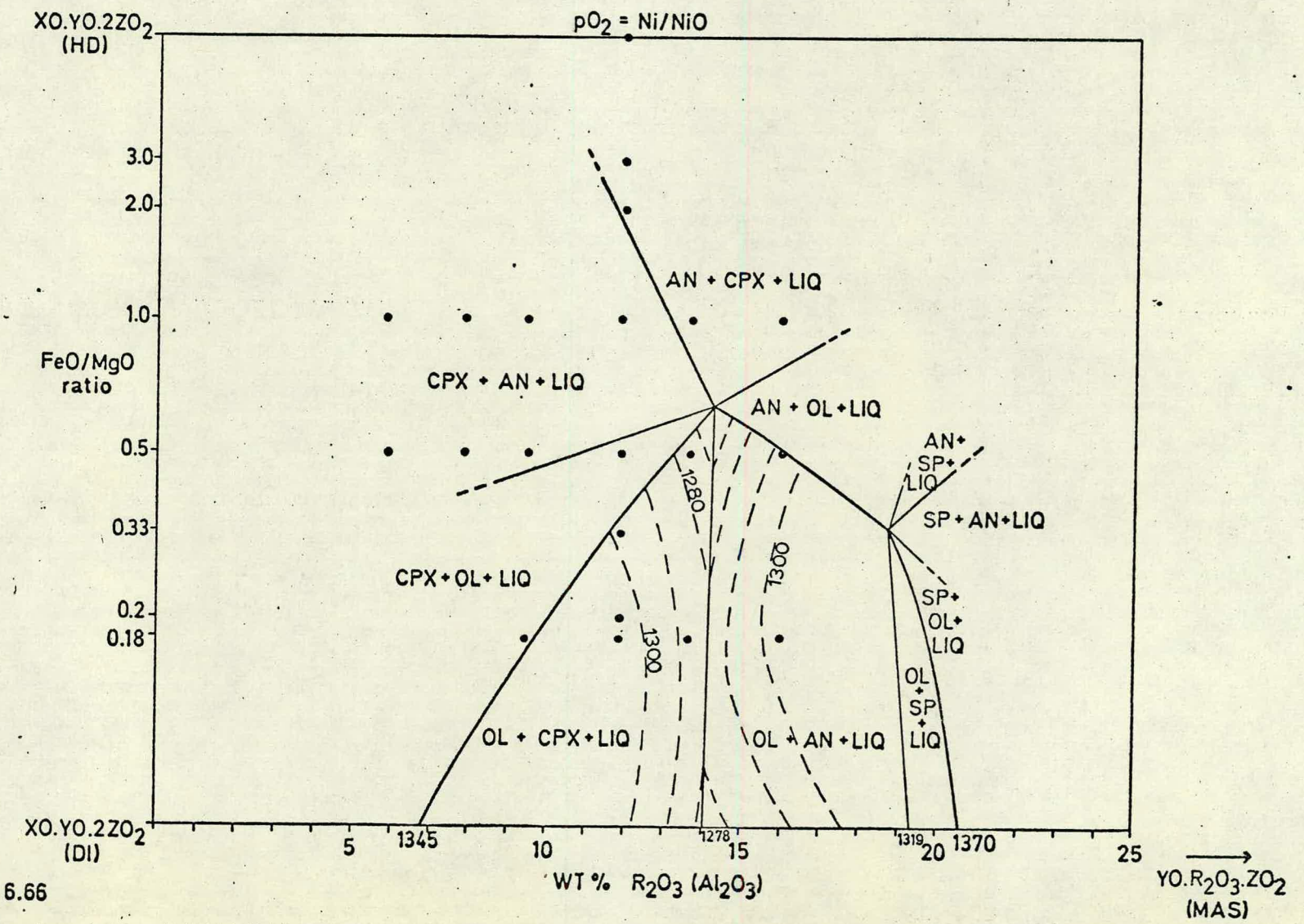
XO.YO.2ZO2
(HD)
pO2 = Ni/NiO
3.0
2.0
1.0
FeO/MgO
ratio
0.5
0.33
0.2
0.18
XO.YO.2ZO2
(DI)
AN + CPX + LIQ
CPX + AN + LIQ
AN + OL + LIQ
AN+
SP+
LIQ
SP + AN + LIQ
CPX + OL + LIQ
SP+
OL+
LIQ
OL
+
SP
+
LIQ
OL + CPX + LIQ
OL + AN + LIQ
1280
1300
1300
5
1345
10
1278
15
1319
20
1370
25
WT % R2O3 (Al2O3)
YO.R2O3.ZO2
(MAS)

Fig 6.66

Figures 6.67 to 6.69

T - X sections for part of the join $XO.YO.2ZO_2$-$5YO.3R_2O_3.5ZO_2$ (Diopside-$M_5A_3S_5$) at FeO/MgO mole ratios of 0.18, 0.5, and 1.0, and the pO_2 of the Ni/NiO equilibrium. The experiments on each composition are shown at the appropriate temperatures by filled circles, the composition names are indicated beneath each composition studied. The phase boundaries are drawn using the combined data plots presented in figures 6.70, 6.71.

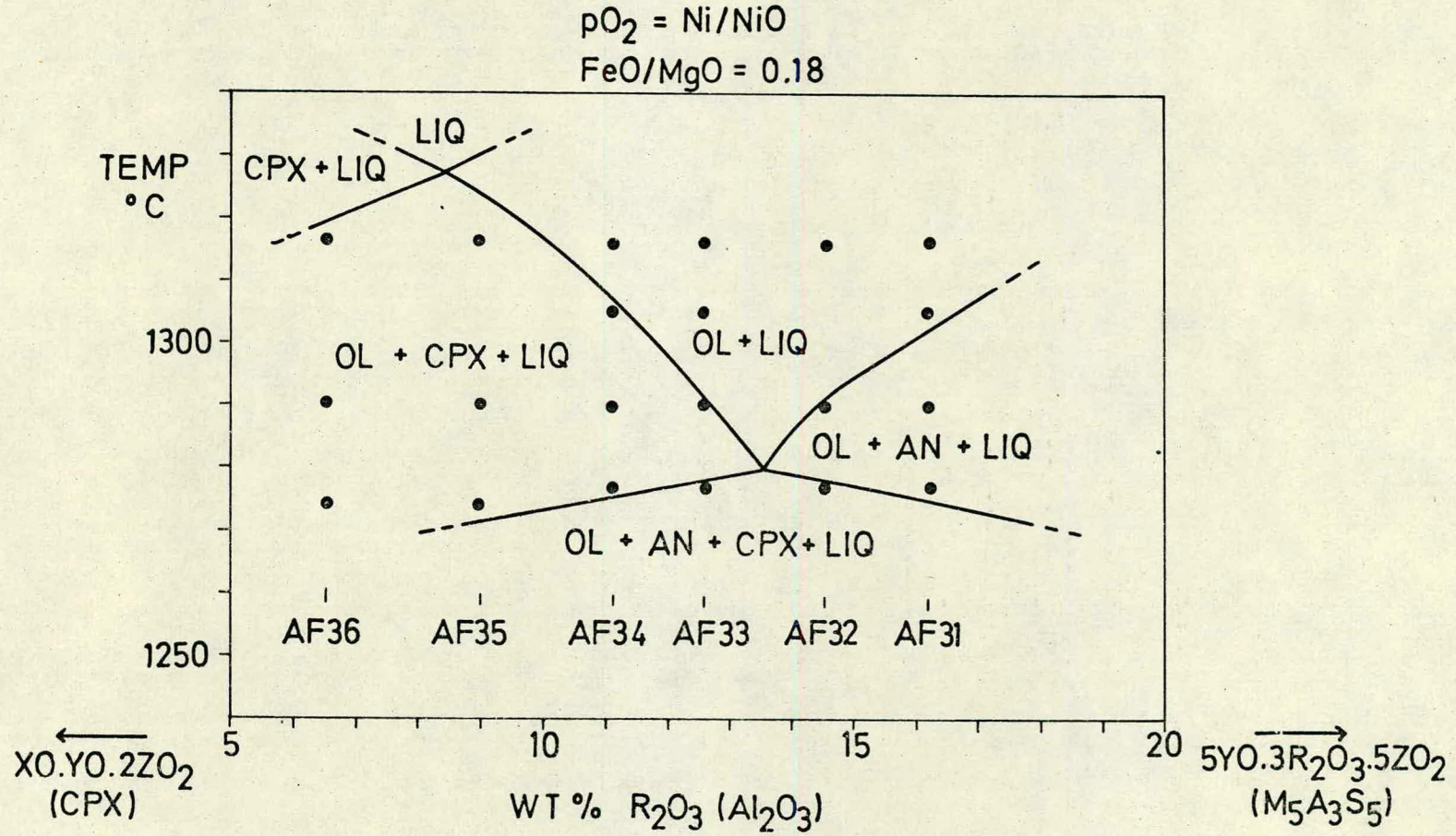
pO_2 = Ni/NiO
FeO/MgO = 0.18
TEMP °C
LIQ
CPX + LIQ
1300
OL + CPX + LIQ
OL + LIQ
OL + AN + LIQ
OL + AN + CPX + LIQ
1250
AF36
AF35
AF34
AF33
AF32
AF31
5
10
15
20
$XO.YO.2ZO_2$
(CPX)
WT % R_2O_3 (Al_2O_3)
$5YO.3R_2O_3.5ZO_2$
($M_5A_3S_5$)

Fig 6.67

Figure 6.68

See figure 6.67

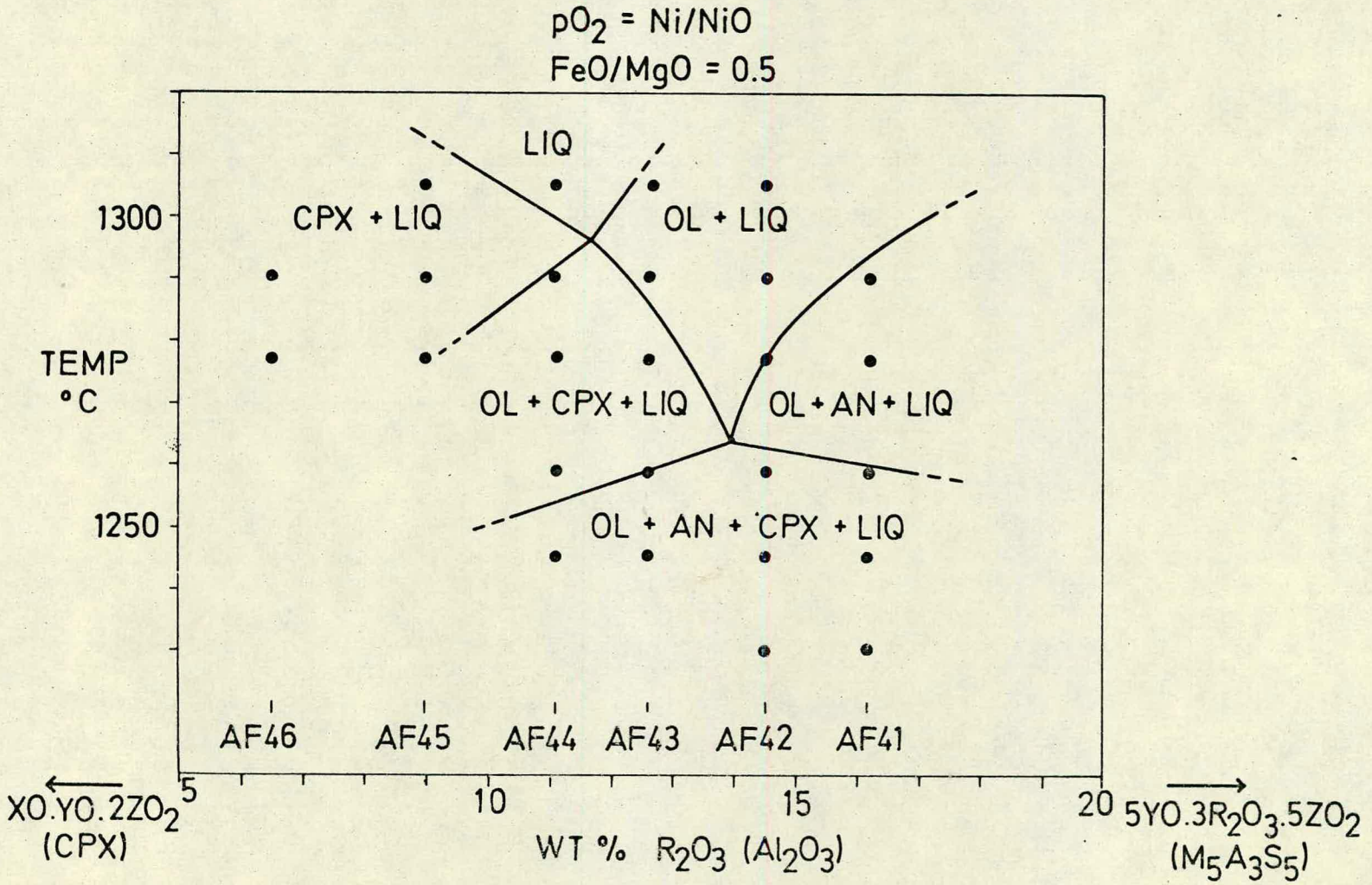
pO_2 = Ni/NiO
FeO/MgO = 0.5
LIQ
CPX + LIQ
OL + LIQ
OL + CPX + LIQ
OL + AN + LIQ
OL + AN + CPX + LIQ
1300
1250
TEMP
°C
AF46
AF45
AF44
AF43
AF42
AF41
5
10
15
20
WT % R_2O_3 (Al_2O_3)
$XO.YO.2ZO_2$
(CPX)
$5YO.3R_2O_3.5ZO_2$
($M_5A_3S_5$)

Fig 6.68

Figure 6.69

See figure 6.67

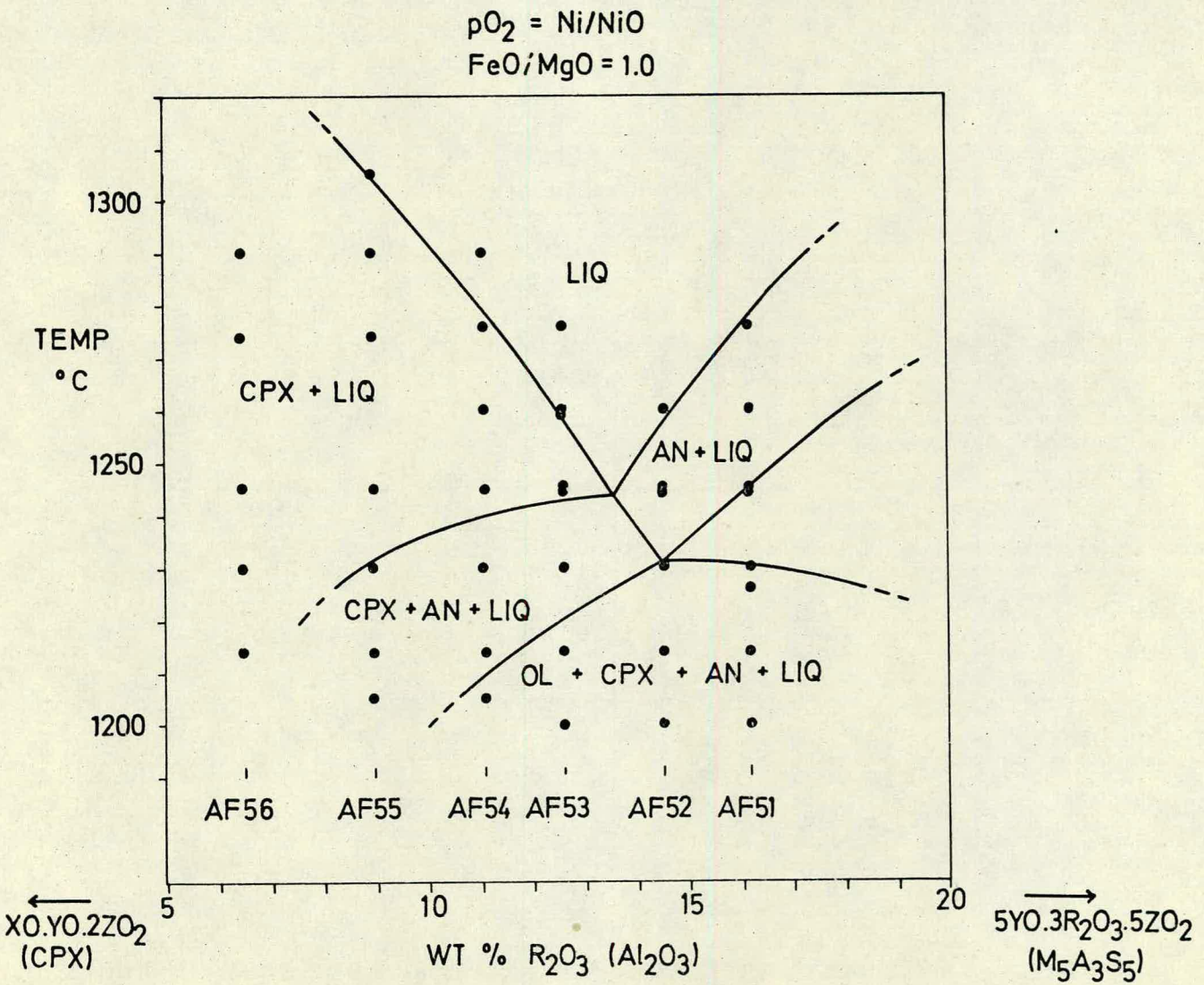
pO_2 = Ni/NiO
FeO/MgO = 1.0
1300
1250
1200
TEMP
°C
LIQ
CPX + LIQ
AN + LIQ
CPX + AN + LIQ
OL + CPX + AN + LIQ
AF56
AF55
AF54
AF53
AF52
AF51
5
10
15
20
WT % R_2O_3 (Al_2O_3)
$XO.YO.2ZO_2$
(CPX)
$5YO.3R_2O_3.5ZO_2$
($M_5A_3S_5$)

Fig 6.69

Figure 6.70

Liquidus diagram for part of the join $XO.YO.2ZO_2$-$5YO.3R_2O_3.5ZO_2$ (Diopside-$M_5A_3S_5$), to show the change in liquidus phase for molecularly equivalent compositions with changing FeO/MgO ratio, at the pO_2 of the Ni/NiO equilibrium. The compositions studied are shown by filled circles, the composition names can be found by referring to the individual T - X sections for this join (figures 6.67-6.69). The phase boundaries are indicated by thick solid lines, the dashed lines are the temperature contours where known.

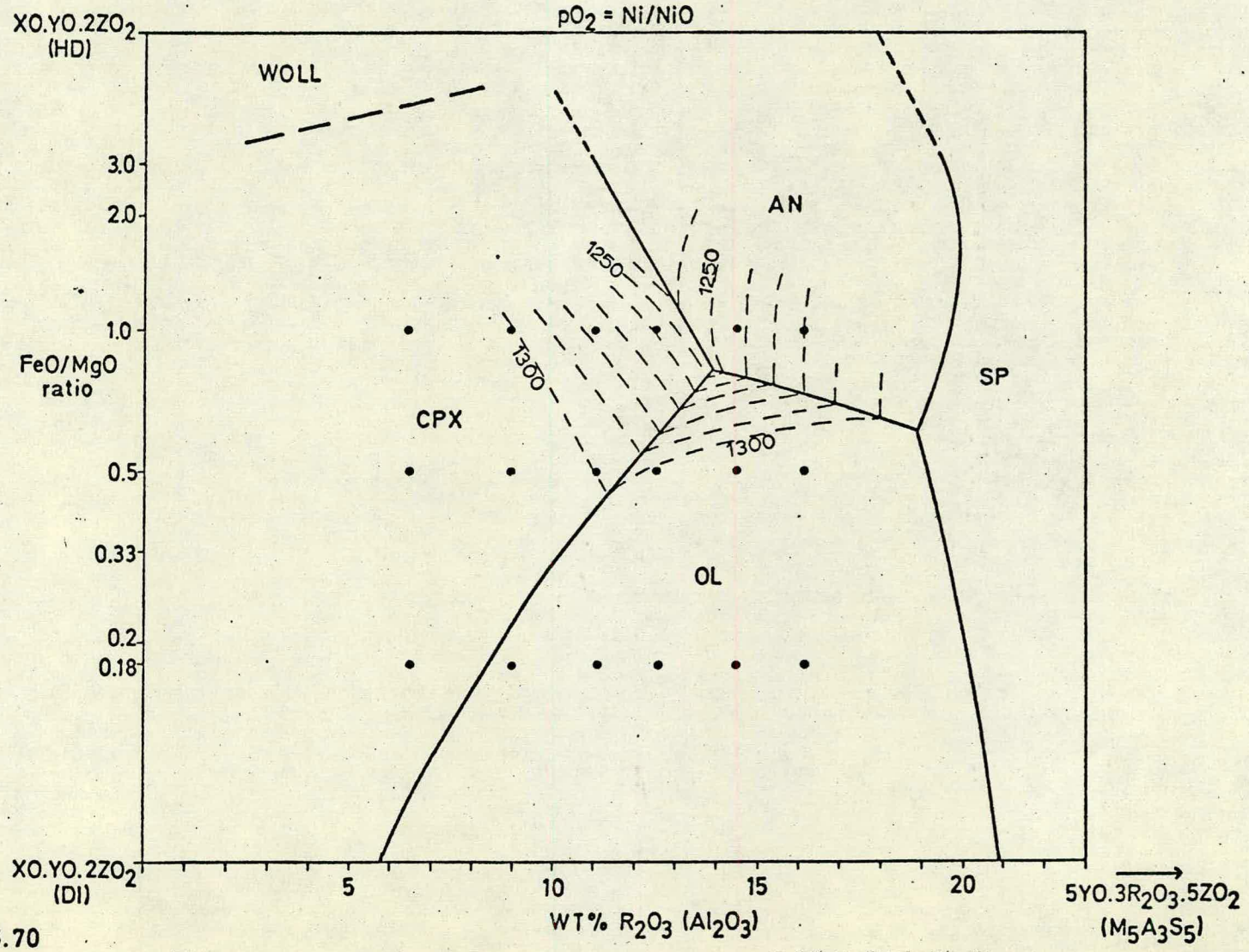
pO2 = Ni/NiO
XO.YO.2ZO2 (HD)
WOLL
AN
SP
CPX
OL
1250
1250
1300
1300
3.0
2.0
1.0
0.5
0.33
0.2
0.18
FeO/MgO ratio
XO.YO.2ZO2 (DI)
5
10
15
20
WT% R2O3 (Al2O3)
5YO.3R2O3.5ZO2 (M5A3S5)

Fig 6.70

Figure 6.71

Diagram to show the change in second phase to crystallise for molecularly equivalent compositions in part of the join $XO.YO.2ZO_2$-$5YO.3R_2O_3.5ZO_2$ (Diopside-$M_5A_3S_5$) with changing FeO/MgO ratio, at the pO_2 of the Ni/NiO equilibrium. The compositions studied are shown by filled circles, the composition names can be found by referring to the individual T - X sections for this join (figures 6.67-6.69). The liquidus phase boundaries are indicated by thick solid lines, the projected phase boundaries within each phase volume by thin solid lines where known. The phase assemblage for each area is indicated. The dashed lines are the temperature contours for the appearance of the second phase in each composition in the join where known.

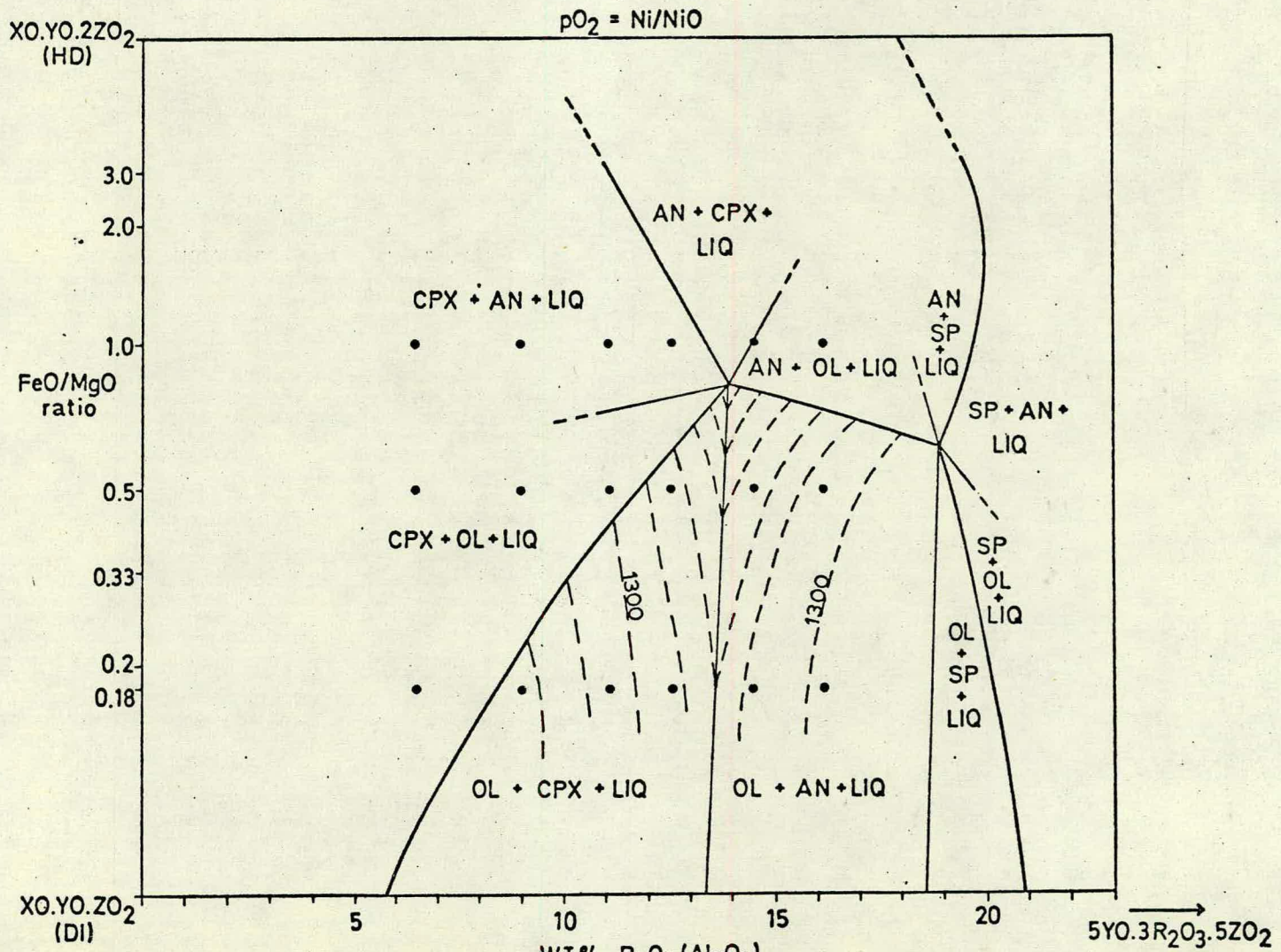
pO2 = Ni/NiO
XO.YO.2ZO2
(HD)
3.0
2.0
1.0
FeO/MgO
ratio
0.5
0.33
0.2
0.18
XO.YO.ZO2
(DI)
AN + CPX +
LIQ
CPX + AN + LIQ
AN
+
SP
+
LIQ
AN + OL + LIQ
SP + AN +
LIQ
CPX + OL + LIQ
SP
+
OL
+
LIQ
1300
1300
OL
+
SP
+
LIQ
OL + CPX + LIQ
OL + AN + LIQ
5
10
15
20
WT% R2O3 (Al2O3)
5YO.3R2O3.5ZO2
(M5A3S5)

Fig 6.71

Figures 6.72 to 6.78

T - X sections for part of the join $YO.ZO_2$-$3XO.R_2O_3.3ZO_2$ (Enstatite-Grossular) at FeO/MgO mole ratios of 0.2, 0.33, 0.5, 1.0, 2.0, 3.0, and X (MgO-free) and the pO_2 of the Ni/NiO equilibrium. The experiments on each composition are shown at the appropriate temperatures by filled circles. The composition names are generated from the information beneath each composition studied, using the format

FeO/MgO mole ratio - moles MgO - 3 - 1 - moles SiO_2.

The phase boundaries are drawn using the combined data plots presented in figures 6.79, 6.80. Some data points are inconsistent with these phase boundaries, but generally only by a small temperature error.

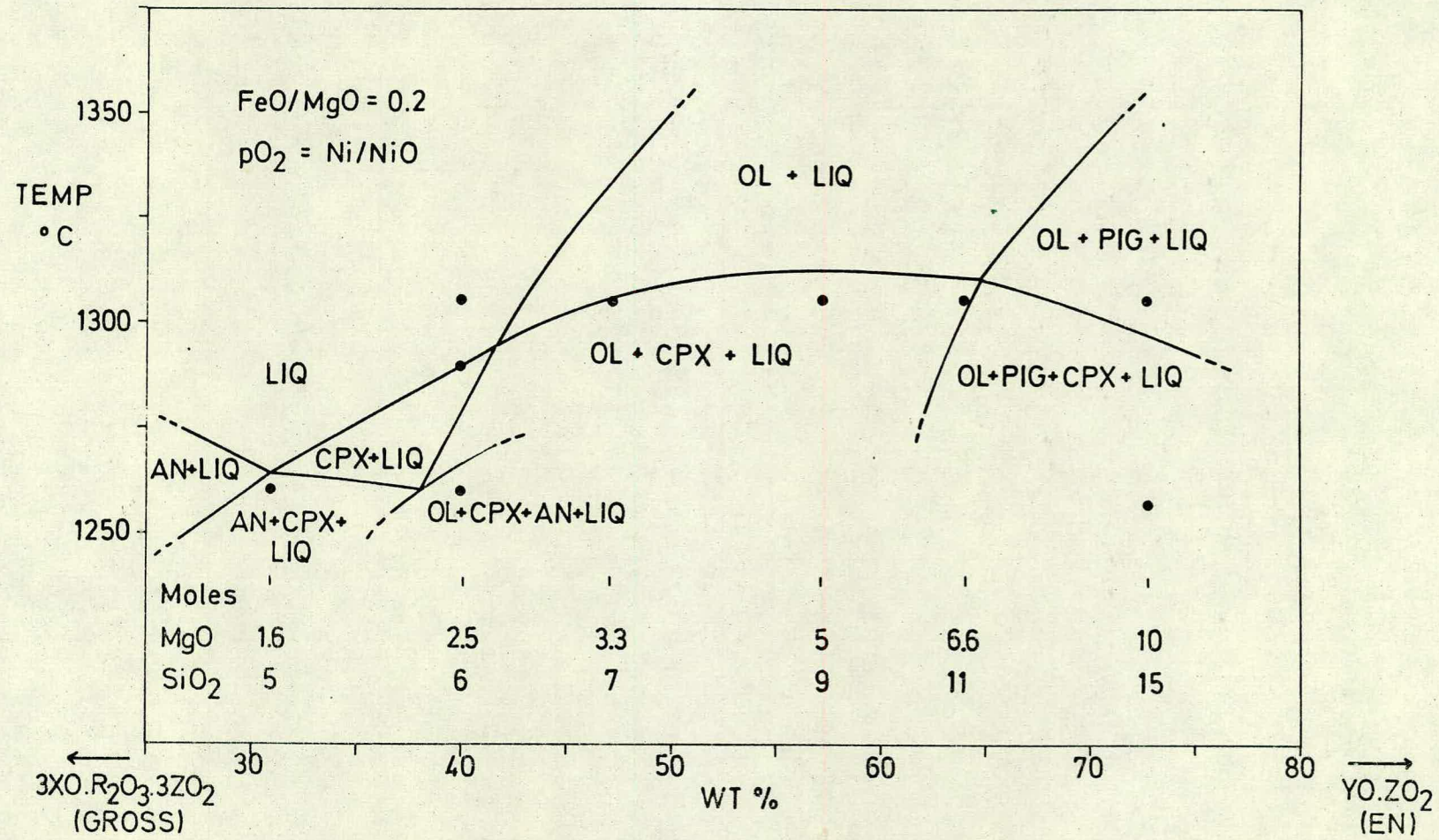
FeO/MgO = 0.2
pO_2 = Ni/NiO
TEMP
°C
1350
1300
1250
OL + LIQ
OL + PIG + LIQ
LIQ
OL + CPX + LIQ
OL+PIG+CPX + LIQ
AN+LIQ
CPX+LIQ
AN+CPX+
LIQ
OL+CPX+AN+LIQ
Moles
MgO 1.6 2.5 3.3 5 6.6 10
SiO_2 5 6 7 9 11 15
30
40
50
60
70
80
WT %
$3XO.R_2O_3.3ZO_2$
(GROSS)
$YO.ZO_2$
(EN)

Fig 6.72

Figure 6.73

See figure 6.72

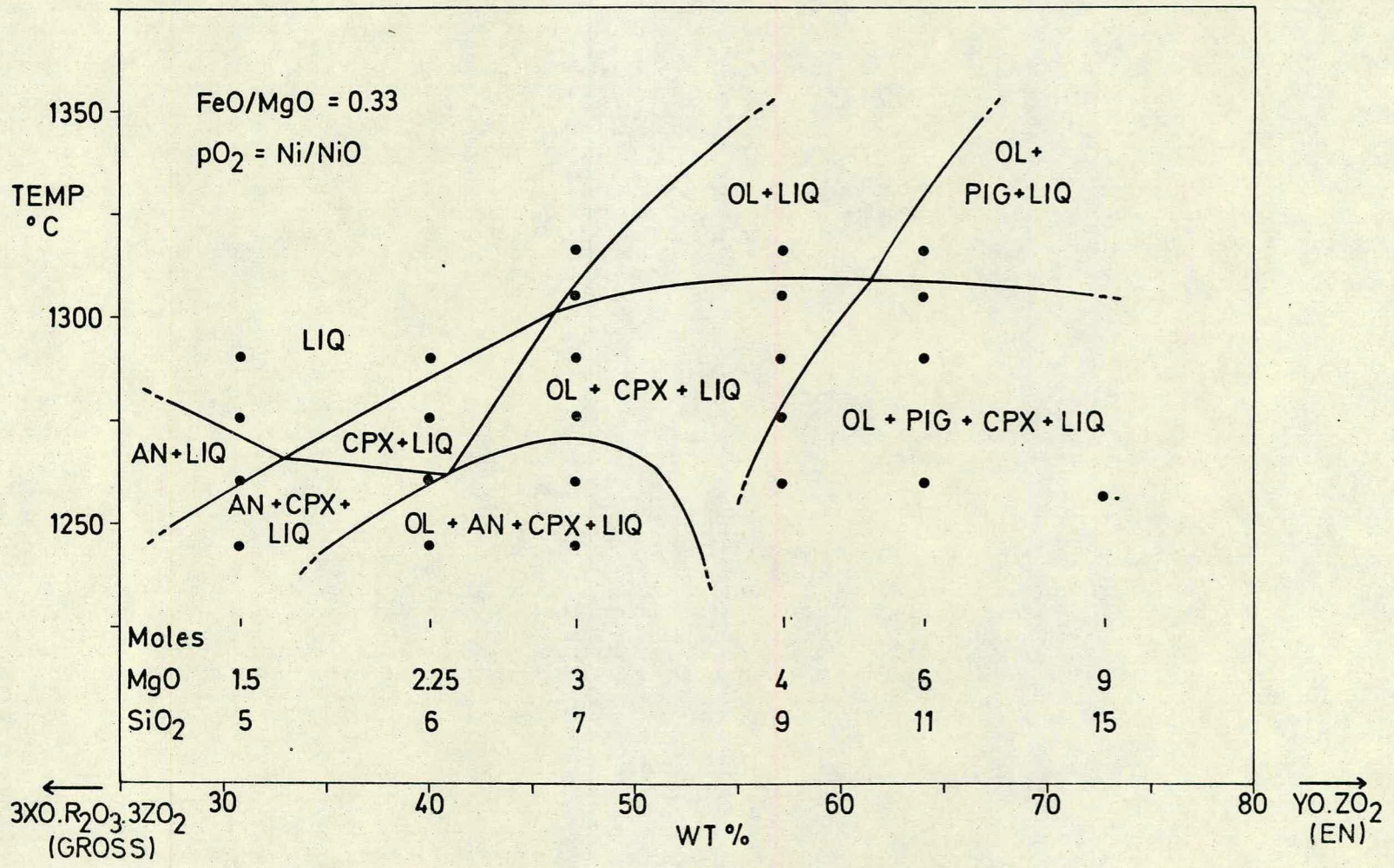
FeO/MgO = 0.33
pO2 = Ni/NiO
TEMP °C
1350
1300
1250
LIQ
OL+LIQ
OL+ PIG+LIQ
OL + CPX + LIQ
OL + PIG + CPX + LIQ
AN+LIQ
CPX+LIQ
AN+CPX+ LIQ
OL + AN + CPX + LIQ
Moles
MgO 1.5 2.25 3 4 6 9
SiO2 5 6 7 9 11 15
30
40
50
60
70
80
WT %
3XO.R2O3.3ZO2 (GROSS)
YO.ZO2 (EN)

Fig 6.73

Figure 6.74

See figure 6.72

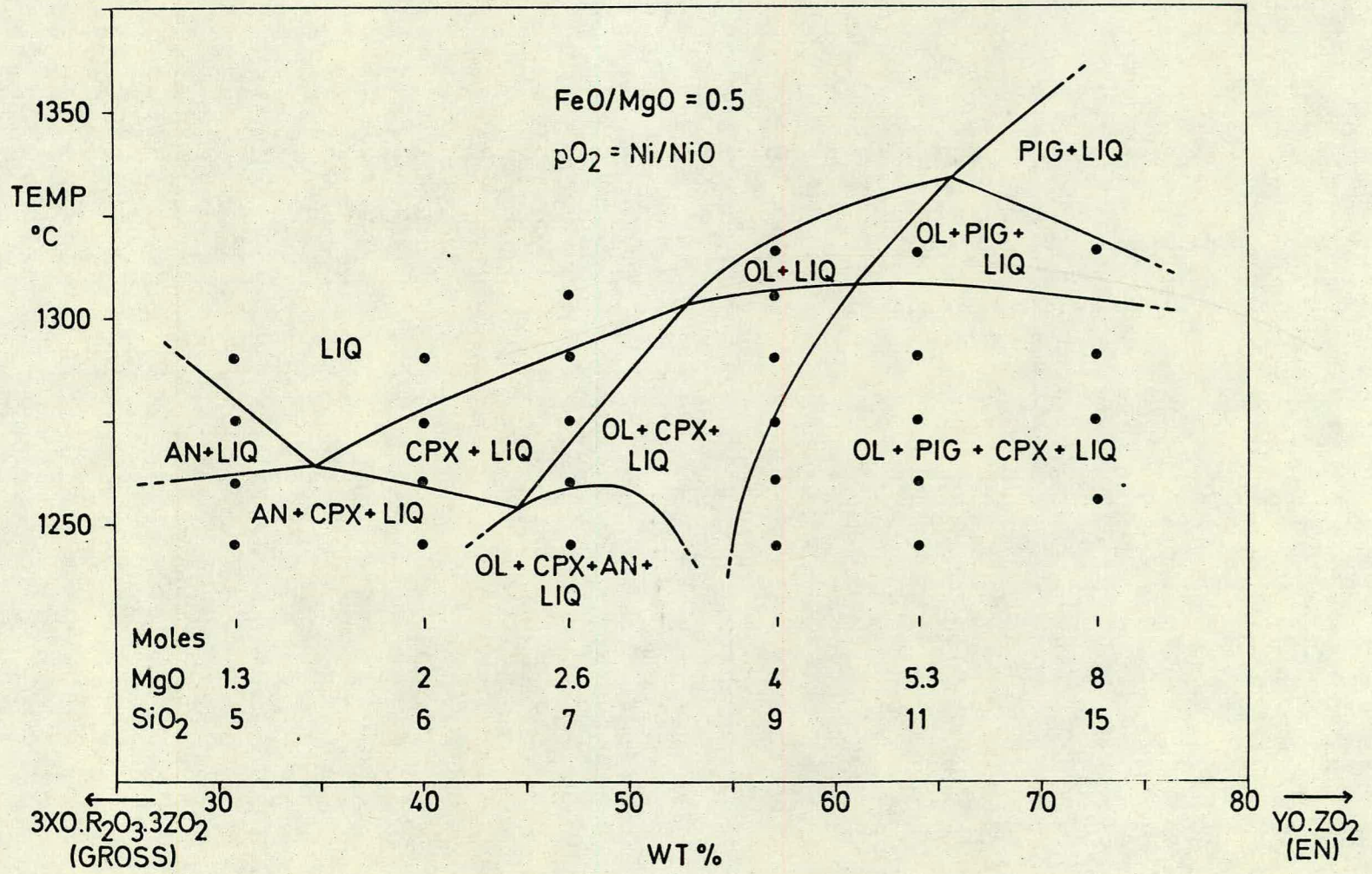
FeO/MgO = 0.5
pO_2 = Ni/NiO
1350
TEMP
°C
1300
1250
LIQ
PIG+LIQ
OL+PIG+
LIQ
OL+LIQ
AN+LIQ
CPX + LIQ
OL+CPX+
LIQ
OL + PIG + CPX + LIQ
AN+CPX+LIQ
OL+CPX+AN+
LIQ
Moles
MgO 1.3 2 2.6 4 5.3 8
SiO_2 5 6 7 9 11 15
30
40
50
60
70
80
$3XO.R_2O_3.3ZO_2$
(GROSS)
WT %
$YO.ZO_2$
(EN)

Fig 6.74

Figure 6.75

See figure 6.72

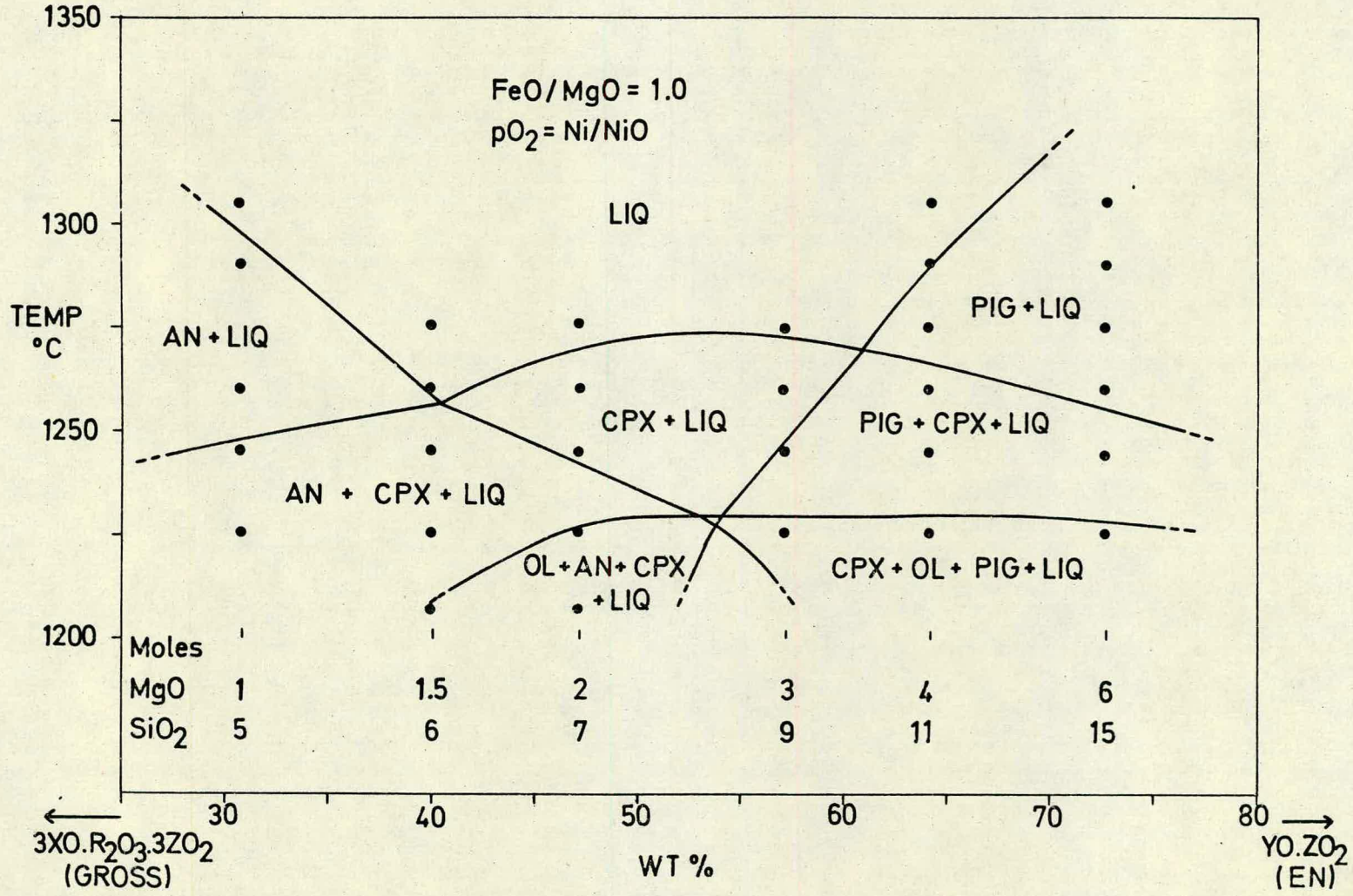
1350
1300
1250
1200
TEMP °C
FeO / MgO = 1.0
pO2 = Ni/NiO
LIQ
AN + LIQ
CPX + LIQ
PIG + LIQ
PIG + CPX + LIQ
AN + CPX + LIQ
OL + AN + CPX + LIQ
CPX + OL + PIG + LIQ
Moles
MgO 1 1.5 2 3 4 6
SiO2 5 6 7 9 11 15
30
40
50
60
70
80
3XO.R2O3.3ZO2 (GROSS)
WT %
YO.ZO2 (EN)

Fig 6.75

Figure 6.76

See figure 6.72

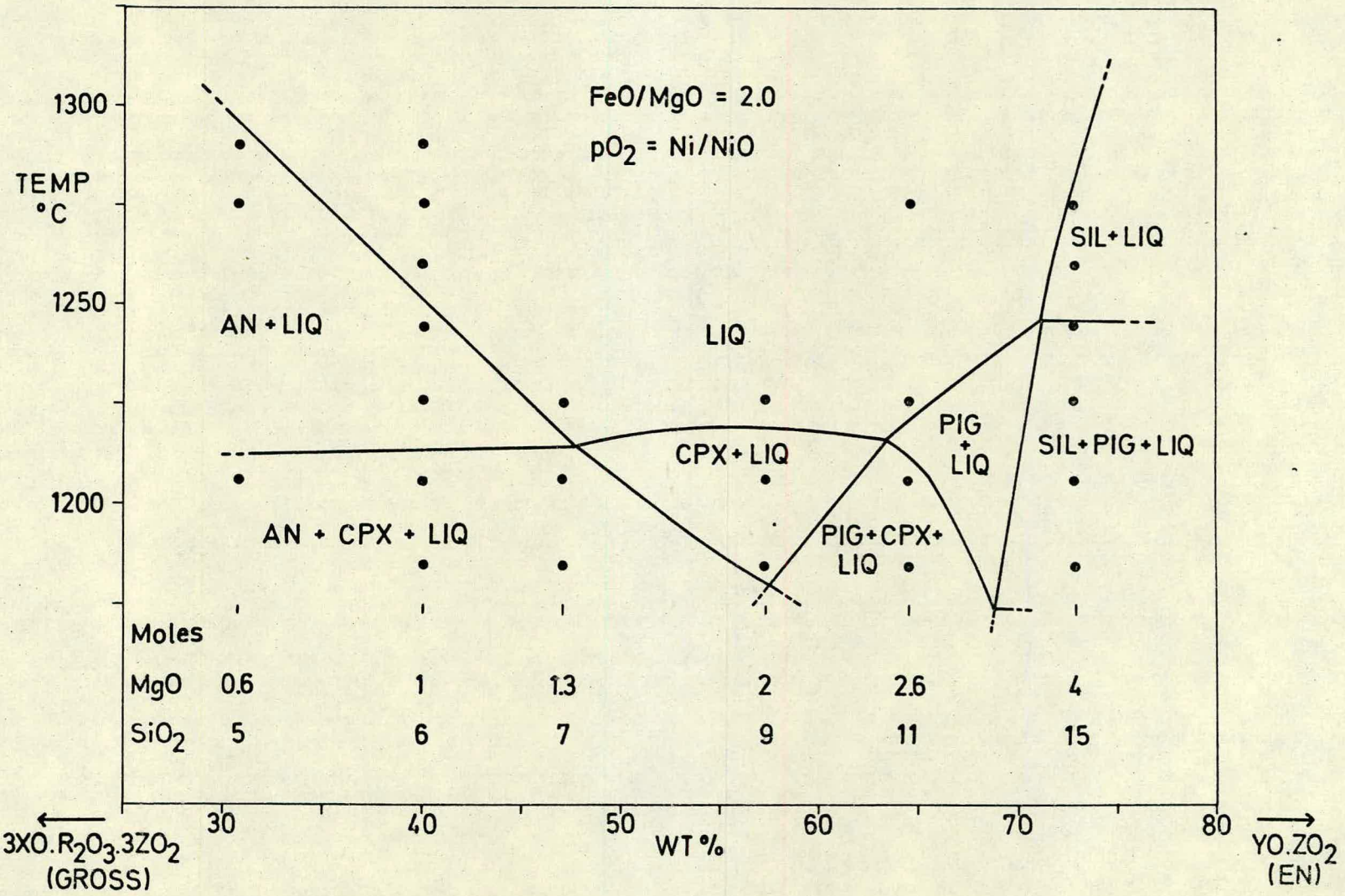
FeO/MgO = 2.0
pO2 = Ni/NiO
TEMP °C
1300
1250
1200
AN + LIQ
LIQ
SIL + LIQ
CPX + LIQ
PIG + LIQ
SIL + PIG + LIQ
AN + CPX + LIQ
PIG + CPX + LIQ
Moles
MgO 0.6 1 1.3 2 2.6 4
SiO2 5 6 7 9 11 15
30 40 50 60 70 80
WT %
3XO.R2O3.3ZO2 (GROSS)
YO.ZO2 (EN)

Fig 6.76

Figure 6.77

See figure 6.72

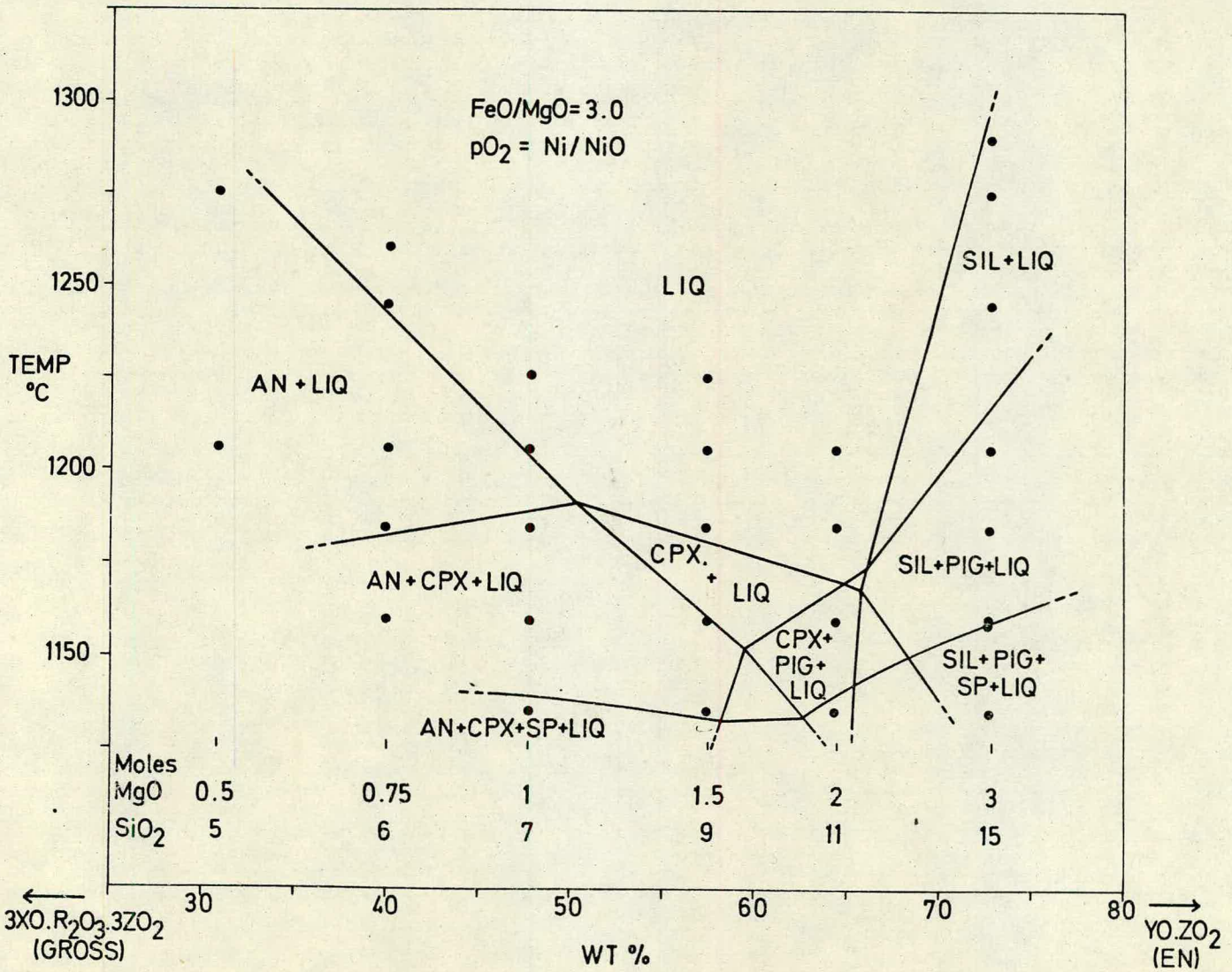
FeO/MgO= 3.0
pO2 = Ni/NiO
1300
1250
1200
1150
TEMP °C
AN + LIQ
LIQ
SIL+LIQ
AN+CPX+LIQ
CPX. + LIQ
SIL+PIG+LIQ
CPX+ PIG+ LIQ
SIL+PIG+ SP+LIQ
AN+CPX+SP+LIQ
Moles MgO 0.5 0.75 1 1.5 2 3
SiO2 5 6 7 9 11 15
30
40
50
60
70
80
3XO.R2O3.3ZO2 (GROSS)
WT %
YO.ZO2 (EN)

Fig 6.77

Figure 6.78

See figure 6.72

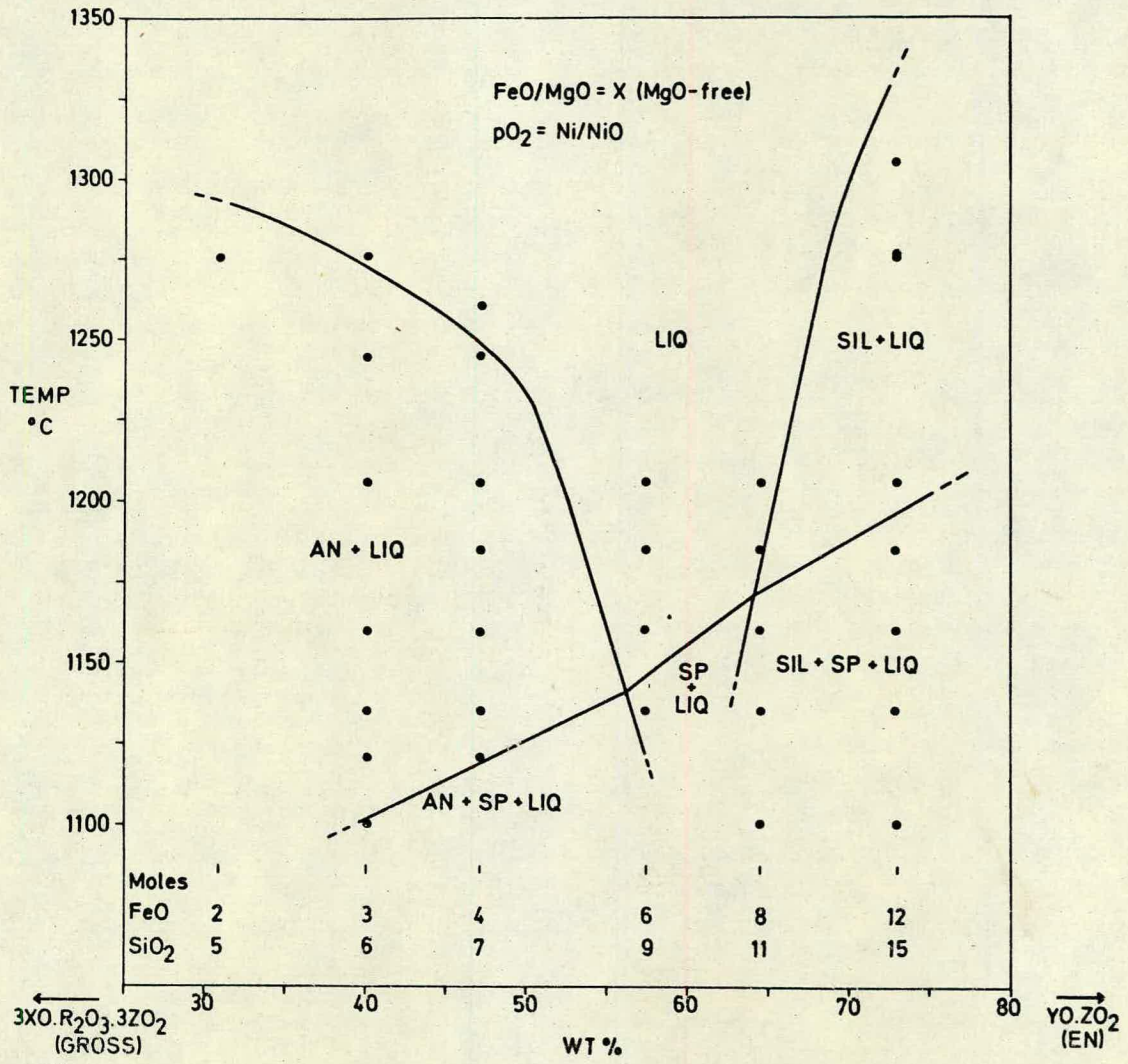
FeO/MgO = X (MgO-free)
pO_2 = Ni/NiO
LIQ
SIL + LIQ
AN + LIQ
SP + LIQ
SIL + SP + LIQ
AN + SP + LIQ
TEMP °C
1350
1300
1250
1200
1150
1100
Moles
FeO 2 3 4 6 8 12
SiO_2 5 6 7 9 11 15
30
40
50
60
70
80
WT %
$3XO.R_2O_3.3ZO_2$ (GROSS)
$YO.ZO_2$ (EN)

Fig 6.78

Figure 6.79

Liquidus diagram for part of the join $YO.ZO_2$-$3XO.R_2O_3.3ZO_2$ (Enstatite-Grossular), to show the change in liquidus phase with changing FeO/MgO ratio for molecularly equivalent compositions, at the pO_2 of the Ni/NiO equilibrium. The compositions studied are shown by filled circles, the composition names can be found by referring to the individual T - X sections for this join (figures 6.72-6.78). The phase boundaries are indicated by thick solid lines, the dashed lines are the temperature contours where known. Data from the join MgO-SiO_2-Fe-O_2 at these pO_2 (figure 6.5) was used along the join "MS"-"FS".

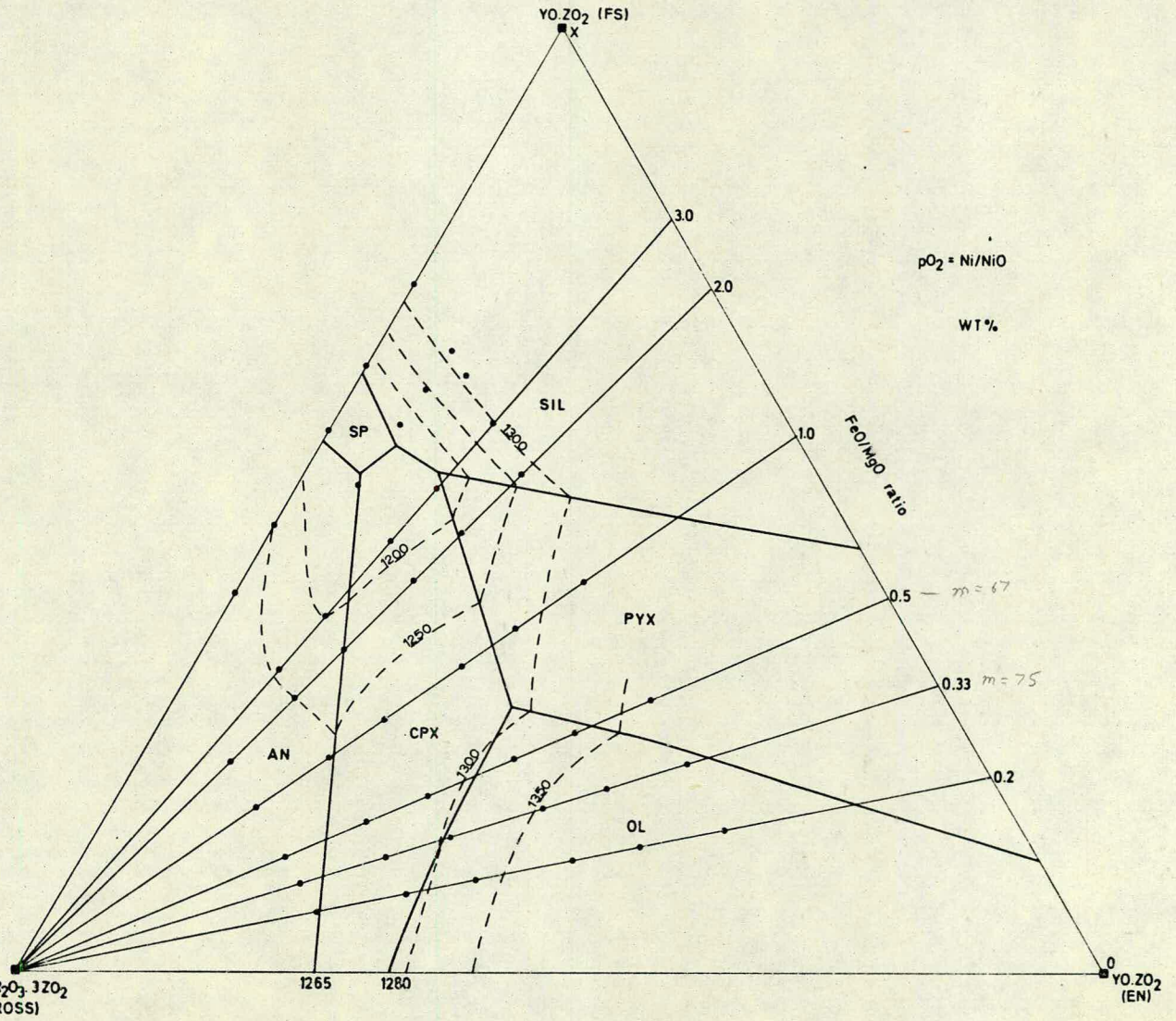
YO.ZO2 (FS)
X
3.0
2.0
1.0
0.5
0.33
0.2
0
FeO/MgO ratio
pO2 = Ni/NiO
WT%
SIL
SP
PYX
CPX
AN
OL
1200
1250
1300
1350
1265
1280
3XO.R2O3.3ZO2
(GROSS)
YO.ZO2
(EN)

Fig 6.79

Figure 6.80

Diagram to show the change in second phase to crystallise for molecularly equivalent compositions in part of the join $YO.ZO_2$-$3XO.R_2O_3.3ZO_2$ (Enstatite-Grossular), with changing FeO/MgO ratio, at the pO_2 of the Ni/NiO equilibrium. The compositions studied are shown by filled circles, the composition names can be found by referring to the individual T - X sections for this join (figures 6.72-6.78). The liquidus phase boundaries are indicated by thick solid lines, the projected phase boundaries within each phase volume by thin solid lines. The phase assemblage for each area is indicated. The dashed lines are the temperature contours for the appearance of the second phase in each composition in the join where known.

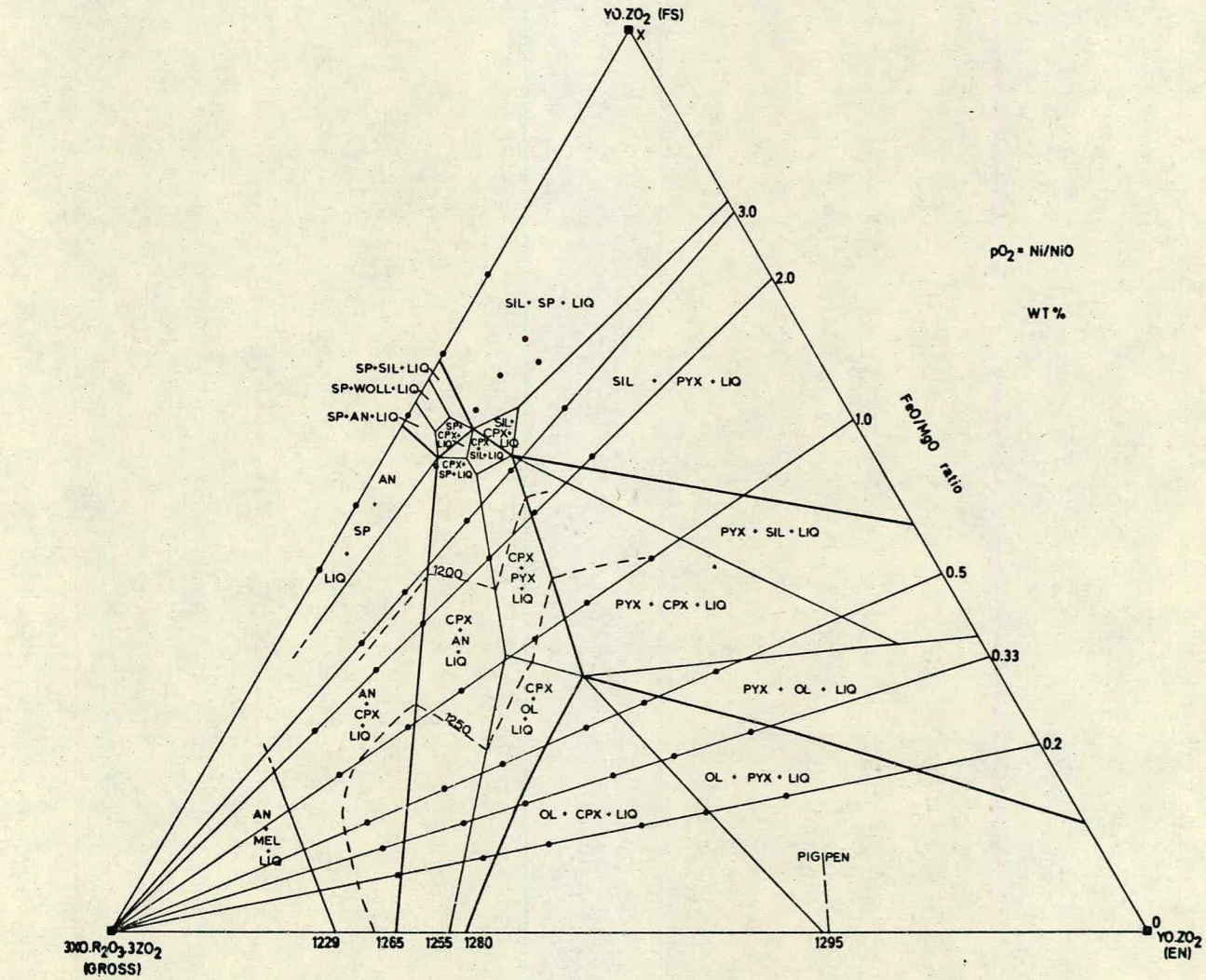
YO.ZO2 (FS)
X
3.0
2.0
1.0
0.5
0.33
0.2
0
pO2 = Ni/NiO
WT %
FeO/MgO ratio
SIL • SP • LIQ
SP•SIL•LIQ
SP•WOLL•LIQ
SP•AN•LIQ
SP • CPX • LIQ
SIL • CPX • LIQ
CPX • SIL • LIQ
CPX • SP • LIQ
SIL • PYX • LIQ
PYX • SIL • LIQ
PYX • CPX • LIQ
PYX • OL • LIQ
OL • PYX • LIQ
OL • CPX • LIQ
AN
SP
LIQ
1200
CPX
PYX
LIQ
CPX
AN
LIQ
AN
CPX
LIQ
1250
CPX
OL
LIQ
AN
MEL
LIQ
PIGEON
3XO.R2O3.3ZO2
(GROSS)
1229
1265
1255
1280
1295
YO.ZO2
(EN)

Fig 6.80

Figures 6.81 to 6.83

T - X sections for part of the join $3XO.R_2O_3.15ZO_2$-YO (C_3AS_{15}-M) at FeO/MgO mole ratios of 0.5, 1.0, and 2.0, and the pO_2 of the Ni/NiO equilibrium. The experiments on each composition are shown at the appropriate temperatures by filled circles. The composition names are generated from the information beneath each composition studied, using the format

FeO/MgO mole ratio - moles MgO - 3 - 1 - moles SiO_2.

The phase boundaries are drawn using the combined data plots presented in figures 6.84, 6.85. Some data points are inconsistent with these phase boundaries, but generally only by a small temperature error.

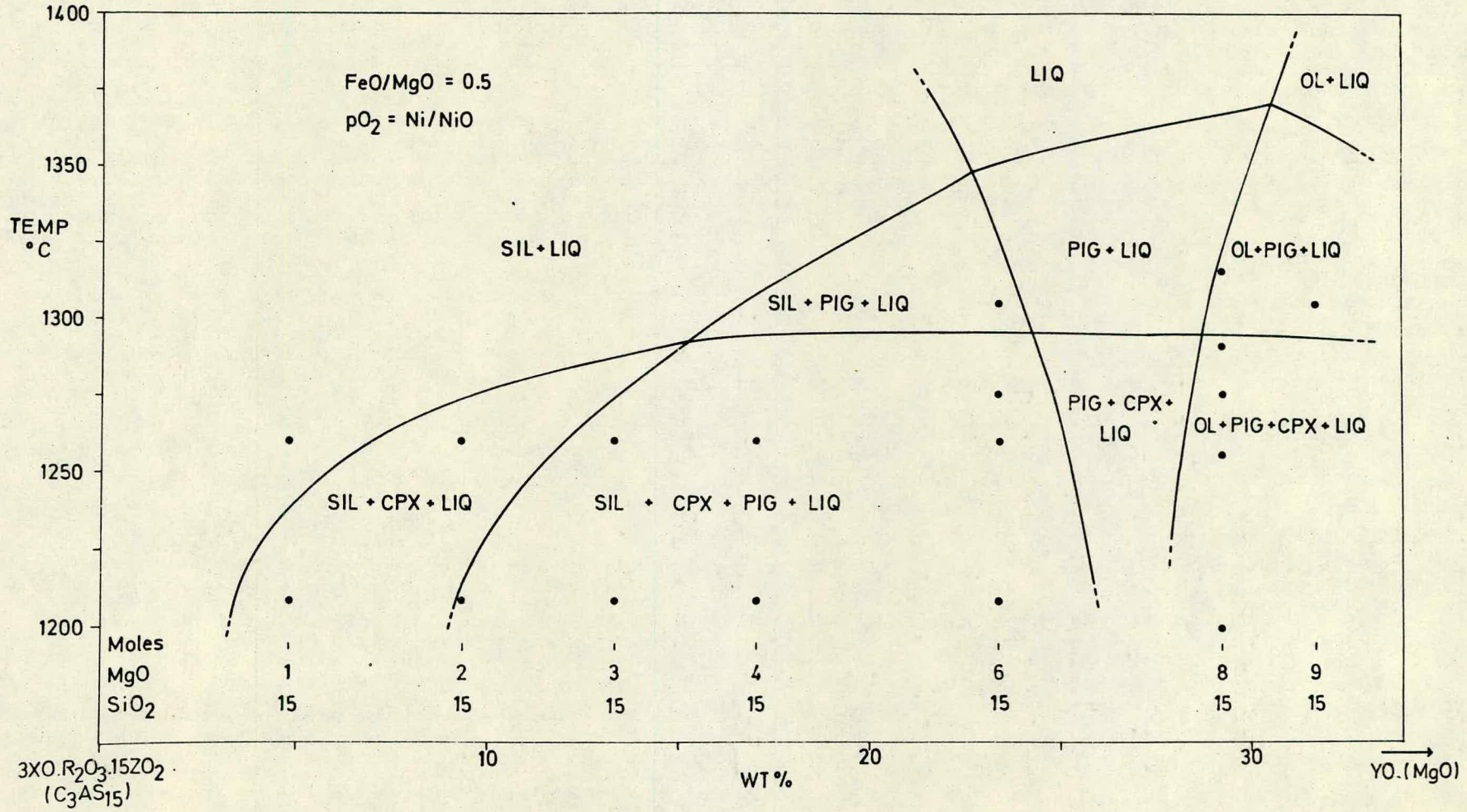
1400
1350
1300
1250
1200
TEMP °C
FeO/MgO = 0.5
pO_2 = Ni/NiO
LIQ
OL + LIQ
SIL + LIQ
PIG + LIQ
OL + PIG + LIQ
SIL + PIG + LIQ
PIG + CPX + LIQ
OL + PIG + CPX + LIQ
SIL + CPX + LIQ
SIL + CPX + PIG + LIQ
Moles MgO
Moles SiO_2
1 15
2 15
3 15
4 15
6 15
8 15
9 15
10
20
30
WT %
$3XO.R_2O_3.15ZO_2$
(C_3AS_{15})
YO.(MgO)

Fig 6.81

Figure 6.82

See figure 6.81

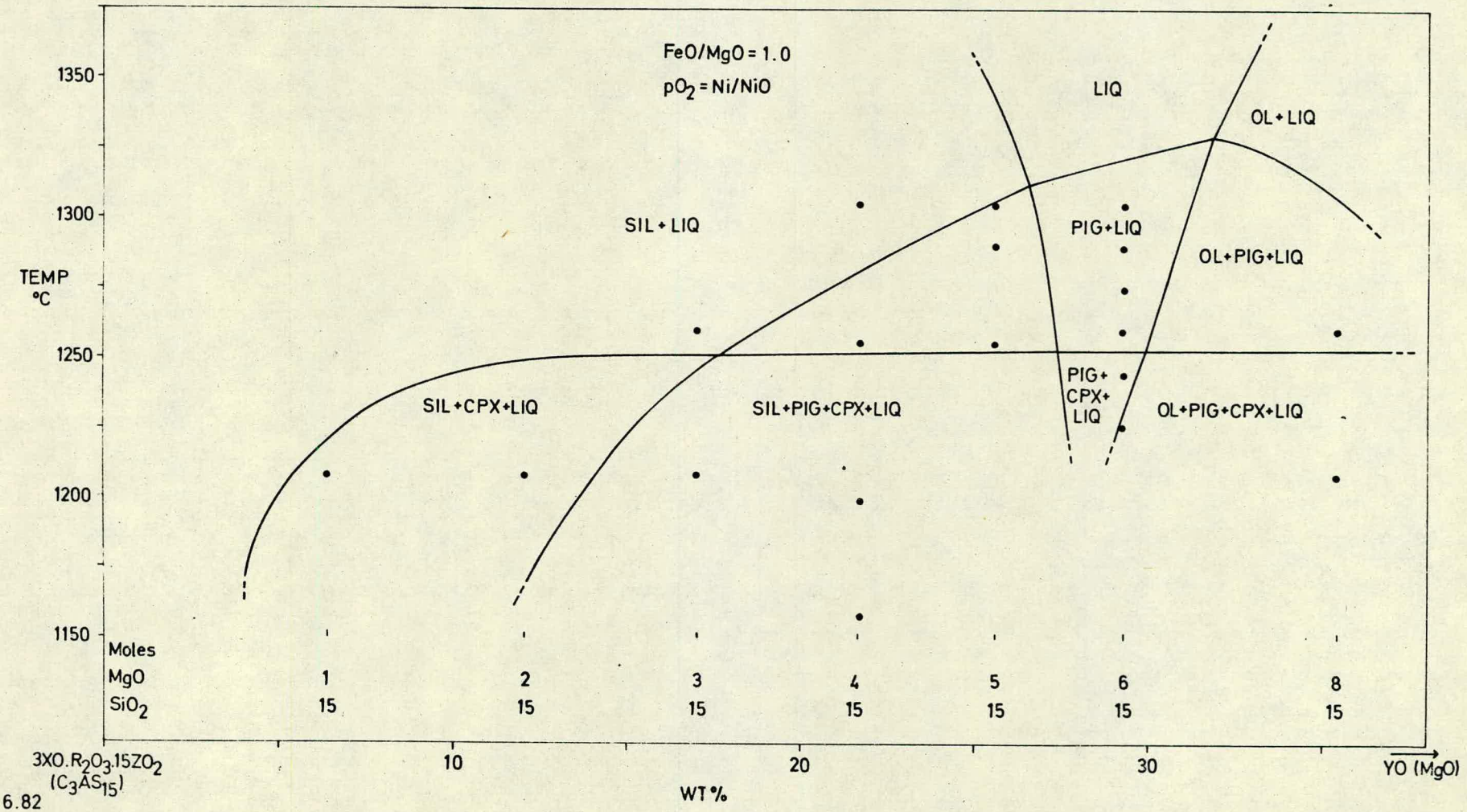
FeO/MgO = 1.0
pO_2 = Ni/NiO
LIQ
OL + LIQ
SIL + LIQ
PIG+LIQ
OL+PIG+LIQ
PIG+ CPX+ LIQ
SIL+CPX+LIQ
SIL+PIG+CPX+LIQ
OL+PIG+CPX+LIQ
TEMP °C
1350
1300
1250
1200
1150
Moles
MgO 1 2 3 4 5 6 8
SiO_2 15 15 15 15 15 15 15
$3XO.R_2O_3.15ZO_2$
(C_3AS_{15})
10
20
30
YO (MgO)
WT %

Fig 6.82

Figure 6.83

See figure 6.81

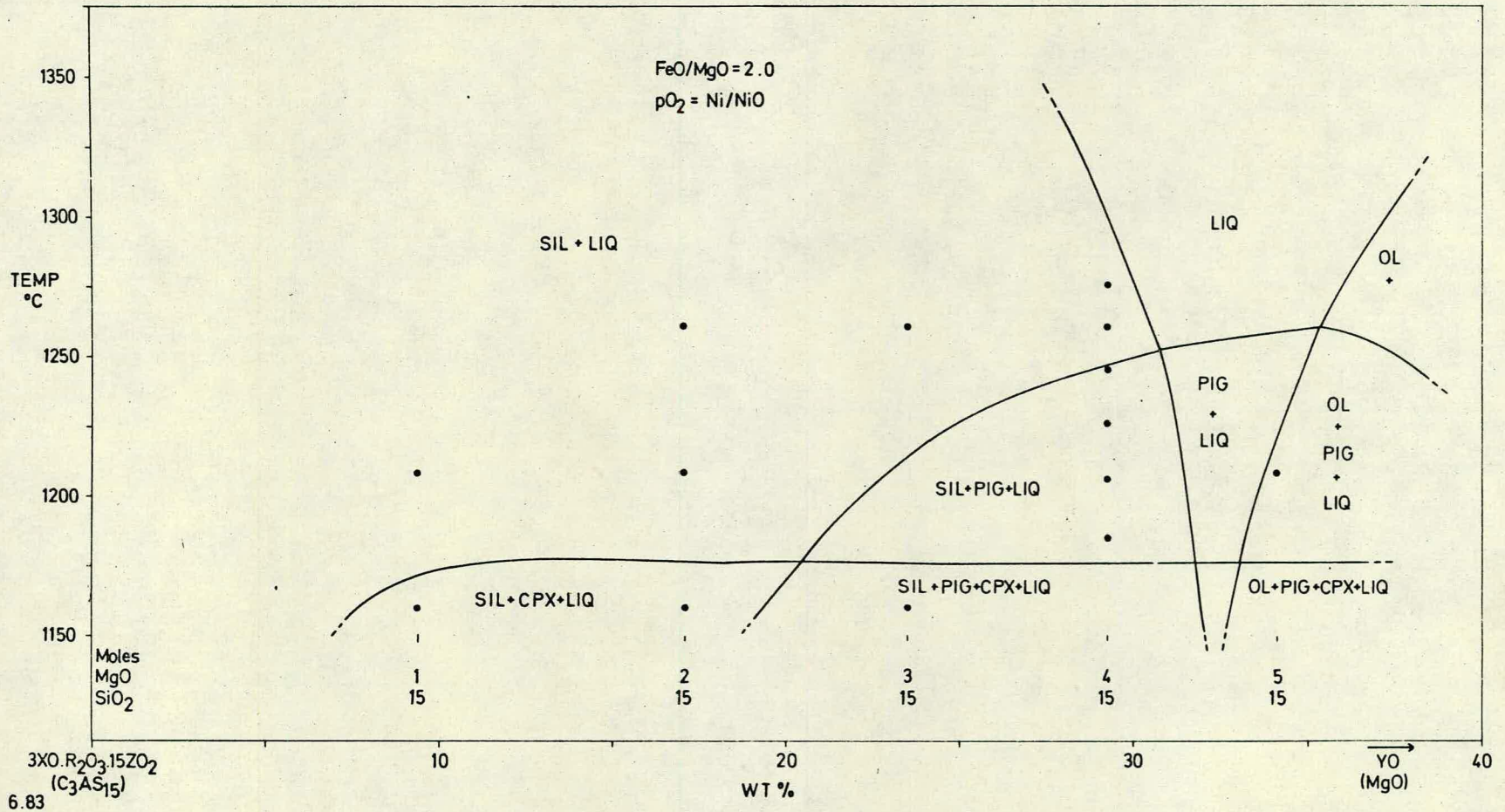
FeO/MgO = 2.0
pO_2 = Ni/NiO
SIL + LIQ
LIQ
OL
+
PIG
+
LIQ
OL
+
PIG
+
LIQ
SIL+PIG+LIQ
SIL+CPX+LIQ
SIL+PIG+CPX+LIQ
OL+PIG+CPX+LIQ
TEMP
°C
1350
1300
1250
1200
1150
Moles
MgO
SiO_2
1
15
2
15
3
15
4
15
5
15
$3XO.R_2O_3.15ZO_2$
(C_3AS_{15})
10
20
30
40
WT %
YO
(MgO)

Fig 6.83

Figure 6.84

Liquidus diagram for part of the join $3XO.R_2O_3.15ZO_2$-YO (C_3AS_{15}-M), to show the change in liquidus phase with changing FeO/MgO ratio for molecularly equivalent compositions, at the pO_2 of the Ni/NiO equilibrium. The compositions studied are shown by filled circles, the composition names can be found by referring to the individual T - X sections for this join (figures 6.81-6.83). The phase boundaries are indicated by thick solid lines.

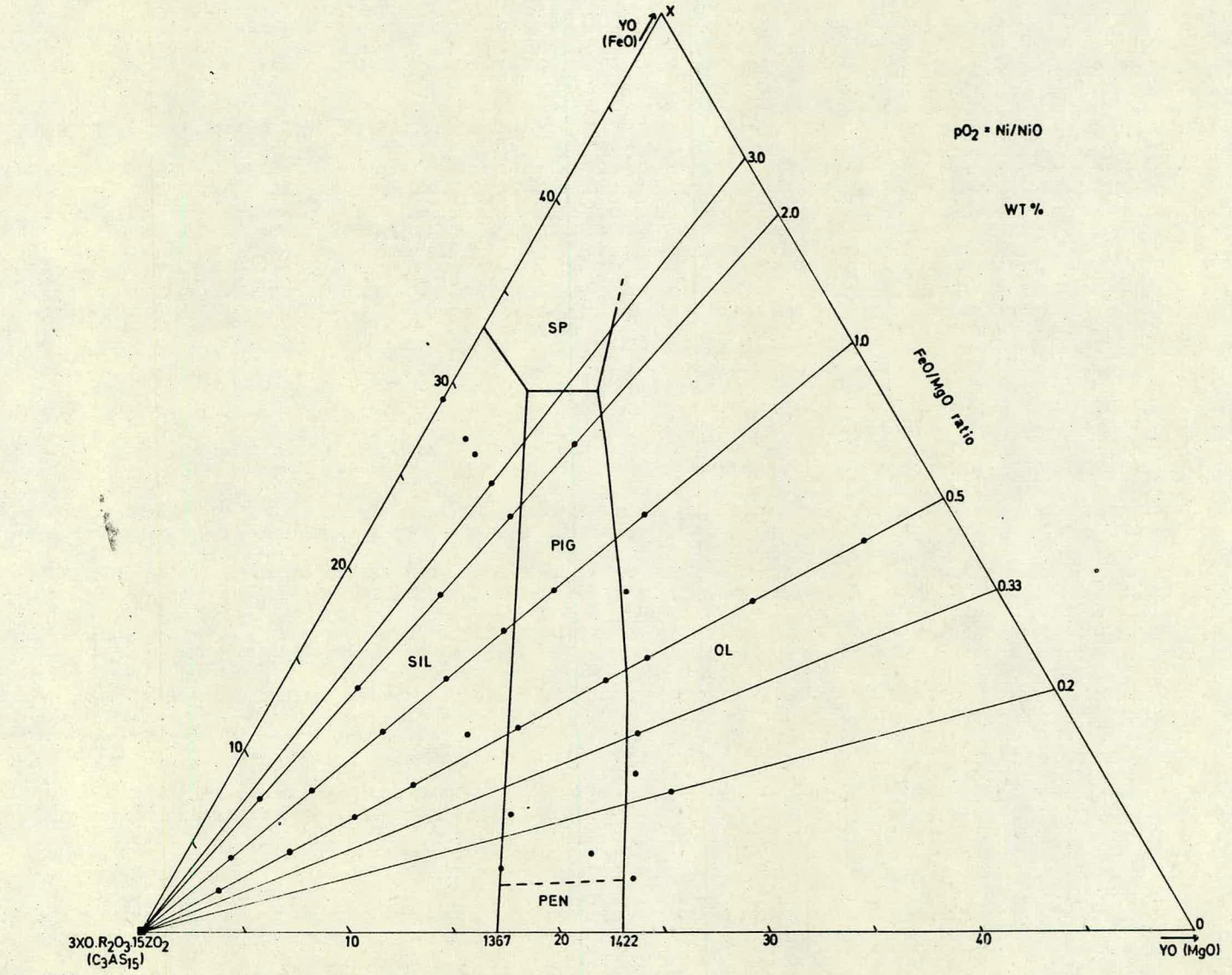
YO
(FeO)
X
pO_2 = Ni/NiO
WT %
3.0
2.0
1.0
0.5
0.33
0.2
0
40
30
20
10
SP
PIG
SIL
OL
PEN
FeO/MgO ratio
$3XO.R_2O_3.15ZO_2$
(C_3AS_{15})
10
1367
20
1422
30
40
YO (MgO)

Fig 6.84

Figure 6.85

Diagram to show the change in second phase to crystallise for molecularly equivalent compositions in part of the join 3 XO.R_2O_3.1.5ZO_2-YO ($C_3AS_{1.5}$-M), with changing FeO/MgO ratio, at the pO_2 of the Ni/NiO equilibrium. The compositions studied are shown by filled circles, the composition names can be found by referring to the individual T - X sections for this join (figures 6.81-6.83). The liquidus phase boundaries are indicated by thick solid lines, the projected phase boundaries within each phase volume are indicated by thin solid lines. The phase assemblage for each area is indicated. The dashed lines are the temperature contours for the appearance of the second phase in each composition in this part of the join, where known.

The thick dashed line marks the approximate maximum extent of pen occurrence in this join. The dash-dot line marks the area in which pen does not react with the liquid, pig therefore not occurring.

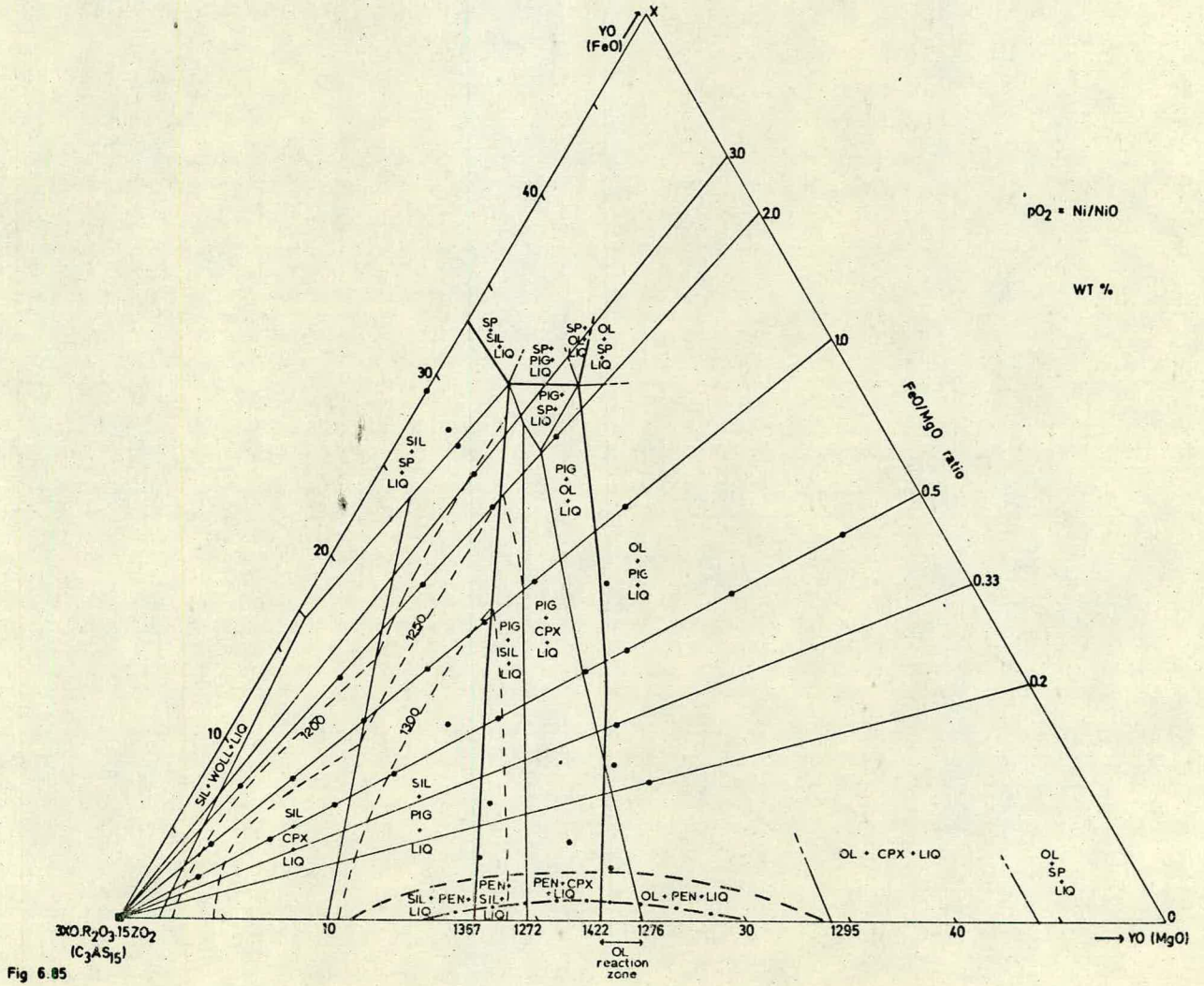
YO (FeO)
X
pO_2 = Ni/NiO
WT %
FeO/MgO ratio
30
40
20
10
2.0
1.0
0.5
0.33
0.2
0
SP + SIL + LIQ
SP + PIG + LIQ
SP + OL + LIQ
OL + SP + LIQ
PIG + SP + LIQ
SIL + SP + LIQ
PIG + OL + LIQ
OL + PIG + LIQ
PIG + ISIL + LIQ
PIG + CPX + LIQ
SIL + WOLL + LIQ
1250
1200
1300
SIL + CPX + LIQ
SIL + PIG + LIQ
OL + CPX + LIQ
OL + SP + LIQ
PEN + SIL + LIQ
PEN + CPX + LIQ
SIL + PEN + LIQ
OL + PEN + LIQ
3XO.R_2O_3.15ZO_2
(C_3AS_{15})
10
1357
1272
1422
1276
30
1295
40
YO (MgO)
OL reaction zone

Fig 6.85

Figures 6.86 to 6.90

Liquidus diagrams for part of the plane $XO.ZO_2$-$YO.ZO_2$-R_2O_3 (CS-MS-A) at FeO/MgO mole ratios of 0.5, 1.0, 2.0, 3.0, and X (MgO-free), and the pO_2 of the Ni/NiO equilibrium. The diagrams show the relationship between the joins $XO.YO.2ZO_2$-$YO.R_2O_3.ZO_2$ (Diopside-MAS), $XO.YO.2ZO_2$-$5YO.3R_2O_3.5ZO_2$ (Diopside-$M_5A_3S_5$), and $YO.ZO_2$-$3XO.R_2O_3.3ZO_2$ (Enstatite-Grossular) studied here, and the join $YO.ZO_2$-$XO.R_2O_3.2ZO_2$:$2YO.ZO_2$ (Enstatite-AnorthiteForsterite piercing point) from Roeder and Osborn (1966), presented as figure 6.16 for these pO_2. The compositions studied are shown by filled circles, the composition names can be found by referring to the T - X sections for the join in question. The phase boundaries are indicated by thick solid lines.

The dashed lines within the olivine phase volume are the projection phase boundaries, indicating the second phase to crystallise for compositions lying in this join. Data for the olivine projection of compositions in the join $YO.ZO_2$-$XO.R_2O_3.2ZO_2$:$2YO.ZO_2$ (Enstatite-AnorthiteForsterite piercing point) from Roeder and Osborn (1966), presented as figure 6.18 for these pO_2, was also used.

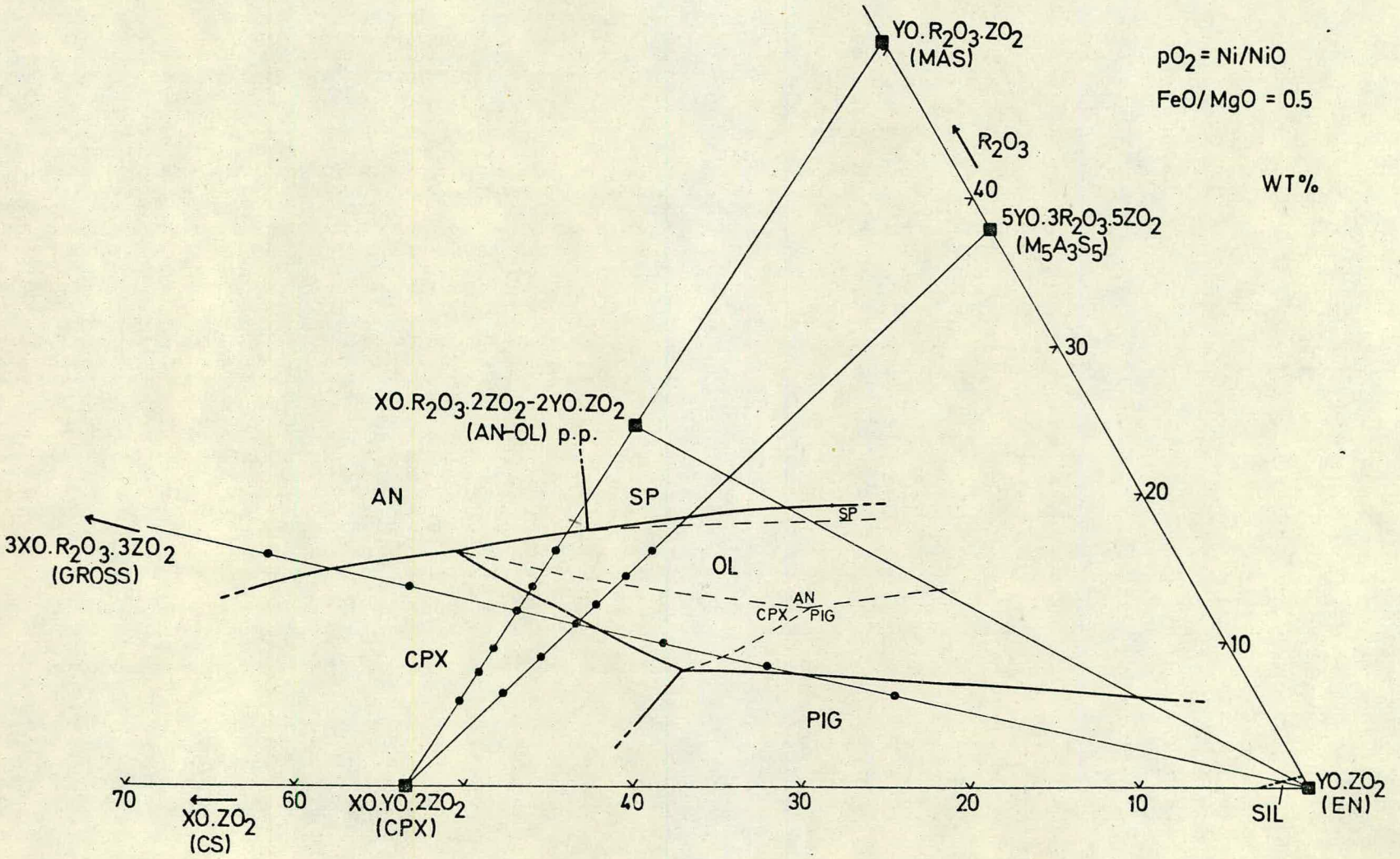
YO.R2O3.ZO2
(MAS)
pO2 = Ni/NiO
FeO/MgO = 0.5
R2O3
WT%
40
5YO.3R2O3.5ZO2
(M5A3S5)
30
XO.R2O3.2ZO2-2YO.ZO2
(AN-OL) p.p.
20
AN
SP
SP
3XO.R2O3.3ZO2
(GROSS)
OL
AN
CPX
PIG
10
CPX
PIG
70
60
XO.YO.2ZO2
(CPX)
40
30
20
10
SIL
YO.ZO2
(EN)
XO.ZO2
(CS)

Fig 6.86

Figure 6.87

See figure 6.86

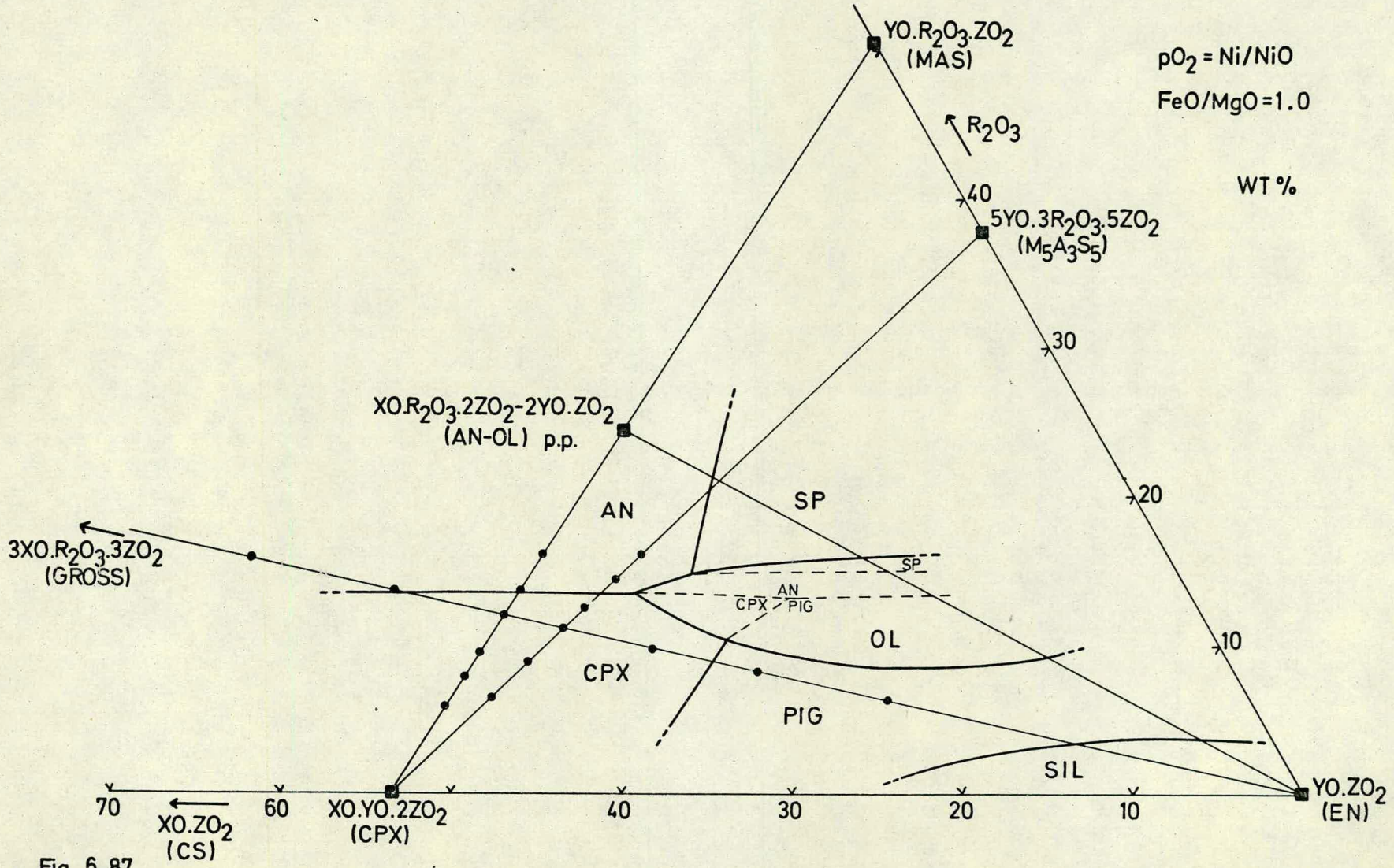
YO.R2O3.ZO2
(MAS)
pO2 = Ni/NiO
FeO/MgO=1.0
R2O3
WT %
40
5YO.3R2O3.5ZO2
(M5A3S5)
30
XO.R2O3.2ZO2-2YO.ZO2
(AN-OL) p.p.
20
AN
SP
3XO.R2O3.3ZO2
(GROSS)
SP
AN
CPX
PIG
OL
10
CPX
PIG
SIL
70
60
XO.YO.2ZO2
(CPX)
40
30
20
10
YO.ZO2
(EN)
XO.ZO2
(CS)

Fig 6.87

Figure 6.88

See figure 6.86

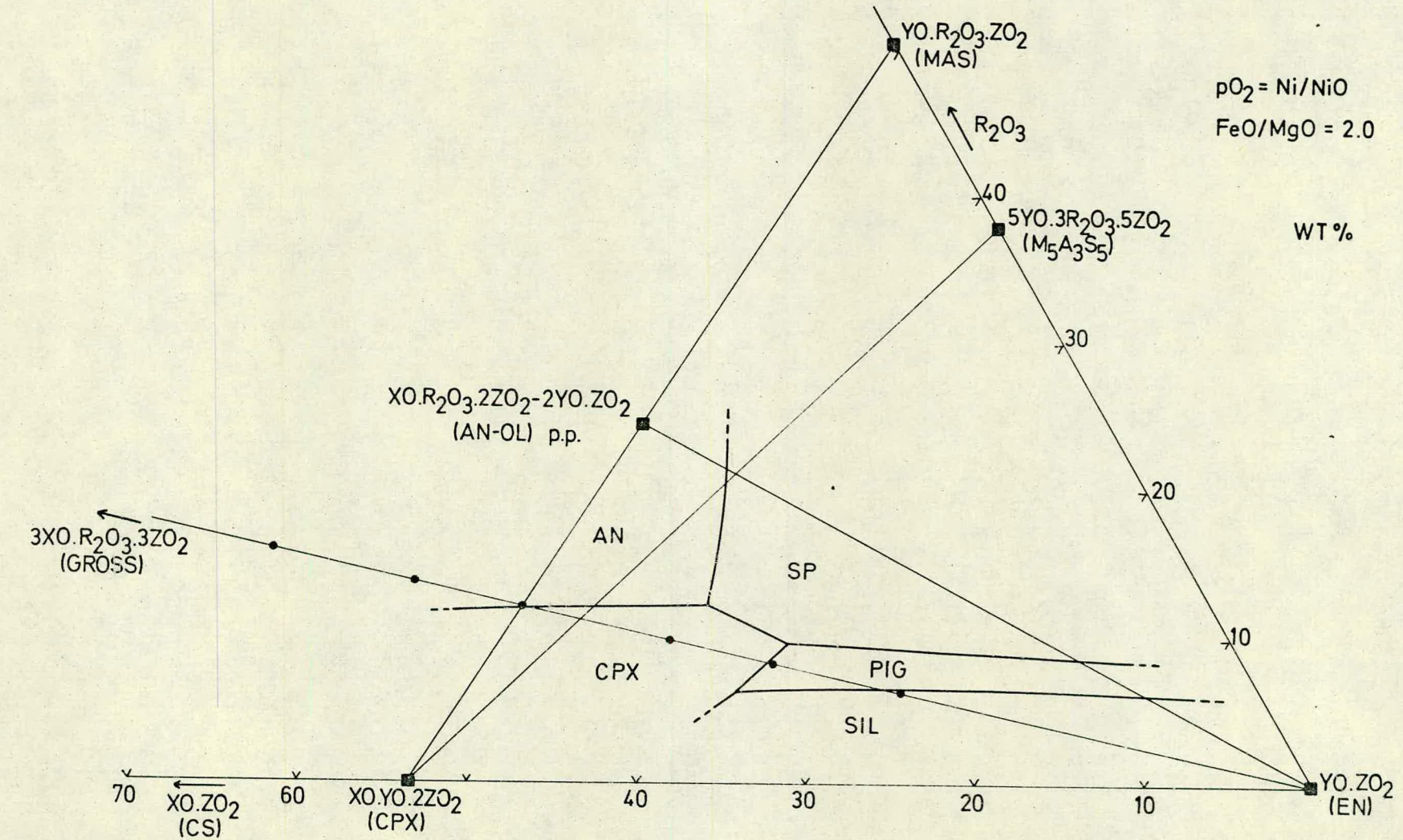
YO.R2O3.ZO2
(MAS)
pO2 = Ni/NiO
FeO/MgO = 2.0
R2O3
40
5YO.3R2O3.5ZO2
(M5A3S5)
WT %
30
XO.R2O3.2ZO2-2YO.ZO2
(AN-OL) p.p.
20
3XO.R2O3.3ZO2
(GROSS)
AN
SP
10
CPX
PIG
SIL
70
XO.ZO2
(CS)
60
XO.YO.2ZO2
(CPX)
40
30
20
10
YO.ZO2
(EN)

Fig 6.88

Figure 6.89

See figure 6.86

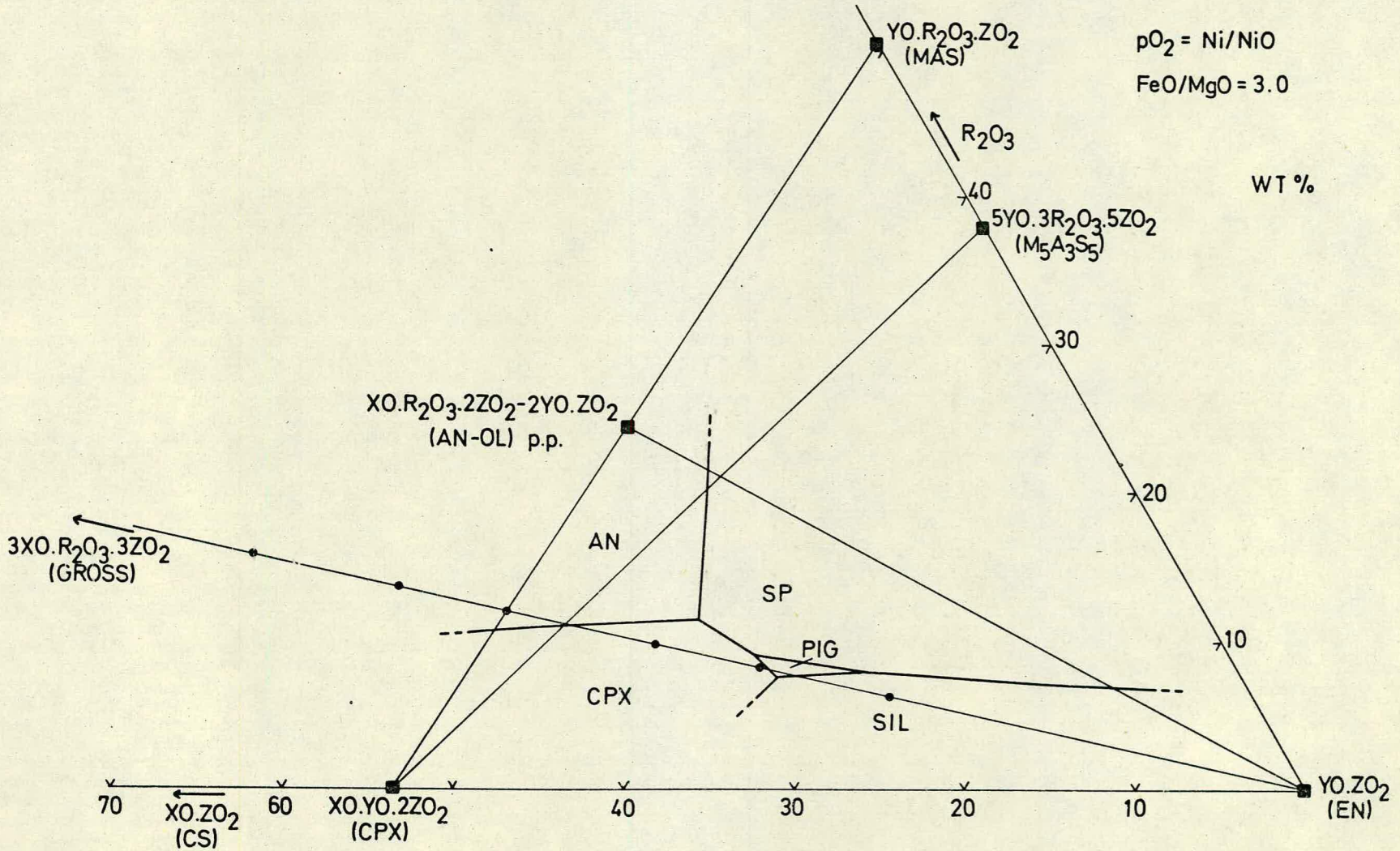
YO.R2O3.ZO2
(MAS)
pO2 = Ni/NiO
FeO/MgO = 3.0
R2O3
WT %
40
5YO.3R2O3.5ZO2
(M5A3S5)
30
XO.R2O3.2ZO2-2YO.ZO2
(AN-OL) p.p.
20
3XO.R2O3.3ZO2
(GROSS)
AN
SP
PIG
10
CPX
SIL
70
XO.ZO2
(CS)
60
XO.YO.2ZO2
(CPX)
40
30
20
10
YO.ZO2
(EN)

Fig 6.89

Figure 6.90

See figure 6.86

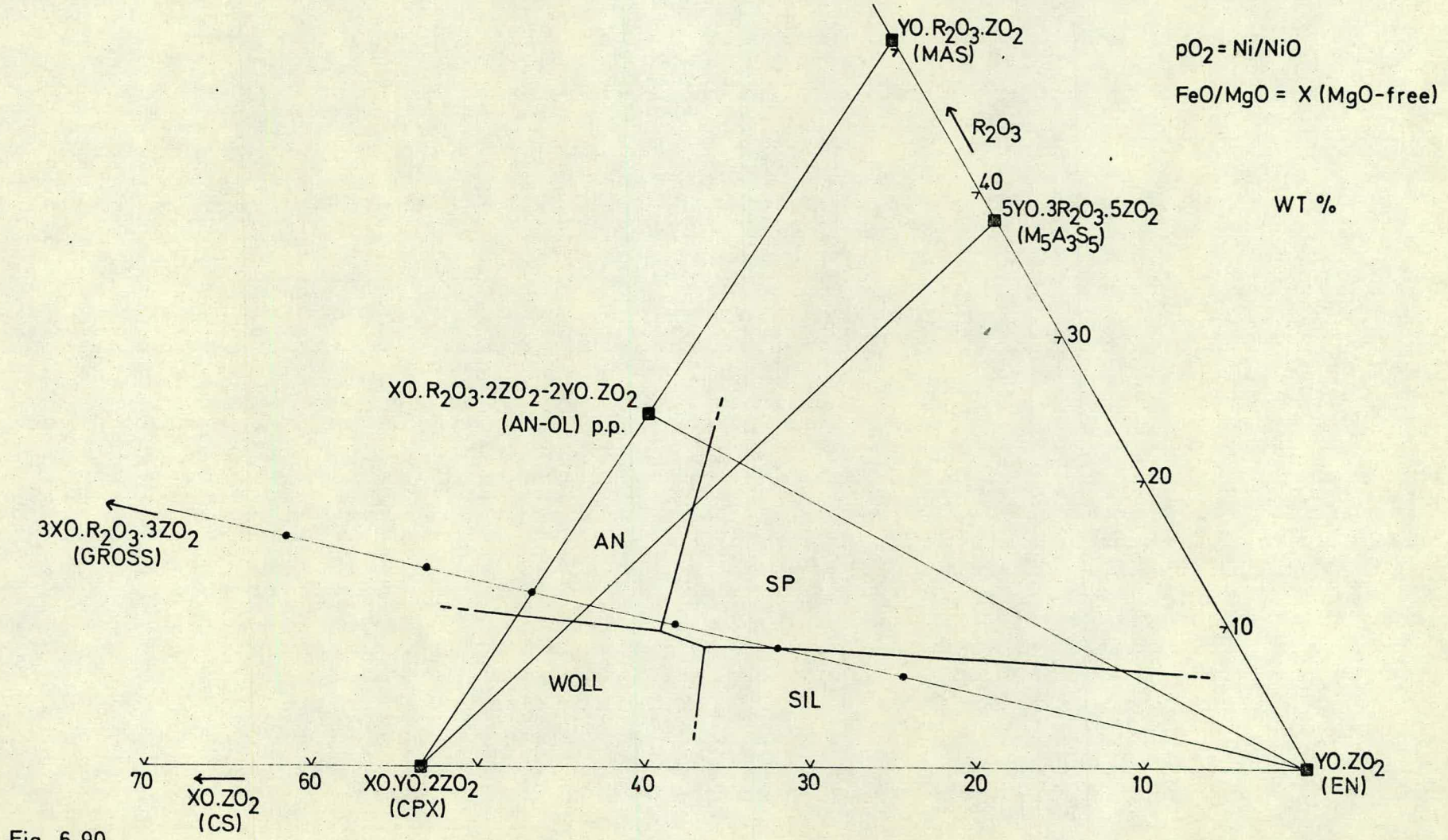
YO.R2O3.ZO2
(MAS)
pO2 = Ni/NiO
FeO/MgO = X (MgO-free)
R2O3
40
5YO.3R2O3.5ZO2
(M5A3S5)
WT %
30
XO.R2O3.2ZO2-2YO.ZO2
(AN-OL) p.p.
20
3XO.R2O3.3ZO2
(GROSS)
AN
SP
10
WOLL
SIL
70
60
XO.ZO2
(CS)
XO.YO.2ZO2
(CPX)
40
30
20
10
YO.ZO2
(EN)

Fig 6.90

Figures 6.91 to 6.95

Liquidus diagrams for part of the plane $3XO.R_2O_3$-YO-ZO_2 (C_3A-M-S) at FeO/MgO mole ratios of 0.5, 1.0, 2.0, 3.0, and X (MgO-free), and the pO_2 of the Ni/NiO equilibrium. The diagrams show the relationship between the joins $YO.ZO_2$-$3XO.R_2O_3.3ZO_2$ (Enstatite-Grossular) and $3XO.R_2O_3.15ZO_2$-YO (C_3AS_{15}-M) studied here, and the join YO-ZO_2 (M-S) at these pO_2 (figure 6.3). The compositions studied are shown by filled circles, the composition names can be found by referring to the T - X sections for the join in question.

The piercing point labelled AD p.p. is the piercing point of the join $XO.R_2O_3.2ZO_2$-$XO.YO.2ZO_2$ (Anorthite-Diopside) in this plane.

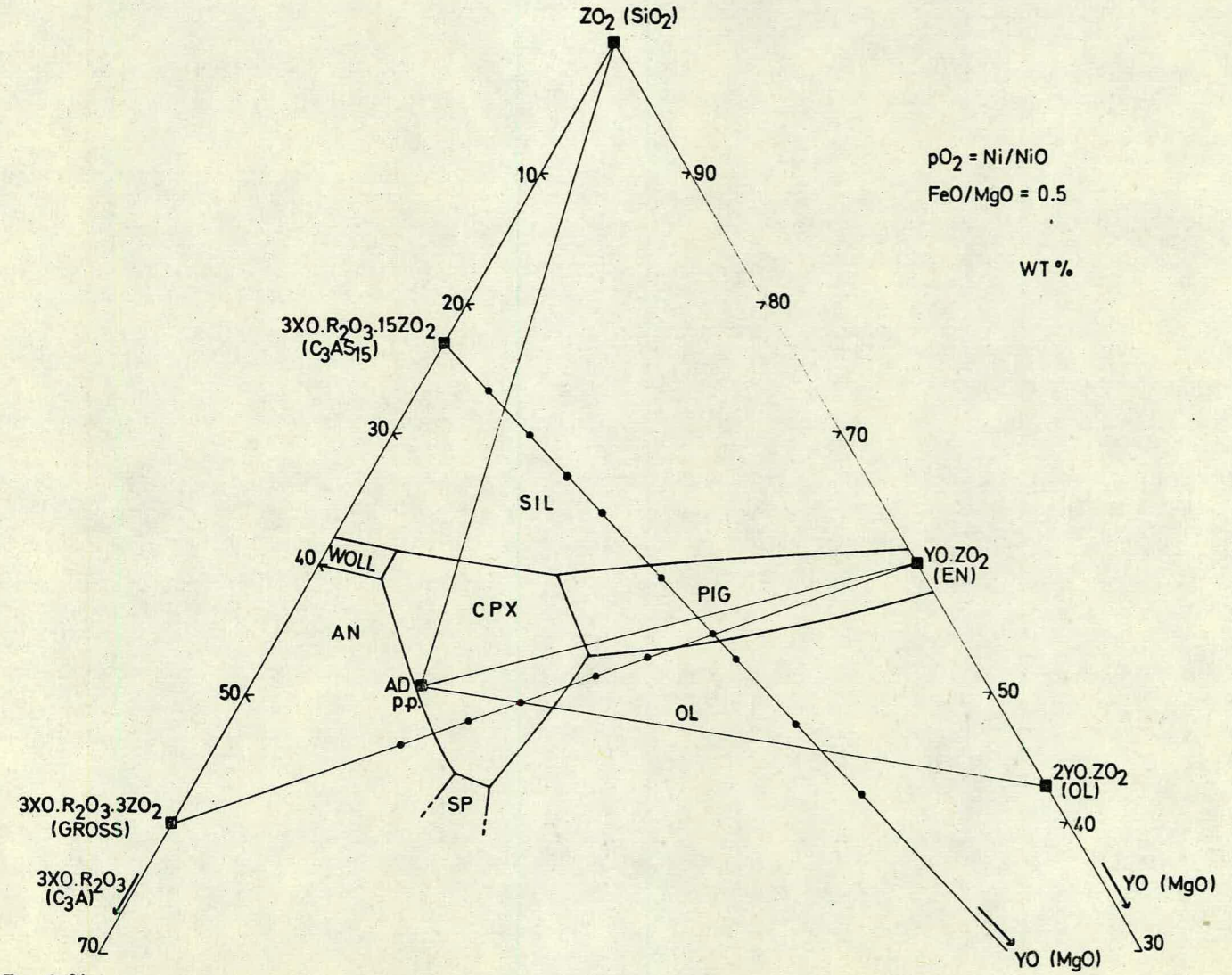
ZO_2 (SiO_2)
pO_2 = Ni/NiO
FeO/MgO = 0.5
WT %
10
90
20
80
$3XO.R_2O_3.15ZO_2$
(C_3AS_{15})
30
70
SIL
40
WOLL
$YO.ZO_2$
(EN)
PIG
CPX
AN
AD
P.P.
50
50
OL
$2YO.ZO_2$
(OL)
$3XO.R_2O_3.3ZO_2$
(GROSS)
SP
40
$3XO.R_2O_3$
(C_3A)
YO (MgO)
YO (MgO)
70
30

Fig 6.91

Figure 6.92

See figure 6.91

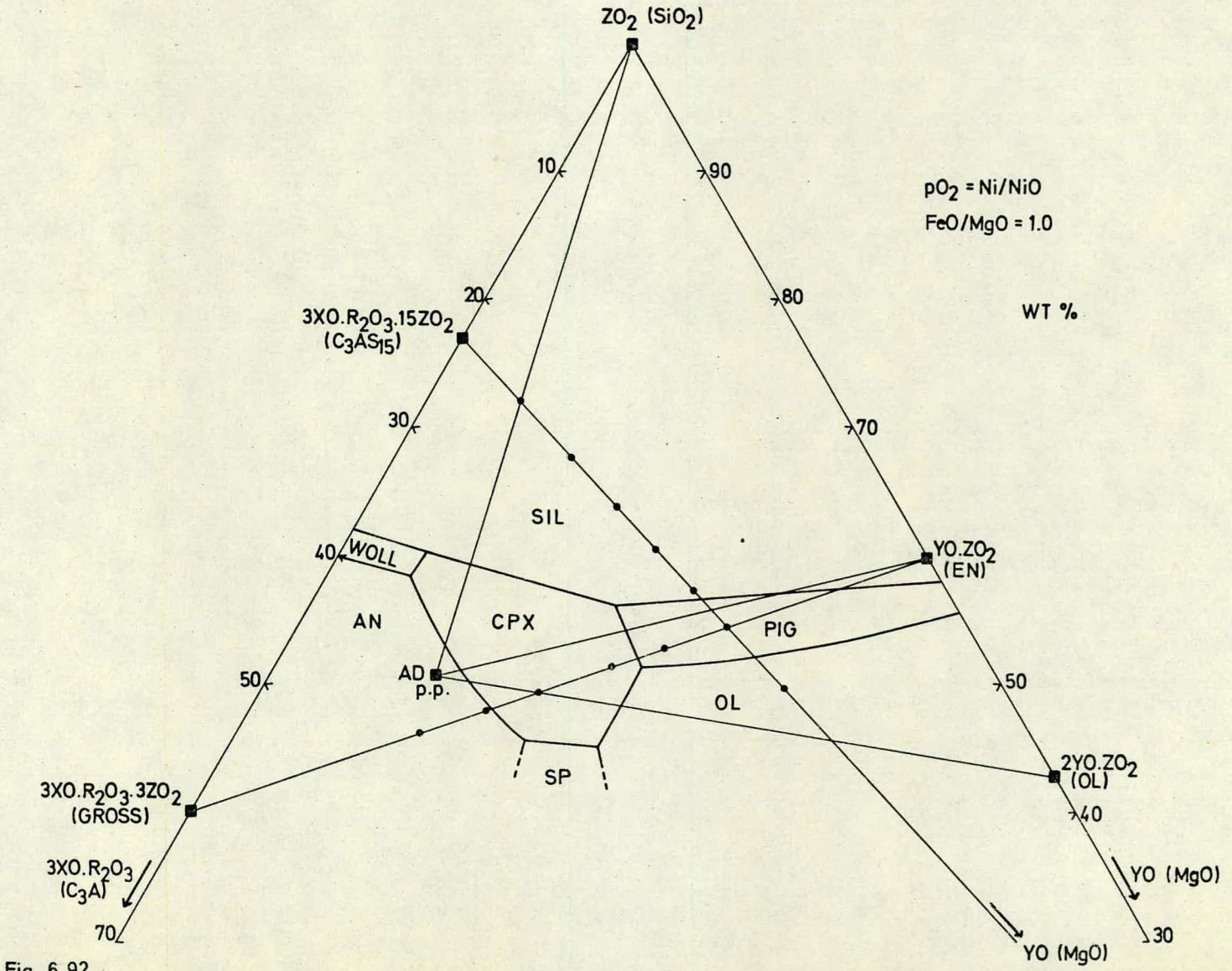
ZO_2 (SiO_2)
10
90
pO_2 = Ni/NiO
FeO/MgO = 1.0
20
80
WT %
$3XO.R_2O_3.15ZO_2$
(C_3AS_{15})
30
70
SIL
40
WOLL
$YO.ZO_2$
(EN)
AN
CPX
PIG
AD
p.p.
50
50
OL
SP
$2YO.ZO_2$
(OL)
$3XO.R_2O_3.3ZO_2$
(GROSS)
40
$3XO.R_2O_3$
(C_3A)
YO (MgO)
70
30
YO (MgO)

Fig 6.92

Figure 6.93

See figure 6.91

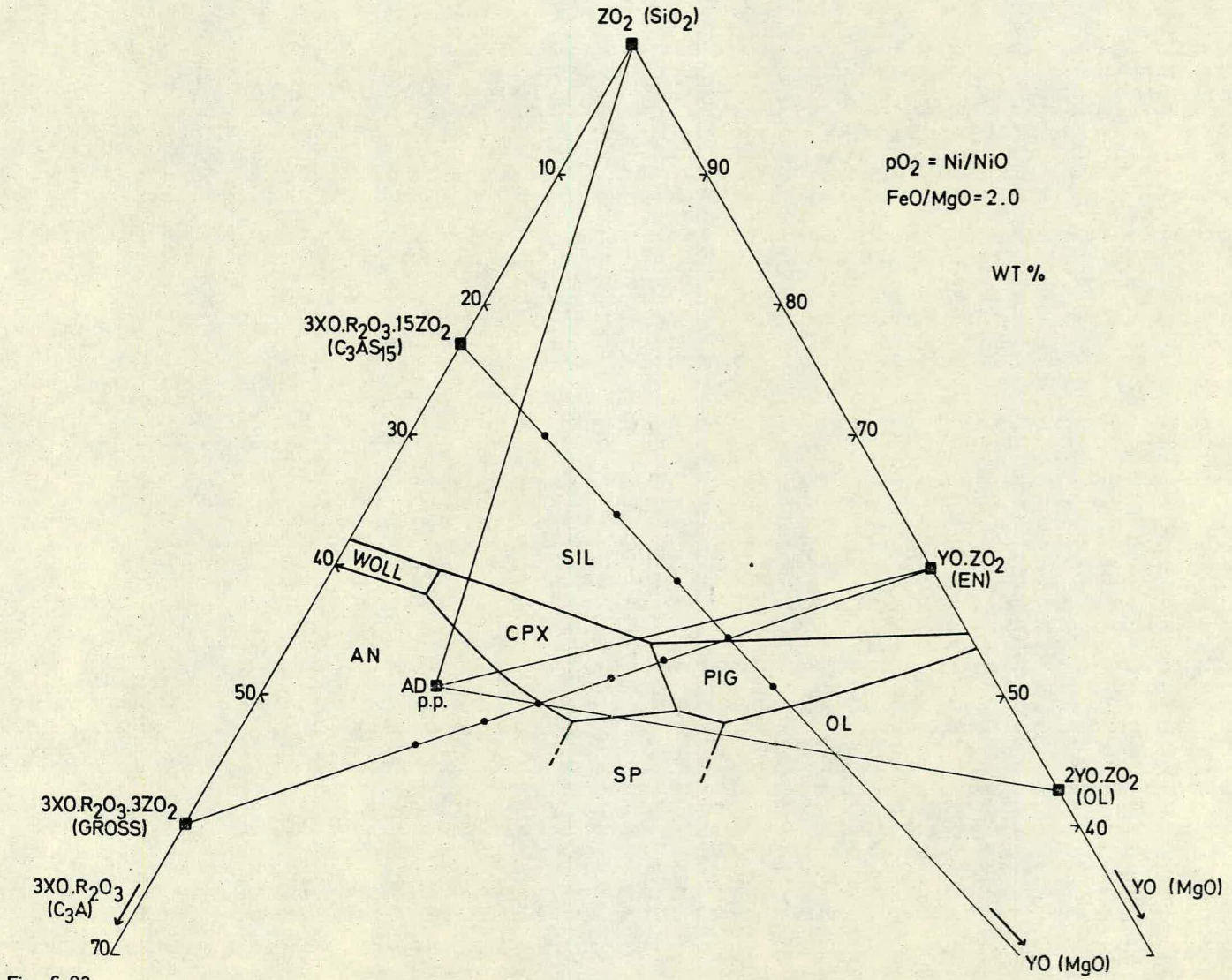
ZO_2 (SiO_2)
pO_2 = Ni/NiO
FeO/MgO = 2.0
WT %
10
90
20
80
30
70
40
50
50
40
70
$3XO.R_2O_3.15ZO_2$
(C_3AS_{15})
WOLL
SIL
$YO.ZO_2$
(EN)
CPX
AN
AD
p.p.
PIG
OL
SP
$2YO.ZO_2$
(OL)
$3XO.R_2O_3.3ZO_2$
(GROSS)
$3XO.R_2O_3$
(C_3A)
YO (MgO)
YO (MgO)

Fig 6.93

Figure 6.94

See figure 6.91

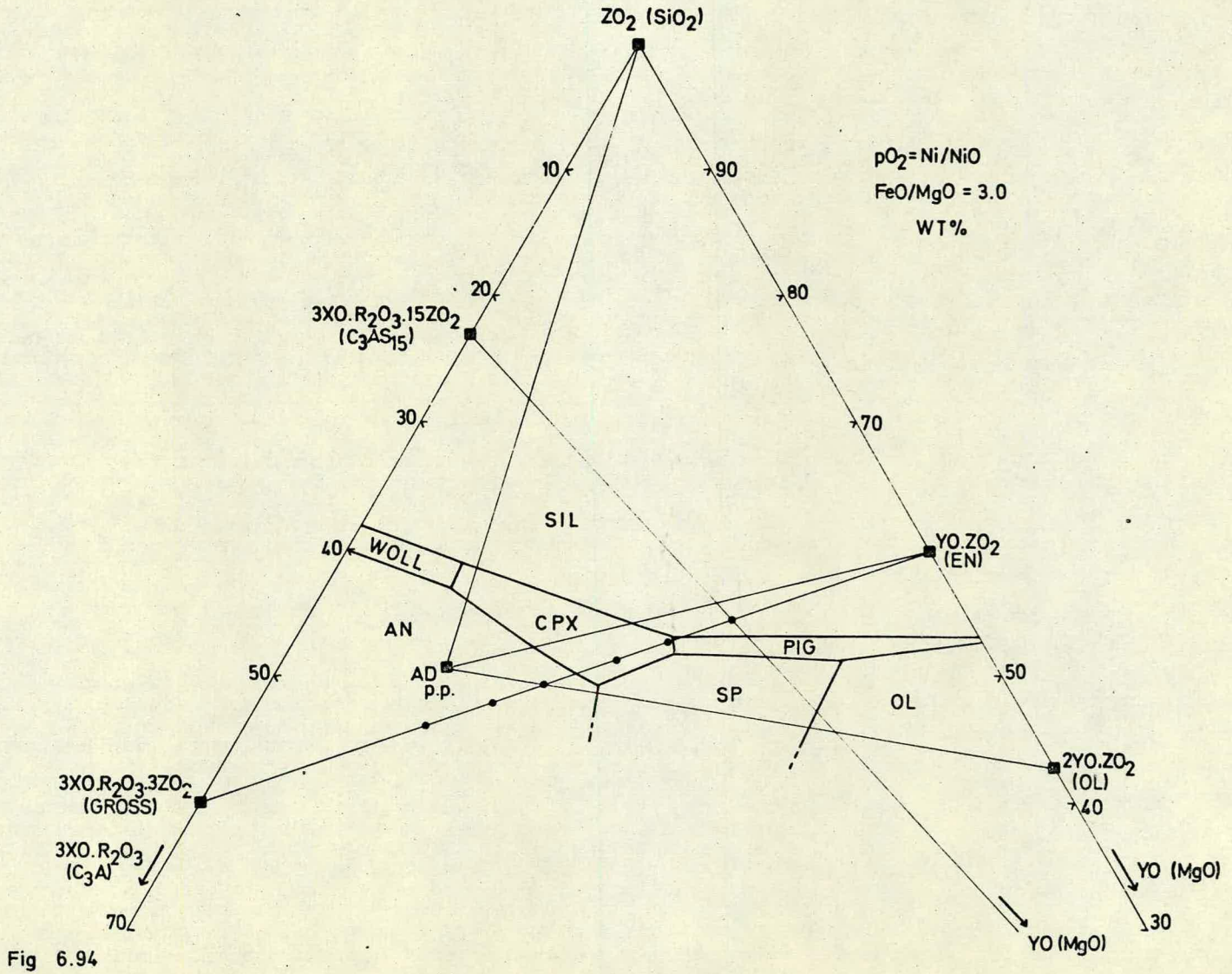
ZO2 (SiO2)
pO2 = Ni/NiO
FeO/MgO = 3.0
WT%
10
90
20
80
3XO.R2O3.15ZO2
(C3AS15)
30
70
SIL
40
WOLL
YO.ZO2
(EN)
AN
CPX
PIG
50
AD
p.p.
SP
OL
50
2YO.ZO2
(OL)
3XO.R2O3.3ZO2
(GROSS)
40
3XO.R2O3
(C3A)
YO (MgO)
70
30
YO (MgO)

Fig 6.94

Figure 6.95

See figure 6.91

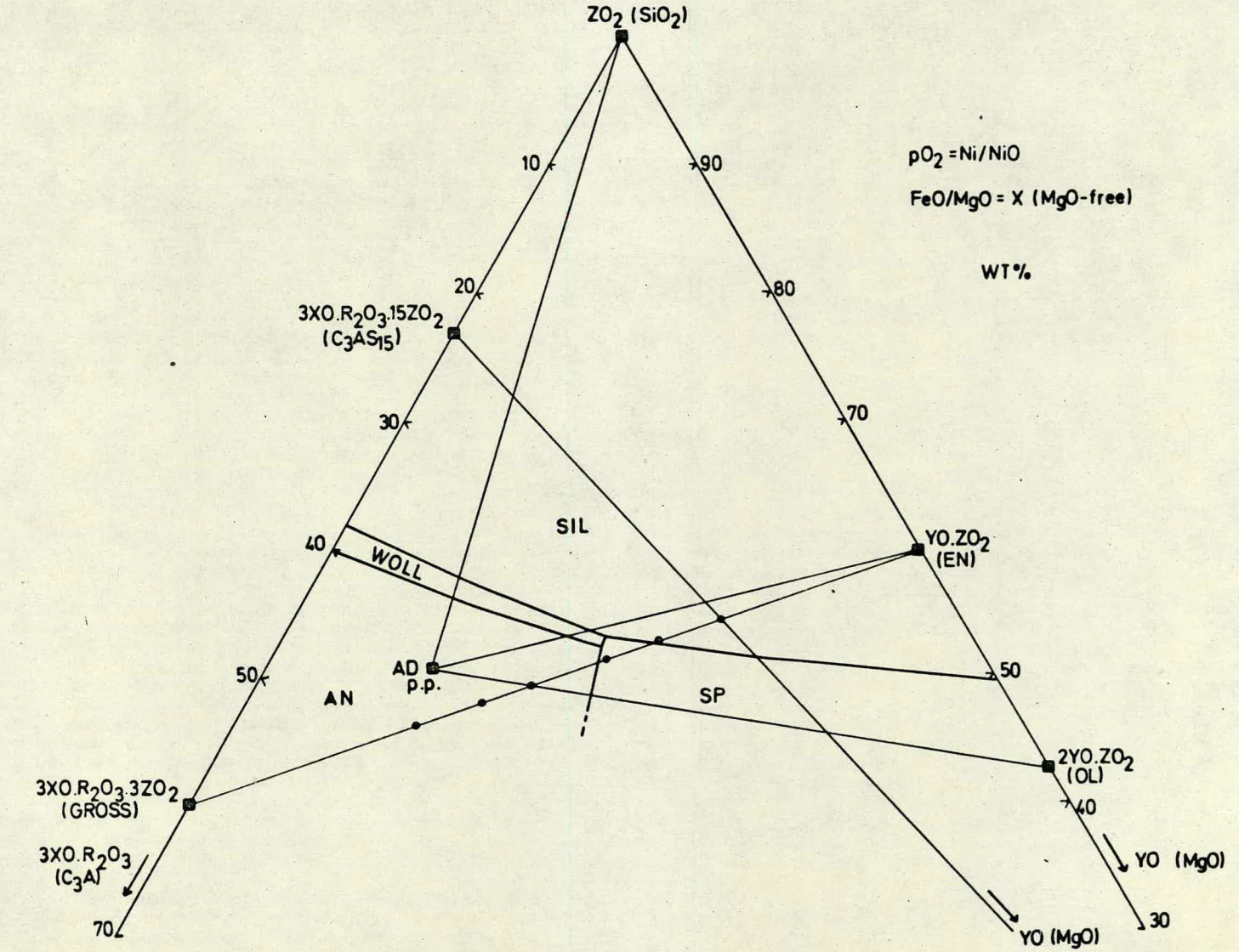
ZO_2 (SiO_2)
10
90
20
80
30
70
40
50
50
70
$3XO.R_2O_3.15ZO_2$
(C_3AS_{15})
SIL
WOLL
$YO.ZO_2$
(EN)
AD
p.p.
AN
SP
$3XO.R_2O_3.3ZO_2$
(GROSS)
$2YO.ZO_2$
(OL)
40
$3XO.R_2O_3$
(C_3A)
YO (MgO)
YO (MgO)
30
pO_2 = Ni/NiO
FeO/MgO = X (MgO-free)
WT%

Fig 6.95

Figure 6.96

A summary figure of the liquidus data for the plane $XO.ZO_2$-$YO.ZO_2$-R_2O_3 (CS-MS-A), combining the L. 6 E 4 piercing points present at each FeO/MgO mole ratio studied (figures 6.86-6.90), to present a multi-Fe/Mg perspective of L. 6 E 3 piercing points which occur in the plane, at the pO_2 of the Ni/NiO equilibrium. The locations of L. 6 E 3 are tentative only. Values in parentheses are 100 x FeO/(FeO+MgO) (wt%), and the arrows indicate the direction of increasing Fe/Mg ratio of the L. 6 E 3.

L. 6 E 3 numbered are

1 = L. 6 E 3 an,ol,sp,cpx,liq (AOMDL)
2 = L. 6 E 3 ol,pyx,cpx,sp,liq (OPDML)
3 = L. 6 E 3 sil,pyx,cpx,sp,liq (SPDML)
4 = L. 6 E 3 cpx,woll,sil,sp,liq (DWSML)
5 = L. 6 E 3 an,sp,woll,cpx,liq (AMWDL)

Abbreviations used for the equilibria are

AMDL = L. 6 E 4 an,sp,cpx,liq
AMWL = L. 6 E 4 an,sp,woll,liq
AODL = L. 6 E 4 an,ol,cpx,liq
AOML = L. 6 E 4 an,ol,sp,liq
AWDL = L. 6 E 4 an,woll,cpx,liq
DWSL = L. 6 E 4 cpx,woll,sil,liq
ODML = L. 6 E 4 ol,cpx,sp,liq
OPDL = L. 6 E 4 ol,pyx,cpx,liq
OPML = L. 6 E 4 ol,pyx,sp,liq
PDML = L. 6 E 4 pyx,cpx,sp,liq
PSDL = L. 6 E 4 pyx,sil,cpx,liq
SMDL = L. 6 E 4 sil,sp,cpx,liq
SMWL = L. 6 E 4 sil,sp,woll,liq
SPML = L. 6 E 4 sil,pyx,sp,liq

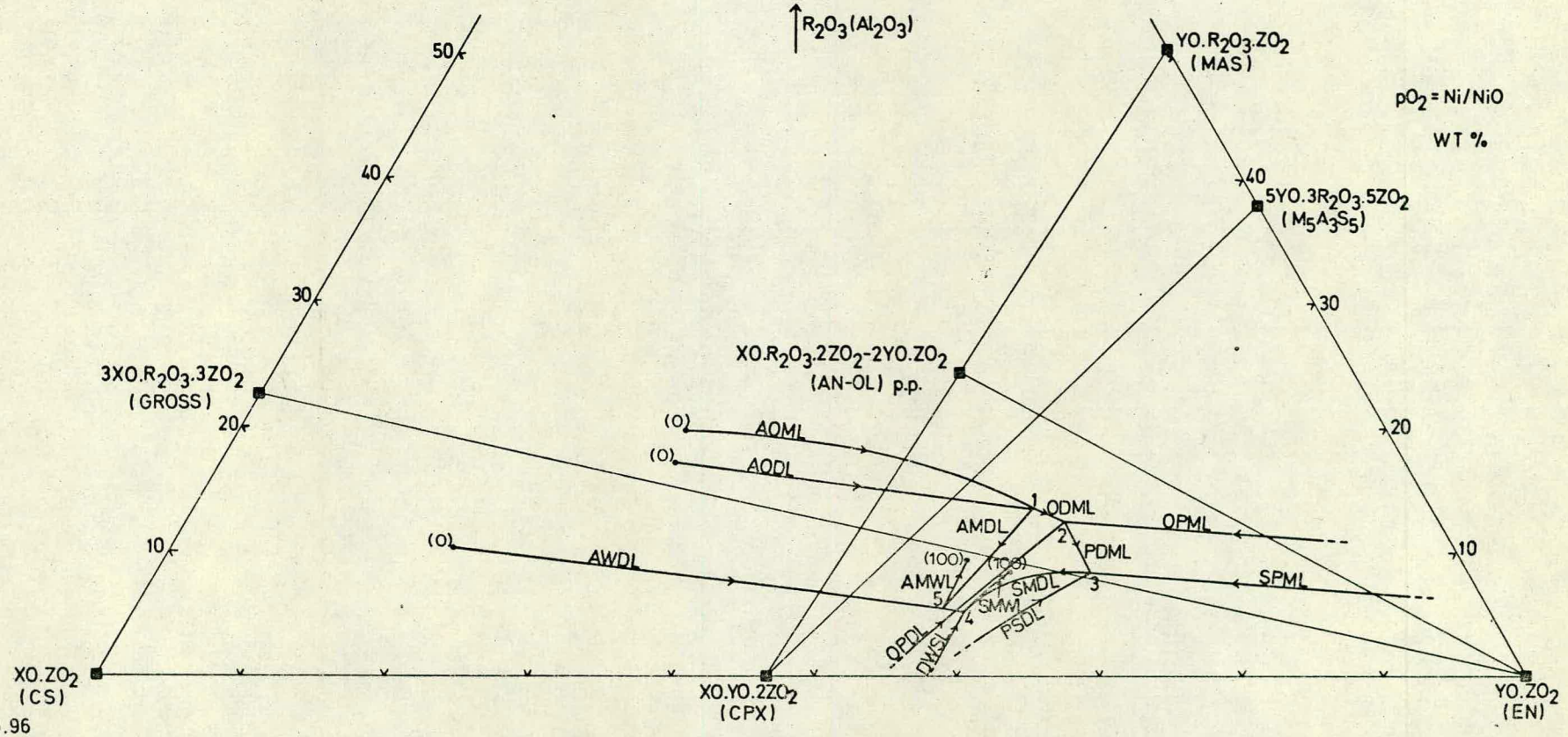
$R_2O_3(Al_2O_3)$
$YO.R_2O_3.ZO_2$
(MAS)
pO_2 = Ni/NiO
WT %
$5YO.3R_2O_3.5ZO_2$
($M_5A_3S_5$)
$3XO.R_2O_3.3ZO_2$
(GROSS)
$XO.R_2O_3.2ZO_2$-$2YO.ZO_2$
(AN-OL) p.p.
$XO.ZO_2$
(CS)
$XO.YO.2ZO_2$
(CPX)
$YO.ZO_2$
(EN)
50
40
30
20
10
(0)
AOML
AODL
AWDL
ODML
OPML
AMDL
PDML
SPML
AMWL
SMDL
SMWL
PSDL
QPDL
QWSL
(100)
(100)
1
2
3
4
5

Fig 6.96

Figure 6.97

A summary figure of the liquidus data for the plane $3XO.R_2O_3$-YO-ZO_2 (C_3A-M-S), combining the L. 6 E 4 piercing points present at each FeO/MgO mole ratio studied (figures 6.91-6.95), to present a multi-Fe/Mg perspective of L. 6 E 3 piercing points which occur in this plane, at the pO_2 of the Ni/NiO equilibrium. The locations of L. 6 E 3 are tentative only. Values in parentheses are 100 x FeO/(FeO+MgO) (wt%), and the arrows indicate the direction of increasing Fe/Mg ratio of the L. 6 E 4.

The piercing point labelled AD p.p. is the piercing point of the join $XO.R_2O_3.2ZO_2$-$XO.YO.2ZO_2$ (Anorthite-Diopside) in this plane.

Abbreviations used for the equilibria are

AMDL = L. 6 E 4 an,sp,cpx,liq
AMWL = L. 6 E 4 an,sp,woll,liq
AWDL = L. 6 E 4 an,woll,cpx,liq
DMWL = L. 6 E 4 cpx,sp,woll,liq
ODML = L. 6 E 4 ol,cpx,sp,liq
OPML = L. 6 E 4 ol,pyx,sp,liq
PDML = L. 6 E 4 pyx,cpx,sp,liq
PODL = L. 6 E 4 pyx,ol,cpx,liq
PSDL = L. 6 E 4 pyx,sil,cpx,liq
SDML = L. 6 E 4 sil,cpx,sp,liq
SDWL = L. 6 E 4 sil,cpx,woll,liq
SMWL = L. 6 E 4 sil,sp,woll,liq
SPML = L. 6 E 4 sil,pyx,sp,liq
AMDWL = L. 6 E 3 an,sp,cpx,woll,liq
SDMWL = L. 6 E 3 sil,cpx,sp,woll,liq

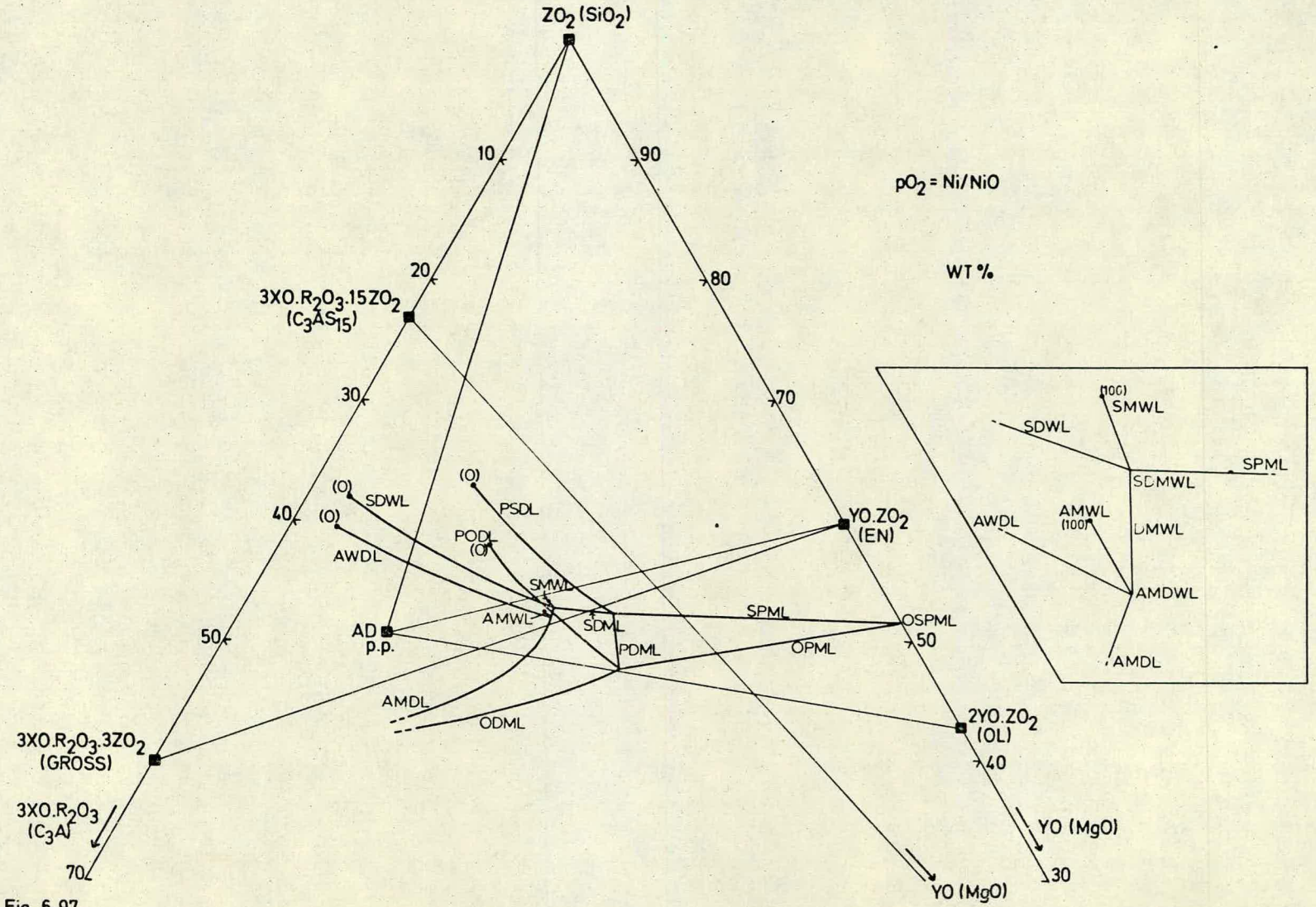
ZO_2 (SiO_2)
10
90
20
80
30
70
40
50
50
40
70
30
$3XO.R_2O_3.15ZO_2$
(C_3AS_{15})
$3XO.R_2O_3.3ZO_2$
(GROSS)
$3XO.R_2O_3$
(C_3A)
$YO.ZO_2$
(EN)
$2YO.ZO_2$
(OL)
YO (MgO)
YO (MgO)
AD
p.p.
OSPML
pO_2 = Ni/NiO
WT %
(0)
SDWL
(0)
AWDL
(0)
PSDL
PODL
(0)
SMWL
AMWL
SDML
SPML
PDML
OPML
AMDL
ODML
(100)
SMWL
SDWL
SPML
SDMWL
AWDL
AMWL
(100)
DMWL
AMDWL
AMDL

Fig 6.97

Figure 6.98

A summary figure of the $2YO.ZO_2$ (olivine) projection into the plane $XO.ZO_2$-$YO.ZO_2$-R_2O_3 (CS-MS-A) combining the L. 6 E 3 data from figures 6.86-6.97 to give an idea of the L. 6 E 2 occurring at the pO_2 of the Ni/NiO equilibrium. Also shown are non-olivine-bearing L. 6 E 2 to obtain a view of silica-bearing equilibria which exist at these pO_2. The locations of L. 6 E 2 are tentative only. Values in parentheses are 100 x FeO/(FeO+MgO) (wt%), and the arrows indicate the direction of increasing Fe/Mg ratio of the L. 6 E 3.

The L. 6 E 2 numbered are

1 = L. 6 E 2 an,ol,pyx,sp,cpx,liq (AOPMDL)

2 = L. 6 E 2 an,pyx,sp,sil,cpx,liq (APMSDL)

3 = L. 6 E 2 ol,pyx,cpx,sil,sp,liq (OPDSML)

Abbreviations used for the equilibria are

AMSDL = L. 6 E 3 an,sp,sil,cpx,liq

AOPML = L. 6 E 3 an,ol,pyx,sp,liq

APDML = L. 6 E 3 an,pyx,cpx,sp,liq

APMSL = L. 6 E 3 an,pyx,sp,sil,liq

APSDL = L. 6 E 3 an,pyx,sil,cpx,liq

DOAPL = L. 6 E 3 cpx,ol,an,pyx,liq

OADML = L. 6 E 3 ol,an,cpx,sp,liq

OMDSL = L. 6 E 3 ol,sp,cpx,sil,liq

OPDSL = L. 6 E 3 ol,pyx,cpx,sil,liq

OPMDL = L. 6 E 3 ol,pyx,sp,cpx,liq

OSPML = L. 6 E 3 ol,sil,pyx,sp,liq

SPMDL = L. 6 E 3 sil,pyx,sp,cpx,liq

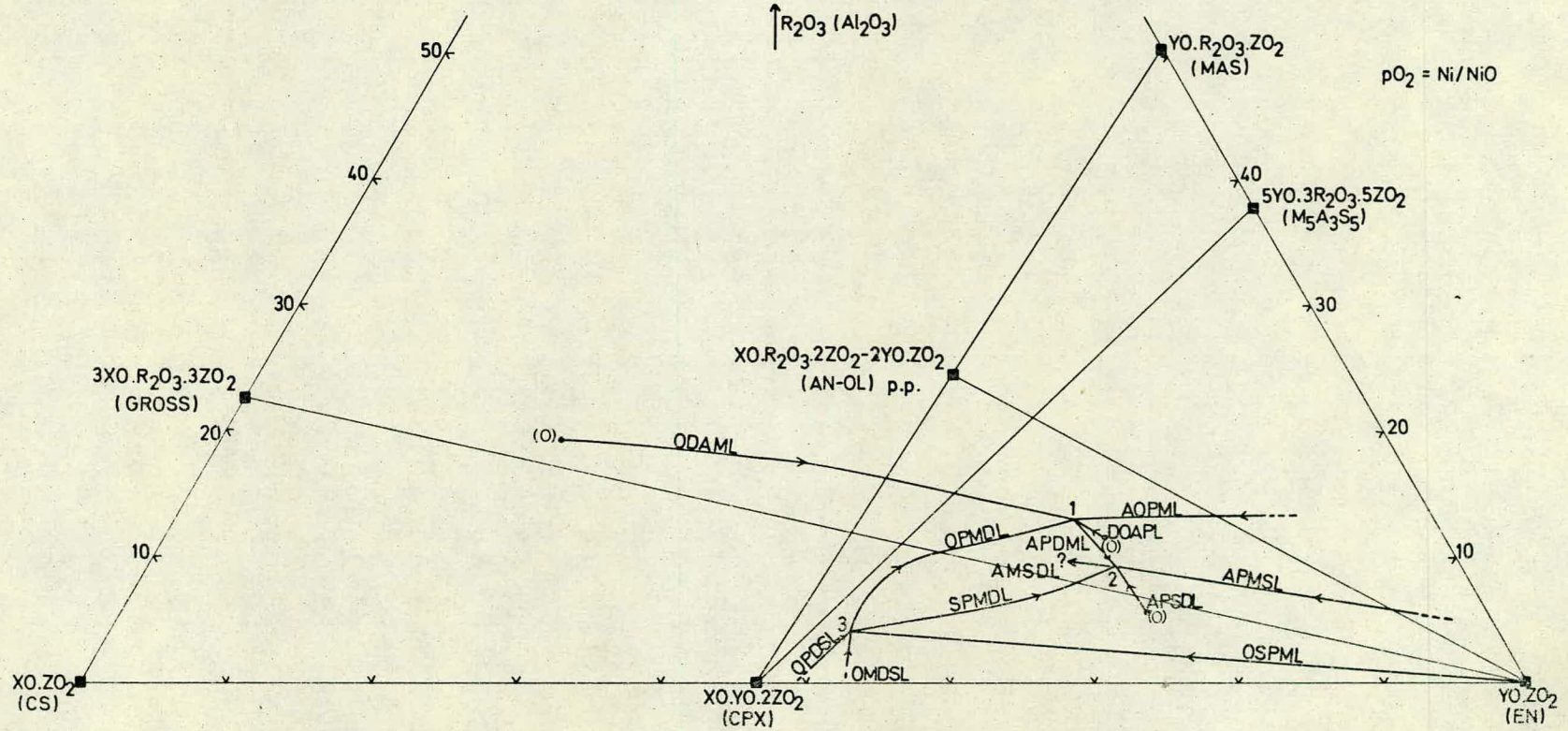
↑R_2O_3 (Al_2O_3)
$YO.R_2O_3.ZO_2$
(MAS)
pO_2 = Ni/NiO
$5YO.3R_2O_3.5ZO_2$
($M_5A_3S_5$)
$XO.R_2O_3.2ZO_2$-$2YO.ZO_2$
(AN-OL) p.p.
$3XO.R_2O_3.3ZO_2$
(GROSS)
$XO.ZO_2$
(CS)
$XO.YO.2ZO_2$
(CPX)
$YO.ZO_2$
(EN)
50
40
30
20
10
(O)
ODAML
AOPML
DOAPL
OPMDL
APDML
AMSDL
APMSL
SPMDL
APSDL
QPDSL
OMDSL
OSPML
1
2
3
WT%

Fig 6.98

Figure 6.99

Liquidus diagram for part of the join $3XO.R_2O_3.15ZO_2$-YO (C_3AS_{15}-M) to show the change in liquidus phase for molecularly equivalent compositions with changing FeO/MgO ratio, in an air atmosphere. The data used was presented by Clarke and Biggar (1972), and is included in Appendix E.3.3. The phase boundaries are shown by thick solid lines. The boundary between opx and pen phase volumes is tentative only.

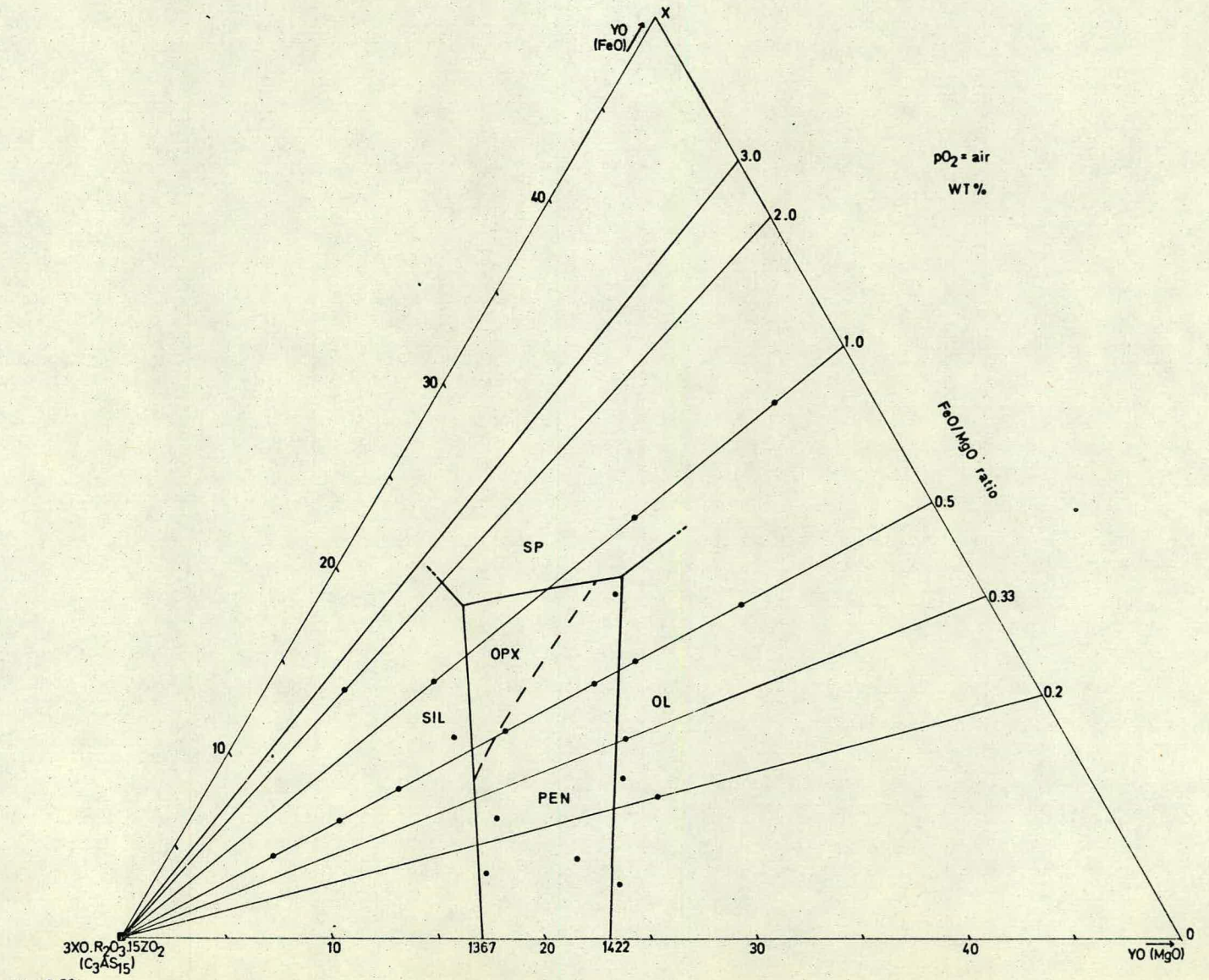
X
YO
(FeO)
3.0
2.0
1.0
0.5
0.33
0.2
0
40
30
20
10
pO2 = air
WT %
FeO/MgO ratio
SP
OPX
SIL
OL
PEN
3XO.R2O3.15ZO2
(C3AS15)
10
1367
20
1422
30
40
YO (MgO)

Fig 6.99

Figure 6.100

The effect of pO_2 on some of the L. 6 E 4 piercing points in the join $YO.ZO_2$-$3XO.R_2O_3.3ZO_2$ (Enstatite-Grossular) with varying FeO/MgO ratio, to obtain the approximate locations of L. 6 E 3 piercing points in this plane. The data from figures 6.37,6.79 are combined in this figure. The arrows on the L. 6 E 4 indicate the direction of more oxidising pO_2, the liquids labelled a being those from the pO_2 of the Fe/FeO equilibrium (figure 6.37), those labelled b from the pO_2 of the Ni/NiO equilibrium (figure 6.79).

The L. 6 E 3 numbered are

1 = L. 6 E 3 sil,cpx,an,ol,liq (SDAOL)
2 = L. 6 E 3 ol,sil,pyx,cpx,liq (OSPDL)
3 = L. 6 E 3 sil,an,cpx,sp,liq (SADML)
4 = L. 6 E 3 sil,cpx,pyx,sp,liq (SDPML)
5 = L. 6 E 3 pyx,cpx,ol,sp,liq (PDOML)

Abbreviations used for the equilibria are

ADOL = L. 6 E 4 an,cpx,ol,liq
AMDL = L. 6 E 4 an,sp,cpx,liq
MDPL = L. 6 E 4 sp,cpx,pyx,liq
OMDL = L. 6 E 4 ol,sp,cpx,liq
OPML = L. 6 E 4 ol,pyx,sp,liq
OSPL = L. 6 E 4 ol,sil,pyx,liq
PDOL = L. 6 E 4 pyx,cpx,ol,liq
SADL = L. 6 E 4 sil,an,cpx,liq
SAML = L. 6 E 4 sil,an,sp,liq
SAOL = L. 6 E 4 sil,an,ol,liq
SDOL = L. 6 E 4 sil,cpx,ol,liq
SDPL = L. 6 E 4 sil,cpx,pyx,liq
SMDL = L. 6 E 4 sil,sp,cpx,liq
SMPL = L. 6 E 4 sil,sp,pyx,liq
ADOIL = L. 6 E 3 an,cpx,ol,Fe,liq
OSPIL = L. 6 E 3 ol,sil,pyx,Fe,liq

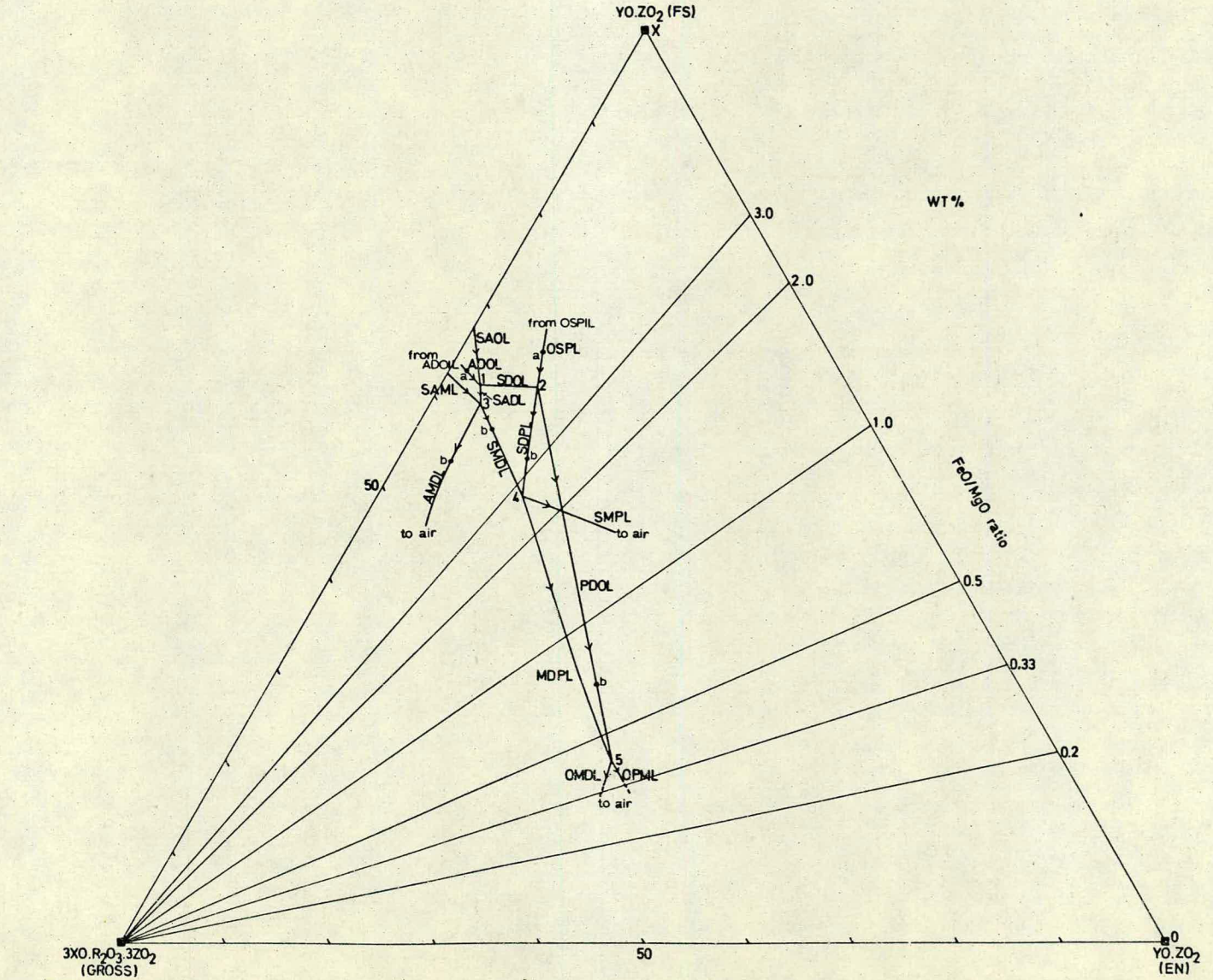
YO.ZO2 (FS)
X
WT%
3.0
2.0
1.0
0.5
0.33
0.2
0
FeO/MgO ratio
from OSPIL
SAOL
OSPL
a
from ADOL
ADOL
a
1
SDOL
2
SAML
3
SAOL
b
SMOL
SDPL
b
AMDL
b
50
to air
SMPL
to air
PDOL
MDPL
b
5
OMDL
OPML
to air
3XO.R2O3.3ZO2
(GROSS)
50
YO.ZO2
(EN)

Fig 6.100

Figure 6.101

The effect of pO_2 on some of the L. 6 E 4 piercing points in the join $3XO.R_2O_3.15ZO_2$-YO (C_3AS_{15}-M) with varying FeO/MgO ratio, to obtain the approximate locations of L. 6 E 3 piercing points in this plane. The data from figures 6.42, 6.84 and 6.99 are combined in this figure. The arrows on the L. 6 E 4 indicate the direction of more oxidising pO_2, the liquids labelled a being those in air (figure 6.99), labelled b those at the pO_2 of the Ni/NiO equilibrium (figure 6.84), and labelled c those at the pO_2 of the Fe/FeO equilibrium (figure 6.42).

Abbreviations used for the equilibria are

OPML = L. 6 E 4 ol,pyx,sp,liq

OSML = L. 6 E 4 ol,sil,sp,liq

OSPL = L. 6 E 4 ol,sil,pyx,liq

SPML = L. 6 E 4 sil,pyx,sp,liq

OSPIL = L. 6 E 3 ol,sil,pyx,Fe,liq

OPSML = L. 6 E 3 ol,pyx,sil,sp,liq

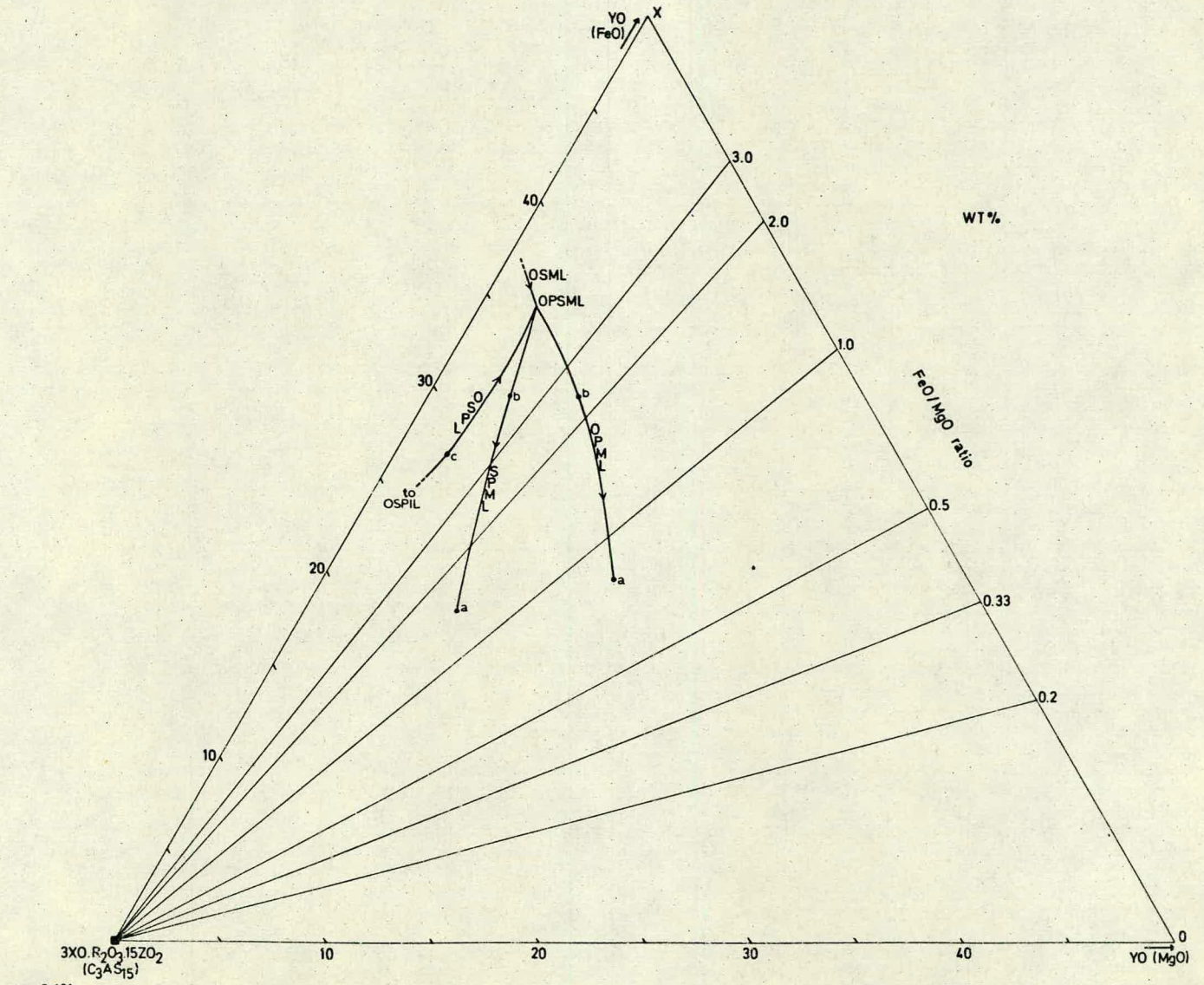
YO
(FeO)
X
3.0
2.0
1.0
0.5
0.33
0.2
0
WT%
FeO/MgO ratio
40
30
20
10
OSML
OPSML
LASO
OSPIL
to
a
b
c
OLSML
3XO.R2O3.15ZO2
(C3AS15)
YO (MgO)

Fig 6.101

Figure 6.102

A flow diagram for part of the system CMAS-Fe-O_2, showing the postulated univariant and divariant equilibria and their relationships presented in the text and figures. The one axis is pO_2, the other has no meaning, since the temperature relationships are not known.

Abbreviations used for the equilibria are

AOPDIL = L. 6 E 2 an,ol,pyx,cpx,Fe,liq

AOPDML = L. 6 E 2 an,ol,pyx,cpx,sp,liq

AOSPDL = L. 6 E 2 an,ol,sil,pyx,cpx,liq

APOSIL = L. 6 E 2 an,pyx,ol,sil,Fe,liq

APOSML = L. 6 E 2 an,pyx,ol,sil,sp,liq

ASPIDL = L. 6 E 2 an,sil,pyx,Fe,cpx,liq

ASPMDL = L. 6 E 2 an,sil,pyx,sp,cpx,liq

OSADIL = L. 6 E 2 ol,sil,an,cpx,Fe,liq

OSADML = L. 6 E 2 ol,sil,an,cpx,sp,liq

OSPIDL = L. 6 E 2 ol,sil,pyx,Fe,cpx,liq

OSPMDL = L. 6 E 2 ol,sil,pyx,sp,cpx,liq

AOSPDIL = L. 6 E 1 an,ol,sil,pyx,cpx,Fe,liq

OSPADML = L. 6 E 1 ol,sil,pyx,an,cpx,sp,liq

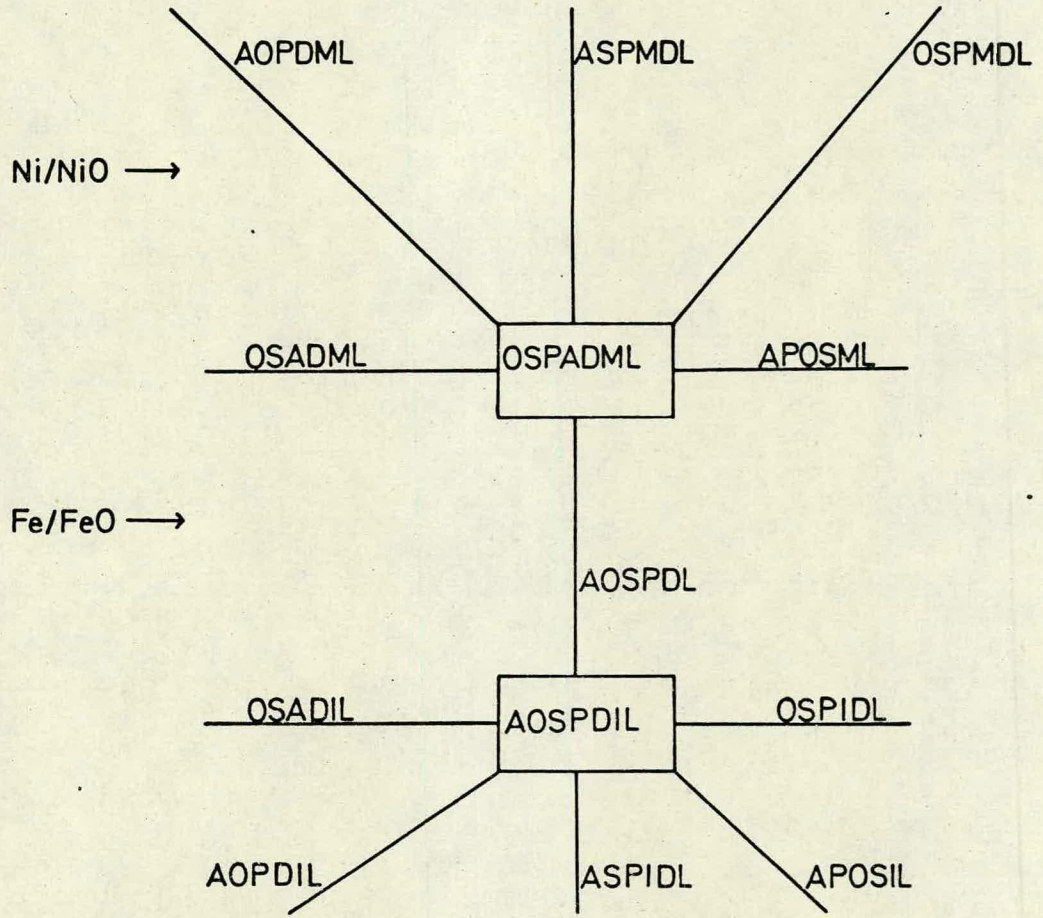
AOPDML
ASPMDL
OSPMDL
Ni/NiO ⟶
OSADML
OSPADML
APOSML
Fe/FeO ⟶
AOSPDL
OSADIL
AOSPDIL
OSPIDL
AOPDIL
ASPIDL
APOSIL

Fig 6.102

CHAPTER 7

THE SYSTEM $CaO-MgO-Al_2O_3-SiO_2-Na_2O-Fe-O_2$

Figures 7.1 - 7.4

Figure 7.1

Multi-pO_2 and multi-Fe/Mg plot of the join $XO.R_2O_3.2ZO_2$-YO-ZO_2 (Anorthite-M-S), showing the piercing points of some of the L. 7 E 4 which pierce this plane when the bulk normative plagioclase ratio is $An_{50}Ab_{50}$ (labelled 50), compared to that when the normative plagioclase is $An_{100}Ab_0$ (labelled 0) from figure 6.10. The data used for the $An_{50}Ab_{50}$ equilibria is from Eggler (1974). The pO_2 of some of the liquids is shown at both plagioclase ratios, the dash-dot line being L. 7 E 5 an,pyx,sp,liq (APML) at the pO_2 of the Ni/NiO equilibrium at both plagioclase ratios.

The piercing point labelled AO p.p. is the piercing point of the join $XO.R_2O_3.2ZO_2$-$2YO.ZO_2$ (Anorthite-olivine) in this plane.

Abbreviations used for the equilibria are

AOPSL = L. 7 E 4 plag,ol,pyx,sil,liq

AOSML = L. 7 E 4 plag,ol,sil,sp,liq

APOML = L. 7 E 4 plag,pyx,ol,sp,liq

APSML = L. 7 E 4 plag,pyx,sil,sp,liq

OPSML = L. 7 E 4 ol,pyx,sil,sp,liq

APOSML = L. 7 E 3 plag,pyx,ol,sil,sp,liq

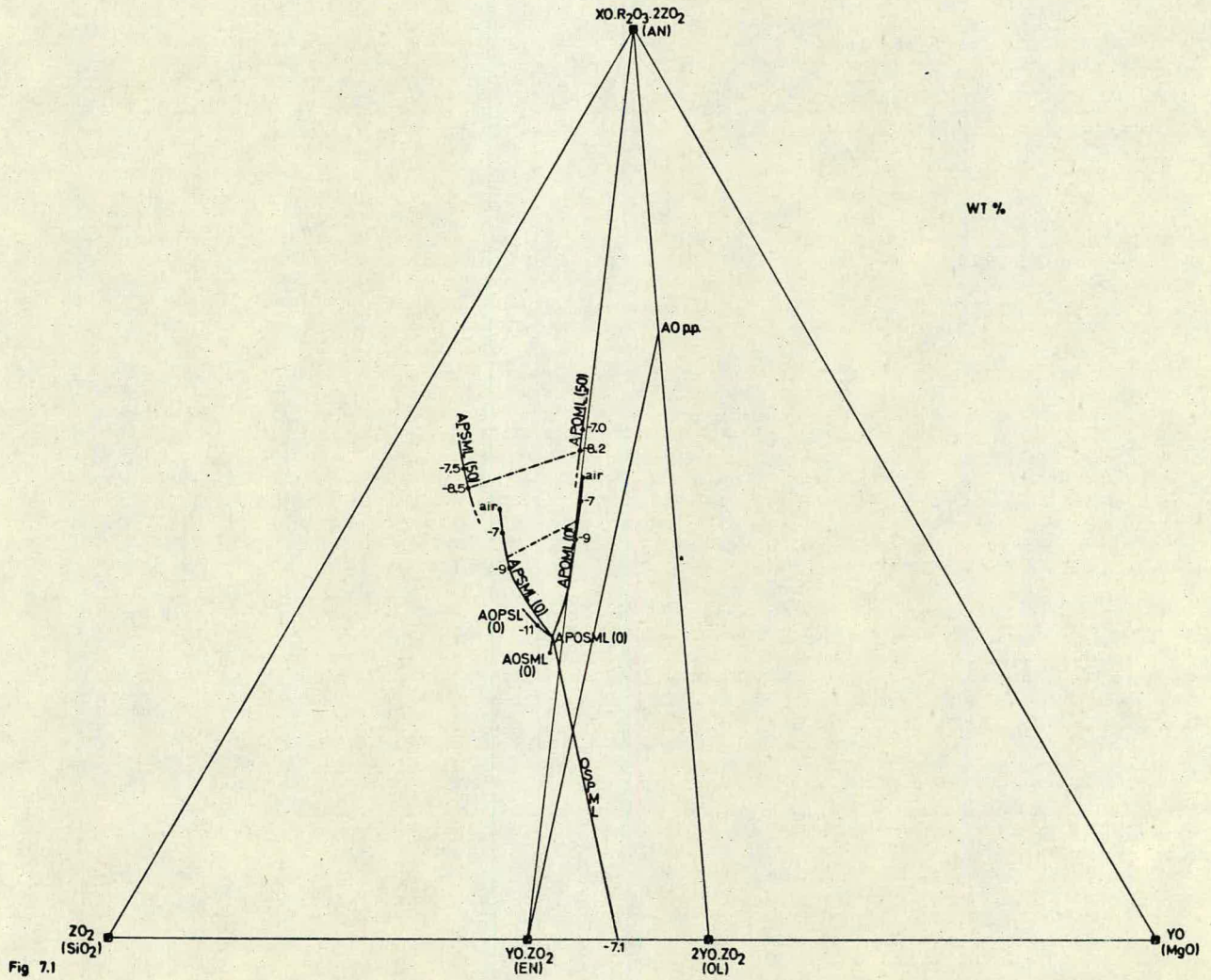
XO.R2O3.2ZO2
(AN)
WT %
AOpp
APSML(50)
APOML(50)
-7.0
-8.2
air
-7.5
-8.5
air
-7
-7
-9
-9
APSML(0)
APOML(0)
AOPSL
(0)
-11
APOSML(0)
AOSML
(0)
FESOO
ZO2
(SiO2)
YO.ZO2
(EN)
-7.1
2YO.ZO2
(OL)
YO
(MgO)

Fig 7.1

Figure 7.2

Multi-pO_2 plot of $XO.R_2O_3.2ZO_2$ (plagioclase) saturation diagrams into part of the plane $MgO-SiO_2-FeO$, using the same data as in figure 7.1. The projected positions of the L. 7 E 4 at bulk normative plagioclase ratios of $An_{100}Ab_0$ (labelled 0), from figure 6.3, can then be compared to those at the ratio $An_{50}Ab_{50}$ (labelled 50). The pO_2 of some of the liquids is shown at both ratios, using the data from Eggler (1974) and Roeder and Osborn (1966).

Abbreviations used for the equilibria are

AOSML = L. 7 E 4 plag,ol,sil,sp,liq

AOSPL = L. 7 E 4 plag,ol,sil,pyx,liq

APOML = L. 7 E 4 plag,pyx,ol,sp,liq

APSML = L. 7 E 4 plag,pyx,sil,sp,liq

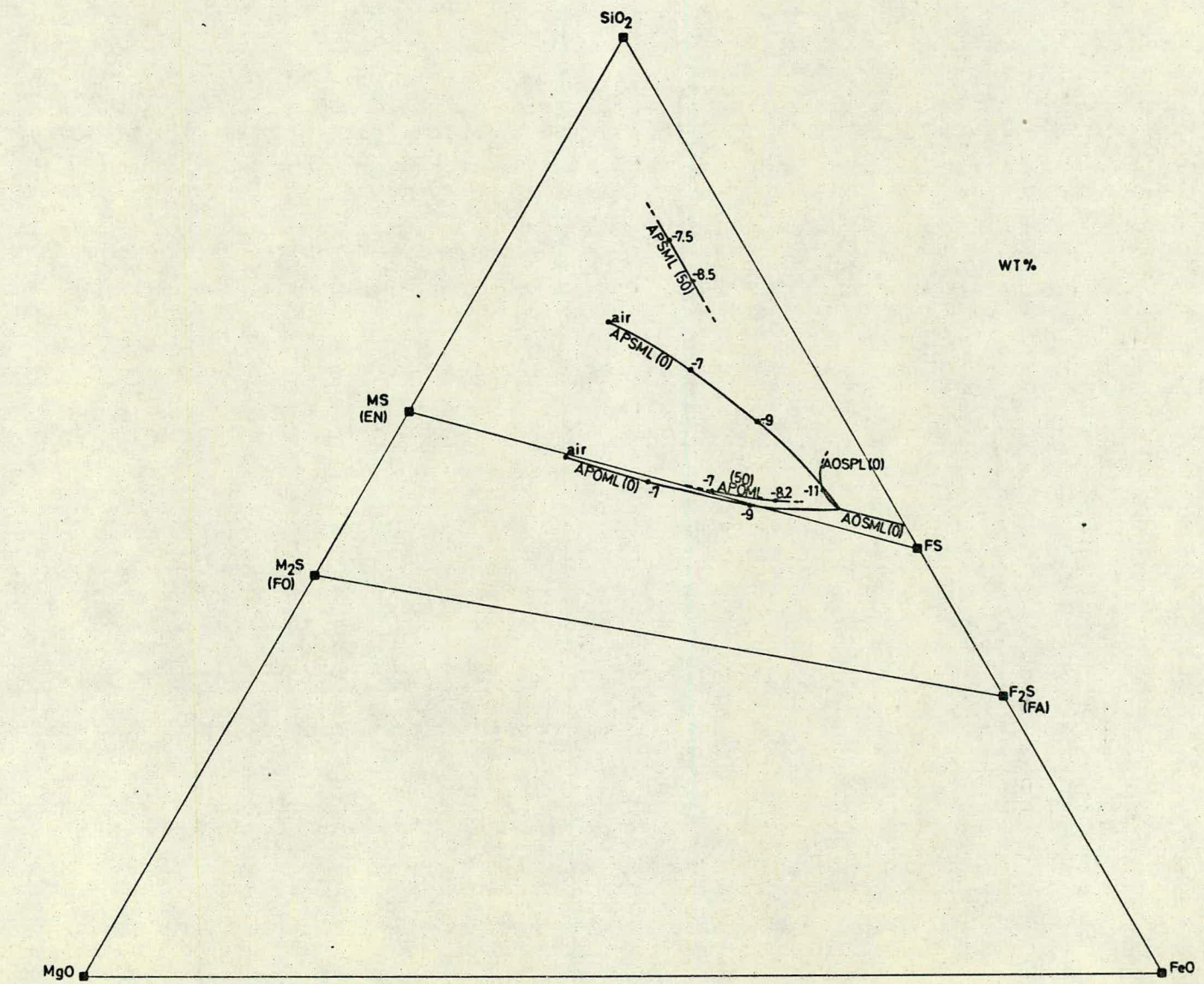
SiO2
WT%
APSML (50)
-7.5
-8.5
air
APSML (0)
-7
-9
MS
(EN)
air
APOML (0)
-7
-7
(50)
APOML
-8.2
-11
-9
AOSPL (0)
AOSML (0)
FS
M2S
(FO)
F2S
(FA)
MgO
FeO

Fig 7.2

Figure 7.3

Temperature versus pO_2 plot of some of the L. 7 E 4 which pierce the join Anorthite-Albite-MgO-SiO_2-Fe-O_2, from Eggler (1974). The small difference in temperature, at constant pO_2, of the equilibria between the bulk normative plagioclase ratios of $An_{100}Ab_0$ (labelled 0) from figure 6.11, and $An_{50}Ab_{50}$ ratio (labelled 50), contrasts with the large difference between the latter and the An_0Ab_{100} ratio (labelled 100) temperatures. The reference curves for the pO_2 of the Ni/NiO and Fe/FeO equilibria are also shown.

L. 7 E 3 plag,pyx,ol,sil,sp,liq (APOSML) with variable An:Ab ratio (0-100) exists between L. 7 E 3 terminations numbered 1 and 2.

Abbreviations used for the equilibria are

AOSML = L. 7 E 4 plag,ol,sil,sp,liq

APOML = L. 7 E 4 plag,pyx,ol,sp,liq

APSML = L. 7 E 4 plag,pyx,sil,sp,liq

OSPAL = L. 7 E 4 ol,sil,pyx,plag,liq

OSPML = L. 7 E 4 ol,sil,pyx,sp,liq

APOSML = L. 7 E 3 plag,pyx,ol,sil,sp,liq

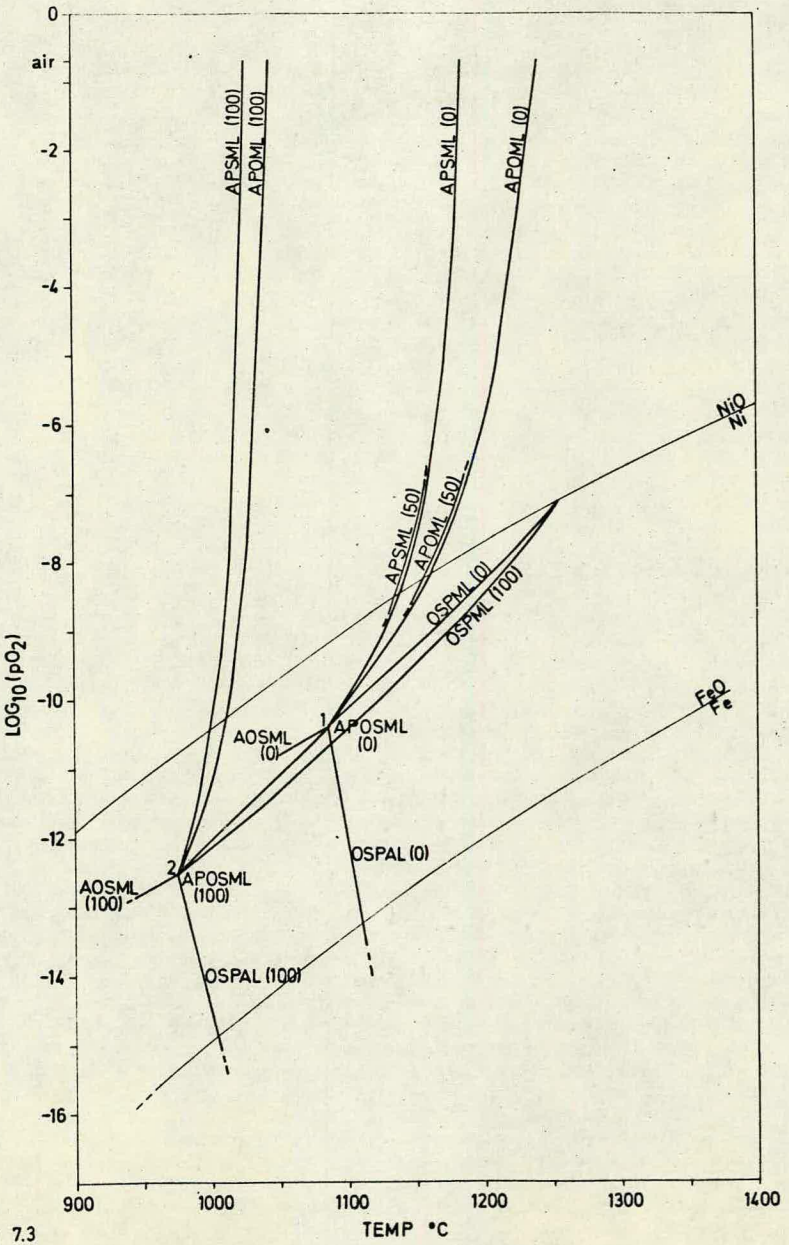
0
air
-2
-4
-6
-8
-10
-12
-14
-16
LOG10(pO2)
900
1000
1100
1200
1300
1400
TEMP °C
APSML (100)
APOML (100)
APSML (0)
APOML (0)
APSML (50)
APOML (50)
OSPML (0)
OSPML (100)
NiO
Ni
FeO
Fe
AOSML (0)
APOSML (0)
1
2
AOSML (100)
APOSML (100)
OSPAL (0)
OSPAL (100)

Fig 7.3

Figure 7.4

A $2YO.ZO_2$ (olivine) projection into part of the plane $XO.ZO_2$-$YO.ZO_2$-R_2O_3 (CS-MS-A), predicted for the combination: FeO/MgO mole ratio = 0.5, pO_2 = Ni/NiO equilibrium, Anorthite/albite bulk normative ratio = $An_{50}Ab_{50}$ (projection boundaries labelled CMASNF). Also shown are the projection boundaries for CMAS only (labelled CMAS) from figure 4.3; for bulk normative plagioclase ratio $An_{50}Ab_{50}$ in CMASN only (labelled CMASN) from figure 5.14; and for FeO/MgO mole ratio = 0.5 at the pO_2 of the Ni/NiO equilibrium only (labelled CMASF) from figure 6.86. The effects of each single change in the ratios is assumed to be cumulative to obtain the predicted projection boundaries.

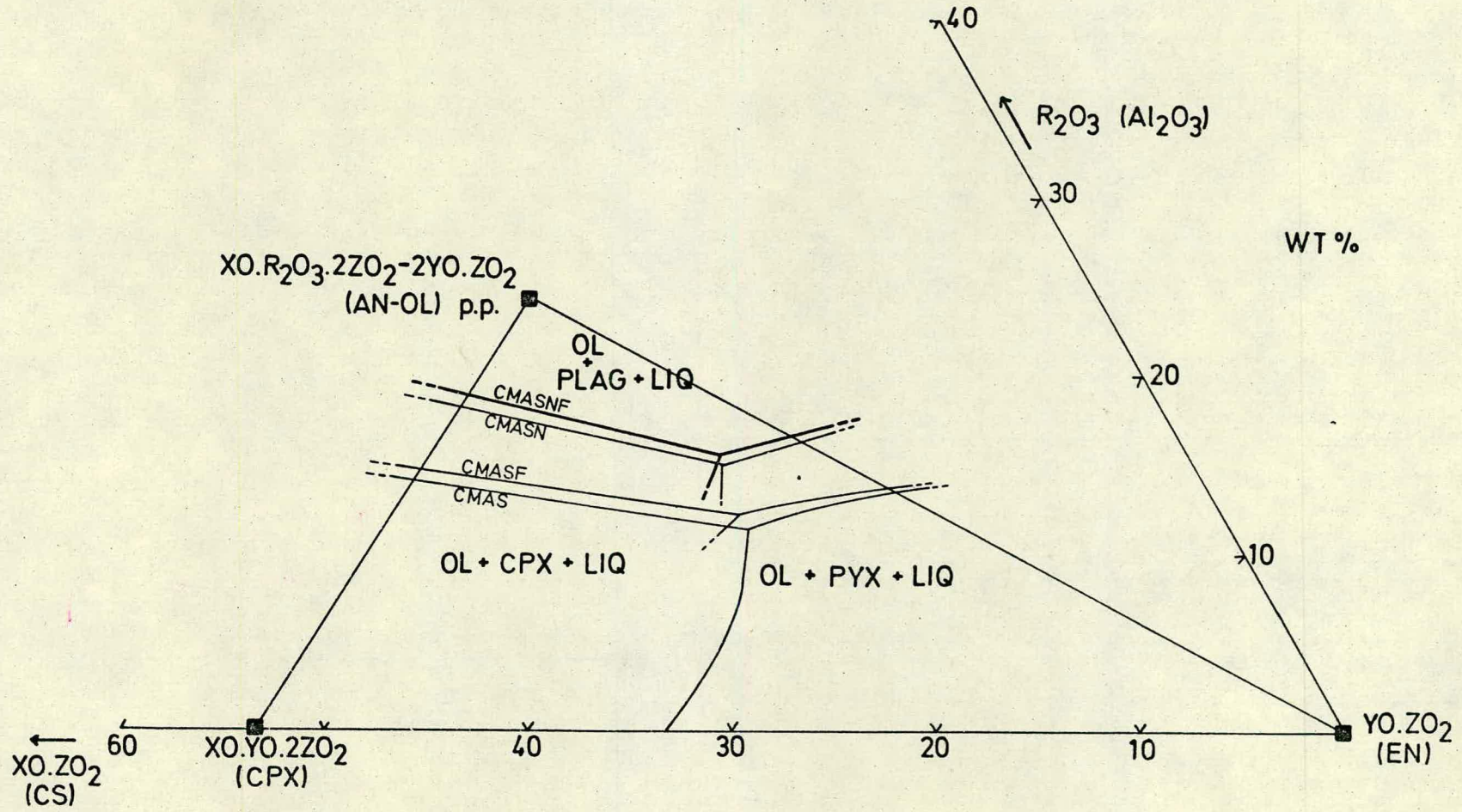
40
R_2O_3 (Al_2O_3)
30
WT %
20
10
$XO.R_2O_3.2ZO_2$-$2YO.ZO_2$
(AN-OL) p.p.
OL
+
PLAG + LIQ
CMASNF
CMASN
CMASF
CMAS
OL + CPX + LIQ
OL + PYX + LIQ
$YO.ZO_2$
(EN)
60
$XO.YO.2ZO_2$
(CPX)
40
30
20
10
$XO.ZO_2$
(CS)

Fig 7.4

CHAPTER 8

MELTING STUDIES ON NATURAL ROCKS

Figures 8.1 - 8.36

Figures 8.1 to 8.25

Temperature versus pO_2 plots of the melting data obtained on each of the Reunion rocks studied. The phase boundaries are labelled with the name of the phase appearing with decreasing temperature unless specified otherwise (for example, liquid out represents liquid disappearing with decreasing temperature).

The melting data obtained by Tilley, et al. (1971) on the same rocks is indicated at the right hand side of the diagram for those rocks studied by both techniques.

The reference curves for the pO_2 of the Fe/FeO and Ni/NiO equilibria are also shown.

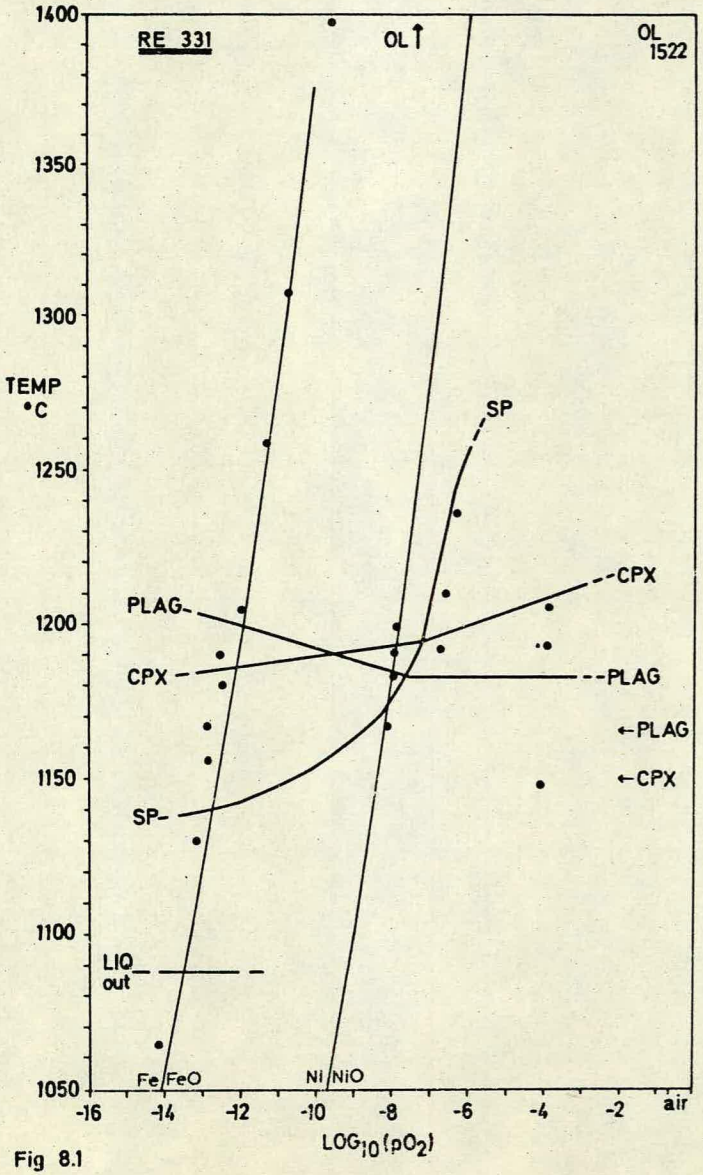
RE 331
OL↑
OL 1522
TEMP °C
1400
1350
1300
1250
1200
1150
1100
1050
SP
CPX
PLAG
CPX
PLAG
←PLAG
←CPX
SP
LIQ out
Fe/FeO
Ni/NiO
-16
-14
-12
-10
-8
-6
-4
-2
air
LOG10(pO2)

Fig 8.1

Figure 8.2

See figure 8.1

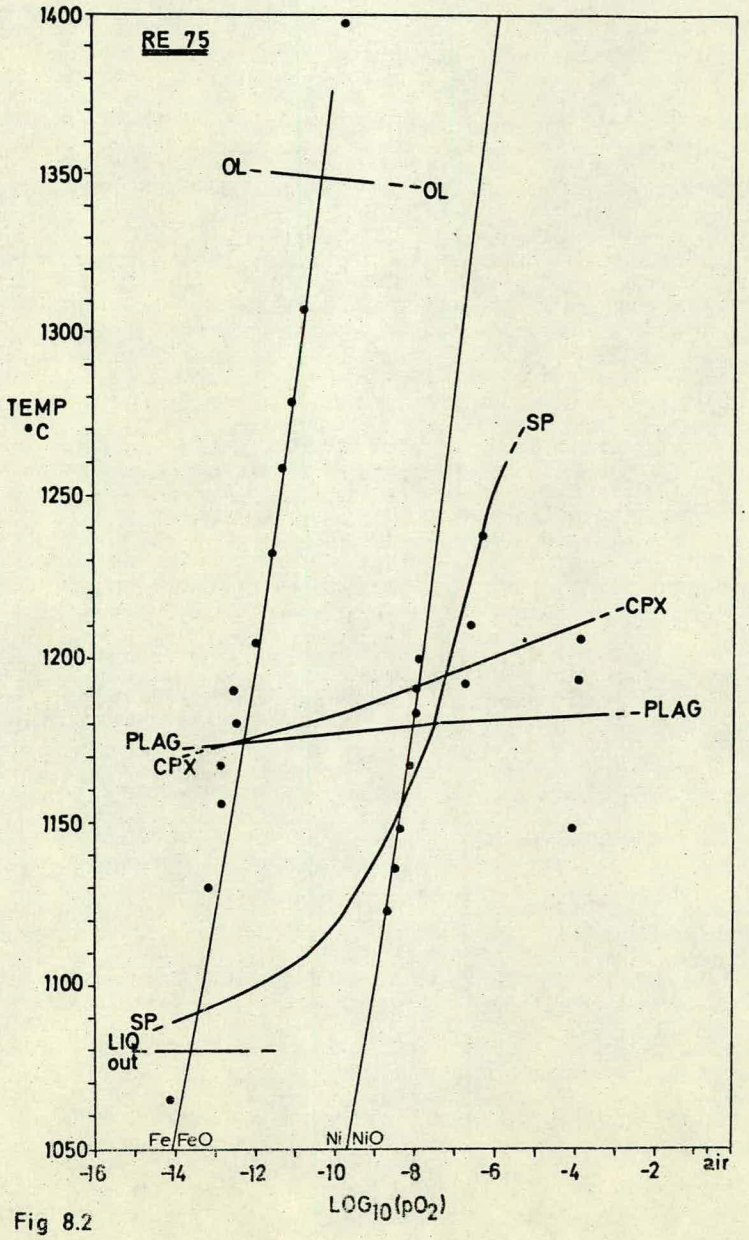
RE 75
1400
1350
1300
1250
1200
1150
1100
1050
TEMP °C
OL
OL
SP
CPX
PLAG
PLAG
CPX
SP
LIQ out
Fe/FeO
Ni/NiO
-16
-14
-12
-10
-8
-6
-4
-2
air
LOG10(pO2)

Fig 8.2

Figure 8.3

See figure 8.1

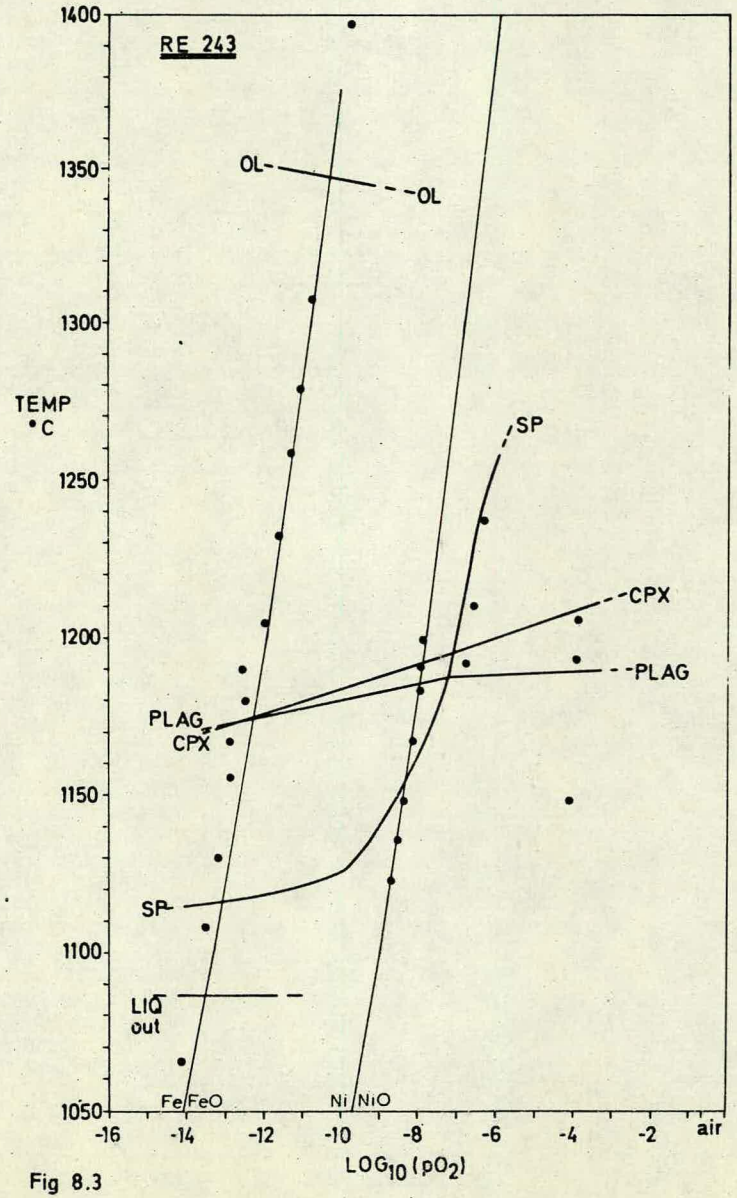
RE 243
OL
OL
SP
CPX
PLAG
PLAG
CPX
SP
LIQ
out
Fe/FeO
Ni/NiO
TEMP
°C
1400
1350
1300
1250
1200
1150
1100
1050
-16
-14
-12
-10
-8
-6
-4
-2
air
LOG10 (pO2)

Fig 8.3

Figure 8.4

See figure 8.1

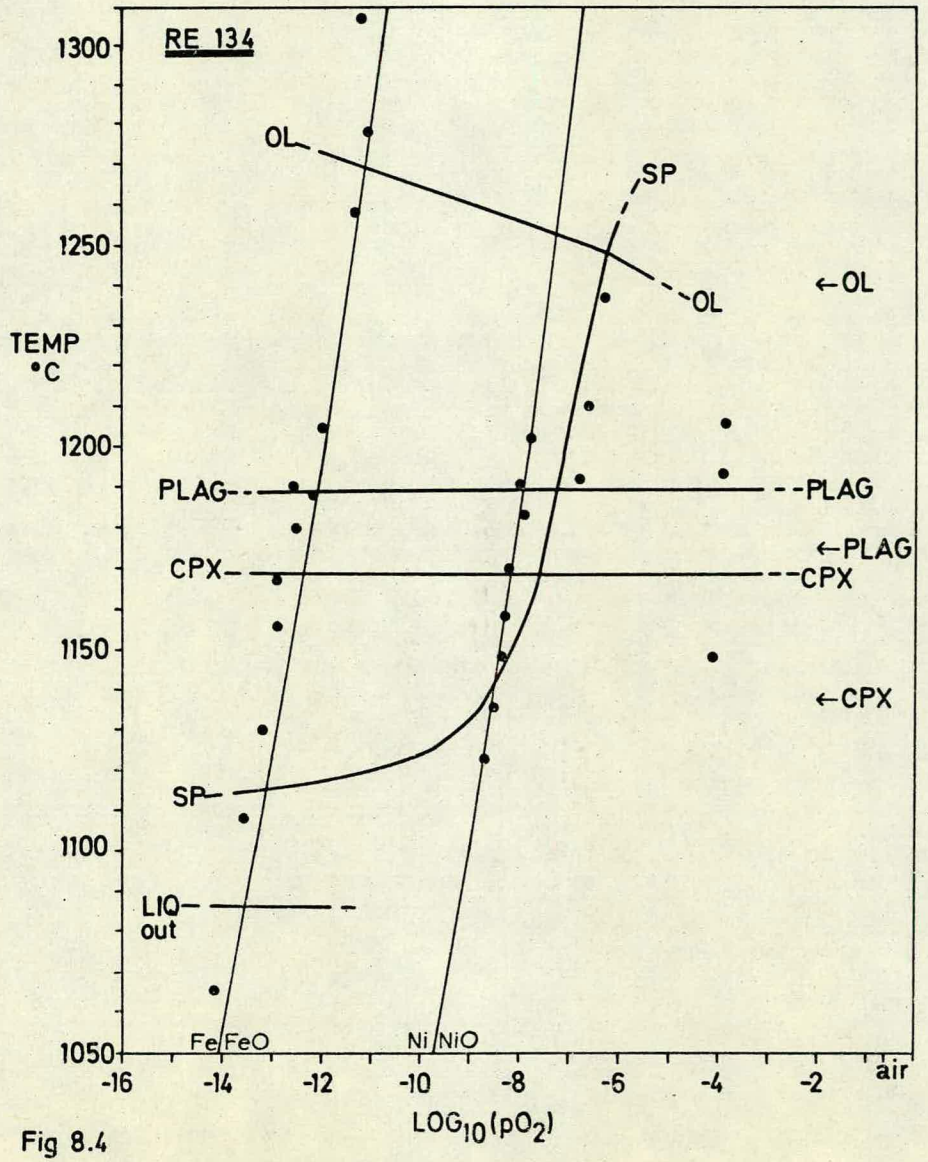
RE 134
OL
SP
OL
←OL
TEMP °C
PLAG
PLAG
←PLAG
CPX
CPX
←CPX
SP
LIQ out
Fe/FeO
Ni/NiO
air
1300
1250
1200
1150
1100
1050
-16
-14
-12
-10
-8
-6
-4
-2
LOG10(pO2)

Fig 8.4

Figure 8.5

See figure 8.1

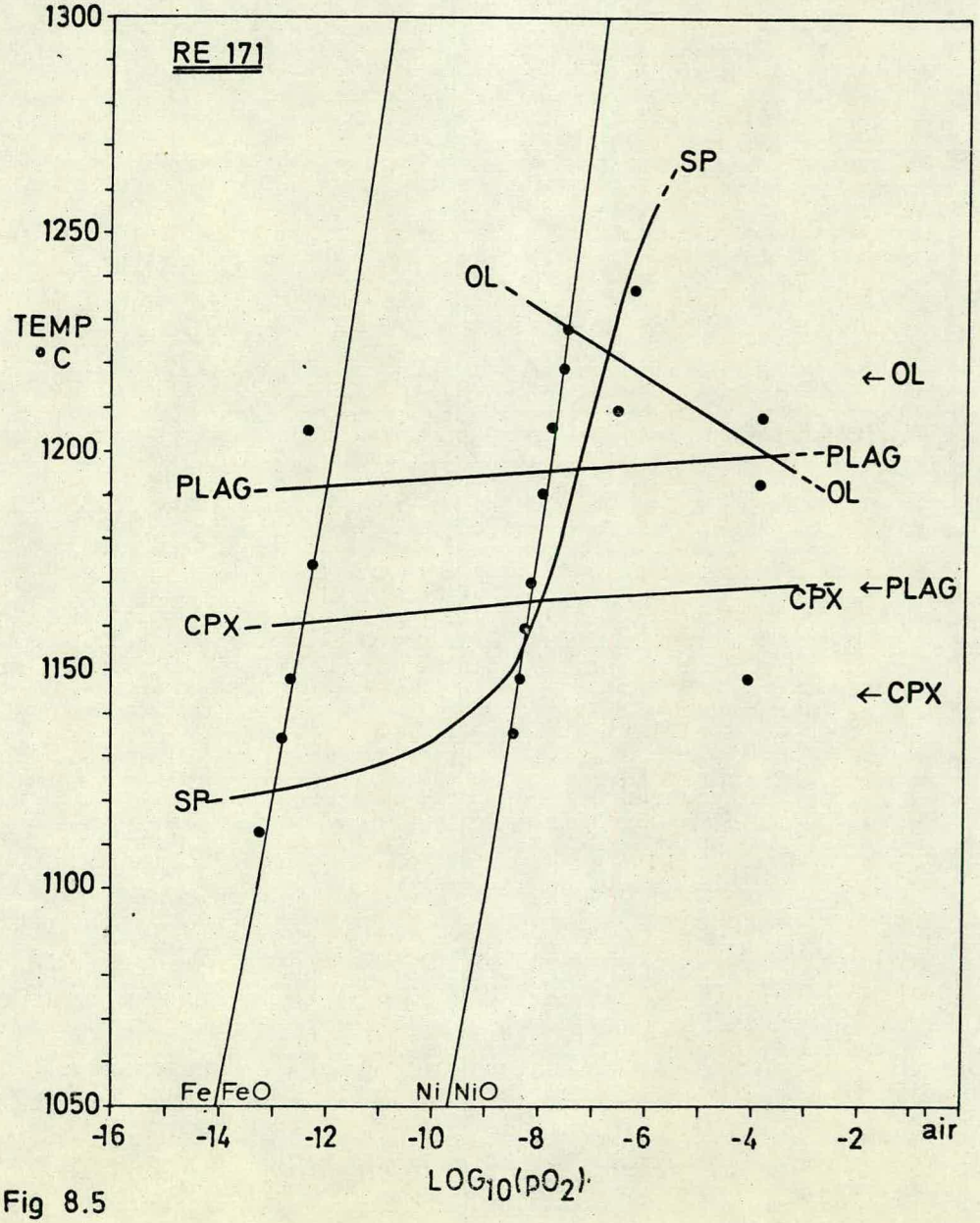
RE 171
1300
1250
1200
1150
1100
1050
TEMP °C
SP
OL
← OL
PLAG
PLAG
OL
CPX
CPX ← PLAG
← CPX
SP
Fe/FeO
Ni/NiO
-16
-14
-12
-10
-8
-6
-4
-2
air
LOG10(pO2)

Fig 8.5

Figure 8.6

See figure 8.1

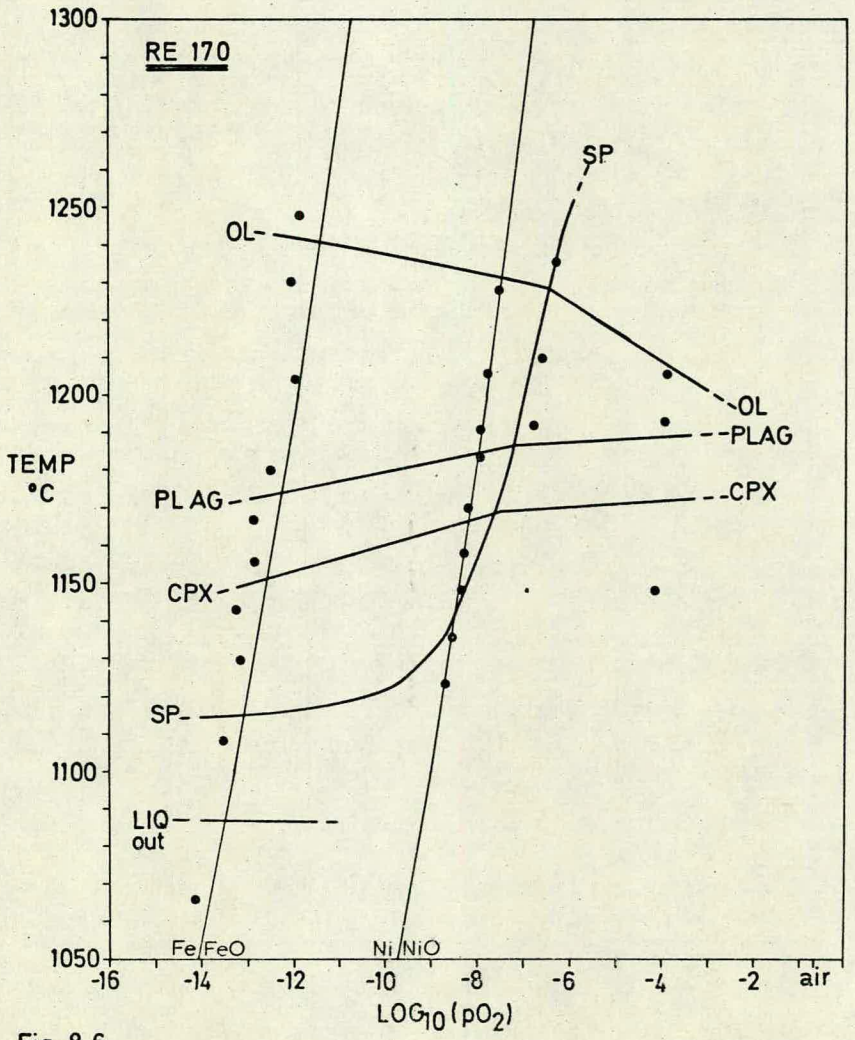
RE 170
1300
1250
1200
1150
1100
1050
TEMP °C
OL
SP
PLAG
CPX
LIQ out
OL
PLAG
CPX
Fe/FeO
Ni/NiO
-16
-14
-12
-10
-8
-6
-4
-2
air
LOG10(pO2)

Fig 8.6

Figure 8.7

See figure 8.1

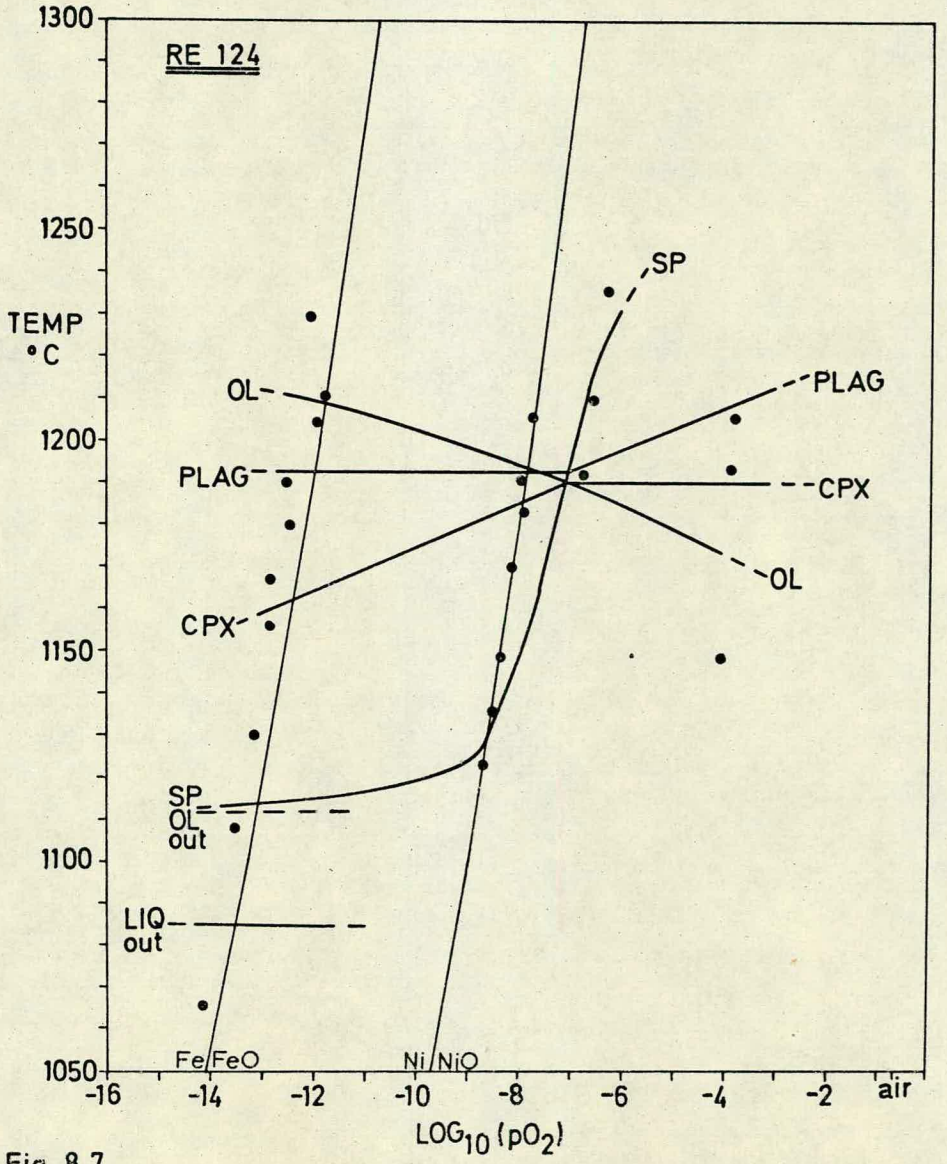
RE 124
1300
1250
1200
1150
1100
1050
TEMP °C
SP
PLAG
OL
PLAG
CPX
OL
CPX
SP
OL out
LIQ out
Fe/FeO
Ni/NiO
-16
-14
-12
-10
-8
-6
-4
-2
air
LOG10 (pO2)

Fig 8.7

Figure 8.8

See figure 8.1

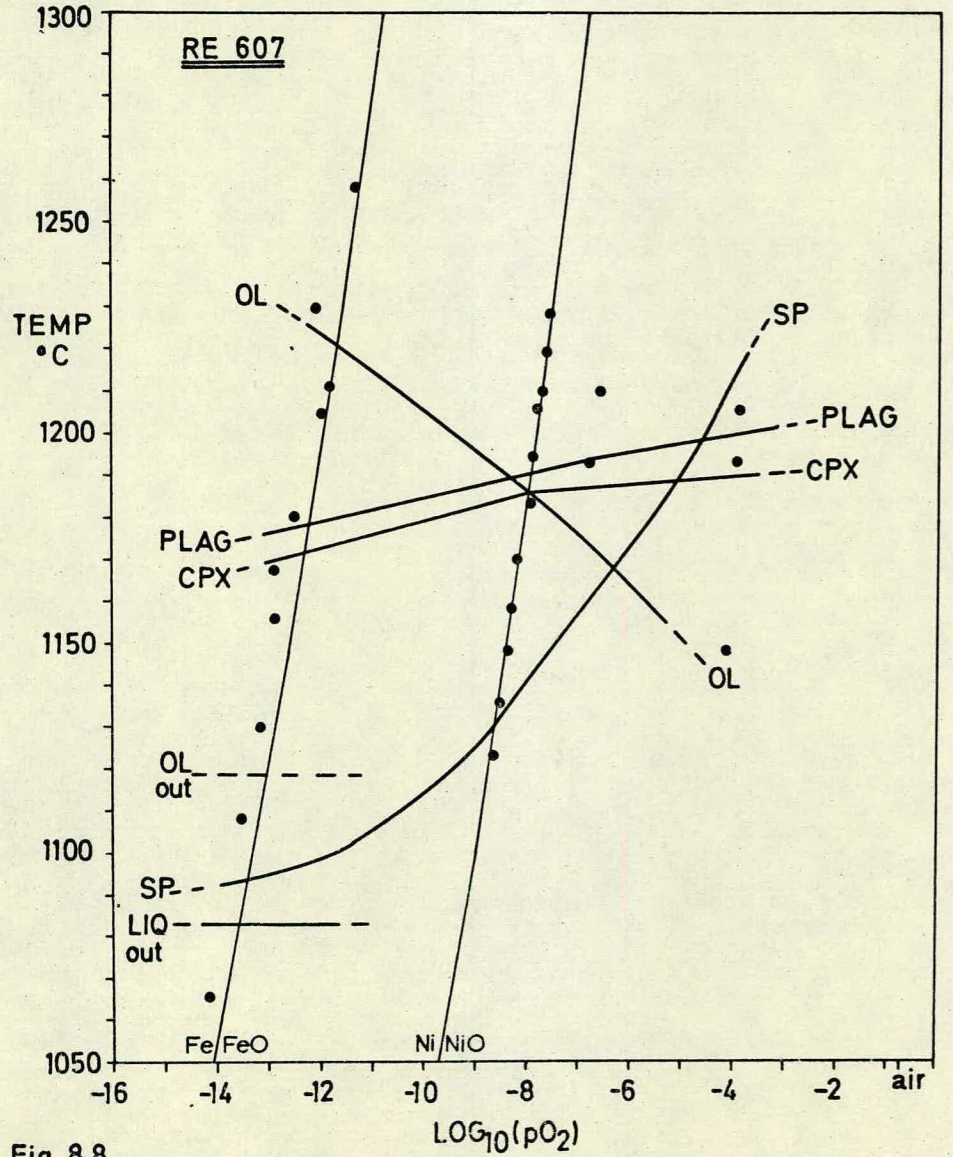
RE 607
1300
1250
1200
1150
1100
1050
TEMP °C
OL
SP
PLAG
CPX
PLAG
CPX
OL
OL out
SP
LIQ out
Fe/FeO
Ni/NiO
-16
-14
-12
-10
-8
-6
-4
-2
air
LOG10(pO2)

Fig 8.8

Figure 8.9

See figure 8.1

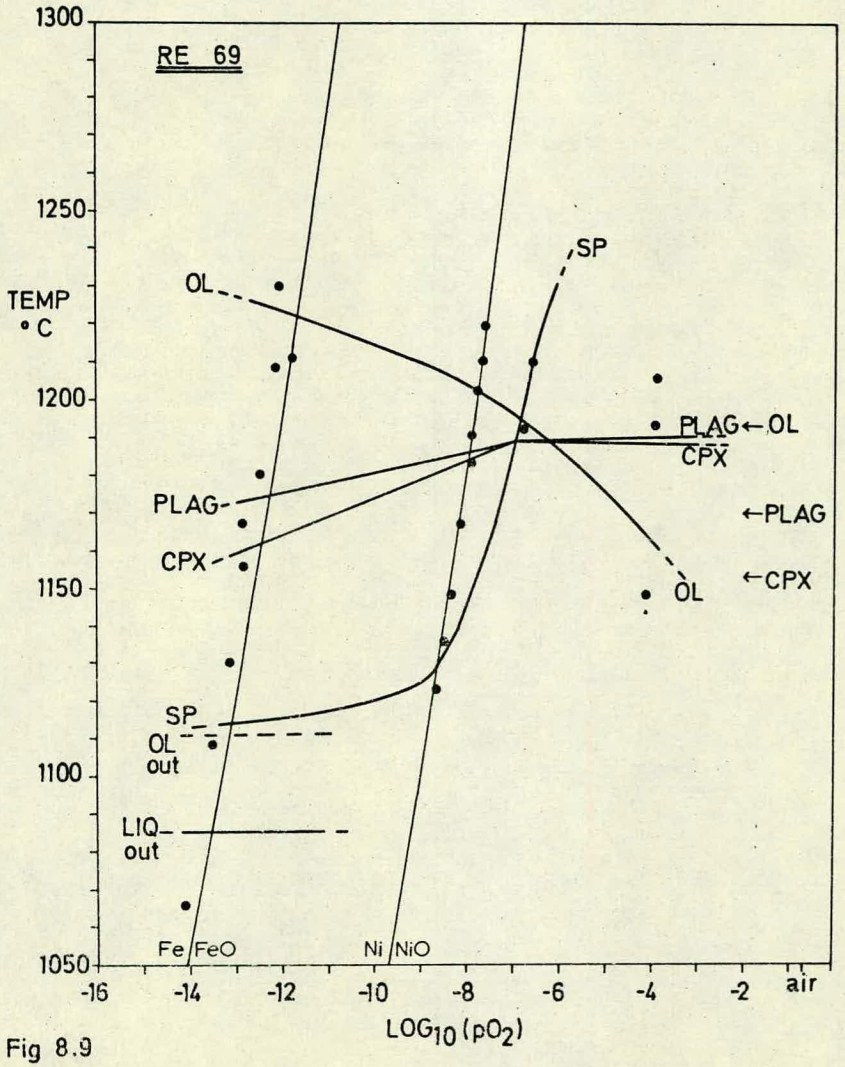
RE 69
1300
1250
1200
1150
1100
1050
TEMP °C
OL
SP
PLAG
CPX
PLAG←OL
CPX
←PLAG
←CPX
OL
SP
OL out
LIQ out
Fe/FeO
Ni/NiO
-16
-14
-12
-10
-8
-6
-4
-2
air
LOG10 (pO2)

Fig 8.9

Figure 8.10

See figure 8.1

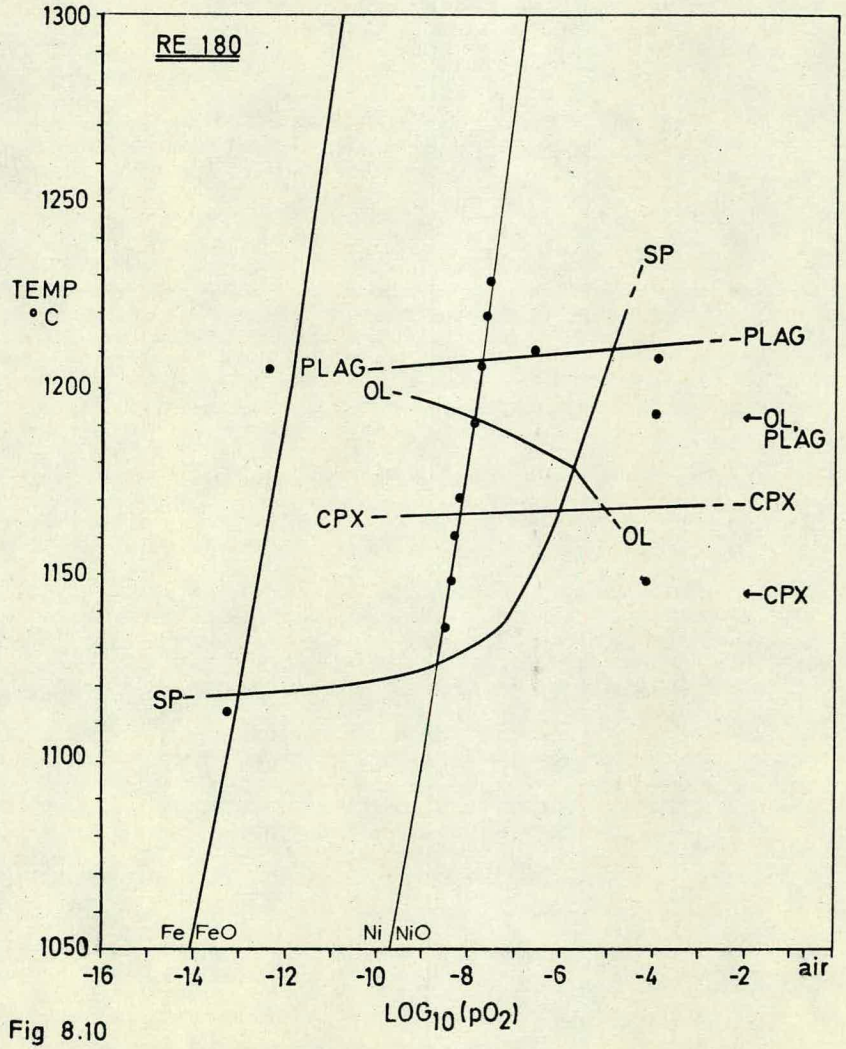
RE 180
1300
1250
1200
1150
1100
1050
TEMP °C
SP
PLAG
PLAG
OL
←OL, PLAG
CPX
CPX
OL
←CPX
SP
Fe FeO
Ni NiO
-16
-14
-12
-10
-8
-6
-4
-2
air
LOG10 (pO2)

Fig 8.10

Figure 8.11

See figure 8.1

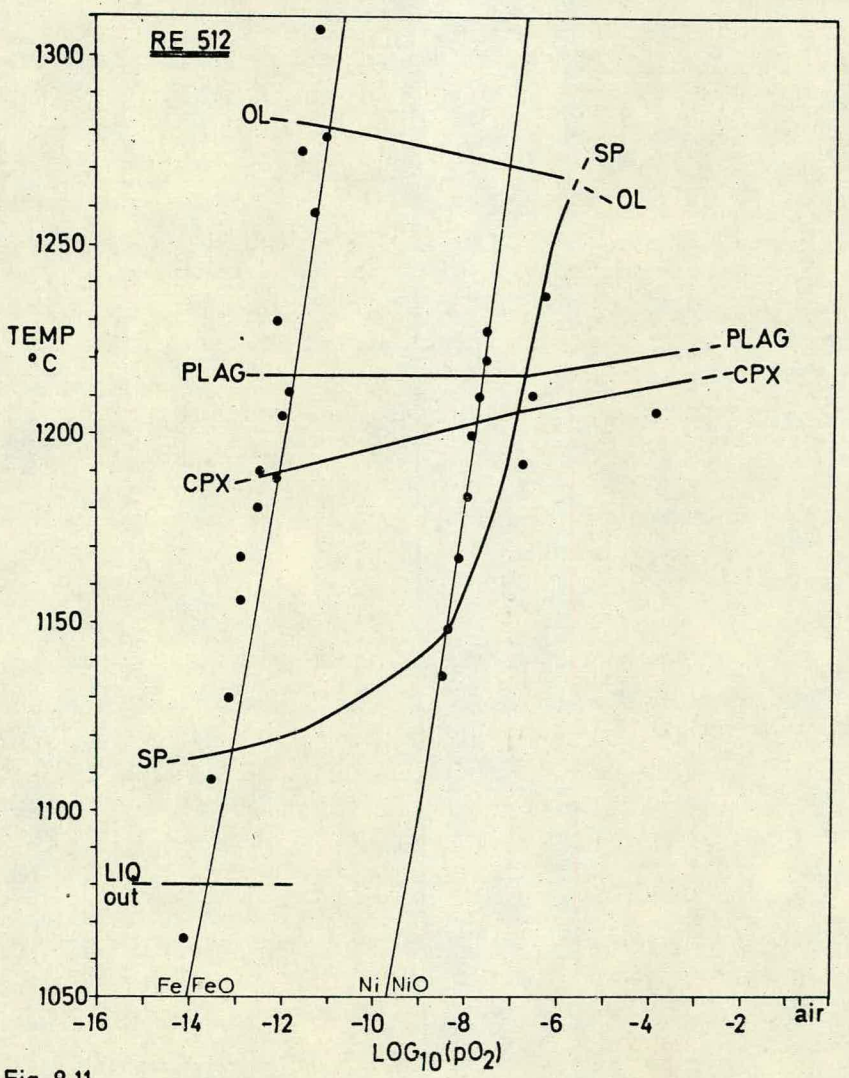
RE 512
1300
1250
1200
1150
1100
1050
TEMP °C
OL
SP
OL
PLAG
PLAG
CPX
CPX
SP
LIQ out
Fe/FeO
Ni/NiO
-16
-14
-12
-10
-8
-6
-4
-2
air
LOG10(pO2)

Fig 8.11

Figure 8.12

See figure 8.1

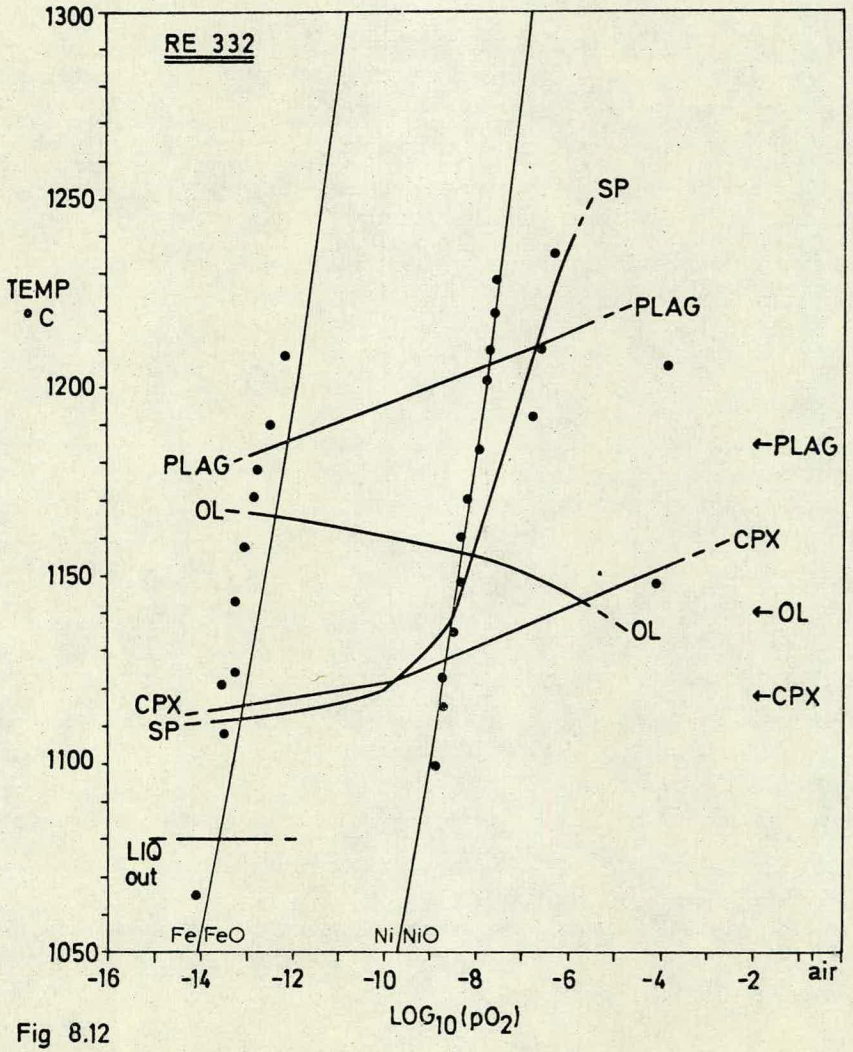
RE 332
TEMP °C
1300
1250
1200
1150
1100
1050
SP
PLAG
PLAG
OL
CPX
OL
CPX
SP
LIQ out
Fe/FeO
Ni/NiO
←PLAG
←OL
←CPX
-16
-14
-12
-10
-8
-6
-4
-2
air
LOG10(pO2)

Fig 8.12

Figure 8.13

See figure 8.1

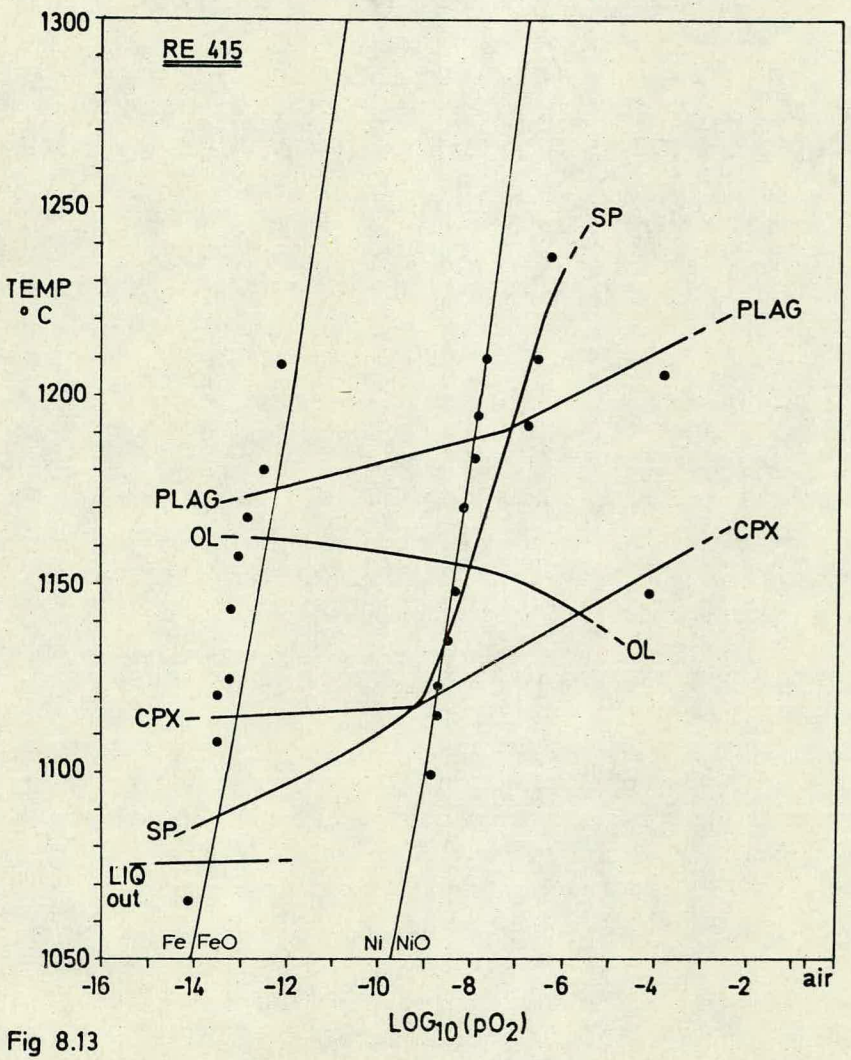
RE 415
1300
1250
1200
1150
1100
1050
TEMP
°C
SP
PLAG
PLAG
OL
CPX
OL
CPX
SP
LIQ
out
Fe FeO
Ni NiO
-16
-14
-12
-10
-8
-6
-4
-2
air
LOG10 (pO2)

Fig 8.13

Figure 8.14

See figure 8.1

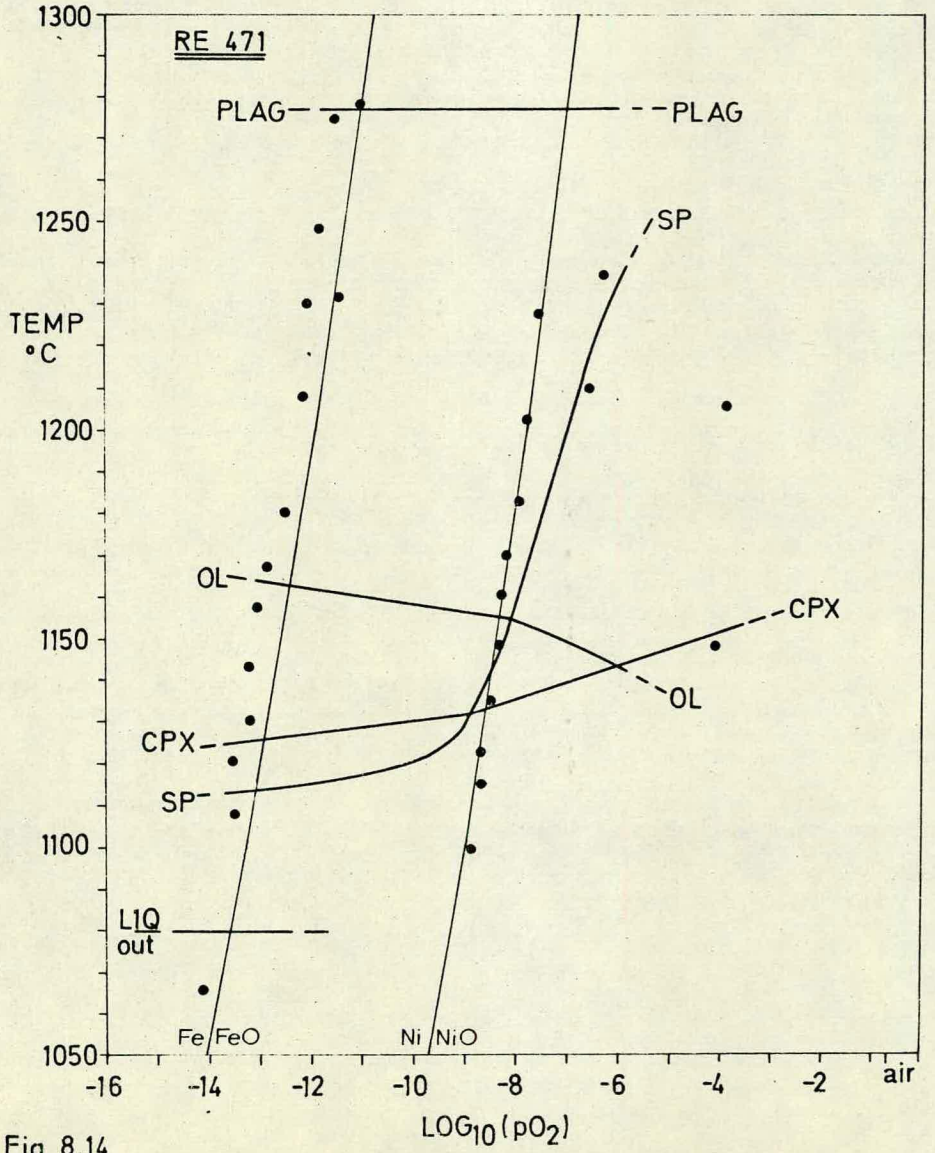
RE 471
PLAG
PLAG
SP
TEMP °C
OL
CPX
OL
CPX
SP
LIQ out
Fe/FeO
Ni/NiO
1300
1250
1200
1150
1100
1050
-16
-14
-12
-10
-8
-6
-4
-2
air
LOG10(pO2)

Fig 8.14

Figure 8.15

See figure 8.1

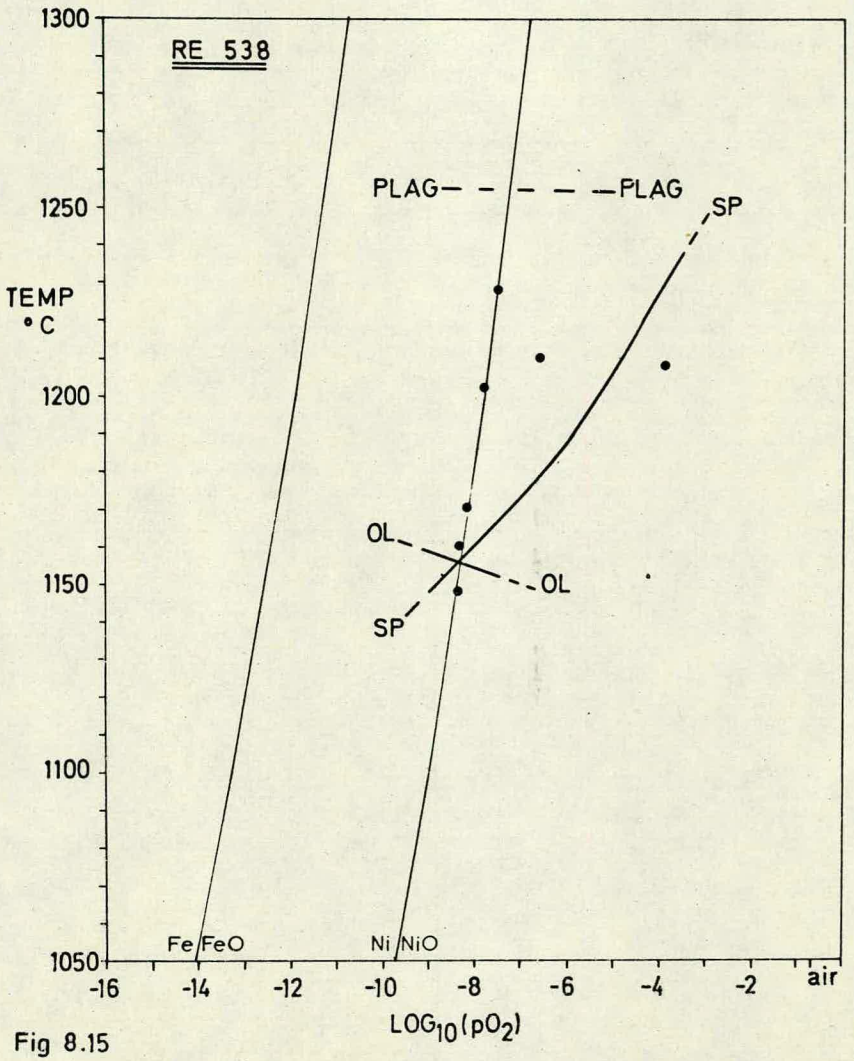
RE 538
1300
1250
1200
1150
1100
1050
TEMP
°C
PLAG
PLAG
SP
OL
OL
SP
Fe/FeO
Ni/NiO
-16
-14
-12
-10
-8
-6
-4
-2
air
LOG10(pO2)

Fig 8.15

Figure 8.16

See figure 8.1

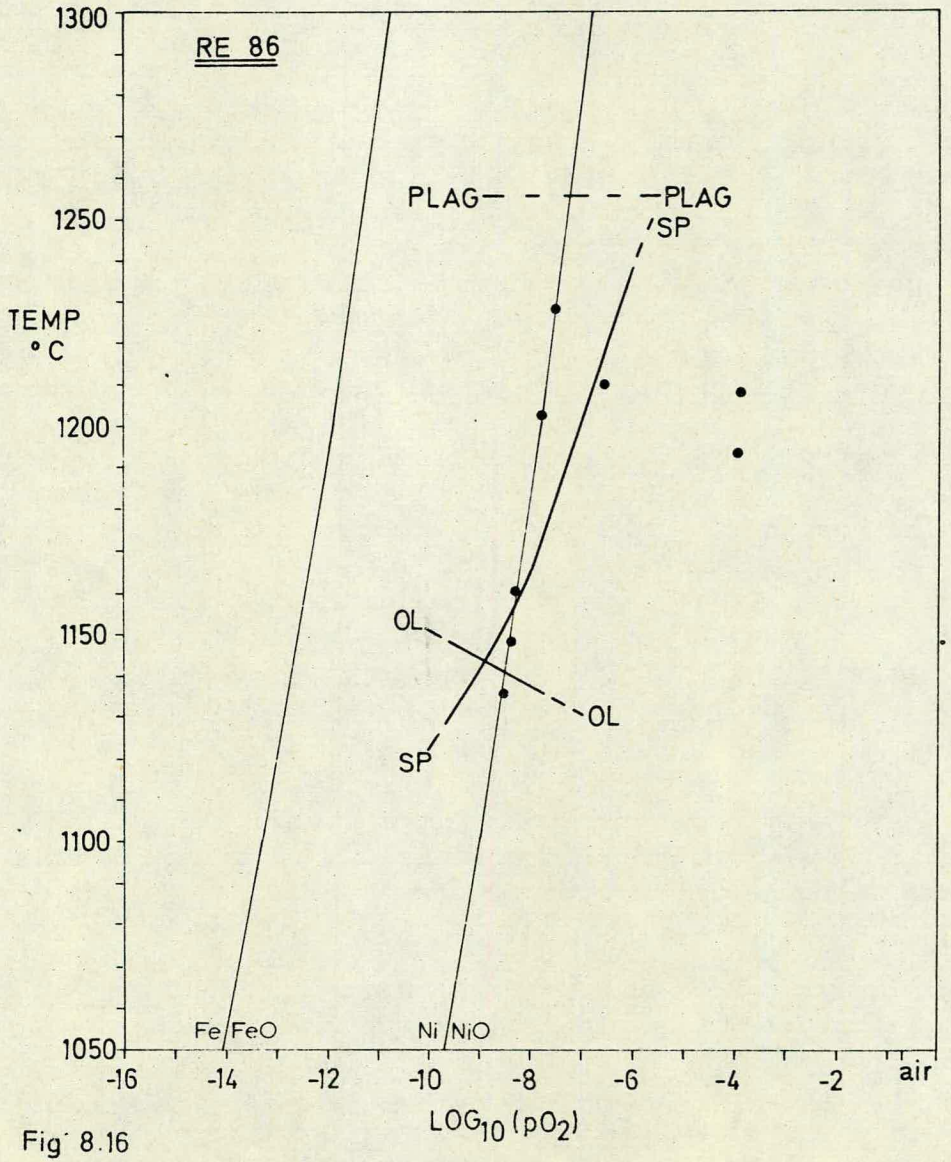
RE 86
PLAG
PLAG
SP
OL
OL
SP
TEMP
°C
1300
1250
1200
1150
1100
1050
Fe/FeO
Ni/NiO
-16
-14
-12
-10
-8
-6
-4
-2
air
LOG10 (pO2)

Fig 8.16

Figure 8.17

See figure 8.1

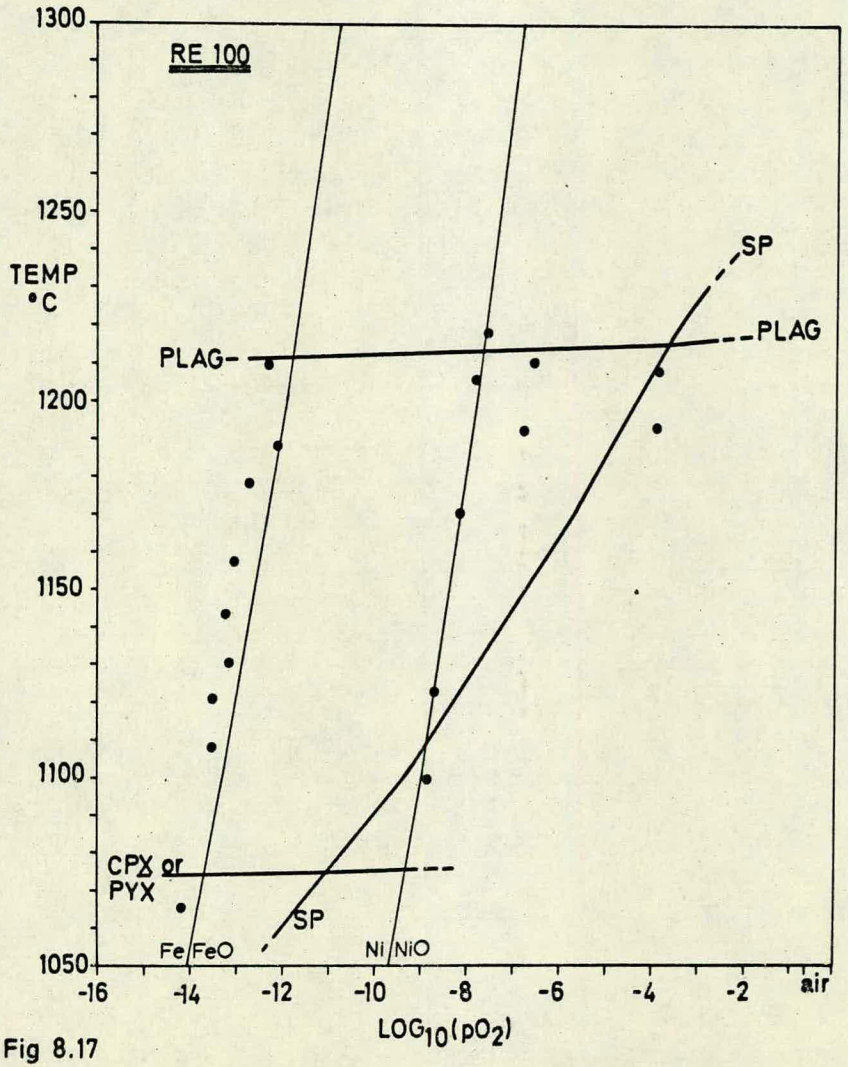
RE 100
1300
1250
1200
1150
1100
1050
TEMP °C
PLAG
PLAG
SP
SP
CPX or PYX
Fe/FeO
Ni/NiO
-16
-14
-12
-10
-8
-6
-4
-2
air
LOG10(pO2)

Fig 8.17

Figure 8.18

See figure 8.1

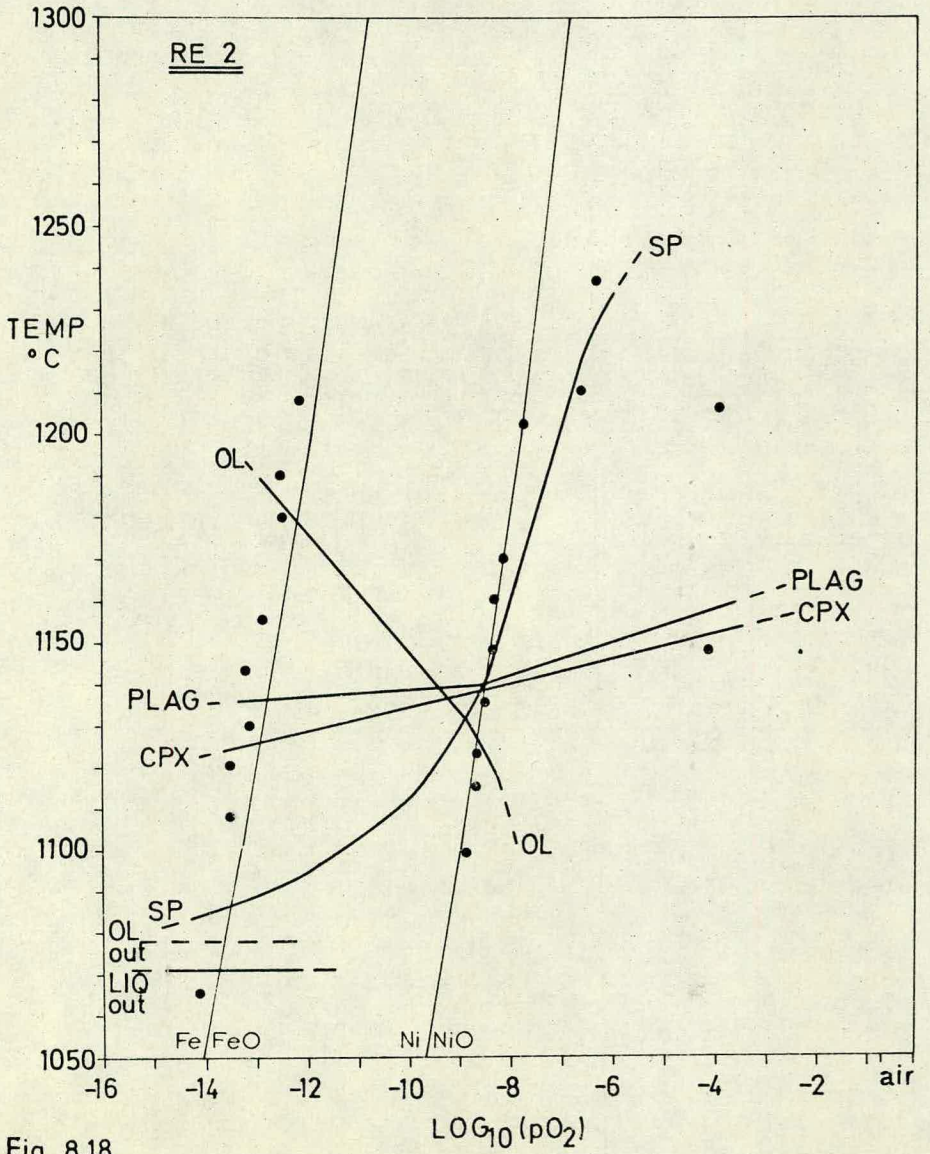
RE 2
1300
1250
1200
1150
1100
1050
TEMP °C
SP
OL
PLAG
CPX
PLAG
CPX
OL
SP
OL out
LIQ out
Fe FeO
Ni NiO
-16
-14
-12
-10
-8
-6
-4
-2
air
LOG10 (pO2)

Fig 8.18

Figure 8.19

See figure 8.1

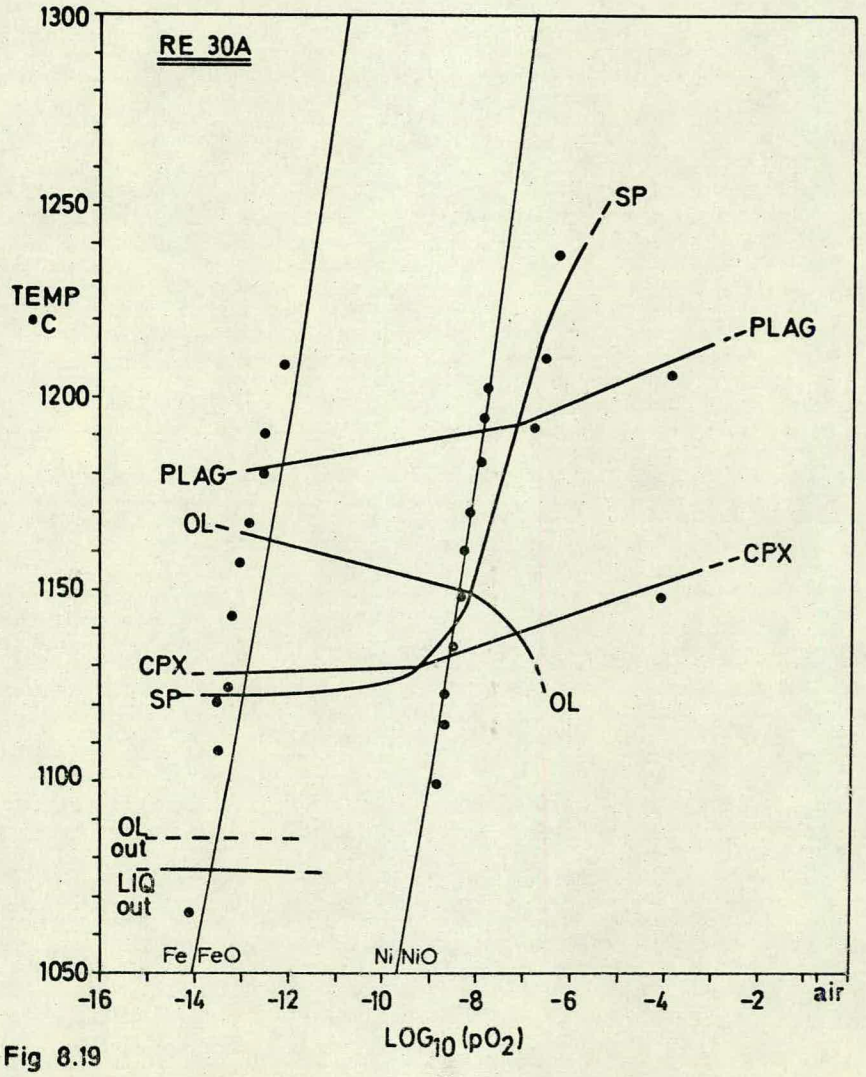
RE 30A
1300
1250
1200
1150
1100
1050
TEMP °C
SP
PLAG
PLAG
OL
CPX
CPX
SP
OL
OL out
LIQ out
Fe/FeO
Ni/NiO
-16
-14
-12
-10
-8
-6
-4
-2
air
LOG10 (pO2)

Fig 8.19

Figure 8.20

See figure 8.1

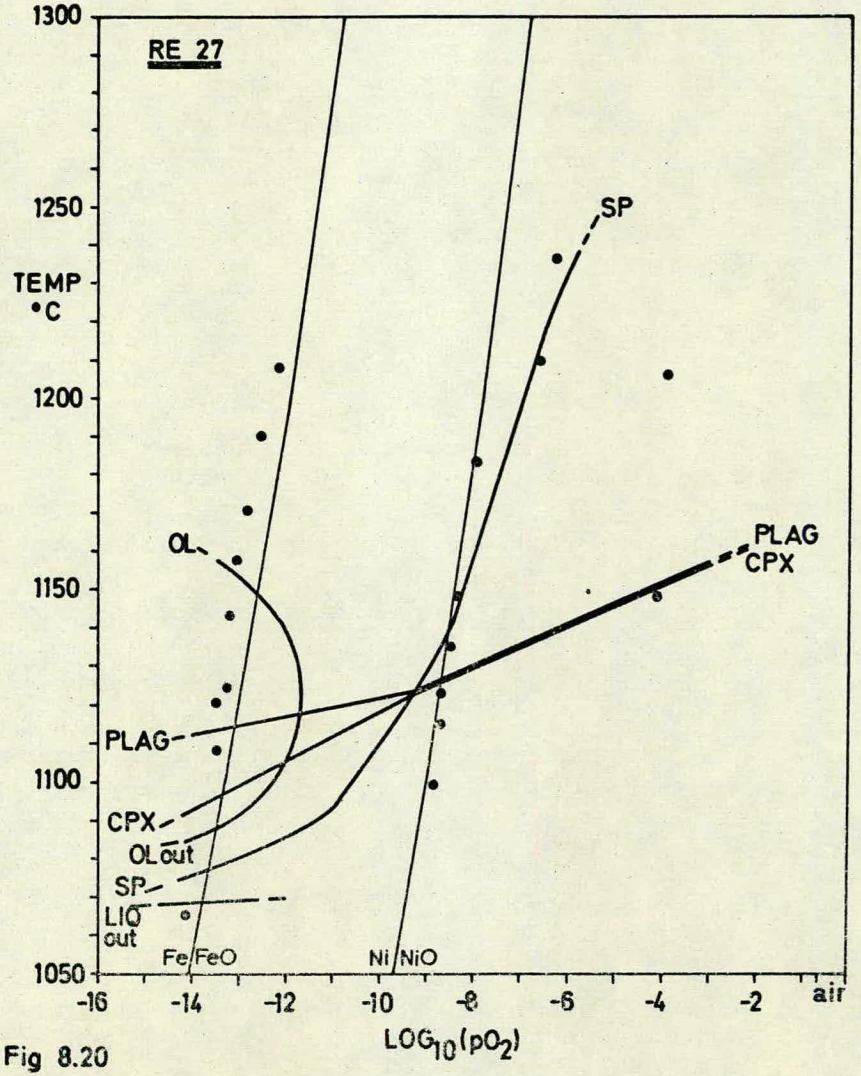
RE 27
1300
1250
TEMP °C
1200
1150
1100
1050
SP
PLAG
CPX
OL
PLAG
CPX
OL out
SP
LIQ out
Fe/FeO
Ni/NiO
-16
-14
-12
-10
-8
-6
-4
-2
air
LOG10(pO2)

Fig 8.20

Figure 8.21

See figure 8.1

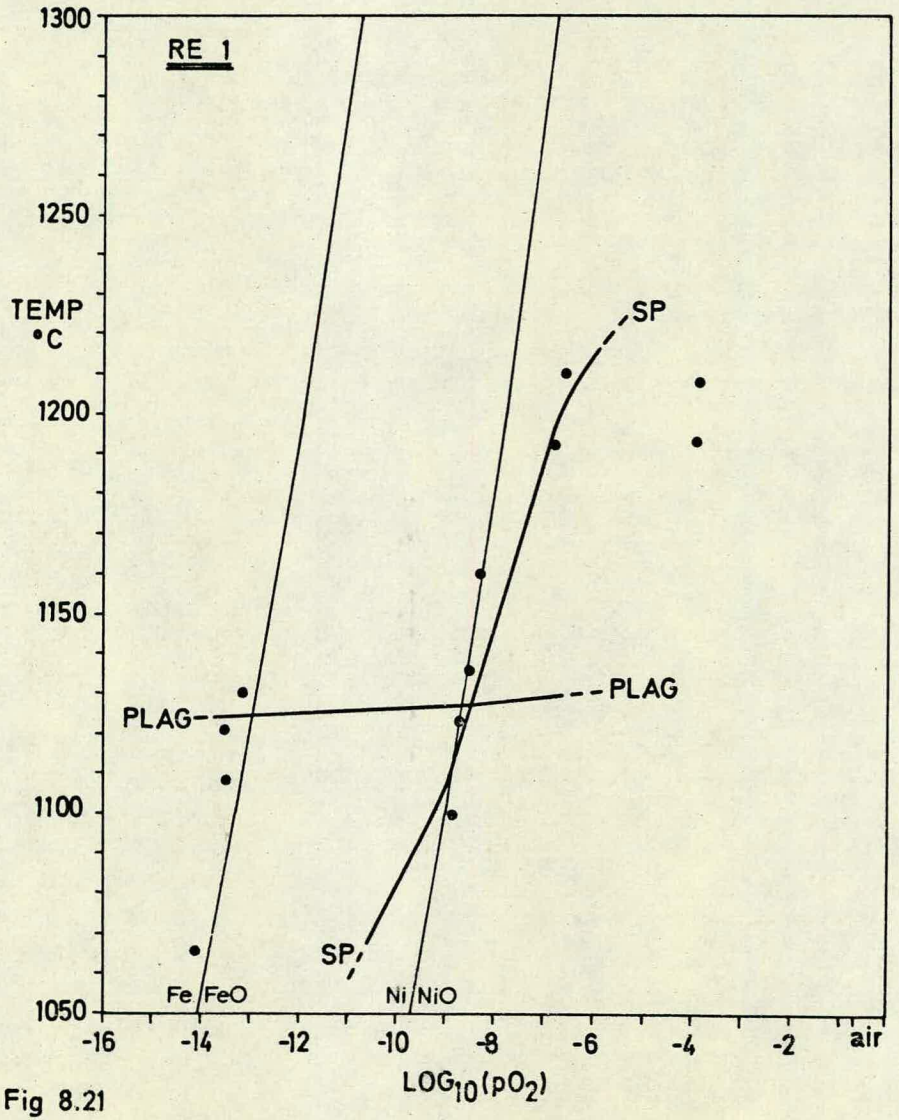
RE 1
1300
1250
TEMP
°C
1200
1150
1100
1050
SP
PLAG
PLAG
SP
Fe FeO
Ni NiO
-16
-14
-12
-10
-8
-6
-4
-2
air
LOG10(pO2)

Fig 8.21

Figure 8.22

See figure 8.1

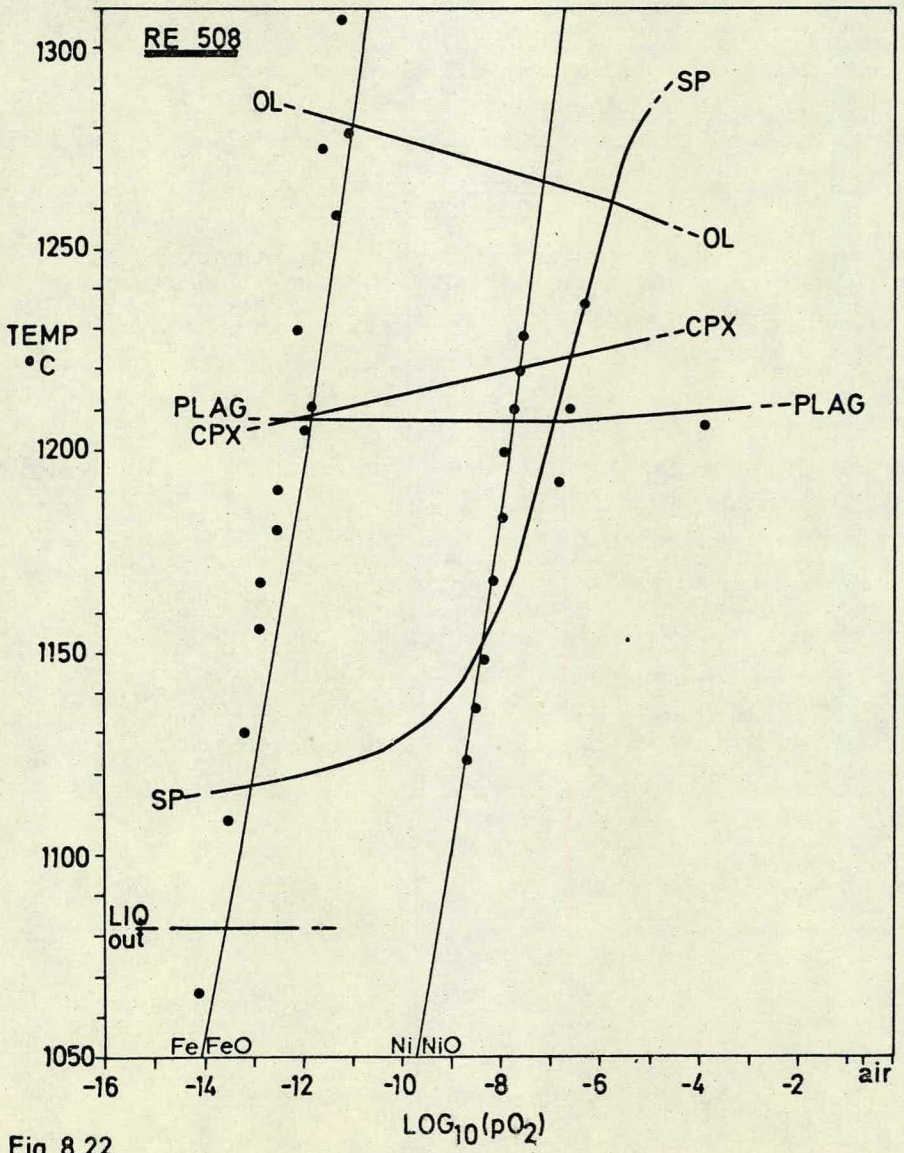
RE 508
OL
SP
OL
CPX
PLAG
CPX
PLAG
SP
LIQ
out
Fe/FeO
Ni/NiO
TEMP
°C
1300
1250
1200
1150
1100
1050
-16
-14
-12
-10
-8
-6
-4
-2
air
LOG10(pO2)

Fig 8.22

Figure 8.23

See figure 8.1

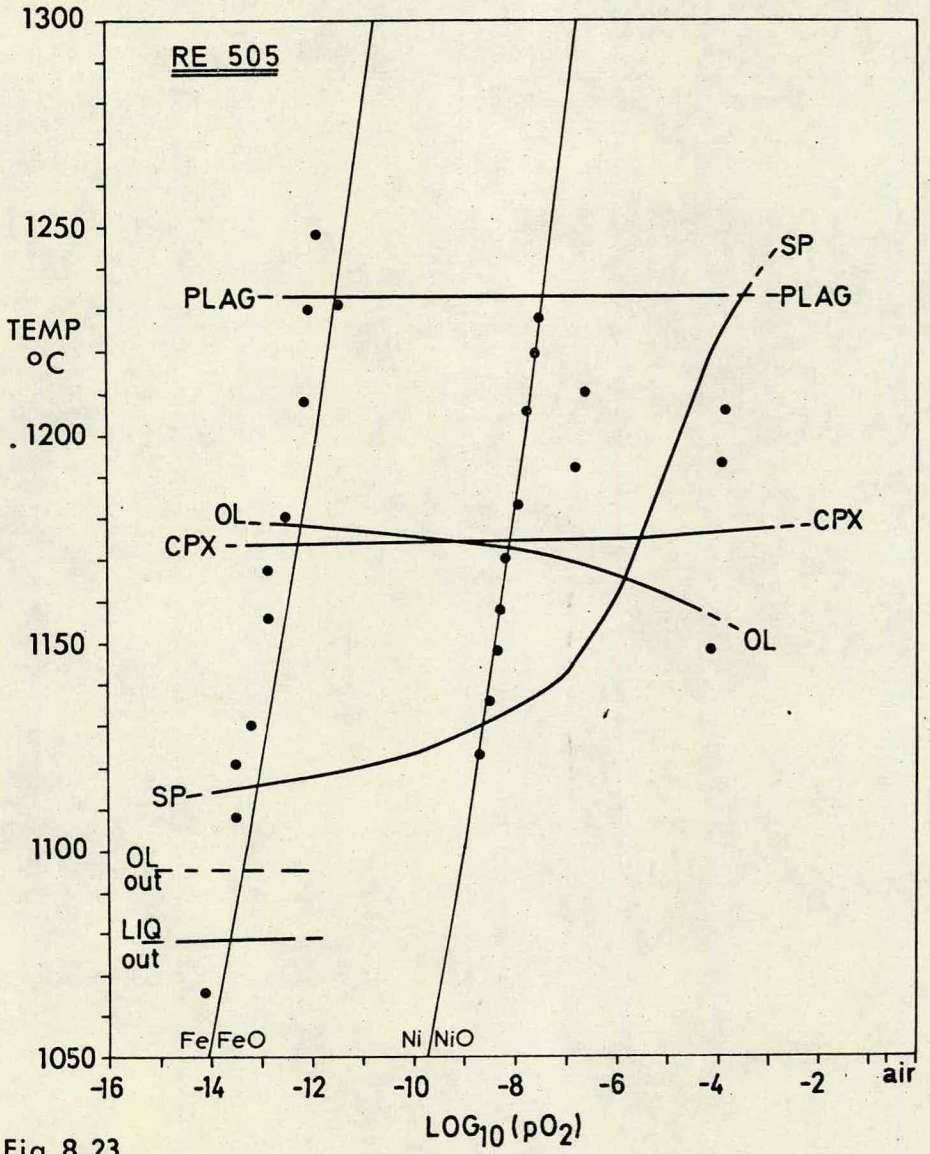
RE 505
1300
1250
1200
1150
1100
1050
TEMP °C
PLAG
SP
PLAG
OL
CPX
CPX
OL
SP
OL out
LIQ out
Fe/FeO
Ni/NiO
-16
-14
-12
-10
-8
-6
-4
-2
air
LOG10 (pO2)

Fig 8.23

Figure 8.24

See figure 8.1

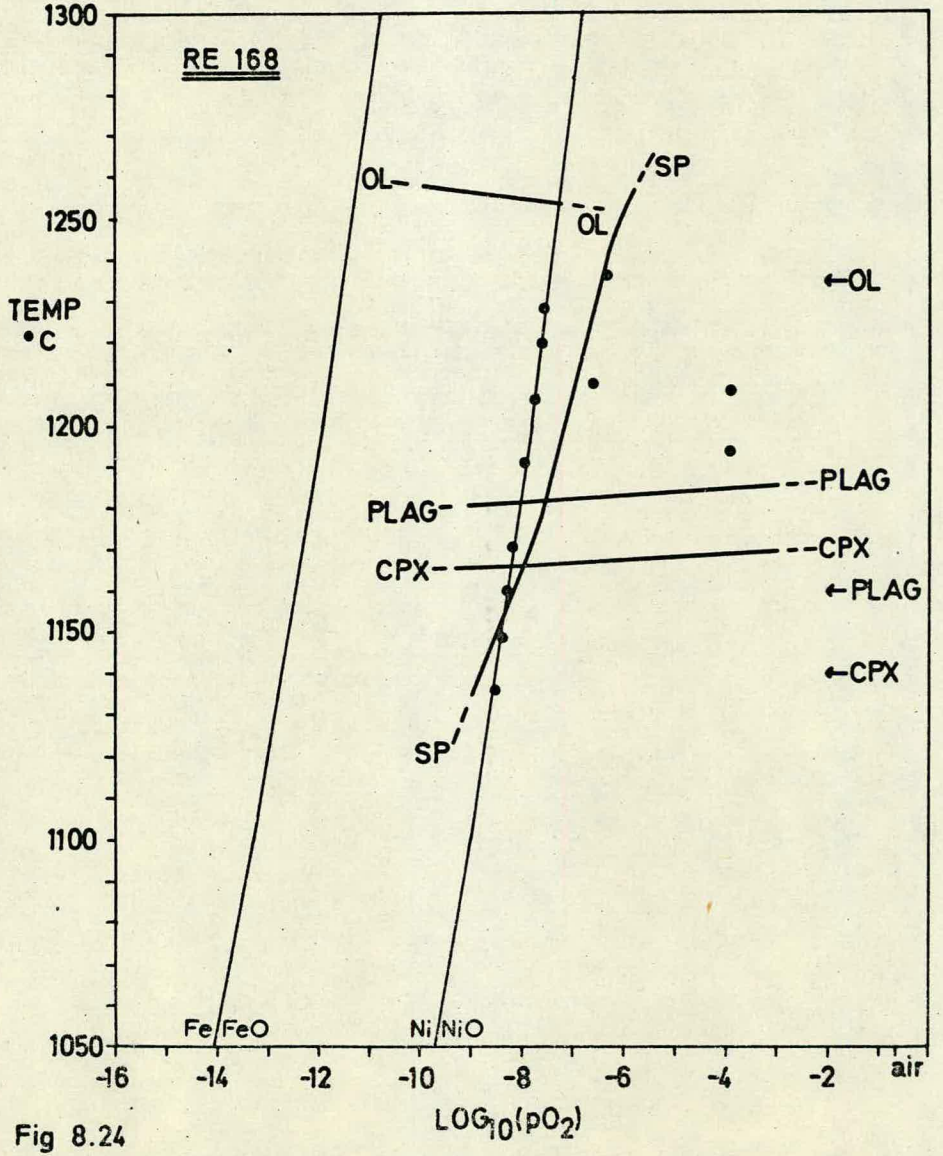
RE 168
1300
1250
1200
1150
1100
1050
TEMP °C
OL
SP
OL
←OL
PLAG
--PLAG
CPX
--CPX
←PLAG
←CPX
SP
Fe/FeO
Ni/NiO
-16
-14
-12
-10
-8
-6
-4
-2
air
LOG10(pO2)

Fig 8.24

Figure 8.25

See figure 8.1

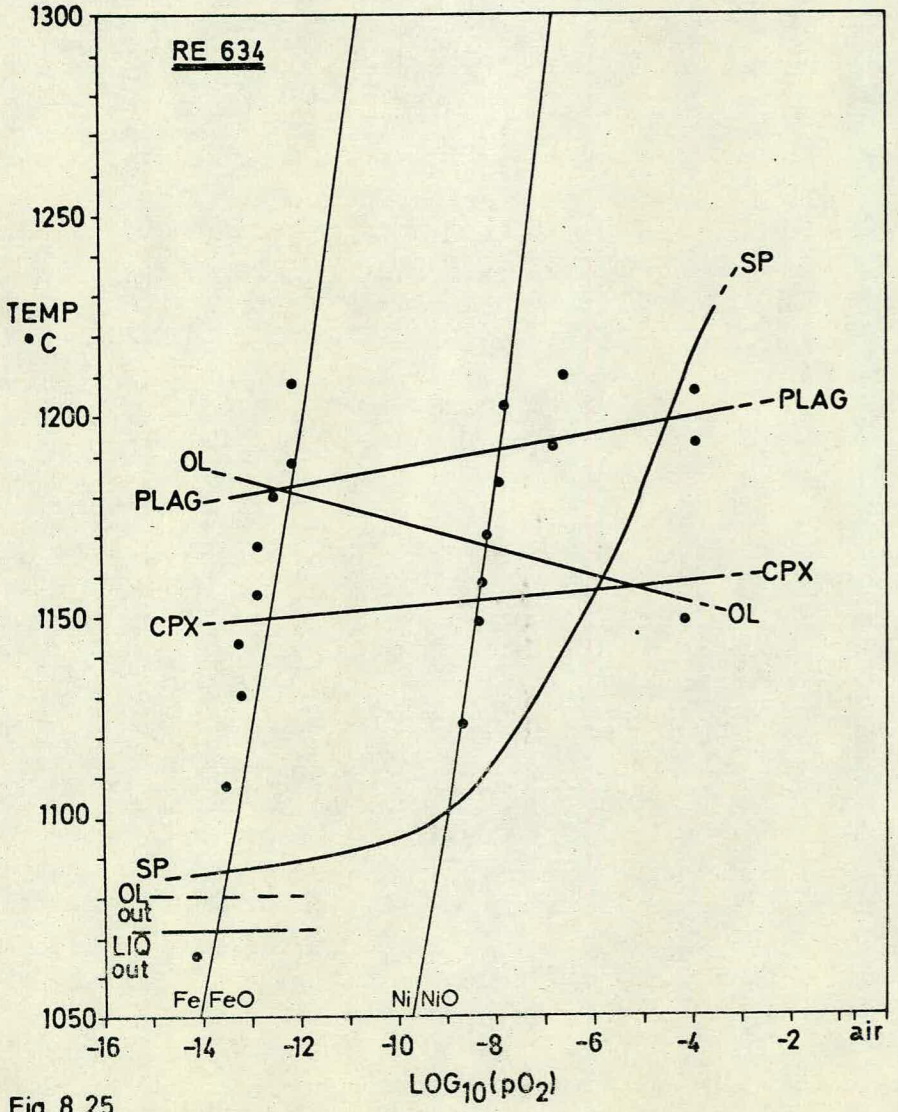
RE 634
1300
1250
1200
1150
1100
1050
TEMP °C
SP
PLAG
OL
PLAG
CPX
OL
CPX
SP
OL out
LIQ out
Fe/FeO
Ni/NiO
-16
-14
-12
-10
-8
-6
-4
-2
air
LOG10(pO2)

Fig 8.25

Figures 8.26A-8.26B

A $2YO.ZO_2$ (olivine) projection into part of the plane $XO.ZO_2$-$YO.ZO_2$-R_2O_3 (CS-MS-A) of the natural rocks studied from the Oceanite Series of Piton des Neiges volcano, Reunion. Also included are the rocks from Piton de la Fournaise and the Nodules. All iron was recast as FeO prior to projecting the analyses. The symbols indicate the second phase to crystallise after olivine for these rocks at the pO_2 of the Fe/FeO equilibrium (figure 8.26A) and Ni/NiO equilibrium (figure 8.26B). The pseudo phase boundary olivine+plagioclase+clinopyroxene+liquid for these rocks is indicated, together with the olivine-bearing projection boundaries from the system CMAS only (labelled CMAS), and that estimated for the system CMASN-Fe-O_2 (labelled CMASNF) for the combination of ratios $An_{50}Ab_{50}$, FeO/MgO mole ratio = 0.5, pO_2 = Fe/FeO or Ni/NiO (as appropriate).

The symbols have the following meanings

- □ plagioclase second
- ◢ clinopyroxene second
- ◪ plagioclase+clinopyroxene second

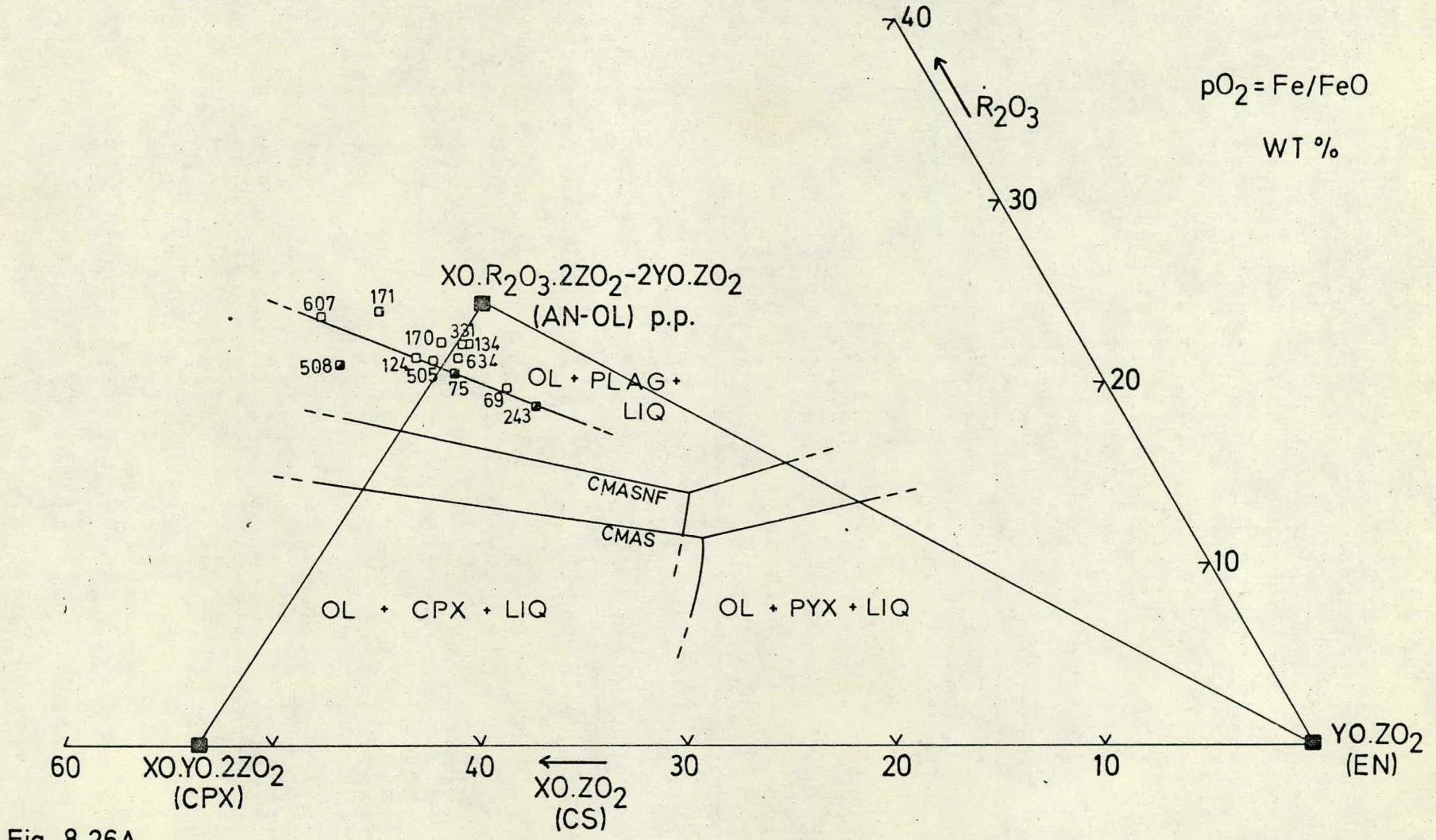
40
R_2O_3
pO_2 = Fe/FeO
WT %
30
20
10
$XO.R_2O_3.2ZO_2$-$2YO.ZO_2$
(AN-OL) p.p.
607
171
170
321
134
634
508
124
505
75
69
243
OL + PLAG + LIQ
CMASNF
CMAS
OL + CPX + LIQ
OL + PYX + LIQ
60
$XO.YO.2ZO_2$
(CPX)
40
$XO.ZO_2$
(CS)
30
20
10
$YO.ZO_2$
(EN)

Fig 8.26A

Figure 8.26B

See figure 8.26A

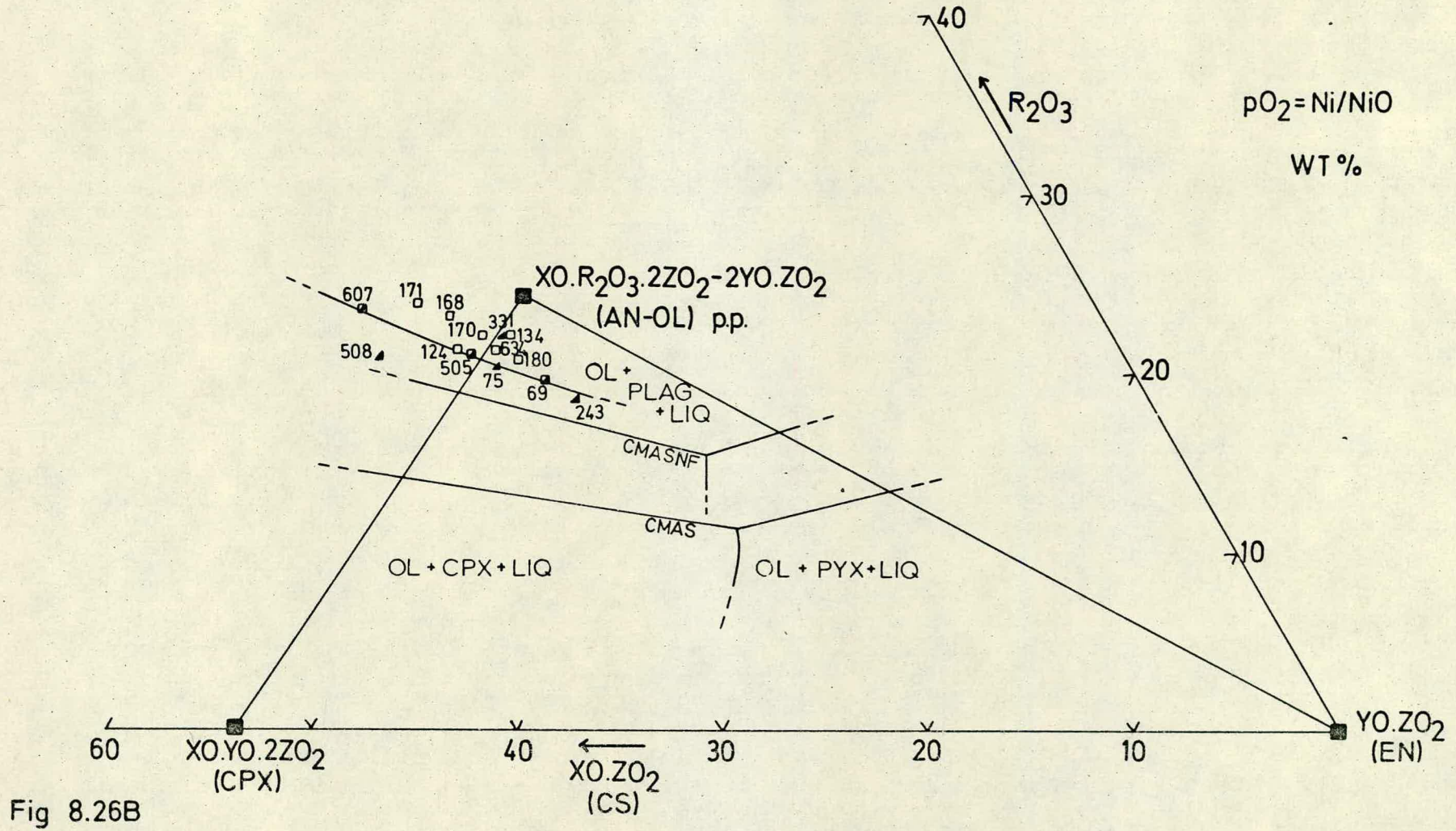
40
R_2O_3
pO_2=Ni/NiO
WT %
30
20
10
$XO.R_2O_3.2ZO_2$-$2YO.ZO_2$
(AN-OL) p.p.
607
171
168
170
331
134
508
124
505
75
69
180
243
OL + PLAG + LIQ
CMASNF
CMAS
OL + CPX + LIQ
OL + PYX + LIQ
60
$XO.YO.2ZO_2$
(CPX)
40
$XO.ZO_2$
(CS)
30
20
10
$YO.ZO_2$
(EN)

Fig 8.26B

Figures 8.27A-8.27B

A $XO.YO.2ZO_2$ (clinopyroxene) projection into part of the plane $XO.R_2O_3$-YO-ZO_2 (CA-M-S) of the natural rocks studied from the Oceanite Series of Piton des Neiges volcano, Reunion. Also included are the rocks from Piton de la Fournaise and the Nodules. All iron in the analyses was recast as FeO prior to projecting the analyses. The symbols indicate the liquidus phase for these rocks at the pO_2 of the Fe/FeO equilibrium (figure 8.27A) and Ni/NiO equilibrium (figure 8.27B). The pseudo phase boundary olivine+plagioclase+clinopyroxene+liquid for these rocks is indicated, the clinopyroxene appearing very shortly after olivine+plagioclase has been reached. The clinopyroxene-bearing projection boundaries from the system CMAS only (labelled CMAS), and that estimated for the system CMASN-Fe-O_2 (labelled CMASNF) for the combination of ratios $An_{50}Ab_{50}$, FeO/MgO mole ratio = 0.5, pO_2 = Fe/FeO or Ni/NiO (as appropriate) are also shown.

The symbols have the following meanings

- ● olivine liquidus
- □ plagioclase liquidus
- ■ olivine+plagioclase liquidus

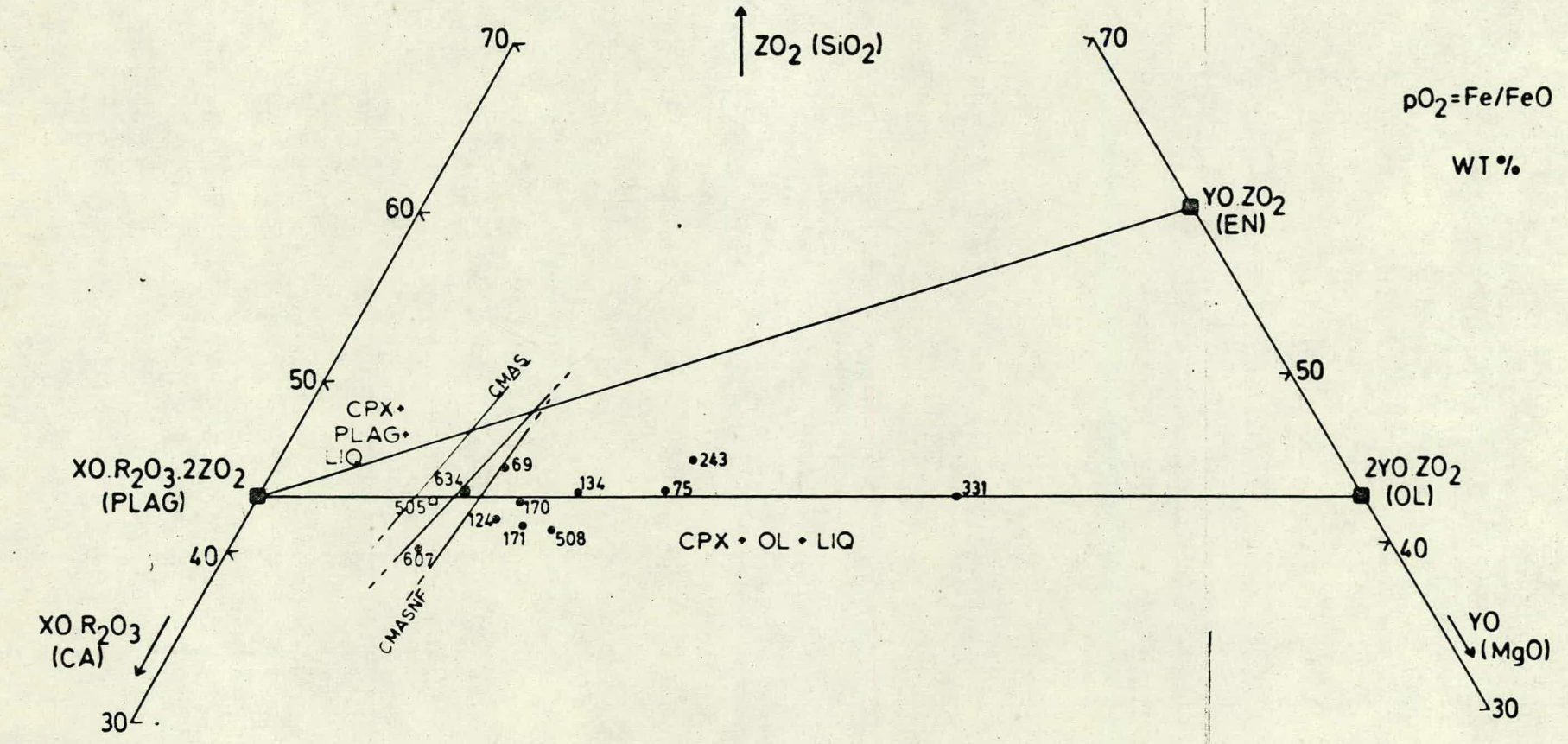
ZO2 (SiO2)
70
60
50
40
30
70
50
40
30
pO2=Fe/FeO
WT %
YO.ZO2
(EN)
XO.R2O3.2ZO2
(PLAG)
2YO.ZO2
(OL)
XO.R2O3
(CA)
YO
(MgO)
CPX+
PLAG+
LIQ
CMAS
CMASNF
CPX + OL + LIQ
634
69
505
124
607
171
170
508
134
75
243
331

Fig 8.27A

Figure 8.27B

See figure 8.27A

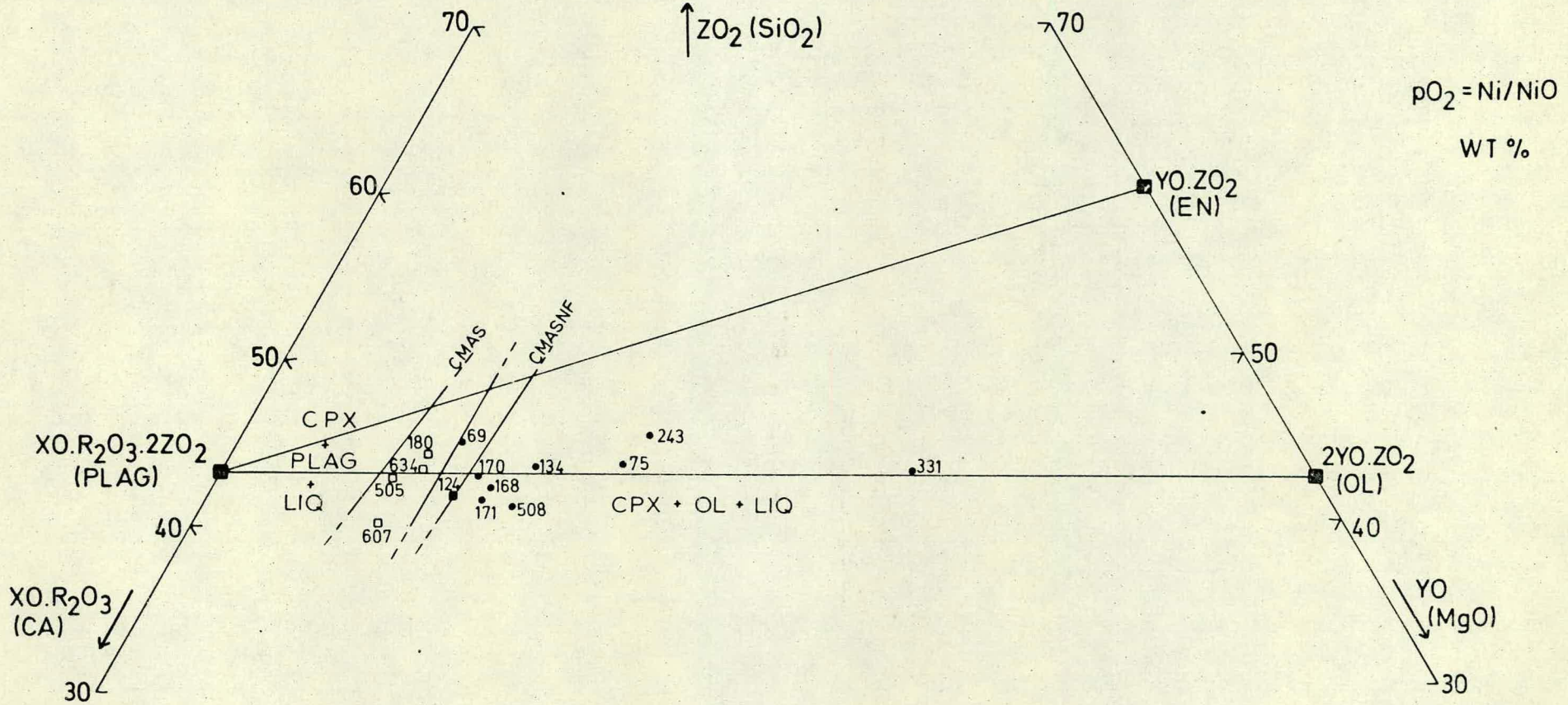
ZO2 (SiO2)
70
60
50
40
30
pO2 = Ni/NiO
WT %
YO.ZO2
(EN)
XO.R2O3.2ZO2
(PLAG)
XO.R2O3
(CA)
2YO.ZO2
(OL)
YO
(MgO)
CMAS
CMASNF
CPX
PLAG
LIQ
180
634
505
607
69
170
124
168
171
508
134
75
243
331
CPX + OL + LIQ

Fig 8.27B

Figures 8.28A-8.28B

A $2YO.ZO_2$ (olivine) projection into part of the plane $XO.ZO_2$-$YO.ZO_2$-R_2O_3 (CS-MS-A) of the natural rocks studied from the Differentiated Series of Piton des Neiges volcano, Reunion. All iron was recast as FeO prior to projecting the analyses. The symbols indicate the second phase to crystallise after olivine, or the first phase if olivine is second, for these rocks at the pO_2 of the Fe/FeO equilibrium (figure 8.28A) and Ni/NiO equilibrium (figure 8.28B). An approximate pseudo phase boundary olivine+plagioclase+clinopyroxene+liquid for these rocks is estimated, and the olivine-bearing projection boundaries from the system CMAS only (labelled CMAS), and that estimated for the system CMASN-Fe-O_2 (labelled CMASNF) for the combination of ratios $An_{50}Ab_{50}$, FeO/MgO mole ratio = 0.5, pO_2 = Fe/FeO or Ni/NiO (as appropriate), are also shown.

The symbols have the following meanings

□ plagioclase second

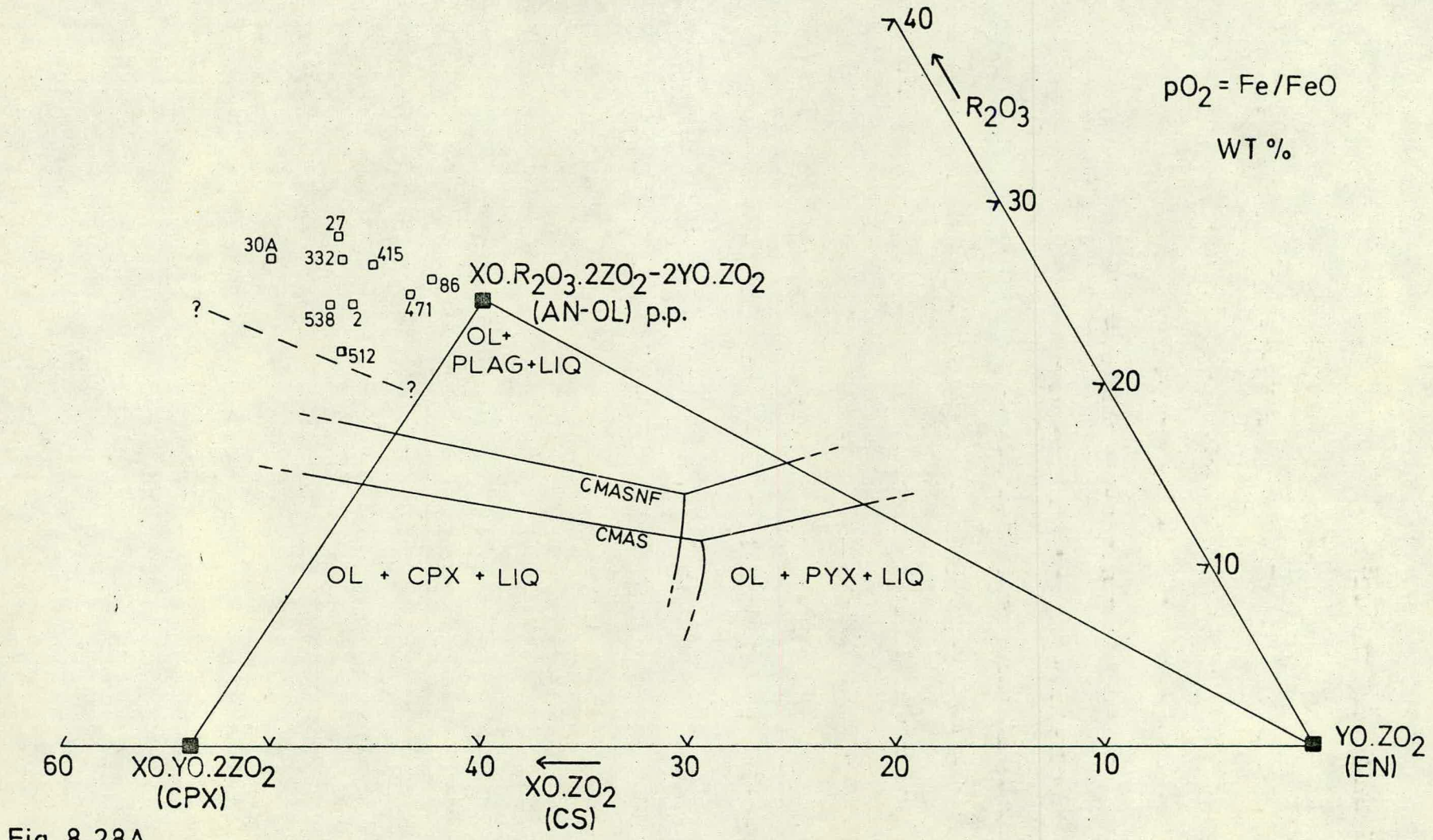
40
R_2O_3
pO_2 = Fe/FeO
WT %
30
20
10
27
30A
332
415
86
471
538
2
512
?
?
$XO.R_2O_3.2ZO_2-2YO.ZO_2$
(AN-OL) p.p.
OL+
PLAG+LIQ
CMASNF
CMAS
OL + CPX + LIQ
OL + PYX + LIQ
60
$XO.YO.2ZO_2$
(CPX)
40
$XO.ZO_2$
(CS)
30
20
10
$YO.ZO_2$
(EN)

Fig 8.28A

Figure 8.28B

See figure 8.28A

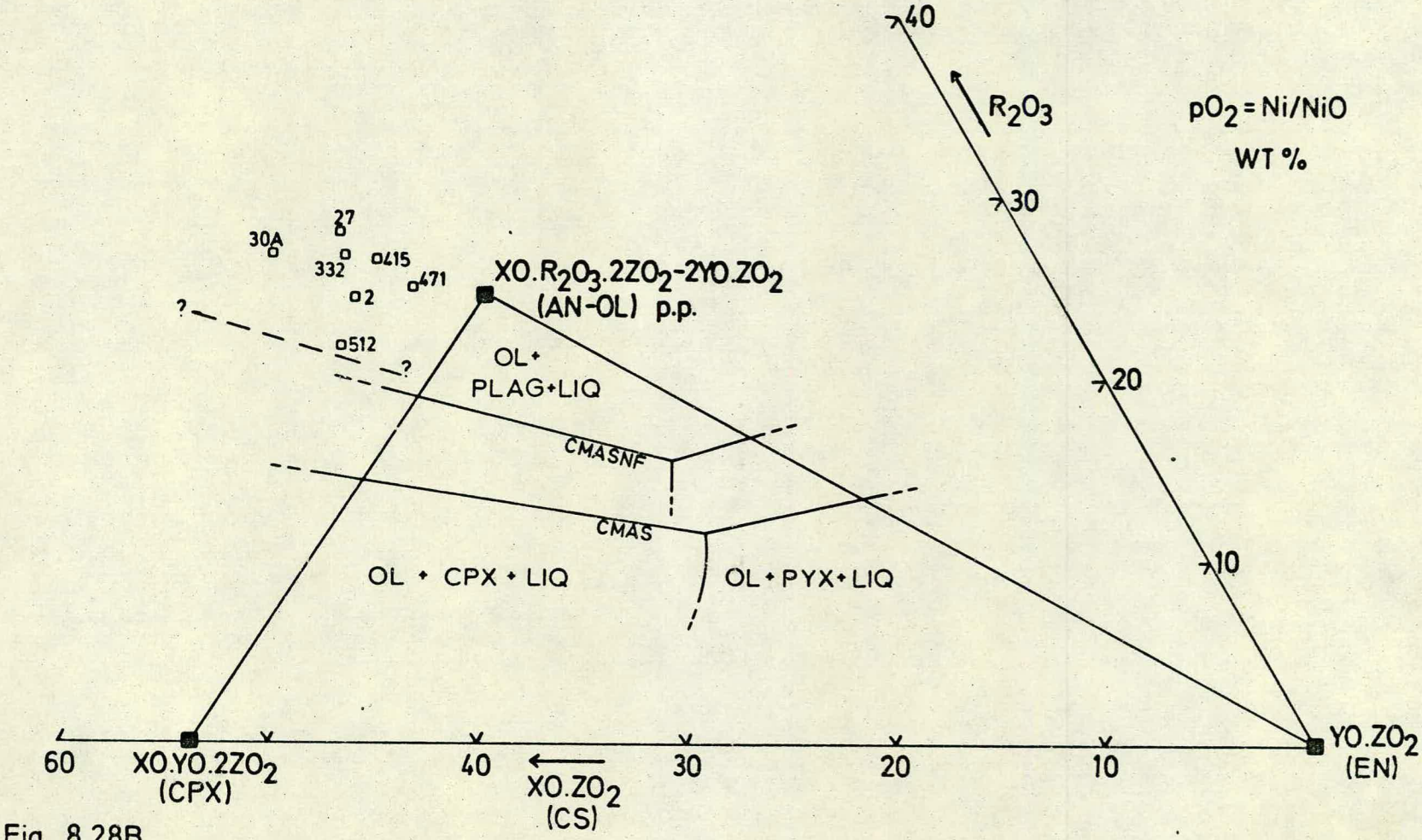
40
R_2O_3
pO_2 = Ni/NiO
WT %
30
20
10
27
30A
332
415
471
2
512
?
?
$XO.R_2O_3.2ZO_2$-$2YO.ZO_2$
(AN-OL) p.p.
OL+
PLAG+LIQ
CMASNF
CMAS
OL + CPX + LIQ
OL + PYX + LIQ
60
$XO.YO.2ZO_2$
(CPX)
40
$XO.ZO_2$
(CS)
30
20
10
$YO.ZO_2$
(EN)

Fig 8.28B

Figure 8.29A-8.29B

A XO.YO.$2ZO_2$ (clinopyroxene) projection into part of the plane XO.R_2O_3-YO-ZO_2 (CA-M-S) of the natural rocks studied from the Differentiated Series of Piton des Neiges volcano, Reunion. All iron was recast as FeO prior to projecting the analyses. The symbols indicate the liquidus phase for these rocks at the pO_2 of the Fe/FeO equilibrium (figure 8.29A) and Ni/NiO equilibrium (figure 8.29B). The pseudo phase boundary olivine+plagioclase+clinopyroxene+liquid for these rocks is indicated, the clinopyroxene appearing very shortly after olivine+plagioclase has been reached. The clinopyroxene-bearing projection boundaries from the system CMAS only (labelled CMAS), and that estimated for the system CMASN-Fe-O_2 (labelled CMASNF) for the combination of ratios $An_{50}Ab_{50}$, FeO/MgO mole ratio = 0.5, pO_2 = Fe/FeO or Ni/NiO (as appropriate) are also shown.

The symbols have the following meanings

- ● olivine liquidus
- □ plagioclase liquidus

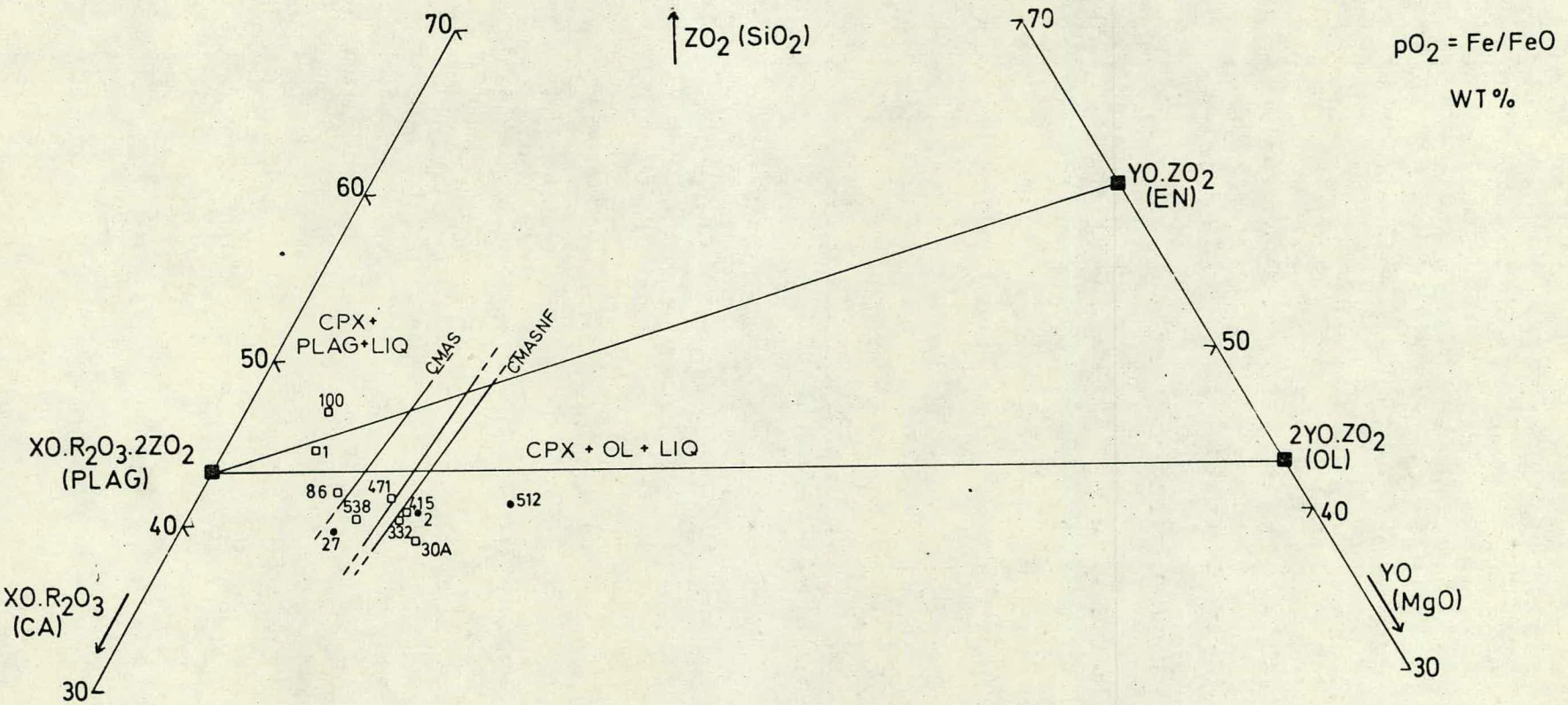
70
60
50
40
30
ZO_2 (SiO_2)
pO_2 = Fe/FeO
WT%
$YO.ZO_2$
(EN)
$XO.R_2O_3.2ZO_2$
(PLAG)
$XO.R_2O_3$
(CA)
$2YO.ZO_2$
(OL)
YO
(MgO)
CPX+
PLAG+LIQ
CPX + OL + LIQ
CMAS
CMASNF
100
1
86
538
471
415
2
27
332
30A
512

Fig 8.29A

Figure 8.29B

See figure 8.29A

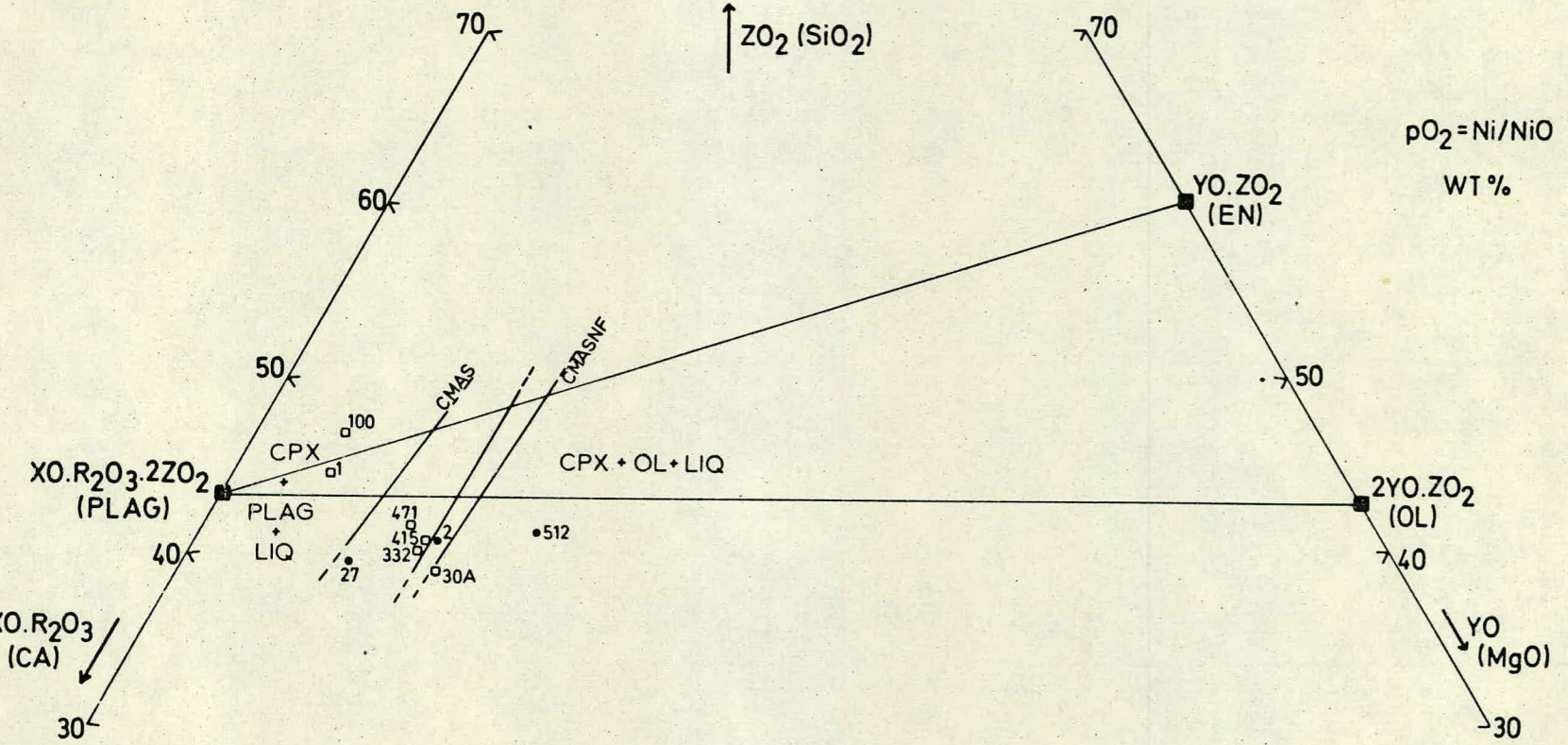
ZO2 (SiO2)
70
60
50
40
30
70
50
40
30
pO2 = Ni/NiO
WT %
YO.ZO2
(EN)
2YO.ZO2
(OL)
YO
(MgO)
XO.R2O3.2ZO2
(PLAG)
XO.R2O3
(CA)
CPX
PLAG
+
LIQ
CPX + OL + LIQ
CMAS
CMASNF
100
1
471
415
332
2
27
30A
512

Fig 8.29B

Figures 8.30A-8.30B

A $XO.YO.2ZO_2$ (clinopyroxene) projection into part of the plane $XO.R_2O_3$-YO-ZO_2 (CA-M-S) of all the natural rocks studied from Reunion Island having olivine or plagioclase liquidus. All iron was recast to FeO prior to projecting the analyses. The symbols indicate the liquidus phase for each of the rocks at the pO_2 of the Fe/FeO equilibrium (figure 8.30A) and Ni/NiO equilibrium (figure 8.30B), to show why the Differentiated Series rocks generally have a plagioclase liquidus, while the Oceanite Series rocks have an olivine liquidus. The pseudo phase boundary olivine+ plagioclase+clinopyroxene+liquid for these rocks is indicated, the clinopyroxene appearing very shortly after olivine+plagioclase has been reached. The clinopyroxene-bearing projection boundaries from the system CMAS only (labelled CMAS), and that estimated for the system CMASN-Fe-O_2 (labelled CMASNF) for the combination of ratios $An_{50}Ab_{50}$, FeO/MgO mole ratio = 0.5, pO_2 = Fe/FeO or Ni/NiO (as appropriate) are also shown.

The symbols have the following meanings

- ● olivine liquidus
- □ plagioclase liquidus
- ■ olivine+plagioclase liquidus

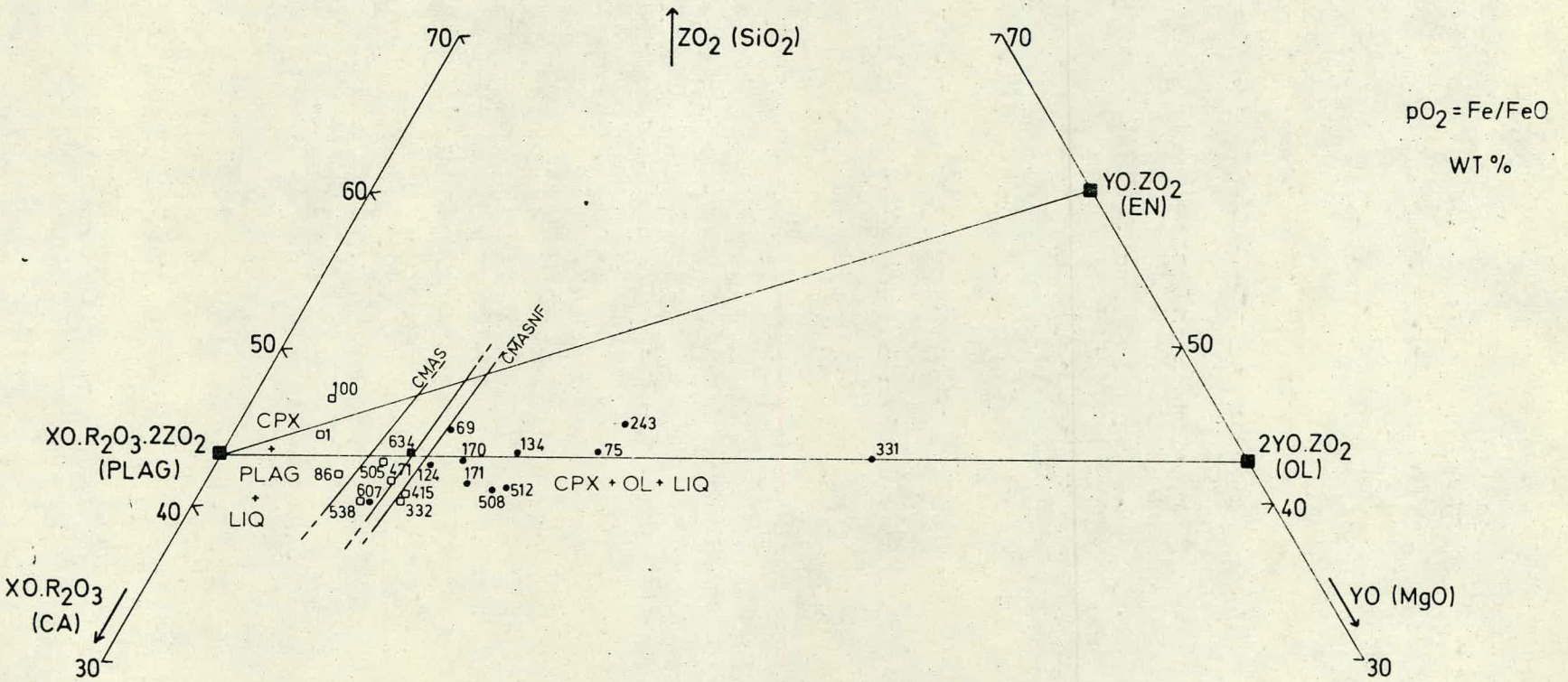
ZO2 (SiO2)
70
60
50
40
30
XO.R2O3.2ZO2
(PLAG)
XO.R2O3
(CA)
YO.ZO2
(EN)
2YO.ZO2
(OL)
YO (MgO)
pO2 = Fe/FeO
WT %
CPX
PLAG
LIQ
CMAS
CMASNF
CPX + OL + LIQ
100
1
634
69
243
170
134
75
331
86
505
471
124
171
607
415
512
538
332
508

Fig 8.30A

Figure 8.30B

See figure 8.30A

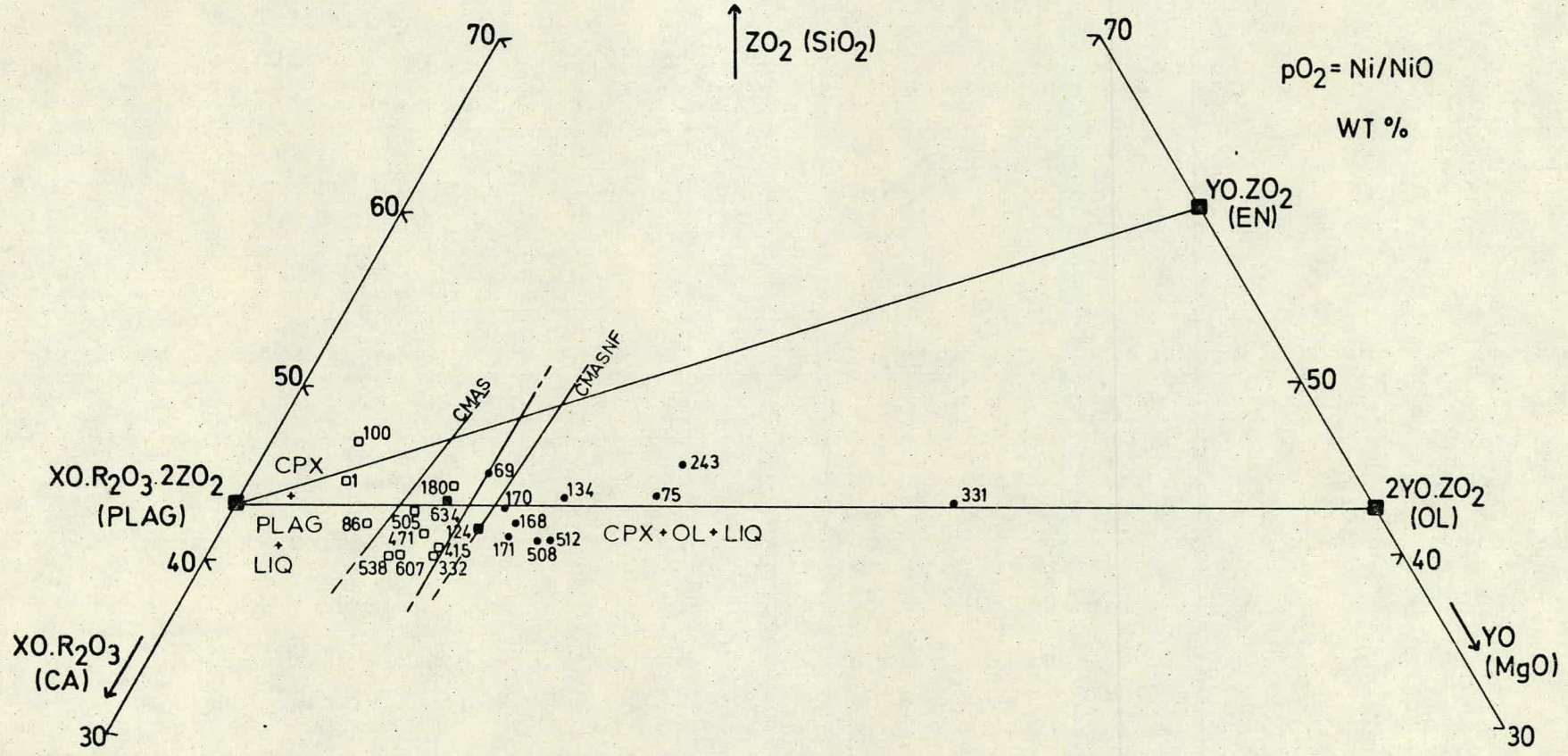
ZO2 (SiO2)
pO2 = Ni/NiO
WT %
70
60
50
40
30
YO.ZO2
(EN)
2YO.ZO2
(OL)
XO.R2O3.2ZO2
(PLAG)
XO.R2O3
(CA)
YO
(MgO)
CMAS
CMASNF
CPX
PLAG
LIQ
CPX+OL+LIQ
100
1
180
69
243
170
134
75
331
86
505
634
471
124
168
415
171
512
508
538
607
332

Fig 8.30B

Figure 8.31

A $XO.YO.2ZO_2$ (clinopyroxene) projection into part of the plane $XO.R_2O_3$-YO-ZO_2 (CA-M-S) of the deduced cotectic liquids in equilibrium with olivine+plagioclase+pyroxenes from the Apollo 11,12 and 15 rocks from Biggar, et al. (1971,1972) and Humphries, et al. (1972a). The arrow indicates the direction of increasing TiO_2 content in these liquids, the boundaries labelled P being the preferred position at simultaneous saturation with TiO_2-rich oxides and the silicates. (The Apollo 11 boundaries are drawn without allowance for TiO_2-rich phase crystallisation). Also shown is the olivine+plagioclase+clinopyroxene+liquid phase boundary estimated for the system CMASN-Fe-O_2 for the combination of ratios $An_{85}Ab_{15}$, FeO/MgO mole ratio = 0.75, pO_2 = Fe/FeO.

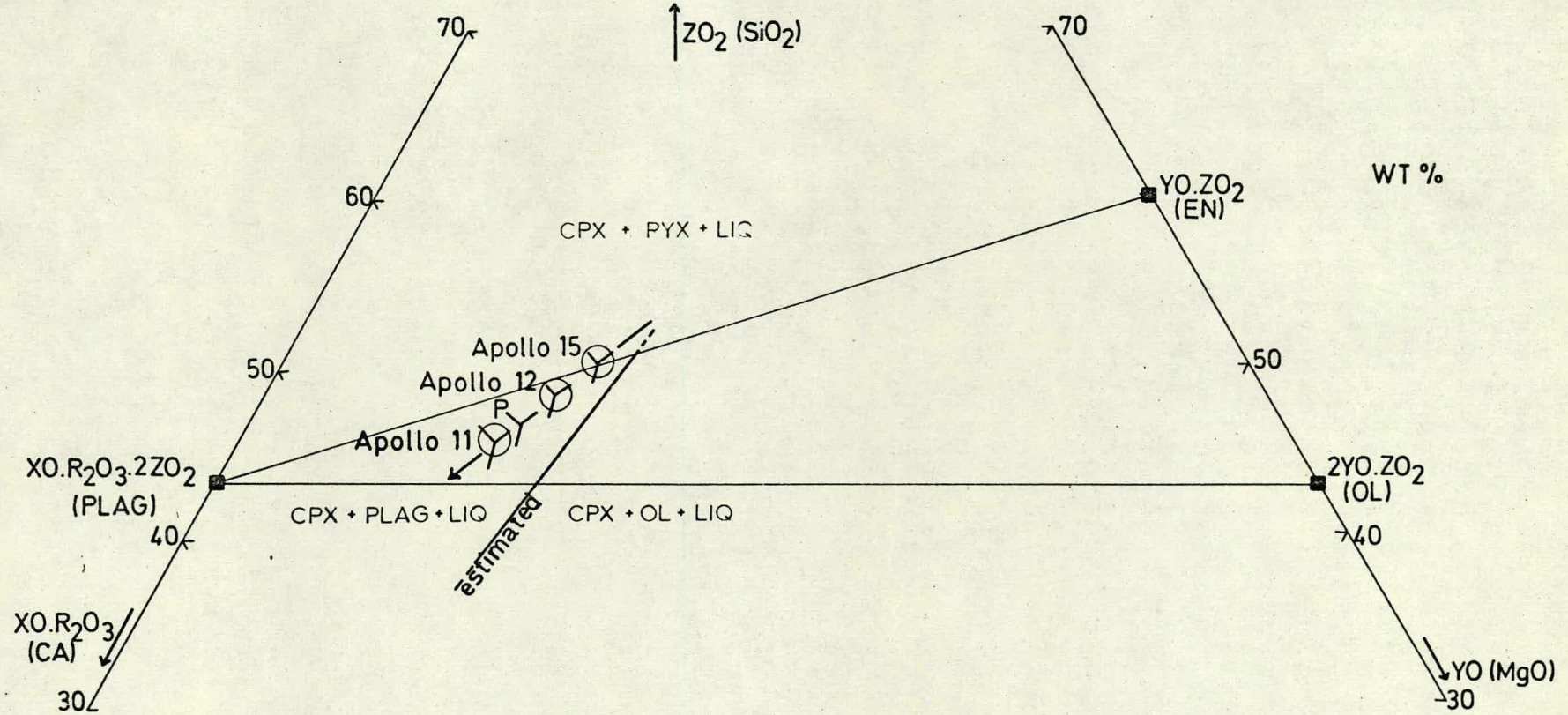
ZO2 (SiO2)
70
60
50
40
30
70
50
40
30
WT %
YO.ZO2
(EN)
2YO.ZO2
(OL)
XO.R2O3.2ZO2
(PLAG)
XO.R2O3
(CA)
YO (MgO)
CPX + PYX + LIQ
Apollo 15
Apollo 12
P
Apollo 11
CPX + PLAG + LIQ
CPX + OL + LIQ
estimated

Fig 8.31

Figure 8.32

A $2YO.ZO_2$ (olivine) projection into part of the plane $XO.ZO_2$-$YO.ZO_2$-R_2O_3 (CS-MS-A) of the deduced cotectic liquids in equilibrium with olivine+plagioclase+pyroxenes from the Apollo 11, 12 and 15 rocks from Biggar, et al. (1971,1972) and Humphries, et al. (1972a). The arrow indicates the direction of increasing TiO_2 content in these liquids, the boundaries labelled P being the preferred position at simultaneous saturation with TiO_2-rich oxides and the silicates. (The Apollo 11 boundaries are drawn without allowance for TiO_2-rich phase crystallisation). Also shown is the olivine+plagioclase+clinopyroxene+liquid phase boundary estimated for the system CMASN-Fe-O_2 for the combination of ratios $An_{85}Ab_{15}$, FeO/MgO mole ratio = 0.75, pO_2 = Fe/FeO.

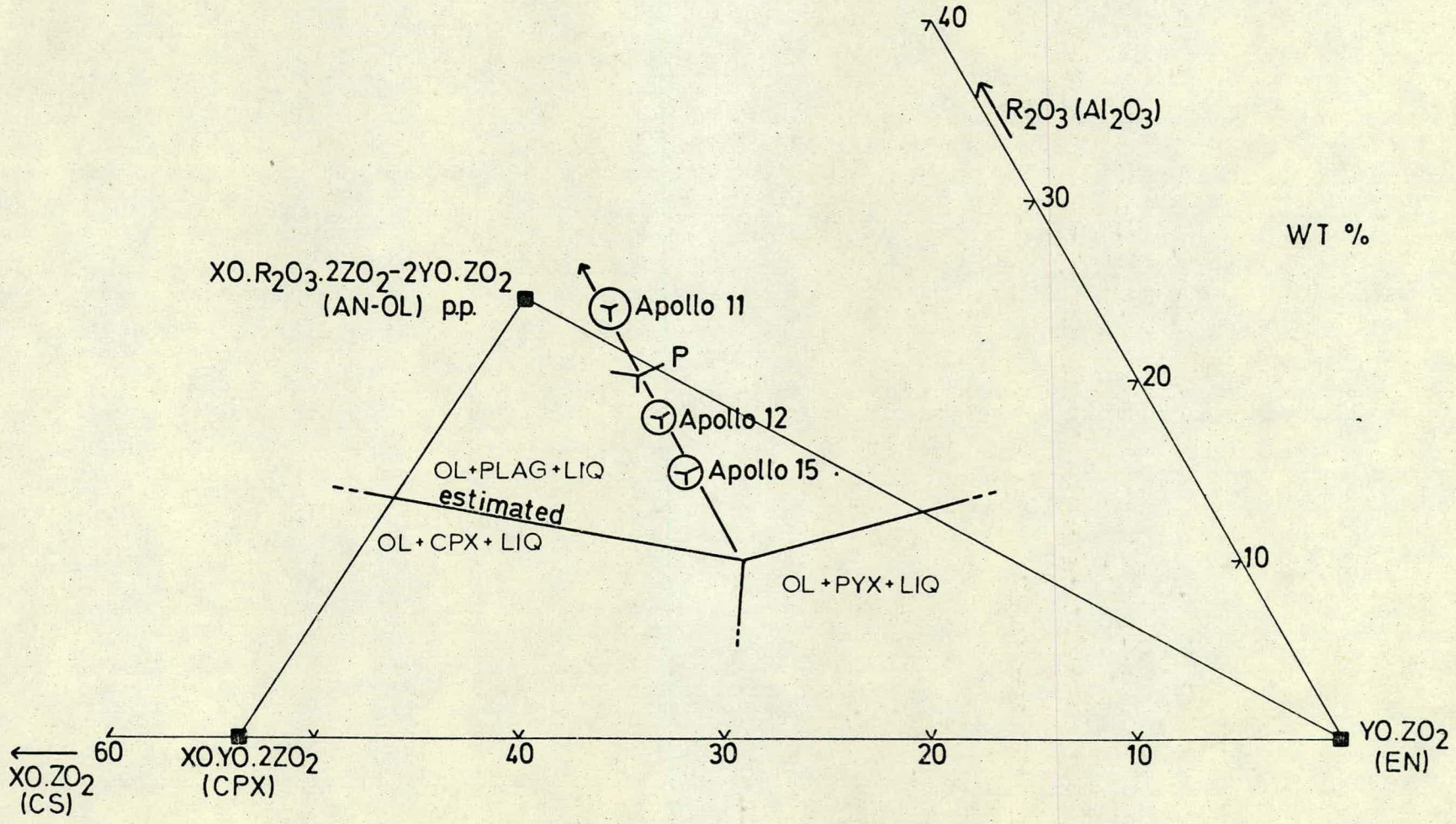
40
R_2O_3 (Al_2O_3)
30
WT %
20
10
$XO.R_2O_3.2ZO_2$-$2YO.ZO_2$
(AN-OL) p.p.
Apollo 11
P
Apollo 12
Apollo 15
OL+PLAG+LIQ
estimated
OL+CPX+LIQ
OL+PYX+LIQ
60
40
30
20
10
$XO.ZO_2$
(CS)
$XO.YO.2ZO_2$
(CPX)
$YO.ZO_2$
(EN)

Fig 8.32

Figure 8.33

Typical melting patterns obtained by Thompson (1972) for natural rocks studied using the argon atmosphere technique. Pattern A agrees with the synthetic system model of Thompson, with all the phases eventually joining the liquidus trend. Pattern B does not agree, the spinel (sp) temperature of appearance increasing with evolutionary sequence, while the clinopyroxene (cpx) appearance decreases throughout and fails to join the liquidus trend.

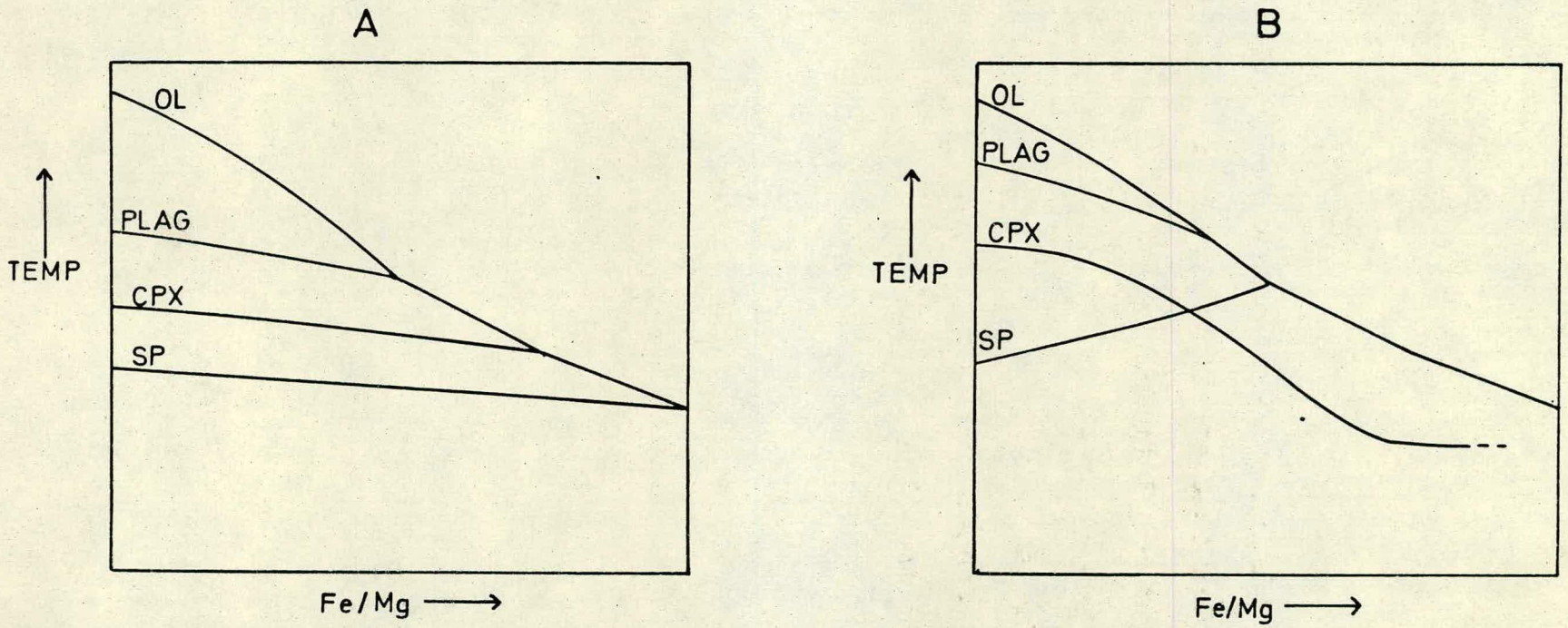

Fig 8.33

Figure 8.34

An oxygen projection of part of the liquidus phase boundaries in the system MgO-SiO-Fe-O_2 into the plane MgO-SiO_2-FeO at $pO_2 = 10^{-6}$, drawn from the analysis presented for this system in figure 6.2. The fractional crystallisation trend of composition Z is shown as the solid line for this pO_2 condition, the equilibrium crystallisation of some of the component compositions of this trend at this pO_2 is also shown (dashed lines).

Inset A presents the equilibrium crystallisation melting pattern which would be obtained for the fractionation series, if studied at $pO_2 = 10^{-6}$ conditions.

Inset B presents the equilibrium constant composition melting pattern for the fractionated series, the pO_2 of the atmosphere in contact with each of the compositions decreasing with decreasing temperature.

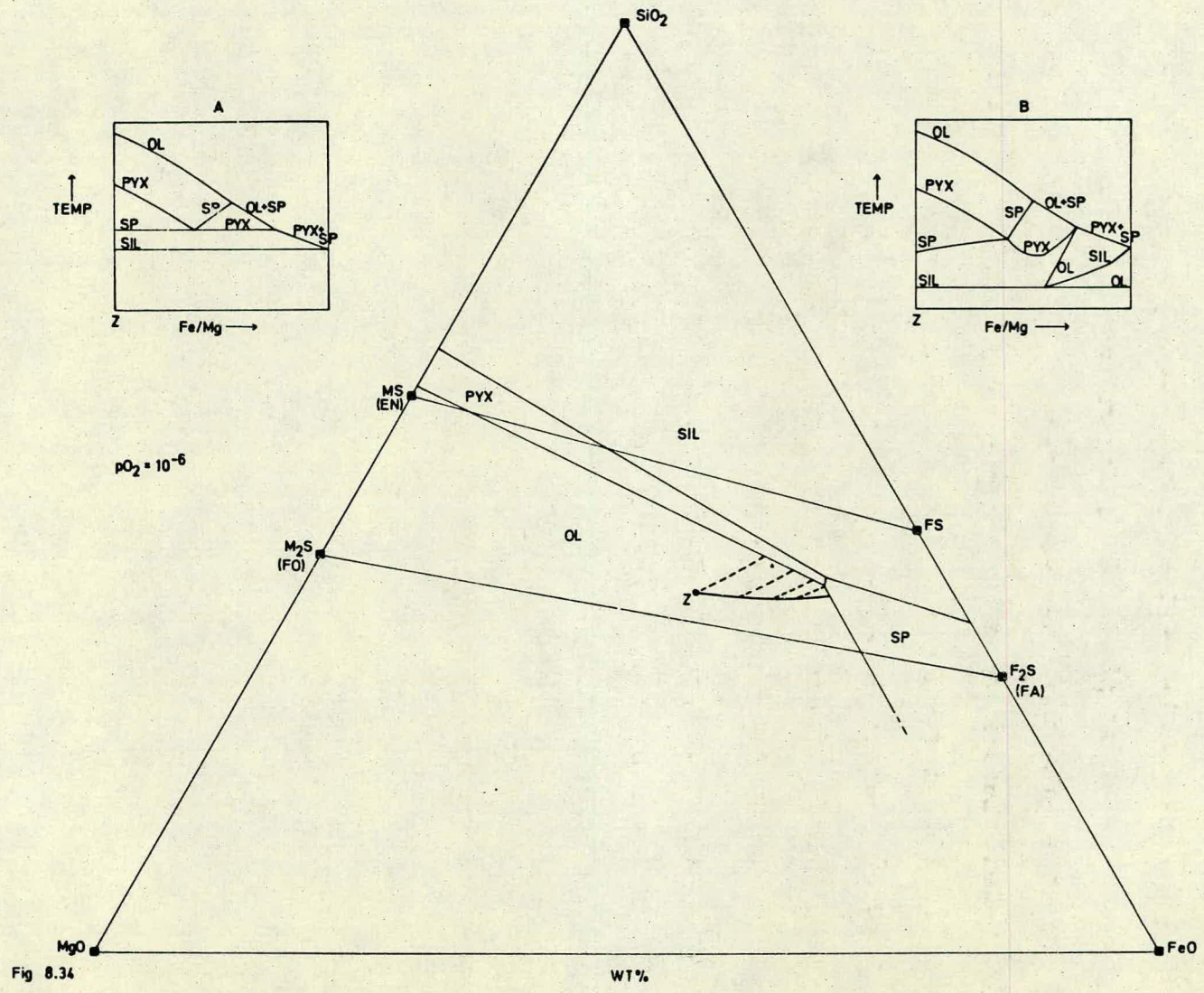
A
OL
PYX
TEMP
SP
SIL
S
OL+SP
PYX
PYX+SP
Z
Fe/Mg
B
OL
PYX
TEMP
SP
OL+SP
PYX+SP
SP
PYX
SIL
OL
SIL
OL
Z
Fe/Mg
SiO2
MS
(EN)
PYX
SIL
pO2 = 10-6
FS
M2S
(FO)
OL
Z
SP
F2S
(FA)
MgO
FeO
WT%

Fig 8.34

Figure 8.35

An oxygen projection of part of the liquidus phase boundaries in the system $MgO-SiO_2-Fe-O_2$ into the plane $MgO-SiO_2-FeO$ at $pO_2 = 10^{-8}$, drawn from the analysis presented for this system in figure 6.2. The fractional crystallisation trend of composition Z, the same composition as in figure 8.34, is shown as the solid line for this pO_2 condition, the equilibrium crystallisation of some of the component compositions of this trend at this pO_2 is also shown (dashed lines).

Inset A presents the equilibrium crystallisation melting pattern which would be obtained for the fractionated series, if studied at $pO_2 = 10^{-8}$ conditions.

Inset B presents the equilibrium constant composition melting pattern for the fractionated series, the pO_2 of the atmosphere in contact with each of the compositions decreasing with decreasing temperature.

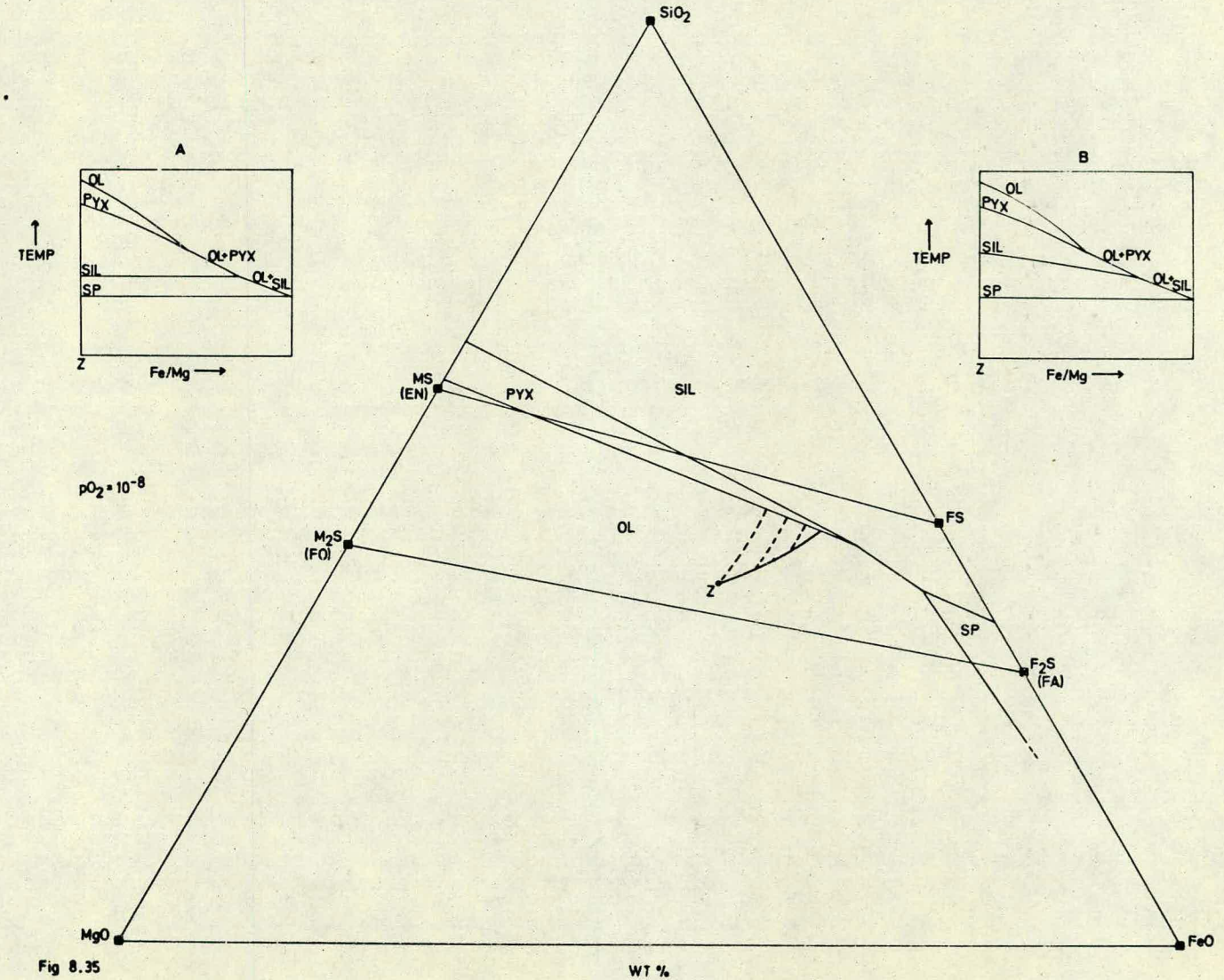
A
OL
PYX
TEMP
OL+PYX
SIL
OL+SIL
SP
Z
Fe/Mg
B
OL
PYX
SIL
TEMP
OL+PYX
OL+SIL
SP
Z
Fe/Mg
SiO2
MS
(EN)
PYX
SIL
FS
M2S
(FO)
OL
Z
SP
F2S
(FA)
MgO
FeO
WT %
pO2 = 10-8

Fig 8.35

Figure 8.36

The melting pattern obtained for some of the rocks of the Oceanite Series, Reunion, at a pO_2 slightly more oxidising than that of the Ni/NiO equilibrium. The pattern obtained is similar to that for the synthetic system at $pO_2 = 10^{-8}$ (figure 8.35).

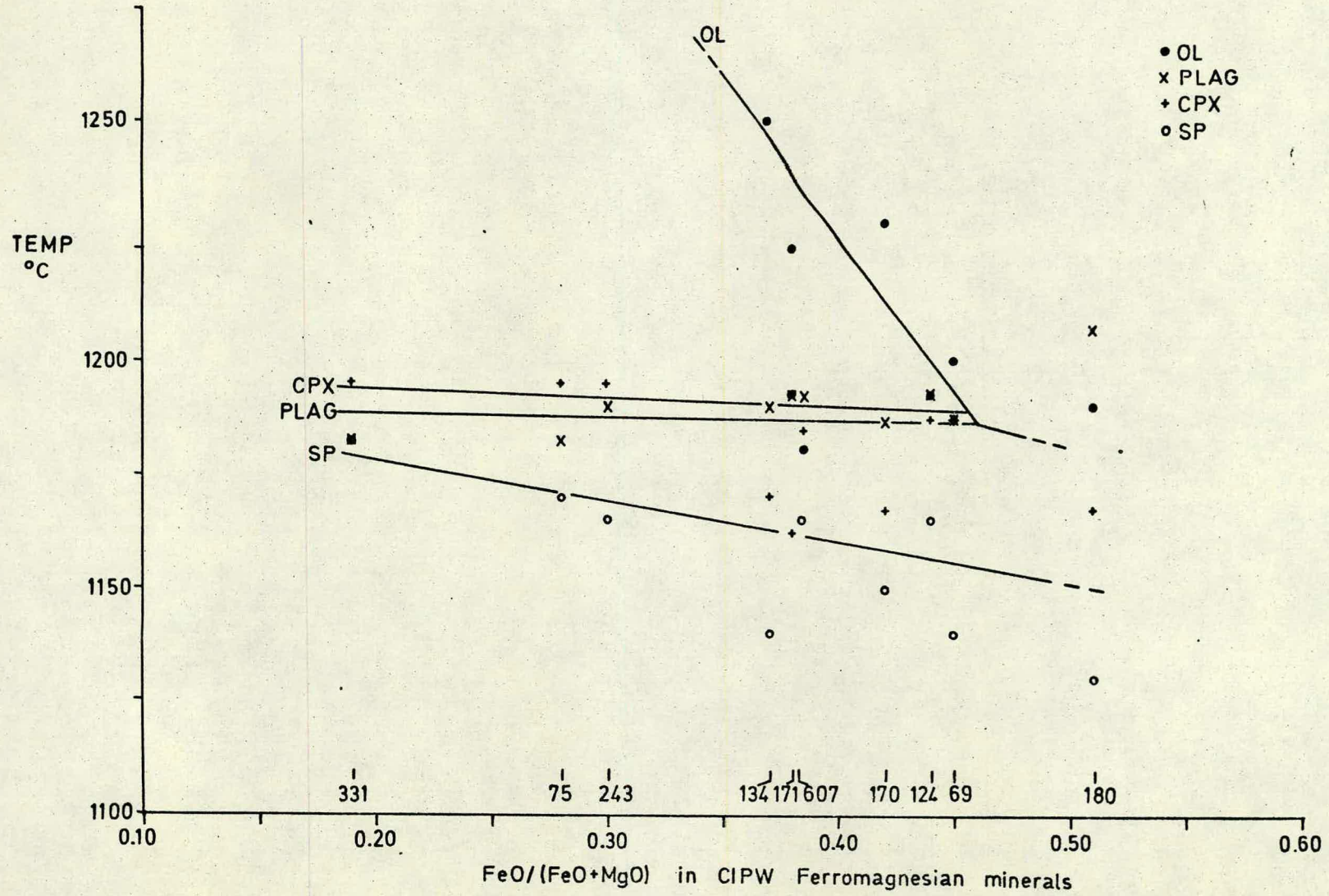
OL
• OL
x PLAG
+ CPX
o SP
TEMP °C
1250
1200
1150
1100
CPX
PLAG
SP
331
75
243
134
171
607
170
124
69
180
0.10
0.20
0.30
0.40
0.50
0.60
FeO/(FeO+MgO) in CIPW Ferromagnesian minerals

Fig 8.36